Spanningsgebaseerde proportionele regeling
van convertorgekoppelde gedistribueerde generatoren in microgrids

Voltage-Based Droop Control
of Converter-Interfaced Distributed Generation Units in Microgrids

Tine Vandoorn

Promotor: prof. dr. ir. L. Vandevelde
Proefschrift ingediend tot het behalen van de graad van
Doctor in de Ingenieurswetenschappen: Werktuigkunde-Elektrotechniek

Vakgroep Elektrische Energie, Systemen en Automatisering
Voorzitter: prof. dr. ir. J. Melkebeek
Faculteit Ingenieurswetenschappen en Architectuur
Academiejaar 2012 - 2013

UNIVERSITEIT
GENT

ISBN 978-90-8578-585-9
NUR 961
Wettelijk depot: D/2013/10.500/18

Ghent University
Faculty of Engineering and Architecture
Department of Electrical Energy,
Systems and Automation (EESA)
Electrical Energy Laboratory (EELAB)

Voltage-Based Droop Control of Converter-Interfaced Distributed Generation Units in Microgrids

Tine Vandoorn

PhD dissertation submitted to obtain the degree of
Doctor of Electromechanical Engineering

Promoter:
Prof. dr. ir. Lieven Vandevelde (UGent – EESA)

Chairman:
Prof. dr. ir. Hendrik Van Landeghem (Director of Education)

Exam commission:
Prof. dr. ir. ing. Jan Desmet (Howest, Kortrijk)
Prof. dr. ir. Chris Develder (UGent – INTEC)
Prof. dr. ir. Johan Driesen (K.U. Leuven)
Prof. dr. ir. Robain De Keyser (UGent – EESA)
Prof. dr. ir. Josep Guerrero (Aalborg University)
dr. ir. Bert Renders (Ingenium)
Prof. dr. ir. Lieven Vandevelde (UGent – EESA)

Dankwoord

Dit werk was niet tot stand gekomen zonder de hulp en vooral de steun van enkele mensen rondom mij, waarvoor een woord van dank zeker gepast is. In de eerste plaats gaat mijn dank uit naar mijn promotor Lieven. Hij heeft me altijd gesteund, me voldoende vrijheid gegeven en ondanks zijn drukke agenda steeds tijd proberen te maken voor mij. Mijn computerproblemen heeft hij aangepakt met enkele magische commando's, waarvoor ik veel bewondering heb.

Mijn (ex-)bureaugenootjes Jeroen, Lieven en Bert verdienen een oprechte vermelding in dit dankwoord. Ze hebben me steeds opnieuw uitgedaagd om een stap verder te gaan en nieuwe pistes te onderzoeken. Hun kritische opmerkingen en de gezamenlijke discussies en redeneringen op ons bord hebben een grote bijdrage geleverd in de kwaliteit van dit werk. Daarnaast heb ik het geluk gehad om altijd in een bureau te vertoeven met een goede sfeer, waarvoor dank. Ik wil Bert bedanken voor de begeleiding bij mijn eerste stappen in de academische wereld, met heel veel goede raad en hulp. Ook Lieven heeft me veel wijsheden, en iets mindere wijsheden, bijgebracht. Ik heb hem moeten missen na zijn vertrek. De leemte in onze bureau die Lieven nagelaten had, heeft Jeroen goed kunnen opvullen. Bedankt om voortdurend mijn schrijfwerk te willen nalezen en voor de hulp met allerhande zaken, zeker tijdens het schrijven van dit werk.
In een paragraaf apart moet toch mijn collega en bureaugenoot Bart komen. Samen aan de opstelling werken was niet alleen productief, maar ook leuk. Je geloof in mij heeft me erg geholpen. Bedankt voor de steun die je me altijd geeft.

Ik wil van de gelegenheid gebruik maken om enkele collega's te bedanken voor de vruchtbare samenwerking. Eerst en vooral wil ik mijn collega's van EELAB, Power-Link en de Howest, in het bijzonder Jan Desmet, bedanken. Een woordje van dank aan onze goedlachse secretaresse Marilyn. Sinds kort hebben Jan, Christof en Brecht ons "netten" team vervoegd, en het is er alleen maar beter op geworden. Ik heb altijd graag geluisterd naar de inzichten van Jeroen De Maeyer over van alles en nog wat, een wijs persoon voor wie ik veel respect heb. Hetzelfde

geldt voor Thomas, bedankt.

Vervolgens wil ik enkele vrienden en vriendinnen via deze weg expliciet bedanken. In de eerste plaats Elke. Enkele van de leukste momenten van mijn leven waren toch met jou. Bedankt om er altijd te zijn en heel vaak mijn dag goed te maken, ook tijdens dit doctoraat. Mijn naamgenootje Tine, Hanne en ons Tanya verdienen zeker een speciaal woordje van dank, hun interesse in mijn doctoraat was veel groter dan ik ooit mocht verwachten. Vervolgens wil ik ook Matthias en Ann-Sofie bedanken. Het is altijd leuk vertoeven bij hen, maar ons avontuur op de ski-latten is iets om nooit te vergeten. Bedankt voor deze, en voor veel andere leuke tijden.

Daarnaast wil ik ook mijn familie, en in het bijzonder mijn grootouders en schoonouders bedanken. Met Dieter, Bert, Joseline en Erik zwoegen op onze bouwwerf was vaak zwaar, maar leuk, werk, bedankt hiervoor. Zonder jullie was dit zeker niet op zo een korte termijn gelukt. Bedankt voor de goede zorgen Joseline en voor de hulp bij de organisatie van de verdediging.

Mama, papa, Bert. Bedankt voor de steun doorheen de jaren, jullie goede zorgen en je grenzeloze liefde. Papa, bedankt om steeds in me te geloven en om mijn doctoraat zo grondig na te lezen. Je inzichten hierover hebben me verrast, maar eigenlijk ben ik dit ook wel een beetje gewoon. Mams, jij bent de persoon bij wie ik altijd terecht kan, je bent de liefste die ik ken. Buiten mijn broer gerekend dan, wiens zacht karakter een leuke standvastigheid is voor me. Altijd leuk als je weer thuis bent broertje. Ten slotte gaat het belangrijkste woordje van dank toch wel uit naar Kristof. Meer dan wie ook maak je mijn verhaaltje compleet.

Tot slot wens ik de lezer een boeiend leesavontuur doorheen dit verhaal.

Maart 2013
Tine

Contents

Summary

The uncertain prices of fossil fuels, concerns about climate change, the dependency of energy supply on other countries and the liberalisation of the energy markets are leading to an increasing penetration of distributed generation (DG) units in the electric power system, a large part of which use renewable energy sources. Despite the numerous advantages of these small-scale units, the current fit-and-forget approach of connecting them to the electrical networks is not a sustainable option. The distribution system is increasingly being confronted with congestion and voltage problems, which limits the further penetration of DG. Hence, a more coordinated approach for integrating DG in the distribution networks is required. Microgrids are designed to provide this coordination by aggregating generators, loads and storage elements. They are likely to play a key role in the evolution of the smart grid. In this sense, the smart grid can emerge as a system of integrated smart microgrids. In the grid-connected mode, microgrids present themselves to the utility network as controllable entities. When necessary, microgrids can also island to deliver reliable power to the local grid elements, e.g., by providing an uninterruptible power supply functionality to hospitals and industrial facilities. Fully off-grid microgrids can enable electrification of remote regions in an economic manner.

In the islanded mode, the microgrid elements are responsible for power sharing and maintaining the power quality in the local network. Microgrids have different characteristics compared to the transmission networks, e.g., this PhD thesis focusses on the low-voltage connected microgrids with resistive network lines opposed to the inductive transmission networks. Microgrids also have a large share of intermittent power sources and power-electronically interfaced grid-elements. Therefore, new control methods for the grid elements in islanded microgrids need to be developed. Like the conventional grid control, microgrid control can be envisioned as a hierarchical control. Locally, the inverters, which interface the DG units to the grid, control their output voltage (islanded microgrid) or current (grid-connected microgrid) to a reference value. This reference value is generally determined by an overlaying primary controller. The primary controller can consist of a power control strategy that enables power sharing between the DG units in

islanded microgrids. It is responsible for the short term stability and reliability of the network. Developing a robust primary control strategy is the core of this PhD thesis. The reference power of this primary controller can, in turn, be altered by an overlaying secondary/tertiary control scheme that is responsible for various objectives such as longer-term economic optimisation.

Chapter 1 introduces the concepts, benefits and challenges of DG, smart grids, microgrids and virtual power plants (VPPs).

Chapter 2 provides an overview of existing primary control strategies for islanded microgrids. To hand a clear overview and enable a clear comparison of the different strategies, the control schemes are given in a coherent manner. Both communication-based controllers and controllers without communication, i.e., droop controllers, are considered. As reliability is key in primary control, it is concluded that communication should be avoided for this purpose. Hence, the droop control scheme is the one further examined in this PhD thesis.

In grid-connected microgrids, the DG units control their terminal current to a certain reference value. In islanded microgrids on the other hand, the power control strategy determines a set-value for the terminal voltage of the inverter that interfaces the primary energy source with the distribution network. Hence, a proper voltage control strategy is crucial for a robust microgrid operation. Chapter 3 discusses the voltage control in islanded microgrids. This chapter deals with the control theory and is not essential for the further development of the primary power control strategy.

Chapter 4 forms the core of this PhD thesis. In this chapter, the voltage-based droop (VBD) control strategy is developed to enable active and reactive power sharing in a single-phase islanded microgrid. This primary controller is responsible for ensuring a stable microgrid operation and uses the voltage as trigger for active power changes of the units. Opposed to many control strategies in literature, the VBD control strategy is based on the specific characteristics of the considered low-voltage microgrids, such as the lack of rotating inertia, the predominantly resistive lines and the high share of intermittent power sources. Because of the usage of constant-power bands, which define an interval in which the voltage may vary without altering the output of the DG units based on the state of the network, the VBD control enables an optimised integration of renewable energy sources. An automatic priority is assigned in the response of the units to load changes, including addressing renewable energy sources for grid support in extreme conditions. An additional control loop is included in the VBD control

strategy such that not only the active and reactive power, but also the harmonic power is properly shared between the different DG units.

Microgrids consist not only of inverter-interfaced DG units, the other grid elements such as the coupling transformer in grid-connected mode, uncontrollable and controllable loads and storage elements are considered in chapter 5. The latter two elements can also contribute in the primary control of the microgrid. Hence, analogously as in the VBD control of the DG units, in section 5.1, the voltage is used for demand dispatch or storage control. Mirrored with VBD control in the DG units, constant-power bands are used. Hence, an automatic priority to change the units' settings is assigned, e.g., such that first, the controllable DG units respond to load changes, next the storage elements and later the controllable loads and less-controllable DG units (such as many renewable sources).
Opposed to in conventional networks, synchronous generators are rather rare in low-voltage microgrids as most DG units are inverter-interfaced. A mismatch between the VBD control strategy and the synchronous generators' controllers exists. Because of the low share of synchronous generators, in section 5.2, the controllers of the SGs are adapted to comply with the VBD control strategy.
Next to the development of the VBD control strategy in chapter 4, a second key element of this PhD thesis is the smart transformer concept presented in section 5.3. The smart transformer is connected at the point of common coupling (PCC) between the utility network and the microgrid. It enables a controlled power exchange between both grids, with the microgrid elements operating as if they were in islanded mode with VBD control. As the microgrid elements automatically respond to smart transformer changes, there is no need for additional communication inside the microgrid. In this way, the smart transformer succeeds to realise one of the most important benefits of microgrids, i.e., their ability to operate as controlled entities . This hands important scaling benefits for the network operator's point of view who does not need to consider each grid element separately any more, which simplifies the market operation of the microgrid.

Except for section 5.3, all previous sections focussed on islanded microgrids. Even in section 5.3, the conventional grid-connected mode was not discussed as a predefined power exchange between microgrid and utility network was achieved. Hence, the utility network was regarded as an undispatchable generator or load. Therefore, chapter 6 studies the VBD control in case of a grid-connected microgrid. Although developed for islanded microgrids, VBD control can pose significant benefits in grid-connected microgrids as well, mainly because the voltage is used as the non-conventional trigger for active power changes. This chapter points out that the VBD control can avoid on-off oscillations in networks

with a high penetration of renewable energy sources, enables to address renewables for grid voltage support when necessary and can even lead to a reduction of the line losses. Also, to allow for microgrid operation in both modes, an additional control loop is included in the VBD control that enables a smooth mode transition.

With the developed control strategy, a robust microgrid operation is possible, i.e., it is a primary control of the microgrid. In chapter 7, the integration of the proposed VBD control in a hierarchical control structure in microgrids is discussed. Some examples are included to clarify the rationale of using secondary/tertiary controllers. The interaction of the developed VBD control and a secondary controller, that changes the former's set points is analysed. Finally, the promising VPP concept is discussed and a hierarchical VPP/microgrid control is presented.

Chapter 8 concludes this PhD thesis and hands some possibilities for further research.

Samenvatting

De onzekere prijzen van fossiele brandstoffen, ongerustheid over klimaatsverandering, afhankelijkheid van andere landen voor energievoorziening en de liberalisatie van de energiemarkten heeft geleid tot een toenemend aandeel decentrale generatoren (DG eenheden) in the elektrisch net. Een groot aandeel van deze DG eenheden wordt gevoed met hernieuwbare energiebronnen. Ondanks de vele voordelen die deze kleine generatoren leveren, is de huidige "fit-and-forget" benadering voor hun connectie in de elektrische netten geen houdbare situatie. De distributienetten worden meer en meer geconfronteerd met congestie en spanningsproblemen, wat de verdere connectie van nieuwe DG eenheden beperkt. Bijgevolg is er een meer gecoördineerde aanpak voor de integratie van DG in het distributienet vereist. Microgrids zijn ontworpen om deze coördinatie te leveren, door aggregatie van generatoren, lasten en opslageenheden. Microgrids zullen hoogstwaarschijnlijk een belangrijke rol spelen in de evolutie van het smart grid. Het smart grid kan immers ontstaan als een systeem van geïntegreerde microgrids. In netgekoppeld bedrijf wordt een microgrid ten opzichte van de rest van het net als een regelbare geheel voorgesteld. Indien vereist, kan een microgrid overgaan naar eilandbedrijf om zo een betrouwbare vermogensvoorziening voor de lokale netelementen te verzekeren, bijvoorbeeld als noodstroomvoeding voor ziekenhuizen en industriële sites. Constant losgekoppelde microgrids kunnen elektriciteitsvoorziening van verafgelegen regio's op een economisch interessante wijze mogelijk maken.
In eilandbedrijf zijn de microgridelementen verantwoordelijk voor de vermogensverdeling en het behoud van een goede netkwaliteit in het lokale netwerk, zonder tussenkomst van een hogergelegen net. Microgrids hebben erg verschillende eigenschappen in vergelijking met het transmissienet, bvb., dit doctoraat concentreert zich op microgrids die gekoppeld zijn aan het laagspanningsnet, dat voornamelijk resistieve netwerklijnen heeft in tegenstelling tot de inductieve hoogspanningslijnen. Daarnaast bevatten microgrids ook een hoge graad aan intermitterende vermogensbronnen en netwerkelementen met een vermogenselektronische koppeling met het net. Bijgevolg zijn er nieuwe regelmethodes voor de netwerkelementen in microgrids in eilandbedrijf vereist. Net als de conventionele netregeling, kan de microgridregeling opgevat worden als een hiërarchische regeling. Lokaal rege-

len de invertoren, die de interface van de DG eenheid met het net vormen, hun uitgangsspanning (microgrid in eilandwerking) of -stroom (netgekoppeld bedrijf) naar een referentiewaarde. Deze referentiewaarde wordt over het algemeen bepaald door een bovenliggende primaire regelaar. De primaire regeling kan bestaan uit een vermogensregeling die de vermogensverdeling tussen de DG eenheden in microgrids in eilandbedrijf verzekert. Ze is verantwoordelijk voor de korte termijn stabiliteit en de betrouwbaarheid van het netwerk. Het uitwerken van een primaire regelstrategie is de kern van dit doctoraat. Het referentievermogen van deze primaire regeling kan gewijzigd worden door een bovenliggend secundair/tertiair regelschema dat verschillende doeleinden kan hebben, zoals de economische optimalisatie van het microgrid op langere termijn.

Hoofdstuk 1 leidt de concepten in en bespreekt de voornaamste voordelen en uitdagingen van decentrale generatoren, slimme netten, microgrids en virtuele centrales.

Hoofdstuk 2 vervolgens levert een overzicht van bestaande primaire regelstrategieën voor microgrids in eilandbedrijf. Om een duidelijk overzicht en een eenvoudige vergelijking tussen deze regelingen mogelijk te maken, worden de regelschema's op een coherente wijze voorgesteld. Zowel regelaars op basis van communicatie als regelaars zonder communicatievereisten, de zogenaamde droopregelaars, worden beschouwd. Aangezien primaire regelaars als hoofddoel hebben om in te staan voor de betrouwbaarheid van het systeem, wordt er in dit hoofdstuk besloten dat communicatie vermeden moet worden hiervoor. Om deze reden wordt het droopregelschema verder onderzocht in deze doctoraatsverhandeling.

In netgekoppelde microgrids regelen de DG eenheden hun klemstroom naar een bepaalde referentiewaarde. In microgrids in eilandbedrijf daarentegen bepaalt de vermogensregeling een referentiewaarde voor de netspanning van de invertor. Bijgevolg is een goede spanningsregeling cruciaal om een robuuste werking van het microgrid te verzekeren. Hoofdstuk 3 bespreekt de spanningsregeling in microgrids in eilandbedrijf. Dit hoofdstuk gaat in op de regelconcepten zelf en is niet essentieel voor de verdere uitwerking van de primaire regeling.

Hoofdstuk 4 vormt het zwaartepunt van dit doctoraat. In dit hoofdstuk wordt de spanningsgebaseerde droopregeling (SBD regeling) ontwikkeld om het actief en reactief vermogen te verdelen tussen de DG eenheden in een éénfasig microgrid in eilandbedrijf. Deze primaire regelaar is verantwoordelijk voor een stabiele microgridwerking en gebruikt de netspanning als parameter om veranderingen teweeg te brengen in het actief vermogen dat geleverd wordt door de eenheden. In tegenstelling tot vele regelstrategieën in de literatuur, is de SBD regeling gebaseerd op de specifieke karakteristieken van microgrids op laagspanning, zoals hun

hoge graad aan moeilijk regelbare bronnen, hun lage inertie en de voornamelijk resistieve lijnen. Wegens het gebruik van de zogenaamde generator-specifieke constante vermogensbanden, die een interval bepalen waarin de klemspanning van een eenheid mag variëren zonder dat deze eenheid zijn output vermogen aanpast naar de toestand van het net, maakt deze regeling een geoptimaliseerde integratie van hernieuwbare energiebronnen mogelijk. Er wordt automatisch een prioriteit ingesteld waarin de eenheden reageren op lastveranderingen, inclusief het aanspreken van hernieuwbare bronnen voor netondersteuning in kritische situaties. Een additionele regellus wordt bijgevoegd bij de SBD regeling om naast het actief en het reactief vermogen ook het harmonisch vermogen gepast te verdelen tussen de verschillende DG eenheden.

Microgrids bestaan echter niet enkele uit invertorgebaseerde DG eenheden. De andere elementen zoals de transformator op het koppelpunt in netgekoppeld bedrijf, de onregelbare en regelbare lasten en de opslagelementen worden beschouwd in hoofdstuk 5. De laatste twee elementen kunnen bijdragen tot de primaire regeling van het microgrid. Om deze reden wordt in sectie 5.1 de spanning gebruikt voor de last- of opslagregeling, analoog als in de SBD regeling van de DG eenheden. Net zoals bij de DG eenheden worden er constante vermogensbanden gebruikt om een automatische prioriteit in de reactie van de eenheden in te stellen. De regelbare DG eenheden reageren bijvoorbeeld eerst op lastveranderingen, pas daarna de opslagelementen en later de regelbare lasten en minder-regelbare DG eenheden zoals vele hernieuwbare bronnen.
In tegenstelling tot in conventionele netwerken, komen synchrone generatoren niet frequent voor in microgrids op laagspanning aangezien de meeste DG eenheden met een invertor aan het net gekoppeld zijn. De conventionele regeling van synchrone generatoren is niet compatibel met de SBD regeling. Wegens het lage aandeel synchrone generatoren wordt in sectie 5.2 de regeling van deze eenheden aangepast om samenwerking met de SBD regeling mogelijk te maken.
Naast de ontwikkeling van de SBD regeling in hoofdstuk 4, is een tweede kernpunt van dit onderzoek het slimme transformator concept dat voorgesteld wordt in sectie 5.3. De slimme transformator is verbonden met het koppelpunt tussen het microgrid en de rest van het net. Het maakt een regelbare vermogensuitwisseling tussen deze twee netten mogelijk, waarbij de microgrid elementen werken alsof ze in eilandwerking waren met de SBD regeling. Op deze manier realiseert de slimme transformator een van de belangrijkste voordelen van microgrids, namelijk hun mogelijkheid om in netgekoppeld bedrijf te werken als een regelbaar geheel. Dit levert belangrijke schaalvoordelen op voor de netwerkoperatoren die niet meer ieder element afzonderlijk moeten beschouwen en het vereenvoudigt de marktwerking van een microgrid.

Buiten sectie 5.3 spitsen alle vorige paragrafen zich toe op de eilandwerking van het microgrid. Zelfs in sectie 5.3 wordt het conventioneel netgekoppeld bedrijf niet beschouwd aangezien een voorafbepaalde vermogensuitwisseling tussen microgrid en distributienetwerk verkregen wordt, waardoor deze laatste als een geregelde generator of last kan gezien worden. In hoofdstuk 6 daarentegen wordt de SBD regeling wel beschouwd in een netgekoppeld microgrid. Hoewel ze ontworpen is voor microgrids in eilandbedrijf, levert de SBD regeling significante voordelen in netgekoppelde microgrids, voornamelijk aangezien de spanning als de onconventionele parameter gebruikt wordt om veranderingen in actief vermogen teweeg te brengen. Dit hoofdstuk toont aan dat de SBD regeling aan/uit oscillaties in netwerken met een hoog aandeel hernieuwbare bronnen kan vermijden, het mogelijk maakt om op de hernieuwbare bronnen te rekenen voor netondersteunende diensten en zelfs kan leiden tot een reductie van de netwerkverliezen. Bovendien wordt in dit hoofdstuk een extra regellus ingevoegd bij de SBD regeling om werking in beide modes, met een vlotte transitie ertussen, mogelijk te maken.

Met de ontwikkelde regeling is een robuuste microgrid werking, dus door middel van een primaire regeling, mogelijk. In hoofdstuk 7 wordt de integratie van de voorgestelde SBD regeling in een hiërarchische regelstructuur in microgrids besproken. Enkele voorbeelden worden gegeven om het gebruik van secundaire/ tertiaire regelaars te duiden. De interactie tussen de voorgestelde SBD regeling en deze secundaire/tertiaire regelaars, die de referentiewaarden van deze eerste wijzigen, wordt geanalyseerd. Ten slotte wordt ook het veelbelovende concept van een virtuele centrale besproken en wordt een hiërarchische regeling tussen deze centrale en een microgrid voorgesteld.

In hoofdstuk 8 wordt een algemeen besluit gevormd over deze doctoraats-verhandeling en worden mogelijkheden voor verder onderzoek aangereikt.

Nomenclature

Parameters

b constant-power band width [p.u.]

C_{dc} dc-link capacitance [F]

CE capacitor energy [J]

C_{f} filter capacitance [F]

f grid frequency [Hz]

f_{s} switching/sample frequency [Hz]

i_{L} filter inductor current (equal to inverter output current) [A]

i_{C} filter capacitor current [A]

i_{g} grid current [A]

I_{dc} dc-side current [A]

J rotating inertia [kg m^2]

KE kinetic energy [J]

K_{g} droop of GVBD control [W]

$K_{\mathrm{P,SG}}$ droop of CPFD control [W/Hz]

K_{f} droop of f/P droop controller [Hz/W]

K_{I} droop of $I_{\mathrm{dc}}/V_{\mathrm{g}}$ droop controller [A/V]

K_{p} droop of P/V droop controller [V/W]

K_{P} droop of $P_{\mathrm{dc}}/V_{\mathrm{g}}$-droop controller [W/V]

K_{Q} droop of Q/f-droop controller [Hz/VAr]

$K_{\mathrm{Q,SG}}$ droop of Q/V_{g}-droop controller of a SG [V/VAr]

$K_{\mathrm{Q,v}}$ droop of Q/V droop controller [V/VAr]

K_{V} droop of $V_{\mathrm{g}}/V_{\mathrm{dc}}$ droop controller [V/V]

L_{f} filter inductance [H]

P ac-side active power (output power of DG unit) [W]

P_{dc} dc-side active power (input power of DG unit) [W]

P_{m} mechanical input power [W]

P_{PCC} power exchange between microgrid and utility through PCC [W]

R_{v} resistive virtual output impedance [Ω]

T_{s} sample period [s]

V_{dc} dc-link voltage [V]

$v_{\mathrm{dc,g}}$ global dc-link voltage [p.u.]

v_{g} grid voltage over the filter capacitor (time function) [V]

V_{g} rms value of the grid voltage v_{g} [V]

$v_{\mathrm{g,droop}}$ v_{g} reference determined by the droop controller [V]

$v_{\mathrm{g,ref}}$ reference of v_{g} [V] (also $v_{\mathrm{g}}^{\star}$)

v_{PCC} PCC voltage [V]

v_{s} voltage at the VSI terminal [V]

ω pulsation or rotational velocity [s^{-2}]

z_{v} virtual output impedance [Ω]

Abbreviations

*	reference value
ACE	area control error
ACSS	averaged current-sharing strategy
AMI	advanced metering infrastructure
APF	active-power filter
ARG	automatic reference generation
AVR	automatic voltage regulator
C-VPP	commercial virtual power plant
CCL	current control loop
CE	capacitor energy
CHP	combined heat and power
CIDG	converter-interfaced DG
CPFD	conventional P/f droop
CSI	current-source inverter
CWDC	current-weighting-distribution control
DCM	distributed control method
DER	distributed energy resource
DG	distributed generation
DNO	distribution network operator
DOE	department of energy
DR	demand response
DSM	demand side management
DSO	distribution system operator
EV	electrical vehicle
FFT	fast- fourier-transform
FLL	frequency-locked loop
GVBD	global voltage-based droop
HCC	highest current control
HV	high-voltage
HVDC	high-voltage direct current
ICCL	inner current control loop
ICT	information and communications technology
LC	local controller
LV	low-voltage
MGCC	microgrid central controller
MO	market operator
MPP	maximum power point
MPPT	maximum power point tracking
MV	medium-voltage
NLL	nonlinear load
nom	nominal values
OLTC	on-load tap changer
ORC	organic Rankine cycle
OVCL	outer voltage control loop
PC	peak value calculation
PCC	point of common coupling
PLL	phase-locked loop

PMSM	permanent-magnet synchronous machine
PR	proportional-resonant
PV	photovoltaic
PWM	pulse-width modulation
ref	reference value
RES	renewable energy sources
RTP	real-time pricing
SG	synchronous generator
SHI	shunt harmonic impedance
ST	smart transformer
T-VPP	technical virtual power plant
TNO	transmission network operator
TSO	transmission system operator
TOU	time-of-use
UPS	uninterruptible power supply
VBD	voltage-based droop
VCL	voltage control loop
VPP	virtual power plant
VSI	voltage-source inverter

Chapter 1

Introduction

1.1 Distributed generation

There has been a significant change in the power system operation and planning, caused by environmental issues, uncertainty of the prices for fossil fuels, concerns about the security of supply and the liberalisation of the electricity markets. The focus is changing from large nuclear and fossil fuel based electrical generators to cleaner technologies. The new-installed, clean generators generally have a low power density and are geographically dispersed. Hence, they are typically available as small distributed generation (DG) units [1–3]. This leads to a fundamental change in the electrical grids. Historically, the system was characterised by centrally produced electricity that flowed from large generators connected to the transmission network to the consumers located at the distribution networks. Recently, this is evolving towards a system with distributed electrical generation on different levels in the grid and subsequent bidirectional power flows, as shown in Fig. 1.1.

1.1.1 Significant growth and drivers

A new evolution in the traditional distribution system is the increasing number of DG units, which are often based on renewable energy sources (RES) such as photovoltaic panels and wind turbines, but can also use other technologies such as in combined-heat and power (CHP) units, microturbines and organic Rankine cycle (ORC) power plants (e.g., for waste heat recovery). RES offer the unique positive characteristics of providing "free" fuel, little to no carbon footprint and a virtually endless supply. DG units and renewables will cover a remarkably increasing portion of the electric power generation, as Fig. 1.2[1] suggests for the case of Europe. For example, by 2020, California is committed to generate 33 % of its electricity

[1] www.eurelectric.org

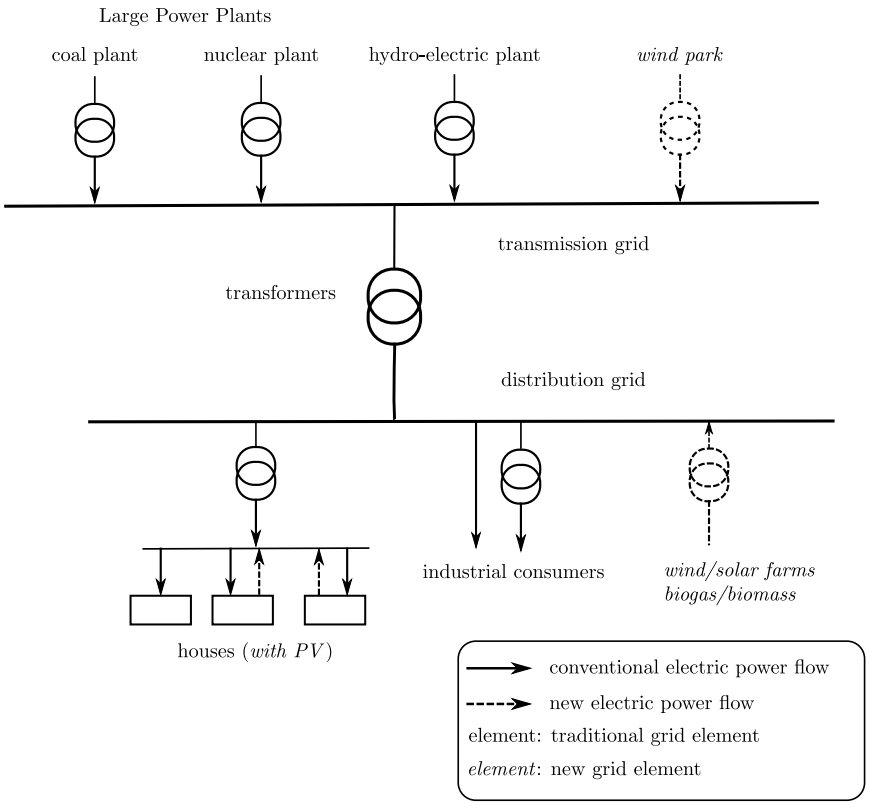

Figure 1.1: Basic scheme of electric power system infrastructure and the recent changes (power flows and new grid elements). Traditional power system: top-down concept with unidirectional power flow. Future power system: distributed concept with bidirectional power flow

by RES, 15 % renewable energy in China[2], and 20 % renewable energy in Australia and the E.U. according to the EU's 20-20-20 targets (or 33 % renewable electricity in the E.U.), with a mandatory target of 13 % renewable energy in Belgium (a target of 20.9 % renewable electricity in 2020) and 18 % renewable energy in Germany (targeting at 35 % renewable electricity).

The main drivers for the increase of DG are [1, 4, 5]:

[2] 15 % of the total energy consumption (electricity, heating and transportation) from renewable sources

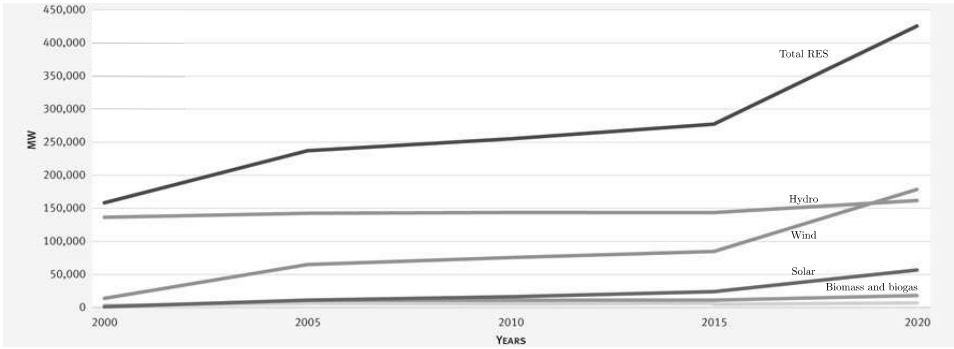

Figure 1.2: RES generation capacity: EU-27 plus Switzerland and Norway

- Environmental drivers:
  - limiting the greenhouse gas emissions;
  - compensating for the closure of nuclear power plants.
- Commercial drivers:
  - liberalisation of the electricity markets with unbundling of transmission, distribution and generation favours small generators;
  - increasing costs and high volatility in the prices of fossil fuels;
  - technological innovations in small generators and power electronics lead to reducing costs of DG technologies;
  - increasing energy usage (Fig. 1.3), certainly in developing countries like China and India, combined with an electrification of the energy usage in the Western world as shown in Fig. 1.4 (e.g., electrification of heating and transportation with heat pumps and electrical vehicles) [6].
- National and regulatory drivers:
  - commitment to decrease the dependency on foreign countries for fuel import: improve the security of supply;
  - public opposition against building new large generators and transmission lines;
  - long lead times to build new large generators and transmission lines;
  - support for the competition policy: many players required to have effective competition [7].

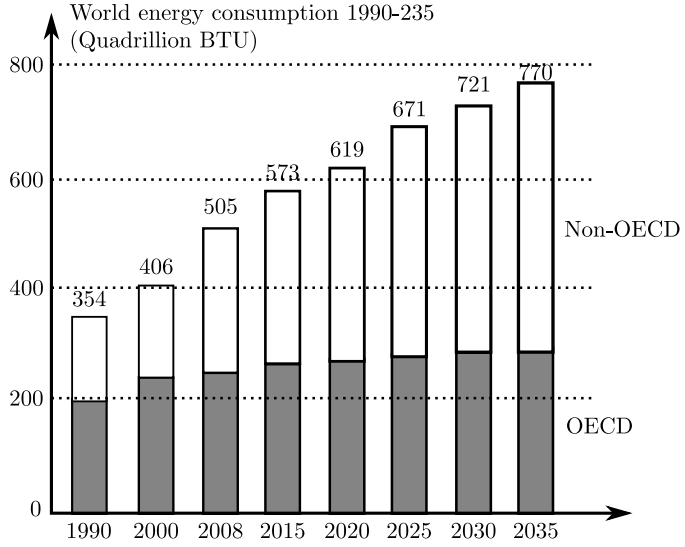

Figure 1.3: Rising energy consumption, especially in non-OECD countries such as India and China (1 BTU ≈ 1kJ

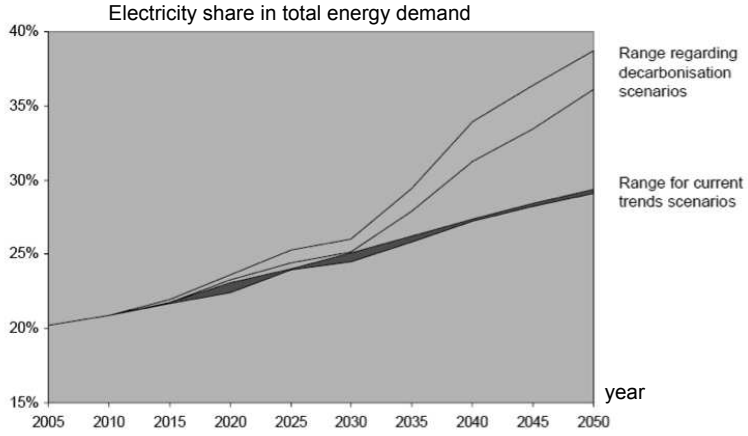

Figure 1.4: Share of electricity in current trend and decarbonisation scenarios (in % of final energy demand). Increasing electricity shares in the total energy demand: electricity will have to play a much greater role than now (almost doubling its share in final energy demand to 36-39 % in 2050) and will have to contribute to the decarbonisation of transport and heating/cooling [8]

1.1.2 Benefits

DG can offer significant advantages, which are summarised in many papers [4, 9–19]. Firstly, DG can present significant environmental advantages, such as limiting the greenhouse gas emissions by using RES, reducing the physical and electrical distance between generation and consumption which can lower the network losses, and offering the possibility to exploit combined head and power (CHP) generation more extensively. By using waste heat for ORC, the efficiency of the system can significantly improve [20].
Secondly, small generators are often favoured above large central generators because of the lower investments, shorter construction times, and as it is easier to select sites for smaller installations. Extension of the transmission network is usually not possible, or has long lead times, due to the "not-in-my-backyard" attitude of the local community. Distributed generation can ease the pressure on transmission system capacity by supplying some of the load with locally-generated power. Furthermore, the increasing and uncertain prices for fossil fuels make large fossil fuel based generators less economically viable, even more so as these generators need to meet considerable environmental requirements.
Further, DG can offer ancillary services, such as voltage control and reserve provision, and thereby, improve the network reliability and power quality. Islanded operation of DG can enable to feed consumers in case of failure of a line, problems in a substation or planned interruptions, hence, it can increase the supply reliability by providing an interruptible power supply (UPS) functionality [19].

1.1.3 Challenges and influence on the grid

Many of the assumed advantages of DG are dependent on the planning, installation and operation of the DG units and the characteristics of the distribution system [11]. Therefore, major efforts are required in the development and integration of sustainable energy systems, leading to a massive reorganisation of the electricity system, both in technological and market terms [21].
Two main issues arise that pose limits on the further penetration of DG. First, there is a lack of coordination in interfacing new DG units in the grid. The further increase of DG is being limited because the electric distribution systems are not designed for the changed, even bidirectional, power flows and the changed voltage profiles in the distribution feeders induced by DG (Fig. 1.5). In this figure, the voltage margins are not depicted. For example, in Belgium, 20 % voltage variation is allowed on the grid, with +10% and -10% compared to the nominal voltage according to the European voltage characteristics standard EN 50160 (voltage characteristics of electricity supplied by public electricity networks). However, this voltage margin has to be shared between the different networks. A common ap-

proach is to allow 4 % voltage variation at transmission level, 6.5 % at medium-voltage level and the other 9.5 % can be used by the low-voltage level[3]. The commonly used basic principle of voltage control in a distribution network is described in [22]. The voltage on the secondary side of a HV/MV transformer is kept within a certain dead band by means of an automatic on-load tap changer (OLCT). When only consumption is considered, this consumption leads to a voltage drop along the MV feeder, which is lowest at minimum consumption and highest at maximum consumption. The further away from the HV/MV transformer, the lower the voltage will be. To compensate for this, MV/LV transformers with different turn ratios are used. The voltage should be such that the voltage magnitude remains in the band set by an undervoltage limit and an overvoltage limit (e.g., the +10/-10 % band) [22]. Hence, the dead band at the HV/MV transformer is normally chosen somewhat above the nominal voltage to allow the voltage drop along the MV and LV feeders. The connection of a DG unit will result in a voltage rise at its terminals. In conclusion, in distribution networks, the voltage is usually only controlled by the HV/MV OLTC transformer. Distribution transformers can generally only be tapped off-line, hence, their contribution in the voltage control is limited. Other means of voltage control such as Flexible AC transmission system (FACTS) devices and switched capacitor banks are described in [23].

Because of the entry of DG, the distribution network has evolved from a passive network to a network that actively reacts to system dynamics [24]. This changed behaviour poses challenges, e.g., in the system planning and protection. Moreover, the power system is more and more overwhelmed with congestion problems [25]. Capacity management as known and treated in the transmission level becomes a main concern in the distribution networks as well. Hence, an increase of DG systems without properly addressing the issues of coordination, can result in a negative impact on the electricity system, such as problems in voltage control and voltage flicker because of sudden changes of DG output, which may jeopardise the reliability and safety of the distribution system [9]. However, DG also brings new opportunities as it can increase the flexibility and performance of the distribution system, which also demands for an organised introduction of DG.

Second, there is a difficult integration of some RES-based DG units, such as wind turbines and photovoltaic panels, due to their intermittence, randomness and uncertainty caused by meteorological factors. This new variability of the generation side (e.g., PV system output in Fig. 1.6[4]) is in addition with the variability of the consumption, and with the limited correlation between this generation and the consumption patterns, for example as shown in Fig. 1.7[5]. Maintaining the balance in

[3] Subsequently, in islanded networks, the full 20 % voltage variation (+10% and -10%) can be used in the (LV) network

[4] www.greenenergynet.com

[5] PJM data: PJM Interconnection serves 13 states and the District of Colombia

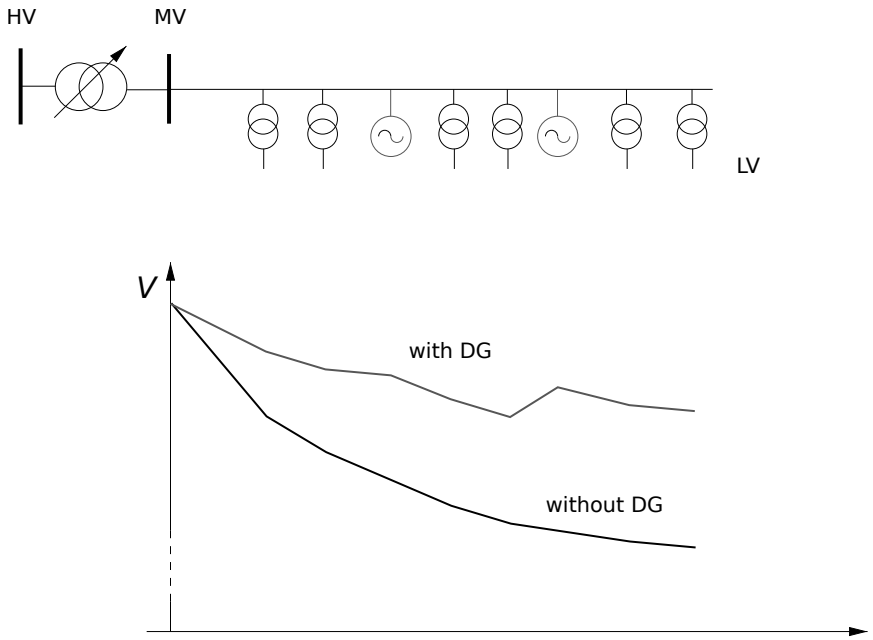

Figure 1.5: Changed voltage profile because of DG. HV/MV transformer, MV feeder. At the MV feeder: MV/LV transformers (generally off-load tap changing transfomers) and DG units are connected. The connection of DG units leads to a voltage increases.

generation and consumption is now mainly done by the large central generators, without contribution of DG. The DG units are operated in a passive manner, where the output is dependent on the availability of the energy source (e.g., wind, solar) and/or the user settings (e.g., heat demand in CHP units). Apart from shutting down the unit in extreme conditions, the state of the electrical power system generally has no influence on the power output of these units. Hence, the fit-and-forget strategy of integrating DG displaces the energy production, but not the flexibility and capacity to provide a reliable power supply at all times. With the increasing share of DG, the situation of not dispatching these units is no longer sustainable such that DG will need to contribute in the frequency control of the electric power system. Moreover, the stochastic behaviour of generation (PV systems, wind turbines, CHP units) and loads lead to less predictable power flows in the distribution networks. Hence, despite the low installed capacity of many DG units, the huge number of these units has a significant impact on the real-time electric power system operation, plan-

Also, the peak in the generation of PV panels at noon is in between the morning and evening peak consumption of typical residential consumers.

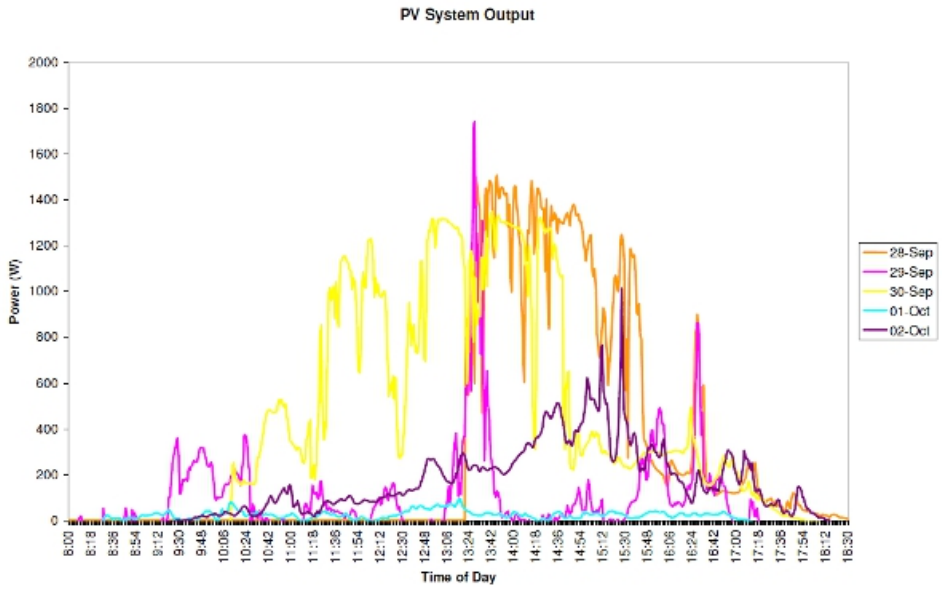

Figure 1.6: PV output for five subsequent days. Significant inter and intra day variations, even when seasonal effect is not yet considered

ning and protection. Committing to a large proportion of renewable energy poses challenges to maintain the reliability of Europe's power system at the current level.

These factors, together with an ageing energy infrastructure, drive the grid to its capacity limits and can result in an inefficient system, a complex and uncoordinated integration of DG units and a decreasing system reliability. Solving these issues within the current grid paradigm could result in increasing system costs, caused by the increased balancing costs, the need for back-up capacity to cope with the variable nature of the loads and many DG technologies and the required reinforcement of the networks [26]. The expected costs to deal with these issues can be mitigated by operating the power system in a more efficient, thus smarter, manner (i.e., smart grid), by integrating DG units in a coordinated manner (microgrids) and by implementing advanced response options such as active DG control and demand response (DR) on a large scale. Hence, important questions are being posed, such as whether the traditional approach for operation and development of the power system is still suitable [27]. An important challenge is, thus, to transform, firstly, the current fit-and-forget strategy where many DG units and loads are not actively dispatched to cope with the grid's needs, to a policy of integrating DG in the planning and operation of the grid. Secondly, to alter the current

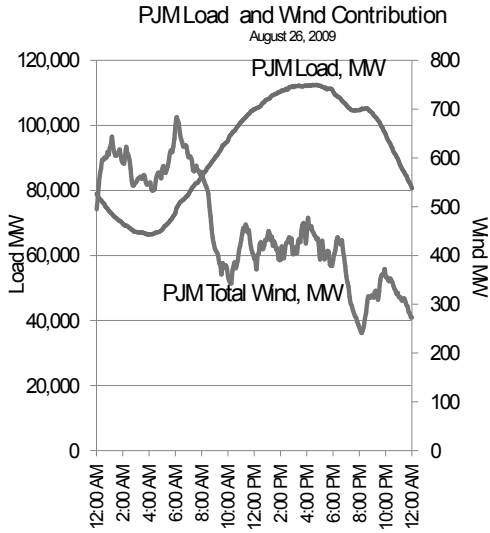

Figure 1.7: Insimultaneity in aggregated load and total wind input: one-day measurement by a regional transmission organisation in the US

load-following strategy, where the generators follow the load profile, to a more generation-following strategy, where the loads act dynamically on changes on the generation side. Integrating dispatch and ancillary services in DG units, such as frequency response, spinning reserve, reactive power support and security of supply contribution, will be required to address these challenges while restraining the costs of the system operation [27].

1.2 Smart grids

An approach to deal with the large increase of decentralised unpredictable power sources, the ageing grid infrastructure and the increasing (peak) consumption, while mitigating the massive investments for this, is to add more intelligence to the power system. The usage of widespread information and communication technologies (ICT) to monitor and manage the distributed energy resources allows the grid to become more efficient and sustainable [6]. These ICT and new remote management abilities couple the grid elements via an interactive intelligent electricity network, the so-called smart grid. New automatic smart meters will enable the distribution network operator (DNO) to have a more frequent and thorough knowledge of the system. There is still discussion about what a smart grid is and what makes a grid intelligent. However, there is consensus that smart

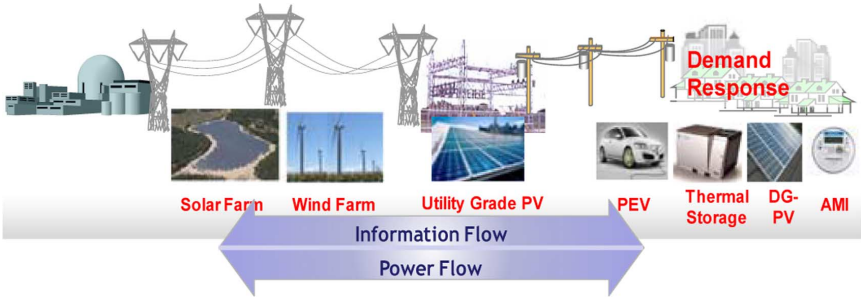

Figure 1.8: Bi-directional communication in a smart grid architecture

grids are more than metering and communication alone: the data should be used to achieve certain objectives Fig. 1.8. The increased system knowledge enables the DNO to faster respond to system disturbances and failure and makes real-time control or, at least, a faster control possible. The latter is presently not possible as the current meters are manually read out less frequently, e.g., only once a year in case of Belgian residential consumers. For example, the DNO can maximise the use of the existing assets by integrating generator and load dispatch, voltage control, control of transformer taps, active/reactive power management and system reconfiguration.

1.2.1 Characteristics

In brief, a smart grid involves the use of sensors, communication, computational ability and control to enhance the overall functionality of the electric power delivery system [28].

According to the U.S. Department of Energy (DOE), the seven defining characteristics of a smart grid are [29]: (1) consumer participation, (2) accommodate both central and distributed generation and storage, (3) enable new products, services and markets, (4) power quality, (5) optimisation of assets, (6) anticipating and responding to system disturbances and (7) operating resiliently to attacks and natural disasters.

Some key components in a smart grid are: distribution automation, energy storage, volt/VAR optimisation, phasor measurement units, community energy storage, microgrids and islanding, demand response and the advanced meter infrastructure (AMI).

An important aspect of the smart grid is that it allows for demand response (DR) on a large scale. Historically, load control has focussed on reducing the overall

electricity consumption (demand side management) and on peak shaving (DR). One technique for DR that has been put into practice is using different tariffs for the day versus night times (Fig. 1.9 left) [30]. Also, direct load control has been introduced, generally with incentives to some large loads that enrol for load shedding. However, apart from direct control of some units and a difference in day and night tariffs, consumer only see averaged prices that do not reflect the instantaneous prices of electricity generation and transportation. Hence, in order to ease the pressure on the grid and increase its capacity to host DG units, while constraining the need to invest in grid reinforcement and backup capacity, consumers should be able to change their consumption based on true production costs. These costs change over time in response to grid contingencies and market prices [28]. In this way, the network operation evolves to a generation-following strategy and the loads help to accomplish for the extra rigidity introduced at the supply side by, e.g., wind turbines and photovoltaic panels (Fig. 1.9 right). The introduction of the smart grids and smart microgrids offers high potential for load response as new smart grid features such as advanced metering and an embedded communication infrastructure make real-time pricing possible. Fig. 1.10 shows the three levels of demand response. On a low level, it focusses on changes in a house or a few houses. The medium level is assigned to control the power flows in a street or small community. The highest level of demand response provides a system-wide support. On each level, demand response can have different objectives as illustrated in this figure. Even small amounts of DR can help significantly in reducing the market prices and the price volatility [28, 31]. It is estimated that roughly 5 to 10 % of the electricity consumption in households can be influenced over time [32]. Although this number may seem small, it can make a major contribution to enabling distributor grid operators to reduce a local critical power load. Typical loads that might be controlled in, e.g., households and small and medium enterprises are loads with a electrical or thermal storage capacity like EV batteries, refrigerators, heat pumps, electrical boilers and freezers, or loads with less stringent timing requirements like dish washers, washing machines and dryers. Electrical vehicles offer a high potential for demand response. On the one hand, they can be used as an energy buffer by changing the charging pattern dependent on the state of the power system. On the other hand, they can provide energy storage by exchanging a bidirectional power flow with the utility network. An important aspect of smart grid research is how to properly compensate the EV owners for their contribution in the grid control, e.g., dealing with the aspect of battery degradation.

The smart grid also promises to be a self-healing system. It makes predictions and takes corrective actions to avoid or mitigate system problems [33]. Self-healing systems play a role in speeding the system recovery.

Another main issue is an ageing grid infrastructure and the subsequent reliability

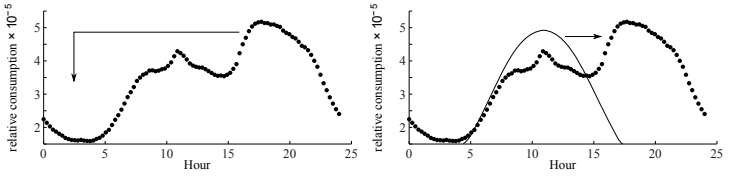

Figure 1.9: Demand response for flattening the load profile or merging consumption and supply

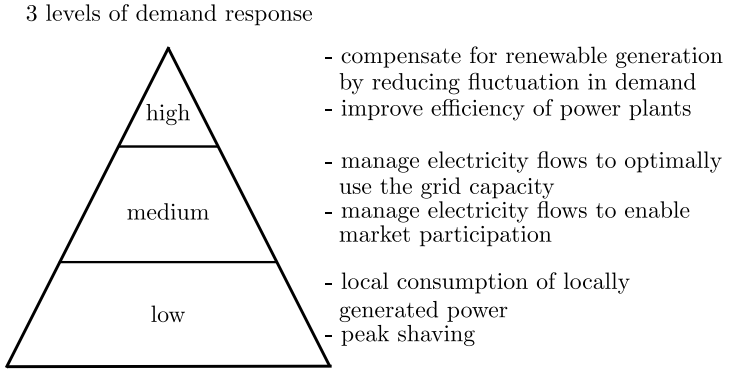

Figure 1.10: Three levels of demand response

concerns. In North America, for example, the average age of power transformers is over 40 years [6] for a typical life span of 40 to 50 years[6]. Many devices are operating well beyond their lifespan. Meanwhile, the demand for electricity continues to rise and a good reliability of the power system in a cost-effective manner remains absolutely crucial. Hence, there is an urgent need for asset management, i.e., repair or replacement of existing assets, in a cost-effective programmatic manner. With the smart grid, asset management can be performed more effectively as it provides a better understanding of the actual condition of the grid and its assets. A focused maintenance scheme and a better understanding of the system can enable a proactive asset management strategy that prevents outages. Even when unplanned outages do occur, smart grid outage management systems can reroute power to minimise the outage's extend and duration and perform the repairs more

[6]The given numbers can differ dependent on the source. According to [34]: in Europe alone, 60 percent of the installed transformers have been in operation for over 25 years. Moreover, the average life expectancy of a transformer is 25 to 30 years in normal operation. From this, the same conclusion of an ageing grid infrastructure can be drawn.

efficiently. More system knowledge will also facilitate the distribution network operator (DNO) in determining the network margins. These margins need to address tasks of capacity management while helping the DNO to achieve an optimal utilisation of the network capacity, which encompasses preventing overloading of assets, optimising asset capital investments, keeping the quality of supply and minimising transport losses.
Next to the smart grid, another approach for upgrading the grid is the super grid, with large-scale transmission of renewable electricity over very long distances. The super grid paradigm can, for example, exploit the potential for wind and solar energy in the deserts of North Africa by connecting these to the European grid via HVDC lines [35]. It can also provide more capacity for transmitting the output of large wind parks in Norths Sea and the Baltic Sea to the rest of Europe. According to [35], the super grid and smart grid can coexist in a super-smart grid, exploiting the benefits of both.

1.2.2 Benefits

The smart grid offers many advantages, such as enabling an increasing share of clean renewable energy, reducing costs, improving the system reliability in the face of increasing intermittency, enabling more customer choices and involvement for their energy management, a more efficient usage of the current assets and help utilisation of electrical vehicles [33].
The focus of what smart grids should accomplish is different on the different continents [36]. In Europe, emphasis is placed on improving the efficiency and reducing the emissions through the use of more decentralised production. In America, there is a strong focus on peak load reduction and dynamic pricing tariffs. China aims at modernising the power system and improving the grid reliability through smart grid development.
The European SmartGrids Technology platform summarises the benefits and objectives of smart grids as follows:

- smart grids significantly reduce the environmental impact of the whole electricity supply system;
- smart grids facilitate the connection and operation of generators of all sizes and technologies;
- smart grids allow consumers to play a part in optimising the operation of the system;
- smart grids provide consumers with more information and better options in choosing their energy supplier;

- smart grids maintain and improve the existing high levels of system reliability, quality, and security of supply
- smart grids maintain and improve the existing services efficiently;
- smart grids foster the development of an integrated European market.

1.2.3 Consumer concerns

With the development of the smart grid, the individual benefits for the consumers should be clear.
Some main barriers to increase the customer acceptance for smart grids are the concerns regarding cost, privacy and security, together with a fear of possible discomfort when they provide flexibility to the grid, e.g., potential disruptions for peak shaving. An important challenge is to overcome the lack of understanding about the smart grid functionalities and increase the customers' knowledge about the explicit benefits for him in specific. Along with lacking awareness about smart grids, consumers are not aware of which appliance are contributing most to their electricity bill. This leads to frustration as, despite best intentions, they are unable to significantly lower their bill [36]. Smart devices can help to address this issue by monitoring the consumption and comparing it with other consumers. End-user acceptance will ultimately determine the success of many aspects of smart grids [36]. Smart grids are now mostly only known as the smart meters, which are costly and have questionable customer benefits. Many protest groups warn against unsafe equipment making the customers vulnerable for theft, annoying marketeers and police investigations. People stating an increase in their electricity price due to smart meters and this information picked up by the press has raised a lot of public opposition against smart meters (Fig. 1.11). Also, smart meters consume more power than the traditional meters. The figures of this range from 1 to more than 20 W. For example, if a (low) 4 W per household more consumption of a smart meter than the traditional meter is assumed, over a year this involves an additional 35 kWh, or roughly 10 EUR yearly for the consumption of the meter alone (there are other possible costs, such as the installation cost, the cost of the communication functionalities and the smart appliances). Whether smart meters are really necessary to make the smart grid happen is still a point of discussion. For example, many smart grid functionalities only need local measurements, no communication. However, the smart meter is only the beginning and may become an enabler of the smart grid. Fig. 1.12 shows the high capital investments in the first step of the smart grid, i.e., the smart meter. For the next steps, such as distribution grid management, which is composed of distribution automation, detection, central and distributed system analysis, correction of disturbances on the grid, etc., a higher value at a

Figure 1.11: Smart meter protest

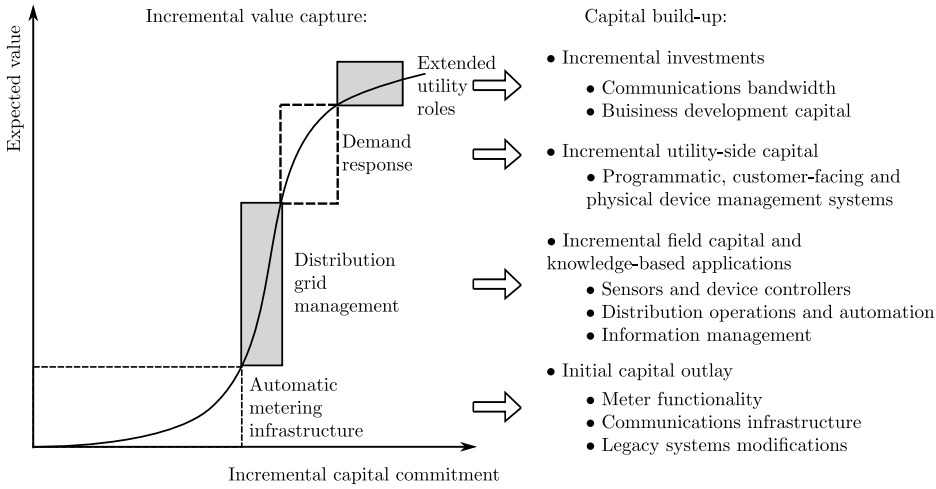

Figure 1.12: Smart meter as enabler of the smart grid

lower cost can be achieved. The figure also emphasises the need for good planning of the sensor and meter capability.

1.3 Microgrids

A microgrid is an interconnection of supply, loads and storage devices, providing both power and heat and cooperating to achieve certain objectives, such as befitting from market participation and reducing the electricity cost through flattening of the aggregated load profile [18, 37]. The key objectives of microgrids are to provide a coordinated integration of DG in the electric power system, to improve the reli-

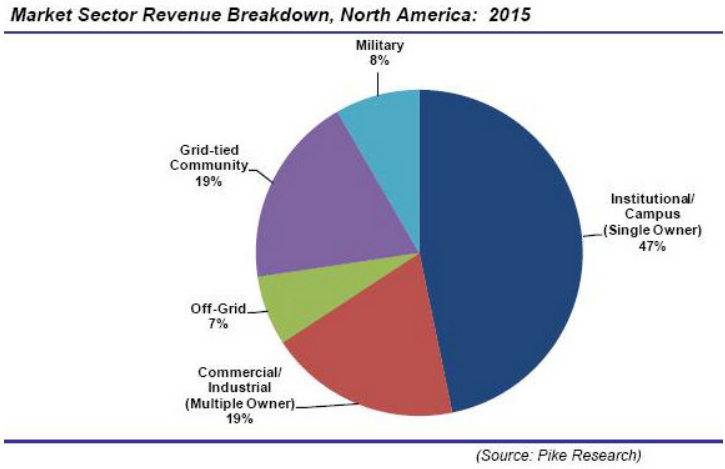

Figure 1.13: Potential of microgrids in North-America by 2015 (remote off-grid microgrids show even larger protential in other parts of the world)

ability, allow a more efficient use of energy and become a controllable entity in the network. These small-scale networks can provide power to a small community, which can range from a housing estate, an isolated rural community; to academic or public communities such as universities or schools; and to industrial sites (illustrated in Fig. 1.13[7]). Industrial parks can be managed as microgrids, e.g., to decrease the energy dependency, operate as low carbon business parks[8] and increase the economic competitiveness (increase the reliability, reduce the purchase of energy, reduce the peak consumption). Microgrids can operate either connect to the utility network in the grid-connected mode or independently from a main grid in the islanded mode as shown in Fig. 1.14. Many of the grid elements are power-electronically interfaced to the microgrid.

1.3.1 Drivers

With the massive penetration of DG, the fit-and-forget principle of integrating them into the electrical power system is no longer a sustainable option and a coordinated approach is required. A systematic approach to capture the emerging potential of DG and to cope with the problems caused by the unconventional behaviour and increasing penetration of DG, is to take a system approach instead of considering each unit separately [38–41]. In the system approach, the generators and

[7] www.pikeresearch.com
[8] www.ace-low-carbon-economy.eu

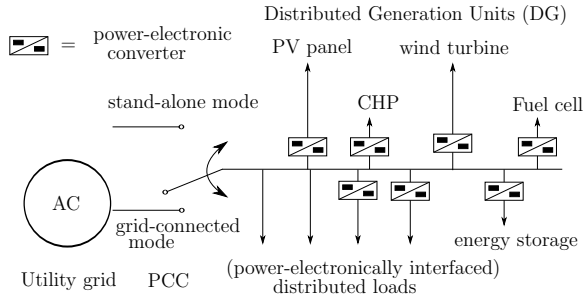

Figure 1.14: Microgrid with (power-electronically interfaced) loads, storage and DG units in stand-alone (islanded) or grid-connected mode

loads are regarded as a subsystem, or microgrid, with a single connection point with the rest of the network. In comparison with a single DG unit, the microgrid has more control flexibility to ensure the system's reliability and power quality requirements [42]. Hence, microgrids are regarded as an important part in the successful integration of massive amounts of DG units and RES [43, 44] and help in power quality issues [18, 45, 46]. In this context, the plug-and-play functionality of the microgrid elements is key [18, 19]. Microgrids also offer potential to integrate local electrical and thermal networks to achieve a coherent generation, storage and load control, and to benefit from CHP generation, which is an important means of efficiency improvement [42].

1.3.2 Benefits

Microgrids can be used to create a new model of generation, consumption and delivery of electrical power and services in a more efficient, robust, sustainable, flexible and environmental-friendly way, while encouraging a much higher level of customer participation [47]. They facilitate the penetration of DG into the utility grid by delivering integration in a coordinated manner and dealing with the unconventional behaviour of DG [40]. Microgrids offer significant benefits in both the grid perspective and the consumer perspective. A key advantage from the grid's point of view is that the microgrid elements are collectively regarded as a single controllable unit, enabling the microgrid to deliver the cost benefits of large units [48]. In this way, utilities do not have to consider each unit separately for their system management. While not always obvious to utilities, microgrids can improve the economics and reliability of their service, help to meet renewable energy obligations, reduce congestion, improve power quality under high penetration levels of DG and support demand response. For example, microgrids can optimise a "troublesome" business complex or university campus, making it more economic

and reliable to serve [6].
From the customers' point of view, the impact of the microgrid on the reliability of the distribution network is relevant, certainly in the future, with more unpredictable generation and higher consumption (peaks) [19, 49, 50]. Reliability is the first requirement of the electric power system. The cost of unreliability can have a considerable impact on the economy. The outage cost in the United States is estimated to amount to some US$ 79 billion per year, among which the momentary outages (< 5min) account for US$ 52 billion [51, 52]. The consequences of grid failure are gigantic because transportation, finance, communication and other critical sectors are dependent on a guaranteed and reliable supply of energy [25]. Most of the reliability improvements will need to be introduced in the distribution system as most outage and power quality issues arise there, over 90 % of all outages in North-America originate in the distribution network according to [33, 52]. To increase the local reliability, back-up gensets and other emergency supplies are often installed near critical loads to provide UPS functionality [53]. The costs of these designated devices, that run only during a limited amount of time, are significant. In this context, microgrids can provide the UPS functionality by exploiting the locally-available DG, storage and loads.
Aggregation of mixed assets in a microgrid can also provide considerable economic benefits to the microgrid subsystems, i.e., by allowing them to participate in the electricity and ancillary services markets.
Other benefits that can arise with the introduction of microgrids is that they can reduce feeder losses, provide reactive power and local voltage support, remove transmission and distribution bottlenecks, provide ancillary services such as heterogeneous power quality and reliability (i.e., differentiation based on the specific needs of the customers), increase efficiency through CHP and provide an easier large-scale integration of DG units [49, 54–57].

1.3.3 Operating modes

Microgrids are connected to the utility network through a single point of connection, the point of common coupling (PCC) as shown in Fig. 1.15. Therefore, they can run in two operating conditions: grid-connected and islanded mode.
In the grid-connected mode, the microgrid supports the utility grid while exchanging power with it. The microgrid can extract power from the grid or deliver power to it, dependent on its generation, consumption and the market policies [46]. For power balancing and energy management, grid-connected microgrids have the following three assets at their disposal [41]:

1. dispatchable distributed energy resource (DER) controllers (DG and optional storage);

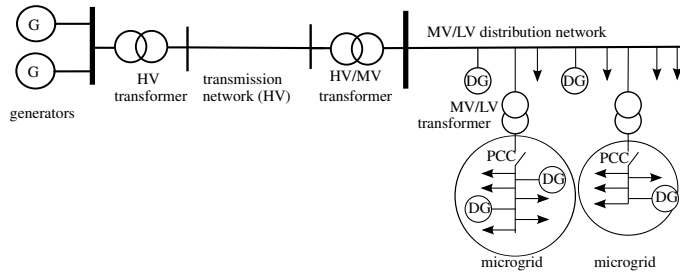

Figure 1.15: Microgrid connected to utility network through the PCC

2. load management;

3. control of the power exchange with the main grid.

Generally, the normal condition of the microgrid is the grid-connected operation. A first advantage is that for the rest of the network, the microgrid can be seen as a controllable entity. This provides significant benefits for both the microgrid participants and the distribution network operator, that does not need to consider all units separately [49, 55–57]. Because of the single connection point between microgrid and distribution network, the power exchange can be determined unambiguously and controlled to a predefined value. Hence, in the electricity markets, not the output power of each unit needs to be measured and traded, but solely the aggregated exchange. Secondly, by aggregating DG units, the installed power can be sufficient to enable the units, that otherwise are too small, to participate in the electricity markets and get better prices for their energy. Also, by aggregating different kinds of units, the risks of deviating predictions of production can be reduced. Thirdly, microgrids can provide ancillary services to the networks, such as reserve provision or reactive power support.
Although the normal operation mode of a microgrid is grid-connected, it also offers the unique characteristic of islanding. In the islanded operation, the microgrid operates independently of the main grid and consequently, the DG units, loads and storage devices are collectively responsible to maintain the integrity of the microgrid without the assistance of a main grid, which is the focus of this PhD thesis. Generally, islanding is not yet allowed because of technical and safety challenges [58]. Also, there is a strange effect that the DNO is responsible in case of incidents, without having control of the islanded microgrid. Hence, a proper development of suitable regulations is required for the integration of microgrids in the distribution networks and for enabling a safe islanded mode [49].
In order to ensure the continuity of supply for the local load, a (short term) islanded mode can occur in case of special situations such as grid faults, outage of the bulk

supply or power quality problems [7, 43, 58, 59]. This offers a potential improvement of the reliability, quality and costs of the system. Hence, microgrids are a good option in applications where electrical energy must be guaranteed at all times such as in hospitals and for servers. For example, for hospitals and industrial facilities, often, interruptible power supplies are installed. Since these facilities often also contain DG units, controllable loads and storage, the operation of their grid as a microgrid in islanded mode can be a favourable alternative. Islanding is also interesting in cases in which the main grid is not robust enough due to factors such as long distances from the main grid [60]. In this way, in extensive, highly dispersed countries such as Canada, USA, Japan, major efforts into microgrid research are being made.
Microgrids can also switch into islanded operation due to planned maintenance operations. In Canada for example, some projects are running concerning intentional islanding to increase the reliability of the power supply in rural feeders and for maintenance without supply interruption [24, 61, 62]. An application is the Hydro-Quebec project for maintenance of a connection line [24].
Although not strictly according to the definition of a microgrid, an islanded microgrid can also exist in case of remote electrification, where no main grid is available due to, e.g., geographical issues. According to the World Bank's 2010 development report, 1.6 billion people in developing countries do not have access to electricity [63]. The most important reason is the extensive investment needed to install grid-connected power lines across large distances and/or rough terrain for expanding the electricity supply to a few people. It is recognised that electricity is a key driver in fast economical growth and to combat poverty. Hence, islanded microgrid projects provide great opportunities to realise sustainable human development. According to IEA (2009), 83 % of the people that do not have access to electricity live in rural areas [64], e.g., over one third of India's rural population. The Indian government targets at providing all its households with electricity in the near future [65]. In case grid connection is not cost-effective to accomplish this, decentralised electric power with local distribution is taken under consideration, i.e., islanded microgrids, with an example in the Sundarbans Islands region in India [65].

1.3.4 Smart microgrids

It is not realistic that the growth of the smart grid would be a revolution. Instead, a gradual evolution is expected [29, 33]. Because of their flexibility and scalability, microgrids are likely to play a key role in the evolution of the smart grid [66] with smart microgrids as small pilot versions (building blocks) of the future power system [67]. Hence, the smart grid will probably emerge as a system of integrated smart microgrids [33]. Smart microgrids are microgrids combined with an overlay-

ing intelligence scheme[9]. The intelligent software implemented in the microgrid can:

- contain energy management systems;
- monitor the system (energy supply, storage and demand) and actively intervene in the consumption/generation;
- identify and maximise energy efficiency opportunities;
- use an extra communication and sensor layer to maximise cost savings and reduce carbon emissions;
- generate a more active participation of the consumers.

A balance between the cost to incorporate intelligence in the grid and the subsequent benefits needs to be made. Furthermore, the infrastructure and control centres for smart grids can be hard to implement on a large scale and this may take many years. Rather than investing in incorporating intelligence on a large scale, investing in small smart microgrids (such as business areas) can be done at a lower cost and more quickly. Also, a high level of intelligence built everywhere in the system is not necessary: different areas require different levels of smartness. The areas that allow more and benefit most from high levels of smartness of the system, such as areas with high penetration of DG, can fit directly into the microgrid concept. In these microgrids, smart features can be installed faster than in the rest of the network with locally higher levels of intelligence than average. In this way, the smart microgrids can enable a new energy strategy while restraining the cost of making the whole system smart.
Essentially, the goals of microgrids and smart grids are the same: to minimise costs, meet the growing demand, integrate more sustainable generation resources by maximising generation assets and increase the efficiency of the power system. Microgrids and smart grids are being tested and demonstrated in many projects such as [24, 37, 60–62, 68–70]:

- the E.U. Microgrids and More Microgrids Projects, with demonstration sites in the Kythnos Island (Greece), in Mannheim-Wallstadt (Germany), Bronsbergen (Netherlands) and Bornholm Island (Denmark);
- the U.S. CERTS microgrid and the U.S. UW microgrid;
- the NEDO microgrid projects in Japan;

[9] In this PhD thesis, no distinction is made between a microgrid and a smart microgrid: microgrids are intrinsically smart. For primary control, the pure microgrid definition would more or less be sufficient. However, when considering a hierarchical microgrid control, smart microgrids are targeted.

- BC Hydro / Hydro Quebec in Canada;
- the smart microgrid U.S. Army Fort Bragg;
- the Linear project in Flanders, Belgium;
- the European SmartGrids Technology platform.

1.4 Virtual power plants

Virtual power plants (VPPs) are a software-based flexible representation of a portfolio of distributed energy resources that can make contracts in wholesale markets and offer services to system operators [71]. VPPs can be classified in technical or commercial VPPs. Ideally, a VPP provides a combination of the two functionalities.

The key objective of commercial VPPs is to allow distributed energy resources to access the electricity markets. Single distributed energy resources generally to not participate in the markets. Often, either the installed power of a single unit is too low to be allowed for market participation. Otherwise, often, the stochastic variations in the produced (or consumed) energy render a risk that is too high for profitable market participation. To deal with these issues, the VPP aggregates distributed energy resources in a virtual unit and interconnects them with an information network.

Technical VPPs are addressed to deliver technical services to the system operator, such as contribution in primary control or ancillary services such as congestion management, voltage control, contribution in reserve provision or reactive power provision.

VPPs and microgrids are similar in the sense that they form an aggregation of distributed energy resources. Microgrids provide a coordinated aggregation on a smaller scale than VPPs, because in opposite to VPPs, they are geographically confined [72]. Microgrids focus on local issues, such as balancing the internal generation and consumption. As VPPs are a virtual aggregation in the sense that they are software-based, they can deal with grid-wide issues. A benefit of microgrids for the DNO is that they are controllable entities. Similarly, but on a larger scale, a benefit of VPPs is that the TNO can regard it as a single unit instead of many individual units. Table 1.1 shows that the concepts have different key aspects and complement each other, e.g., with microgrids as elements of an overlaying VPP. More details about VPPs are given in § 7.4.

Table 1.1: Aspects: microgrid - VPP (key = key aspect, conc = concern, / = of no concern).

	VPP	Microgrid
Market participation	key	conc
Reliability	conc	key
System stability	conc	key
Demand response	conc	key
Geographically confined	/	key
Asset flexibility (address different assets for different needs)	conc	/

1.5 Outline of research questions addressed in this PhD thesis

For the microgrid and smart grid concepts to become a reality on a large scale, some issues need to be handled. A first major issue is how to fulfill the reliability advantages that microgrids promise. Hereto, a robust islanded microgrid operation is key, which is the main contribution of this PhD thesis, by developing the "voltage-based droop control" for DG units in chapter 4.
A second major issue is how to handle the significant amount of DG units in the electrical power system. As islanded microgrids can be seen as miniature versions of the future grids, this PhD thesis focusses on achieving an optimal integration, operation and coordination of DG units, especially based on renewable energy sources, in the islanded networks. The developed voltage-based droop (VBD) control coordinates the DG units to achieve a stable operation and enables to address the renewables to contribute in the grid control instead of merely turning off when grid problems, such as overvoltages, occur. As the VBD control uses the grid voltage as the prime indicator of the "state" of the microgrid, the loads and storage equipment can also contribute in the grid control by means of controllers that comply with the control of the DG units, which is discussed in chapter 5. In this way, the loads can assist in dealing with the variability of many DG units, hence, contribute in achieving a better integration of DG in the power system. The latter addresses a third major issue, the contribution of different grid elements, including loads, in the grid operation.
The developed VBD control strategy can also be applied in grid-connected microgrids, which is analysed in chapter 6. Like in the islanded mode, the renewables can easily be addressed for grid control in the grid-connected mode as well. In this way, on-off oscillations of these units can be avoided, while the renewable energy capturing is maximised. Hence, the usage of VBD control in grid-connected

networks can help addressing some major challenges of distribution networks in the scope of increased DG penetration, e.g., congestion and voltage problems. As discussed in § 6.1, usage of VBD control in grid-connected networks can have a beneficial effect on the line losses as well.
When using a "smart transformer" (§ 5.3) at the PCC of the microgrid, the VBD control allows to obtain a controlled active power exchange between microgrid and utility network, without the need for extensive inter-unit communication. This facilitates the participation of the microgrid elements (hence, of renewable energy sources) in the electricity markets.

1.6 Conclusions

In order to improve and increase the integration of DG in the electric power system, to obtain a more efficient power system and to embed new smart grid features, the microgrid concept has been developed. The normal operating mode of a microgrid is grid-connected, but microgrids have the unique capability to operate in islanded mode as well.
The highest potential for microgrids is in places without (economically feasible) electricity access, where the conventional access is unreliable (countries without meshed grids, long rural feeders), places where a higher reliability than average is required (hospitals, data centres, industrial parks) and areas that benefit from being regarded as a single controllable entity (e.g., by delivering ancillary services to the market and achieving a lower energy dependency).
Analogous as microgrids, an important objective of smart grids is to reduce the carbon footprint, reduce the dependency on fossil fuels and optimise the network performance (e.g., remove bottlenecks and maximise asset utilisation). Smart grids support the introduction of RES while maintaining a stable, reliable and affordable electricity supply. Microgrids are often seen as a smart grid solution to achieve these objectives.

Chapter 2

Conventional primary control strategies for islanded microgrids

Islanded microgrid control by DG units can be divided into three categories as illustrated in Fig. 2.1. The controllers on the lowest level are responsible for controlling the terminal voltage of the DG unit to a certain reference value. This reference value is determined by the mid-level primary controller. The primary controller is responsible for achieving a stable microgrid operation. Hence, it takes care of the power sharing between the DG units. The set points of the primary controller can be altered by higher level secondary/tertiary controllers. These controllers take care of microgrid optimisation and economical issues, and are not necessarily a part of the DG unit. The main focus of this thesis is the primary control strategy.
The main control aim for DG units in islanded microgrids is to obtain an accurate power sharing while achieving a proper control of the amplitude of the microgrid

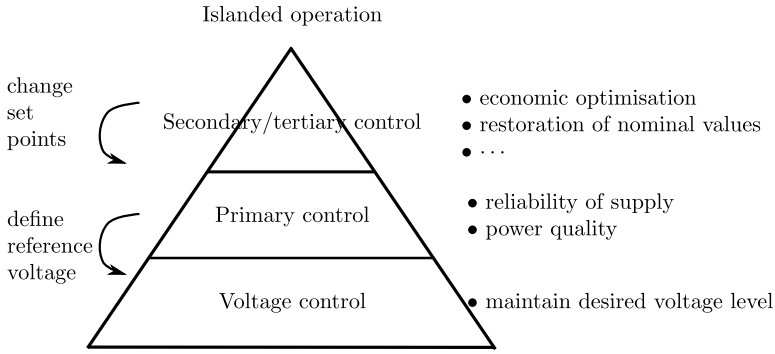

Figure 2.1: Hierarchical DG unit control: three levels

voltage and the frequency [10]. As most DG units are power-electronically interfaced to the grid, specific control strategies have been developed for the converter interfaces of the DG units in islanded microgrids. Centralised control, based on a communication infrastructure, has been investigated. However, it is often impractical and costly to distribute the dynamic control signals, which are characterised by their relatively high bandwidth[1] [10]. Moreover, problems concerning the reliability of the centralised control approach can counteract the positive reliability boost that is gained by implementing DG in microgrids [10]. To overcome these limitations, the decentralised approach has been presented, often based on the droop control strategy, which mimics the droop characteristics of the large synchronous generators. This chapter gives an overview of existing microgrid control strategies for the active and reactive power sharing between the DG units, i.e., primary control, in islanded microgrids.

2.1 Simplest method to connect inverters in parallel

The simplest method to connect inverters in parallel is to physically add an inductor at the output of the inverters and control their output voltage to a fixed reference [73]. However, a bulky inductor increases the size and cost of the system. In case the load current contains harmonics, the output voltage will also be strongly distorted by the inductors. Another implementation is to include a series resistor at the output of the individual sources [74]. The main disadvantage is the increase of power losses.

With these output impedances and in case of equal line impedances and output voltages, the output current of the converters will be shared equally. However, in real situations, the parameters of the converters have deviations from their nominal values. The load sharing is sensitive to phase angle differences, line impedances, output LC filter values and so on. When two power sources are only connected through a line impedance, the smallest phase or amplitude deviation causes circulating currents between the converters and, hence, a power sharing that is not controlled. This sensitivity is the reason why converters controlled at fixed frequency

[1] In the last years, the cost of communication per Mbit/s has significantly decreased. The communication latency is dependent on, e.g., the chosen protocol, medium and distance. Whether the latency is an issue is, thus, also dependent on the scale of the microgrid. This PhD thesis does not focus on a specific size of the microgrid, thus, in some cases, latency can be an issue. Hence, concerning the cost (of bandwidth and equipment) and latency, the usage of communication for primary control is always impractical compared to strategies that do not rely on inter-unit communication. Still, the main reason to avoid communication for the primary control is the reliability aspect. For secondary, slower control, full benefit of communication can be taken as latencies and bandwidth are generally not an issue. Also, the communication equipment is often already installed or will be installed anyway.

f and voltage V can not operate in parallel [75]. There is always a voltage difference caused by the tolerance of the sensors, references, temperature drift, ageing components and clock differences.

2.2 Control strategies with communication

The primary control strategies with communication achieve good voltage regulation and power sharing. Also, opposed to the droop controllers discussed further, the output voltage is generally closer to its nominal value. However, these strategies need communication lines between the modules. Communication lines are expensive and/or vulnerable. They could also reduce the system reliability and expandability and limit the flexibility of the system.

2.2.1 Central control / concentrated control

In the central control method, a central controller coordinates the power-electronic interfaces in the microgrid to obtain a good voltage quality by properly sharing the active power P and reactive power Q between the DG units in steady-state [40]. A communication link between the central controller and each unit is required. Central control has the advantage of using simple control algorithms in the converters. However, large expenses for the communication lines and a supervisory control centre are required. Hence, central control is difficult to implement in highly distributed and large systems [40]. Central control also makes it difficult to expand the system [76].
A possibility for central control is to use the single master operation, with one unit in the grid-forming mode[2] controlling its terminal voltage to a fixed reference value. The power sharing can be achieved by using a central controller that measures the total load power and distributes the weighted value (for example, with weighting according to the ratings of the DG units) to all units. The other DG units operate in grid-following mode, following the grid voltage and changing their output power according to the centrally communicated signals. The synchronisation can be achieved by using a phase locked loop (PLL). However, it is difficult to achieve a fast response for power distribution control due to the inherently relatively slow response of the PLL [77].
The simplest central control method, the **central-limit control (CLC)**, is discussed in [78–80] and the control scheme is depicted in Fig. 2.2[3]. The power sharing

[2]The difference between grid-forming and grid-following controllers is discussed in chapter 3 on page 57. In brief, grid-forming controllers are voltage-controlled, while grid-following controllers are current-controlled. At least one grid-forming controller is required in an islanded microgrid.

[3]The load is considered as a black-box and is not specified. It can be a controlled load, an RL load, a constant-power load, a power-electronically interfaced load, etc. Some concerns about the

and voltage regulation are controlled centrally and the subsequent commands are distributed through a communication link. A central controller defines the set value of the current for each module. This reference current i_{ref} is a fraction of the load current i_{load}. The latter current is measured by the central controller. For N equal modules, i_{load} is evenly distributed between the modules ($i_{\mathrm{ref}} = i_{\mathrm{load}}/N$), i.e., i_{ref} is the central-limit reference current (the mean value of all source currents). It is also possible to connect units with different power-ratings to the system. Then, for each unit, a different reference current is needed and the central controller uses individual weighting functions instead of the factor $1/N$ for all units. Of course, the sum of the N weighting functions should be equal to one. The central controller also determines a voltage correction term v_{e} to control the measured load voltage v_{o} to its reference value v_{ref} and communicates this voltage v_{e} to all modules. To determine the central v_{ref}, several options exist as is discussed in [79]. The local controllers of each module control their output current to the reference current received from the central controller. The output v_{c} of the current controller is added to v_{e}. The output voltage of each module equals $v_{\mathrm{e}} + v_{\mathrm{c}}$ and is generated by using pulse-width modulation (PWM). The shared signals that require a communication link are v_{e} and i_{ref}.

An advantage of this method is that current sharing is forced during all times, also during transients. During transients, the current loop is responsible for maintaining proper power sharing between the modules. The voltage loop will recover the voltage. This accurate power sharing in steady-state as well as during transients is not achieved by the master/slave control schemes for example, in which the master unit delivers most of the compensation current during the transients. The main disadvantage is that both v_{e} and i_{ref} have to be distributed to all converters by using a high-bandwidth communication link to synchronise the units [17].

Note that the line impedances are generally not considered explicitly in this paragraph (§ 2.2). In § 2.3 on the other hand, which discusses the controllers without communication, the line impedances are mostly taken into account. Neglecting the line impedances in the control strategies is a significant disadvantage, as the definition of load voltage v_{o} becomes unclear when the microgrid consists of a feeder with multiple loads. The methods that rely on communication are generally developed for UPS purposes, which are significantly smaller than microgrids. Hence, neglecting the line impedance can be acceptable in the UPS case, but mostly not in microgrids.

In the **power deviation method**, the load current i_{load} is (centrally) measured and divided by the number of operating inverters N (or by using a weighting factor) to obtain i_{ref}. This information is fed to all modules. From $i_{\mathrm{ref}} - i_{\mathrm{L,i}}$ and v_{o}, the

capacitance of the loads, e.g., with respect to resonances with the LC filters of the DG units and other loads, may arise in the future, this domain is not yet widely investigated in literature.

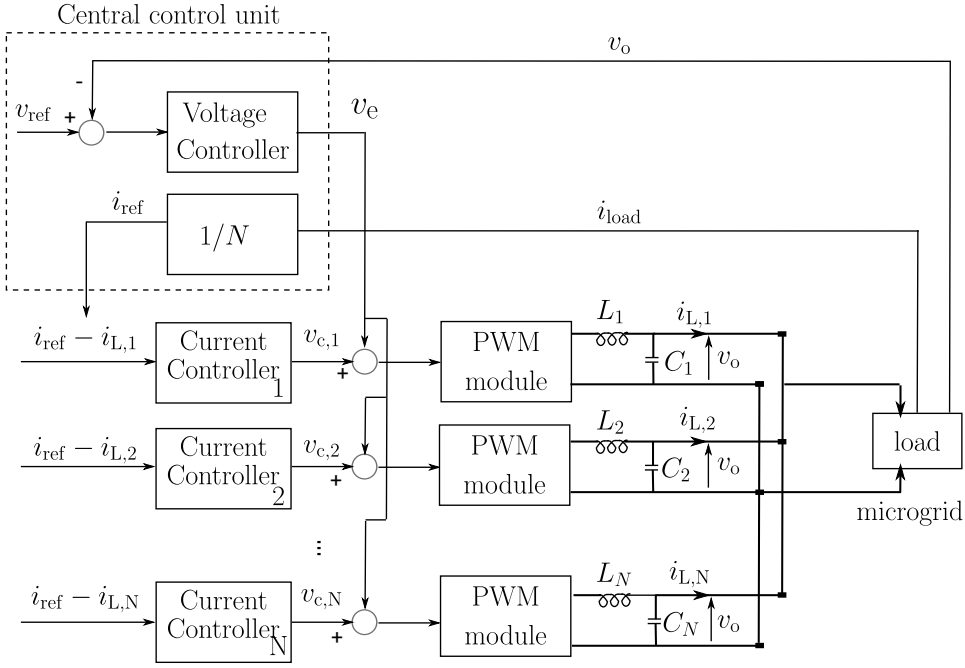

Figure 2.2: Central-limit control principle

power deviation, i.e., the active component ΔP and the reactive component ΔQ, are evaluated. In [81] and Fig. 2.3 the inverters are connected to the common bus via a series inductance. The power deviation method is based on the theory that the active and reactive power are separately determined by the phase angle and amplitude of each module's output voltage, respectively, which will be discussed further. The power angle is dynamically controlled by slightly changing the inverter frequency. The reactive power deviation ΔQ, the common grid voltage reference V_{ref} and the inverter output voltage V_{o} determine the reference amplitude $V_{\mathrm{g}}^{\star}$ of the inverter's output voltage. The active power deviation ΔP and the frequency reference f_{ref}, determine the new frequency set value $f^{\star}$.

2.2.2 Master/slave control

In the master/slave control strategy, voltage as well as current controllers are used. In central-limit control, the converters share the total load current by using weighting factors. A disadvantage is, thus, that if the sum of these factors differs from one, due to for example the shut down of a unit or a programming fault, the load current continues to decrease or is not shared properly [80]. In master/slave con-

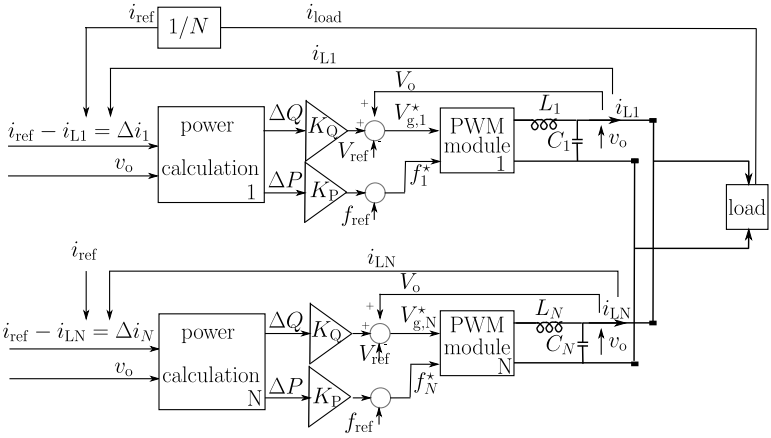

Figure 2.3: Power deviation control

trol on the other hand, the master only has voltage control, no current control. Hence, this unit delivers the transient current and compensates for wrong weighting factors. The master module is responsible for output voltage regulation and to specify the reference current of each inverter. The slave units track the current command provided by the master to achieve an equal current distribution. It is well-known that a master/slave control can realise excellent current sharing performance with easy implementation, even with non-identical modules. However, master/slave control does not achieve redundancy as the slave units depend on the master module. Another drawback is that as the master output current is not controlled, high output current overshoot during transients can occur [82]. The slave units react slower to the transient current demand such that the master needs to provide the compensation current [17]. Communication signals of relatively high bandwidth, i.e., instantaneous current and voltages, are distributed throughout the system.
Different strategies for assigning the master are possible, such as [83]:

- dedicated: master is a fixed module;
- rotary: master is arbitrarily chosen;
- highest rms current: master is the module with maximum rms current.

A. Without central controller

The master/slave control scheme without central controller consists of a single master and a set of slave inverters without additional central controller [17, 82–84].

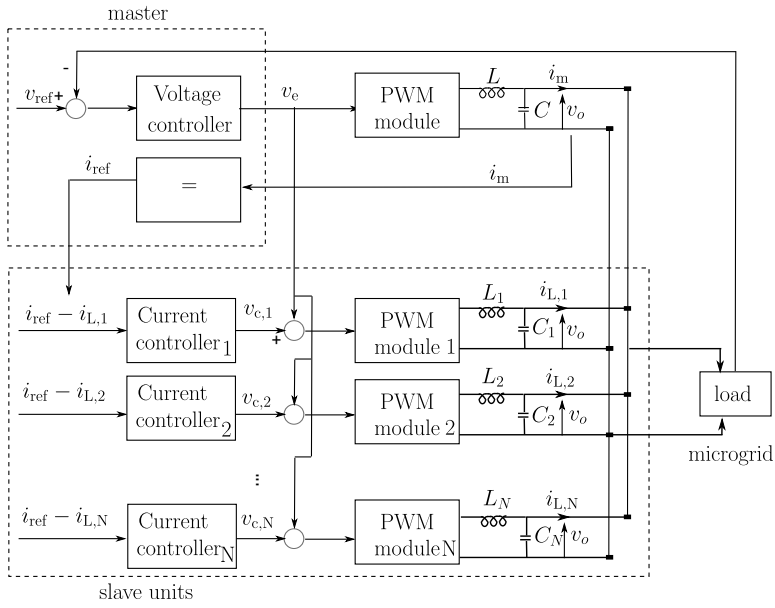

Figure 2.4: Master/slave control principle without central controller

The master operates as a voltage-source inverter (VSI) in order to control the load voltage as shown in Fig. 2.4. It also measures the total load current and determines the set value of the current for each slave unit. The slave units operate in current-control mode acting as current-source inverters (CSIs). In the master/slave control method of Fig. 2.4, derived from its dc/dc variant in [82], the reference current of the slaves equals the master output current $i_{\mathrm{m}} = i_{\mathrm{ref}}$. A current controller controls the slave's output current $i_{\mathrm{L,i}}$ to i_{ref}. The output of the slave's current controller v_{c} is added to a master-signal v_{e} and forms the input of the pulse-width modulation (PWM). The signal v_{e} can be seen as a feed-forward term. The master module controls v_0 to v_{ref} via a voltage controller with output v_{e}, which is directly used for the PWM signal generation of the master.

An advantage of this strategy is that voltage recovery is obtained by the voltage controller of the master and the current control loops of the slaves together [17]. A disadvantage is that both current sharing signals (i_{m}) and voltage (v_e) feedback signals are distributed by using a relatively high bandwidth communication link as instantaneous values are communicated [17]. The current sharing is accurate in steady-state, but during the transients, large differences between master and slave currents can occur due to the limited bandwidth of the communication. The master delivers most of the compensation current during transients.

For the master/slave communication scheme, several possibilities exist. In a first one, the master unit sends its signals to all other units. Therefore, the number of interconnections can become quite large. However, if any slave fails, the system would still be operational, leading to a certain degree of redundancy. In a second implementation, the units are arranged in a ring configuration. Therefore, the master unit sends its signals only to one (first) or two (first and last) slave units. This reduces the number of interconnections, but can compromise the redundancy. With both configurations, the reliability of the power system is determined to a large extent by the reliability of the master unit [85]. Therefore, in [85], a rotating priority window, providing random selection of the master is suggested to increase the reliability. In [86], extended monitoring by two redundant monitoring systems is performed. These systems define one of the healthy blocks as the master.

B. With central controller

A second variant on master/slave control is the control strategy with a central controller as shown in Fig. 2.5. This approach is based on a method for operating UPS systems in parallel and is described in [17,77,87–89]. The master is responsible for the voltage control and is, thus, a VSI, while the slaves take care of the current control in the CSI mode. Opposed to the control method without central controller, the master current is not equal to the reference current and the master does not provide this reference current to the slave units anymore. This task is performed by a central control unit, that calculates the central-limit reference current ($i_{\mathrm{ref}} = i_{\mathrm{load}}/N$) and distributes this to all slave units. Compared to the method without central controller, the voltage reference value is not shared, the only distributed signal is i_{ref}. Hence, the voltage control is achieved by the master unit alone.

The advantages and disadvantages are analogous to those of the master/slave control without central controller. Like in the previous master/slave control during transients, the master tries to recover the output voltage, which may lead to large master current transients [17]. This can become critical in large systems wherein the master has to provide the transients of the whole system. Only one signal has to be distributed, but still, a high bandwidth of the communication link is required. There is always a time or phase delay between the output current of each slave unit and the load current [77].

An advantage of this method is that in grid-connected mode, the grid can be regarded as the master. Therefore, there is no need for specific control methods for grid-connected and islanded operation. Also, good load sharing is achieved. However, because of the presence of a single central controller and a master, the system is not redundant.

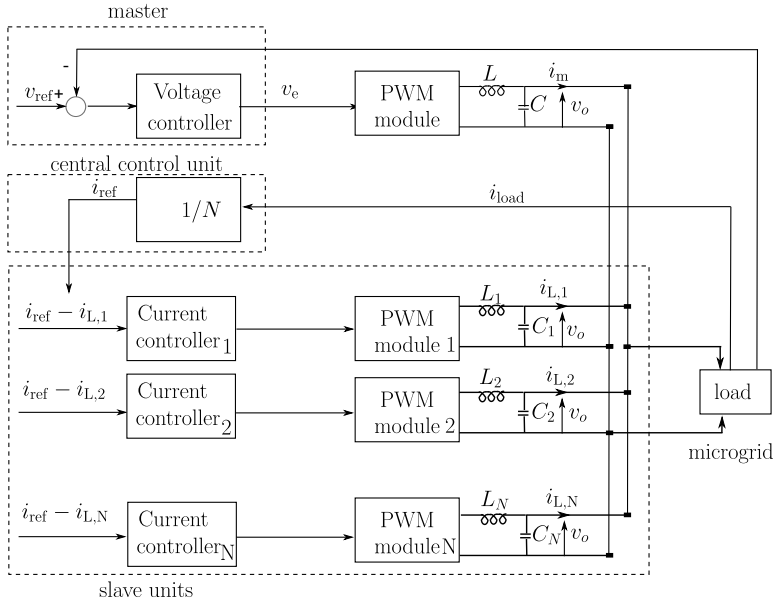

Figure 2.5: Master/slave control principle with central controller

C. Auto-master-slave control

In [90], an auto-master-slave control strategy is proposed, which is a variant of the master/slave control. The main principle is depicted in Fig. 2.6.

The control circuitry employs an active power and a reactive power share communication bus interconnecting all the paralleled units [90]. All inverters measure their output power. The inverter with the highest output power becomes the master. The master of real power drives P_{bus}, which becomes the reference signal for the other units. In the master, $\Delta P = 0$, while for the slaves $\Delta P = P_{\text{bus}} - P_i$. By using ΔP, the frequency compensation value Δf is calculated. As for the master, $\Delta P = 0$ in steady-state, the master works at the reference frequency $f = f_{\text{ref}}$. For the reactive power, an analogous regulation is adopted in [90], also including a master unit for the reactive power. The value ΔQ determines the reference voltage amplitude of the units. The bus signals P_{bus} and Q_{bus} are almost dc and the noise can be eliminated easily, so the information can be transferred over long distances [90]. This is in contrast to the master/slave and central control schemes, where instantaneous values of voltage and/or current need to be distributed.

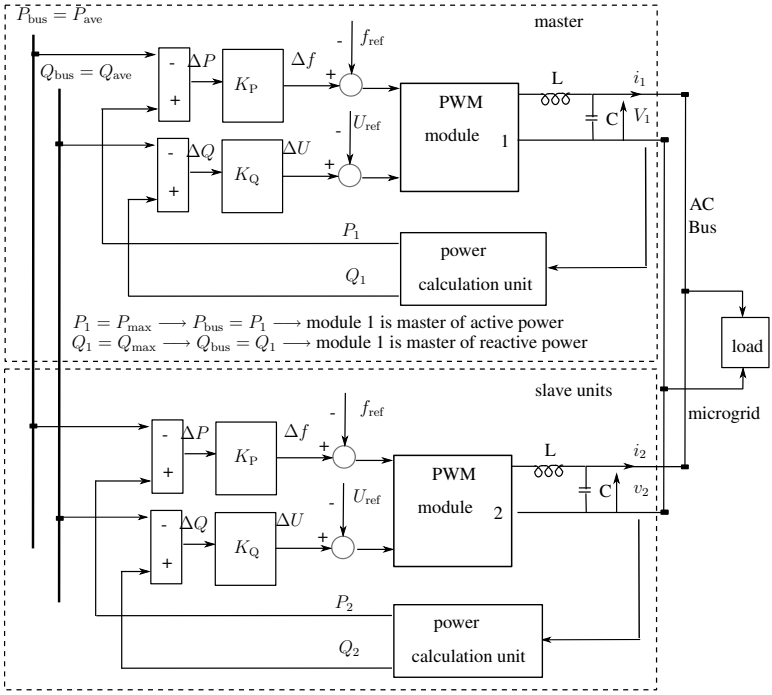

Figure 2.6: Auto-master-slave control principle

2.2.3 Instantaneous(-average) current sharing

Another control strategy that depends on inter-unit communication is the instantaneous current sharing technique. Opposed to the master/slave control scheme, no master controller is present. The method is similar with the central-limit control principle, but here, the line impedance is taken into account. Average current sharing requires a current sharing bus and a reference synchronisation for the voltage. The voltage and current references are shared signals among the modules. The objective of the shared information is to determine the deviation of the individual output current from the desired value [91]. Since the output currents of the inverters are regulated at every switching cycle, the instantaneous-current sharing scheme has a good performance both on current sharing and voltage regulation [91]: even if the output currents contain harmonics, the inverters can share the output currents equally. However, interconnections between the inverters are necessary. This limits the flexibility of the system and degrades the redundancy [91].

The control principle is depicted in Fig. 2.7. Each inverter is connected to the load through an impedance Z_i. By taking this impedance into account, there is no com-

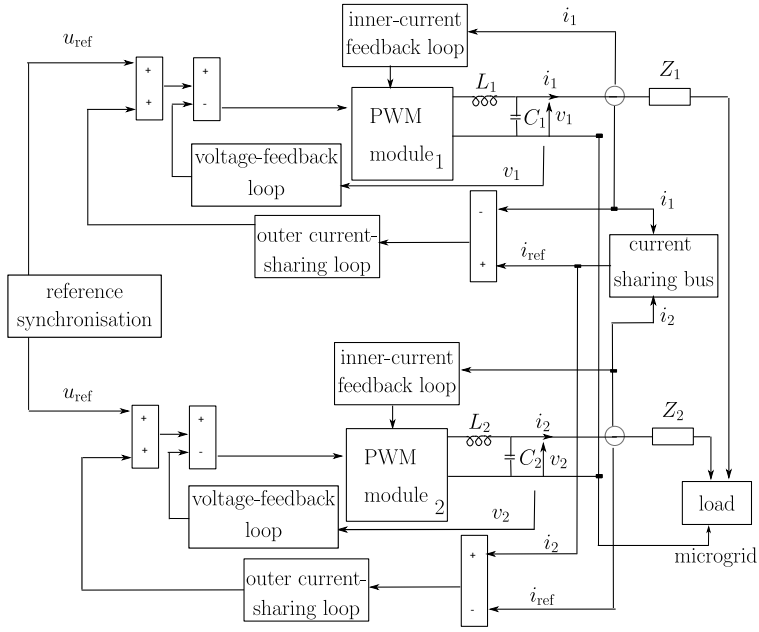

Figure 2.7: Instantaneous average current sharing

mon voltage reference of the DG units that is equal to the load voltage v_{o}. The references of the voltage-feedback loops are synchronised to make the output voltages of all inverters in phase [92]. This common synchronisation reference is the first input of the voltage control loop. The output of the outer current-sharing loop is added to this value such that each inverter contributes the same power to the load [91]. Each inverter provides a measurement of its output current to the current-sharing bus, which generates a common current reference i_{ref} [91,93]. The value i_{ref} minus the measured terminal current of the DG units forms the input of the outer current sharing loop.

The reference i_{ref} can be the highest output current, the output current of the inverter with the highest clock frequency or the averaged output current [91]. A disadvantage of the highest current control (HCC) is that the sensed highest output current can include noise, which deteriorates the performance of the current distribution and output voltage regulation. In addition, non-identical component characteristics and input voltage variation of the paralleled inverters might also deteriorate the system performance [94]. In [94, 95], the averaged current-sharing strategy (ACSS) is used to achieve an equal current distribution and to reduce noise effects occurring at the converter switching transition. In [96], the average current

sharing method is combined with load current feed-forward to improve the output characteristics. However, with the HCC and ACSS, it is difficult to achieve a weighted current distribution control when the paralleled inverters have different power ratings [97]. Therefore, a current-weighting-distribution-control (CWDC) is used in [97] to achieve a weighted output current distribution among the inverters. This allows for inverters with different power ratings, as opposed to the case where the factor $1/N$ is used for the current distribution. The control strategy is analogous to the other instantaneous current sharing strategies and is depicted in Fig. 2.8. First, the average current is calculated, which is defined as (with N the number of units):

$$i_s = \frac{\sum_{\mathrm{i}=1}^{N} i_{\mathrm{L,i}}}{N} \tag{2.1}$$

Then, for each unit, the reference current is calculated by using a weighting function:

$$i_{\mathrm{ref,j}} = i_s \frac{P_{\mathrm{j,nom}}}{(\sum_{\mathrm{i}=1}^{N} P_{\mathrm{i,nom}})/N} \tag{2.2}$$

The value $P_{\mathrm{i,nom}}$ represents the nominal active power output of inverter i. For the weighting function, the ratings of the units (apparent power S) can be used as well instead of the nominal active power.
The power sharing is affected by the line impedances. For example, for two units that are scheduled to provide the same amount of active power (equal P_{nom}), perfect power sharing is achieved when the actually delivered active power is equal for the two units as well. In this control strategy however, these units deliver the same current, hence, if $Z_1 > Z_2$, then $V_1 > V_2$. In this case, the first unit delivers more active power than the second one, despite their equal P_{nom}. To improve the current and power sharing when the line impedance is different among the inverters, adaptive gain scheduling is introduced in the instantaneous average current sharing control scheme in [93].

2.2.4 Peak-value based current sharing

In [98, 99], peak-value based current sharing is used to obtain accurate power sharing and smooth mode transfer. One converter operates with a voltage dual-loop controller to control the ac-bus voltage to a reference value. For this, an inner current control and an outer voltage control loop with proportional-resonant (PR) controllers are used. The other converters only have a current control loop with a PR controller. The control strategy is summarised in Fig. 2.9. The reference amplitude of the current-controlled inverters is determined by the obtained cur-

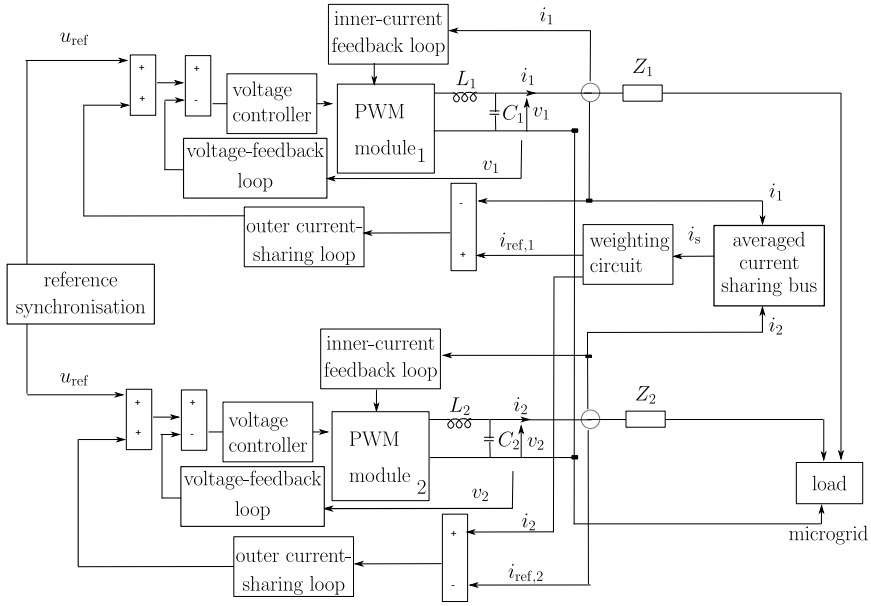

Figure 2.8: Current-weighting-distribution-control

rent amplitude of the voltage-controlled inverter by using peak value calculation (PC) and is communicated via a communication bus [99]. The reference phase is determined by using a PLL that calculates the phase angle of the load voltage v_{o}. An automatic reference generation (ARG) calculates the current reference of the current-controlled units in order to minimise the current peak difference and phase difference. Only the magnitude and phase information of the ac current need to be communicated [99]. The frequency information is not transmitted because it is automatically tracked by the PLL (opposed to the master/slave control scheme).

2.2.5 Circular chain control

In the circular chain control (3C) scheme depicted in Fig. 2.10, the modules are connected in a circular configuration and each module tracks the inductor current of the previous one. In this way, equal current distribution is achieved [100]. An outer voltage control loop is used, such that each module controls its output voltage v_{o} to a reference value v_{ref}. As shown in Fig. 2.10, the line impedances are neglected. The output of the voltage controller, together with the measured inductor current of the module and that of the subsequent one, form the input of the inner current control loop.

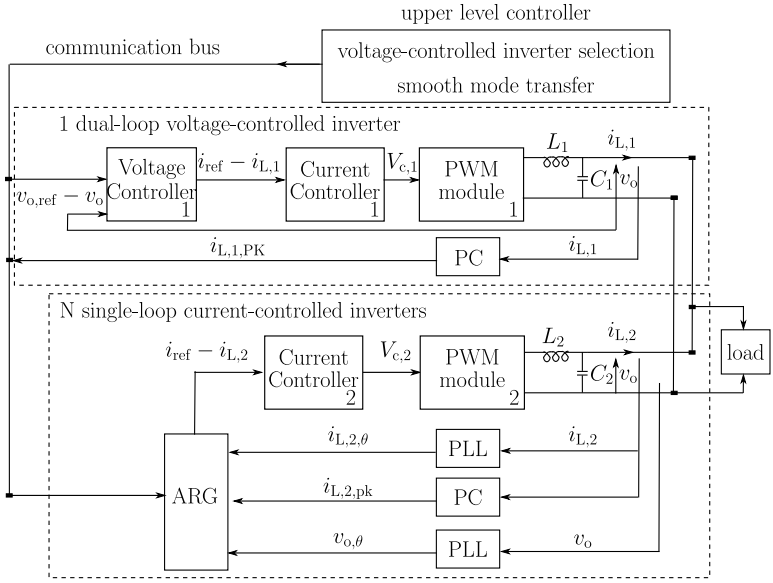

Figure 2.9: Peak-value based current sharing (pk = peak value; θ = phase angle)

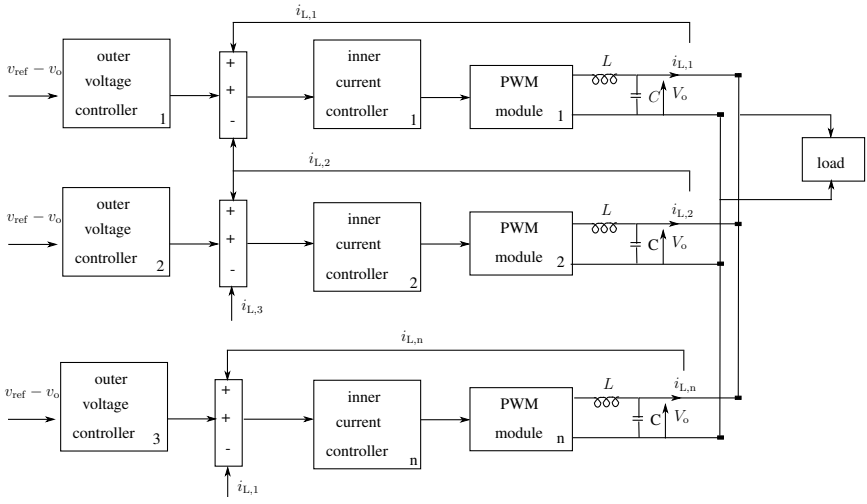

Figure 2.10: Circular chain control

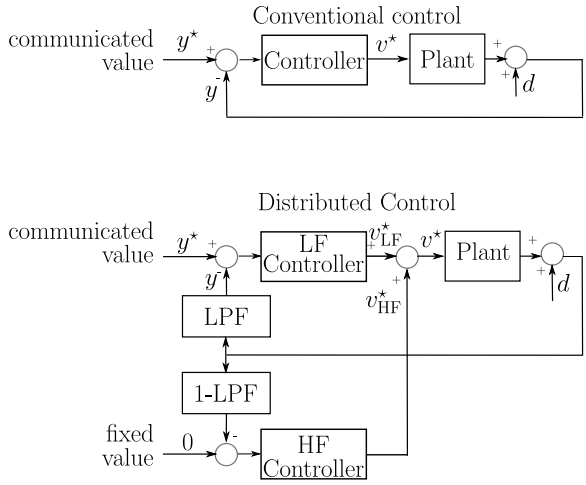

Figure 2.11: Conventional control scheme versus distributed control scheme

2.2.6 Distributed Control

Another method to parallel converters is the distributed control method (DCM) [17, 101]. It is important in distributed control to reduce the number of communication lines to improve the ease of implementation and the reliability. The shared bus can consist of signals such as the voltage reference, the current reference and an averaged feedback voltage. By using a shared bus between the modules, the system will keep running in case a module breaks down.

The DCM of [17] uses low-bandwidth communication to maintain instantaneous power sharing and high power quality under various loads. In the previous methods, if the bandwidth of the distributed signals decreases, the disturbance rejection will be compromised as higher frequency components are not regulated. Therefore, in the DCM, a central controller provides fundamental frequency power sharing between the different converters by distributing a low-bandwidth signal to all converters. Power quality aspects are dealt with within the local controllers, by means of higher-frequency signals. The difference between the conventional control schemes and the DCM method of [17] is shown in Fig. 2.11, with d a disturbance. In the conventional control scheme, a signal y is controlled to its reference value $y^\star$, with controller output $v^\star$. In communication-based control algorithms, $y^\star$ is a communicated signal. In the DCM, a remote central controller regulates the low-frequency components of y, by determining $v^\star_{\mathrm{LF}}$ and communicating it to the plant by means of a low-bandwidth signal. For the higher frequency components, a high-bandwidth signal is locally controlled to zero.

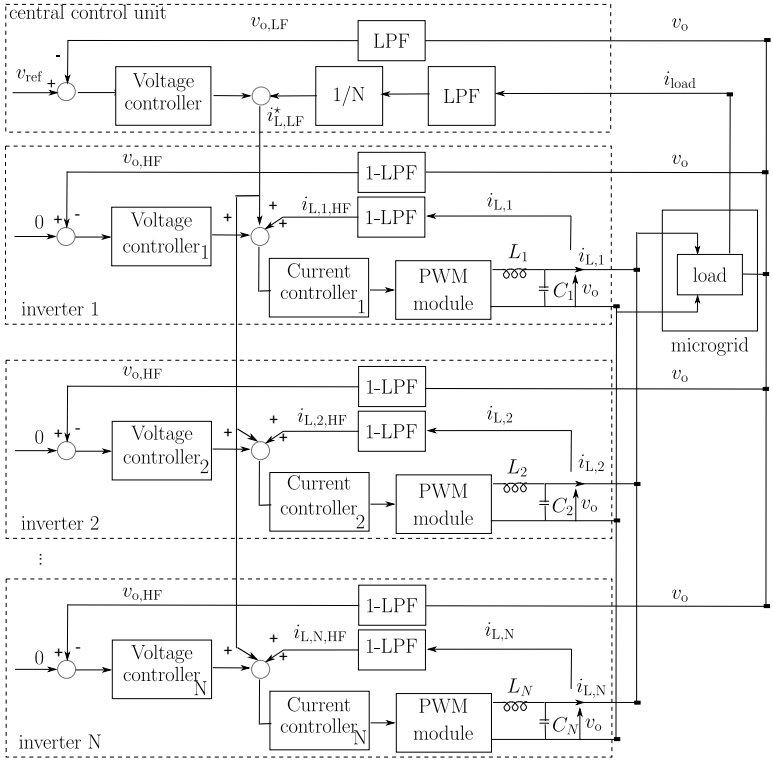

Figure 2.12: Distributed control method (HF = high-frequency, LF=low-frequency

The DCM scheme is shown in Fig. 2.12. The central controller controls the low-frequency components of the load voltage to $v_{\rm ref}$ and determines the low-frequency reference $i^\star_{\rm L,LF}$ for the converters. This reference signal can be transmitted to the individual units via a communication link of limited bandwidth [17, 101]. Steady-state and low-frequency issues are, thus, centrally controlled. The control is distributed between this low-bandwidth central controller and high-bandwidth local controllers. The local controllers are responsible for rejecting high-frequency disturbances, such as harmonic suppression, without the use of a communication channel [17, 101]. They control the high-frequency components of the load voltage to zero. The current controller's input is formed out of three components. The first component consists of the central $i^\star_{\rm L,LF}$ for fundamental frequency power sharing and voltage regulation. The second input of the current controller is the local voltage controller's output, which determines the high-frequency component of the inverters output current $i_{\rm L,i,HF}$. The third is the measured high-frequency component of the output current.

In conclusion, voltage regulation and fundamental power sharing are controlled centrally. The DCM is distributed in the sense that the higher frequency components are dealt with by local controllers. However still, a single point of failure is present, namely the (communication link of the) central controller. The main advantage of the method proposed in [17, 101] is that the control topology uses a communication link of limited bandwidth to maintain power sharing between the units.
The distributed control can be seen as a variant on the master/slave control. In distributed control, only low-bandwidth communication is required and the harmonic support is done locally, opposed to in the master/slave control scheme.

2.2.7 Angle droop

In [102], angle droop control is presented. This is a control method that uses communication for phase angle referencing. In the conventional droop control method, which is discussed in § 2.3.1, P and Q are controlled through the frequency and amplitude of the reference voltage. In angle droop control on the other hand, the phase angle, relative to a system-wide common reference (a phase angle reference), is used for the P control instead of the grid frequency:

$$\delta = \delta_0 - m(P - P_0) \tag{2.3}$$

$$V = V_0 - n(Q - Q_0). \tag{2.4}$$

Mostly, GPS signals are used to obtain the reference angle. In this way, no inter-unit communication is required.

2.3 Control strategies without communication

The usage of communication often needs to be avoided for the primary control as primary objective of the primary controller is to maintain the stability of the system [4]. Overlaying secondary and tertiary controllers, which can change the set points of the primary controllers, e.g., for economic optimisation, generally rely on communication.
The strategies that operate without inter-unit communication for the primary control are based on droop control. Operation without a communication link is often essential when connecting remote inverters. It also makes it easy to achieve redundancy and avoids the complexity, high costs and the requirement of high reliability of a supervisory system. Also, such systems are more easy to expand because of

the plug and play features of the modules. Therefore, especially for long distances and high-bandwidth requirements, communication lines are often avoided. Other advantages of droop controllers are that they can easily deal with units of different power ratings and offer great flexibility and reliability. Nevertheless, droop control also has some inherent drawbacks, such as the trade-off between power sharing accuracy and voltage deviations, unbalance in harmonic current sharing and dependency on the system impedance. To overcome these issues, some variations on the conventional droop controllers have been presented, such as injecting high-frequency signals (i.e., > 50 or 60 Hz) in the power lines as discussed in § 2.3.3. Another disadvantage is that the local controllers in the converters are more complex than when a central controller is used, i.e., next to a voltage control, the units also need a power control block [76].

2.3.1 P/f droop control

A well-known way to realise a plug and play feature for each DG unit is employing the conventional droop control [42]. In the transmission system, the synchronous generators are equipped with P/f droops. When the extracted electrical active power of the power station is larger than its input mechanical power, the generator will slow down because energy is being extracted from its rotating inertia. Hence, the frequency of its terminal voltage will lower. In this way, the phase angle of the voltage will decrease and because of the line characteristics, also the ac power will decrease. The frequency is a global parameter, i.e., equal in the entire system and the rotational speed of the generators is directly linked to the frequency. Hence, each generator will measure its speed and droops it in a P/f droop with negative slope to change its input mechanical power. In this way, accurate power sharing between different generators is obtained.

A. Conventional P/f droop control

Droop control was introduced for standalone microgrid control in [4, 15, 18, 40, 103–106]. The P/f droop control method mimics the operation of synchronous generators in the transmission system. In the conventional power system, the droop control method changes P as a function of the grid frequency, and is based on the inertia of the synchronous machines ($P(f)$). As the converter-based microgrids generally lack this inertia, the P/f droop method in microgrids is based on the line characteristics. The power flow equations from a source E_1 with phase angle δ to a voltage E_2 with phase angle 0 (phase angles are relative values) through an inductive line impedance jX can be approximated by (see § 4.1) (with $\sin\delta \approx \delta$

and $\cos\delta \approx 1$ for low phase angle differences δ):

$$P \approx \frac{E_1 E_2 \delta}{X}, \tag{2.5}$$

$$Q \approx \frac{E_1}{X}(E_1 - E_2). \tag{2.6}$$

For this reason, in inductive networks, a linkage between active power and phase angle and between reactive power and voltage amplitude exists. For the control, the frequency is used instead of the phase angle as the units do not know the initial phase value of the other units. Another reason is that, due to component tolerances for example, minor differences in the frequency of a signal can occur although the same reference frequency is used. Hence, it is necessary to compensate for the difference between the crystal clock generators [83].

In the P/f droop control method, the P of the generators is drooped with the measured terminal frequency ($P(f)$). However, in converter-based microgrids, measurements of the instantaneous frequency are not straightforward, while measuring the active power is easier [104]. Also, the frequency of a converter-system can be controlled independently, opposed to the frequency of a synchronous generator that is linked to its rotational speed. Therefore, generally, a droop with f as a function of the measured P ($f(P)$) is proposed, which is analogous to determining P as a function of the measured f ($P(f)$) [107]:

$$\omega_i = \omega_{\mathrm{ref}} + K_{\mathrm{f}}(P_i - P_{\mathrm{i,ref}}), \tag{2.7}$$

with ω the angular pulsation ($\omega = 2\pi f$) and K_{f} the droop. Preferably, the droops are coordinated to make each DG system supplying real power in proportion to its power capacity [42]:

$$K_{\mathrm{f}} = \frac{\omega_{\mathrm{ref}} - \omega_{\mathrm{min}}}{P_{\mathrm{i,ref}} - P_{\mathrm{i,max}}} < 0. \tag{2.8}$$

In case multiple DG units are connected in parallel, they share the load according to their droops analogously as in the conventional power system. Similarly, the amplitude of the voltage is drooped with the measured reactive power:

$$V_i = V_{\mathrm{ref}} + K_{\mathrm{Q,v}}(Q_i - Q_{\mathrm{i,ref}}), \tag{2.9}$$

$$K_{\mathrm{Q,v}} = \frac{V_{\mathrm{ref}} - V_{\mathrm{min}}}{Q_{\mathrm{i,ref}} - Q_{\mathrm{i,max}}} < 0. \tag{2.10}$$

The choice of K_{f} and $K_{\mathrm{Q,v}}$ influences the network stability [9].
The control algorithm with conventional droop control is depicted in Fig. 2.13. The unit operates as a voltage source with voltage and frequency determined by local control loops [4]. Only the steady-state power and voltage (i.e., 'ref' or 'nom' values) are communicated by using secondary controllers in a microgrid management scheme. An advantage of the droop method is its simplicity because no extra interconnections among the inverters are required. Therefore, high modularity, flexibility (i.e., plug and play) and good reliability can be achieved. However, the performance of the voltage regulation and the transient responses are lower, and the harmonic currents cannot be shared properly with the conventional P/f droop control method. Because of the proportional controllers without integral term (i.e., droops), the frequency and voltage in the microgrid are not constant but load-dependent. Hence, there is an inherent trade-off between the voltage control against the accuracy of Q and P sharing [108, 109]. In choosing the droop coefficients, there is also a trade-off between the magnitude of the droop and the stability. Large droops speed up the load sharing, but can cause instability. Smaller droops slow down the control [110]. A slow dynamic response is obtained as low-pass filters are required to calculate the average P and Q [108]. Another disadvantage of this method is the inability to provide rejection of the voltage harmonic content [101]. Still, the independence of communication for the primary control outweighs these disadvantages in most cases.
Some solutions to the aforementioned issues have been discussed in literature. A virtual output impedance [111], frequency restoration [112] and a derivative controller [10,113,114] can be included in the droop method. Also, the primary droops can be overlayed with a communication-based, slower secondary controller that can change the droop characteristic.

B. Variants on P/f droop control

Different variants on P/f droop control have been presented to cope with some issues like a line-impedance dependency, inaccurate P or Q regulation and slow transient response [115].

Derivative term To improve the dynamics of the system, a derivative term is included in the adaptive derivative droop in [10]:

$$\omega = \omega^{\star} + K_{\mathrm{f}}(P_i - P_{\mathrm{i,ref}}) + K_{f,d}\frac{dP_i}{dt}, \tag{2.11}$$

$$V_i = V_{\mathrm{ref}} + K_{\mathrm{Q,v}}(Q_i - Q_{\mathrm{i,ref}}) + K_{Q,v,d}\frac{dQ_i}{dt}. \tag{2.12}$$

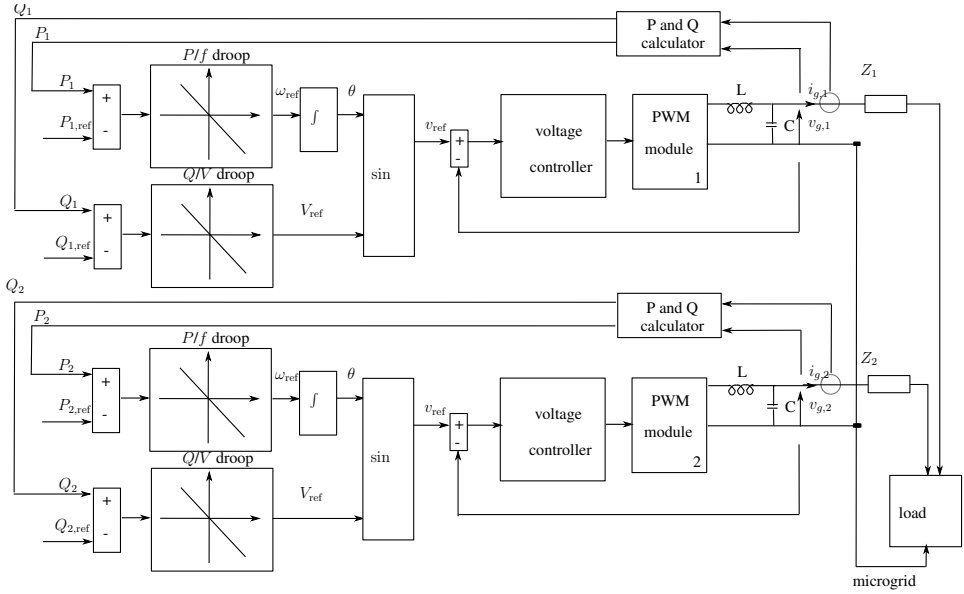

Figure 2.13: Conventional droop control: P/f droops and Q/V droops

In small microgrids, large load changes can be expected, hence, adaptive (hatted-values (ˆ)) transient derivative droops are used in [10] to add damping and to avoid large start-up transients and circulating currents:

$$\omega = \omega^{\star} + K_{\mathrm{f}}(P_i - P_{\mathrm{i,ref}}) + \hat{K}_{f,d}\frac{dP_i}{dt}, \tag{2.13}$$

$$V_i = V_{\mathrm{ref}} + K_{\mathrm{Q,v}}(Q_i - Q_{\mathrm{i,ref}}) + \hat{K}_{Q,v,d}\frac{dQ_i}{dt}. \tag{2.14}$$

A pole placement problem changes $\hat{K}_{f,d}$ and $\hat{K}_{Q,v,d}$ [10].

Virtual output impedance To avoid P-Q coupling, a virtual output inductor can be included, which introduces a predominantly inductive impedance without the need for further line impedance information. In [111, 113], a virtual inductive output impedance is implemented in the inverter by including fast control loops in the droop control method as shown in Fig. 2.14. The input of the voltage controller

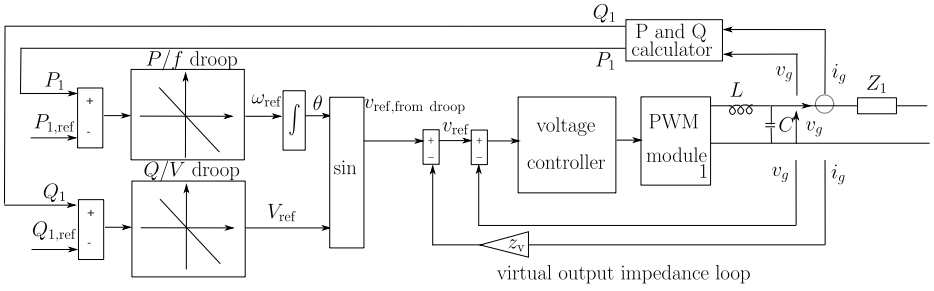

Figure 2.14: P/f droops and Q/V droop with virtual output impedance

becomes [42]:

$$v_{\text{ref}} = v_{\text{ref,from droops}} - L_{\text{virt}} \frac{di_{\text{g}}}{dt}. \tag{2.15}$$

A concern from the virtual inductor control scheme is the derivation of the line current i_{g} [42]. Differentiation can cause high-frequency noise amplification, which in turn may destabilise the voltage control scheme especially during a transient [42]. A common approach to avoid noise amplification is to add a low-pass filter to the measured grid current [42,108,116]. However, this approach is subjected to a tradeoff between the high frequency noise attenuation and the fundamental component phase and gain errors (or tradeoff between the overall control scheme stability and the virtual inductor control accuracy) [42]. Therefore, another method uses a high-pass filter instead of a pure derivative [111]:

$$v_{\text{ref}} = v_{\text{ref,from PQ droops}} - \frac{s}{s + \omega_C} L_{\text{virt}} i_{\text{g}}. \tag{2.16}$$

The virtual output impedance method is effective in preventing the P-Q coupling, but can increase the reactive power sharing error due to increased voltage drops. Therefore, in [42], the reactive power control is improved by on-line estimating the voltage drops and the local load demand.

In addition, soft start is included in [108] to avoid initial current peaks:

$$L_{\text{virt}} = L^{\star}_{\text{virt,f}} + (L^{\star}_{\text{virt,0}} - L^{\star}_{\text{virt,f}}) e^{-\text{t}/\text{T}_{\text{start}}}, \tag{2.17}$$

with $L^{\star}_{\text{virt,0}}$ and $L^{\star}_{\text{virt,f}}$ the initial and final values of the virtual output impedance and T_{start} the time constant of the soft start operation.

Frame transformation To avoid P/Q coupling, next to the virtual output impedance method, virtual P and Q frame transformation has been proposed [117]. A transformation matrix with angle ϕ, that is dependent on the R/X value of the lines, is used to calculate the virtual powers P' and Q':

$$\begin{bmatrix} P' \\ Q' \end{bmatrix} = \begin{bmatrix} \cos\phi & -\sin\phi \\ \sin\phi & \cos\phi \end{bmatrix} \begin{bmatrix} P \\ Q \end{bmatrix}, \tag{2.18}$$

with $\phi = \pi/2 - \theta = \arctan(R/X)$.
The P/f droop becomes:

$$\omega_i = \omega_{\text{ref}} + K_{\text{P}}(P'_i - P'_{\text{i,ref}}). \tag{2.19}$$

This is equal to:

$$\omega_i = \omega_{\text{ref}} + K_{\text{P}}\frac{X}{Z}(P_i - P_{\text{i,ref}}) + K_{\text{P}}\frac{R}{Z}(Q_i - Q_{\text{i,ref}}). \tag{2.20}$$

For the reactive power,

$$V_i = V_{\text{ref}} + K_{\text{Q}}(Q'_i - Q'_{\text{i,ref}}) = E_{\text{ref}} + K_{\text{Q}}\frac{X}{Z}(Q_i - Q_{\text{i,ref}}) + K_{\text{Q}}\frac{R}{Z}(P_i - P_{\text{i,ref}}). \tag{2.21}$$

The droops are, thus, equal to those of (2.7) and (2.9), but with P and Q replaced by P' and Q' respectively. In this way, despite the non-zero R/X value of the lines, P/Q decoupling is achieved as if the network would have been purely inductive. In general, the value X/R is not accurately known in the point of coupling, but according to [117], an estimation of R/X is sufficient.
Another method that uses frame transformation is presented in [118]. Here, the transformation angle is continually adapted to reach a minimum current and accurate power sharing. However, according to [119], the slow dynamics of the added current droop can make this method impractical.
As the virtual power frame (P'-Q') cannot directly and accurately share the actual power, in [120, 121], a virtual frequency-voltage (ω' - E') frame is used. This method also achieves a decoupled power control and an improved system stability.
In [122], an adaptive droop controller is presented in which the grid's phase angle is estimated by using a PLL to determine the frame transformation angle.

Harmonic power sharing An interesting method to share the harmonic burden is the usage of G/H droops, with G the harmonic conductance and H the harmonic var (volt-ampere reactive). This method is presented in [14] and is shown in

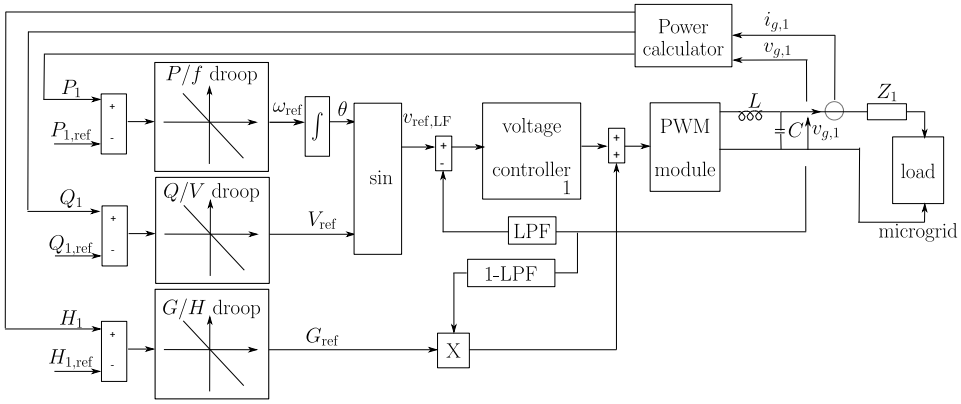

Figure 2.15: Harmonic power sharing: P/f, Q/V and G/H droops

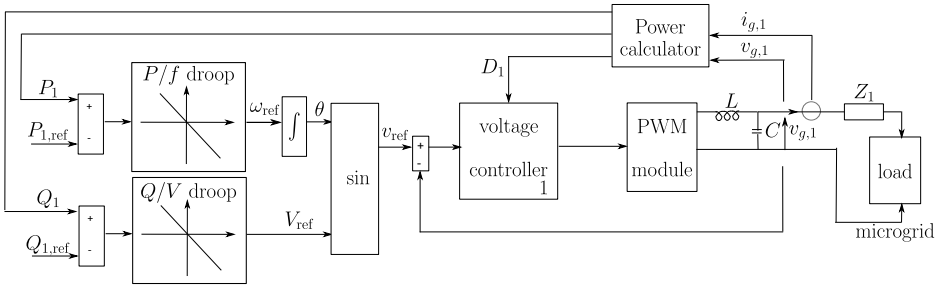

Figure 2.16: Harmonic power sharing: sharing the distortion by adapting the bandwidth of the voltage controller

Fig. 2.15. The harmonic power H is calculated according to the instantaneous reactive power theory [123]. This method is based on inductive lines, thus, the G-H droop control cooperates with P-f and Q-V droop controllers for the fundamental components.

In [124], a variant of the G/H droop is presented. The distortion D is calculated by using $S^2 = P^2 + Q^2 + D^2$. The distortion is shared by adapting the gain (and bandwidth) of the voltage controller dependent on D as shown in Fig. 2.16. The downside is a reduction in voltage waveform quality.

In [108], an additional current harmonic loop is added in the control strategy for properly sharing nonlinear loads. Selective harmonic current sharing is used to treat the significant output-current harmonics separately by using bandpass filters.

Virtual inertia In normal operating conditions, the frequency is limited by the narrow margins of the primary controllers, the presence of rotating inertia in the system and the frequency-dependent consumption of, e.g., electrical motors. The primary control stabilises the frequency after an event, but has no significant effect on the initial frequency deviations. As the number of generators and loads that are not directly coupled to the network is steadily increasing, the available inertia decreases (certainly in islanded microgrids) [125]. This decreased inertia results in faster and larger frequency deviations after an event, which may cause problems in the network [126–131]. To emulate rotating inertia, the DG units can be operated as virtual synchronous generators (VSGs). VSGs require additional reserve, which enables them to damp initial transients and stabilise the system. The additional control power can support the frequency stability even before the primary reserve is activated, hence, contributes to the pre-primary reserve of the microgrid. Different variants of a VSG exist, such as VSGs based on frequency measurements in [126, 127], VSGs based on power measurements in [128, 132] and synchronverters, which are inverters that operate based on the mathematical model of synchronous generators [131, 133].

2.3.2 P/V droop control

Low-voltage networks are mainly resistive, leading to the usage of P/V droop controllers. A disadvantage of this method is that the compatibility with the large central generators can be lost if the DG units need to contribute in the load sharing evenly with the synchronous generators. In the islanded operation considered here, this is not an issue. Also, using P/V droops, not with the objective of providing primary control, but for voltage regulation in grid-connected low-voltage networks has significant advantages as illustrated in chapter 6. The main advantage of P/V droop control is that there is a better match between the control strategies and the characteristics of the considered networks.

A. P/V droop control

While the P/f droop control method works well in a power grid with mainly inductive line impedances, it leads to a concern when implemented in a low-voltage microgrid, where the feeder impedance is not inductive and the line resistance should not be neglected [42]. This is especially true for DG units without grid-side inductor or transformer, where the output inductance is very small [42]. In case of mainly resistive lines, the power flow equations become:

$$P \approx \frac{E_1}{R}(E_1 - E_2) \tag{2.22}$$

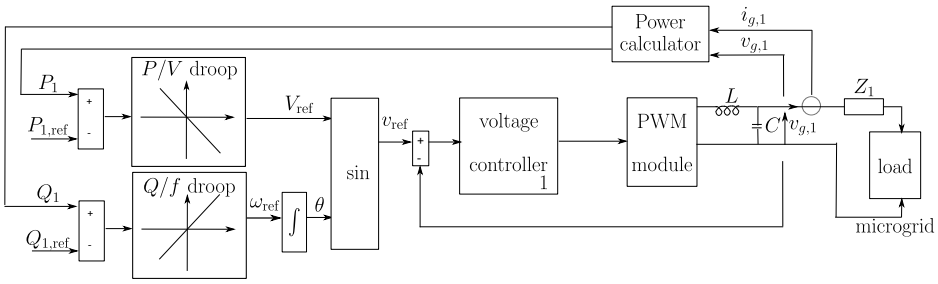

Figure 2.17: P/V droop control: P/V droops and Q/f droops

$$Q \approx \frac{-E_1 E_2 \delta}{R}. \tag{2.23}$$

Consequently, the active power is mainly linked with the voltage difference, while the reactive power is mainly linked with the phase angle, which is dynamically determined by the frequency. This leads to P/V and Q/f droops as opposed to the conventional P/f and Q/V droops [75, 104, 134–136]. The active and reactive power is measured and drooped to obtain the rms voltage and its frequency respectively:

$$V_i = V_{\text{ref}} + K_{\text{p}}(P_i - P_{\text{i,ref}}), \tag{2.24}$$

$$\omega_i = \omega_{\text{ref}} + K_{\text{Q}}(Q_i - Q_{\text{i,ref}}), \tag{2.25}$$

with $K_p < 0$ and $K_Q > 0$. The control scheme is depicted in Fig. 2.17.
In [136], the P/V droops are compared with the P/f droops. It is concluded that the former are better in resistive networks as they give a more damped response.

B. Variants on P/V droop control

Virtual output impedance A resistive virtual output impedance can be enforced by subtracting a proportional term of the output current from the reference voltage [113]:

$$v_{\text{ref}} = v_{\text{ref,from droops}} - i_{\text{g}} R_{\text{v}} \tag{2.26}$$

The main advantages are P/Q decoupling and an enhanced stability and dynamic response of the studied system (a more damped system) [113, 115].
In [137], this is extended with G-H droops in combination with the P-V and Q-f droops.

Voltage-based droop control The conventional droop controller is not designed for integration in renewable energy sources. Meanwhile, the voltage-based droop (VBD) controller of chapter 4 seamlessly integrates renewables in the power sharing control of the microgrid. In the VBD control strategy, the P/V droop controller is divided into two droop controllers and constant-power bands are included as depicted in Fig. 4.3. Note that the conventional P/V droop control of Fig. 2.17 also requires an additional controller for the dc-link balancing, which is achieved by the $V_{\mathrm{g}}/V_{\mathrm{dc}}$ droop controller in the VBD control scheme.
In [136], a dead band around the nominal voltage and frequency is used as well. This dead band prevents control actions for each V_{g} and f deviation, which may lead to stability problems such as oscillations in the system [136].
In [138], an additional loop is included in the VBD control strategy to ensure controllable harmonic power sharing.

Derivative term To also improve the dynamics of the system, a derivative term is included in [113]:

$$V_i = V_{\mathrm{ref}} - K_{\mathrm{p}}P - K_{\mathrm{p,d}}\frac{dP}{dt} \tag{2.27}$$

$$\omega_i = \omega_{\mathrm{ref}} + K_{\mathrm{Q}}Q + K_{\mathrm{Q,d}}\frac{dQ}{dt} \tag{2.28}$$

The controller does not include integrating terms as this would induce an unstable system [113].

2.3.3 Frequency-based signal injection

Several current sharing techniques based on frequency encoding of the current-sharing information have been presented. The network lines are used for the communication to achieve the power sharing (power-line communication). This method has significant advantages, particularly concerning its reliability as no interconnections between the modules are required, avoiding single-point of failure mechanisms, analogous as the P/f and P/V droops. With the frequency-encoding approach, the designer can select the frequency range over which the current-sharing

information is communicated and can use this design freedom to achieve objectives such as noise minimisation [139].

In [110], a small ac signal is injected in the system as control signal for P and Q (and the distortion current). The control scheme is shown in Fig. 2.18. For example for Q, the measured Q is drooped with droop $K_{\mathrm{ripple,K}}$ to obtain the frequency f_{Q} of the ripple component in the output voltage:

$$f_{\mathrm{Q}} = f_{\mathrm{Q},0} + K_{\mathrm{ripple,K}} Q. \tag{2.29}$$

A signal $V_q \cos(2\pi f_{\mathrm{Q}} t)$ is added to the reference voltage of for example, 230V/50Hz, with V_q a constant value. For two DG units, $f_{\mathrm{Q},1} \approx f_{\mathrm{Q},2}$ such that in the system analysis, phase angle deviations instead of frequency differences can be considered. Hence, if Q_1 increases, then $f_{\mathrm{Q},1} > f_{\mathrm{Q},2}$ and the phase angle of the first unit will keep increasing relatively to that of the second one. From the power flow equations in inductive lines, it follows that the active power at the considered frequency f_{Q} of the first unit will increase $P_{\mathrm{f_{Q,1}}} > P_{\mathrm{f_{Q,2}}}$. A PLL is used to measure this frequency component in the current, the voltage is known as it is a controlled variable. With both values, the active power in this frequency component ($P_{\mathrm{f_Q}}$) is obtained. For the reactive power sharing, this active power $P_{\mathrm{f_Q}}$ is drooped to obtain the reference amplitude of the fundamental voltage such that $V_{\mathrm{g},1}$ will decrease:

$$V_{\mathrm{g},1} = V_{\mathrm{g,ref}} - K_Q P_{\mathrm{f_Q}}. \tag{2.30}$$

In this way, a Q/V droop is achieved, but indirectly through the frequency component f_{Q}. A disadvantage of this method is its complexity and the need to measure and generate high-frequency components.

In [110], the harmonic distortion D caused by nonlinear loads is shared in an analogous manner. A control signal with a frequency that is drooped with D is injected. The power in this injected control signal is then used to adjust the bandwidth of the voltage loop of the inverter.

In Fig. 2.19, the method of [139] is depicted. Each module injects into the current-sharing bus a signal with a frequency that is related to its output current, or better, power. The resulting signal is available for each module. Each module employs a frequency estimator to calculate a weighted average ω_{est} of the frequency content of the aggregate signal [139]. This signal is used to change the reference current of the inner current control loop of the unit.

In Fig. 2.20, the method of [139, 140] is depicted where the switching ripple of the modules is used as the perturbation source. Each converter is controlled such that its average current or power is directly related to its switching frequency. The aggregate output ripple voltage contains information about the output of the indi-

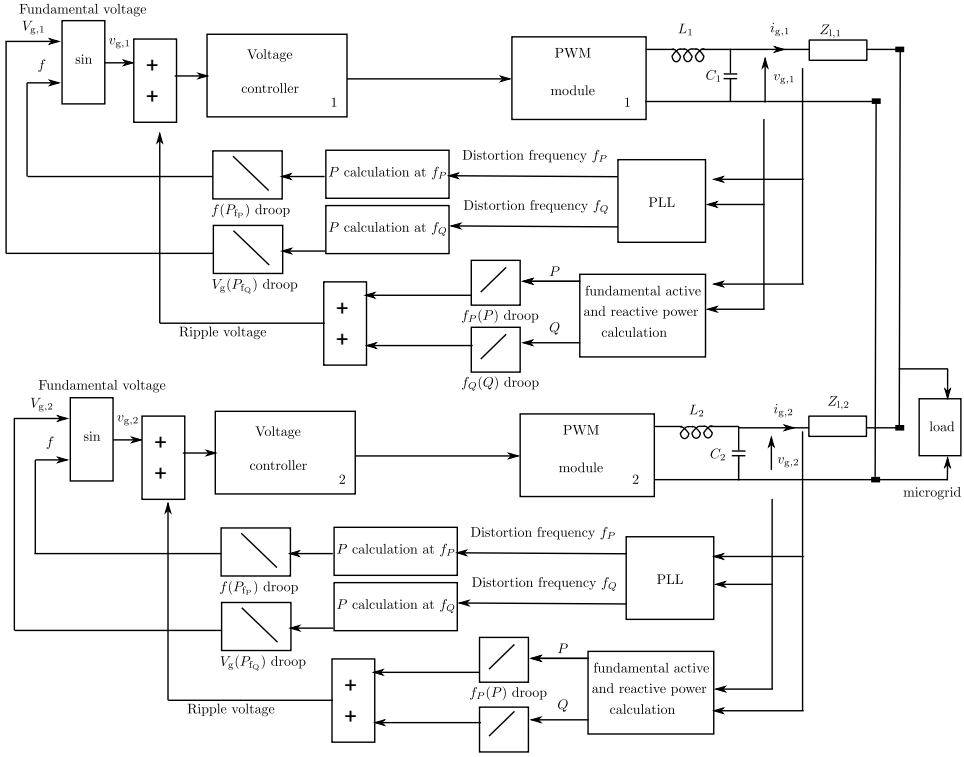

Figure 2.18: Frequency based signal injection

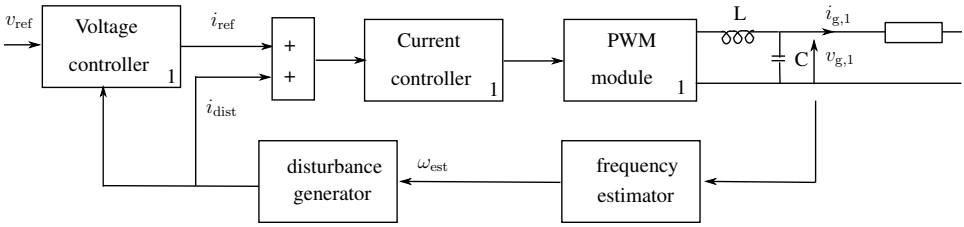

Figure 2.19: Frequency based signal injection with perturbation generator

vidual modules. This approach has the benefit that no additional ripple is injected into the output to encode the current sharing information, and controlling the switching frequency of the converters is typically straightforward.

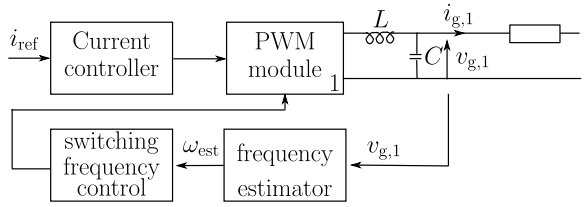

Figure 2.20: Frequency based signal injection with changing the switching frequency

2.4 Comparison of controller performances

Table. 2.1 provides an overview of the controller performances on some of the most important evaluation criteria. The usage of inter-unit communication for primary control (+ denotes not required, - denotes required) is a distinct disadvantage for the reliability of the islanded microgrid.
Concerning the bandwidth requirements, some controllers need to send full waveforms (- sign), others send the low-frequency (e.g., 50 Hz waveform) components (-/0 sign), while others only need to send average values for the primary control (0 sign). The controllers that do not require communication are again indicated by the + sign.
Many controllers, especially the communication-based, originate from UPS systems. In these systems, there was often only one load, or a limited amount of separate loads. Hence, measuring the load current was swift and easy. However, microgrids generally have multiple dispersed loads, hence, a requirement of measuring the load current and/or voltage is a distinct disadvantage (+ denotes not required, - denotes required). In this context, the controllers that rely on load current measurements also often use "the" load voltage for the control, which is not a definable parameter in microgrids with multiple loads and where the line impedances are not neglected.
Although often neglected, the line impedance can influence the power sharing between each two DG units, i.e., equally-rated units can deliver a different amount of power because of the line impedance effect. The master/slave control strategy for example determines the reference current of the slave units, hence, although equally-rated DG units have an equal output current, different line impedances result in a changed power sharing. In P/f droop control, the power sharing is not modified by the line impedance. In P/V droop control, i.e., VBD control, it is discussed in § 6.1 that the power sharing modification can have a beneficial effect with respect to the network line losses.
Microgrids have a large share of power-electronically interfaced DG units, which

lack the inertia the conventional grid control is based on. Also, the considered microgrids are low-voltage networks, which have mainly resistive line parameters as discussed in § 4.1. Therefore, without modification to cope with this issue, the P/f droop control is not directly applicable in these networks. Conversely, an advantage of P/f droop control over the P/V droops is the direct similarity with the conventional grid control.

2.5 Conclusions

In this chapter, an overview of primary control strategies for islanded microgrids is given. Concerning the reliability of the system, methods that do not depend on communication are more suitable for the primary control. Methods injecting a high-frequency signal are generally rather complex due to the requirement of measuring a small signal. This can also negatively affect the robustness of the system. Hence, only droop controllers are considered in this PhD thesis.
The content of this chapter has been published in [141].

Table 2.1: Performance comparison of primary controllers

	Requirement of inter-unit communication for primary control	Communication bandwidth requirement for primary control	Measuring "the" load current/voltage in dispersed microgrids	Influence of grid impedance on power sharing ratio	Applicability in resistive networks without inertia	Similarity with conventional grid control
Central	-	-	-	-	+	-
Master/slave	-	-	-	-	+	-
Auto-master-slave	-	0	+	0	-	0
IACS	-	-	+	-	+	-
Peak value based	-	0	-	-	+	-
Distributed	-	-/0	-	-	+	-
P/f droop	+	+	+	0	-	+
P/V droop	+	+	+	+	+	0

Chapter 3

Voltage control in islanded microgrids

The DG units in islanded microgrids can consist of grid-forming (Fig. 3.1) and grid-following units[1] (Fig. 3.2). Because of the lack of a utility grid, at least one grid-forming unit should be present in an islanded microgrids. A grid-forming controller "forms" the grid voltage, which implies a voltage control strategy. This voltage controller is a key issue in islanded microgrids. Grid-following controllers are current-controlled and have widely been studied [142, 143].

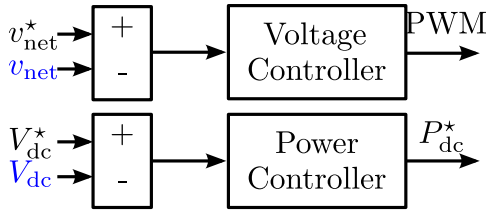

Figure 3.1: Grid-forming controllers

This chapter focusses on the voltage control of grid-forming converters in islanded microgrids. Due to their limited number of parameters and straightforward implementation, in practice, PID controllers and variants on PID control are used in a wide range of applications [144–146], including converter control [147, 148]. This

[1] In literature, sometimes the grid-forming units are classified in grid-supporting and grid-forming units. The grid-forming units, then, point out DG units with voltage control with fixed reference. Only one such unit can be connected to the power system. Grid-supporting units are in this context the voltage controlled units with variable reference. In this PhD thesis, no distinction between those units is made, both are called grid-forming units, referring to the voltage-controlled units.

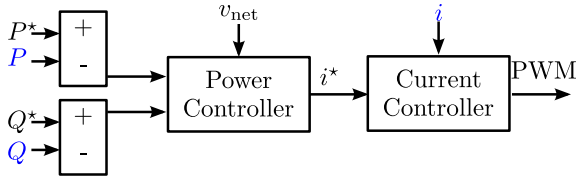

Figure 3.2: Grid-following controllers

chapter gives theoretical insight into the system envisaged for control purposes, completed by experimental validation. The efficient use of all available signals (i.e., voltage and current) at different locations in the system is a key issue. For this, direct control and cascaded control are compared. Only cascaded control uses grid current measurements for the voltage control. Next to current measurements, also the effect of adding grid voltage measurements to the output of the controllers is studied. As a result of the theoretical analysis, simple yet effective control strategies arise as intrinsic solutions to the problem. It is shown that, for the cascaded control, a P controller in series with PI control is sufficient, while direct control requires the usage of a PID controller.

In § 3.1, the microgrid circuit is analysed. Next, PID type controllers for direct and cascaded control are theoretically examined in § 3.2. These controllers are tuned and compared by means of simulations in § 3.3 and experiments in § 3.4. The appendix A discusses some other control strategies, such as sliding mode and fuzzy logic control. The extension to optimised voltage control is not the focus of this PhD thesis.

3.1 Circuit analysis

The considered single-phase (extension to three-phase microgrids is not the focus of this PhD thesis) microgrid configuration is depicted in Fig. 3.3. The energy source is represented as a constant dc-voltage source as the voltage control, not the power control, is analysed in this chapter. It is interfaced to the grid with a voltage-source inverter (VSI), consisting of two legs of semiconductor switches in parallel. The VSI switches T_1-T_4 are controlled in a full-bridge configuration by using pulse-width modulation (PWM) with duty ratio $\delta \in [-1, 1]$. They determine $v_{\text{s}} = \delta v_{\text{dc}}$, if averaged over one switching period, with v_{s} the ac-side voltage and v_{dc} the dc-side voltage of the VSI. For the attenuation of high-frequency switching components, an LC-filter is introduced in the system. The inductor current, or equivalently, the VSI output current i_{L} equals $i_{\text{C}} + i_{\text{g}}$, with i_{C} the filter capacitor current and i_{g} the microgrid current.

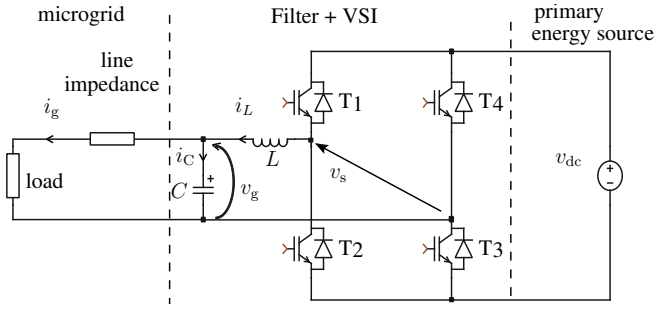

Figure 3.3: VSI, interface between the microgrid and an energy source. Single-phase islanded microgrid represented as a load and a line impedance. The VSI needs to control the microgrid voltage v_g.

The control strategy implemented in the VSI forces the grid voltage v_g towards a reference value $v_g^\star$. The reference voltage $v_g^\star$ is determined by the power control strategy of chapter 4. The microgrid is represented by an unknown, variable load connected to a power source through a line impedance. This load is a black-box from the DG unit's point of view, it can consist of loads as well as other DG units and storage elements. Despite this lack of knowledge concerning the microgrid and its variable parameters, the control strategy must provide an easily implementable and accurate method for tracking a sinusoidal voltage.

The control of the VSI is usually obtained in the rotating dq-reference frame (thus, a three-phase system) synchronous to the grid voltage, for example in [17, 101, 149, 150]. An advantage of this method is that the i-th harmonic of the signal with a 50 Hz fundamental component can easily be evaluated by using a low-pass filter after transformation to a reference frame rotating with i times the fundamental pulsation. A disadvantage of this method is the numerical complexity, because of the need for a harmonic reference. By using the Clarke and Park transformations, the quantities in a three-phase balanced sinusoidal system in steady-state are transformed into dc-Park components, which is an advantage for the controllers. However, in three-phase asymmetrical systems or in systems with voltage harmonics, the Park transformation does not result in dc-quantities. In single-phase systems, the Park or Clarke transformations are even not applicable. For these reasons, in this PhD thesis, the control is performed in the time domain by using conventional stationary-frame regulators without transformation of reference frame. To improve the controller's performance, a feed-forward term is included, further details of which are given in § 3.2 and [151].

The differential equations describing the system illustrated in Fig. 3.3 are given by:

$$L\frac{di_{\mathrm{L}}(\mathrm{t})}{dt} = v_{\mathrm{s}}(\mathrm{t}) - v_{\mathrm{g}}(\mathrm{t}), \tag{3.1}$$

$$C\frac{dv_{\mathrm{g}}(\mathrm{t})}{dt} = i_{\mathrm{L}}(\mathrm{t}) - i_{\mathrm{g}}(\mathrm{t}). \tag{3.2}$$

The switch voltage v_{s} can be written in terms of the dc-link voltage v_{dc} by introducing the duty ratio δ of the switches:

$$v_{\mathrm{s}}(\mathrm{t}) = \delta(\mathrm{t})v_{\mathrm{dc}}(\mathrm{t}) \tag{3.3}$$

For the tuning of the controllers, $v_{\mathrm{dc}}(\mathrm{t})$ is considered as a constant parameter, V_{dc}. The differential equations are transformed to the Laplace domain:

$$sLi_{\mathrm{L}}(\mathrm{s}) = v_{\mathrm{s}}(\mathrm{s}) - v_{\mathrm{g}}(\mathrm{s}) \tag{3.4}$$

$$sCv_{\mathrm{g}}(\mathrm{s}) = i_{\mathrm{L}}(\mathrm{s}) - i_{\mathrm{g}}(\mathrm{s}) \tag{3.5}$$

The general scheme equivalent to the model of (3.4)-(3.5) is that of the LC filter illustrated in Fig. 3.4. In practice, i_{g} is varying, which poses challenges for the controller. The signal i_{g} represents the load from the consumer. It is a stochastic, unknown disturbance in the considered system (i_{g} is a variable, unknown function $f(\cdot)$ of v_{g}). If this is an independent disturbance, classical feedback control strategies can be applied. However, if such a control is applied blindly, it may lead to sub-optimal results, since the assumption that i_{g} is an independent variable is false.

3.2 PID-type control: theoretical analysis

Proportional-Integral-Derivative (PID) controllers are commonly-used feedback controllers. A PID controller calculates an error value as the difference between a measured process variable and a desired set point. The controller attempts to minimise the error by adjusting the process control inputs. The PID controller algorithm involves three separate constant parameters: the proportional, the integral and derivative values, denoted P, I, and D.

The DG units' VSIs are equipped with pulse-width modulation (PWM), involving

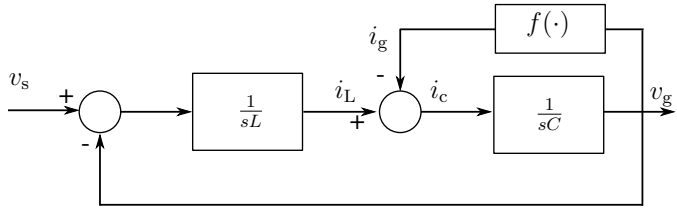

Figure 3.4: Considered system: dynamics of the LC filter

a sample frequency and switching frequency, which are equal in the considered voltage control loop. Therefore, discrete control is used. For the tuning of the discrete controllers, several methods are possible:

- tuning in the discrete z-domain;
- tuning in the continuous s-domain, including a Padé approximation for delay time and determining the discrete variant of the obtained PID controller.

The last option is discussed here. Nevertheless, the first method has already proven to give good results [152, 153].
For the purpose of control of the grid voltage v_{g}, the source voltage v_{s} needs to be manipulated. However, the system has inherent feedback loops. Hence, in the context of providing good control performance of microgrids, irrespective of load disturbances, it is necessary to understand the dynamics of the system. In the remainder of this section, several aspects to understand the system and develop an appropriate control strategy are presented, structured in two main parts: direct and cascaded PI(D) control.

3.2.1 Direct PID control

This paragraph proves that a PI controller is not sufficient in the direct control. A PID controller is really necessary, which is not the case in cascaded control.

A. Without forward voltage compensation

If i_{g} could be measured, then (hypothetically) one can compensate for the feedback $f(\cdot)$ from v_{g} in the scheme of Fig. 3.4, by injecting at the same point where i_g enters the loop, an i_{g}-signal with an opposite sign. Of course, this is not physically possible. However, based on the theoretical developments hereafter, a practical

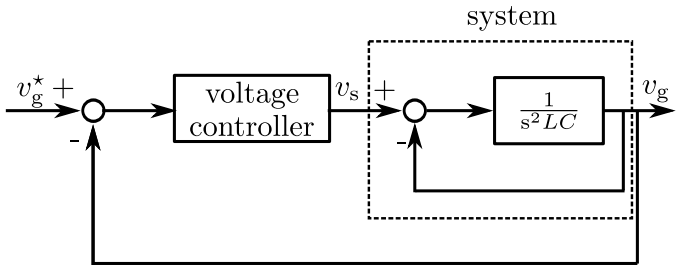

Figure 3.5: Closed loop scheme for voltage control, when i_g in Fig. 3.4 is compensated. Direct PID control

solution will be given (see § B.). Assuming that the ideal case of perfect compensation would be possible, the equivalent basic scheme will be the same as in Fig. 3.4, but with the signal i_g removed. In this case, a significant observation can be made: the derivative of v_g is proportional to i_L (it will be shown further how this observation can be used):

$$\frac{v_g}{i_L} = \frac{1}{sC}. \tag{3.6}$$

In this case, if only voltage control would be used, it follows that the transfer function of the system becomes:

$$\frac{v_g(s)}{v_s(s)} = \frac{1}{1 + s^2 LC}, \tag{3.7}$$

with the corresponding scheme given in Fig. 3.5, showing the inherent feedback in the system.

For the controller, the root locus of the system is studied. The system has two complex poles $j\frac{1}{\sqrt{LC}}$ and $-j\frac{1}{\sqrt{LC}}$. The corresponding root locus of the closed loop if a PI control is used, is given in Fig. 3.6 (left). As a PI controller adds a real pole and a zero in the origin, it follows that a PI controller cannot stabilise the system, hence derivative action is absolutely necessary. The corresponding root locus of the closed loop if a PID control is used, is given in Fig. 3.6 (right). In this case, a stable closed loop is obtained, at the expense of increased noise effects (due to differentiation) and the necessity of adding noise filters in the physical system.

However, as discussed above, i_g can not be perfectly compensated for. When returning to the initial scheme of Fig. 3.3 (or (3.4) and (3.5)), the following is valid:

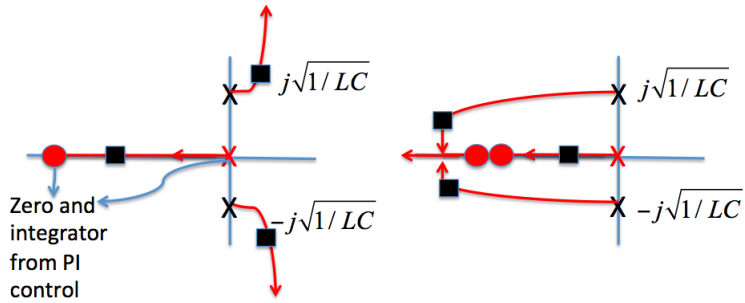

Figure 3.6: Left: Root locus for the closed loop with a PI controller. Right: Root locus for the closed loop with a PID controller.

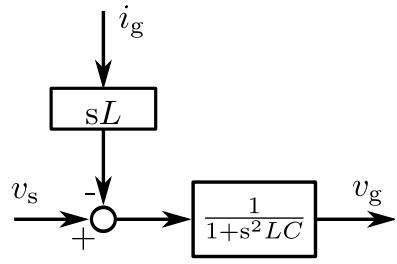

Figure 3.7: Equivalent scheme for direct control

$$v_g = \frac{1}{sC} i_C = \frac{1}{sC}(i_L - i_g) = \frac{1}{sC}(\frac{1}{sL}(v_s - v_g) - i_g), \tag{3.8}$$

such that:

$$\frac{v_g(s)}{i_g(s)} = \frac{-sL}{1 + s^2LC}. \tag{3.9}$$

The system of Fig. 3.4 can then be reformed to Fig. 3.7. In this equivalent scheme, i_g interacts, by a known transfer function $-sL$, on the manipulated variable v_s. Opposed to the configuration of Fig. 3.4, in Fig. 3.7, i_g enters the loop at a position that can be manipulated.

Since the current i_g can be measured, it can be compensated by adding the opposite term to the output of the PID controller C(s) as depicted in Fig. 3.8.

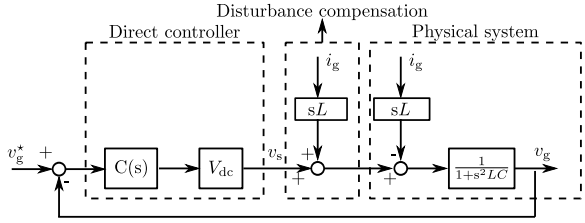

Figure 3.8: Equivalent scheme for direct control, compensation of i_g

However, this involves adding the derivative of a measured signal to the output of a controller, which could induce stability problems, e.g., under the influence of derivatives of measurement disturbances and noise. Therefore, compensation of i_g is not used in the direct PID control scheme and the disturbance by i_g is neglected. The PID controller is tuned according to the following second-order system model:

$$\frac{\Delta v_g}{\delta^\star} = \frac{V_{dc}}{1 + s^2 LC}. \tag{3.10}$$

This involves two issues:

- tuning of a PID controller;
- $f(\cdot)$ is unknown and especially variable in small-scale microgrids.

Therefore, in the next paragraph, the influence of voltage compensation to provide additional information about the microgrid state, is discussed.

B. With forward voltage compensation

Analogous to i_g, also v_g can be compensated for. Hence, to achieve a better system performance, a duty-ratio feed-forward ($\delta_{ff} \in [-1, 1]$) is included [154]:

$$\delta_{ff}(t) = \frac{v_g(t)}{v_{dc}(t)}. \tag{3.11}$$

As $v_{dc}(t)$ is fairly constant, $v_{dc}(t) \approx V_{dc}$. Fig. 3.9 shows the system of Fig. 3.4, including the controller C(s) and the compensation of v_g. This compensates for the systems inner feedback loop of v_g, such that the controller can be tuned according to the transfer function

$$\frac{v_g}{v_s} = \frac{1}{s^2 LC}, \tag{3.12}$$

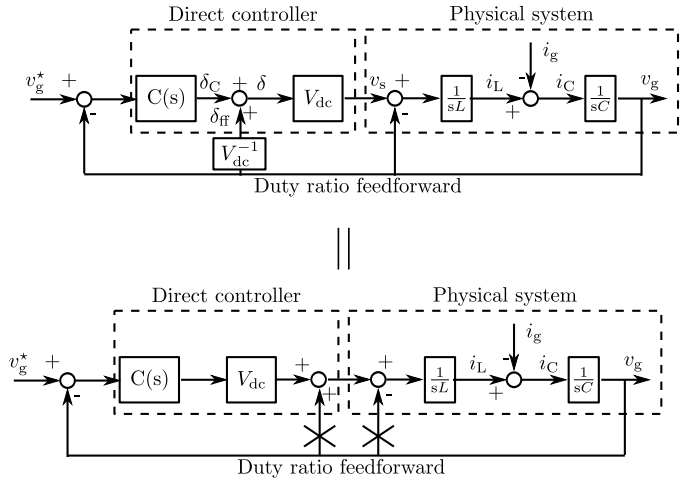

Figure 3.9: Direct control with duty ratio feedforward of v_g ($\delta_{ff} = \frac{v_g}{V_{dc}}$)

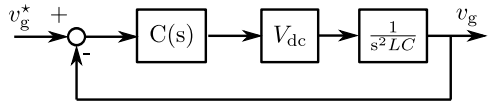

Figure 3.10: Tuning direct PID controller

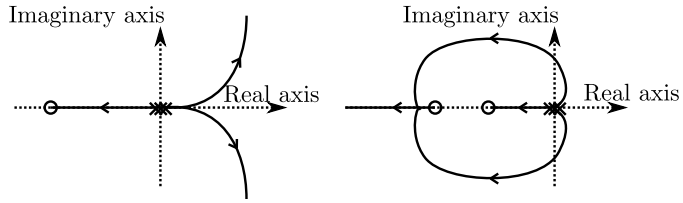

Figure 3.11: Root locus analysis direct controller with feedforward of v_g. Left: PI controller; right: PID controller

when the disturbance i_g is neglected as shown in Fig. 3.10. The latter approximation is less crucial than in the case without forward voltage compensation, as δ_{ff} already gives information about the microgrid loading. The root locus analysis on this system in Fig. 3.11 proves that a PID controller is required in this case as well. The main advantage of a direct PID control is its simple and straight-forward imple-

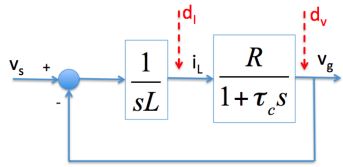

Figure 3.12: Equivalent scheme of the LC filter, with inherent feedback from i_{g} (through a resistor R) included in the loop, with $\tau_C = RC$. Notice two disturbance inputs d_{I} and d_{V}.

mentation. The currents i_{g} and i_{L} do not need to be measured, hence disturbances in these measurements have no influence on the performance of the system. On the other hand, this leads to an inherent lack of system knowledge as the current i_{g} delivers important microgrid information. Also, as only the voltage is controlled, there is no direct control over the current, which may lead to large transient currents [54].

3.2.2 Cascaded PI control

In the direct PID control, the measurements of i_{g} and i_{L} were not used. Using these measurements for the control is possible in cascaded control. Therefore, first, it is studied whether cascaded control is possible. The main factor in this study is having an inner loop that is sufficiently faster than the outer loop. Secondly, the implementation of cascaded control is described.
In cascaded voltage control, the grid voltage is controlled by using both an inner current control loop (ICCL) and an outer voltage control loop (OVCL). A fast current controller is used in the inner loop, having a reference current obtained by the outer-loop voltage regulation. An advantage of the inner current control loop is its easy current-limit function. More advantages of the inner current control loop are described in [17].

A. Possibility of using cascaded control

In practice, i_{g} is varying, posing challenges for the controller. This signal represents the load from the consumer, which is a variable, unknown function $f(\cdot)$ of v_{g}. Let us consider for simplicity that the current i_{g} is related to the grid voltage by a varying load which can be represented in its simplest form by a resistor R $\left(f(\cdot) = R^{-1}\right)$. This leads to the scheme in Fig. 3.12. Note that in § D., a practical solution is given such that the tuning of the controllers becomes independent of the load (here assumed as R).

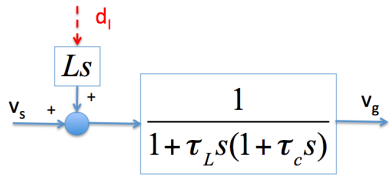

Figure 3.13: Equivalent scheme of the LC filter, based on the derived transfer functions.

The question that now arises is whether measuring the current i_{L} would be useful for the control purposes. For this analysis, the equivalent loop transfer functions for the circuit from Fig. 3.4 are derived, with $\tau_C = RC$. The transfer function from the manipulated variable to the output is given by:

$$\frac{v_{\mathrm{g}}}{v_{\mathrm{s}}} = \frac{\frac{R}{sL(1+\tau_c s)}}{1+\frac{R}{sL(1+\tau_c s)}} = \frac{1}{1+\tau_L s(1+\tau_c s)} \tag{3.13}$$

with $\tau_L = \frac{L}{R}$ (τ_L and τ_C are both varying with the load R). The transfer function from the disturbance d_I to the output is given by:

$$\frac{v_{\mathrm{g}}}{d_{\mathrm{I}}} = \frac{\frac{R}{1+\tau_c s}}{1+\frac{R}{sL(1+\tau_c s)}} = \frac{Ls}{1+\tau_L s(1+\tau_c s)} \tag{3.14}$$

Based on these transfer functions, the scheme from Fig. 3.12 can be re-arranged as in Fig. 3.13.

The combination of Figs. 3.12 and 3.13 leads to the block scheme of the system to be controlled, shown in Fig. 3.14, where the current i_{L} appears explicitly in the loop. $P_m(s)$ denotes the transfer function of the system to be controlled by a master controller; $P_s(s)$ denotes the transfer function to be controlled by a slave controller. Compared to Fig. 3.12, Fig. 3.14 has no internal feedback loop.

From this representation, it is easy to see that cascaded control can be applied if the signal i_{L} is available as a measurement. At this moment, it is necessary to verify whether cascaded control would be useful. The speed of response of the two transfer functions $P_m(s)$ and $P_s(s)$ is determined by the locations of the poles. The pole of the master transfer function is given by $s = -\frac{1}{\tau_c}$. For the two poles of the slave transfer function, the root locus analysis [155] is applied to the characteristic equation $1 + \frac{1}{\tau_c \tau_L}\frac{1}{s(s+\frac{1}{\tau_c})}$. This is shown in Fig. 3.15 (left). It follows that the location of the poles depends on the term $1/LC$, but they are always located to the right of $s = -\frac{1}{\tau_c}$. This implies that $P_s(s)$ is slower than $P_m(s)$.

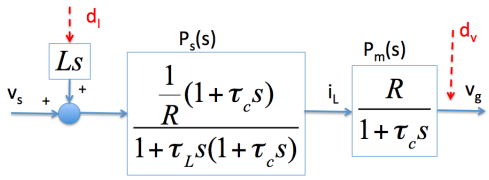

Figure 3.14: Equivalent scheme of the LC filter, including i_{L} as an explicit signal in the loop.

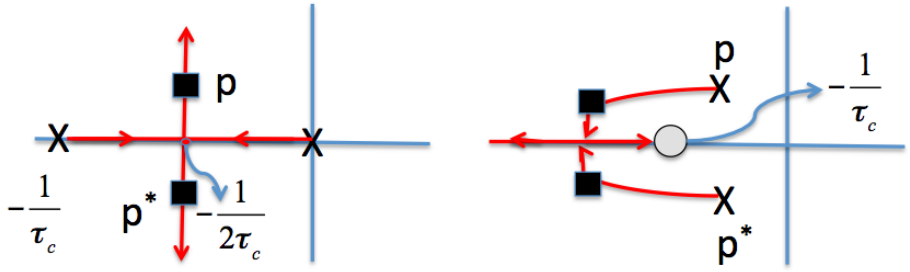

Figure 3.15: Left: Root locus for the open loop $P_s(s)$. Right: Root locus for the closed loop of the slave control, with a gain controller and i_{L} used in a slave feedback loop.

The above conclusion was made in the context that the current i_{L} is not measured. Consider now the case when i_{L} is measured and used in a slave feedback loop, e.g., by using a simple P-controller with gain K_s. This feedback loop is given by the transfer function

$$\frac{K_s P_s(\mathrm{s})}{1 + K_s P_s(\mathrm{s})} \tag{3.15}$$

The denominator can be rewritten as:

$$1 + K \frac{(s + 1/\tau_c)}{(s - p)(s - p^*)} \tag{3.16}$$

with p and p^* being the poles of the open loop $P_s(\mathrm{s})$ (determined in Fig. 3.15 (left)) and K the loop gain. After applying root locus analysis to this characteristic equation, the obtained location of the poles is depicted in Fig. 3.15 (right). The conclusions from this analysis are twofold: 1) the poles of the slave loop (3.15) can

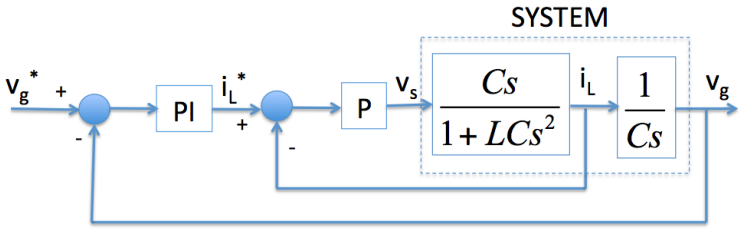

Figure 3.16: Cascaded closed loop control scheme with inherent derivative action from the current loop on i_{L}.

be placed to the left of $s = -\frac{1}{\tau_c}$, for suitable values of the gain K; and 2) the zero from the slave loop (3.15) cancels the pole of the master transfer function $P_m(s)$. Hence, the system with slave loop is faster than the open loop transfer function in Fig. 3.14, and cascaded control is, thus, useful.

B. Benefits and implementation of cascaded control

Without feedforward of i_{g} At this point, it becomes interesting to consider the benefits of adding a slave loop. Recall here the observation from (3.6) that i_{L} is proportional to the derivative of v_g. This fact implies that an inner loop can be introduced (current loop) to replace the explicit derivative action in the PID controller, as is clarified in Fig. 3.16. Using an inner loop with feedback from i_L is, thus, equivalent to using D-action in the master PID controller. However, it does not have the mentioned noise sensitivity. The scheme of the closed loop becomes that of Fig. 3.16, with P the proportional controller of the inner loop and a PI controller in the outer loop.
The root locus analysis on the inner loop of Fig. 3.16, with transfer function:

$$\frac{i_{\mathrm{L}}}{v_{\mathrm{s}}} = \frac{Cs}{1 + s^2 LC}, \tag{3.17}$$

is shown in Fig. 3.17. From this figure, it follows that a P controller is sufficient to stabilise the ICCL. The closed loop transfer function becomes:

$$\frac{i_{\mathrm{L}}}{i_{\mathrm{L}}^{\star}} = \frac{CPs}{1 + CPs + s^2 LC} \tag{3.18}$$

For large P, the transfer function becomes approximately equal to one.
In the fast inner current control loop, the measured inverter current i_L(t) is com-

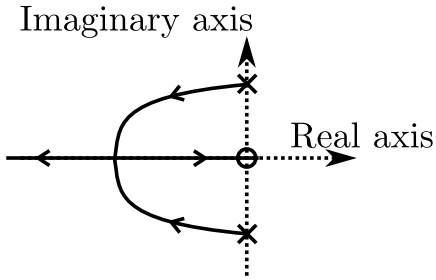

Figure 3.17: Root locus on inner current control loop: P controller

pared with its set value i_L^*(t). The obtained current error is presented to a discrete proportional controller. The output of the current controller is the set value of the switching voltage v_{s}^*(t) or, equivalently, the duty-ratio δ(t). To obtain better disturbance rejection, a duty-ratio feed-forward branch is added to the output of the current controller [154]. The sum of the duty-ratio and the duty-ratio feed-forward is the input of the PWM-unit, which calculates the switching signals for the inverter.

Design of ICCL and OVCL The design of the current controller is based on:

$$L\frac{\mathrm{d}i_{\mathrm{L}}(t)}{\mathrm{dt}} = v_{\mathrm{s}}(t) - v_{\mathrm{g}}(t) = \delta(t).v_{\mathrm{dc}} - v_{\mathrm{g}}(t). \tag{3.19}$$

Transformation to a small signal model in the Laplace domain results in

$$\hat{i}_L(s) = \frac{V_{\mathrm{dc}}\hat{\delta}(s)}{sL} + \frac{\delta_0\hat{v}_{\mathrm{dc}}(s)}{sL} - \frac{\hat{v}_g(s)}{sL}, \tag{3.20}$$

with δ_0 the average duty-ratio and where hatted values $\hat{x}$ denote small deviations from the steady state value of x. This equation shows that the current of the inverter i_{L} is determined by variations of the control variable $\hat{\delta}$, but also by variations of the grid voltage $\hat{v}_{\mathrm{g}}$ and the inverter dc-bus voltage $\hat{v}_{\mathrm{dc}}$. The latter two variations can be considered as disturbances. Implementing a duty-ratio feed-forward δ_{ff}(t) decreases the influence of these disturbances [154]. This results in a better current tracking [156]. By using the following transfer function of duty-ratio to inverter current:

$$\frac{\hat{i}_L(s)}{\hat{\delta}(s)} = \frac{V_{\mathrm{dc}}}{sL} \tag{3.21}$$

the inner regulator can be tuned. The output of this regulator is $\Delta\delta^\star$ and the input of the VSI switches equals $\delta = \Delta\delta^\star + \delta_{\rm ff}$ when voltage compensation is used.
In the OVCL, the reference grid voltage $v_{\rm g}^*$ is compared to its measured value v_g and controlled by a second PI-regulator. The PI-regulator to control the grid voltage $v_{\rm g}$ is tuned by using the transfer function

$$\frac{\hat{v_g}}{\hat{i_c}} = \frac{1}{sC} \tag{3.22}$$

and a Padé approximation for delay time as a result of the sample and hold procedure. The output of the outer PI-regulator is $\Delta i_{\rm C}^*$, with $\Delta i_{\rm C}^*$ a small-signal deviation from the steady state $i_{\rm C}^*$. The input of the inner PI-regulator is

$$\Delta i_{\rm L} = i_{\rm L}^\star - i_{\rm L} \tag{3.23}$$

with

$$i_{\rm L}^\star = (i_{\rm g} + i_{\rm C})^\star \approx i_{\rm g} + i_{\rm C}^\star = i_{\rm g} + \Delta i_{\rm C} + i_{\rm C}, \tag{3.24}$$

with $i_{\rm C} = sCv_{\rm g}^\star$ the steady state value, thus, $i_{\rm C}$.
By implementing a controller with two loops in series, an additional advantage is created as the inverter current i_L can easily be limited.

C. Feedforward of $v_{\rm g}$

Starting again from Fig. 3.4, and similar to injecting $i_{\rm g}$ into the system, a measurement of $v_{\rm g}$ can be injected to the output of the P controller in the inner loop as illustrated in Fig. 3.18. Notice that, opposed to injecting $i_{\rm g}$, injecting $v_{\rm g}$ is physically possible. The effect of adding $v_{\rm g}$, i.e., $\delta_{\rm ff}$ will compensate for the physically-present feedback from the $v_{\rm g}$ signal (see Fig. 3.18).

D. Practical solution to inject $i_{\rm g}$

In Fig. 3.18 with perfect compensation of the internal loop with $v_{\rm g}$, the transfer function of the system $i_{\rm L}^\star$ to $i_{\rm L}$ is $\frac{1}{1+Ls/K}$. In the ideal case of perfect models and perfect measurements and assuming a P controller with a gain K sufficiently large, the loop from $i_{\rm L}^*$ to $i_{\rm L}$ is approximately equal to 1. This implies that $i_{\rm L} \cong i_L^*$, which immediately suggests the physical solution to inject $i_{\rm g}$ at the output of the master controller (a PI-controller), leading to the final configuration depicted in Fig. 3.19. In this way, the internal feedback of $i_{\rm g}$ is compensated for as explicitly shown in Fig. 3.19. This figure also shows that the ICCL can be simplified by the transfer function $\frac{1}{sL}$ and the OVCL by $\frac{1}{sC}$.

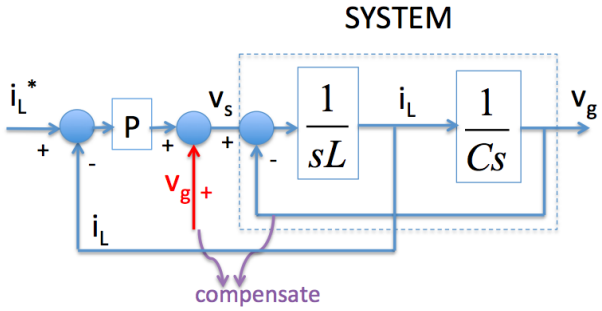

Figure 3.18: Schematic representation of injecting v_g in the inner loop.

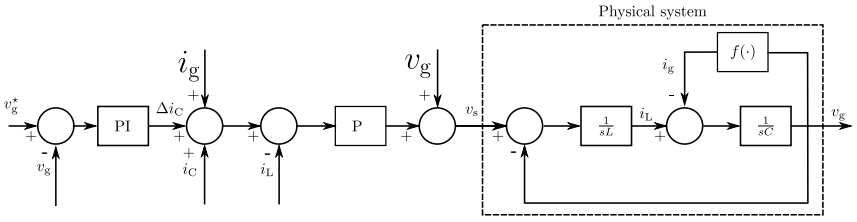

Figure 3.19: Final configuration with practical solution for injecting i_g and v_g into the closed loop control scheme. The internal feedback of v_g is compensated by the feedfworward term. The ICCL can be approximated as zero, such that also i_g is compensated for.

To summarise, the theoretical analysis suggests the following: 1) cascaded control from i_L is always useful, and 2) compensating for the signals v_g and i_g is beneficial for the overall control performance.
Notice that - thanks to the i_g injection - the tuning of the controllers became independent of the load.

E. Implementation of cascaded control

Fig. 3.20 shows the implementation of the cascaded control. For the inner loop, e.g., a P, PI or PD controller can be used.
An advantage of the cascaded control according to [17] is that non-linearities due to the switching of the converter and external disturbances are dealt with in this loop. Opposed to in the direct control, an over-current protection can easily be included in the ICCL. The disadvantage of need for more measurements is not applicable as these currents will be measured anyway in the overlaying controllers to calculate

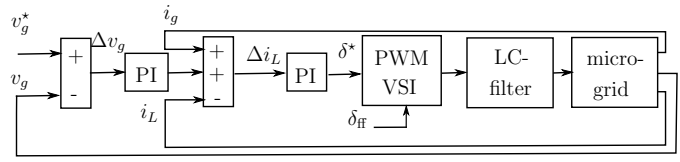

Figure 3.20: Cascaded PIPI control

the active and reactive power. A disadvantage is the usage of two controllers that both need to be tuned, with a sufficiently different bandwidth. Furthermore, these controllers are tuned under nominal conditions of the filter parameters L en C en dc-link voltage v_{dc}. Significant variation of these parameters require retuning of the controllers.

The reference value $i_{\text{L}}^\star$ consists of:

- The output of the PI controller of the OVCL with transfer function $\frac{1}{sC}$: $\Delta i_{\text{C}}^\star$;
- The feed forwarded steady state current through the filter capacitor C: i_{C}, which is calculated using the reference voltage $v_{\text{g}}^\star$ ($i_{\text{C}} = sCv_{\text{g}}^\star$). This stabilises the system and improves the dynamic response by rapidly compensating for near-future variations in the load voltages whose rate of change is indirectly sensed by measuring the capacitor currents [157].
- The measured grid current i_{g}.

The input of the ICCL equals $i_{\text{L}}^\star - i_{\text{L}}$. The estimated current i_{C} is added to the output of the voltage controller, as although this is a small current, simulations show that this has an effect on the tracking performance of the cascaded controller. In order to study the effect of including i_{c} in the reference value $i_{\text{L}}^\star$, two cases are compared. The simulations are preformed on a small microgrid with one DG unit and a load $R = 25\ \Omega$, a line impedance of $r_l = 0.411\frac{\Omega}{km}$ and a line of length 800 m, hence, $R_l = 0.33\ \Omega$. For $i_{\text{C}} = 0$ A, Fig. 3.21(a) shows the simulation results. When including i_{C}, the result is given in Fig. 3.21(b). A clear improvement in voltage tracking is concluded.

F. Cascaded versus direct control: conclusions

For the direct control, a PID controller is required. For cascaded control, at least a PI-P combination is needed.
If the current i_g is available for control, the best control structure is a cascaded configuration with a PI master controller and a P slave controller. When i_{g} is used,

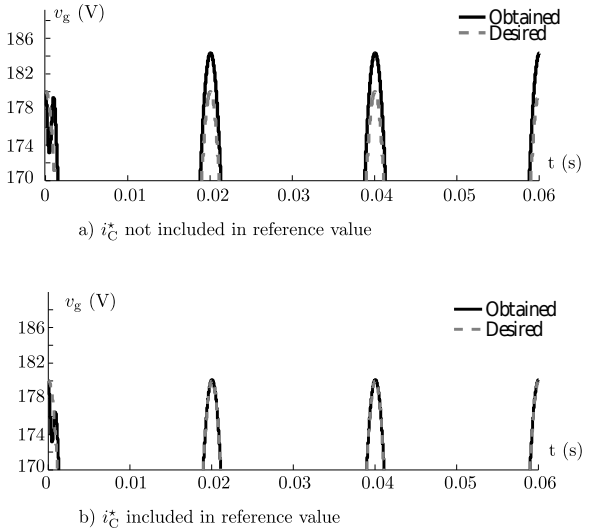

Figure 3.21: Influence of adding $i_C^\star$ to the output of the OVCL

there is an advantage which is extremely important from practical point of view: thanks to the i_g injection, the tuning of the controllers became independent of the load (R). This is a significant benefit from control point of view, since in practice the load is varying and not known.

3.3 Tuning of the controllers

In the time domain (continuous form), a PID controller is given by:

$$u(t) = K_p e(t) + K_i \int_0^{t_k} e(\tau)d\tau + K_d \frac{d}{dt} e(t), \tag{3.25}$$

with as Laplace transform:

$$G(s) = K_p + \frac{K_i}{s} + K_d s = \frac{K_d s^2 + K_p s + K_i}{s}. \tag{3.26}$$

In order to design a digital implementation of a PID controller, the standard form of the PID controller is discretised. Approximations for first-order derivatives can

be made by backward finite differences. For the integral term

$$\int_0^{t_k} = e(\tau)d\tau = \sum_{i=1}^{k} e(t_i)\Delta t \tag{3.27}$$

and the derivative term

$$\frac{de(t_k)}{dt} = \frac{e(t_k) - e(t_{\mathrm{k}-1})}{\Delta t} \tag{3.28}$$

are obtained. Therefore:

$$u_{t_k} = K_p e_{t_k} + K_i \sum_{i=1}^{k} e_{t_i}\Delta t + K_d \frac{e_{t_k} - e_{t_{k-1}}}{\Delta t} \tag{3.29}$$

$$u_{t_k} = K_p e_{t_k} + K_i e_{t_k}\Delta t + (u_{t_{k-1}} - K_p e_{t_{k-1}} - \frac{K_d}{\Delta t}(e_{t_{k-1}} - e_{t_{k-2}}) + K_d \frac{e_{t_k} - e_{t_{k-1}}}{\Delta t} \tag{3.30}$$

Hence,

$$u_{t_k} = u_{t_{k-1}} + e_{t_k}(K_p + K_i\Delta t + \frac{K_d}{\Delta t}) + e_{t_{k-1}}(-K_p - 2\frac{K_d}{\Delta t}) + e_{t_{k-2}}\frac{K_d}{\Delta t} \tag{3.31}$$

or simplified,

$$u_{t_k} = u_{t_{k-1}} + e_{t_k}k_1 + e_{t_{k-1}}k_2 + e_{t_{k-2}}k_3. \tag{3.32}$$

The z-transform becomes:

$$G(z) = \frac{k_1 z^2 + k_2 z + k_3}{z(z-1)} \tag{3.33}$$

Another method to derive the discrete form of (3.26) uses the bilinear transformation (Tustin's method) with

$$s \approx \frac{2}{T}\frac{1 - z^{-1}}{1 + z^{-1}}. \tag{3.34}$$

In this case:

$$G'(z) = \frac{k_1' z^2 + k_2' z + k_3'}{z^2 - 1} \tag{3.35}$$

This transfer function has two poles, $z = 1$ and $z = -1$, the latter one makes the system marginally stable. In order to deal with this, a proper transfer function of the PID controller G(s) in (3.26) needs to be used. The discrete form of a PI controller equals:

$$u_{t_k} = u_{t_{k-1}} + e_{t_k}(K_p + K_i\Delta t) - K_p e_{t_{k-1}} \tag{3.36}$$

with K_i and K_p the design parameters. The PI(D) controllers are tuned based on root locus analysis and bode plots.

3.3.1 Direct PID control

The direct PID controller is tuned by using Matlab Sisotool, with system (3.10):

$$P(s)\frac{1}{1+s^2LC}, \tag{3.37}$$

with $L = 2$ mH, $C = 3$ μF and $P(s)$ a Padé approximation for delay time ($T_s = 1/f_s$). The parameters of the LC filters are chosen according to some common design rules. The cut-off frequency is chosen at 2kHz ($\frac{1}{2\pi\sqrt{LC}} = 2055$ Hz), which enables to deal with frequencies up to the 40th harmonic (the European standard EN50160, which is commonly used to evaluate the supply voltage in MV and LV networks, gives restrictions on the THD of the supply voltage including harmonics up to the order 40). The capacitance should be small enough that the reactive power provision is less than 5 % of the nominal active power of the DG unit. For setting this, a small 1 kW unit is anticipated (for larger units, the chosen capacitance, will, thus, be on the safe side). In 230 V networks, a 3 μF capacitor delivers 50 VAr, which complies with the design specification for reactive power. The capacitance is not chosen smaller as a large value has a positive effect on the voltage quality, making the voltage controller more easy to tune. Of course, DG units of significantly higher ratings or connected to other voltage levels can require other filter parameters. The Padé approximation is included as the PWM control uses discrete time steps with the sample frequency, with:

$$P(s) = \frac{1}{\frac{s^3T_s^3}{3!} + \frac{s^2T_s^2}{2!} + sT_s + 1}, \tag{3.38}$$

with T_s the sampling period. The following PID controller is tuned:

$$\mathrm{PID}_1(s) = \frac{6.4e^{-6}s^2 + 0.0012s + 1000}{s}, \tag{3.39}$$

with as discrete-time equivalent following Tustin's method:

$$\mathrm{PID}_1(z) = \frac{0.2822z^2 - 0.462z + 0.2798}{z^2 - 1}, \tag{3.40}$$

which is not a stable transfer function. Therefore, (3.39) is transferred to a proper transfer function[2], with τ sufficiently small ($1/\tau$ sufficiently larger than the bandwidth of the system):

$$\mathrm{PID}(s) = \frac{6.4e^{-6}s^2 + 0.0012s + 1000}{s(1 + \tau s)}, \tag{3.41}$$

with as discrete-time equivalent following Tustin's method for $\tau = 10^{-5}$:

$$\mathrm{PID}(z) = \frac{0.2016z^2 - 0.33z + 0.1999}{z^2 - 0.5174z - 0.4286}. \tag{3.42}$$

This PID controller is tuned for bandwidth and phase margin. The control circuit has the following characteristics: settling time $T_{\mathrm{set}} = 3.9$ ms, overshoot $\%\mathrm{OS} = 0$, phase margin $\mathrm{PM} = 40.8°$, gain margin $\mathrm{GM} = 28.8$ dB and open loop bandwidth $f_{\mathrm{b}} = 2.05$ kHz. The open loop root locus and bode plots are depicted in Fig. 3.22.

3.3.2 Cascaded PI controllers

The PI controller of the inner current control loop is tuned by using the transfer function

$$\frac{V_{\mathrm{dc}}}{sL} \tag{3.43}$$

combined with a Padé approximation P for delay time. The following controller in the z-domain is obtained:

$$\mathrm{PI_I} = \frac{0.04594z - 0.0318}{z - 1}. \tag{3.44}$$

In cascaded PI control, it is important to achieve a fast inner control loop and a slower outer control loop. Therefore, the $\mathrm{PI_I}$ controller is tuned primarily according to a desired bandwidth and phase margin, here 1.9 kHz and 30° respectively as depicted in Fig. 3.23. The PI controller of the outer voltage control loop has a

[2] A proper transfer function is a transfer function in which the degree of the numerator does not exceed the degree of the denominator.

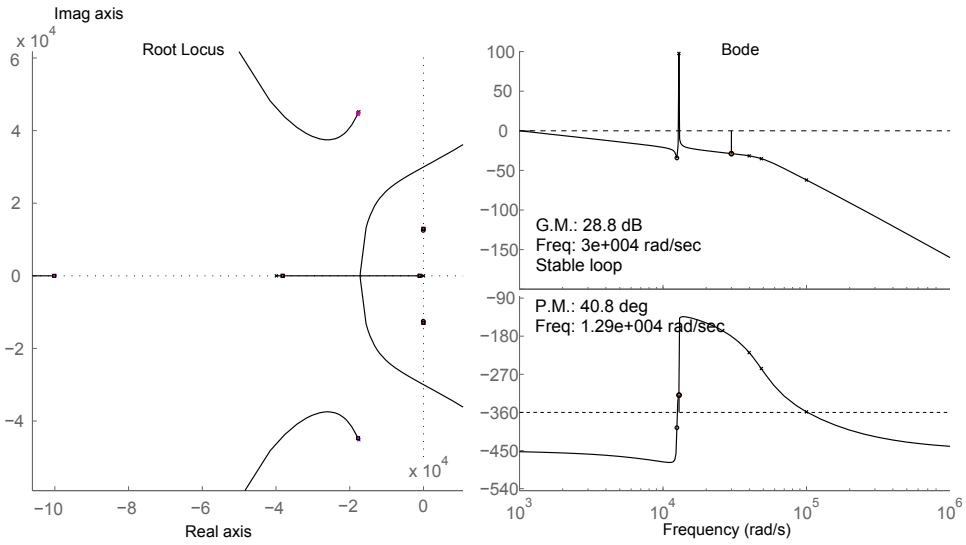

Figure 3.22: Direct PID controller: root locus and bode plot

lower bandwidth and is tuned according to:

$$\frac{\mathrm{PI_I}\frac{V_{\mathrm{dc}}}{sL}P}{1+\mathrm{PI_I}\frac{V_{\mathrm{dc}}}{sL}P}\frac{1}{sC}P \tag{3.45}$$

with Padé approximation P. Note that the inner current control loop can also be neglected in cascaded control in case of sufficient different bandwidths of the control loops leading to tuning according to $\frac{P}{sC}$. The following controller is obtained

$$\mathrm{PI_V} = \frac{0.006539z - 0.006055}{z-1}, \tag{3.46}$$

which has a bandwidth of 455 Hz and a phase margin of 49° as depicted in Fig. 3.24.

3.3.3 Controllers comparison

By means of simulations, the controllers are compared. The dc-link voltage equals 450 V, the filter parameters are $L = 2$ mH and $C = 3$ μF. Three cases are studied. For the cases load 1 and load 2, a microgrid with one DG unit is considered. In the third case, a microgrid with two DG units is considered. The parameters of the loads are chosen to comply with residential loads (e.g., the 25 Ω load has a 2 kW

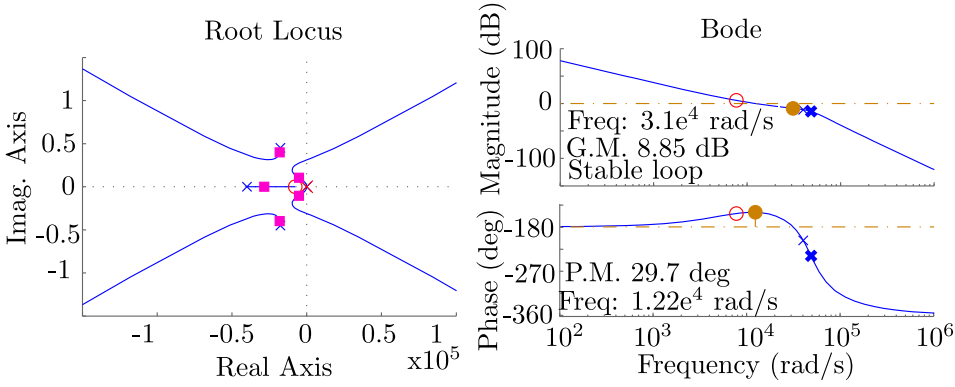

Figure 3.23: Root Locus of the $\mathrm{PI_I}$ *control loop*

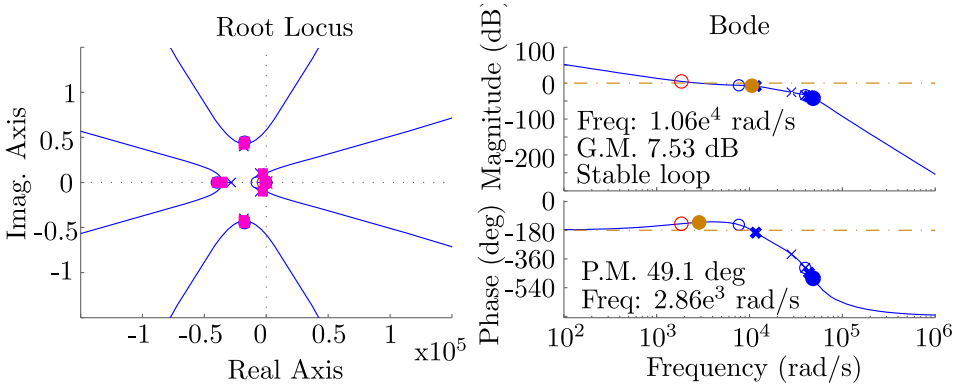

Figure 3.24: Root Locus of the $\mathrm{PI_V}$ *control loop*

consumption in a 230 V network). The 0.1 H inductive load leads to an 31.4 Ω impedance, hence, a power factor $\cos\phi$ of 0.6 when put in series with the 25 Ω load. This is a bad power factor, but the other loads have no inductive term and the power factor is here chosen small to magnify the effect of phase differences between the voltage and current of the DG unit. The line impedance is chosen according to a 0.4 Ω/km line (EAXVB cable combined with smaller, thus with higher resistance, connection cable to load, see table 4.2) and a realistic, but low, line length. Here, a low line length is chosen to magnify the effect of load changes.

- Load 1
  In the first case, the system configuration is depicted in Fig. 3.25. The RL

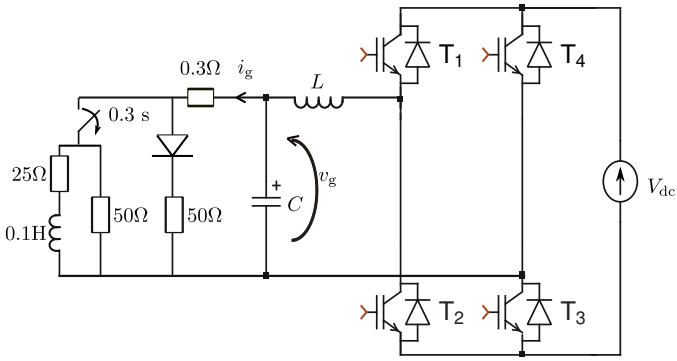

Figure 3.25: Comparison of direct PID and cascaded PI control: system configuration

load turns off at $t = 30$ ms. The reference voltage $v_g^\star$ is a 50 Hz, 230 V rms sine wave. After 15 ms, the rms value changes to 195 V and after 20 ms, again to 230 V.

- Load 2
  In load 2, the same microgrid configuration, including the reference and load change, is used as in load 1. Although the controllers are tuned with the filter parameters given above, in this case, the real filter parameters are twice these values. In this way, the sensitivity to model faults can be studied. Also, after 25 ms, the robustness to measurement noise is studied. Therefore, a band-limited white noise in the measurements of v_g, i_g and i_L is included varying between -10 V and +10 V or -5 % and +5 % for the voltages and -0.5 A and +0.5 A for the currents.

For the direct PID controller, the simulation results with both reference loads are depicted in Fig. 3.26. For the first load, an accurate steady-state tracking is obtained. The total tracking error e, defined as:

$$e = \sqrt{\frac{1}{N}\frac{1}{V_{g,ref}\sqrt{2}}\sum_{i=1}^{N}(v_{g,ref}(i) - v_g(i))^2}, \tag{3.47}$$

with $V_{g,ref} = 230\ V$, equals 0.0289 over the simulation time of 0.6 s. For the second load in Fig. 3.26(c,d), the PID controller shows a good parameter sensitivity but a low robustness to measurement error. The error e in this case equals 0.2796. For the cascaded PI controllers, the simulation results with both reference loads are depicted in Fig. 3.27. The error e for the first load equals 0.0226 and for the second

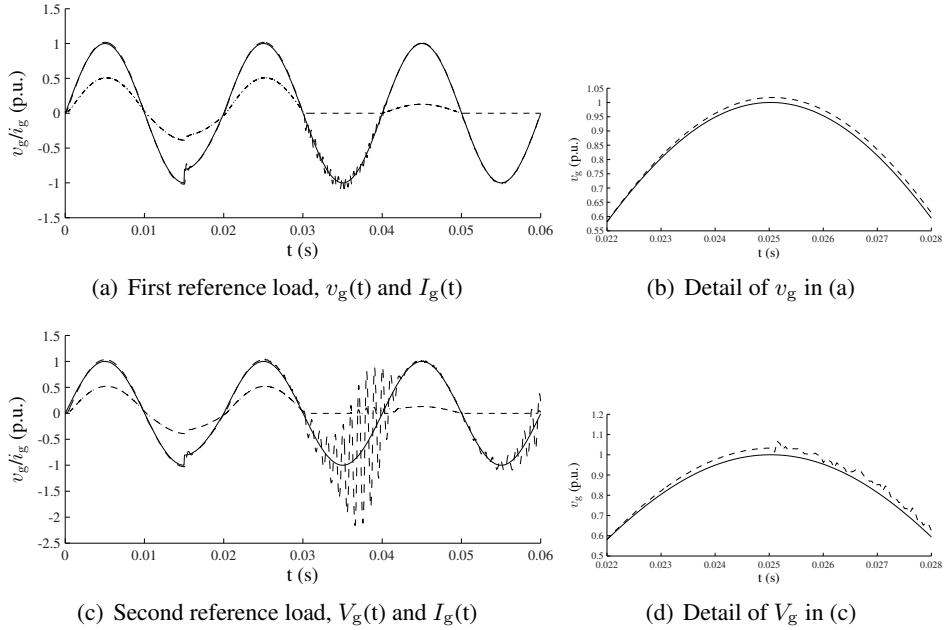

(a) First reference load, v_{g}(t) and I_{g}(t)

(b) Detail of v_{g} in (a)

(c) Second reference load, V_{g}(t) and I_{g}(t)

(d) Detail of V_{g} in (c)

Figure 3.26: Direct PID control (— = $v_{\mathrm{g}}(\mathrm{t})$ (p.u.); ---- = $v_{\mathrm{g}}^{\star}(\mathrm{t})$ (p.u.), -.-.-. = $i_{\mathrm{g}}(\mathrm{t})$ (p.u.))

load $e = 0.0376$. The robustness of this controller is, thus, clearly better than that of the direct PID control.
In a third case, the direct and cascaded PI(D) controllers are included in a basic microgrid configuration with two DG units, as illustrated Fig. 3.28. In the microgrid, $C_{\mathrm{dc}} = 1.5$ mF, $P_{\mathrm{nom},1} = 1500$ W, $P_{\mathrm{nom},2} = 750$ W. Voltage-based droop control is used with $K_{\mathrm{v}} = -1$, $K_p = -P_{\mathrm{nom}}/50$ W/V, $K_q = 1 \cdot 10^{-4}$ Hz/VAr, $z_v = 3\Omega$, $b = 0$ % (the parameters are discussed in chapter 4).
Fig. 3.29 and Fig. 3.30 show the obtained results with direct PID control and the cascaded PI control respectively. Again, the tracking performance is slightly better in the case of the cascaded PI controller.

3.4 PID control comparison: experiments

In the following section, a comparison is made between the direct and cascaded control as well as between different duty ratio feed-forward strategies. First, some simulations are discussed, next, the same cases are analysed in the experiments. A lower switching and sampling frequency as in the previous paragraph is considered, namely 10 kHz, although 20 kHz for low-power converters in grid-connection applications is also possible in practice. The experiments are based on [158].

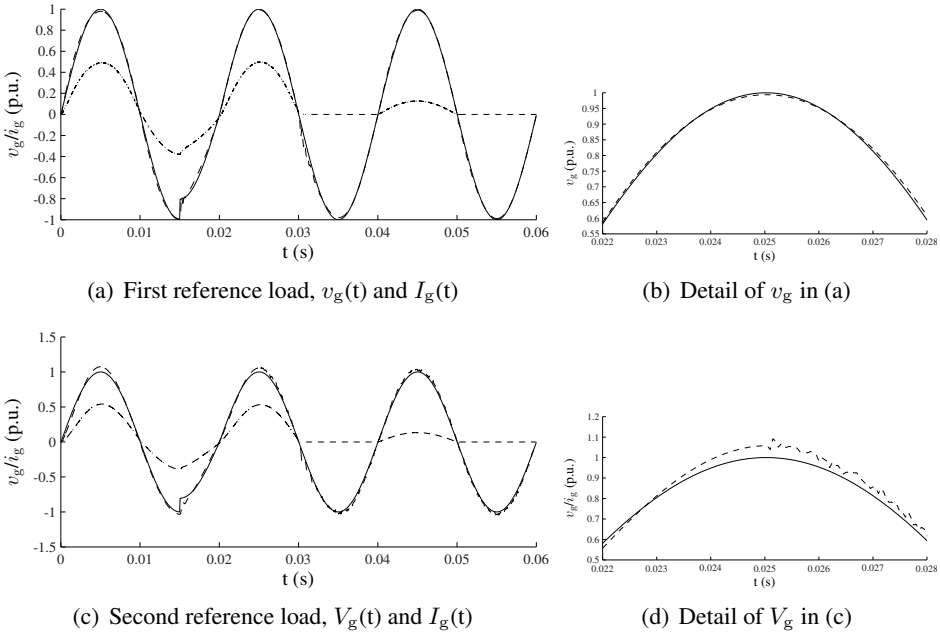

(a) First reference load, v_{g}(t) and I_{g}(t)

(b) Detail of v_{g} in (a)

(c) Second reference load, V_{g}(t) and I_{g}(t)

(d) Detail of V_{g} in (c)

*Figure 3.27: Cascaded PI control (— = $v_{\mathrm{g}}(\mathrm{t})$ (p.u.); **----** = $v_{\mathrm{g}}^{\star}(\mathrm{t})$ (p.u.), -.-.-. = $i_{\mathrm{g}}(\mathrm{t})$ (p.u.))*

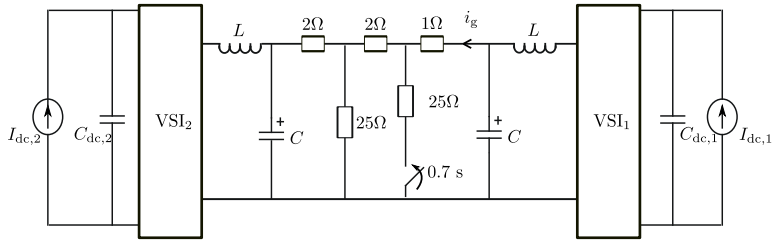

Figure 3.28: Comparison of direct PID and cascaded PI control: microgrid configuration with two DG units

As suggested in the previous section, direct control implies the necessity of a PID controller, while for cascaded control, a PI-P combination is sufficient. Hence, direct and cascaded control, with the suggested PID-type controllers are compared. The cases with and without adding v_{g} to the output of the controller (forward voltage compensation) are compared for the direct as well as the cascaded con-

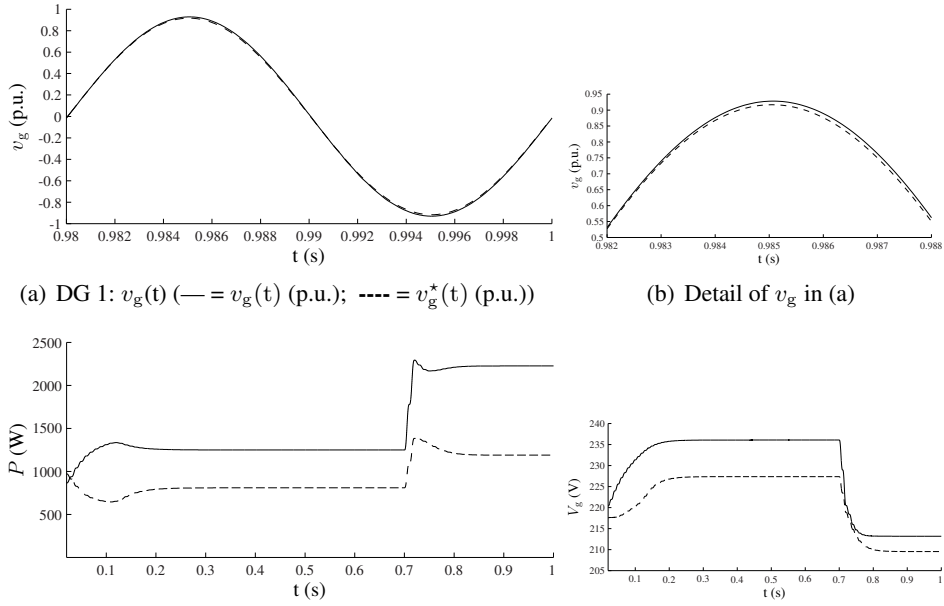

(a) DG 1: v_{g}(t) (— = $v_{\mathrm{g}}(\mathrm{t})$ (p.u.); ---- = $v_{\mathrm{g}}^{\star}(\mathrm{t})$ (p.u.))

(b) Detail of v_{g} in (a)

(c) Active power Delivered to network (— = DG 1; ---- = DG 2)

(d) Terminal rms voltage V_{g} (— = DG 1; ---- = DG 2)

Figure 3.29: Direct PID control in microgrid with two DG units

trol structure.

3.4.1 Simulation results

For the tuning of the controllers, per unit voltages and currents are used with reference values of 400 V and 10 A respectively. The dc-link voltage equals 400 V, the filter inductance L 2.2 mH and filter capacitance C is 5 μF. The equal per unit reference and dc-link voltage result in a convenient implementation of the forward voltage compensation, i.e., adding v_{g} to the output of the controller. The reason is that in the averaged model of the VSI with pulse-width modulation, v_s equals δv_{dc}, with $v_{\mathrm{dc}} = 1$. In the experimental part, a 25 Hz network is considered. In the figures, the reference voltage for the per unit calculation equals $230\sqrt{2}$ V and the reference current is 20 A.
The following reference loads are used:

- Firstly, the set point voltage equals 230 V rms. At $t = 30$ ms, this set point value drops to 195 V and is restored at $t = 40$ ms. A resistive load of 65 Ω and an RL load of 65 Ω in series with 310 mH, thus with $\cos\phi = 0.8$, are present. The former load turns off at $t = 50$ ms and the last one at $t = 70$ ms.

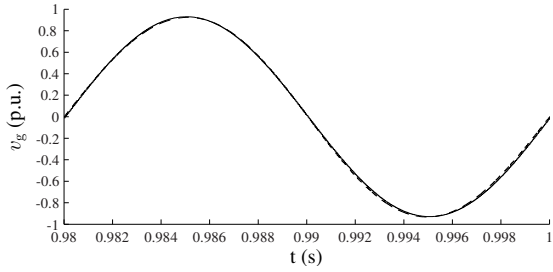

(a) DG 1: v_g(t) (— = v_g(t) (p.u.); ---- = $v_g^\star$(t) (p.u.))

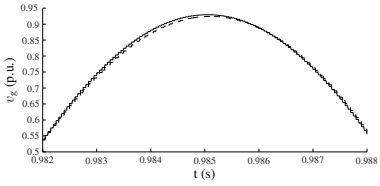

(b) Detail of v_g in (a)

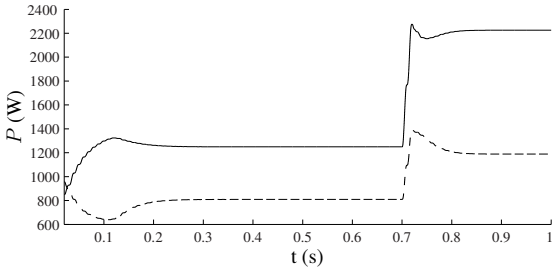

(c) Active power Delivered to network (— = DG 1; ---- = DG 2)

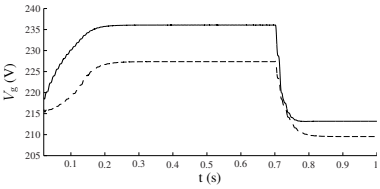

(d) Terminal rms voltage V_g (— = DG 1; ---- = DG 2)

Figure 3.30: Cascaded PI control in microgrid with two DG units

- Secondly, the values of C and L are doubled compared to the values for which the controllers are tuned. In this way, parameter sensitivity to model faults can be studied. Next, after 0.5 s, the robustness to measurement noise is studied by including band-limited white noise in the measurements of i_g, i_L and v_g varying between -5% and $+5\%$. This 5% value is a high value, in practice, a lower measurement error can be assumed. In the simulation plots, the measurements, thus including this noise, are depicted.

A. Direct control

The grid voltage v_g(t) is controlled to its reference value $v_g^\star$(t). In this control scheme, i_g is regarded as a disturbance and there are no measurements of current required.

Without forward voltage compensation For the direct control without adding v_g to the output of the controller (forward voltage compensation), the following

PID controller is tuned:

$$C(z) = 0.24573 \frac{z^2 - 2.2z + 2.066}{z(z-1)} \tag{3.48}$$

With this controller, the control circuit has the following characteristics: settling time $T_s = 1.84$ ms, overshoot %OS = 25.8, phase margin PM = 48.8°, gain margin GM = 6.33 dB and open loop bandwidth $f_b = 1.71$ kHz. From the Bode plot, it follows that the phase lag for 25 Hz (which is the frequency of the reference signal) equals 4.2°. This is compensated by including a phase-lead in the reference signal. This controller is referred to as PID 1.
For the first reference load, a good regime voltage tracking is obtained as shown in Fig. 3.31 (a,b). The transient after the load switching shows some oscillations. That the phase-lag compensation significantly affects the controller performance, is shown in Fig. 3.31(c,d), where the phase-lag compensation of 4.2° is omitted. This leads to a larger regime error.
The PID 1 controller does not obtain a stable operation with the second reference load. A stable operation is achieved for the adapted second reference load where L remains unchanged as depicted in Fig. 3.31(e,f). Hence, this controller is sensitive to L. The results from $t > 50$ ms show that the controller is sufficiently robust for measurement error.
For PID 1, an important difficulty is that accurate phase-lag calculation is required, depending on an accurate system model. To overcome this issue, a variant of the PID 1 controller uses the same PID controller as the previous case, but with adding the set point voltage $v_{\mathrm{g}}^{\star}$ to its output. This controller is referred to as PID 2. The phase-lag compensation in the reference signal is omitted in PID 2 and the control scheme is depicted in Fig. 3.32. This leads to a more robust control design.
The simulation results in case of the first reference load are depicted in Fig. 3.33. Similar steady-state voltage tracking and transient results are obtained as in case of the direct control without $v_{\mathrm{g}}^{\star}$ compensation and with phase-lag compensation. Like the previous controller, this controller does not obtain a stable operation with the second reference load. For the adapted second reference load, when L remains unchanged, similar results as in Fig. 3.31(e,f) are obtained.

With forward voltage compensation Second, forward voltage compensation of v_{g} is implemented by adding the measured voltage v_{g} to the output of the controller as depicted in Fig. 3.34. A new PID controller is tuned because the system changes from H to $\frac{H}{1-H}$ due to this forward compensation. The following PID controller is tuned:

$$C(z) = 0.67432 \frac{(z - 0.868)(z - 0.3)}{z(z-1)} \tag{3.49}$$

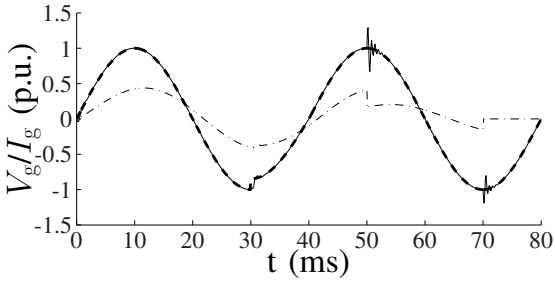

(a) First reference load, with phase-lag compensation: V_{g}(t) and I_{g}(t)

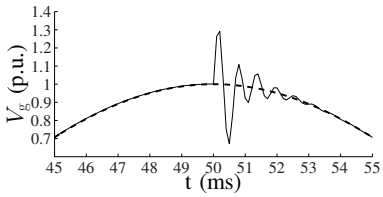

(b) Detail of V_{g} in (a)

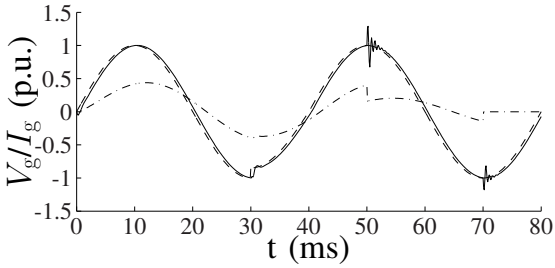

(c) First reference load, without phase-lag compensation: V_{g}(t) and I_{g}(t)

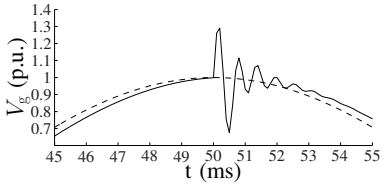

(d) Detail of V_{g} in (c)

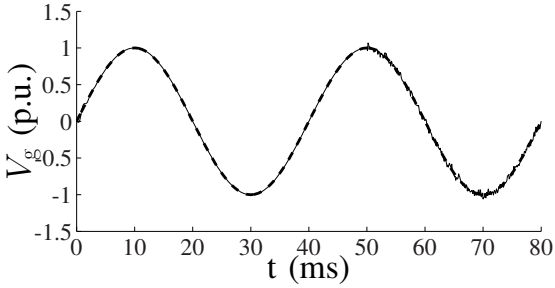

(e) Adapted second reference load, with phase-lag compensation: V_{g}(t)

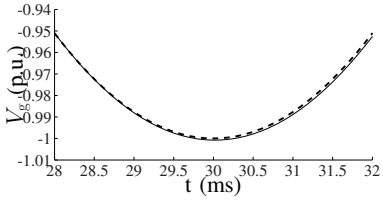

(f) Detail of V_{g} in (e)

*Figure 3.31: PID 1 - Direct control without forward compensation (— = $v_{\mathrm{g}}(\mathrm{t})$ (p.u.); **----** = $v_{\mathrm{g}}^{\star}(\mathrm{t})$ (p.u.), -.-.-. = $i_{\mathrm{g}}(\mathrm{t})$ (p.u.))*

With this controller, the control circuit has the following characteristics: $T_s = 1.76$ ms, %OS = 46.5, PM = 40°, GM = 6 dB, $f_b = 776$ Hz. From the Bode plot, it follows that the phase for 25 Hz (which is the frequency of the reference signal) equals 0.115°. This small value is not compensated by including a phase-lead in the reference signal. This controller is referred to as PID 3.

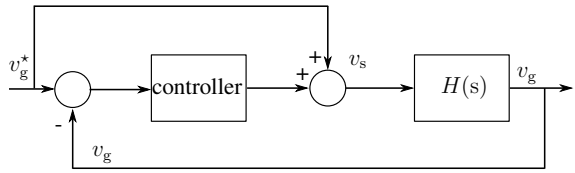

Figure 3.32: Direct control with $v_g^\star$ added to the output of the PID controller (feed forward compensation

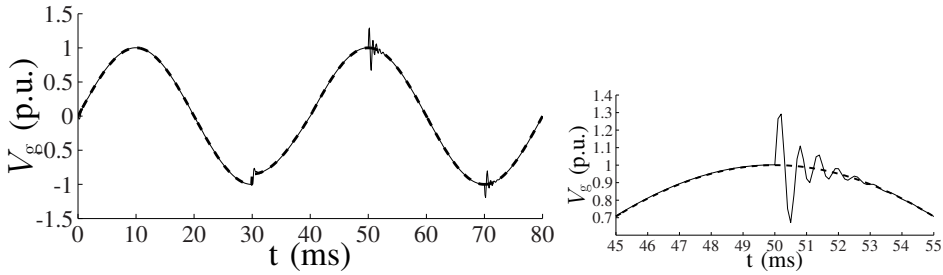

(a) First reference load: $V_g(t)$ and $I_g(t)$ (b) Detail of V_g in (a)

Figure 3.33: PID 2 - Direct control with adding $v_g^\star$ to the output of the PID controller (— = $v_g(t)$ (p.u.); ---- = $v_g^\star(t)$ (p.u.) , -.-.-. = $i_g(t)$ (p.u.))

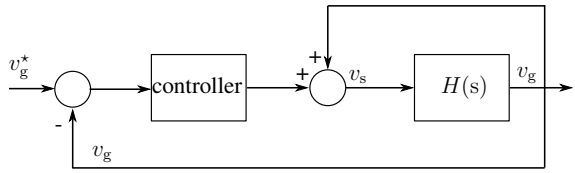

Figure 3.34: Direct control with v_g added to the output of the PID controller (feed forward compensation)

In case of the first reference load in Fig. 3.35(a,b), a slightly less accurate steady-state tracking is obtained, but PID 3 results in a significant improvement in transient behaviour compared to the previous case. This slightly less accurate regime tracking can be due to the lower bandwidth of this controller. For the second load in

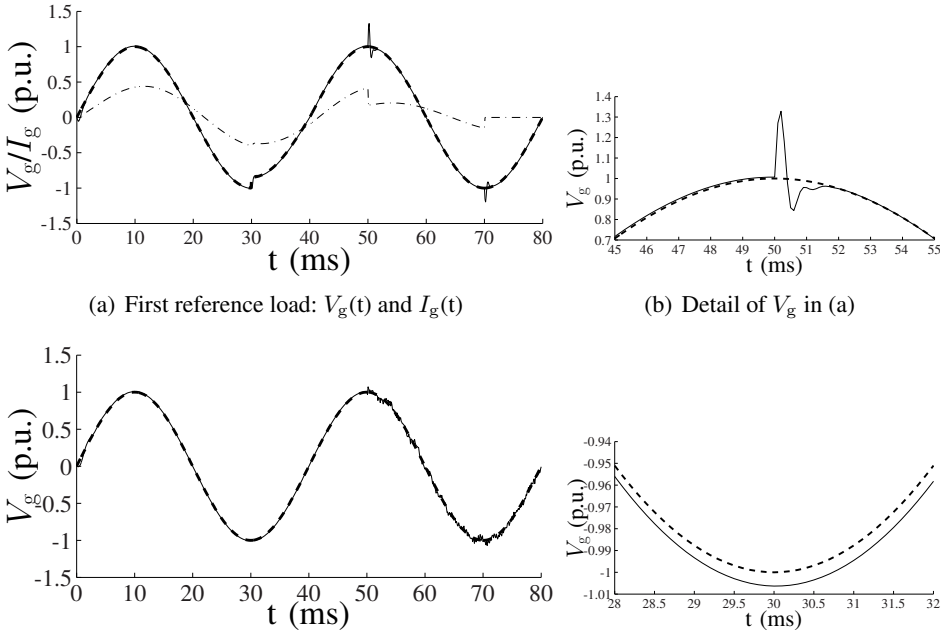

(a) First reference load: $V_{\mathrm{g}}(\mathrm{t})$ and $I_{\mathrm{g}}(\mathrm{t})$

(b) Detail of V_{g} in (a)

(c) Second reference load: $V_{\mathrm{g}}(\mathrm{t})$

(d) Detail of V_{g} in (c)

Figure 3.35: PID 3 - Direct control with forward compensation of v_{g} *(—* $= v_{\mathrm{g}}(\mathrm{t})$ *(p.u.);* **----** $= v_{\mathrm{g}}^{\star}(\mathrm{t})$ *(p.u.),* -.-.-. $= i_{\mathrm{g}}(\mathrm{t})$ *(p.u.))*

Fig. 3.35(c,d), the PID 3 controller outperforms PID 1 and PID 2, by reaching a stable operation despite the model faults in both L and C.

B. Cascaded control

As discussed in § 3.2, the usage of cascaded control is possible in the considered system. Including current measurements that are not present in the direct control is beneficial for the overall controller performance. In this paragraph, the latter two conclusions are investigated in simulation and the effect of extra voltage measurement (forward voltage compensation) is studied as well.

Without forward voltage compensation For cascaded control without adding v_{g} to the output of the controller (forward voltage compensation) as suggested in Fig. 3.16, theoretically, a P controller is sufficient in the current control loop. However, to obtain a sufficient phase margin, a PD controller with a small D action

is used in the following simulations:

$$C(z) = 0.3455\frac{z - 0.22}{z}. \tag{3.50}$$

With this controller, the current control loop has the following characteristics: PM = 30.1°, GM = 7.78 dB, $f_b = 2.01$ kHz (open loop bandwidth). For the voltage controller, the following PI controller is tuned:

$$C(z) = 0.35134\frac{z + 2}{z - 1}. \tag{3.51}$$

With this controller, the voltage control loop has the following characteristics: T_s=1.22 ms, PM = 63.5°, GM = 6 dB, %OS= 10.4 and $f_b = 497$ kHz (open loop bandwidth). From the Bode plot, it follows that the phase lag for 25 Hz (which is the frequency of the reference signal) equals -3.03°, which is compensated by a phase-lead in the reference voltage. This controller is referred to as PIPD 1.

The simulation results in case of the first load are depicted in Fig. 3.36(a,b). An accurate steady-state tracking is obtained, analogous to the PID 1 and PID 2 control strategies and better than for the PID 3 option. For the second load in Fig. 3.36(c,d), a good robustness to model faults and noise are obtained.

Analogous as in the previous paragraph, PIPD 2 consists of the same PI-PD controller as the previous case but with addition of the set point voltage $v_{\mathrm{g}}^{\star}$ to the output of the controller to avoid the phase-lag compensation. PIPD 1 and PIPD 2 have similar results, as it was the case in the direct control with PID 1 and PID 2.

With forward voltage compensation Second, a forward compensation of the measured voltage v_{g} is included. For this, a PI-P control strategy is sufficient. The P controller of the inner current control loop equals 0.35811 giving this loop a $f_b = 1$ kHz and PM= 53.9°. The PI controller of the outer voltage control loop equals

$$1.9823\frac{z - 0.81}{z - 1}, \tag{3.52}$$

giving the controlled system T_s =2.14 ms, PM = 40°, GM = 6 dB, %OS = 40.6 and $f_b = 695$ kHz (open loop bandwidth). This controller is referred to as PIP 3.

The simulation results depicted in Fig. 3.37 show that because of the addition of v_{g} in the controller's output, a better transient behaviour compared to PIPD 1 is obtained. This is analogous as in the direct control strategy. Again, the regime results are slightly less accurate.

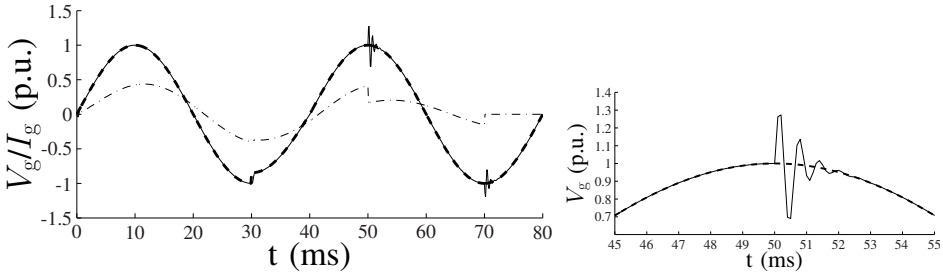

(a) First reference load: $V_{\mathrm{g}}(\mathrm{t})$ and $I_{\mathrm{g}}(\mathrm{t})$ (b) Detail of V_{g} in (a)

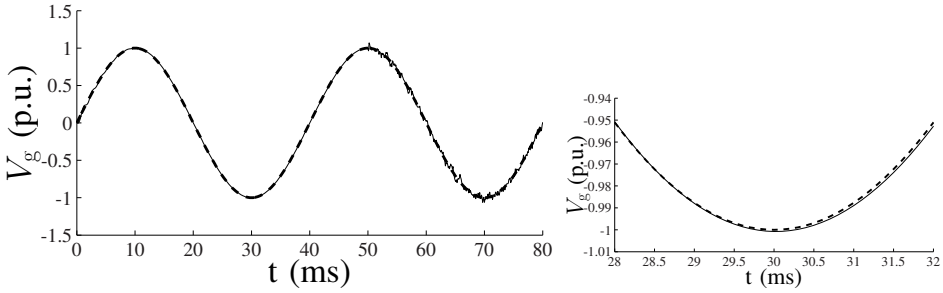

(c) Second reference load: $V_{\mathrm{g}}(\mathrm{t})$ (d) Detail of V_{g} in (c)

Figure 3.36: PIPD 1 - Cascaded PI-PD control (— = $v_{\mathrm{g}}(\mathrm{t})$ (p.u.); ---- = $v_{\mathrm{g}}^{\star}(\mathrm{t})$ (p.u.), -.-.-. = $i_{\mathrm{g}}(\mathrm{t})$ (p.u.))

C. Conclusion: comparison of controllers

The performance of all controllers is summarised in Table 3.1. In this table, the voltage error e is given, which is defined as:

$$e = \sqrt{\frac{1}{N}\sum_{\mathrm{i}=1}^{N}(v_{\mathrm{g,i}} - v_{\mathrm{g,i}}^{\star})^2}. \tag{3.53}$$

The voltages in $39.9 \leq t \leq 49.9$ ms are compared. In this way, for the first reference load, the regime performance is compared and for the second one, the parameter sensitivity, because the robustness to measurement noise is similar for all controllers.

The PID 1-2 en PIPD 1-2 controllers have similar results in e. The PID 1 and PIPD 1 controllers require the knowledge of the phase lag, while PID 2 and PIPD 2 need addition of $v_{\mathrm{g}}^{\star}$ to the output. From a practical point of view, the latter is preferable, despite the slightly better performance of the PID 1 and PIPD 1 controllers compared to their PID 2 and PIPD 2 variants respectively.

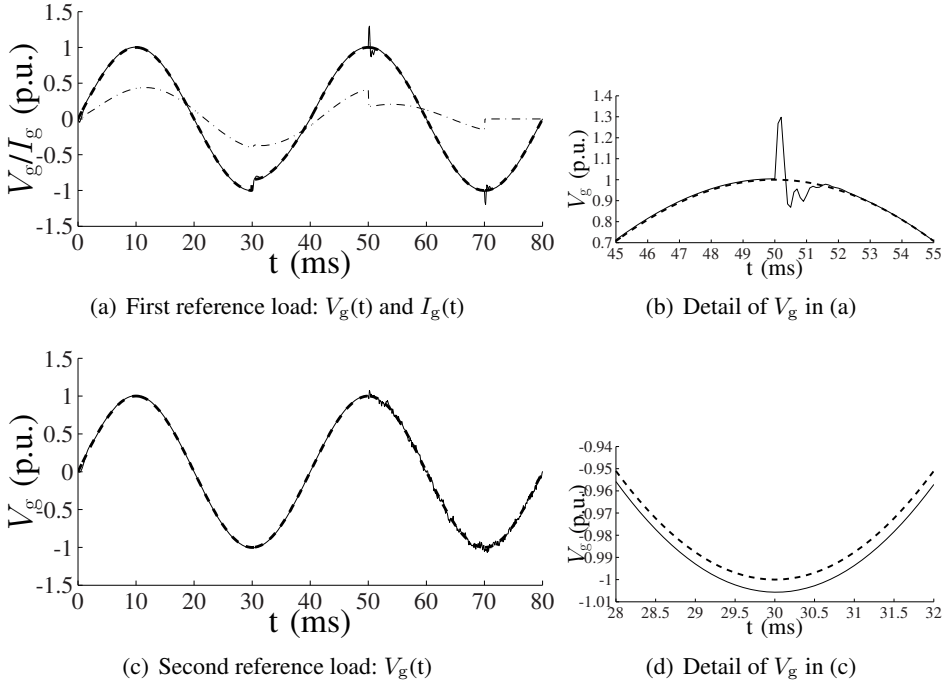

(a) First reference load: $V_{\mathrm{g}}(\mathrm{t})$ and $I_{\mathrm{g}}(\mathrm{t})$

(b) Detail of V_{g} in (a)

(c) Second reference load: $V_{\mathrm{g}}(\mathrm{t})$

(d) Detail of V_{g} in (c)

Figure 3.37: PIP 3 - Cascaded PI-P control with forward compensation of v_{g} *(—* $= v_{\mathrm{g}}(\mathrm{t})$ *(p.u.);* **----** $= v_{\mathrm{g}}^{\star}(\mathrm{t})$ *(p.u.), , -.-.-.* $= i_{\mathrm{g}}(\mathrm{t})$ *(p.u.))*

Table 3.1: Steady-state performance controllers

	e (load 1)	e (load 2)
PID 1	0.0443	unstable
PID 2	0.0520	unstable
PID 3	0.1674	0.1160
PIPD 1	0.0237	0.0258
PIPD 2	0.0494	0.0404
PIP 3	0.0944	0.0944

Although the PID 1 and 2 controllers have a good regime tracking, they are very sensitive to model faults of L. The PID 3 controller is less sensitive to these model faults, shows a better transient behaviour, but a slightly less accurate steady-state performance compared to the other direct controllers.
In the cascaded control, a good parameter robustness is obtained. The PIPD 1 and 2 controllers have similar results and achieve a slightly better steady-state tracking

performance than PID 1 and 2. The transient results are similar, but as discussed above, their model robustness is a very important advantage. The PIP 3 controller has the advantage that the current control loop only requires a P-controller and it achieves a very good transient response, but a slightly less accurate regime tracking compared to PIPD 1 and 2. Compared to PID 3, its steady-state voltage tracking and model robustness are better.
To summarise, from these simulations, it follows that using cascaded control of VSIs in islanded microgrids is possible, by adding current measurements in the control system. Cascaded control allows for using the system knowledge that can be gained through a measurement of i_{g} for the control. In cascaded control, PI controllers can be used, whereas the direct control requires PID controllers, which are harder to tune and implement. Also, the ICCL allows for a direct handling of the current, e.g., with respect to over-current limitation. The analysis above has shown that cascaded control is especially beneficial when considering model inaccuracies. Also, the regime error is lower in cascaded control compared to direct control. When adding a grid voltage measurement to the output of the controller, both direct and cascaded control show a better transient response and parameter sensitivity. Without the forwarding of this voltage measurement, either phase-lag compensation in the reference signal or adding the reference voltage to the controller's output is required for a good controllers performance.

3.4.2 Experimental Results

The previous theoretical and simulation results have been verified on an experimental set-up, see also [158]. A full bridge single phase converter is used with the same parameters as in the simulations. This converter was designed in the lab based on a Fuji IGBT Intelligent Power Module (IPM). A Freescale 56F8367 digital signal processor is used to implement the different controllers and generate the PWM switching signals for the converter. Both direct and cascaded controllers are digitally implemented with a differential equation and will now be discussed. The same load is used in all the experiments, which is an RL load (2.5 A, $\cos\phi = 0.8$). The figures in this section show the set point and measured grid voltage and the measured grid current. Also, the difference e_v between the set point and measured grid voltages is shown.

A. Direct control

Without forward compensation The PID 1 controller does not use forward compensation. Analogous as in the simulations, this leads to a phase-lag in a steady-state situation, which was compensated by a phase-lead in the reference signal in the experiments. Fig. 3.38 shows the measurement results. Note that when

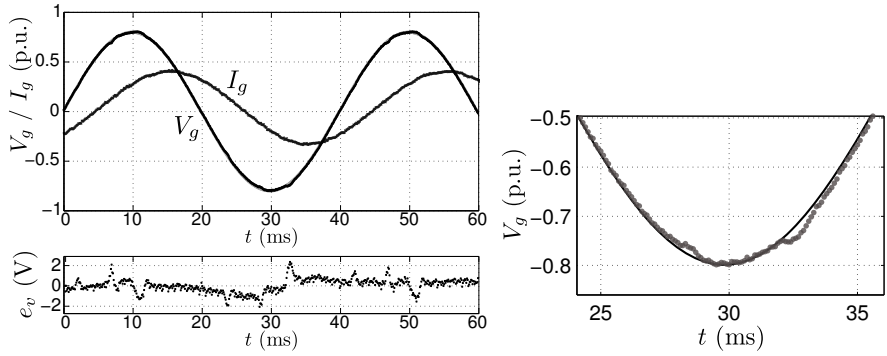

(a) V_g(t) and e_v(t) (b) Detail of V_g

Figure 3.38: PID 1 - Direct control without forward compensation of v_g: Experiment, RL load (2.5 A, $\cos\phi = 0.8$)

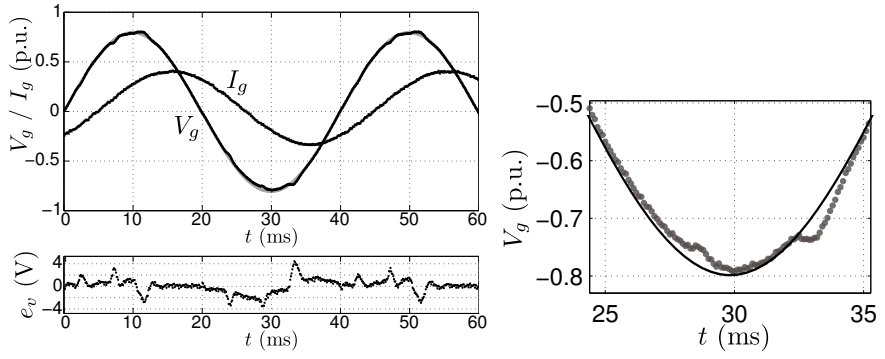

(a) V_g(t) and e_v(t) (b) Detail of V_g

Figure 3.39: PID 3 - Direct control with forward compensation of v_g: Experiment, RL load (2.5A, $\cos\phi = 0.8$)

this voltage controller is used in combination with other controllers, such as the power controllers of chapter 4, this phase-lead often becomes impractical.
The measurement shows good steady-state tracking of the set point voltage, but an accurate phase-lag compensation was necessary to achieve this.

With forward compensation The PID 3 controller uses forward compensation of the voltage measurement v_g. Therefore, the phase-lag of PID 1 is not longer present such that a phase-lag compensation is unnecessary. Fig. 3.39 shows a measurement of the PID 3 controller.

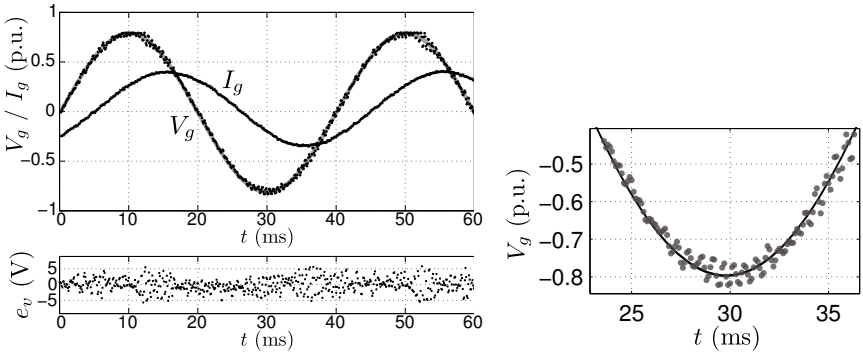

(a) V_{g}(t) and e_v(t) (b) Detail of V_{g}

Figure 3.40: PIPD 1 - Cascaded PI-PD control: Experiment, RL load (2.5A, $\cos\phi = 0.8$)

This figure clearly shows that a good steady-state tracking of the set point is maintained, although the phase-lag compensation was omitted. Thanks to the forward compensation, this satisfactory performance is achieved. Like in the simulations, a slightly better steady-state voltage tracking is obtained by the PID 1 controller compared to PID 3. However, this conclusion can be relativised by noise and measurement inaccuracies.

B. Cascaded control

Without forward compensation The PIPD 1 controller does not use forward compensation. Hence, a phase lag compensation is needed to achieve a good steady state tracking. Fig. 3.40 shows a measurement of the PIPD 1 controller.
Again, good steady state tracking is achieved, but phase-lag compensation was needed. Also, the derivative action of the PD current controller results in an increased sensitivity to noise in the measurements.

With forward compensation The PIP 3 controller uses forward compensation of the measured voltage v_g, such that a phase-lag compensation becomes unnecessary. Also, the derivative action of the current controller was omitted. Fig. 3.41 shows the measurement results of the PIP 3 controller.
Although no phase compensation was applied, the PIP 3 controller has a good steady-state tracking performance thanks to the forward compensation of v_g. Therefore, the result is similar to that of the PIPD 1 controller.
This shows that using cascaded control is possible for voltage control in islanded microgrids. In the experiments, a good performance is obtained with all four con-

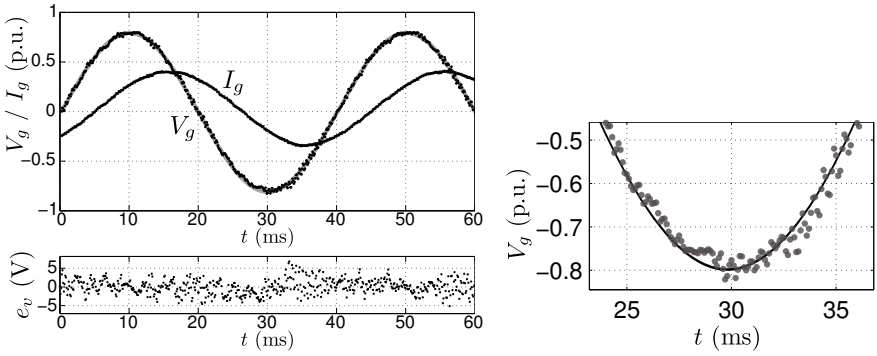

(a) V_{g}(t) and e_v(t) (b) Detail of V_{g}

Figure 3.41: PIP 3 - Cascaded PI-P control with forward compensation of v_g: Experiment, RL load (2.5A, $\cos\phi = 0.8$)

trollers. Clearly, like in the simulations, either phase-lag compensation or forward voltage compensation is required to achieve a good tracking performance.

3.5 Conclusions

A theoretical analysis of voltage control in islanded microgrids shows that cascaded control is possible and using measured current signals in this control scheme is beneficial for the overall system performance. Also, for cascaded control, a combined PI-P controller is sufficient while direct control requires the usage of a PID controller for a stable operation. This is demonstrated by means of both simulation and experimental results. In both the direct and the cascaded control, phase-lag compensation is required to compensate for the phase-lag that is otherwise present in the regime voltage tracking. To avoid this, forward voltage compensation, thus adding a measurement of the grid voltage to the output of the controller, shows good results. By using these simple yet effective PID-type controllers, accurate voltage control is obtained in islanded microgrids.
The content of this chapter has been published in [159].
Although voltage control is not the main objective of this PhD thesis, other control strategies such as sliding-mode control, linear quadratic regulation, fuzzy logic control and hysteresis control are discussed and compared in Appendix A.

Chapter 4

Voltage-based droop control

This chapter presents the voltage-based droop (VBD) control strategy of DG units in an islanded microgrid. The microgrids considered here are single-phase low-voltage networks, with multiple DG units (multiple connection points) which mostly have a power-electronic interface. There is a single point of common coupling (PCC) between the microgrid and the distribution network. In this chapter, and in chapters 5-6, extensive case studies to validate the developed control strategies are performed in MatLab Simulink, extended with the Plecs library for modelling the DG units upto the level of the converter switches. Although this increases the simulation time, it allows for detailed dynamic studies. The simulation experiments are generally built up in a similar structure. First, some small set ups, e.g., consisting of one or two DG units, are studied to clarify the effects focused on. Next, some more extensive set ups, upto an IEEE feeder, are discussed in dynamical situations. Most of these large set ups are used multiple times in this PhD thesis, with some small changes dependent on the specific effect that is analysed.
In this chapter, first, the power flow equations in the considered networks are studied as these form the basics for the VBD control. Second, the active power balancing and sharing by using the VBD control strategy is presented. Next, the Q/f droop controller is considered for reactive power balancing and sharing. In § 4.4, the VBD control strategy is modified by an extra term to enable harmonic power sharing. In § 4.5, a method to adapt the VBD controller to achieve exact power sharing, if required, is suggested. Finally, in § 4.6, the analogy between conventional grid control and VBD control is studied.

4.1 Power flow equations

The simple system of Fig. 4.1, consisting of a power source, a line and a load is considered to derive the power flow equations. The complex power $\underline{S}$ injected into

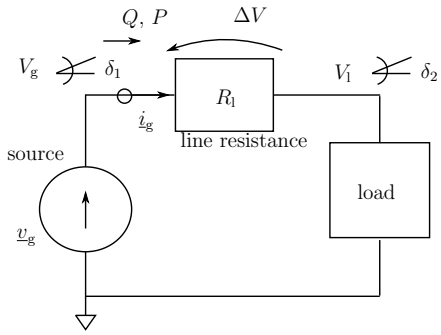

Figure 4.1: Simple system to study power flow equations

the grid by a power source is given by:

$$\underline{S} = \underline{v}_{\mathrm{g}} \underline{i}_{\mathrm{g}}^{\star} \tag{4.1}$$

with $\underline{v}_{\mathrm{g}}$ the voltage of the power source: $\underline{v}_{\mathrm{g}} = V_g e^{j\delta_1}$ in the complex notation, $\underline{i}_{\mathrm{g}}$ the line current and $\underline{i}_{\mathrm{g}}^{\star}$ the complex conjugate of $\underline{i}_{\mathrm{g}}$. This power source is connected to a load with voltage $\underline{v}_{\mathrm{l}} = V_{\mathrm{l}} e^{j\delta_2}$ through a line impedance $\underline{Z}_{\mathrm{l}} = R_{\mathrm{l}} + jX_{\mathrm{l}}$:

$$\underline{i}_{\mathrm{g}} = \frac{\underline{v}_{\mathrm{g}} - \underline{v}_{\mathrm{l}}}{R_{\mathrm{l}} + jX_{\mathrm{l}}}. \tag{4.2}$$

The load's phase angle δ_2 can be chosen as zero as voltage angles are relative quantities, therefore, $\underline{v}_{\mathrm{l}} = V_{\mathrm{l}}$. The active power can be written as

$$P = \frac{V_{\mathrm{g}}}{Z_{\mathrm{l}}^2} \left[R_{\mathrm{l}} (V_{\mathrm{g}} - V_{\mathrm{l}} \cos\delta_1) + X_{\mathrm{l}} V_{\mathrm{l}} \sin\delta_1 \right]. \tag{4.3}$$

The reactive power equals:

$$Q = \frac{V_{\mathrm{g}}}{Z_{\mathrm{l}}^2} \left[-R_{\mathrm{l}} V_{\mathrm{l}} \sin\delta_1 + X_{\mathrm{l}} (V_{\mathrm{g}} - V_{\mathrm{l}} \cos\delta_1) \right]. \tag{4.4}$$

A general assumption is that the phase angle variations are limited in the network, hence, $\delta_1 \approx \delta_2$, $\sin\delta_1 \approx \delta_1$ and $\cos\delta_1 \approx 1$. By using these approximations, P and Q can be expressed as:

$$P \approx \frac{V_{\mathrm{g}}}{Z_{\mathrm{l}}^2} \left[R_{\mathrm{l}} (V_{\mathrm{g}} - V_{\mathrm{l}}) + X_{\mathrm{l}} V_{\mathrm{l}} \delta_1 \right], \tag{4.5a}$$

$$Q \approx \frac{V_\mathrm{g}}{Z_\mathrm{l}^2}\left[-R_\mathrm{l}V_\mathrm{l}\delta_1 + X_\mathrm{l}(V_\mathrm{g} - V_\mathrm{l})\right]. \tag{4.5b}$$

In resistive networks:

$$P \approx \frac{V_\mathrm{g}}{R_\mathrm{l}}(V_\mathrm{g} - V_\mathrm{l}) \tag{4.6a}$$

$$Q \approx \frac{-V_\mathrm{g}V_\mathrm{l}}{R_\mathrm{l}}\delta_1. \tag{4.6b}$$

From (4.6a) and (4.6b), it is concluded that a decoupling of P and Q is achieved in microgrids with resistive characteristics. Q is predominantly dependent on the phase difference over the line (which is dynamically dependent on the frequency), while P is determined mainly by the voltage difference over the line.

In inductive networks, the active power P and reactive power Q can be expressed as:

$$P \approx \frac{V_\mathrm{g}V_\mathrm{l}}{X_\mathrm{l}}\delta_1 \tag{4.7a}$$

$$Q \approx \frac{V_\mathrm{g}}{X_\mathrm{l}}(V_\mathrm{g} - V_\mathrm{l}). \tag{4.7b}$$

Like in the case of resistive networks, a decoupling of P and Q is achieved. P is predominantly dependent on the phase difference over the line (which is dynamically dependent on the frequency), while Q is determined mainly by the voltage difference over the line. This leads to the well-known P/f and Q/V linkage in transmission networks. This dependency is the opposite of that in resistive networks.

In [75, 104], typical line parameters for low-voltage (LV), medium-voltage (MV) and high-voltage (HV) networks are compared. The results are depicted in Table 4.1. This table shows that LV microgrids are mainly resistive, while the HV networks are clearly inductive. The LV networks considered in Table 4.1 are rural networks. In Table 4.2, some parameters of commonly used cables in LV networks, the EAXVB and (older) BAXB cables, are given [160]. A typical Belgian LV network has a total R/X-ratio of 2-5. The total line impedance is dependent on the transformer (mainly X), the line impedance in the grid (some cable details are given in Table 4.2) and the impedance of the connection line to

Table 4.1: Typical line parameters

Type	$r\ [\frac{\Omega}{km}]$	$x\ [\frac{\Omega}{km}]$	I_N	$\frac{R}{X}$
LV	0.642	0.083	142	7.73
MV	0.161	0.190	396	0.85
HV	0.06	0.191	580	0.31

Table 4.2: BAXB and EAXVB cables in LV grids

	BAXB	EAXVB
section (mm^2)	$3 \times 95 + 54.6$	4×150
resistance (Ω/km)	0.410	0.265
inductance (mH/km)	0.243	0.248
R/X	5.37	3.40

the load (which often has a smaller section, thus a higher resistance/km and R/X). In general, the R/X-ratio varies between 2 and 8 in LV networks.

4.2 Active power control

As discussed in chapter 2, a widely-known control method for islanded microgrids is the active power/frequency (P/f) droop control, similar to the droop control in conventional grids. In this control strategy, local measurements of voltage and frequency are used as a communication link for the power sharing between the generators connected to the microgrid. Because of the droop functions, changes of the power delivered to the grid cause changes of the voltage and frequency settings, or vice versa [4, 15, 18, 104–106, 108, 117, 161]. Accordingly, in case of multiple inverters, the power will be shared between the generators based on their droop characteristics. The main advantage of this control strategy is that it does not require inter-unit communication and mimics the synchronous generator control in the transmission network.

However, some problems arise when using the P/f droop control strategy as this controller is not based on the specific characteristics of the microgrids. Consequently, the voltage-based droop (VBD) control strategy for converter-interfaced DG units in islanded microgrids is presented in this PhD thesis. Like in the P/f

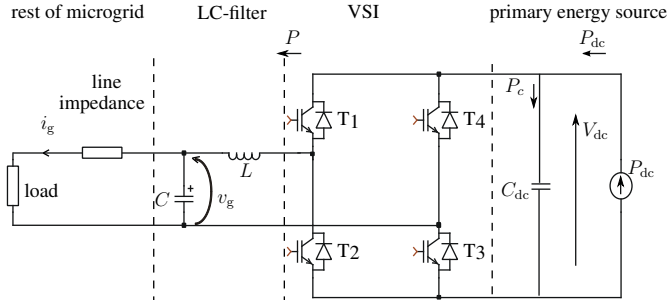

Figure 4.2: Grid architecture for the case of one power source: dc-side (power source or current source), VSI, ac side (consisting of line impedances and the rest of the microgrid, which is a black box)

droop control, no critical communication between the inverters is required. The specific characteristics of the microgrid, that differ significantly from those of the traditional power system, are taken into account. Firstly, in conventional grids, when an unbalance occurs between the generated power of the sources and the electrical power consumption, the power is instantly balanced by the rotating inertia in the system, resulting in a change of frequency. Because the grid elements in microgrids are mainly power-electronically interfaced or consist of resistive loads, islanded microgrids lack this significant inertia. Thus, while the conventional grid control is based on the spinning reserve, for microgrid control, this feature is not inherently available. Secondly, as low-voltage distribution grids are mainly resistive, the active power through a power line mainly depends on the voltage amplitude, unlike in transmission grids where the active power is mainly linked with voltage phase-angle changes across the line. Therefore, active power/voltage (P/V) droops have been presented in [104, 134, 135], opposed to the conventional P/f droops. In this PhD thesis, the reference voltage amplitude (see Fig. 4.2) is determined by the V_g/V_{dc} droop control instead of the P/V droop in the conventional P/V droop control strategy. V_g is the rms value of the grid voltage v_g and V_{dc} the dc-bus voltage of a primary energy source in Fig. 4.2. With the VBD control strategy, changing the sources generated power is postponed until a certain threshold voltage is reached. This leads to an optimised integration of renewable energy sources, as it enables to address them to take part in the load sharing. By using the VBD control, also, (smart) loads and storage elements can adjust their power consumption according to the voltage levels, which will be discussed in chapter 5.

The overall control principle of the VBD control principle, when harmonics are not considered, is shown in Fig. 4.3. The Q controller is discussed in § 4.3 and the voltage controller in chapter 3. Concerning the active power controller, two droop

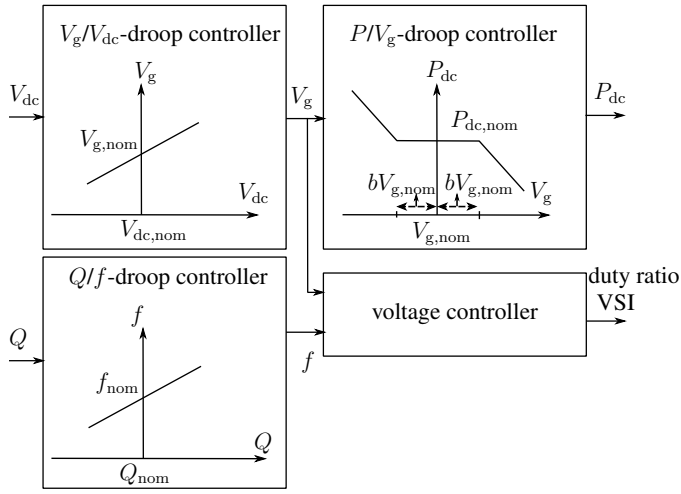

Figure 4.3: VBD control: active and reactive power control. Combined operation of the droop controllers to determine the set value of the grid voltage.

controllers are implemented:

- the V_g/V_{dc} droop controller: enables power balancing between the ac and dc-side of the VSI;
- the P_{dc}/V_g droop controller: enables voltage limiting and includes the constant-power band to delay the active power changes of the renewables to more extreme voltages compared to those of the dispatchable DG units.

In the converter, a digital control using pulse width modulation (PWM) with sampling period T_s is implemented. The VBD controller provides the discrete reference values for the voltage control block. The reference value $v^{\star}_{g,k} = \sqrt{2}V_{g,k}\sin(\alpha_k)$ is obtained from V_g (V_g/V_{dc} droop controller) and f (Q/f droop controller) at the discrete instant k according to

$$v^{\star}_{g,k} = \sqrt{2}V_{g,k}\sin(\alpha_{k-1} + 2\pi f_k T_s). \tag{4.8}$$

The droop controllers are discussed below.

4.2.1 V_g/V_{dc} droop controller

The primary function of the V_g/V_{dc} droop controller is to balance the ac and dc-side of the VSI. A secondary function is limiting of the dc-link voltage.

A. Control principle

The DG units' configuration is depicted in Fig. 4.2. The dc-side of the converter consists of a dc-link capacitor C_{dc} and a current source or power source, as opposed to chapter 3, where the dc-side consists of a voltage source.
The $V_{\mathrm{g}}/V_{\mathrm{dc}}$ droop controller is based on two intrinsic features of the considered microgrid and the DG unit:

- The (transient) storage capabilities of the dc-link capacitor:
  In case the load (P) increases, while the dc-power (P_{dc}) remains the same, power is extracted from the dc-link capacitor (P_{c}). This will induce a decreasing dc-link voltage. Vice versa, a sudden decrease of load will be balanced by the dc-link capacitor absorbing energy, resulting in a higher dc-link voltage. Therefore, changes of V_{dc} indicate a power unbalance between the generated power by the primary energy sources (P_{dc}) and the power injected in the microgrid (P).

- Low-voltage microgrid characteristic:
  As low-voltage grids are mainly resistive, there is a significant linkage between P and V_{g} in the lines. Also, a change of V_{g} will lead to a changed active power consumption in the resistive loads.

Therefore, in the V_g/V_{dc} droop control principle, a Proportional (P) controller with slope K_{V} is used to control the dc-bus voltage V_{dc} by changing V_{g} [162]:

$$V_{\mathrm{g}} = V_{\mathrm{g,nom}} + K_{\mathrm{V}}(V_{\mathrm{dc}} - V_{\mathrm{dc,nom}}). \tag{4.9}$$

A natural balancing in the VSI is obtained with the $V_{\mathrm{g}}/V_{\mathrm{dc}}$ droop controller. By changing the rms grid voltage, the power absorbed by the loads and lines in the islanded microgrid changes. This leads to the restoration of the power balance across the ac and dc-side of the VSI as a small voltage change is not harmful for the grid elements. Also, some (intelligent) loads and power supply elements can further change their power consumption (§ 5.1) and some power sources can change their power production (§ 4.2.2) according to the voltage levels. This enables voltage limiting.
In the single-phase grid configuration with full bridge converter, the dc-bus voltage has a ripple of twice the fundamental grid frequency. Therefore, the bandwidth of the P controller is set in order to avoid this ripple occurring in the grid voltage [163], by operating at a sample rate of 100 Hz. If a higher control frequency for this controller would be used, further measures need to be taken to avoid the appearance of the 100 Hz variations of V_{dc} in v_{g}. Generally, a moving average scheme is

included such that:

$$V_{\mathrm{g}}(k) = V_{\mathrm{g,nom}} + K_{\mathrm{V}} \left[\frac{(V_{\mathrm{dc}}(k) - V_{\mathrm{dc,nom}}) + (V_{\mathrm{dc}}(k-1) - V_{\mathrm{dc,nom}})}{2} \right], \quad (4.10)$$

and where the time difference between two discrete steps is 0.01 s. Another possibility to avoid the 100 Hz variation in V_{dc} occurring in the reference rms grid voltage is the usage of a low-pass filter on the measurement of V_{dc}.

B. Discussion

With the V_g/V_{dc} droop control strategy, frequent changes of P_{dc} are avoided as V_{g} can deviate from its nominal value. The capability of the voltage to deviate from its nominal value ([43]) is, thus, effectively used. To prevent the voltage exceeding certain levels, a limiting mechanism should be added. This limiting procedure can be provided by DG units, intelligent loads and storage elements, that can change their power exchange with the grid dependent on the voltage. With the combination of $V_{\mathrm{g}}/V_{\mathrm{dc}}$ droop control and a voltage limiting method, changing P_{dc} can be postponed to more extreme voltages if compared to the conventional case with the P/V or P/f droop controller only. Therefore, the DG units, that are often renewable energy resources, and their storage elements are not unnecessary burdened with frequent (small) power changes.
In the P/V droop control strategy, either the rms voltage V_{g} needs to be tracked to change P_{dc} ($P_{\mathrm{dc}}(V_{\mathrm{g}})$) or the ac power needs to be measured to change V_{g} ($V_{\mathrm{g}}(P)$). By using the V_g/V_{dc} droop controller in the VBD control strategy, neither V_{g} needs to be tracked as it is output of the V_g/V_{dc} droop, nor P needs to be measured to be used as input of a control block. Instead, V_{dc} needs to be measured, which is significantly easier as it is a dc value.

C. Examples

The $V_{\mathrm{g}}/V_{\mathrm{dc}}$ droop control principle is applied to a microgrid, that, in a first simulation, is fed by one power source. Next, a case with two DG units is considered.

One DG unit In the first simulation, the islanded microgrid consists of a line resistance $R_l = 1.5\ \Omega$ in series with a load $R = 33\ \Omega$. The case where the line impedance is not purely resistive is studied in § 4.2.3. The controller filter parameters are: $L = 2$ mH and $C = 3\ \mu$F and only the $V_{\mathrm{g}}/V_{\mathrm{dc}}$ droop control is used. The nominal dc-link voltage $V_{\mathrm{dc,nom}}$ equals 450 V and $C_{\mathrm{dc}} = 1.5$ mF. Note that the simulations are performed upto the level of the switches, including switching ripple. The plots are sampled with the switching frequency as this is also the case for the VSI control and measurements. The nominal reference microgrid voltage

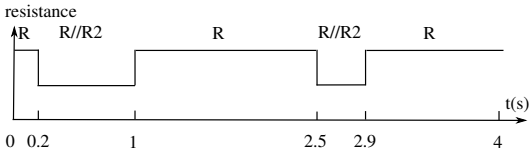

Figure 4.4: Time line of the change of load resistance, '//' denotes 'in parallel'

$v^{\star}_{\mathrm{g,nom}}$ is a 50 Hz voltage, with an rms value $V_{\mathrm{g,nom}}$ of 230 V. The power P_{dc} delivered by the source is constant and equals 2100 W. In order to study the controller performance to large transients, a variable load is implemented: e.g. after 0.2 s, a second load R_2 of 33 Ω is turned on in parallel with R. The time line of Fig. 4.4 shows the load change in the microgrid. The slope of the $V_{\mathrm{g}}/V_{\mathrm{dc}}$ droop control K_{V} equals $\frac{0.5}{\sqrt{2}}$. The sample frequency of this controller equals 100 Hz, as discussed above.

For verification of the $V_{\mathrm{g}}/V_{\mathrm{dc}}$ droop control strategy, the theoretical steady-state microgrid voltage can be calculated, e.g., for a microgrid loaded with R:

$$P = \frac{V_{\mathrm{g}}^2}{R_{\mathrm{tot}}} = \frac{V_{\mathrm{g}}^2}{(R + R_l)}, \tag{4.11}$$

$V_{\mathrm{g}} = 269.2$ V. If R_2 is turned on in parallel with R: $V_{\mathrm{g}} = 194.4$ V. This voltage is lower than in the first case with only R as the power delivered by the source remains the same with a lower overall microgrid impedance.

The simulation results of the rms microgrid voltage V_{g} are depicted in Fig. 4.5(a)[1]. The changes of the rms voltage due to the variations of the load resistance, are clearly shown in this figure. The 100 Hz variation of the dc-link voltage is clearly shown in Fig. 4.5(c). Due to the use of a P controller, V_{dc} can deviate from $V_{\mathrm{dc,nom}}$. The grid voltage rms values match the theoretical calculations. The power P delivered to the microgrid is shown in Fig. 4.5(b). From this figure, it is concluded that during steady-state, P is constant and equal to the output power P_{dc} of the power source. Just after the load changes, transients in the power P delivered to the microgrid occur because the $V_{\mathrm{g}}/V_{\mathrm{dc}}$ droop controller has a finite bandwidth. For example at a time $t = 1$ s, when R_2 turns off, the overall load decreases. To maintain the power balance between the power source and the rest of the microgrid, some power is being delivered to the dc-link capacitor C_{dc}. Therefore, the dc-link voltage increases as shown in Fig. 4.5(c). The $V_{\mathrm{g}}/V_{\mathrm{dc}}$ droop controller reacts on the raise of V_{dc} by increasing the set value of V_{g} until no more power is exchanged

[1] In order to determine the rms values, a moving average over one fundamentel period (0.02 s) of the grid voltage is taken.

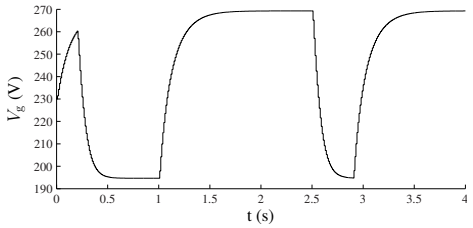

(a) Terminal voltage V_{g}

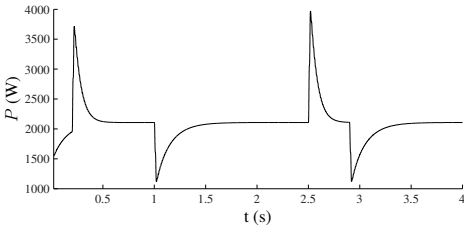

(b) Output power P

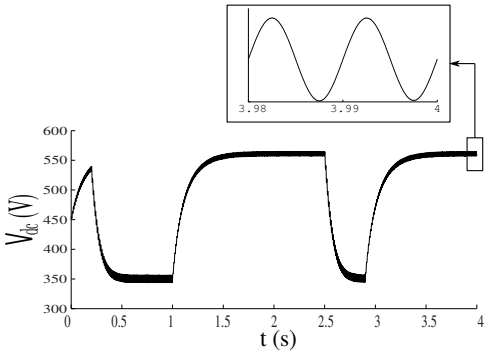

(c) Dc-link voltage V_{dc}

Figure 4.5: One power source: $V_{\mathrm{g}}/V_{\mathrm{dc}}$ droop control

with C_{dc} and V_{dc} remains constant. Subsequently, again a steady-state is reached and the power P delivered to the electrical network equals the dc-power P_{dc}. The voltages obtained in this simulation are larger than those generally tolerated in microgrids as power flexibility is not yet included in this example.

Two DG units In a second case, the V_g/V_{dc} droop controlled microgrid is fed by two DG units as shown in Fig. 4.6. The same parameters and loads as in the previous case are considered, except $P_{\mathrm{dc,nom},1} = 700$ W and $P_{\mathrm{dc,nom},2} = 1400$ W. By using Fig. 4.6, the power balancing for the case of two power sources is discussed. E.g., first, only one power source with power P_{dc1} is turned on. Only the $V_{\mathrm{g}}/V_{\mathrm{dc}}$ droop controller is considered, hence, $P_{\mathrm{dc1}} = P_{\mathrm{dc,nom},1}$. The $V_{\mathrm{g}}/V_{\mathrm{dc}}$ droop controller of this power source controls the rms voltage to V_{g1} in order to achieve a constant dc-link voltage, and $V_{\mathrm{g1}} > V_{\mathrm{l}}$, with V_{l} the rms value of the load voltage v_{l}. As the second DG unit is turned off, in open circuit: V_{g2} equals V_{l}. Next, the second source with power P_{dc2} turns on. At first, V_{g2} remains constant and equal to V_{l} and therefore, P_2 remains zero. In order to maintain the power balance, the dc-link voltage V_{dc2} increases because the dc-link capacitor power P_{C2} equals P_{dc2}.

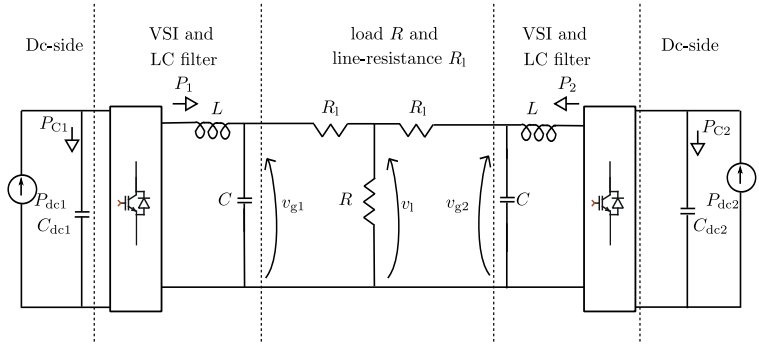

Figure 4.6: Two VSIs: microgrid configuration

Therefore, the V_g/V_{dc} droop control of this second source changes the set value of V_{g2}. Power is injected in the rest of the microgrid and V_{g2} increases. The power delivered to the load, here represented as R, increases and therefore, the voltage V_l will increase. If V_{g1} remains constant, the power P_1 delivered to the microgrid by source 1 decreases as the difference $(V_{g1} - V_l)$ is lower. Therefore, under constant P_{dc1}, the dc-link voltage of source 1 will increase and the controller will increase V_{g1}. This process goes on until steady-state is reached.

The microgrid rms voltages, V_{g1} and V_{g2}, are depicted in Fig. 4.7(a). The power P_1 and P_2 delivered to the microgrid are equal to the nominal power of 700 W and 1400 W respectively, except during the load changes. In this case, $K_{V,1} = 0.5/\sqrt{2}$, $K_{V,2} = 1/\sqrt{2}$, leading to steady-state dc-link voltages $V_{dc,1} = 544$ V and $V_{dc,2} = 503$ V. Note that by changing the droop of this controller, V_{dc} can be forced closer to its nominal value, dependent on the specifications of the dc-link. For example, for $K_{V,1} = K_{V,2} = 0.5/\sqrt{2}$, $V_{dc,1} = 542$ V and $V_{dc,2} = 553$ V. Hence, a lower $K_{V,2}$ leads to a higher deviation of the dc-link voltage from its nominal value as the terminal ac voltage remains approximately constant because of the power balance with equal loads.

A stable operation is obtained, but the obtained voltages exceed the voltage limits as no power flexibility is incorporated in the control. Therefore, the P_{dc}/V_g droop controller is included in the next paragraph. Also, a relatively large line resistance (i.e., an urban microgrid with long lines) is considered enabling the same study-case as with the combination V_g/V_{dc} droop and P_{dc}/V_g droop control. For multiple DG units, low line resistance can give oscillations in the system. Hence, in § 4.2.3, a solution will be discussed to deal with low resistances.

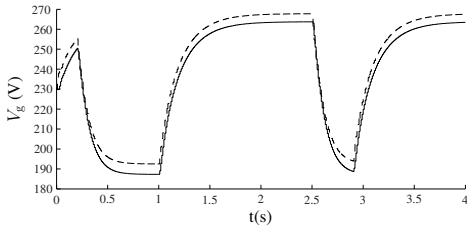

(a) Terminal voltage V_{g}

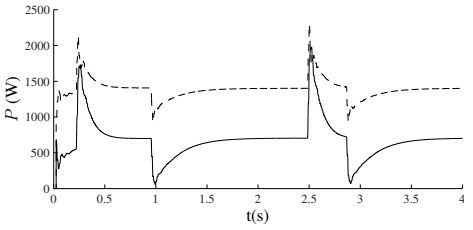

(b) Output power P

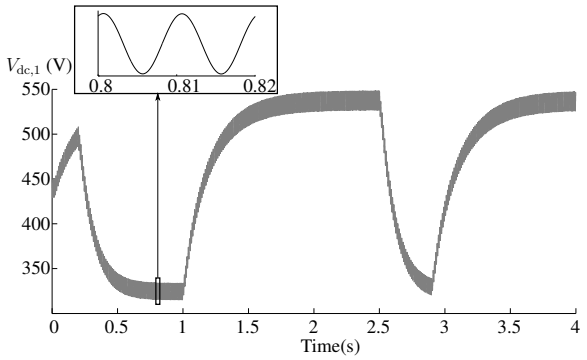

(c) Dc-link voltage V_{dc}

Figure 4.7: Two power sources: $V_{\mathrm{g}}/V_{\mathrm{dc}}$ droop control

Conclusions The control strategy shows a good performance for a constant as well as a variable load. With this control strategy, frequent changes of P_{dc} are avoided as V_g can deviate from its nominal value. Still, combination of V_g/V_{dc} droop control with a voltage limiting method is required.

4.2.2 VBD control

The VBD control strategy is based on two control algorithms, with their operation dependent on the rms microgrid voltage as shown in Fig. 4.3. In a voltage band around the nominal microgrid voltage, only the $V_{\mathrm{g}}/V_{\mathrm{dc}}$ droop control strategy is applied, keeping the generated power constant and where V_{g} is drooped with V_{dc}. If the microgrid voltage exceeds this band, a $P_{\mathrm{dc}}/V_{\mathrm{g}}$ droop controller is turned on in addition to the $V_{\mathrm{g}}/V_{\mathrm{dc}}$ droop controller. Opposed to the conventional P/V droop control, which is only implemented in dispatchable DG units, the $P_{\mathrm{dc}}/V_{\mathrm{g}}$ droop controller is implemented in both the renewable and dispatchable DG units, which will be discussed in this section.

A. *Control principle*

The V_g/V_{dc} droop control strategy delays changing the output power of the generators by slightly varying V_g. All electrical equipment in the microgrid is designed to withstand some voltage deviation from its nominal value. Still, the variations of V_g need to remain in a tolerated voltage band (for example 0.9-1.1 $V_{g,nom}$) [43]. Therefore, it is necessary to also control the active power of the DG units. In the low-voltage, thus resistive, microgrids, there is a linkage between active power and grid voltage. Hence, a P_{dc}/V_g droop controller is used that changes P_{dc} according to V_g, while avoiding communication and central controllers. Changing P_{dc} can be done in several ways. For instance, P_{dc} can be decreased by storage charging, by lowering the generated power P_{gen}, load increase or by using dump loads. For an increase of P_{dc}, battery discharge, demand-side management (potentially driven by the emerging smart grid concept) or an increase of P_{gen} can be incorporated in the control. The method of changing the power delivered to the dc-link does not inherently change the control method and can be determined according to the specific application. For PV panels for example, the control of the dc-dc converter, e.g., a chopper, including maximum power point tracking (MPPT), is not considered.

The P_{dc}/V_g droop controller only operates when the terminal voltage exceeds a certain threshold voltage, which is determined by the adjustment voltages $V_{g,up}$ and $V_{g,low}$. In case these adjustment voltages are not exceeded, P_{dc} remains unchanged and only the V_g/V_{dc} droop control strategy is used. This operating mode is called constant-power operation. The total width of the constant-power band equals $h = 2b = V_{g,up} + V_{g,low}$. The parameter '$b$' is called 'the constant-power band width' as in this PhD thesis, a symmetrical constant-power band ($h = 2b$) is considered. Summarised, the P_{dc}/V_g droop controller operates according to:

$$P_{dc} = \begin{cases} P_{dc,nom} - K_P(V_g - (1+b)V_{g,nom}) & \text{if } V_g > (1+b)V_{g,nom} \\ P_{dc,nom} & \text{if } (1-b)V_{g,nom} < V_g < (1+b)V_{g,nom} \\ P_{dc,nom} - K_P(V_g - (1-b)V_{g,nom}) & \text{if } V_g < (1-b)V_{g,nom} \end{cases} \tag{4.12}$$

The droop K_P is generally determined according to the ratings of the units, such that $\frac{P_{dc,nom}}{K_P}$ is equal for each DG unit. For constant-current sources, an analogous I_{dc}/V_g droop controller, instead of P_{dc}/V_g droop controller, can be implemented. The index 'nom' refers to nominal values, but is not necessarily equal to the rating of the unit. In the dispatchable DG units, $P_{dc,nom}$ is generally determined according to unit scheduling in the electricity markets. This is often based on (but not necessarily equal to) the ratings of the units, which in turn corresponds to the operating point with optimal efficiency. Hence, $P_{dc,nom}$ can vary in time. For the renewable DG units, $P_{dc,nom}$ generally is the instantaneous maximum power point (MPP), hence, also not constant in time.

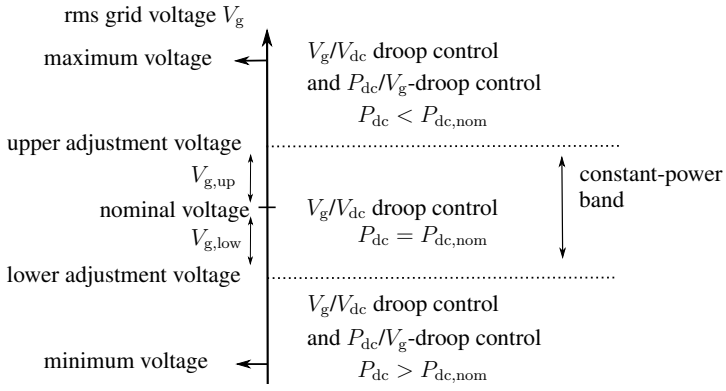

Figure 4.8: P_{dc} control as a function of V_g: adjustment voltages $V_{g,up}$ and $V_{g,low}$

By setting a proper b, VBD control enables an automatic priority allocation for the primary control. Based on the terminal voltage, an example of this priority list for power changes is: 1) dispatchable DG units, 2) storage, 3) highly controllable loads, 4) less dispatchable DG units (including local storage, deviating from the MPP, and local load changes), 5) less controllable loads, 6) load shedding of the other loads.
The combined operation of the V_g/V_{dc} and P_{dc}/V_g droops is shown in Fig. 4.8. This figure shows that if V_g, calculated according to the V_g/V_{dc} droop control, exceeds the upper adjustment voltage $V_{g,nom} + V_{g,up}$, the P_{dc}/V_g droop controller decreases P_{dc}, and it increases P_{dc} if V_g is lower than $V_{g,nom} - V_{g,low}$. In these two conditions, the two droop controllers operate together. Otherwise, with only the V_g/V_{dc} droop controller, P_{dc} remains equal to $P_{dc,nom}$.
An overview of the VBD control strategy is given in Fig. 4.9.

B. Adjustment voltages

The adjustment voltages $V_{g,up}$ and $V_{g,low}$ depend on the flexibility of the power source, which is depicted in Fig. 4.10. This figure shows that the P_{dc}/V_g function is abstract and can be modified according the characteristics of the source.
For example, a distinction can be made between variable and non-variable power sources. For variable, controlled (often non-renewable) power sources, a narrow constant-power band can be handled such that the dispatchable units decrease their output power with increasing voltage and vice versa for low voltages. Therefore, small variations of V_g from $V_{g,nom}$ address the P_{dc}/V_g droop controller to change P_{dc}. This enables to fully exploit the power control capability of the power source. In this way, less voltage variation in the microgrid is obtained as the power source acts dynamically to limit the voltage changes by changing its output power. After a

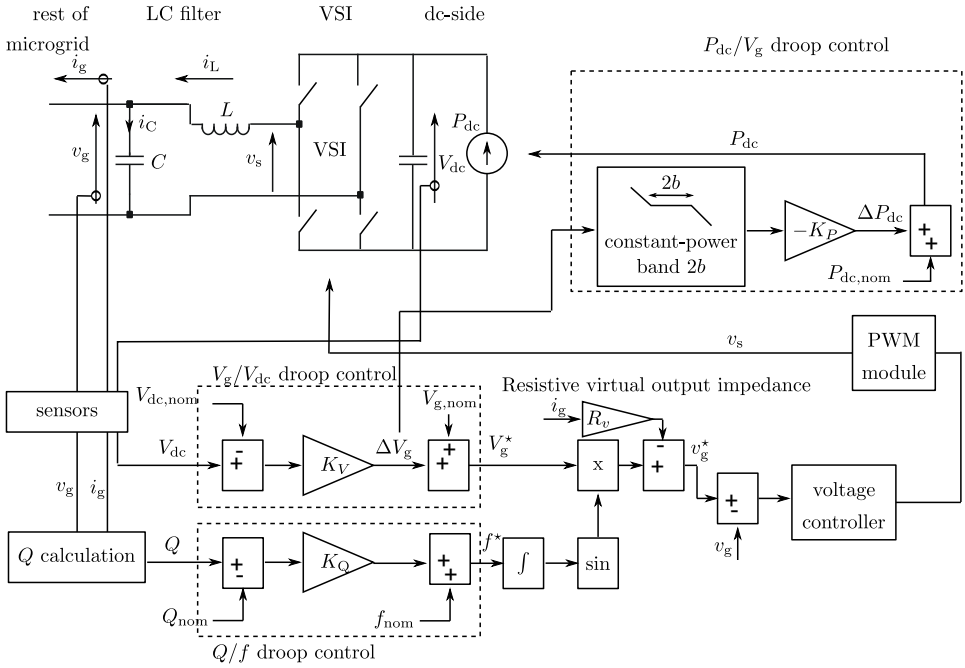

Figure 4.9: VBD control: P_{dc}/V_g droops, Q/f droops, V_g/V_{dc} droop controller and constant-power bands. The resistive virtual output impedance is explained further

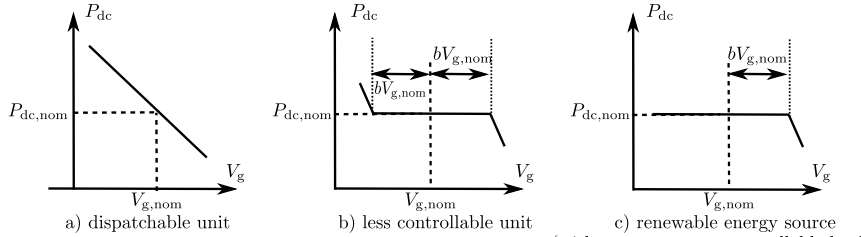

Figure 4.10: Fully dispatchable versus fully undispatchable DG unit. Dispatchable units have a small constant power band; fully undispatchable DG units have a very wide constant-power band.

small load change compared to the scheduled (nominal) load, only these units will act in the power sharing by changing their output power. The less dispatchable DG units will not act as long as their voltage is inside the constant-power bands.

For non-variable or slightly-variable power sources (often intermittent renewable or combined heat and power units with heat as primary driver), a wide constant-

power band can be applied. The variable intermittent, often renewable, units, deliver nominal power to the network in case the voltage is in the constant-power band. Further, in case the terminal voltage exceeds this band, the power of the DG unit is changed, e.g., by including small storage elements, load response, or by abandoning the MPP. E.g., if only a renewable source is present, the power band is characterised according to Fig. 4.10(c) as only a power decrease is possible[2]. Fig. 4.10(b) represents, for example, a combination of a renewable energy source and a controllable load. The power can decrease by the renewable source through deviation from the maximum power point, and a power increase is equivalent with a load decrease (load shifting). By properly setting the constant-power band widths, changing the output power of the less dispatchable power sources is delayed to more extreme terminal voltages compared to the dispatchable DG units. It is only addressed to limit too large voltage variations in the microgrid. Because of the increasing share of renewable energy sources, active dispatching of these units in small-scale microgrids will be required, e.g. to avoid over-voltage tripping. This control strategy makes this possible without inter-unit communication, while still delaying the power changes of the renewables. Note that the width of the constant-power band should be lower than that of the voltage margins. Otherwise, these units will not contribute in the voltage support and the power sharing.
In conclusion, by setting the value b, the priority in which the units react on load variations is automatically set, dependent on variations of the voltage from its nominal value. For small variations, the dispatchable DG units and storage elements (small b) will react. Only for more extreme voltages, the other units, such as controllable loads or renewables will react as well. Hence, with a proper combined usage of $V_{\mathrm{g}}/V_{\mathrm{dc}}$ and $P_{\mathrm{dc}}/V_{\mathrm{g}}$ droop controllers in the VBD control, a higher degree of renewables (contributing in voltage support) and a more efficient usage of the renewable energy (other grid elements such as the loads can act on the voltage as well) can be expected.
As VBD control is a primary control strategy, dealing with the stability of the microgrid, further optimisation can be made by using a secondary controller, e.g., to return to the MPP by changing the consumption or by coordinating the DG units to achieve fuel savings.

Conclusion By combining the $V_{\mathrm{g}}/V_{\mathrm{dc}}$ and P/V_{g} droop controllers, the advantages of both control strategies can be exploited, frequent power changes are avoi-

[2] A nominal operation different from the maximum power point is presently unrealistic from a economics and ecological point of view to capture as much as possible renewable energy. Note that in the future, with a large share of renewable sources, this principle may need to change by operating the renewables just below the MPP to always have some primary reserve and to enable them to participate in the voltage support (high voltages are most likely at times of high renewable energy input).

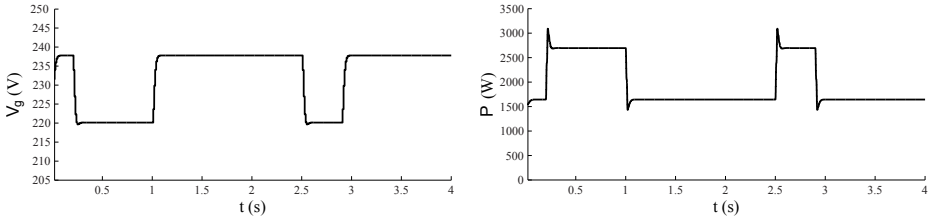

(a) Terminal voltage V_g (b) Output power P

Figure 4.11: One power source: VBD control with $b = 0$ %

ded, no communication for the primary control is required and the tolerated voltage deviation from its nominal value is effectively used for the control without violation of the voltage limits. Also, the VBD controller takes into account the specific characteristics of the islanded microgrid, such as the lack of inertia, resistive lines and high share of renewables. It offers high flexibility to address different kinds of distributed energy resources to ensure a stable microgrid operation. This is achieved in a pre-defined priority list, without need for communication. This control goes beyond the state of the art that uses the fit-and-forget approach for integrating DG, which poses limits on the number of renewable sources in the network.
This active power control strategy of the generators allows to use the microgrid voltage as a trigger for active load control in § 5.1 as the abstract nature of the $P_\mathrm{dc}/V_\mathrm{g}$ droop control makes it possible to use an analogous control in the loads and storage elements as well.

C. Examples

With the $V_\mathrm{g}/V_\mathrm{dc}$ droop controller, a stable microgrid operation is obtained. In order to also avoid voltage limit violation, also a $P_\mathrm{dc}/V_\mathrm{g}$ droop controller is included in the following examples.

One DG unit The same case as in the previous secion (§ A.) is considered, but with VBD control instead of $V_\mathrm{g}/V_\mathrm{dc}$ droop control only.
In a first case, $b = 0$ %, such that the DG unit represents a fully dispatchable unit. The obtained simulation results are depicted in Fig. 4.11. Clearly, the voltage swings are significantly lower compared to the case with only $V_\mathrm{g}/V_\mathrm{dc}$ droop control and the voltage stays inbetween the 10 % limits. The cost of this is a change of output power of the DG unit.
When using a higher constant-power band, e.g., a not fully dispatchable DG unit with $b = 5$ %, the microgrid voltage differs more from its nominal value as is

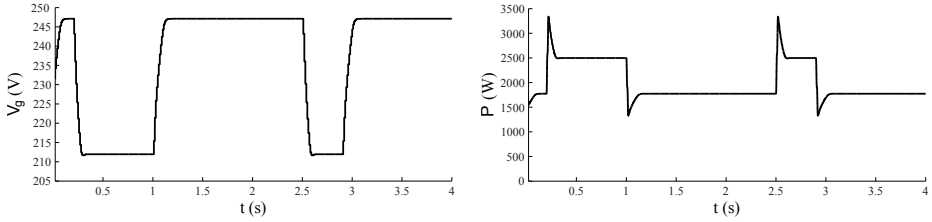

(a) Terminal voltage V_{g} (b) Output power P

Figure 4.12: One power source: VBD control with $b = 5$ %

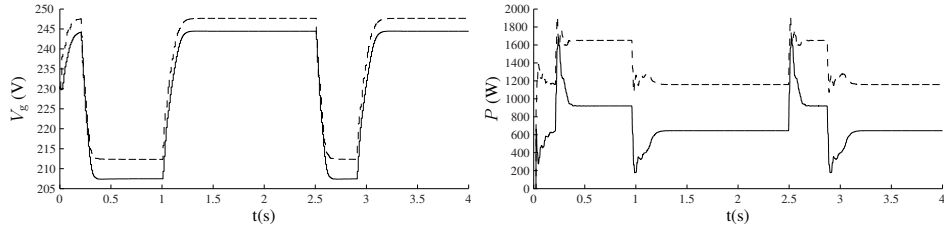

(a) (b)

Figure 4.13: Two power sources: VBD control with $b = 5$ % (— = VSI 1, --- = VSI 2). a) rms microgrid voltage V_{g}, b) power P delivered to the microgrid

shown in Fig. 4.12. Still, no voltage limit violation occurs.

Two DG units The same microgrid configuration as with the $V_{\mathrm{g}}/V_{\mathrm{dc}}$ droop controller is considered. Fig. 4.13 shows the obtained results for the case with $P_{\mathrm{dc}}/V_{\mathrm{g}}$ droop and constant-power bands of 5 %. It is shown that by implementing the $P_{\mathrm{dc}}/V_{\mathrm{g}}$ droop controller, e.g., in case of high voltages, the delivered power is lower than the nominal power to force the voltage closer to its nominal value. In Fig. 4.14, DG 2 has a small constant-power band (0 %), while that of DG 1 remains 5 %. DG 2 reacts more on deviations of the voltage from its nominal 230 V value. Also, the terminal voltage of both units is closer to the nominal voltage.
The same is also simulated where VSI 2 is a current-controlled source, with varying current:

- $t = 0$ s to $t = 0.5$ s: $I_{\mathrm{dc}} = I_{\mathrm{dc,nom}}$
- $t = 0.5$ s to $t = 2$ s: $I_{\mathrm{dc}} = I_{\mathrm{dc,nom}} + I_{\mathrm{dc,var}}$
- $t = 2$ s to $t = 2.2$ s: $I_{\mathrm{dc}} = I_{\mathrm{dc,nom}}$

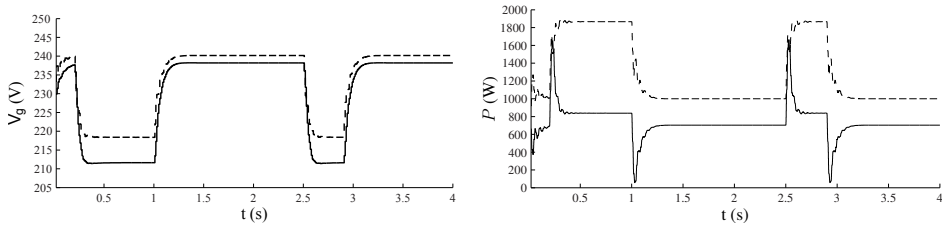

(a) (b)

Figure 4.14: Two power sources: VBD control with $b = 5$ % for DG 1 and $b = 0$ % for DG 2(— = VSI 1, --- = VSI 2). a) rms microgrid voltage V_{g}, b) power P delivered to the microgrid

- $t = 2.2$ s to $t = 3$ s: $I_{\mathrm{dc}} = I_{\mathrm{dc,nom}}/2$
- $t = 3$ s to $t = 3.8$ s: $I_{\mathrm{dc}} = I_{\mathrm{dc,nom}}/2 + I_{\mathrm{var}}$.

$I_{\mathrm{dc,nom}}$ equals 1.5 A and $I_{\mathrm{dc,var}}$ is a randomly varying component (e.g., PV panel with time-varying irradiation), $I_{\mathrm{dc,var}}$ is maximum 10 % of $I_{\mathrm{dc,nom}}$. For VSI 2, the $I_{\mathrm{dc}}/V_{\mathrm{g}}$ droop controller is only activated with a very large constant-power band representing a fully undispatchable DG unit with the only flexibility of fully turning off in case of voltage limit violation. VSI 1 is equipped with the $P_{\mathrm{dc}}/V_{\mathrm{g}}$ droop control with $b = 5$ % and $P_{\mathrm{dc,nom1}} = 1000$ W. To clearly show the effect of the varying output power of VSI 2, the load remains constant and equal to $R = 33\ \Omega$ with $R_{\mathrm{l}} = 1.5\ \Omega$. The obtained results are depicted in Fig. 4.15. From $t = 0$ s to $t = 0.5$ s, the start-up transient is shown. Then, because of the ripple in the generated power of VSI 2, a ripple in the output power P and the microgrid voltage is depicted. Still, a stable operation is obtained, and the changes of the power of VSI 2 are compensated by VSI 1. At $t = 2.2$ s, the output power of VSI 2 significantly decreases, which is also depicted in the microgrid voltage. It is also shown that VSI 1 then increases its output power as the constant-power band of 5 % is exceeded.

Three DG units The simulation case is extended to an islanded microgrid consisting of three power sources depicted in Fig. 4.16. One of these sources is a current-controlled source with $V_{\mathrm{g}}/V_{\mathrm{dc}}$ and $I_{\mathrm{dc}}/V_{\mathrm{g}}$ droop control. A wide constant-power band $b = 10$ % is included in this unit. The other two power sources use a combination of the $V_{\mathrm{g}}/V_{\mathrm{dc}}$ and $P_{\mathrm{dc}}/V_{\mathrm{g}}$ droop control principles with $b = 5$ %. The nominal power of sources 1 and 2 equal 1.2 and 2 kW respectively, while source 3 has current $I_{\mathrm{dc,nom}} = 2$ A for a nominal dc-link voltage of 450 V. In this simulation, the loads consist of a combination of R ($R = 33\ \Omega$), RL (33 Ω//0.5 H) loads,

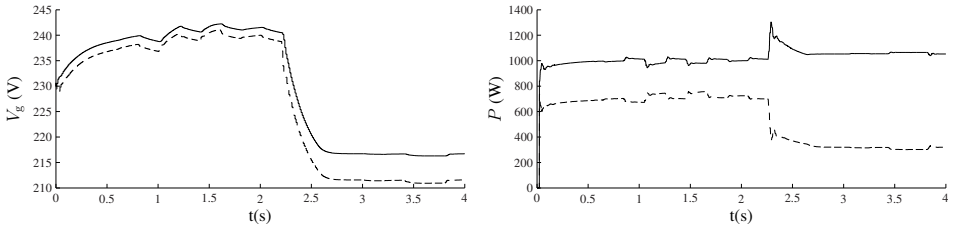

Figure 4.15: Two sources (including variable output of PV panel), constant load, VBD control (— = VSI 1, --- = VSI 2). a) rms microgrid voltage V_g, b) power P delivered to the microgrid

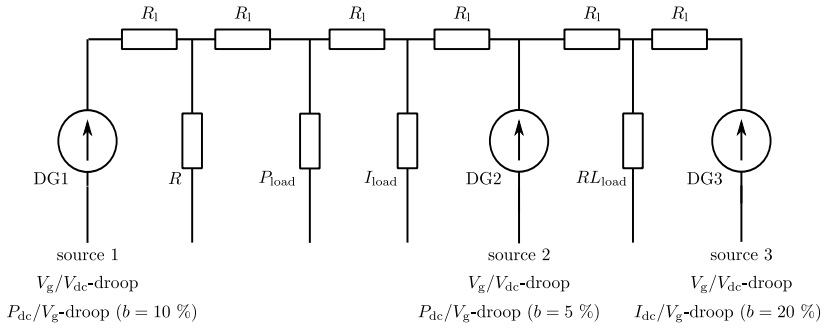

Figure 4.16: Three VSIs: constant-power and current loads

resistive lines ($R_l = 1\ \Omega$), a constant-power load (P_{load}) (845 W, 125 VAr) and a constant-current load ($I_{\text{load}} = 2$ A in phase with the voltage of DG2). Because of the inductive load, also reactive power control in a Q/f droop according to (2.25) (and further discussed in § 4.3) is included. The simulation results are depicted in Fig. 4.17. It is shown that a stable operation is obtained in the extended microgrid. The terminal rms voltage of DG 3 is larger than that of the other two as, in this simulation, the main part of the load is located between the first two sources.

Realistic microgrid configuration Finally, a more realistic microgrid (with respect to the grid configuration) with multiple feeders and different types of DG units is studied. The microgrid configuration is depicted in Fig. 4.18. The DG units vary in the extend to which they are controllable, thus, the constant-power band b varies. Also, both current-controlled and power-controlled sources are included. Furthermore, a dynamical current-controlled source, such as a PV panel, is in-

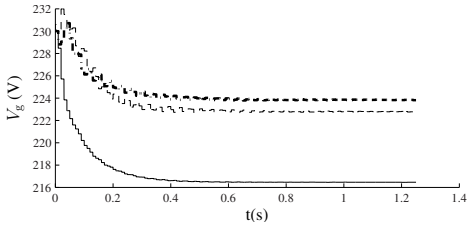

(a) rms microgrid voltage V_{g}

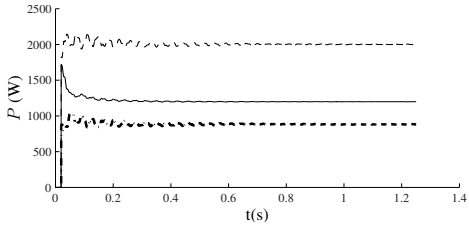

(b) active power P delivered to the microgrid

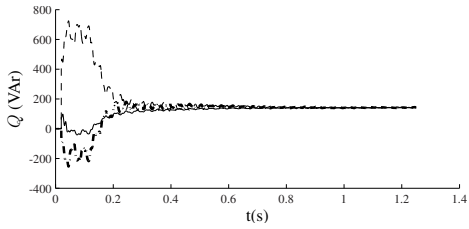

(c) reactive power Q delivered to the microgrid

Figure 4.17: Extended microgrid with VBD control: three power sources, R and RL loads, constant-power load and constant-current load (— = VSI 1, --- = VSI 2, -·-·-· = VSI 3).

cluded in the simulation. This current source delivers 1.5 A from $t = 0$ s until $t = 0.5$ s and then has a linearly increasing current until, at $t = 1.4$ s, $I_{\mathrm{dc},3}$ equals 2.22 A. At $t = 1.4$ s, its output drops to 1.11 A. The details of the other generators are shown in Fig. 4.18, with nominal values: $P_{\mathrm{dc,nom},1} = 1000$ W, $P_{\mathrm{dc,nom},2} = 1500$ W, $P_{\mathrm{dc,nom},4} = 2000$ W, $I_{\mathrm{dc,nom},5} = 3$ A and $P_{\mathrm{dc,nom},6} = 700$ W. Also, a combination of different loads is included, such as constant-power loads, current loads, RL loads and nonlinear loads (NLLs). The NLLs are modelled as single-phase rectifiers. The NLL L_4 and the RL load L_9 turn off after $t = 1.8$ s. From $t = 0$ s to $t = 1$ s, the variable resistive load L_{12} increases in discrete steps, from 500 to 36 Ω.

The simulation results are depicted in Fig. 4.19. From $t = 0$ s to 1.4 s, this simulation clearly shows the linear increase of output power of DG 3, both in P and V_{g}. As the load L_{12} linearly increases as well from $t = 0$ s to $t = 1$ s, the other power sources do not significantly change their output power in this time interval. When the output of DG 3 halves at $t = 1.4$ s, a small transient in power where all other generators slightly increase their output power and a small voltage decrease are clearly shown. At $t = 1.8$ s, when two loads turn off, a clear increase in V_{g} and a transient are shown in the simulation. At the end of the simulation, clearly the output power of the generators is strongly linked with their nominal power, and the changes are forced by the $P_{\mathrm{dc}}/V_{\mathrm{g}}$ droop controller.

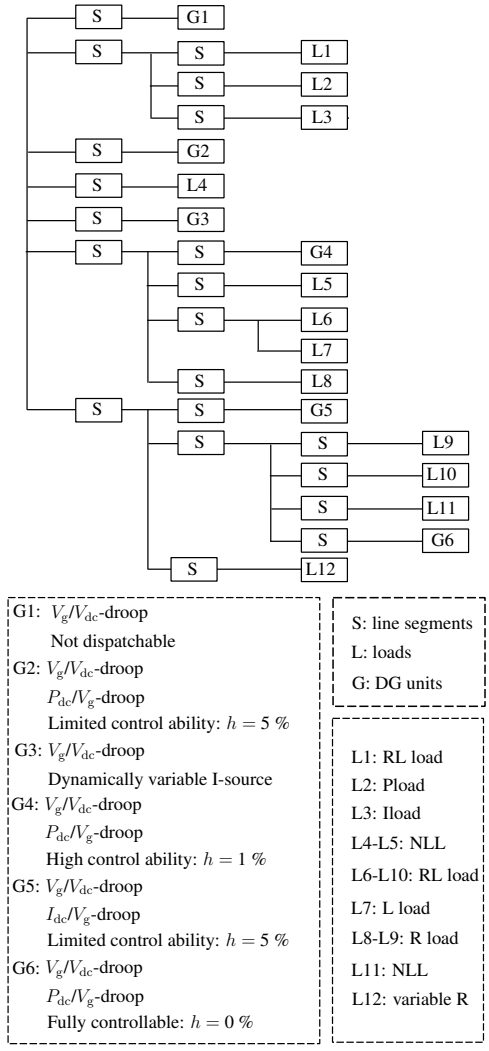

Figure 4.18: Configuration of a realistic microgrid

Extended microgrid: IEEE 13 Node Test Feeder Also, a variant of the IEEE 13 Node Test Feeder in Fig. 4.20 is studied. The IEEE 13 Node Test Feeder is modified for application as a low-voltage network in islanded mode. The simulation details of the nodes are summarised in Fig. 4.21, showing that a combination of various loads (resistive, inductive, constant-power and switching loads) is used. There are three converter-interfaced DG (CIDG) units connected to the feeder, with details summarised in Table 4.10. The units use a resistive virtual output impedance $z_v =$

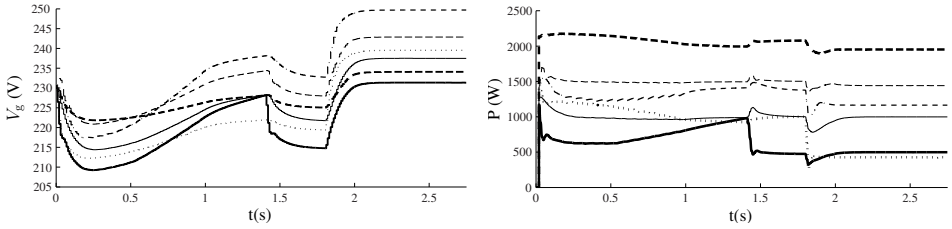

(a) rms microgrid voltage V_{g} (b) active power P delivered to the microgrid

Figure 4.19: Realistic microgrid: six power sources, R and RL loads, constant-power load and constant-current load, variable sources and loads (— = VSI 1, --- = VSI 2, ▬ = VSI 3, ▬ ▬ = VSI 4, -.-.-. = VSI 5, ... = VSI 6).

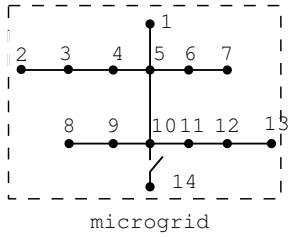

Figure 4.20: IEEE 13 Node Test Feeder

Table 4.3: CIDG units in test feeder: details

CIDG	$P_{\mathrm{dc,nom}}$	constant-power band
CIDG1	$P_{\mathrm{dc,nom},1} = 3.15$,W	$b = 0$ %
CIDG2	$P_{\mathrm{dc,nom},2} = 6$ kW	$b = 0$ %
CIDG3	$P_{\mathrm{dc,nom},3}$:	$b = 8$ %
	t <0.3 s: 6.3 kW	
	t >0.3 s: 4.2 kW	

3Ω, which will be discussed in § 4.2.3. The results are depicted in Fig. 4.22. A stable microgrid operation is obtained. The decreased output power of CIDG3 at $t = 0.3$ s is clearly picked up by the other two DG units. Also, the load decrease at node 16 at $t = 0.4$ s and at nodes 4 and 14 at $t = 0.5$ s lead to acceptable transients that are rapidly mitigated by the VBD controllers.

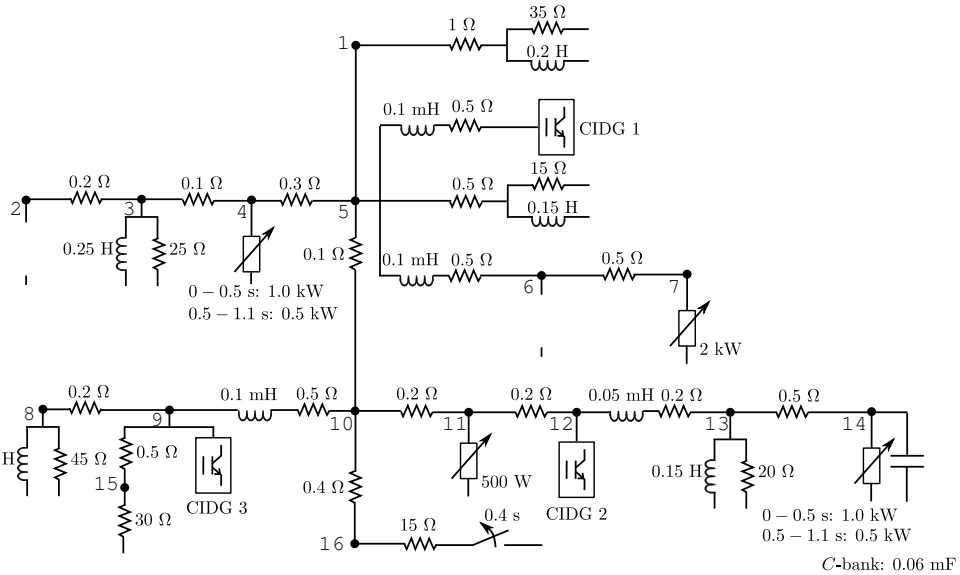

Figure 4.21: Considered 13 Node Test Feeder

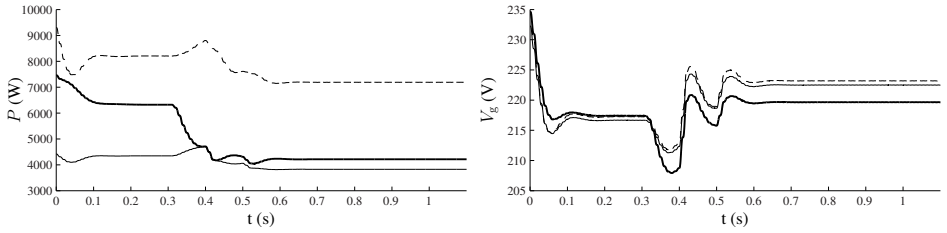

(a) Active power P delivered to the microgrid

(b) rms microgrid voltage V_g

Figure 4.22: Extended microgrid, IEEE 13 node test feeder (— = VSI 1, --- = VSI 2, ▬ = VSI 3)

From these simulations, it is concluded that the controllers obtain a stable islanded microgrid operation, share power according to the droops and constant-power band widths of the sources, limit the voltage, take into account the specific characteristics of the sources by setting the constant-power band, and do no require inter-unit communication.

4.2.3 Resistive virtual output impedance

The previous cases considered line resistances that were relatively high. The reason was that low resistances may provide insufficient damping to achieve a stable microgrid operation. Typical EAXVB cables have a line resistances ranging from 0.1 to $0.4\ \Omega$/km. To deal with low line resistances, the so-called resistive virtual output impedance loop is included in the VBD control strategy.

A. Control principle

The virtual output impedance control loop has been proposed in literature to fix the output impedance of the inverter, to increase the stability of the system and to share linear and nonlinear loads. Therefore, virtual inductive, resistive and complex impedances can be used [113, 114, 116]. In this PhD thesis, a resistive output impedance z_v is chosen as this provides more damping in the system [164] and complies with the power control strategies of the loads and generators, where the active power is changed based on the grid voltage:

$$v_{\mathrm{g,ref}} = v_{\mathrm{g,droop}} - z_v i_g, \tag{4.13}$$

with $v_{\mathrm{g,ref}}$ the reference voltage, which forms the input of the voltage controller, $v_{\mathrm{g,droop}}$ the voltage obtained by the VBD controller and i_g the grid current. The virtual impedance loop is depicted in Fig. 4.23.

B. Examples

The resistive virtual output impedance is included in a basic microgrid and a comparison is made between the cases with and without z_{v}. In the realistic microgrid of Fig. 4.21, z_{v} was already included.
The basic microgrid configuration of Fig. 4.24 is considered, with $R = 25\ \Omega$, $R_{\mathrm{l1}} = 1\ \Omega$ and $R_{\mathrm{l2}} = R_{\mathrm{l3}} = 0.2\ \Omega$. One of the loads turns on after 0.7 s. The voltage controller consists of the two cascaded PI controllers discussed in § 3.3.2. In the first case, VBD control with $P_{\mathrm{dc}}/V_{\mathrm{g}}$ droops is used. The DG units are modelled as power sources, with $K_{\mathrm{P}} = -\sqrt{2}P_{\mathrm{nom}}/50$ W/V, $P_{\mathrm{nom,1}} = 2$ kW, $P_{\mathrm{nom,2}} = 1.5$ kW and both units operate without constant-power band, i.e., are fully dispatchable units. The results in Fig. 4.25 show that in order to cope with small line resistances, virtual output impedance is required to achieve a stable microgrid operation.
The resistive virtual impedance method can also enable the VBD control to cope with inductive lines. The same example as in the previous case is considered, but the lines are not purely resistive anymore, but inductive with $jX = j2\Omega$. First, the case with $z_{\mathrm{v}} = 0$ and second, the case with $z_{\mathrm{v}} = 3\Omega$ (thus $R/X = 1.5$) are

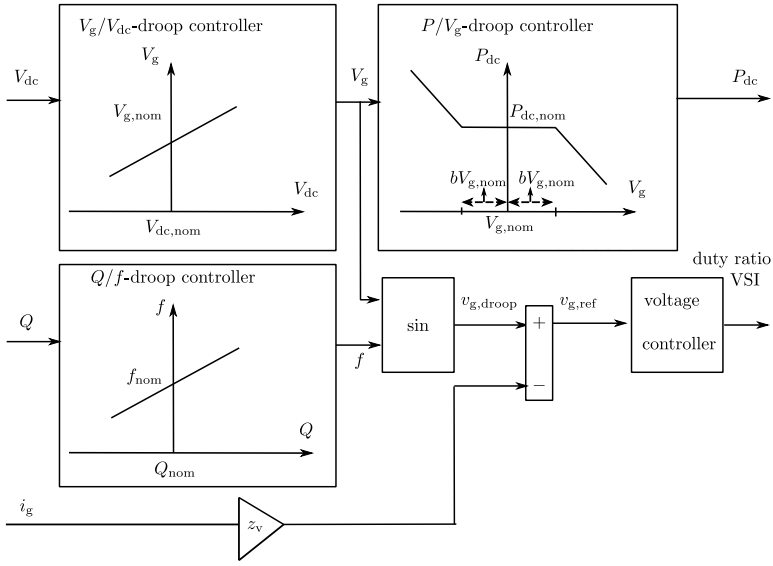

Figure 4.23: Virtual impedance loop in VBD controller

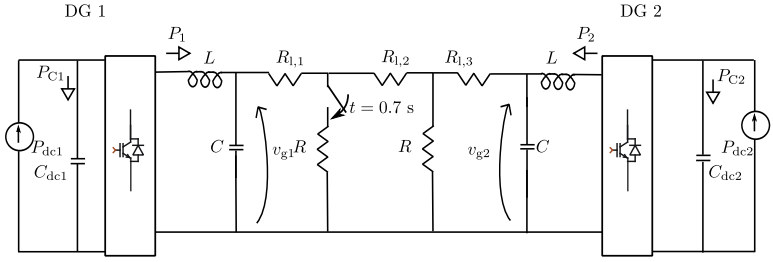

Figure 4.24: Two VSIs with resistive virtual output impedance: microgrid configuration

studied. The results for the case of current sources, with $I_{dc,1} = P_{nom,1}/V_{dc,nom}$, $I_{dc,2} = P_{nom,2}/V_{dc,nom}$, $V_{dc} = 450$ V, $K_p = -\sqrt{2}I_{dc}/50$ A/V, are shown in Fig. 4.26. For power sources, analogous results are obtained.

In conclusion, including resistive virtual impedance stabilises the microgrid control.

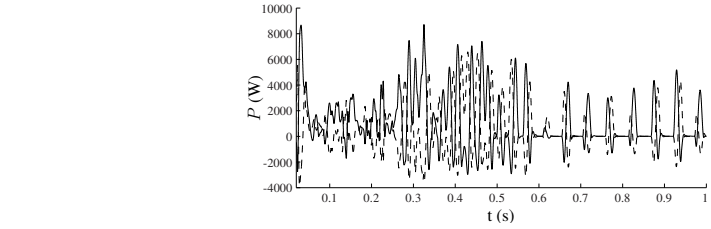

(a) $z_{\mathrm{v}} = 0\Omega$

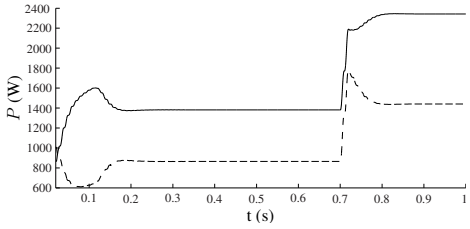

(b) $z_{\mathrm{v}} = 3\Omega$

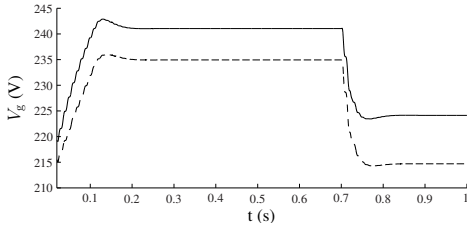

(c) $z_{\mathrm{v}} = 3\Omega$

Figure 4.25: Influence virtual output impedance (— = VSI 1, --- = VSI 2); a,b) active power P delivered to the microgrid; c) rms microgrid voltage V_{g}

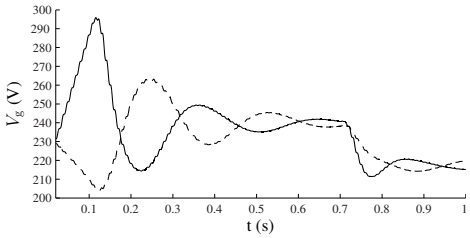

(a) $z_{\mathrm{v}} = 0\Omega$

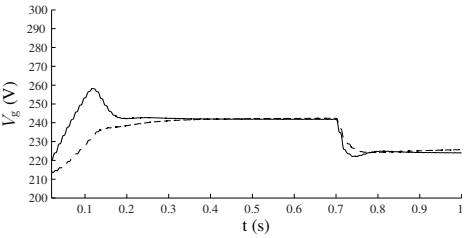

(b) $z_{\mathrm{v}} = 3\Omega$

Figure 4.26: Virtual output impedance to cope with inductive lines, current sources (— = VSI 1, --- = VSI 2); rms microgrid voltage V_{g}

4.3 Reactive power control

In the previous paragraphs, mostly, the loads were considered as purely active power consumers. Of course, also the reactive power needs to be shared between the DG units, e.g., according to their ratings. Analogous to the VBD control, communication should be avoided for the primary reactive power control. The reactive power controller is a reactive power/frequency (Q/f) droop controller.

4.3.1 Control principle

As discussed in § 4.1, the reactive power flow in resistive networks is linked with the phase angle differences over the lines. Hence, in the considered microgrids, the reactive power of the power sources can be controlled by a Q/f droop. From (4.6b), an increase of Q leads to a decreased phase angle δ_1 of the voltage of the power source. Note that this statement is valid from a generators point of view for the current reference, with a positive current flowing from generator to load. A possible droop characteristic for two VSIs is shown in Fig. 4.27(a), with positive slopes K_{Q} as the relationship reactive power/voltage phase angle or frequency in (4.6b) has a minus sign:

$$f = f_{\mathrm{nom}} + K_{\mathrm{Q}}(Q - Q_{\mathrm{nom}}) \tag{4.14}$$

By using the obtained value of f, the reference voltage $v_{\mathrm{g,ref,droops}}$ is determined according to (4.28).

Starting from $Q_1 = Q_2 = 0$ VAr for example, the microgrid settings change, causing an increase of Q with ΔQ in Fig. 4.27(b). In this example, the controller of VSI 2 reacts very fast compared with VSI 1. Therefore, this second inverter changes its settings to deliver all the extra reactive power ΔQ: $Q_2 = \Delta Q$, while Q_1 remains zero. Therefore, starting from $f_1 = f_2 = 50$ Hz while Q was zero, now, $f_2 > f_1$. Accordingly, the angle of the grid voltage of VSI 2 will keep increasing compared to that of VSI 1. From (4.6b), it follows that the delivered Q of VSI 2 will decrease, while Q_1 increases. With the Q/f droop, this will induce an increase of f_1 and a decrease of f_2 until $f_1 = f_2 = f_{\mathrm{e}}$ in the steady-state condition of Fig. 4.27(c). In steady-state, the reactive power will be shared according to the droop characteristics of the primary energy sources and independent of the time constant of the units. In this example, VSI 2 will deliver the major part of the reactive power change as its slope is smaller.

4.3.2 Examples

In the following example, two primary energy sources, with $P_{\mathrm{dc,1}} = 1400$ W and $P_{\mathrm{dc,2}} = 2800$ W are paralleled with the islanded microgrid shown in Fig. 4.28. As the reactive power is studied, only the $V_{\mathrm{g}}/V_{\mathrm{dc}}$ droop controller is implemented in the units. The microgrid load is represented by two RL-elements connected to the generators and each other via line resistances as shown in Fig. 4.28, with $R_{\mathrm{l,1}} = R_{\mathrm{l,2}} = 0.4\ \Omega$, $R_{\mathrm{l,3}} = 0.2\ \Omega$ and for the loads $Z_{\mathrm{load,1}}$ and $Z_{\mathrm{load,2}}$: $L = 0.1$ H and $R = 25\ \Omega$. The inverters start-up from 230 V at $t = 0$ s.

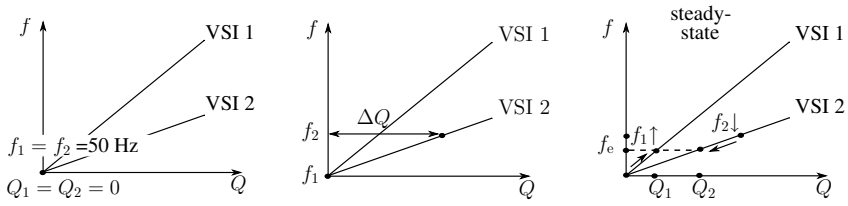

(a) VSIs with different slopes for Q/f droop control

(b) Microgrid change with ΔQ: initially delivered by VSI 2

(c) Steady-state, the VSIs operate at the same frequency

Figure 4.27: Q/f droop of two VSIs

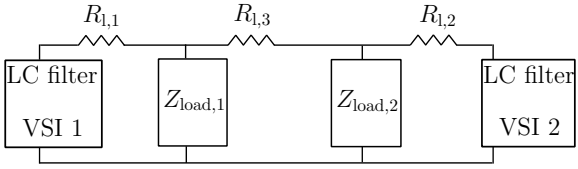

Figure 4.28: Microgrid load

A. Without Q-control

In this case, only the active power of the VSIs is controlled, while the reactive power control is not considered.

Symmetrical microgrid configuration In this first simulation, the microgrid configuration as described above is applied, which is symmetrical as $R_{\mathrm{l},1} = R_{\mathrm{l},2}$ and $Z_{\mathrm{load},1} = Z_{\mathrm{load},2}$. As Q/f droops are not yet included, both inverters deliver grid voltage $V_{\mathrm{g,i}} \sin(2\pi f_0 t)$, with $i = 1, 2$, $f_0 = 50$ Hz and $V_{\mathrm{g,i}}$ determined by the $V_{\mathrm{g}}/V_{\mathrm{dc}}$ droop controller for active power balancing. The frequency of both inverters is equal and remains constant, such that their grid voltages remain in phase.
The reactive power delivered by both power sources is depicted in Fig. 4.29(a). The determination of power is only accurate after one fundamental period, hence the initial value of zero. In steady-state, both sources deliver reactive power to the grid with $Q_1 = 824$ VAr and $Q_2 = 2425$ VAr. The exact reactive power distribution is determined by the microgrid characteristics and the grid voltage amplitude of the VSIs. As $P_2 > P_1$, the $V_{\mathrm{g}}/V_{\mathrm{dc}}$ droop controller forces $V_{\mathrm{g},2} > V_{\mathrm{g},1}$ and, thus with (4.6b), $Q_2 > Q_1$.
During start-up, for the second power source, the power P_2 injected into the microgrid is lower than its generated power $P_{\mathrm{dc},2}$. Therefore, the dc-bus voltage of this power source increases as shown in Fig. 4.29(d), and the active power $V_{\mathrm{g}}/V_{\mathrm{dc}}$

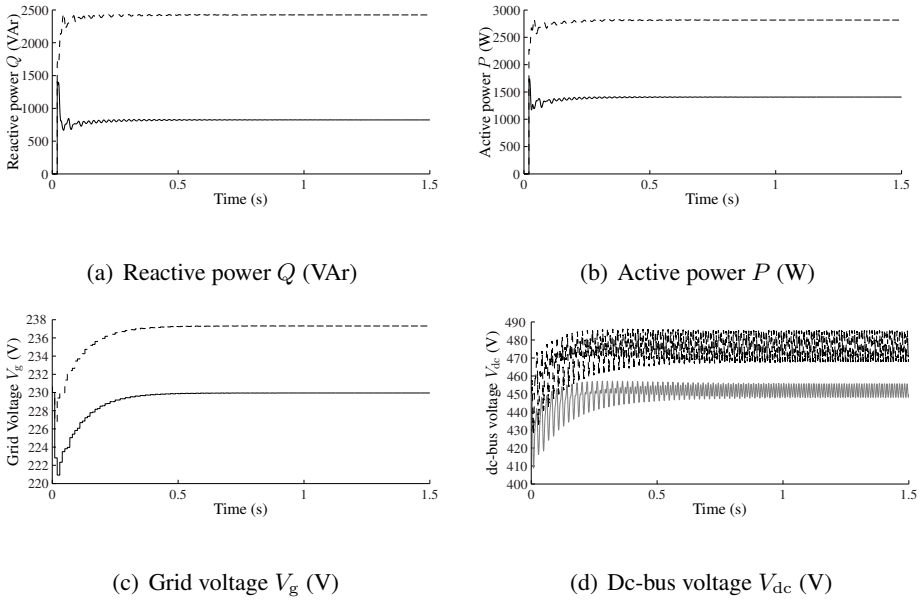

(a) Reactive power Q (VAr)

(b) Active power P (W)

(c) Grid voltage V_{g} (V)

(d) Dc-bus voltage V_{dc} (V)

Figure 4.29: P control, no Q control, symmetrical microgrid (— = VSI 1; --- = VSI 2)

droop controller increases V_{g} in Fig. 4.29(c). This process goes on until steady-state is reached, with $P_1 = P_{\mathrm{dc},1}$ and $P_2 = P_{\mathrm{dc},2}$ in Fig. 4.29(b). Because of the full-bridge configuration of the single-phase microgrid, a 100 Hz bus ripple is shown in V_{dc}.

Asymmetrical microgrid configuration In this simulation, the microgrid is asymmetrical as the line impedances are different: $R_{\mathrm{l},1} = 0.4\Omega$ and $R_{\mathrm{l},2} = 0.8\Omega$. The terminal voltage does not change significantly ($V_{\mathrm{g},2}$ becomes 238.1 V instead of the previous 237.3 V and $V_{\mathrm{g},1}$ remains the same) because the loads remain the same. Hence, following from the load flow equations, the increased line resistance near DG2, will lead to this unit delivering less reactive power to the network than DG1. This is also shown in the simulation as in steady-state, the delivered reactive powers are $Q_1 = 1490$ VAr and $Q_2 = 1708$ VAr, see Fig. 4.30. In this way, the amount of reactive power delivered to the network becomes significantly dependent on the line impedance. Q/f droop control solves this issue.

B. With Q-control

In the following simulations, the Q/f droop control principle is implemented in each VSI. The reactive power Q injected into the grid is measured and its value is

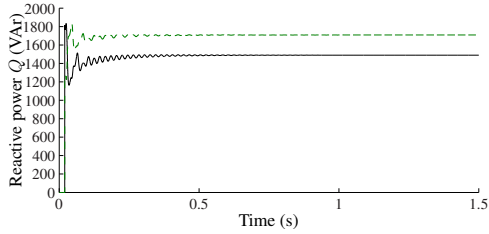

Figure 4.30: P control, no Q control, asymmetrical microgrid: reactive power Q (VAr) (—- = VSI 1; ---- = VSI 2)

drooped in order to define the grid voltage frequency f. Several cases of the slope are examined:

- $K_{\mathrm{Q},1} = K_{\mathrm{Q},2} = 5 \cdot 10^{-5}$ Hz/VAr;
- $K_{\mathrm{Q},1} = 2 \cdot K_{\mathrm{Q},2}$;
- $K_{\mathrm{Q},2} = 2 \cdot K_{\mathrm{Q},1}$.

The $V_{\mathrm{g}}/V_{\mathrm{dc}}$ droop controller is turned on at $t = 0$ s and the reactive power droop controller is started after 100 ms to clearly show its effect. Some cases are studied in order to show that droop control is required for two reasons. Firstly, without droop control, the reactive power sharing becomes very dependent on the line characteristics (part A). Secondly, droop controllers can avoid high circulation currents (parts B and C).

A. Influence of droop First, the symmetrical microgrid is considered and the following results are obtained.

A. 1. $K_{\mathrm{Q},1} = K_{\mathrm{Q},2}$ The delivered reactive power is depicted in Fig. 4.31(a), where it is shown that in steady-state, both VSIs deliver the same Q: $Q_1 = Q_2 = 1629$ VAr. During start-up, the simulations show that $Q_2 > Q_1$. The reason is that the grid voltage $V_{\mathrm{g},2}$ is higher than $V_{\mathrm{g},1}$ because of the $V_{\mathrm{g}}/V_{\mathrm{dc}}$ droop effect as the second power source delivers more P. As $Q_2 > Q_1$, after 100 ms, the Q/f droop controller induces $f_2 > f_1$ as is shown in Fig. 4.31(b) and, thus, Q_2 will decrease while Q_1 increases.
The terminal voltage and output active power are shown in Figs. 4.31(c) and 4.31(d) respectively. The transients are analogous to the previous case and in steady-state: $P_1 = P_{\mathrm{dc},1}$ and $P_2 = P_{\mathrm{dc},2}$ because only the $V_{\mathrm{g}}/V_{\mathrm{dc}}$ droops are included. As the generated power of VSI 2 is larger than that of VSI 1, $V_{\mathrm{g},2} > V_{\mathrm{g},1}$ in this symmetrical microgrid configuration.

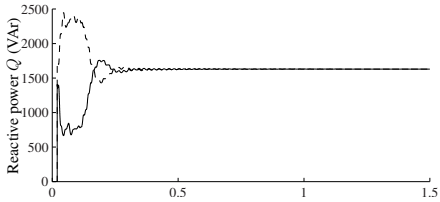

(a) Reactive power Q (VAr)

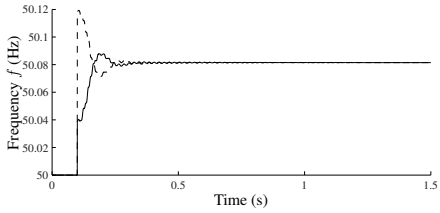

(b) Frequency f (Hz)

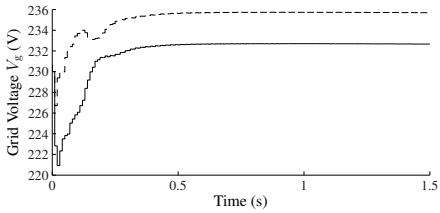

(c) Grid voltage V_{g} (V)

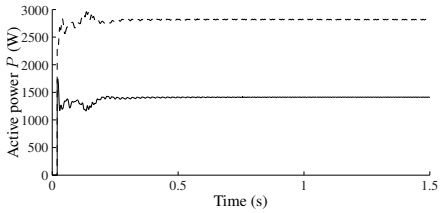

(d) Active power P (W)

Figure 4.31: Q and P-control, $K_{\mathrm{Q},2} = K_{\mathrm{Q},1}$ (— = VSI 1; ---- = VSI 2)

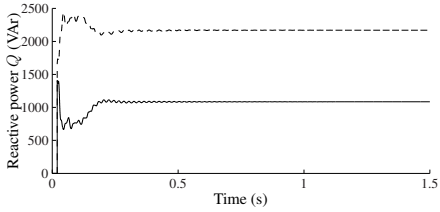

(a) Reactive power Q (VAr)

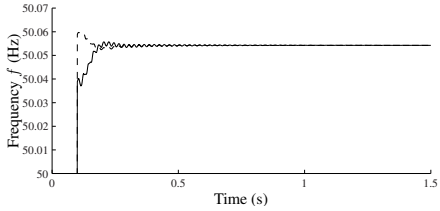

(b) Frequency

Figure 4.32: Q and P-control, $K_{\mathrm{Q},1} = 2K_{\mathrm{Q},2}$ (— = VSI 1; ---- = VSI 2)

A. 2. $K_{\mathrm{Q},1} = 2K_{\mathrm{Q},2}$ The reactive power injected into the microgrid is depicted in Fig. 4.32. As the slope of VSI 2 is smaller than that of VSI 1, in steady-state conditions, Q_2 will be higher than Q_1 and the simulations prove that $Q_2 = 2Q_1$. The details are summarised in Table 4.4.

A. 3. $K_{\mathrm{Q},2} = 2K_{\mathrm{Q},1}$ As the slope of the droop characteristic of VSI 1 is smaller than that of VSI 2, $Q_1 > Q_2$, see Table 4.4.

Table 4.4: Q injection into the symmetrical microgrid

	Q_1 (VAr)	Q_2 (VAr)
Without Q-control	824	2425
With Q-control ($K_{\mathrm{Q},1} = K_{\mathrm{Q},2}$)	1629	1629
With Q-control ($K_{\mathrm{Q},1} = 2K_{\mathrm{Q},2}$)	1085	2170
With Q-control ($2K_{\mathrm{Q},1} = K_{\mathrm{Q},2}$)	2170	1085

A. 4. Q-limitation In this simulation, the case with $K_{\mathrm{Q},1} = K_{\mathrm{Q},2}$ is studied under the symmetrical microgrid and with the implementation of a Q-limiting function. The droop characteristic is now composed of a piece-wise linear curve. If the reactive power of unit 1 surpasses a certain limit, the slope increases, limiting the reactive power. In this simulation, if Q_1 exceeds 1500 VAr, the droop increases with a factor 10. For the case without Q limitation, it was shown that $Q_1 = Q_2$, but because of the Q limitation of VSI 1: $Q_1 < Q_2$, i.e., $Q_1 = 1503$ VAr and $Q_2 = 1630$ VAr.
In the asymmetrical microgrid, the Q/f droop controller obtains reactive power sharing according to the droops as well, e.g., if $K_{\mathrm{Q},1} = K_{\mathrm{Q},2}$, $Q_1 = Q_2 = 1602$ VAr and for $K_{\mathrm{Q},1} = 2K_{\mathrm{Q},2}$, $Q_1 = 1053$ VAr and $Q_2 = 2Q_1 = 2106$ VAr. In this way, the reactive power sharing is independent of the line characteristics. Without Q/f droops, the reactive sharing was determined by the microgrid configuration, i.e., $Q_1 = 1490$ VAr and $Q_2 = 1708$ VAr.

B. (Initial) Phase difference Generally, before connecting a new VSI to the microgrid, it is synchronised to it. Due to, e.g., a problem in this synchronisation procedure, the phase of the microgrid and the VSI voltage may not match, which can lead to circulating currents if there is no Q control in the resistive network. In the following simulations, this is studied as VSI 2 is switched on with a voltage angle that is different from the microgrid voltage angle, or equivalently, the phase angles of the paralleled VSIs differ.

B. 1. With Q-control: $K_{\mathrm{Q},2} = K_{\mathrm{Q},1}$ In this simulation, the initial voltage-phase of VSI 2 is 5 degrees higher than that of VSI 1. This phase difference will be cleared by the reactive power controller. Still, reaching steady-state is delayed compared to the case with $\delta \approx 0$ due to this phase difference.
Fig. 4.33(a) shows the reactive power injected into the microgrid. Due to the initial phase difference, initially, circulating currents are obtained, this can be seen in the

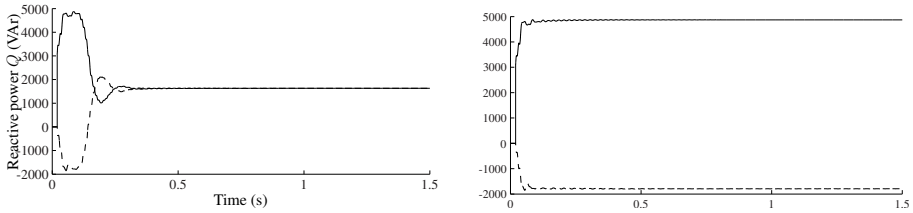

(a) P and Q-control, $K_{\mathrm{Q},2} = K_{\mathrm{Q},1}$ (b) P-control, no Q control

Figure 4.33: Phase difference 5 degrees: reactive power Q (— = VSI 1; ---- = VSI 2)

large values of Q and the different sign of Q_1 and Q_2. As VSI 2 initially leads VSI 1 by 5 degrees, the initial reactive power delivered by VSI 2 is smaller than that of VSI 1, which follows from (4.6b). Nevertheless, after this start-up transient, a steady-state is obtained, where $Q_1 = Q_2$ as $K_{\mathrm{Q},1} = K_{\mathrm{Q},2}$.

B. 2. Without Q-control The phase difference between the sources is also simulated for the case that no Q-control is implemented, and the results are shown in Fig. 4.33(b). Unlike with Q-control, this phase difference is not eliminated by the controllers. Therefore, it results in large circulating currents, even in steady-state.

C. Frequency difference In the following paragraph, a frequency difference between the power sources is simulated, which can be due to, e.g., the crystal-clock tolerances causing a mismatch of the set value of 50 Hz. This can also lead to circulating currents if this frequency difference is not eliminated. In the following simulations, the frequency of VSI 1 equals exactly 50 Hz. VSI 2 operates at 50.01 Hz, while assuming that a 50 Hz waveform is achieved.

C. 1. With Q-control: $K_{\mathrm{Q},2} = K_{\mathrm{Q},1}$ The frequency difference will be cleared by the reactive power controller. This results in transients that are larger and have a longer duration compared to the case without frequency difference, but does not result in large circulating power flows as shown in Fig. 4.34(a). In steady-state, $f_2 = f_1$, but: $f_{2,nom} = 50.01$ Hz $> f_{1,nom} = 50$ Hz, leading to $Q_2 < Q_1$ in accordance with (4.14), even with $K_{\mathrm{Q},2} = K_{\mathrm{Q},1}$.

C. 2. Without Q-control Unlike with Q-control, the frequency difference is not eliminated by the power controller. The phase angle difference will keep increasing. Therefore, it results in large circulating currents and reactive power flows as shown in Fig. 4.34(b).

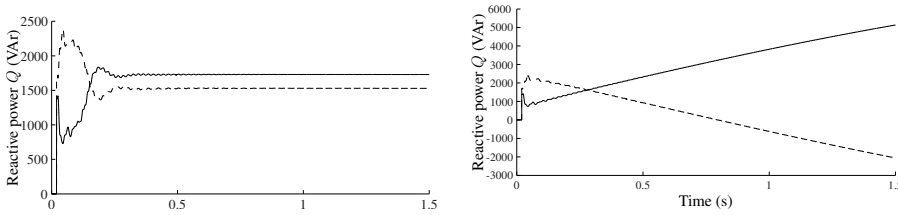

(a) Q and P control (b) P control, no Q-control

Figure 4.34: Initial frequency difference: reactive power Q (VAr) (— = VSI 1; ---- = VSI 2)

4.4 Harmonic power sharing

The VBD control strategy[3] achieves active and reactive power balancing and sharing between multiple DG units in islanded microgrids. However, to deal with harmonic and nonlinear loads, the power control strategies of chapter 2 in general, and the VBD control strategy specifically, need to be modified. Otherwise, the DG units that are voltage-controlled form short-circuits for harmonic currents. Therefore, in this section, the shunt harmonic impedance method for harmonic damping in the grid-connected mode is adapted for application in islanded microgrids. The VBD control strategy of the DG units is extended with programmable resistive behaviour towards harmonics. In this way, harmonic current sharing between the DG units can be achieved in a controllable manner, e.g., according to the ratings of the units.

4.4.1 Introduction and literature overview

The controllers that are developed for the DG units in islanded microgrids mainly focus on the fundamental active and reactive power sharing. However, two important issues that need to be addressed as well are the power quality and harmonic current sharing. The usage of converter-based DG units, combined with a large amount of nonlinear and unbalanced loads, can contribute to a degraded power quality [165–167]. Many types of power-electronic equipment produce current harmonics, distorting the line voltage, which may propagate throughout the distribution system and cause unfavourable effects [168]. In small-scale electrical networks, such as islanded microgrids, the ratio harmonic distorted loads versus

[3]The VBD control strategy consists of the $V_{\mathrm{g}}/V_{\mathrm{dc}}$ and $P_{\mathrm{dc}}/V_{\mathrm{g}}$ droop controllers combined with a Q/f droop controller, a voltage controller, a virtual output impedance loop and constant-power bands.

linear loads can be larger than in the large electrical networks. The resulting effect is even more manifest in networks with high line impedances, such as the low-voltage distribution networks considered here, because the nonlinear currents these loads extract lead to larger harmonic voltage drops. Power quality is, thus, an important issue in microgrids [17]. To mitigate the adverse impacts, common methods such as network upgrade can show good results but are costly [169]. For filtering, both passive and active filtering techniques have been studied, a review of active power filters is given in [170, 171]. Traditional active-power filters (APFs) are located in the proximity of large nonlinear loads to generate harmonic currents of the same amplitude and opposite phase as those of the load. These techniques can be based on the instantaneous reactive power theory [172]. Another possibility to compensate a nonlinear load can be based on APFs that are controlled by neural filtering [166]. Also, central APFs can be uses to mitigate harmonic propagation [165, 173].

Instead of installing APFs especially designed to improve the power quality, DG units can have a positive effect as well. For the grid-connected operation of a microgrid, in literature, several methods to achieve harmonic mitigation in a network by using ancillary services from inverter-interfaced DG units are discussed. In [174], the DG units in the microgrid are equipped with a power quality compensator, consisting of both a shunt and a series inverter to enhance the power quality of the microgrid. In [149, 175], a resistive-APF functionality is included in several DG units with adjustable damping at harmonic frequencies. In [176, 177], the shunt harmonic impedance (SHI) method with programmable harmonic resistance (PR), the PR-SHI method, is presented to redesign the converter-connected DG units to have a positive effect on the distortion of the electrical network. The above-mentioned methods have been presented for converters that are connected to the utility network. These methods can be used or modified for application in an islanded microgrid, e.g., by using the PR-SHI method in some grid-following units in an islanded microgrid to achieve a good power quality. However, achieving controllable harmonic current sharing between different DG units is not dealt with by these methods.

When using droop control (P/f droops, P/V droops or VBDs), the harmonic load is not shared in a controllable manner. Instead, as the grid-forming DG units deliver sinusoidal voltages with fundamental frequency, they almost form short-circuits for harmonic currents. An interesting method to share the harmonic burden is the usage of G-H droops, with G the harmonic conductance and H the harmonic var (volt-ampere reactive), in [14]. The harmonic power H is calculated according to the instantaneous reactive power theory [123]. This method is based on inductive lines, thus the G-H droop control cooperates with P-f and Q-V droop controllers for the fundamental components. In [137], this is extended with G-H droops in

combination with P-V and Q-f droops in resistive microgrids. In [108], a current harmonic loop is added in the control strategy for properly sharing nonlinear loads. Selective harmonic current sharing is used such that the significant output-current harmonics are treated separately by using band-pass filters.
In this section, the PR-SHI method of [176–178], that is developed for improving the power quality in the grid-connected mode, is modified to enable non-selective controllable harmonic current sharing in islanded microgrids. Therefore, based on the PR-SHI method, an extra term dependent on the distorted current is added to the reference voltage that is provided by the VBD control strategy. With the combination of the VBD control and the modified PR-SHI method, the DG units have a controllable resistive behaviour towards harmonics. By changing the PR, the harmonic current sharing can be influenced, e.g., according to the ratings of the DG units. The advantages of the PR-SHI method in grid-connected mode, namely, easy to interpret and implement, and a swift extraction of the distorted current, are combined with the advantages of the droop-based control, e.g., no communication required for fundamental power and harmonic current sharing.
By changing the VBD control strategy of the DG units with a modified version of the PR-SHI method, controllable harmonic current sharing between DG units is achieved in islanded microgrids. In this section, first an overview of PR-SHI in grid-connected mode is given, next the modified PR-SHI for islanded microgrids, that is implemented in the VBD control strategy, is presented. Finally, some examples are discussed.

4.4.2 PR-SHI for grid-connected DG units

In the grid-connected case, the DG units behave as so-called grid-following units that are current-controlled. A specified amount of power, often determined by MPPT, is injected into the electric power system by measuring the grid voltage and controlling the injected current. Often unity power factor is used.
In the traditional power system, the power sharing, and thus the harmonic sharing, is mainly a task of the central generators and centrally designated devices. In [165], a shunt harmonic impedance (SHI) is proposed as a central damper for grid resonance. This converter is designed to behave as a low grid impedance for harmonics and an open chain for the fundamental component of the grid voltage [176]. The PR-SHI method of [176,177] does not use designated devices, but utilises a secondary control function in the DG units to add damping into the system in a distributed manner.
With the PR-SHI method, converter-connected DG systems behave as controlled resistive impedances for harmonic voltage components while also delivering fundamental power to the power system. The PR-SHI method uses a phase-locked loop (PLL) to extract the nominal voltage (fundamental component with nominal amp-

litude) from the measured voltage. A current is then injected which constitutes of two components. The first component represents the fundamental component to inject a specified amount of power in the network as grid-connected mode is assumed for the PR-SHI method. The second component is proportional to the voltage distortion in order to obtain a resistive behaviour towards voltage harmonics and to include harmonic damping. The control strategy is summarised in Fig. 4.35. The reference value of the inductor current $i_{\mathrm{L}}^{\star}(t)$ can be written as:

$$i_{\mathrm{L}}^{\star} = g_1 V_{\mathrm{g,nom}} \sin\theta_{\mathrm{PLL}} + g_{\mathrm{h}}(v_{\mathrm{g}} - V_{\mathrm{g,nom}} \sin\theta_{\mathrm{PLL}}), \tag{4.15}$$

with $V_{\mathrm{g,nom}}$ the nominal amplitude of the grid voltage $v_{\mathrm{g}}(t)$, g_1 the fundamental conductance (in Ω^{-1} or S) and g_h the harmonic conductance (Ω^{-1}). The phase angle θ_{PLL} of the sinusoidal reference signal is locked to the phase of the fundamental component of the mains voltage by using a PLL.

Eq. (4.15) is discussed in [179]. The first term of this equation, $g_1 V_{\mathrm{g,nom}} \sin\theta_{\mathrm{PLL}}$, represents the fundamental current. The second term reacts on every deviation from v_{g} compared to its nominal value $V_{\mathrm{g,nom}} \sin\theta_{\mathrm{PLL}}$. As discussed in [179], this allows for the DG unit to inject harmonic currents proportional to the amount with which the grid voltage is distorted. This may lead to an improvement in the harmonic distortion of the feeder. The second term also becomes non-zero when a voltage dip occurs. Then, the DG unit will contribute in grid support by injecting a higher current. In [160], this method is extended for unbalanced networks. The second term is adapted for its three-phase application and enables to provide grid support in the unbalanced systems. Hence, when applied in grid-connected networks, the amount of voltage waveform improvement that can be obtained by one unit is limited by the ratings of the unit. However, the total power quality improvement can be significant because of the large number of DG units [179].

The conductance g_1 is adapted by the dc-link voltage controller to obtain a constant dc-bus voltage V_{dc}, because the DG units are modelled as dc-current sources I_{dc}. In this way, the generated dc-power is equal to the ac power delivered to the electrical network, and the dc-link voltage remains constant. The value $i_{\mathrm{L}} - i_{\mathrm{L}}^{\star}$ is sent to a current controller. The output of this controller, together with a duty ratio feed-forward δ_{ff} term according to [154], forms the duty ratio for the pulse-width modulator.

By using the PR-SHI method, a programmable harmonic input impedance is achieved, which can be used to reduce the harmonic distortion in the utility grid [180]. The PR-SHI control strategy also allows the setting of a harmonic input resistance (g_h^{-1}) independent of the fundamental input impedance, and thus, independent of the power level of the converter [176, 180]. Hence, the converter is able to maintain its damping potential over a wide range of power levels. This PR-SHI method is very promising because it may swiftly extract the distorted voltage, without neces-

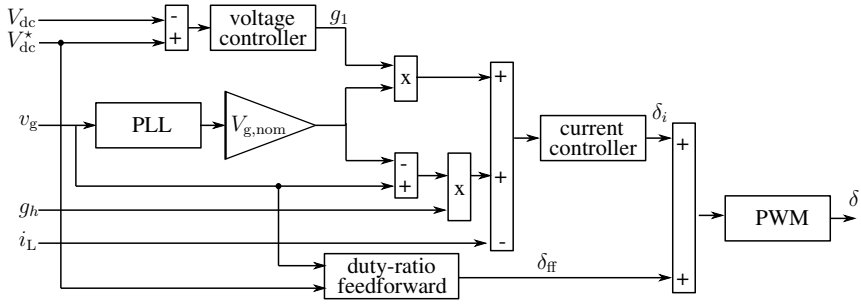

Figure 4.35: Harmonic damping for grid-connected DG units

sity of the instantaneous reactive power theory, and also, the two components in the injected current are easy both to interpret and to implement in practice. The benefits of this control strategy have been discussed in [160, 168, 175, 180, 181].

4.4.3 PR-SHI for islanded microgrids: control principle

In islanded microgrids, the considered DG units are grid-forming, as opposed to the grid-following units in the grid-connected mode. The voltage at their terminals is controlled according to the VBD control strategy. This droop controller enables fundamental active and reactive power sharing but does not deal with harmonic issues. Therefore, the grid-forming DG units in the islanded microgrid can be represented as short-circuits for harmonic currents. In order to achieve controllable harmonic current sharing, the PR-SHI method is modified for usage in islanded microgrids. With the combination of the VBD control strategy and the modified PR-SHI method, fundamental power sharing, voltage control and harmonic current sharing between multiple DG units are achieved.
Summarised, the PR-SHI method, which was developed for improving the voltage quality (unbalance mitigation, grid support in case of voltage dips and improvement of harmonic distortion) in grid-connected networks, is here adapted for application in islanded microgrids, targeting at achieving a controllable sharing of harmonics in the microgrid.

A. Combination of VBD control and modified PR-SHI

In order to achieve controllable harmonic current sharing, the control principle of Fig. 4.36 is used. An extra term $v_{\rm g,h}$ (h are the harmonic components) determined

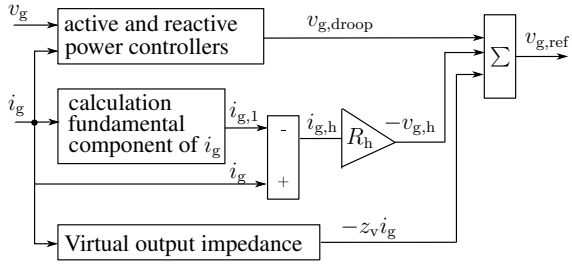

Figure 4.36: Control scheme harmonic power sharing islanded mcirogrid

by the harmonic loop is added to the reference voltage of the VSI, $v_{\mathrm{g,ref}}$, such that:

$$v_{\mathrm{g,ref}} = v_{\mathrm{g,droop}} - z_v i_g - v_{\mathrm{g,h}}. \tag{4.16}$$

The term $v_{\mathrm{g,h}}$ is dependent on the harmonic current $i_{\mathrm{g,h}}$ according to:

$$v_{\mathrm{g,h}} = R_{\mathrm{h}} i_{\mathrm{g,h}}, \tag{4.17}$$

with R_{h}, a programmable harmonic impedance.
A phase-locked loop (PLL) can be used to extract the fundamental component $i_{\mathrm{g,1}}$ of the measured grid current i_{g}. The harmonic component $i_{\mathrm{g,h}}$ is then derived from:

$$i_{\mathrm{g,h}} = i_{\mathrm{g}} - i_{\mathrm{g,1}}. \tag{4.18}$$

In this way, (4.17) becomes analogous to the second term of the PR-SHI method in (4.15). The harmonic impedance R_{h} is programmable, analogously to g_h in [180]. This enables to control the harmonic current sharing between DG units in an islanded microgrid, e.g. according to the ratings of the DG units.

B. Bode plot of impedance of the VSI

In this paragraph, the influence of the harmonic current sharing strategy, the impedance of the LC filter at the terminals of the inverter and the voltage control strategy on the total impedance of the VSI ($v_{\mathrm{g}}/i_{\mathrm{g}}$) over a wide frequency range is studied. The bode plots of this impedance, with and without harmonic impedance are compared. The bode plot is derived in analogy with [111]. The open-loop output-voltage dynamics of the converter follow (3.1) and (3.2) with the parameters as defined in Fig. 3.3. Averaged over one switching cycle (e.g., $\hat{v}_{\mathrm{g}}$ represents

the average value of $v_{\mathrm{g}}(\mathrm{t})$) and in the Laplace domain, this becomes:

$$\hat{v}_{\mathrm{s}}(\mathrm{s}) = \hat{v}_{\mathrm{g}}(\mathrm{s}) + sL\hat{i}_{\mathrm{g}}(\mathrm{s}) + s^2LC\hat{v}_{\mathrm{g}}(\mathrm{s}). \tag{4.19}$$

A PID controller, with duty ratio feedforward ($v_{\mathrm{ref}}(\mathrm{s}) = v_{\mathrm{g}}^{\star}$) as in [154], is used for tracking the output voltage:

$$\hat{v}_s(\mathrm{s}) = v_{\mathrm{ref}}(\mathrm{s}) + \frac{k_d s^2 + k_p s + k_i}{s}(v_{\mathrm{ref}}(\mathrm{s}) - \hat{v}_{\mathrm{g}}(\mathrm{s})). \tag{4.20}$$

Combination of (4.19) and (4.20) gives:

$$\begin{aligned}\hat{v}_{\mathrm{g}}(\mathrm{s}) = {} & \frac{k_i + s(1+k_p) + k_d s^2}{k_i + s(1+k_p) + s^2 k_d + s^3 LC} v_{\mathrm{ref}}(\mathrm{s}) \\ & + \frac{-s^2 L}{k_i + s(1+k_p) + s^2 k_d + s^3 LC}\hat{i}_{\mathrm{g}}(\mathrm{s}).\end{aligned} \tag{4.21}$$

Hence,

$$\hat{v}_{\mathrm{g}}(\mathrm{s}) = G(\mathrm{s})v_{\mathrm{ref}}(\mathrm{s}) - Z_0(\mathrm{s})\hat{i}_{\mathrm{g}}(\mathrm{s}) \tag{4.22}$$

Bode plot of output impedance Three cases are studied: 1) $z_v = R_{\mathrm{h}} = 0\Omega$; 2) $z_v \neq 0\Omega$ and $R_{\mathrm{h}} = 0\Omega$; and 3) $z_v \neq 0\Omega$ and $R_{\mathrm{h}} \neq 0\Omega$. In the first case, $z_v = R_{\mathrm{h}} = 0\Omega$. Hence, $v_{\mathrm{ref}}(\mathrm{s}) = v_{\mathrm{g,ref}}(\mathrm{s})$, with $v_{\mathrm{g,ref}}$ directly determined by the VBD controller.
For the second case $z_v \neq 0\Omega$ and $R_{\mathrm{h}} = 0\Omega$, $v_{\mathrm{ref}}(\mathrm{s})$ becomes $v_{\mathrm{g,ref}}(\mathrm{s}) - z_{\mathrm{v}}\hat{i}_{\mathrm{g}}(\mathrm{s})$. The output impedance of the inverter then equals $Z_0(s) + z_v$ (in the following $z_v = 3\ \Omega$).
In the third case, a resistive harmonic impedance R_{h} is included as well, the output impedance of the inverter is calculated analogously (here, $R_{\mathrm{h}} = 10\ \Omega$).
The bode plots of the output impedance of the inverter are depicted in Fig. 4.37. In case $z_v = R_{\mathrm{h}} = 0\Omega$, a low impedance for the fundamental component and the low harmonics (e.g. 5th, 7th harmonic) is obtained. Also, the DG unit has a mainly inductive character. The influence of z_v on the bode plot is clearly visible. For the most important harmonics, commonly restricted to the 40th order harmonic, the bode plot shows a resistive output impedance (10 dB or 3 Ω). By including the programmable resistance R_{h}, the impedance of the harmonics and fundamental component can be different. The impedance of the significant harmonics (not the fundamental) has increased to 22.2 dB or 13 Ω ($R_{\mathrm{h}} + z_v$). When using an additional low-pass filter on $R_{\mathrm{h}} i_{\mathrm{g,h}}$ to avoid the measurement noise of i_{g}, analogous results are obtained. Still, for frequencies around the switching frequency (here, 20 kHz), a sufficiently high output impedance of the inverter is obtained.

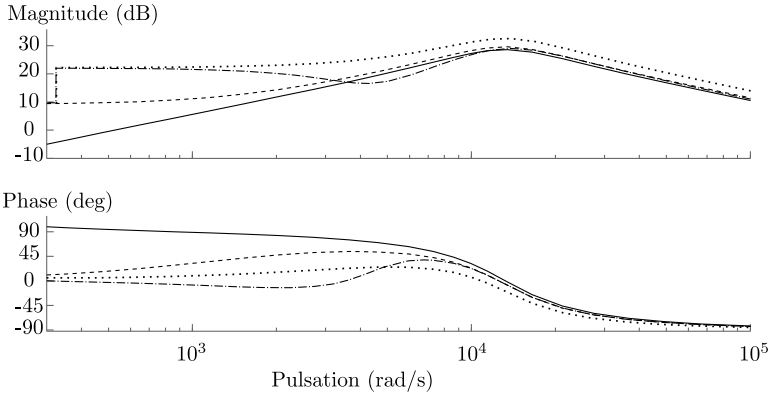

Figure 4.37: Bode plot of output impedance of inverter (— = $z_{\rm v} = R_{\rm h} = 0\Omega$; ---- = $z_{\rm v} = 3\ \Omega$ and $R_{\rm h} = 0\Omega$, $\cdots$ = $z_{\rm v} = 3\ \Omega$ and $R_{\rm h} = 10\ \Omega$, ·---· = $z_{\rm v} = 3\ \Omega$ and $R_{\rm h} = 10\ \Omega$ with low pass filter on the measurement of $i_{\rm g,h}$ with cut-off frequency 5 kHz)

Bode plot of closed-loop voltage control Note that the converter uses an LC filter to attenuate the switching ripple, here $L = 2$ mH and $C = 3\mu$F. Consequently, the cut-off frequency equals 2 kHz. The higher order harmonics are, thus, mitigated by the LC filter. Also, the bandwidth of the voltage controller is properly tuned such that the closed-loop voltage controller has a bandwidth of slightly less than 2 kHz as shown in Fig. 4.38. This bode diagram is derived from the direct control scheme in chapter 3 and by taking into account the duty ratio feedforward $\delta_{\rm ff}$ that is added to the output of the controller [154]. Hence,

$$v_s = (\delta + \delta_{\rm ff})V_{\rm dc} = \delta V_{\rm dc} + v_{\rm g,ref} \tag{4.23}$$

and

$$\frac{v_{\rm g}}{v_{\rm g,ref}}({\rm s}) = \frac{{\rm P(s)} \cdot {\rm V_{dc}} \cdot \frac{1}{1+{\rm s^2LC}} \cdot (1 + {\rm PID(s)})}{1 + {\rm P(s)} \cdot {\rm V_{dc}} \cdot \frac{1}{1+{\rm s^2LC}} \cdot {\rm PID(s)}}, \tag{4.24}$$

with P the Padé approximation for delay time in (3.38) and PID(s) the voltage controller given by (3.39). For the harmonic control this means that:

- the harmonics with frequency higher than 2 kHz are attenuated by the LC filter, thus, cannot be controlled by the DG unit (e.g., generally harmonics upto the 40-th harmonic or 2 kHz in the considered 50 Hz network are taken into account [182]).
- the harmonics with frequency lower than the bandwidth of the voltage controller can be dealt with by the voltage control loop

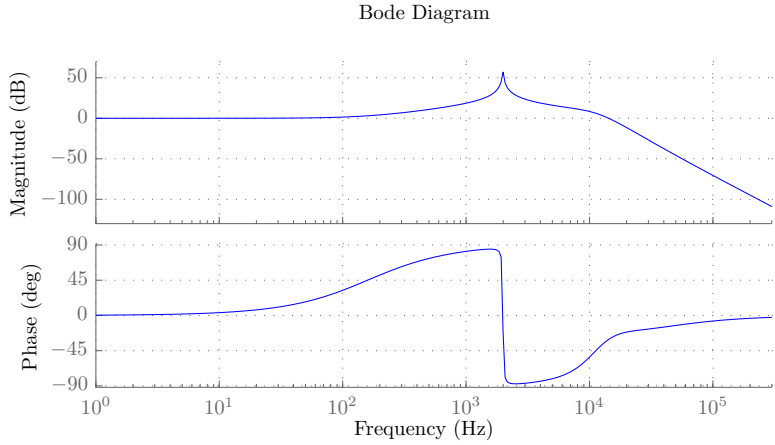

Figure 4.38: Bode plot closed-loop voltage control

- the harmonics with frequency between the bandwidth of the voltage controller and the 2 kHz cut-off frequency of the LC filter cannot exactly be controlled by the voltage control loop, e.g., due to attenuation as depicted in Fig. 4.38.

Summarised, the harmonics that can be shared are determined by the bandwidth of the voltage control loop, which in turn is dependent on the switching frequency of the VSI. The latter is linked with the ratings of the DG unit, small DG units are considered here because of the connection to a low-voltage microgrid.

C. Influence of R_h in concept case

By using the PR-SHI method modified according to (4.16) for usage in islanded microgrids combined with the VBD control strategy, controllable harmonic current sharing between DG units can be obtained. This is clarified in this concept case. First, the statement that the DG unit with droop control behaves as short-circuit for harmonics is illustrated. Secondly, harmonic resistance is included in the VBD control. In the simulation according to Fig. 4.39, the DG unit is presented as voltage source v_g of 230 V rms and 50 Hz. A resistive load and a harmonic load, represented as a harmonic current source that injects a 5-th harmonic current (250 Hz) of 3 A amplitude, are included and the line impedances are neglected. A simplified steady-state situation is considered, more details concerning the harmonic content of nonlinear loads are given in [183]. If the output impedance of the VSI is neglected as well, the VSI can be considered as a short circuit for harmonics as depicted in Fig. 4.39, because the terminal voltage is purely sinusoidal while the

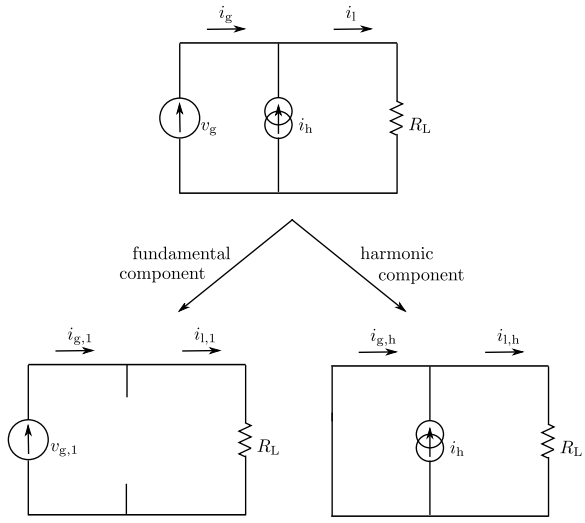

Figure 4.39: VSI can be considered as a short circuit for harmonics

current contains harmonics. The amplitudes of the obtained harmonics after Fast-Fourier-Transform (FFT) are summarised in Table 4.5. These results show that the DG unit delivers the harmonic current content of the nonlinear load ($I_{g,5} = 3$ A while $I_{l,5} = 0$ A). In case multiple DG units are included, an important disadvantage is, thus, that the current i_h would be shared based on the line impedances between the DG units and the nonlinear loads, instead of on the ratings of the DG units. Table 4.5 also shows the total harmonic distortion (THD). The THD of v_g is zero as a pure fundamental voltage is generated. The current i_l is nearly pure sinusoidal, which is shown in the zero value of the THD of i_l. As the voltage source absorbs all the harmonic current, the THD of i_g is not zero.

In the next case, the DG unit behaves resistively towards harmonics, Fig. 4.40, with $R_h = R_L = 10\Omega$. The simulation results are summarised in Table 4.5. In order to provide resistance towards harmonics, the THD of the grid voltage v_g is not zero any more. This is a consequence of the strategy that enables harmonic current sharing, in this case between the DG unit and the load. As R_h equals R_L in this example, the harmonic current is evenly distributed between the load and the DG unit. Therefore, by changing R_h, the harmonic current content of the DG unit can be modified. Further, it will be shown that in practical cases, this control strategy enables us to control the harmonic current sharing between different DG units.

It is concluded that without extra measures, a grid-forming inverter (voltage controlled inverter), becomes a short-circuit for harmonic currents. Therefore, if a non-

Table 4.5: Proof of concept, with n the order of the harmonic, I_{g} current of the DG unit, I_{l} load current, I_{h} current of harmonic current-source

	$R_{\mathrm{h}} = 0\Omega$		$R_{\mathrm{h}} = 10\Omega$	
	$n = 1$	$n = 5$	$n = 1$	$n = 5$
I_{g} (A)	32.5	3	32.5	1.5
I_{l} (A)	32.5	0	32.5	1.5
I_{h} (A)	0	3	0	3
V_{g} (V)	325	0.067	325	14.9
V_{l} (V)	325	0.067	325	14.9
THD(v_{g})	0		0.046	
THD(v_{l})	0		0.046	
THD(i_{s})	0.0931		0.046	
THD(i_{l})	0		0.046	

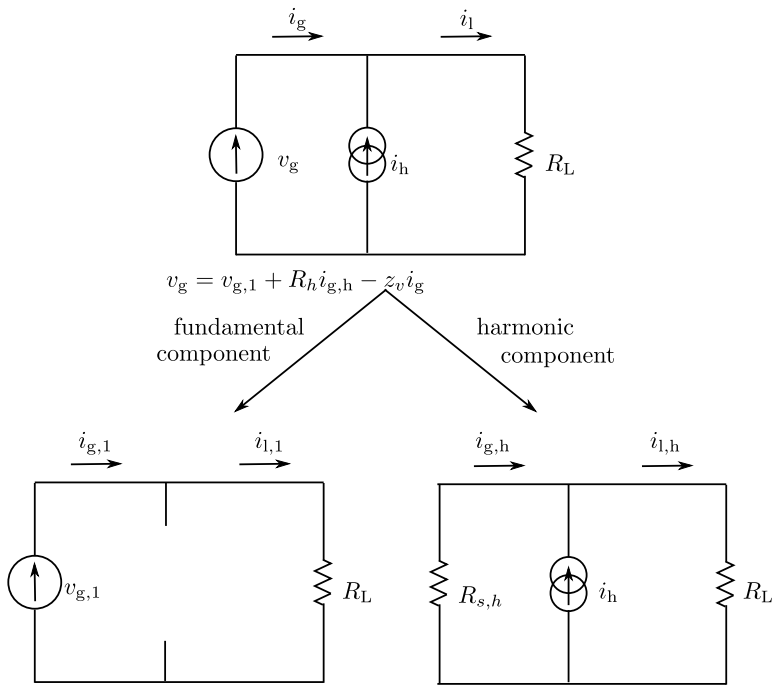

Figure 4.40: VSI with resistive harmonic impedance

linear load is included in the network, the DG unit delivers the total harmonic current. If a nonlinear load is included in a network with multiple DG units, they all behave as short-circuits towards harmonic currents and the harmonic current sharing will be determined by the electrical distance between the units, instead of their ratings. By including resistive behaviour towards harmonics, the harmonic current delivered by the DG units can be controlled such that sharing according to the ratings is obtained. Note that in order to provide harmonic current sharing, the output voltage is not purely sinusoidal at fundamental frequency any more because of (4.16). This can be seen in the THD of the voltages and current. Resistive behaviour towards harmonics leads to a lower THD of the current. The price to pay for this resistive behaviour is more harmonic content in the voltage.

4.4.4 Examples

A. Harmonic current sharing between DG units

In the following paragraph, the power sharing between two DG units in a microgrid is studied. The configuration of Fig. 4.41 is analysed and the line impedances R_{l} are not neglected in this example. The load $R_{\mathrm{l}} + R_{\mathrm{L}}$ equals 25 Ω with lines $R_{\mathrm{l}} = 1\ \Omega$. Purely resistive lines are assumed in the considered low-voltage microgrid. Two fully dispatchable ($b = 0$), equally rated DG units are considered with dc-current $I_{\mathrm{dc,nom}} = 4$ A and $V_{\mathrm{dc,nom}} = 450$ V. A nonlinear load injecting a 5-th harmonic current with 3 A amplitude is connected to the microgrid.
In a first simulation case, $R_{\mathrm{h},1} = R_{\mathrm{h},2} = 0\ \Omega$ and $z_{\mathrm{v}} = 0\ \Omega$. Therefore, except for the output impedance of the inverters, both inverters have short-circuit behaviour towards harmonics. In a second case, a virtual impedance is included such that: $R_{\mathrm{h},1} = R_{\mathrm{h},2} = 0\ \Omega$ and $z_{\mathrm{v}} = 3\ \Omega$. This virtual impedance delivers damping in the system, it is a resistance for both the fundamental component and the harmonics, but it does not represent a programmable harmonic impedance. In the next simulation, $R_{\mathrm{h},1} = 0\ \Omega$, while $R_{\mathrm{h},2} = 22\ \Omega$ and $z_{\mathrm{v}} = 3\ \Omega$. The second DG unit has a programmable resistive behaviour towards harmonics. Finally, $R_{\mathrm{h},1} = R_{\mathrm{h},2} = 22\ \Omega$. The simulation results are summarised in Table 4.6.
In the first case, without virtual output impedance nor harmonic impedance, the harmonic current of the nonlinear load is shared by the DG units. An equal distribution is only obtained because of the equal line resistances R_{l} from the DG units to the harmonic load. The sharing of the nonlinear current is, thus, determined by the line impedances. Therefore, the harmonic current sharing is not controllable by the control strategy of the DG unit. Because the line impedances are not neglected in this simulation, the branch of the DG units does not form a short-circuit, thus, the load absorbs some harmonic current. The fundamental current is equally shared between the units because they have equal ratings, equal control strategies and as a

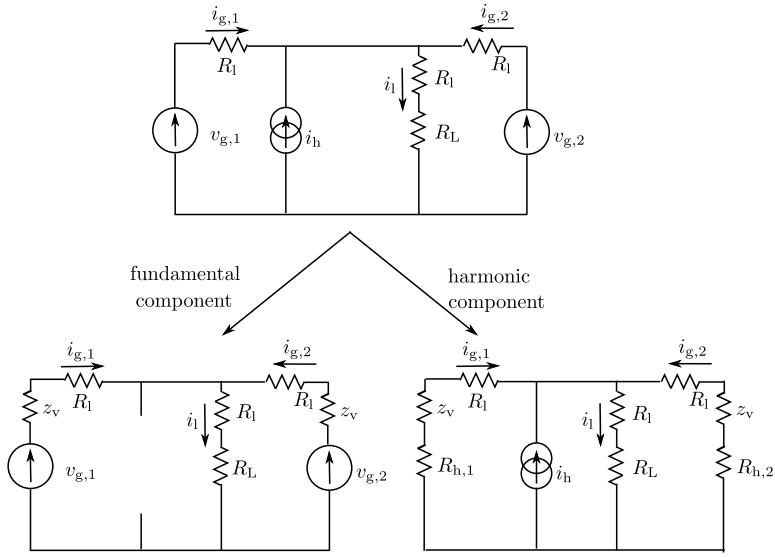

Figure 4.41: Configuration harmonic power sharing between two DG units

symmetrical microgrid is assumed ($P_1 = P_2 = 1.2$ kW).
In the second case, a virtual impedance z_v is included in the units. As z_v is present for both the fundamental component and the harmonics, the harmonic content in the DG units' voltages increases slightly because of their resistive behaviour towards both the fundamental and harmonic components. The DG units deliver most of the harmonic current of the harmonic load because $z_v << Z_L$. The fundamental current of the units has slightly increased because the harmonic power they provide has slightly decreased.
In the third simulation, the second DG unit has a high harmonic impedance. Therefore, the control strategy avoids that this unit contributes significantly in the harmonic current sharing, so, the total harmonic distortion in $i_{g,2}$ is lower. Also, $i_{l,h} \approx i_{g,2,h}$ because the harmonic impedance of load and second DG unit are nearly equal: $Z_{h,load} = R_L + R_l \approx Z_{h,DG2} = R_l + z_v + R_{h,2}$. The first DG unit, with low R_h, delivers most of the harmonic current. The fundamental component of the second DG unit has slightly increased ($P_1 = 1.1$ kW and $P_2 = 1.2$ kW).

In case of equal ratings of the DG units, a logical choice is $R_{h,1} = R_{h,2}$. In this case, the harmonic current is evenly shared between the units. It is concluded that by setting R_h, the harmonic current sharing between the DG units can be controlled, e.g., according to their ratings.

Summarised, R_h is included to achieve controlled harmonic current sharing

Table 4.6: Harmonic current sharing between DG units in a microgrid, with n the order of the harmonic

	$R_{\mathrm{h},1} = R_{\mathrm{h},2} = 0\,\Omega$ $z_{\mathrm{v}} = 0\Omega$		$R_{\mathrm{h},1} = R_{\mathrm{h},2} = 0\,\Omega$ $z_{\mathrm{v}} = 3\Omega$		$R_{\mathrm{h},1} = 0\Omega, R_{\mathrm{h},2} = 22\,\Omega$ $z_{\mathrm{v}} = 3\Omega$		$R_{\mathrm{h},1} = R_{\mathrm{h},2} = 22\,\Omega$ $z_{\mathrm{v}} = 3\Omega$	
	$n=1$	$n=5$	$n=1$	$n=5$	$n=1$	$n=5$	$n=1$	$n=5$
I_{g1} (A)	6.78	1.45	6.83	1.38	6.21	2.23	6.92	0.98
I_{g2} (A)	6.78	1.45	6.83	1.38	7.57	0.43	6.92	0.98
I_{h} (A)	0	3	0	3	0	3	0	3
I_{l} (A)	13.56	0.15	13.66	0.28	13.78	0.45	13.84	1.04
THD(i_{g1})	0.22		0.20		0.36		0.14	
THD(i_{g2})	0.22		0.20		0.08		0.14	
THD(v_{g1})	0.015		0.02		0.03		0.07	
THD(v_{g2})	0.015		0.02		0.03		0.07	

between the DG units: units with high R_{h} take less part in the harmonic current sharing compared to those with low R_{h}.

B. Microgrid case

In this paragraph, a more realistic microgrid case is studied. The islanded microgrid consists of three DG units, several linear loads (both resistive and inductive), a nonlinear load and some harmonic loads. A low-voltage microgrid (230 V rms, 50 Hz) is considered, with DG units delivering power in the order of kW. The DG units have the following characteristics:

- G1: the first DG unit represents a fully dispatchable DG unit. The active power control algorithm uses $V_{\mathrm{g}}/V_{\mathrm{dc}}$ droop control combined with $I_{\mathrm{dc}}/V_{\mathrm{g}}$ droop control to change the output current of G1. The nominal dc-current of this unit equals 2 A, after 0.6 s this drops to 1 A.
- G2 represents a fully dispatchable DG unit as well, with nominal dc-current equal to 3 A.
- G3 represents an undispatchable unit, with constant dc-current of 1.5 A. The balancing algorithm of this unit uses the $V_{\mathrm{g}}/V_{\mathrm{dc}}$ droop control strategy only.

The details of the configuration are summarised in Fig. 4.42. A 3-rd and 5-th harmonic load injecting harmonic current of 3 A and 5 A respectively are included. Also, a nonlinear load N consisting of a rectifier is included in the network. A

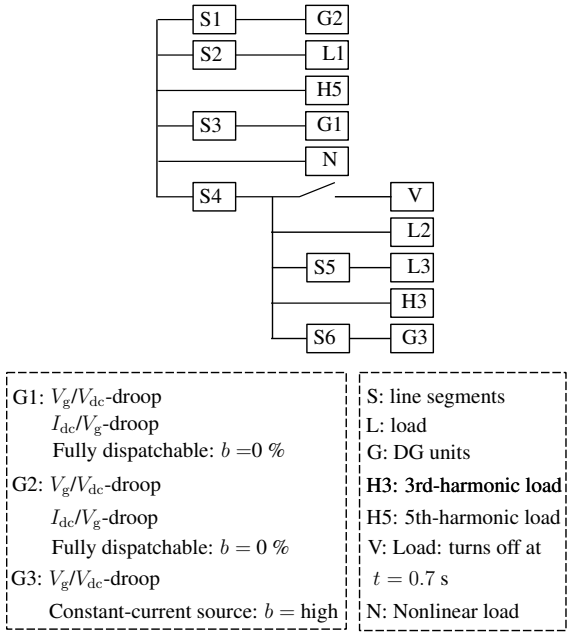

Figure 4.42: Configuration harmonic current sharing in a microgrid case

resistive load V of 50 Ω turns off after 0.7 s. Also, resistive line parameters are assumed because of the low-voltage microgrid. Note that even if a small inductance in the lines is included, a stable operation is obtained as well, because of the usage of resistive virtual output impedance of the converter such that a high R/X is obtained [184]: $S_1 = S_6 = 3\ \Omega$, $S_3 = 4\ \Omega$, $S_4 = S_5 = 1\ \Omega$. For the loads: $S_2 + L_1 = 25\ \Omega$, $L_2 = 50\ \Omega$ and L_3 consists of 50 Ω in parallel with 0.15 H inductance.

In the first simulation, the harmonic resistance R_h of all units equals 22 Ω and the virtual output impedance z_v equals 3 Ω. The results are depicted in Fig. 4.43. The dc-current of the generators remains constant in the first 100 ms, because in the simulation, the I_{dc}/V_g droop controller is turned on with a delay of 100 ms. After a start-up transient, increased by the delayed turning on of the active and reactive power controllers, a steady-state is reached. At $t = 0.6$ s, the dc-current of G1 drops, which is clearly shown in Fig. 4.43c, this leads to a small transient in the terminal voltage v_g of the DG units. At 0.7 s, a resistive load turns off. Therefore the dc-side power is higher than the ac-side power. The dc-bus voltage of the converter-connected DG units will increase accordingly. All V_g/V_{dc} droop controllers react according to the rise of V_{dc} by increasing V_g. The I_{dc}/V_g droop

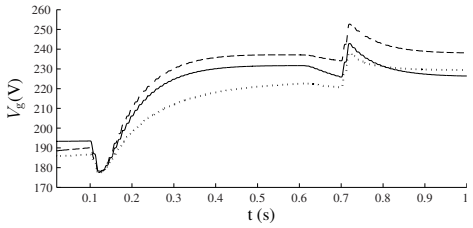

(a) Terminal voltage $V_{\rm g}$

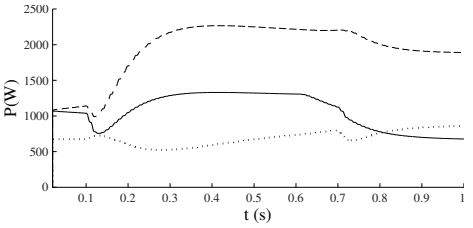

(b) Output power P

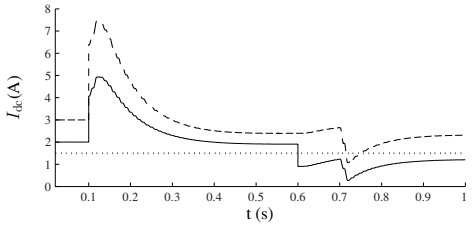

(c) Dc-current $I_{\rm dc}$

Figure 4.43: Microgrid case with $R_{\rm h,1} = R_{\rm h,2} = R_{\rm h,3} = 22\ \Omega$ (— = G 1; ---- = G 2, $\cdots$ = G 3)

controllers of G1 and G2 decrease the output current of the sources. The current of G3 remains constant because this represents an undispatchable DG unit. Again, a stable steady-state is reached. At $t = 1$ s, the steady-state values of the terminal rms voltages are: $V_{\rm g,1} = 226.4$ V, $V_{\rm g,2} = 238.1$ V and $V_{\rm g,3} = 229.5$ V, which are well within the limits of the microgrid voltage (e.g. 10 %). The delivered active powers at that instant are: $P_1 = 677$ W, $P_2 = 1890$ W and $P_3 = 861$ W, which follow the ratings of the DG units.

The harmonic current sharing results are also summarised in Table 4.7. The fundamental current is shared between the DG units according to their ratings for the dispatchable units G1 and G2. The 3-rd and 5-th harmonic components are evenly shared between the units as the harmonic impedance of these units is the same.

For the second simulation case, $R_{\rm h,1} = 0\ \Omega$ and $R_{\rm h,2} = R_{\rm h,3} = 22\ \Omega$, the results are summarised in Table 4.7. Compared to the previous case, the harmonic impedance of G1 is lower, thus, the harmonic current content of this unit is larger. The harmonic content of G2 and G3 are, again, evenly distributed because of the equal $R_{\rm h}$.

These cases show that in a microgrid with a combination of different DG types and nonlinear loads, the harmonic current sharing can be controlled by setting $R_{\rm h}$.

Table 4.7: Harmonic current sharing between DG units in a realistic microgrid, with n the order of the harmonic

$R_{\mathrm{h},1} = R_{\mathrm{h},2} = R_{\mathrm{h},3} = 22\ \Omega$					
	$n=1$	$n=2$	$n=3$	$n=4$	$n=5$
$I_{\mathrm{g},1}$ (A)	4.26	0.27	0.57	0.08	0.99
$I_{\mathrm{g},2}$ (A)	11.27	0.33	0.60	0.07	1.02
$I_{\mathrm{g},3}$ (A)	5.34	0.28	0.68	0.07	0.99
N	2.87	1.41	0.15	0.35	0.25
$R_{\mathrm{h},1} = 0\ \Omega$, $R_{\mathrm{h},2} = R_{\mathrm{h},3} = 22\ \Omega$					
	$n=1$	$n=2$	$n=3$	$n=4$	$n=5$
$I_{\mathrm{g},1}$ (A)	3.91	0.70	1.44	0.17	2.46
$I_{\mathrm{g},2}$ (A)	11.92	0.21	0.38	0.04	0.67
$I_{\mathrm{g},3}$ (A)	5.11	0.16	0.47	0.04	0.65
N	2.93	1.36	0.09	0.31	0.18

4.5 Improvement of active power sharing ratio

Microgrids provide a coordinated integration of distributed generation units in the electrical power system. By operating in islanded mode, microgrids can increase the reliability of the system or electrify remote areas. For the power sharing and voltage control in low-voltage microgrids, active power/grid voltage droop control is highly suitable. In order to optimise the integration of renewable energy sources in the microgrid, a variant of this droop control, the voltage-based droop (VBD) control, has been presented. A well-known concern about droop controllers is the inherent trade-off between voltage control and power sharing. Therefore, in this section, an additional control loop is included in the VBD control to improve the active power sharing ratio. In this way, accurate power sharing is achieved, i.e., the DG units respond to load changes exactly according to their droops. Although this modification relies on communication, it does not jeopardise the reliability of the microgrid as if the communication is lost, the basic VBD control still operates without the need for communication, ensuring a stable microgrid operation.

4.5.1 Accurate power sharing

Although a stable microgrid operation is of the first importance, sometimes, accurate power sharing is important as well to achieve a fair contribution of DG units in the microgrid control. A disadvantage of droop control is that there is always a trade-off between the voltage control and the accuracy of the power sharing. The accuracy of power sharing or power sharing ratio reflects the contribution of each unit to cope with load variations compared to the other units. Perfectly accurate power sharing is achieved when the load variations are picked up by the DG units exactly according to their droops. These droops are dependent on the ratings of the units and the controllability of the energy source. For example, gas-fired power stations, which are highly controllable, contribute more to the primary control to cope with load variations than nuclear power plants. This is analogous for DG units, fully-controllable DG units contribute to the power sharing proportionally to their rated power, but less controllable units (such as many renewables) will contribute less.

The grid voltage is a local parameter and can be different in different network locations, which can affect the power sharing ratio. Therefore, in the P/f - Q/V droop control, the reactive power (Q) sharing ratio can differ from the droop ratio, i.e. inaccurate reactive power sharing. Equally, the active power sharing ratio can be inaccurate in the P/V - Q/f droop controllers.

Several solutions to increase the power sharing accuracy have been presented in literature, focussing on the P/f - Q/V droop controllers. In [110], a small high-frequency signal is injected in the system as control signal for P and Q. However, the circuitry required to measure the small real power variations in this signal adds to the complexity of the control [185]. In [185], each unit regulates its terminal voltage based on the reference voltage that is obtained from, firstly, the conventional Q/V droops and, secondly, a correction term based on the measured load voltage. An analogous method to achieve accurate power sharing by introducing load voltage feedback is presented in [186].

In this section, the method of [185] is modified to improve the active power sharing ratio in low-voltage networks. The modifications are twofold. Firstly, the paper [185] focusses on Q/V droops, while here, the P/V droops in the VBD control are adapted. Secondly, in microgrids, there is not a single load voltage. In microgrids, the loads and DG units are distributed in the network and the line impedances in between cannot be neglected. Hence, this paragraph suggests to communicate the active power output of the units instead of the load voltage to achieve accurate power sharing.

In § 4.5.2, the method of [185] for Q/V droops is summarised. The active power sharing ratio with the VBD control is improved in § 4.5.3. This is achieved by, firstly, analogously to [185] communicating the load voltage, and secondly, by

communicating output active power measurements. In § 4.5.4, the IEEE 13 node test feeder is studied in order to show the improvement of the power sharing ratio by using this active power correction in a dynamical situation with multiple DG units, VBD control and various loads.

4.5.2 Power sharing of conventional controllers

The droops are coordinated to make each DG system supplying active and reactive power in proportion to its power capacity. For the P/f droops, accurate power sharing is always obtained:

$$\frac{\Delta P_1}{\Delta P_2} = \frac{K_{\mathrm{f},2}}{K_{\mathrm{f},1}}, \tag{4.25}$$

with $\Delta P_i = P_i - P_{\mathrm{i,ref}}$, because the frequency is equal everywhere in the network. The latter is not valid for the terminal voltages V of the DG units, which can differ due to different line impedances. This can affect the accuracy of the reactive power sharing. Hence, the reactive power sharing is only accurate if

$$\frac{\Delta Q_1}{\Delta Q_2} = \frac{K_{\mathrm{Q,v},2}}{K_{\mathrm{Q,v},1}}. \tag{4.26}$$

To improve the reactive power sharing ratio, in [185], the Q/V droop controller is changed. Each unit regulates its terminal voltage based on, firstly, the reference voltage V_{i} that is determined by the Q/V droop and, secondly, the communicated load voltage V_l. A correction voltage $V_{\mathrm{i,corr}}$ is determined

$$V_{\mathrm{i,corr}} = K_{\mathrm{f,corr}} \int (V_i - V_l) dt, \tag{4.27}$$

with $K_{\mathrm{f,corr}}$ a correction factor. Hence, the terminal voltage magnitude of the DG unit is controlled to $V_{\mathrm{i,corr}}$, whereas with conventional Q/V droops, it is controlled to V_{i}. In this way, two DG units can share the reactive load accurately. The integrator gain $K_{\mathrm{f,corr}}$ can be varied to achieve the desired speed of response without affecting the voltage regulation [185].

4.5.3 Improved active power sharing in VBD control

In this section, first, the method of [185], which is developed for Q/V droops, is modified to comply with the P/V droops in the VBD control. Accurate power sharing is achieved, but the load voltage needs to be communicated. As in microgrids, there is no common load voltage, in the second paragraph, the output power of the DG units is communicated. In this way, the VBD control is adapted to achieve

accurate power sharing between the DG units in a microgrid.

A. Load voltage amplitude communication

Control principle In [185], the accuracy in power sharing of the Q/V droop controller is improved by communicating the load voltage magnitude to all DG units. Based on this technique, in this paragraph, a modification to the VBD control is made to improve the accuracy of the active power sharing, as here P/V droops are used.
In order to improve the accuracy of the active power sharing, the reference voltage $v_{\mathrm{g,droop}}$, which is the input of the voltage controller, is changed compared to the case with the original VBD controller. In (4.28), instead of using the voltage amplitude V_{g}, which is the output of the V_g/V_{dc} droop controller, the reference voltage is calculated by using a correction voltage $V_{\mathrm{g,corr}}$:

$$v^{\star}_{\mathrm{g,droop,k}} = V_{\mathrm{g,corr,k}} \sin(\alpha_{\mathrm{k-1}} + 2\pi f_{\mathrm{k}} T_s). \tag{4.28}$$

The correction voltage is obtained from a measurement of the load voltage V_{l}, which is communicated to the DG unit:

$$V_{\mathrm{g,corr}} = K_{\mathrm{corr}} \int (V_{\mathrm{g}} - V_{\mathrm{l}}) \mathrm{dt}, \tag{4.29}$$

analogously as in (4.27). The correction voltage is implemented in discrete time (z-domain):

$$V_{\mathrm{g,corr,k}} = K_{\mathrm{corr}} \frac{T_{\mathrm{s}}}{z-1} (V_{\mathrm{g,k}} - V_{\mathrm{l,k}}) + V_{\mathrm{g,nom}}. \tag{4.30}$$

The control scheme is summarised in Fig. 4.44.
The VBD control strategy is a primary controller, focussing on the reliability of the microgrid, and hence, does not use communication. By including the correction voltage, communication is used. However, this does not jeopardise the reliability of the system. If the communication of V_{l} fails, the controller falls back to the core VBD control, thus, without voltage correction. This controller achieves a stable operation, but, the active power sharing ratio can deviate a little from its pre-determined value. Also, the communication of V_{l} does not require a high bandwidth as only the amplitude of the signal needs to be communicated and not the instantaneous value.

Example The correction voltage is used to achieve a better active power sharing ratio in the simple microgrid of Fig. 4.6. This microgrid consists of two DG units and one load. A resistive virtual output impedance $R_{\mathrm{v}} = 3\ \Omega$ is included. The

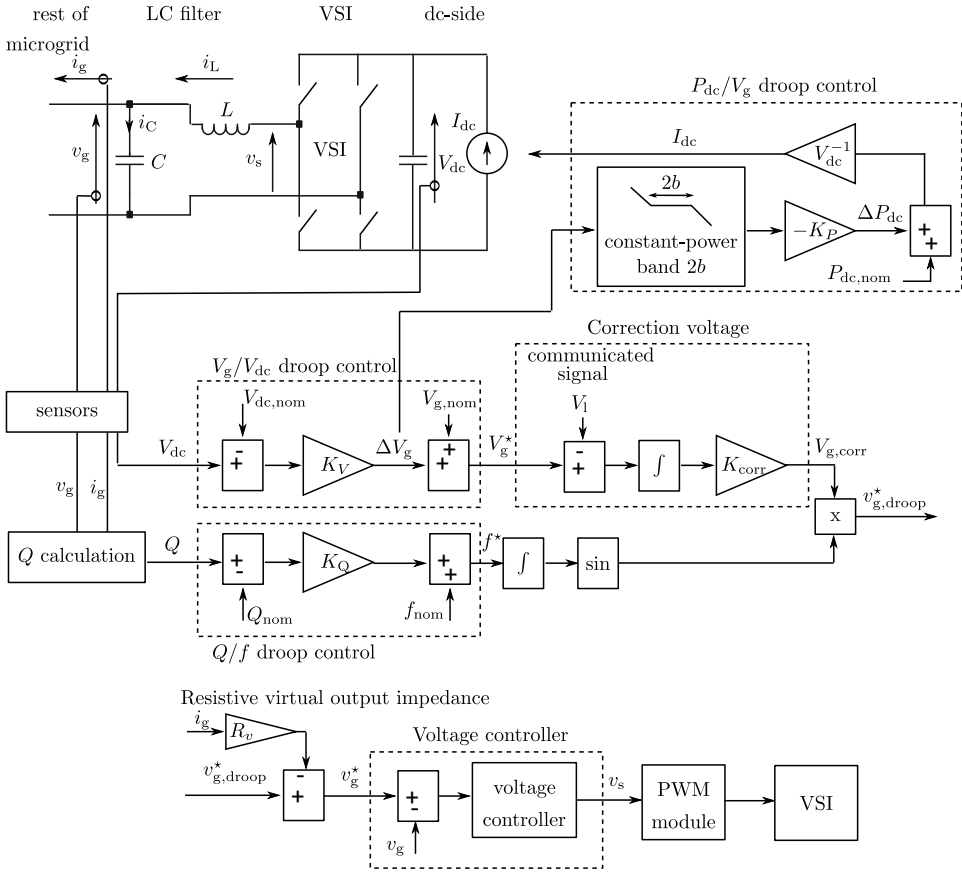

Figure 4.44: VBD control with voltage correction and virtual output impedance

following parameters are used: $L = 2$ mH, $C = 3$ μF, $C_{dc} = 1.5$ mF, $V_{dc,ref} = 450$ V, $V_{g,ref} = 230\sqrt{2}$ V, $f_{nom} = 50$ Hz, $R_{l,1} = 1$ Ω, $R_{l,2} = 0.3$ Ω, $R = 25$ Ω in case of a resistive load (R-load) or $P = 2500$ W for a constant-power load (P-load), $b = 0$ %, $P_{nom,1} = 2000$ W and $P_{nom,2} = 1000$ W. The droops are $K_V = 0.5$ V/V for the V_g/V_{dc} droop controller, $K_{p,1} = P_{nom,1}/50$ W/V, $K_{p,2} = P_{nom,2}/50$ W/V for the P/V_g droop controller and $K_Q = 1 \cdot 10^{-4}$ Hz/VAr for the Q/f droop controller. When voltage correction $V_{g,corr,k}$ is used, K_{corr} equals 50 and $T_s = 50$ μs.

Without voltage correction, accurate power sharing, i.e.,

$$\Delta P_1/\Delta P_2 = \frac{P_1 - P_{nom,1}}{P_2 - P_{nom,2}} = 2 \tag{4.31}$$

Table 4.8: Voltage correction : load voltage amplitude (V_l) communication

case	P_1 (W)	P_2 (W)	$\Delta P_1/\Delta P_2$
no V_l correction, R-load	1257	879	6.1
V_l correction, R-load	1546	775	2.0
no V_l correction, P-load	1502	1060	-8.3
V_l correction, P-load	1710	854	2.0

would only be achieved when $P_{\mathrm{nom},1}/P_{\mathrm{nom},2} = R_{\mathrm{l},2}/R_{\mathrm{l},1}$, which is obviously not the case. From the obtained simulation results in Table 4.8, it follows that perfect power sharing is obtained when communicating the load voltage to the DG units and using it for the control in a correction voltage.

B. Output active power communication

Control principle An issue with the communication of V_l as used in the previous paragraph and [185], is that it conflicts with the extended microgrid configurations. Microgrids consist of feeders with different loads and DG units connected at different places in the network. The line impedances cannot be neglected in these cases. Subsequently, a general V_l does not exist in the microgrid. Therefore, in this paragraph, the active power output of the DG units is communicated to the other units and a method is presented to adapt the VBD control to achieve accurate power sharing.
When using active power communication, the power sharing accuracy can be enforced directly. In this case, the correction voltage for DG unit i is obtained by using

$$V_{\mathrm{g,corr,k,i}} = K_{\mathrm{corr}} \frac{T_\mathrm{s}}{z-1} \left(\frac{P_{\mathrm{nom,i}}}{P_{\mathrm{nom,j}}} - \frac{P_i}{P_j}\right) + V_{\mathrm{g,k,i}}, \tag{4.32}$$

with P_j the communicated output active power of another unit j and $V_{\mathrm{g,k,i}}$ the output of the $V_\mathrm{g}/V_\mathrm{dc}$ droop controller.

Example The same case as in the previous paragraph is studied with $K_{\mathrm{corr}} = 200$ V/W. The obtained results are depicted in Table 4.9. It follows that by using P correction, perfect power sharing is achieved as well. For three DG units, the control strategy remains the same, the units can relate their active power to a chosen unit j, for example, by choosing the closest unit. In the next paragraph, a more extended microgrid with multiple DG units is studied.

Table 4.9: Active power communication

case	P_1 (W)	P_2 (W)	$\Delta P_1/\Delta P_2$
no P correction, R-load	1257	879	6.1
P correction, R-load	1440	720	2.0
no P correction, P-load	1502	1060	-8.3
P correction, P-load	1715	857	2.0

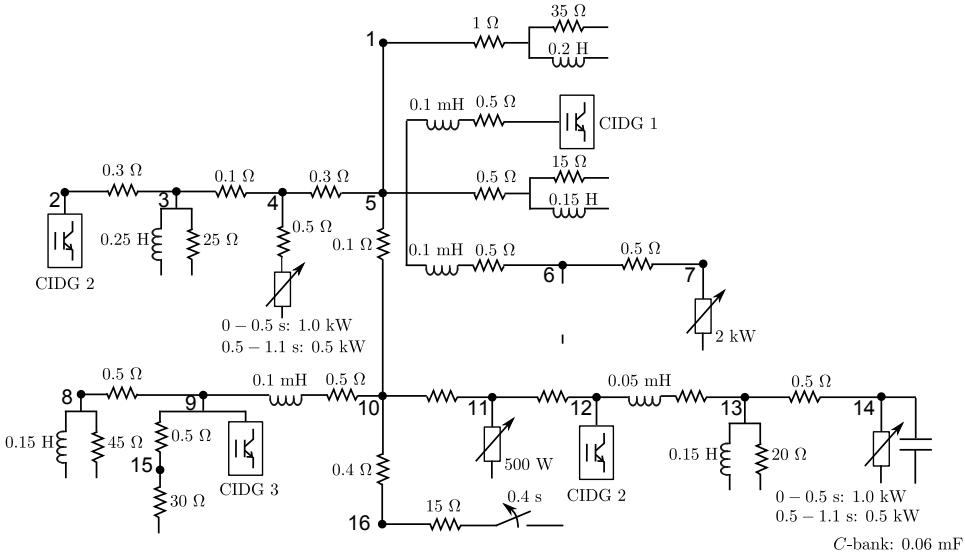

Figure 4.45: Considered 13 Node Test Feeder

4.5.4 Case study

A variant of the IEEE 13 Node Test Feeder, as shown in Fig. 4.20 is studied. The IEEE 13 Node Test Feeder is modified for application as a low-voltage network in islanded mode. The simulation details of the nodes are summarised in Fig. 4.45, showing that a combination of various loads (resistive, inductive, constant-power and switching loads) is used. There are three converter-interfaced DG (CIDG) units connected to the feeder, with parameters summarised in Table 4.10. The units use a resistive virtual output impedance $z_{\mathrm{v}} = 3\Omega$. A dynamical load and DG unit profile is included as the output of DG 3 and some loads vary in time.

The simulation results in Figs. 4.46 and 4.47, for VBD control without and with P

Table 4.10: CIDG units in test feeder: parameters

CIDG	$P_{\mathrm{dc,nom}}$	b
DG1	$P_{\mathrm{dc,nom},1} = 3.15$ kW	0 %
DG2	$P_{\mathrm{dc,nom},2} = 6$ kW	0 %
DG3	$P_{\mathrm{dc,nom},3}$:	8 %
	t <0.3 s: 6.3 kW	
	t >0.3 s: 4.2 kW	
DG4	$P_{\mathrm{dc,nom},1} = 1.5$ kW	10 %

Table 4.11: Simulation results extended microgrid

DG unit	P_{nom}	no P corr	P corr
DG1	3.15 kW	3.8 kW	3.1 kW
DG2	6.0 kW	5.00 kW	6.0 kW
DG3	4.2 kW	4.2 kW	4.2 kW
DG4 ($b = 10$ %)	1.5 kW	1.5 kW	1.5 kW
P_1/P_2	0.52	0.77	0.52
P_1/P_4	2.10	2.55	2.10

correction respectively, show a stable microgrid operation. The decreased output power of CIDG3 at t =0.5 s is clearly picked up by the other two DG units. Also, the load decrease at node 16 at $t = 0.4$ s and at nodes 4 and 14 at $t = 0.5$ s lead to acceptable transients that are mitigated fast by the VBD controllers. When comparing the cases with and without P control, on the one hand both control strategies achieve a stable microgrid operation, which is the main function of primary control. On the other hand, by including P control, accurate power sharing according to the droops is achieved as illustrated in Table 4.11.

For the sharing between three units, the same case is studied but with $b = 0$ % in DG 4 instead of 10 %, such that this becomes a dispatchable DG unit. The results of this case, and with other values for nominal power, are shown in Table 4.12. It is concluded that the accuracy of power sharing is improved by using P communication and a P correction term in the voltage controller.

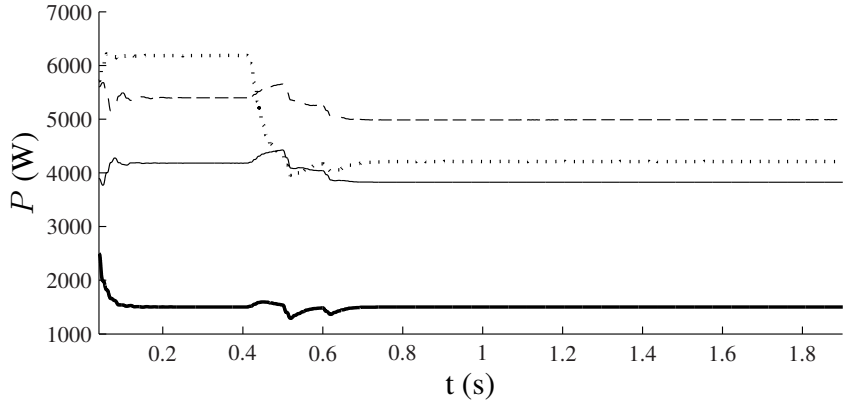

(a) Output power P

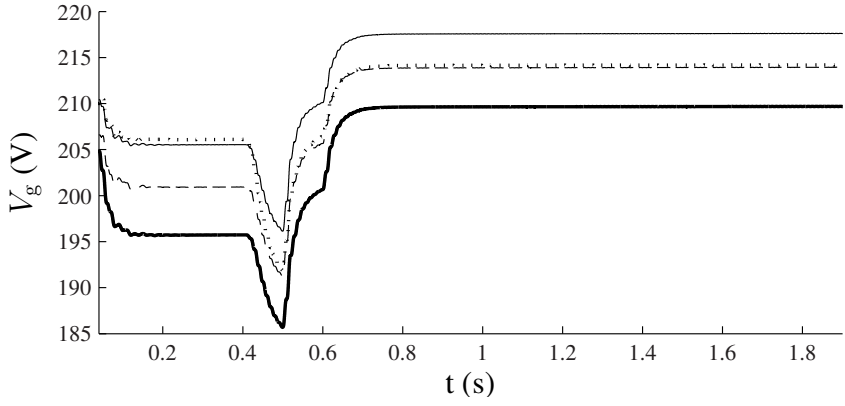

(b) Terminal voltage V_g

Figure 4.46: 13 node test feeder: without communication of P (— = DG1; ---- = DG2, · · · = G3; ▬ = DG4)

4.5.5 Conclusion

In this section, the power sharing ratio of P/V droop control in general and VBD control in specific is improved through a correction term that uses communication. With VBD control, a stable microgrid operation is obtained but the power sharing is not perfectly accurate. Possibly, some DG units are slightly more burdened to cope with load variations than others, which can cause discussions concerning fairness. Therefore, an additional control loop is included to achieve accurate power sharing. A power correction term is calculated in each dispatchable DG unit by using the

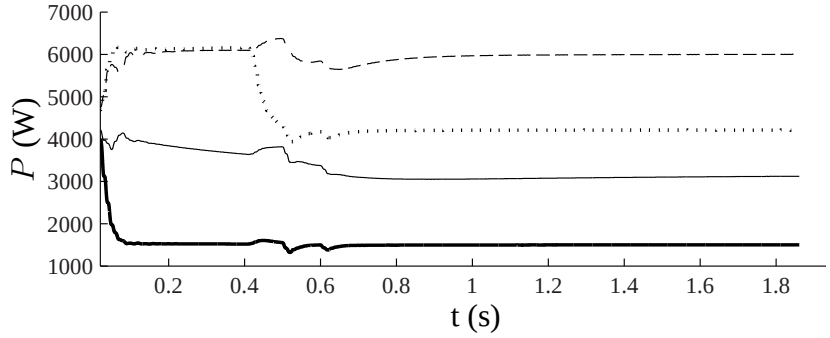

(a) Output power P

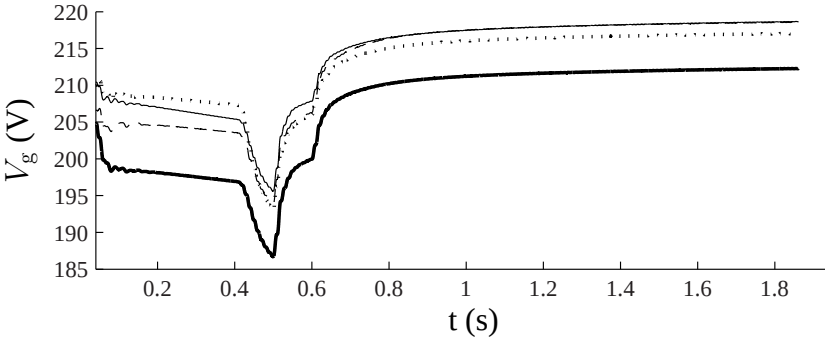

(b) Terminal voltage V_g

Figure 4.47: 13 node test feeder: with communication of P (— = DG1; ---- = DG2, ··· = DG3; ▬ = DG4)

communicated signals of the DG units' output power. The output of the V_g/V_{dc} droop controller together with this power correction term determines the reference grid voltage amplitude. This section shows that in this way, a perfect power sharing ratio, i.e., according to the droops, is obtained. If the communication fails, the control strategy falls back to the core VBD controller achieving a stable operation, which is the aim of primary control, and this controller still has a reasonably good power sharing ratio.

In § 6, it is demonstrated and analysed that the core VBD controller can achieve a changed power sharing ratio (i.e., not only determined by the droops of the units but also by the line impedances), with this change in the sense that the line losses

Table 4.12: Simulation results extended microgrid: other reference power and/or b for DG 4

DG unit	desired	no P corr	P corr
DG1	4.0 kW	3.78 kW	3.95 kW
DG2	6.5 kW	4.68 kW	6.48 kW
DG3	4.5 kW	4.4 kW	4.4 kW
DG4 ($b = 10$ %)	3.0 kW	3.00 kW	2.99 kW
P_1/P_2	0.62	0.81	0.62
P_1/P_4	1.33	1.26	1.33
DG1	3.15 kW	3.64 kW	3.65 kW
DG2	6.0 kW	4.80 kW	6.94 kW
DG3	4.2 kW	4.20 kW	4.20 kW
DG4 ($b = 0$ %)	1.5 kW	2.52 kW	1.74 kW
P_1/P_2	0.52	0.76	0.52
P_1/P_4	2.10	1.44	2.10
$\Delta P_1/\Delta P_2$		-0.41	0.52
$\Delta P_1/\Delta P_4$		0.48	2.04
DG1	4.0 kW	3.72 kW	3.61 kW
DG2	6.5 kW	4.61 kW	5.86 kW
DG3	4.5 kW	4.4 kW	4.4 kW
DG4 ($b = 0$ %)	3.0 kW	3.34 kW	2.70 kW
P_1/P_2	0.62	0.81	0.62
P_1/P_4	1.33	1.11	1.33
$\Delta P_1/\Delta P_2$		0.15	0.61
$\Delta P_1/\Delta P_4$		-0.82	1.30

are lowered. Hence, this change is beneficial for the network operator and from an environmental point of view. Therefore, the implications of using the VBD controller with the communication-based addition to achieve perfect power sharing, as presented in this section, are twofold. Firstly, some investments have to be made in the communication infrastructure. This is however negligible as these investments are generally already made, or will be made anyway, e.g., to enable smart grid features (e.g., changing P_{nom} in a secondary communication-based control strategy). Secondly, the power sharing is generally in the sense that the line losses are slightly higher than in the case with the core VBD controller. The effect on the reliability of the system is negligible as discussed above. The benefit is that the power sharing is exactly equal to the set value.

4.6 Global VBD control

In this section, the developed VBD control is analysed in comparison with the conventional grid control, referred to as the conventional active power/frequency droop (CPFD) control. Both the VBD control and the CPFD control operate without communication and focus on the primary grid control to ensure a stable network operation. The main difference is that the CPFD controllers use frequency as trigger for active power changes, while the VBD controller is triggered by the dc-link voltage.

4.6.1 Introduction

The theoretical analogy between conventional grid control by means of synchronous generators (SGs) and resistive islanded microgrid control through converter-interfaced distributed generation (CIDG) units is studied. There is an analogy between the rotating inertia of SGs and the dc-link capacitor of CIDG units, as they form the storage capacity for transient active power changes. A second analogy is present between the grid frequency in case of SGs and the dc-link voltage of DG units, as they show the state of the network. The conventional grid control is based on the frequency as a global parameter, which is thus equal throughout the power system. Frequency changes show differences between the mechanical power and the ac power. The SGs act on changes of frequency through their P/f droop controllers, without inter-unit communication. For CIDG units, a difference between dc-side power and ac-side power is visible in the dc-link voltage of each unit. Opposed to grid frequency, this is not a global parameter. Thus, in order to make a theoretical analogy, a global measure of the dc-link voltages is required. A control strategy based on this global voltage, the global dc-link voltage-based droop (GVBD) control, is presented, and the analogy with the conventional grid control is studied. In order to make the theoretical analogy complete, communication is required to determine the global parameter representing the dc-link voltage of all DG units, the so-called global dc-link voltage.

The GVBD control follows the theoretical analogy with conventional grid control, but requires inter-unit communication. In this section, it is shown that the VBD control for CIDG units approximates this analogy closely, but avoids inter-unit communication. Therefore, this control strategy is straightforward for implementation as it is close to what control engineers are used to. Also, it has some specific advantages for the integration of renewables in the network as is discussed in § 4.2.

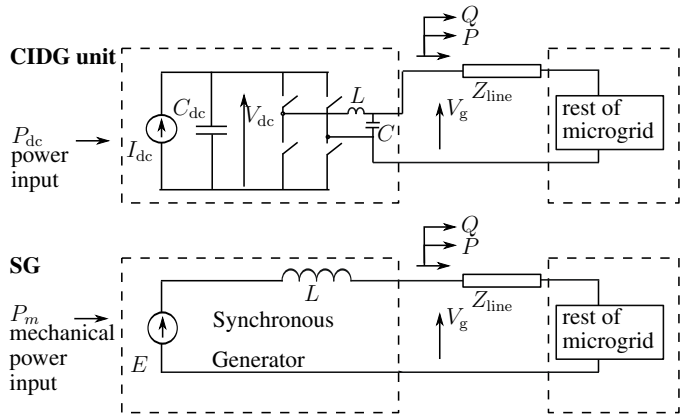

Figure 4.48: Synchronous generator (SG) versus voltage-source inverter (VSI) in case of a converter-interfaced DG (CIDG) unit

4.6.2 Conventional grid control

The CPFD control, for large centralised SGs connected to the transmission network, is largely based on the rotating inertia of the network. In case of a difference between the mechanical input power P_m and the electrical output power P in Fig. 4.48, the rotational speed of the generator will change. The grid frequency f is directly coupled with the rotational speed. Therefore, in case of a load change in the network, the SGs will all measure a changed grid frequency, as frequency is a global parameter. The CPFD control strategy of the SGs is designed such that the prime movers react on the frequency changes by means of a droop control mechanism:

$$P_{\mathrm{m}} = P_{\mathrm{m,nom}} - K_{\mathrm{P,SG}}(f - f_{\mathrm{nom}}) \tag{4.33}$$

with $K_{\mathrm{P,SG}}$ the droop coefficient or statism of the generator. $K_{\mathrm{P,SG}}$ is tuned according to the type of energy source and the ratings of the SGs.

4.6.3 Control of CIDG units in an islanded microgrid

Islanded microgrids are generally fed with CIDG units (see Fig. 4.48). These units generally have no rotating inertia or are not directly coupled to the grid (thus, the rotational speed of the generator is not directly coupled with the grid frequency), just like the loads. Therefore, the islanded microgrids lack the inertia where the conventional grid control is largely based on. Also, in the considered resistive networks, there is mainly a linkage between the active power and the voltage instead

of the phase angle. Therefore, the VBD control strategy is used.

4.6.4 Analogy conventional grid control/microgrid control

A. Parameter for active power change

A change of consumption or generation instantly affects the dc-link voltages of the DG units, because of the presence of dc-link capacitors. This is analogous to the change of grid frequency in conventional networks. If the CIDG units are controlled by control strategies that keep the dc-link voltage equal to a predefined value (e.g., proportional-integral controller), only the transient state is visible in V_{dc}. However, in the VBD control, V_{dc} is controlled to a constant but not necessary predefined value (proportional controller). Therefore, V_{dc} shows the overall system state. A high V_{dc} indicates a low load burden, while a low dc-link voltage is present in case of a heavily loaded network.

However, opposed to the grid frequency, V_{dc} is not a global parameter, thus, for the analogy between conventional grid control and islanded microgrid control, a global parameter representing the state of all units is required. This global parameter can be obtained from the balancing energy. In the conventional system, the kinetic energy (KE) stored in the system equals:

$$\mathrm{KE} = \frac{1}{2} J \omega^2 \tag{4.34}$$

with J the total rotating inertia of the system and $\omega = 2\pi f$. Changes of f show differences between P_{m} and P that are balanced by a changed KE of the system. In the islanded microgrid, the balancing energy is obtained from the energy in the dc-link capacitors (capacitor energy CE):

$$\mathrm{CE} = \sum_{\mathrm{i}=1}^{\mathrm{N}} \frac{1}{2} C_{\mathrm{dc,i}} V_{\mathrm{dc_i}}^2 \tag{4.35}$$

with N the number of dc-link voltages. A complete analogous energy equation is obtained. Hence, a change of CE compared to the nominal value can be used as the required global parameter:

$$e_{\mathrm{dc,g}} = \frac{1}{N} \sum_{i=1}^{N} \frac{C_{\mathrm{dc,i}} V_{\mathrm{dc,i}}^2 - C_{\mathrm{dc,nom,i}} V_{\mathrm{dc,nom,i}}^2}{C_{\mathrm{dc,nom,i}} V_{\mathrm{dc,nom,i}}^2} \tag{4.36}$$

This is analogous to

$$\frac{1}{N}\frac{J\omega^2 - J\omega_{\mathrm{nom}}^2}{J\omega_{\mathrm{nom}}^2}. \tag{4.37}$$

Hence, $e_{\mathrm{dc,g}}$ and ω (or f) can be used as parameters in $P/e_{\mathrm{dc,g}}$ and the conventional P/f droop controllers that are implemented in an analogous way. Here, the considered units have equal nominal dc-link voltages and capacitances. Therefore, and to limit the computational burden, also the dimensionless parameter $v_{\mathrm{dc,g}}$ can be used instead of $e_{\mathrm{dc,g}}$:

$$v_{\mathrm{dc,g}} = \frac{1}{N}\sum_{i=1}^{N}\frac{V_{\mathrm{dc,i}} - V_{\mathrm{dc,nom,i}}}{V_{\mathrm{dc,nom,i}}} \tag{4.38}$$

$v_{\mathrm{dc,g}}$ is called the global dc-link voltage. However, if the difference between the capacitance of the dc-link capacitors is significant, using e_{dc} instead of $v_{\mathrm{dc,g}}$ is the logical approach to make a control in resistive microgrids that is analogous to the CPFD control in conventional networks.

B. Droop controller based on global dc-link voltage

The global $v_{\mathrm{dc,g}}$ is drooped, with a negative slope, to determine the dc-power of the unit as shown in Fig. 4.49:

$$P_{\mathrm{dc}} = P_{\mathrm{dc,nom}} - K_{\mathrm{g}} v_{\mathrm{dc,g}}. \tag{4.39}$$

This is analogous to (4.33) by linking f with $v_{\mathrm{dc,g}}$. The droop K_{g} can be tuned in the same way as the statism of conventional generators. A low value of K_{g} is included in little-dispatchable units and/or units with low P_{nom}, while a high K_{g} is used in case of dispatchable units and/or units with high P_{nom}.
Note that in order to determine V_{dc} in a single-phase system, a sample rate of twice the fundamental grid frequency is required to filter the ripple in the dc-link voltage caused by the full-bridge configuration of the VSI. Therefore, for the communication of $v_{\mathrm{dc,g}}$, an important advantage is that only low-bandwidth communication is required. Also, if this communication fails, instead of the global $v_{\mathrm{dc,g}}$, the local V_{dc} can be used in the droop to determine P_{dc}.
With the controller in (4.39) alone, V_{g} would remain constant. This would lead to an inadequate operation in the resistive network because in this case, the active power sharing is determined by the line impedances instead of the ratings of the DG units. Therefore, the $V_{\mathrm{g}}/V_{\mathrm{dc}}$ droop controller is used.
In conclusion, in the analogy between GVBD control of CIDG units and CPFD control of SGs, the dc-link capacitor C_{dc} has the function of the rotating inertia J

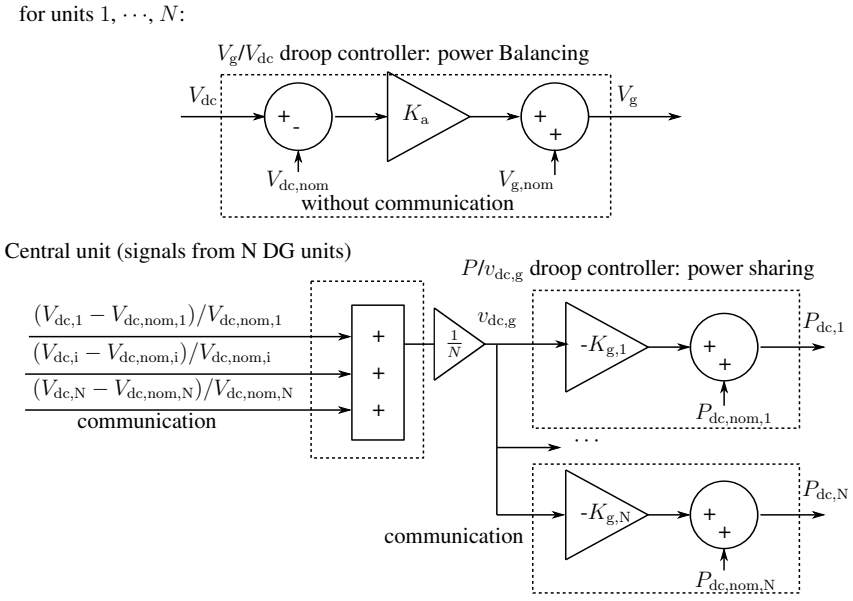

Figure 4.49: GVBD control (here a dispatchable DG unit is considered: $b = 0$), $v_{dc,g}$ is communicated to each CIDG unit and used in the $P_{dc}/v_{dc,g}$ droop control. This controller cooperates with the V_g/V_{dc} droop controller.

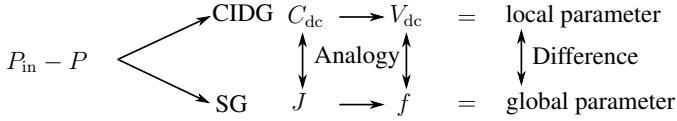

Figure 4.50: Analogy between J and C_{dc}; V_{dc} and f (P_{in} is the input power of the unit: $P_{in} = P_m$ in case of a SG, and $P_{in} = P_{dc}$ in case of a CIDG unit)

in the conventional grid control and the global dc-link voltage $v_{dc,g}$ functions as the grid frequency f as depicted in Fig. 4.50.

C. *VBD control as variant of GVBD control without inter-unit communication*

In SGs with CPFD control, P is drooped with f, while in the analogy of CIDG units with GVBD control, P is drooped with $v_{dc,g}$. The VBD control strategy, consisting of V_g/V_{dc} and P_{dc}/V_g droop controllers, matches the GVBD control strategy very

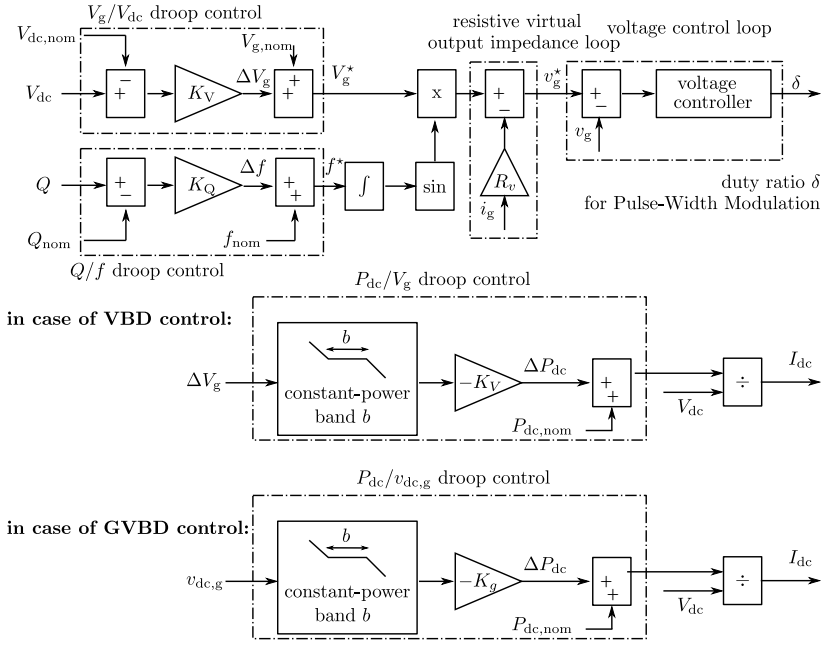

Figure 4.51: Control algorithm of GVBD and VBD control

closely in resistive networks. As illustrated in Fig. 4.51, the P_{dc}/V_g droop controller in VBD control is analogous to the $P_{dc}/v_{dc,g}$ droop controller in GVBD control because of the linear relationship between V_{dc} and V_g through the V_g/V_{dc} droop controller. An exact match in the analogy between VBD control and CPFD control is not possible, opposed to the case of GVBD droop control, because the VBD control does not use inter-unit communication. Therefore, not the global $v_{dc,g}$ is known but only the local V_{dc} is visible for each DG unit separately.

The analogy is, thus, precise if the microgrid is fed by only one dispatchable unit ($v_{dc,g}V_{dc,nom} = V_{dc} - V_{dc,nom}$). It is also precise in case of a combination of one dispatchable unit and several units operating in the constant-power band (with $P_{dc} = P_{dc,nom}$). In case of multiple dispatchable units, the analogy is approximately valid if it is considered in a local manner. The local nature of the VBD control is one of its intrinsic advantages. In case of, e.g., high renewable generation and a low local load, the grid voltage will locally increase. This is because of the usage of constant-power bands. Because of the local nature of these high voltages, only dispatchable DG units located electrically nearby and local loads (see chapter 5) will change their generated power. This can decrease the line losses and avoid congestion problems as locally consumed power is locally generated.

In conclusion, VBD control is similar to GVBD control, with the latter being completely analogous to conventional grid control. Therefore, this control strategy can be implemented in a manner close to what control engineers are used to. The local nature of VBD control, opposed to GVBD and CPFD control, has some important advantages, as discussed above.

4.6.5 Islanded microgrids: CPFD control with SGs versus GVBD and VBD control with CIDG units

In this paragraph, first, a basic microgrid is studied consisting of two generators and two loads. The cases of GVBD control and CPFD control are compared in order to study the theoretical analogy between both control strategies. Second, the same case with VBD control is considered to prove that this control strategy follows the analogy with CPFD control closely, without need for inter-unit communication, opposed to the GVBD control. Finally, the three controllers (GVBD, VBD and CPFD control) are studied in a more realistic microgrid with dynamic events and three generators.

A. CIDG units with GVBD control

In this first case, two DG units G_1 and G_2 are feeding a constant-power load $P_{\text{load},1}$ of 2 p.u. ($P_{\text{ref}} = 1$ kW) in islanded mode as depicted in Fig. 4.52. After 1 s, a second load of 1 p.u. turns on as well. The VSIs have an LC filter with $L = 2$ mH and $C = 3$ μF, the nominal grid voltage equals 1 p.u. rms ($V_{\text{ref}} = 230$ V). The dc-link capacitances C_{dc} equal 1.5 mF and the input dc-current I_{dc} equals $P_{\text{dc}}/V_{\text{dc}}$, with P_{dc} determined according to (4.39) and V_{dc} the dc-link voltage. The two DG units have nominal power $P_{1,\text{nom}} = 0.9$ p.u. and $P_{2,\text{nom}} = 1.2$ p.u. The line impedances are assumed as purely resistive and $Z_{\text{line}} = 0.009$ p.u. A resistive virtual output impedance $z_v = 0.056$ p.u. is included in the VSI. Note, that the nominal voltage in (4.9) is adapted according to z_v:

$$V_{\text{g,nom}} = V_{\text{ref}} + z_v \frac{P_{\text{nom}}}{V_{\text{ref}}}. \tag{4.40}$$

The global measure of V_{dc} is determined according to (4.38), with $N = 2$. This parameter $v_{\text{dc,g}}$ is then drooped according to the GVBD control strategy, with a negative slope K_g to determine the dc-power of the unit. In the following simulations: $V_{\text{dc,nom}} = 450$ V, $K_{\text{V}} = \frac{0.5}{\sqrt{2}}$, $K_{\text{g},1} = 100 V_{\text{dc,nom}} \frac{2P_{1,\text{nom}}}{P_{1,\text{nom}}+P_{2,\text{nom}}}$ and $K_{\text{g},2} = K_{\text{g},1} \frac{P_{2,\text{nom}}}{P_{1,\text{nom}}}$. For the reactive power control, Q/f droop control with $K_Q = 1 \cdot 10^{-4}$ Hz/VAr is used. The simulation results are depicted in Fig. 4.53.
At $t = 1$ s, a small transient is depicted as the second load turns on. In steady-state,

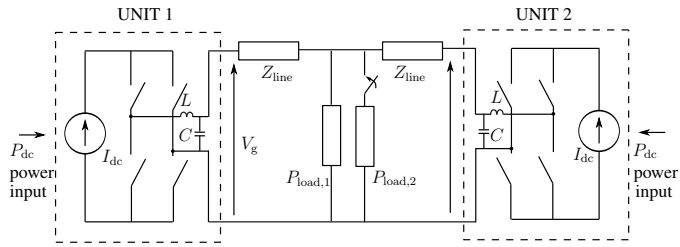

Figure 4.52: Configuration: microgrid with two generation units and two constant-power loads

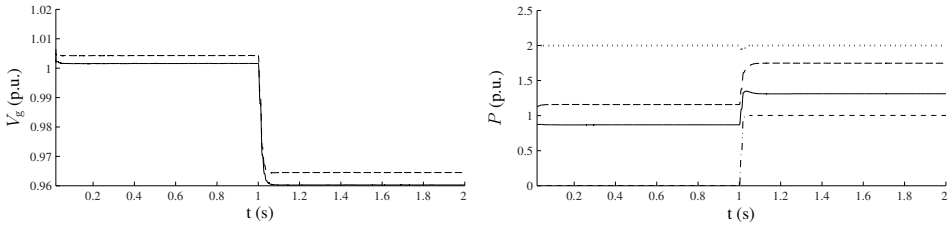

(a) Terminal voltage V_{g} (b) Output power P

Figure 4.53: GVBD: DG units act on global measure of V_{dc} (— = G1; ---- = G2, ⋯ = load 1, -·-·- = load 2)

with total load 3 p.u., $P_1 = 1.311$ p.u. and $P_2 = 1.748$ p.u. The power is shared according to the ratings of the DG units as $\frac{\Delta P_1}{\Delta P_2} = \frac{P_1 - P_{1,\text{nom}}}{P_2 - P_{2,\text{nom}}} = 0.75$.
For $0 < t < 1$ s, $v_{\text{dc,g}} = \frac{0.435}{V_{\text{dc,nom}}}$ p.u. This slightly positive value of $v_{\text{dc,g}}$ implies that $P_1 + P_2 < P_{\text{nom,1}} + P_{\text{nom,2}} = 2.1$ p.u. In $1 < t < 2$ s, $v_{\text{dc,g}} = \frac{-4.795}{V_{\text{dc,nom}}}$ p.u., which has decreased because of the extra load. Therefore, the generated powers of the DG units increase and accurate load sharing is obtained.

B. SGs equipped with CPFD control

The same microgrid is studied, but with SGs instead of DG units. Each SG is represented as an emf E in series with an inductance L (and a small equivalent stator resistance of $0.18 \cdot 10^{-3}$p.u.). The combination of the inductive lines and the SG inductance equals $j0.028$ p.u. The inertia of the SGs equals 0.18 kgm^2. CPFD control is used, i.e. (4.33), with $K_{\text{P,SG,i}} = 8000\pi \frac{P_{\text{i,nom}}}{P_{1,\text{nom}} + P_{2,\text{nom}}}$, $i = 1, 2$. For the reactive power control, Q/V droops are implemented. In the simulations, by comparing the ac power P with P_m and by using the inertia of the SG, the change

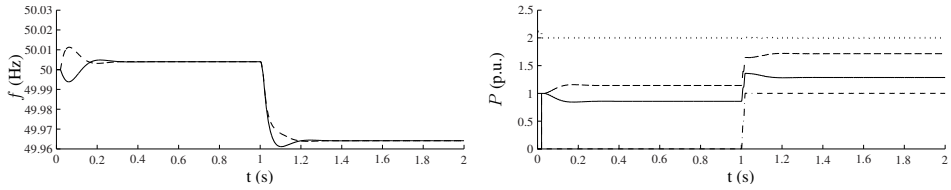

(a) Frequency f (b) Output power P

Figure 4.54: SGs equipped with CPFD control, inductive lines (— = G1; ---- = G2, ⋯ = load 1, -·-·- = load 2)

of frequency is calculated. The frequency, together with the obtained rms voltage from the Q/V droops, determine the back-emf E of the SG. The simulation results are depicted in Fig. 4.54.

After a start-up transient and a transient because of the changing load, a stable operation is obtained. As only primary control is implemented, in steady-state $f_1 = f_2$, but not necessarily equal to f_{nom}. In steady-state, $P_1 = 1.29$ p.u. and $P_2 = 1.71$ p.u., thus, with power sharing according to the ratings of the units. Also in steady state, $P_1 + P_2 = P_{\text{load},1} = 3$ p.u. because the line impedances are assumed as purely inductive, opposed to the previous case.

C. CIDG units with VBD control

The same case as with the other CIDG units is studied, but with $P_{\text{dc}}/V_{\text{g}}$ droop control without communication instead of the $P_{\text{dc}}/v_{\text{dc,g}}$ droop control. The line parameters are equal to those in the GVBD control scenario. The droop K_P of the $P_{\text{dc}}/V_{\text{g}}$ droop controller equals $\sqrt{2}P_{\text{nom}}/50$ W/V. The results depicted in Fig. 4.55 show that in steady-state, $P_1 = 1.33$ p.u. and $P_2 = 1.74$ p.u. The power is not exactly shared according to the ratings of the units as $\Delta P_1/\Delta P_2 = 0.80$. Exact power sharing is achieved when $R_{\text{line},1}/R_{\text{line},2} = P_2/P_1$, then, $P_1 = 1.31$ p.u. and $P_2 = 1.75$ p.u. The power sharing is, thus, partly dependent on the line parameters. Because of this issue, using the $v_{\text{dc,g}}$ droop control with communication as secondary control next to the primary VBD control without communication can give good results. On the other hand, in the VBD control, the individual V_{dc} can vary differently from $v_{\text{dc,g}}$. This can be advantageous for the line losses in the network.

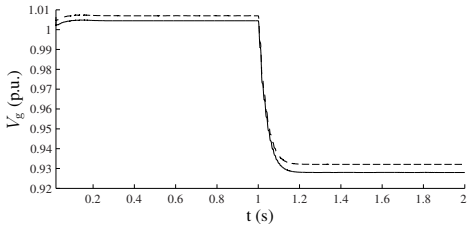

(a) Terminal voltage V_{g} (b) Output power P

Figure 4.55: VBD: DG units act on local parameters (— = G1; ---- = G2, , ⋯ = load 1, -·-·- = load 2)

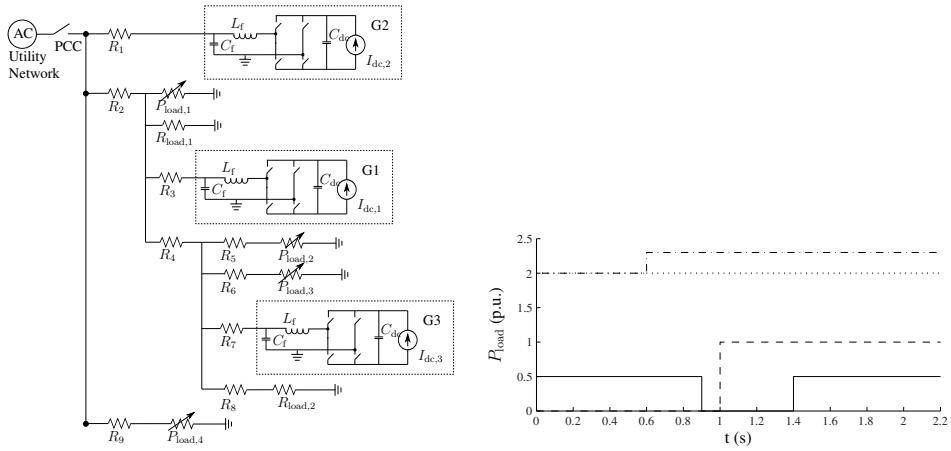

(a) Islanded microgrid (b) Constant-power loads (— = $P_{\mathrm{load},1}$; ---- = $P_{\mathrm{load},2}$, -·-·- = $P_{\mathrm{load},3}$, ⋯ = $P_{\mathrm{load},4}$)

Figure 4.56: Microgrid configuration)

D. Microgrid

In the following simulation, the microgrid of Fig. 4.56(a) is studied. There are four constant-power loads, with load profile shown in Fig. 4.56(b), two resistive loads $R_{\mathrm{load},1}$ and $R_{\mathrm{load},2}$ and three DG units. To limit the simulation time, an averaged converter model is used and the configuration parameters are summarised in Table 4.13. The combination of the line resistances and the resistive virtual output impedances of the DG units (R_1, R_3 and R_7) equals 0.057 p.u.

Table 4.13: Microgrid case: parameters

Parameter	value	parameter	value
C_{dc}	1.5 mF	$R_{\mathrm{load},2}$	1.42 p.u.
$V_{\mathrm{dc,nom}}$	450 V	K_{V}	$0.5/\sqrt{2}$ V/V
$V_{\mathrm{g,ref}}$	230 V	$K_{\mathrm{g},1}$	$90\frac{P_{\mathrm{nom},1}}{P_{\mathrm{nom},1}+P_{\mathrm{nom},2}}\frac{\mathrm{kW}}{\mathrm{V}}$
P_{ref}	1 kW	$K_{\mathrm{g},2}$	$90\frac{P_{\mathrm{nom},2}}{P_{\mathrm{nom},1}+P_{\mathrm{nom},2}}\frac{\mathrm{kW}}{\mathrm{V}}$
f_{nom}	50 Hz	$K_{\mathrm{g},3}$	0 kW/V
$p_{\mathrm{nom},1}$	2.5 p.u.	K_{Q}	0.0001 Hz/VAr
$p_{\mathrm{nom},2}$	3 p.u.	$K_{\mathrm{P},1}$	$P_{\mathrm{nom},1}/50$ W/V
$p_{\mathrm{nom},3}$	2 p.u.	$K_{\mathrm{P},2}$	$P_{\mathrm{nom},2}/50$ W/V
R_1,R_3,R_7,R_8	0.057 p.u.	$K_{\mathrm{P},3}$	0 W/V
R_2,R_4,R_5,R_6	0.006 p.u.	$K_{\mathrm{P,SG},1}$	$8\pi\frac{P_{\mathrm{nom},1}}{P_{\mathrm{nom},1}+P_{\mathrm{nom},2}}\frac{\mathrm{kW}}{\mathrm{Hz}}$
R_9	0.006 p.u.	$K_{\mathrm{P,SG},2}$	$8\pi\frac{P_{\mathrm{nom},2}}{P_{\mathrm{nom},1}+P_{\mathrm{nom},2}}\frac{\mathrm{kW}}{\mathrm{Hz}}$
$R_{\mathrm{load},1}$	0.95 p.u.	$K_{\mathrm{P,SG},3}$	$8\pi\frac{P_{\mathrm{nom},2}}{P_{\mathrm{nom},1}+P_{\mathrm{nom},2}}\frac{\mathrm{kW}}{\mathrm{Hz}}$

CIDG units with GVBD control In the first case, GVBD control is considered with $v_{\mathrm{dc,g}}$ calculated from the dc-link voltages of G1 and G2. G3 is considered as a non-dispatchable generator: from $0 < t < 1$ s, G3 operates at $P_{\mathrm{nom},3}$, from $1 < t < 1.5$ s, the generated power decreases with 25 %; from then on, the generated power increases again to $1.25P_{\mathrm{nom},3}$. Next to the $P_{\mathrm{dc}}/v_{\mathrm{dc,g}}$ droops with slope K_{g}, also the $V_{\mathrm{g}}/V_{\mathrm{dc}}$ droop with slope K_{V} and Q/f droops with slope K_{Q} are used in the DG units. The results are depicted in Fig. 4.57(a).

After a start-up transient, a stable operation is obtained. The undispatchable DG unit G3 delivers its nominal power, despite the load changes, and hence, does not take part in the power sharing. The other two DG units take part in this power sharing by acting on the load changes. For example, in steady-state, $P_1 = 2.23$ p.u., $P_2 = 2.68$ p.u., thus, accurate power sharing is obtained as

$$\Delta P_1/\Delta P_2 = P_{\mathrm{nom},1}/P_{\mathrm{nom},2} = 0.83. \tag{4.41}$$

Therefore, the GVBD control works well, showing that making an analogy between CPFD control and microgrid control with resistive line parameters is possible, but communication is required.

SGs with CPFD control In the analogous CPFD control, instead of DG units, the microgrid is powered by directly coupled SGs. The three units are equipped with P/f droop control. In this way, these units take part in the power balancing

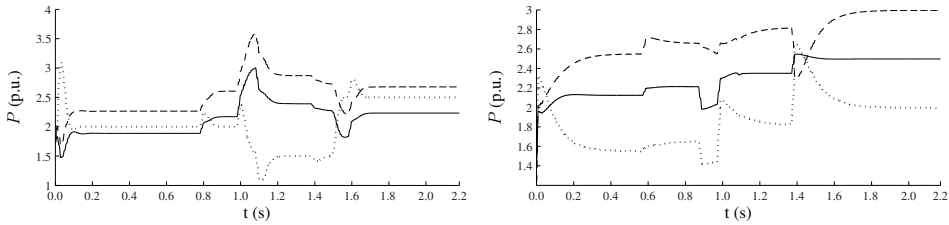

(a) DG units with GVBD control

(b) SGs with CPFD control

Figure 4.57: Output power P (— = G1; ---- = G2, $\cdots$ = G3)

as most SGs are dispatchable opposed to many small DG units. As the networks powered by SGs are generally high-voltage networks, the lines here are considered as mainly inductive. Except for this, the considered microgrid is the same as in the previous case. Next to the P/f droops with slope $K_{\mathrm{P,SG}}$, also Q/V droops with slope $0.01/\sqrt{2}$ V/VAr are used. The results are depicted in Fig. 4.57(b).
For example, at $t = 2.20$ s, $P_1 = 2.50$ p.u., $P_2 = 3.00$ p.u. and $P_3 = 2.00$ p.u.; while at $t = 1.4$ s, $P_1 = 2.35$ p.u., $P_2 = 2.81$ p.u. and $P_3 = 1.82$ p.u. In steady-state, the power is exactly shared according to the ratings of the SGs without communication.

CIDG units with VBD control The same microgrid configuration as with the GVBD control is studied, but with VBD control. Next to the $P_{\mathrm{dc}}/V_{\mathrm{g}}$ droops with slope K_{P}, also the $V_{\mathrm{g}}/V_{\mathrm{dc}}$ droops with slope K_{V} and Q/f droops with slope K_{Q} are used. The results are depicted in Fig. 4.58.
After a start-up transient, a stable operation is obtained. In steady-state at $t = 2.2$ s, $P_3 = 2.5$ p.u. as this is the undispatchable DG unit; $P_1 = 2.3$ p.u., $P_2 = 2.6$ p.u., thus, $\Delta P_1/\Delta P_2 = 0.50$. This illustrates a well-known characteristic of droop control without communication, namely the inherent trade-off between accuracy of power sharing and voltage deviations [83, 110, 111]. It also shows that the GVBD control can help to optimise the power sharing according to the ratings of the units, e.g., when included as a secondary control strategy, requiring communication. VBD control is used as primary control because of reliability reasons as it does not depend on communication links to achieve a proper microgrid operation.

4.6.6 Conclusion

In this paragraph, the CPFD control in inductive networks based on the rotating inertia of the SGs and the control of resistive microgrids by means of CIDG units

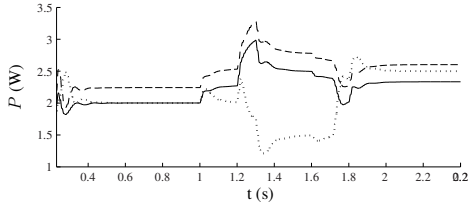

Figure 4.58: Microgrids with DG units controlled by VBD control, output power P (— = G1; ---- = G2, $\cdots$ = G3)

lacking inertia, are compared. The theoretical analogy between the rotating inertia and the dc-link capacitor on one hand and the grid frequency and the dc-link voltage on the other hand are studied. A control strategy based on this analogy is presented, which is called the GVBD control. Opposed to CPFD control, the GVBD control requires inter-unit communication. This is because the dc-link voltage is not a global parameter, opposed to grid frequency. With the GVBD control, accurate power sharing, a stable operation, and an operation similar to conventional grid control are obtained.
The VBD control is based on the same principles as the GVBD control but without inter-unit communication, which benefits the reliability of the system. Therefore, it is a control strategy for resistive islanded microgrids that approaches the analogy with CPFD control closely, so an operation similar to that of the conventional network can be obtained. The local nature of this control strategy can lead to a possible reduction of line losses and congestion problems.

4.7 Conclusions

Because of the mainly resistive line parameters and the lack of inertia in islanded microgrids, voltage-based droop control is very promising for active power sharing between DG units. The method does not require inter-unit communication which benefits the robustness. Also, an optimised integration of renewable energy sources can be achieved because the voltage-based droop control strategy does not require communication to delay the power changes of the renewable DG units compared to those of the dispatchable units and uses power curtailment instead of on/off control of renewable energy sources.
The Q/f droop controller is well-suited for cooperation with VBD control. Its usage is also based on the resistive lines in the considered microgrids and it does not require inter-unit communication.
However, if no extra measures are taken, the DG units can be represented as a short-circuit for harmonic currents and the DG units electrically closest to the harmonic

load, will deliver most harmonic currents. Therefore, the VBD control strategy is modified to provide controllable harmonic current sharing. A modified version of the PR-SHI method is implemented in the VBD control strategy. This enables the DG units to become programmable resistances for harmonic currents. In this way, harmonic current sharing between the DG units can be achieved in a controllable manner and without inter-unit communication.

An inherent characteristic of droop control is the trade-off between power sharing accuracy and voltage control. Therefore, an additional control loop can be included in the VBD control to improve the power sharing, i.e., obtaining a power sharing that is exactly according to the droops. However, inter-unit communication is required for this purpose, but this is not a significant disadvantage concerning the reliability of the system. A more important disadvantage is that the local nature of the original VBD control and the subsequent advantage of a reduction of line losses, which is clarified in this fifth section and chapter 6, is lost.

In the final section, the theoretical analogy between conventional P/f droop control in the transmission networks and VBD control in low-voltage microgrids is illustrated. Hereto, the GVBD control is developed as communication is required to fully make this analogy valid. VBD control approximates the conventional grid control closely and has the advantage that its local nature can reduce line losses and mitigate congestion problems.

The content of this chapter has been published in the papers [138, 184, 187, 188]. The content of § 4.5 is submitted for publication.

Chapter 5

Control of other microgrid elements

The previous chapter focussed on the control of the DG units in an islanded microgrid by introducing the VBD control scheme. In this chapter, an analogous control strategy is presented for the other microgrid elements. First, the active loads and storage elements can also participate in the primary control of the islanded microgrid. By using VBD control in all grid elements, an automatic priority to act on load variations is set. This is achieved by setting a proper constant-power band. Note that demand dispatch generally consists of three elements: prediction, planning and control. As here, the real-time control is addressed to maintain a stable microgrid operation, it is called a primary load control strategy, analogous to the primary control of the DG units. In the second section, the synchronous generator control is modified to comply with the VBD control strategy. Finally, in § 5.3, the transformer at the PCC is operated as a "smart transformer". In this way, the power exchange between microgrid and utility network can be controlled and a virtual islanded operating condition is possible.

5.1 Loads and storage elements

The VBD control is developed for the VSI interfaced DG units in islanded microgrids. Because of the small size of the microgrid and the high share of renewables with an intermittent character, new means of flexibility in power balancing are required to ensure a stable operation. Hence, the other grid elements also need to contribute in the control. Therefore, a novel demand dispatch strategy is presented. The demand dispatch is triggered by the microgrid voltage level.

5.1.1 Introduction

Some factors in microgrids lead to an increased need for active load control. Firstly, a large share of the DG units in the microgrid are not centrally dispatched. These DG units generate power when the energy source is available, which can not be scheduled nor predicted with certainty. This lowers the power flexibility and decreases the system reliability. Secondly, high consumption peaks arise in islanded microgrids because of their small scale.

A novel demand dispatch strategy is presented, with the rms voltage as trigger. This is enabled by using the VBD control strategy in the DG units as it influences the microgrid voltage as a measure of the level of loading versus generation in the microgrid. In VBD control, the renewables only act on extreme voltage deviations to change their active power. Hence, large voltages indicate times with a high renewable energy input and a low load burden and vice versa for low voltages. In this way, the voltage shows the critical instants at which the contribution of storage and controllable loads is required. Therefore, the control of the active loads and the generators can use the same trigger, namely the microgrid voltage. The demand dispatch strategy shifts the load to have a lower consumption in case of a low microgrid voltage and to a higher consumption in case of high voltages. Hence, the demand dispatch does not require inter-unit communication, which is an important advantage concerning reliability issues. The controllers are responsible for the primary control of the microgrid and can be overlayed with a secondary (communication-based) controller.

Short-term storage of energy is needed to cope with the fluctuations in power demand or accommodate sudden changes of generation. A microgrid is not a stiff system: the small generators neither store significant amounts of energy in a mechanical inertia nor necessarily respond quickly to sudden changes of load. Hence, short-term storage elements, possibly distributed with the generators, can permit the inverters to follow rapid changes while giving time to the generators to respond [189]. The stability, power quality and reliability of supply can, thus, be improved thanks to the usage of energy storage. In [51], a review of microgrid-oriented energy storage technologies can be found. The presented demand dispatch and VBD control strategies are applicable for the storage equipment as well. Storage can be operated in an analogous manner as the fully dispatchable DG units (zero constant-power bands) or the less dispatchable units (non zero constant-power bands). Of course, the specific constraints of the storage equipment, such as the charging levels, need to be taken into account. This is similar with the load constraints in the demand dispatch strategy. Here, the focus is on the demand dispatch strategy, rather than on storage control or taking the specific constraints into account. The latter can be performed by a slower secondary controller.

5.1.2 Demand dispatch in islanded microgrids

A. Historical demand dispatch strategies

It is estimated that the potential of demand dispatch is huge: in [190] for example, it is estimated that up to 33 % of all loads could have at least some level of demand dispatch control without a significant impact on the end users. Some loads that are good candidates for demand dispatch are discussed in [190]. In [30], some techniques of demand side management (DSM[1]) that have been put into practice, such as night-time control and direct control, are summarised. Also, under-frequency or under-voltage load shedding are investigated [191]. Historically, demand dispatch has focussed on reducing the overall electricity consumption and on peak shaving to help reducing the generation margin [30]. However, with the high degree of unpredictable sources and the high peak loads, the active load control must go further than the historical response. Therefore, more recently, it has begun to be considered for supply reliability services [192]. In the future, demand dispatch will become more embedded as customers will be able to purchase smart appliances and use new technologies to automate their responses [193]. The smart grid will further enable demand dispatch as it provides real-time targeted communication with individual loads to provide remote load control [190]. From the consumers point of view, new products and services arise by demand dispatch, helped by the development of the smart grid as in the emerging smart grid paradigm, active load control is an important ingredient [194, 195]. For the network operators, demand dispatch will increase the control flexibility to maintain a reliable system operation. Smart grid communication enables to optimise load shedding as well. For example in [196], by detecting the voltage change rate and profile, the load shedding amount is calculated, which requires some level of communication or system knowledge.

In microgrids with a high share of (renewable) uncontrollable sources, demand dispatch can be represented as a form of standing reserve for managing the demand-supply balance. Consequently, it can provide an increased supply reliability, despite the inflexibility of the power sources. Therefore, in this section, a novel demand dispatch strategy is specifically designed for application in an islanded microgrid. The demand dispatch is performed as a primary control without communication, and mainly for increasing the reliability of the islanded microgrid.

[1] DSM is a combination of methods to engage customers in having a more energy-efficient consumption and to shift their consumption when required. DSM consists, thus, of energy efficiency and demand response (DR) programs. DR manages the customer consumption in response to supply conditions. Demand dispatch is equal to DR and enables the load to follow the generation, instead of the current strategy where the generation follows the load variations.

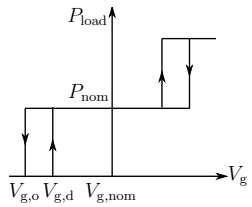

Figure 5.1: Implementation of demand dispatch to change the load: relay function

B. Presented demand dispatch strategy

By using the VBD control method for the generators, the possibility of the microgrid voltage to vary between certain limits is effectively used. Therefore, the microgrid voltage can be applied to communicate an excess or deficit of power in the islanded microgrid, which is mainly due to the renewable power in case of proper application of the adjustment voltage.
The implementation of the demand dispatch strategy with a relay (hysteresis) function is displayed in Fig. 5.1. For example, in case an active load senses a terminal voltage that is lower than $V_{\mathrm{g,o}}$, if possible (which depends on the state of the load), it switches off or decreases its power consumption. If the microgrid voltage rises back to $V_{\mathrm{g,d}}$, it turns back on. Because of the relay with $V_{\mathrm{g,d}}$ larger than $V_{\mathrm{g,o}}$, frequent load switching or changing are avoided. The implementation of the demand dispatch strategy for load increases, or equivalently, load shifting towards high-voltage periods is analogous. Similar to the VBD control of the DG units, the relay function also has a constant-power band with $b = \frac{V_{\mathrm{g,nom}} - V_{\mathrm{g,o}}}{V_{\mathrm{g,nom}}}$. The value b can be set analogously as that of the generators. Further, the relay function can be extended from load shedding to a more complete active load control that includes gradual load changes in a stepwise or linear relay function.

C. Discussion

As the presented demand dispatch strategy is performed with the emphasis of increasing the reliability of the microgrid by providing assistance in the balancing, it is performed without communication. Hence, the rms microgrid voltage is the trigger for the demand dispatch. Therefore, if a remote communication signal for external demand control is lost, still, the demand dispatch, which is crucial in small islanded microgrids, can cooperate with the control of the generators to balance the power in the microgrid with a short response time. Communication can however be effectively used for secondary demand dispatch features, e.g., for optimal management of the load changes.
Customer acceptance to load control is widely studied, e.g. in [197]. For each

strategy, the basic requirement for customer acceptance is financial benefit. The pricing aspect is out of the scope of this PhD thesis. However, it is suggested that by extending the control strategy with smart grid features, a compensation for this grid support can be established. In [198], a distinction is made between time-based (temporarily changes of electricity prices) and incentive-based demand dispatch. The incentive-based control is a direct control, which implies that a service provider can directly influence the loads and DG units [6]. Examples include direct load control of residential water heaters and air conditioning loads in California [199]. The advantages of direct control are achieving prompt and predictable reactions. The drawbacks arise from the communication and optimisation efforts involved in controlling a large number of devices, and often a low customer acceptance [6]. Time-based control is an indirect control that uses price signals based on which the consumer decides to change its load or generation. Disadvantages arise from the possibility of avalanche effects and simultaneous reactions to the signal, and from the inherent forecasting errors due to the necessity to predict the reaction of the consumers to different price signals. Hence, a combination of strategies will mostly be required.
The main contribution of the demand dispatch strategy in this section is to increase the reliability of the islanded microgrid. Therefore, the incentive-based strategy could give good results, e.g., by presenting a lower distribution cost in case the load contributes to the demand dispatch. This can, for example, be monitored by the utility by means of smart grid applications. The time-based response would be harder to implement because the microgrid voltage is the trigger, which is highly influenced by the neighbour microgrid elements. However, new possibilities could arise in making the price partially dependent on the local voltage.

D. Conclusion

An advantage of this demand dispatch strategy based on the local microgrid voltage is that it can lead to a better usage of the available (renewable) energy. The reason is that the consumers optimise their consumption according to the microgrid voltage level, which depends on the instantaneous production. For example, when customers shift their consumption towards high-voltage times, they mainly use renewable power. The reason is the usage of the VBD control in the DG units. This requires that the constant power band width b of the generators and loads are properly set to obtain the desired priority list for active power changes. Secondly, a possible advantage is also the reduction of the line losses in the microgrid. E.g., if a renewable power source switches on, the closest loads will sense a higher terminal voltage and therefore, shift their consumption in time. In this way, averaging over a specified time period and assuming that the total consumption for each load remains constant in this period, the consumption is temporarily shifted to zones with an in-

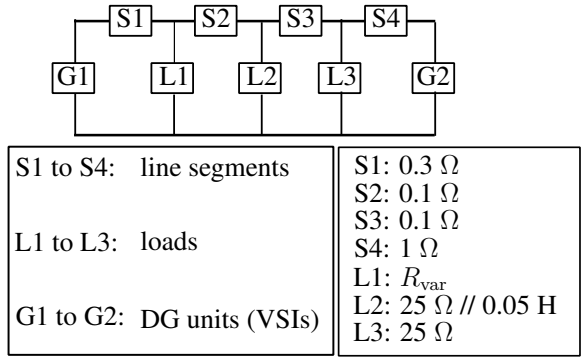

Figure 5.2: Microgrid configuration: basic example

stantaneous higher production, decreasing the overall line losses. Both advantages lead to an increased reliability and a better exploitation of the islanded microgrids. In § 5.1.3 and 5.1.4, some examples to illustrate this demand dispatch strategy and its advantages are discussed.

5.1.3 Simulation results: basic demand dispatch

In the following, demand dispatch is studied in a small islanded microgrid. The power sources are controlled with the $V_{\mathrm{g}}/V_{\mathrm{dc}}$ droop (in this case, there is no $P_{\mathrm{dc}}/V_{\mathrm{g}}$ droop control that limits the voltage variations as b is large in the considered (renewable) DG units) and Q/f droop control strategies, resulting in a constant active power of the power sources. This is a basic example where, e.g., two solar panels with MPPT feed the microgrid. The dc-link of each power source is connected to a capacitor, which forms a small storage capacity for transient ride-through. As in this case, the output power of the sources is fixed, the only control mechanism for the voltage support (obtaining a good quality of voltage amplitude and frequency) in the microgrid lies in the loads or storage elements. Except for the dc-link capacitor, storage is not considered in this example, but the loads are changed by means of the demand dispatch strategy of § 5.1.2.

The microgrid of Fig. 5.2 is considered. The two power sources are connected to the microgrid via VSIs with $L = 2$ mH and $C = 3$ μF. The dc-link capacitors are 1.5 mF and the generated powers, $P_{\mathrm{dc},1}$ and $P_{\mathrm{dc},2}$, equal 2 kW and 3 kW for G1 and G2 respectively. The reactive power controller starts after 100 ms, and with equal droops K_{Q} for the two VSIs. At $t = 0$ s, the active power balancing is initiated and the microgrid voltages start from 230 V, which is considered as an equivalent grid-connected operation mode.

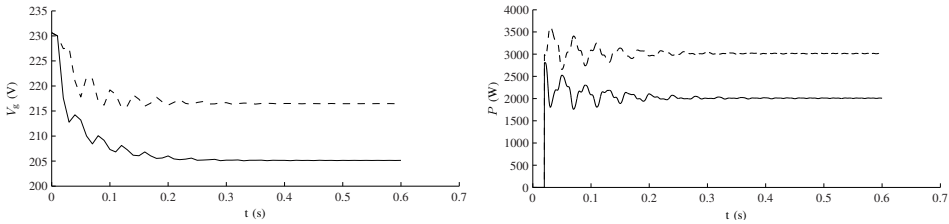

(a) Microgrid voltage (b) Active power to the electrical network

Figure 5.3: Constant dc-power, constant loads (— = VSI 1; ---- = VSI 2)

In the simulations presented below, in the simple microgrid, the cases with and without demand dispatch are compared, showing that demand dispatch leads to an operating condition that is closer to the nominal one, which increases the microgrid reliability.

A. Constant load

In this first example, the generated active powers and the loads remain constant, with a constant load R_{var} of 25 Ω. Hence, no power flexibility is included, not in the loads nor in the DG units. The simulation results are depicted in Fig. 5.3. Note that power measurements are only valid after one fundamental period of 20 ms, hence the zero initial values. Fig. 5.3(b) shows the power settling through a transient stage, until constant power is reached, which is equal to the generated power $P_{\mathrm{dc},1} = 2$ kW and $P_{\mathrm{dc},2} = 3$ kW. In Fig. 5.3(a), it is shown that in steady state, $V_{\mathrm{g},1}$ and $V_{\mathrm{g},2}$ are equal to 205.1 V and 216.5 V respectively. Thus, the terminal voltage of VSI 1 exceeds the 10 % limit, with 230 V as nominal microgrid voltage.

B. Load decrease or increase

In this case, the microgrid voltage is used as a trigger for the demand dispatch by using the relay principle of Fig. 5.1. If the microgrid voltage at the terminal of the active load R_{var} drops below $V_{\mathrm{g,o}} = 210$ V, R_{var} changes from 25 Ω to 50 Ω. In the relay function, $V_{\mathrm{g,d}}$ equals 225 V. The simulation results are depicted in Fig. 5.4. The active load control is delayed with 100 ms compared to the active power control of the generators in order to show the separate effects. Therefore, analogous to the previous simulation, the load terminal voltage, which is lower than $V_{\mathrm{g},1}$, decreases below $V_{\mathrm{g,o}}$. Then, the demand dispatch strategy is activated and the load changes to 50 Ω. The load does not change back to its initial value,

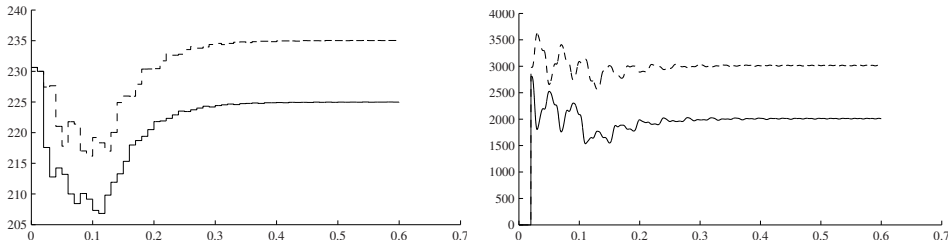

(a) Microgrid voltage (b) Active power to the electrical network

Figure 5.4: Constant dc-power, demand dispatch (—- = VSI 1; ---- = VSI 2)

as in steady-state, its terminal voltage equals 217.9 V which is lower than $V_{\mathrm{g,d}}$. In steady state, $V_{\mathrm{g},1}$ and $V_{\mathrm{g},2}$ are equal to 225 V and 235 V respectively. Now, because of the higher R_{var}, and thus, the temporarily lower power consumption, $V_{\mathrm{g},1}$ and $V_{\mathrm{g},2}$ remain in the 10 % limits, without changing the generated power. Therefore, the demand dispatch offers a high potential for obtaining a good voltage quality and reliability in the islanded network.

C. Extended load control

The demand dispatch strategy can go further than only on/off control. The load can depend on the microgrid voltage level in a linear or a piecewise manner as depicted in Fig. 5.5, which is analogous to the on/off relay function of Fig. 5.1. This piecewise relay function is included in the following simulation where in steady-state, the load is changed from 25 to 43.8 Ω to contribute in the stabilisation of the islanded microgrid. From Fig. 5.6, it follows that the voltage at the terminals of the DG units are 221 V and 232 V. The terminal voltage of R_{var} equals 214 V in this case. By using this control function and dependent on the chosen relay, the demand dispatch strategy can be used more optimally, avoiding unnecessary total load shut down or too high load changes.

5.1.4 Simulation results: microgrid demand dispatch

In the following simulations, the more extended microgrid configuration of Fig. 5.7 is studied. The microgrid consists of three power sources:

- VSI 1
  This power source applies the VBD control strategy with adjustment voltages of $V_{\mathrm{nom}} \pm 1\%$ ($b = 1$ %). An example of this is a power source that has a limited flexibility (storage or fuel intake).

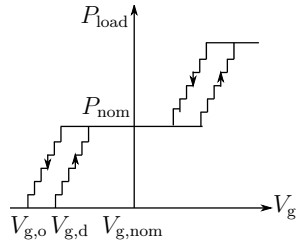

Figure 5.5: Implementation of extended demand dispatch

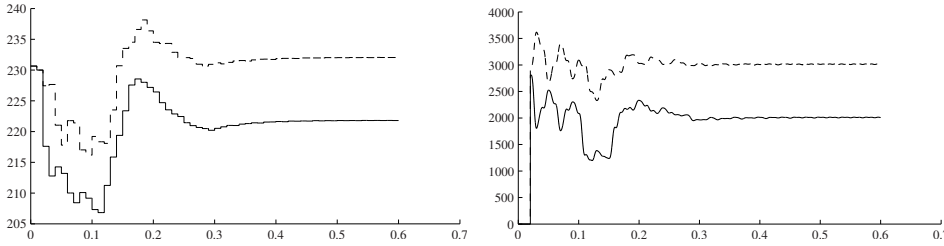

(a) Microgrid voltage (b) Active power to the electrical network

Figure 5.6: Constant dc-power, demand dispatch in continuous manner (—- = VSI 1; ---- = VSI 2)

- VSI 2
  This power source operates with VBD control with ($b = 0$ %). An example of this is a power source that is flexible in power change.

- VSI 3
  VSI 3 operates at constant power with a $V_{\text{g}}/V_{\text{dc}}$ droop control strategy (large b). This can be a renewable energy source that operates according to an MPPT algorithm. Of course, P_{dc} can vary in time because of external factors, such as the irradiation of the PV panels, but the control strategy itself does not change the delivered output power. Therefore, the output power of VSI 3 is not determined by the state of the rest of the microgrid. The only controllability possible in this power source is turning off in case of too high terminal voltages or a faulted electrical network. In practical applications however, it is recommended to follow the MPPT as long as possible, but in case the microgrid stability is jeopardised, the generator should also contribute in the power sharing by abandoning the MPPT and including adjustment voltages that are high but do not exceed the voltage limits. In this simulation

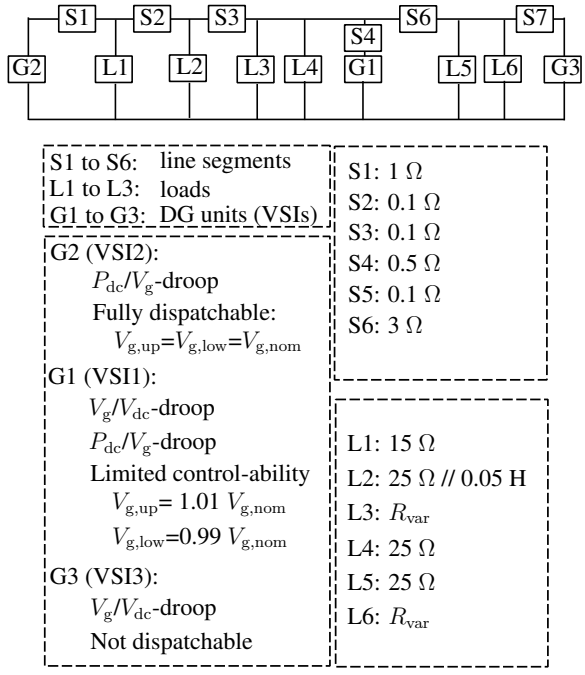

Figure 5.7: Microgrid configuration: extended example

however, as the demand dispatch strategy is studied, this VSI 3 does not have this ability of soft curtailment.

The nominal generated powers are as follows: $P_{dc,1} = 4500$ W, $P_{dc,2} = 3500$ W and $P_{dc,3} = 2500$ W. For the reactive power control, Q/f droop control is applied, with equal droops for the power sources. As the microgrid is a low-voltage distribution network, at first instance, the line impedances are purely resistive. In the last simulation case, also inductive line elements are included. The loads considered here are a combination of variable and non-variable loads.

In the simulations presented below, first, the islanded microgrid without demand dispatch is studied. Secondly, a power source is lost in this microgrid, showing an insufficient generated power and an operation close to the microgrid voltage limits. More flexibility in this microgrid is needed, and therefore, in the third simulation case, the demand dispatch is activated. This shows a more reliable microgrid operation. The last two simulation cases mimic a dynamic profile, with more dynamic events such as losing a generator and changing the demand dispatch dependent on the needs of the loads.

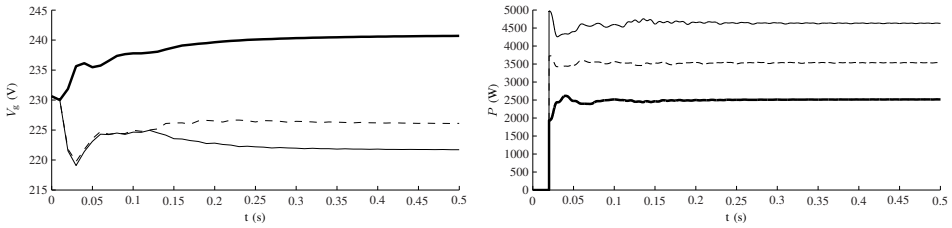

(a) Microgrid voltage

(b) Active power to the electrical network

Figure 5.8: Basic configuration: constant loads (— = VSI 1; ---- = VSI 2; ▬ = VSI 3)

A. Basic configuration

At first instance, the variable loads remain constant, with variable load 1 (L3) turned off and variable load 2 (L6) equal to 25 Ω. The simulation results are depicted in Fig. 5.8.

For the active power controllers during start-up, e.g., the dc-link voltage of VSI 1 decreases. Therefore, the $V_{\mathrm{g}}/V_{\mathrm{dc}}$ droop controller of VSI 1 decreases $V_{\mathrm{g},1}$ until steady-state is reached, where $V_{\mathrm{dc},1}$ remains constant. Because of the microgrid configuration and load profile, $V_{\mathrm{g},1}$ is less than $V_{\mathrm{g},2}$ and $V_{\mathrm{g},3}$, despite its higher nominal power.

From simulations, it follows that $P_1 = 4631$ W, $P_2 = 3535$ W and $P_3 = 2500$ W. The first two power sources change their generated powers, or use storage elements, as the microgrid voltages exceed the adjustment voltages of 1 % (227.7-232.3 V) and 0 % (230 V) respectively. The terminal microgrid voltages are $V_{\mathrm{g},1} = 221.7$ V, $V_{\mathrm{g},2} = 226.7$ V and $V_{\mathrm{g},3} = 240.7$ V.

B. Loss of a power source

In this simulation, VSI 3 is switched off. The simulation results are depicted in Fig. 5.9. From simulations, it follows that: $P_1 = 4886$ W and $P_2 = 3772$ W, which are higher than in the previous case because of the loss of power source 3. The terminal voltages $V_{\mathrm{g},1} = 203.8$ V and $V_{\mathrm{g},2} = 209.7$ V are lower for the same reason. In this microgrid, the sources are not sufficient anymore to feed the loads, and the allowable microgrid voltage limits can be exceeded. To solve this, larger $P_{\mathrm{dc}}/V_{\mathrm{g}}$ droops are an option, but make the control more difficult concerning stability issues and stress the power sources significantly. It is well-known that in small isolated power systems, load changes can have a larger impact than in large interconnected systems. Therefore, the presented demand dispatch strategy is

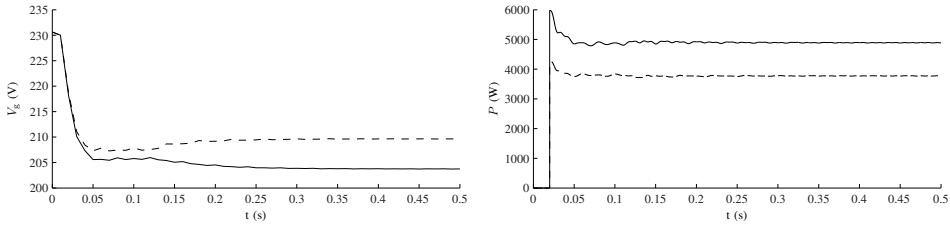

(a) Microgrid voltage (b) Active power to the electrical network

Figure 5.9: Loss of VSI 3: constant loads (— = VSI 1; ---- = VSI 2)

included in the following simulation.

C. *Demand dispatch*

Demand dispatch is included in the microgrid, for the case of the loss of VSI 3 with $R_{\mathrm{var},1}$ now switched on to make the demand dispatch even more urgent. Without demand dispatch, this would have induced even lower microgrid voltages than in the previous simulation case where $R_{\mathrm{var},1}$ was off. A relay function analogous to Fig. 5.1 is used for the demand dispatch control, with $V_{\mathrm{g,o}} = 0.9V_{\mathrm{g,nom}}$ and $V_{\mathrm{g,d}} = 0.92V_{\mathrm{g,nom}}$ for changing $R_{\mathrm{var},1}$ from 25 Ω to 50 Ω and $R_{\mathrm{var},2}$ from 25 Ω to shut down. Practically, more steps in the load changes (upto continuous variations) according to Fig. 5.5 can be included, which is not the case in this simulation.
Because of the activation of the demand dispatch, the variable load $R_{\mathrm{var},1}$ changes from 25 to 50 Ω and $R_{\mathrm{var},2}$ turns off. The simulations start, again, from 230 V. The simulation results are depicted in Fig. 5.10, where in steady-state: P_1 and P_2 equal 4793 W and 3685 W respectively. This is lower than in the previous case, because of the lower load-burden ($R_{\mathrm{var},1}$ is switched on, but is a small load, while $R_{\mathrm{var},2}$ is turned off), while $V_{\mathrm{g},1} = 210.4$ V and $V_{\mathrm{g},2} = 215.7$ V are now higher. The microgrid voltage limits, here 10 % [43], are not exceeded in this case.

D. *Dynamic profile*

Here, a dynamic microgrid profile is simulated. Note that the transients follow very quickly. The reason is to have short simulation times, as the steady-state conditions give no further information. Starting from 230 V without demand dispatch:

- $t = 0$ s: all VSIs operate at 100 % (nominal) power ;
- $t = 0.35$ s: VSI 3 switches off;

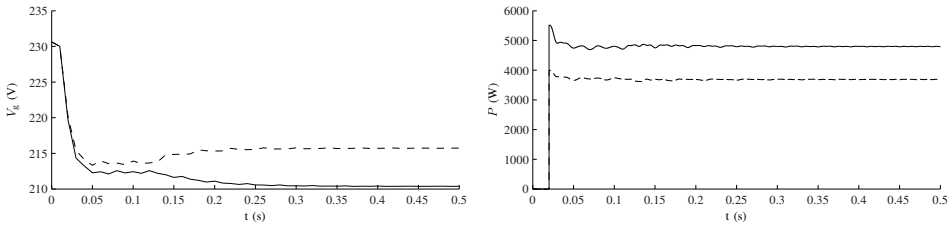

(a) Microgrid voltage (b) Active power to the electrical network

Figure 5.10: Loss of VSI 3: variable loads (— = VSI 1; ---- = VSI 2)

- $t = 0.36$ s: start of the demand dispatch for both variable loads according to the previous case. The demand dispatch operates with a delay, for stability reasons, to include measurement and responsive delay and for practical reasons in the implementation in the loads.
- $t = 0.70$ s: VSI 3 starts operating at 50 %;
- $t = 0.85$ s: demand dispatch turns off for the first variable load, such that $R_{\mathrm{var},1} = 25\ \Omega$, as, e.g., its power consumption can not be delayed any further.
- $t = 1$ s: the nominal power of VSI 2 falls down to 75 %.

The simulation results are shown in Fig. 5.11. The following dynamic results are obtained:

- term 1, $0 < t < 0.35$ s:
  After a start-up transient, the generated powers reach: $P_1 = 4839$ W, $P_2 = 3702$ W, $P_3 = 2500$ W, with $V_{\mathrm{g},1} = 208.4$ V, $V_{\mathrm{g},2} = 213.9$ V and $V_{\mathrm{g},3} = 226.9$ V. The generated powers are higher, with a lower obtained microgrid voltage than in the simulation case § A., because $R_{\mathrm{var},1}$ is now activated.
- term 2, $0.36 < t < 0.70$ s:
  At 0.36 s, the demand signal of both variable loads turns on, and $R_{\mathrm{var},1}$ changes to 50 Ω and $R_{\mathrm{var},2}$ turns off. After a transient because of the disconnection of VSI 3 and the start-up of the demand dispatch, $P_1 = 4802$ W, $P_2 = 3680$ W, $P_3 = 0$ W. Despite the loss of VSI 3, the other power sources need to deliver slightly less power because of the contribution of the now activated demand dispatch. Without demand dispatch, of course, the other power sources would have delivered more power to cope with the loss of

VSI 3.
The effect of the demand dispatch on the microgrid voltages is clearly shown if compared to Fig. 5.9(a), where a large voltage decrease was obtained. Here, even small voltage rises are obtained because of the demand dispatch. Again, this is due to the combined effect of the loss of VSI 3 (decreasing voltage) and the activated demand response (increasing voltage).
Note that the voltage $V_{\mathrm{g},3}$ is slowly decreasing as the figure shows the voltage across the filter capacitor of VSI 3, which is de-charging over a parasitic resistance as VSI 3 is disconnected from the electrical network.

- term 3, $0.70 < t < 0.85$:
  In this case, in steady-state, the sources operate at about $P_1 = 4650$ W, $P_2 = 3575$ W, $P_3 = 1250$ W. As expected, VSI 1 and VSI 2 deliver less power as VSI 3 is turned on again.

- term 4, $0.85 < t < 1.00$:
  At 0.85 s, the demand signal of variable loads 1 is turned off, thus, $R_{\mathrm{var},1} = 25\ \Omega$. In this case, in steady-state, the sources operate at about $P_1 = 4766$ W, $P_2 = 3664$ W, $P_3 = 1250$ W. The first and second power source increase their power production or use some storage capacity as the first variable load started consuming again. The power of the third generator remains constant as it uses $V_{\mathrm{g}}/V_{\mathrm{dc}}$ droop control only. Also, the positive effect of the demand dispatch strategy is shown as the microgrid voltages now deviate more from their nominal values because of the lacking contribution of $R_{\mathrm{var},1}$ in the demand dispatch. Hence, the demand dispatch strategy helps to stabilise the microgrid.

- term 5, $1.00 < t$:
  From the simulations, it follows that $P_1 = 4843$ W, $P_2 = 2919$ W, $P_3 = 1250$ W and $V_{\mathrm{g},1} = 206.3$ V, $V_{\mathrm{g},2} = 207.6$ V, $V_{\mathrm{g},2} = 210.6$ V. The ac-power of the second power source is decreased, this decrease is however less than 75 % because of the $P_{\mathrm{dc}}/V_{\mathrm{g}}$ droop controller and because, as P_2 lowered, P_1 has increased.

The reactive power and microgrid frequency show the same profile, because of the droop action of the Q/f droop controller. Also, as the droop slopes and nominal values of the three sources are equal, in steady-state, they deliver the same reactive power.
In general, by including the demand dispatch strategy triggered by the microgrid voltage, the load can actively contribute to the stabilisation of the microgrid.

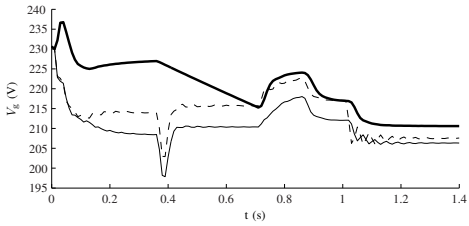

(a) Microgrid voltage

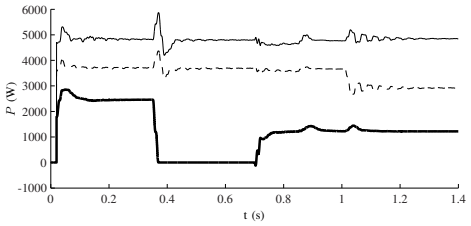

(b) Active power to the electrical network

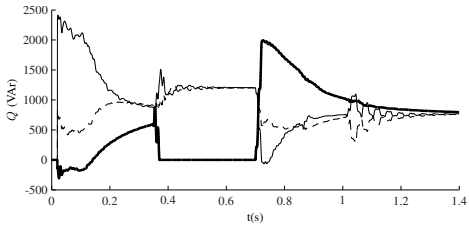

(c) Reactive power to the electrical network

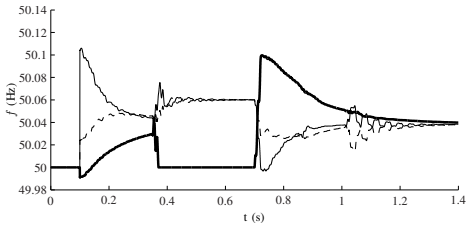

(d) Frequency

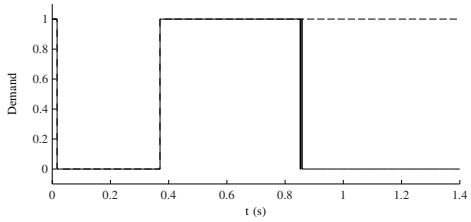

(e) Demand signal (— = $R_{\mathrm{var},1}$; ---- = $R_{\mathrm{var},2}$)

Figure 5.11: Dynamic profile: variable loads (— = VSI 1; ---- = VSI 2; ▬ = VSI 3)

E. Dynamic profile, inductive line parameters

Although the high R/X value in low-voltage networks makes it is a good assumption of having merely resistive lines, there is always some inductance present in the lines (R/X not infinite). Therefore, in this case, some inductance will be included in the lines. The line resistance S1 becomes 1 Ω in series with an inductance of 1 mH. The latter gives a R/X ratio of 3.2, which is realistic in low-voltage networks [200]. Between variable load 2 and the 25 Ω load, a line inductance of 1 mH is included and the line impedance between variable load 1 and the 25 Ω load becomes 0.5 mH. The simulation results are shown in Fig. 5.12, where no

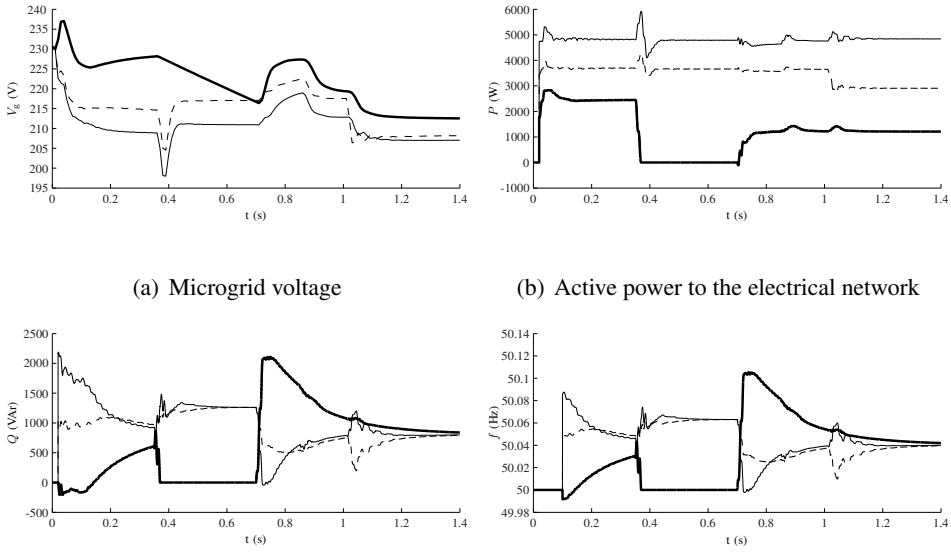

(a) Microgrid voltage

(b) Active power to the electrical network

(c) Reactive power to the electrical network

(d) Frequency

Figure 5.12: Dynamic profile: variable loads and slightly inductive line parameters (— = VSI 1; ---- = VSI 2; ▬ = VSI 3)

major differences compared with Fig. 5.11 are present. Finally: $P_1 = 4838$ W, $P_2 = 2905$ W, $P_3 = 1250$ W and $V_{g,1} = 207.0$ V, $V_{g,2} = 208.5$ V, $V_{g,3} = 212.5$ V. In the final steady-state condition, the reactive powers of the sources are equal to 810 VAr approximately, whereas in the case without inductance in the lines, this was 770 VAr.

5.1.5 Conclusions

A novel method for demand dispatch control in islanded microgrids is presented. It is shown that because of the application of VBD control for the generators and the P-V linkage in weak low-voltage electrical networks, the rms voltage is a good measure for the power production versus consumption level in the microgrid. Therefore, the loads can temporarily adjust their power consumption according to the voltage level to enable demand dispatch. This section renders a proof of concept for the microgrid voltage as a trigger for a novel demand dispatch strategy in islanded microgrids. With this strategy, it is possible to increase the flexibility in the microgrid, i.e., the part in the microgrid that is contributing to the power sharing, which gives more security for a stable operation. Furthermore, there is no need

for a communication link for the primary active and reactive power control of the generators nor for the active load control. It is shown that the presented demand dispatch strategy improves the reliability of islanded microgrid and can lead to a reduction of the line losses. With the combination of the VBD control algorithm and the presented active load control, the renewable energy can be exploited optimally, potentially allowing higher amounts of renewable DG units in islanded microgrids.

5.2 Synchronous generators

Most generators in a low-voltage microgrid are interfaced to the network with a power-electronic interface, i.e. a converter. However, still some directly-coupled Synchronous Generators (SGs) can be present in the microgrid. These generators have different characteristics compared to the converter-based DG (CIDG) units, such as the presence of rotating inertia. Also, their control is mostly based on P/f and Q/V droops, opposed to the P/V and Q/f droops in the VBD control strategy. To integrate both SGs and CIDG units in an islanded microgrid, their control strategies should be adjusted to each other. As the DG units form the major part of the generators in the islanded microgrid, the control of the SGs is changed to introduce converter behaviour. The SGs are equipped with P/V and Q/f droop controllers that are adjusted to take into account the rotating inertia.

5.2.1 Introduction

When directly-coupled SGs are included in an islanded network, their control strategy conflicts with the VBD control or other P/V_{g} droop-type controllers of the CIDG units. Generally, the control of the SGs uses the frequency as a parameter to trigger active power change, while the CIDG units have the terminal voltage as the trigger parameter. Also, the presence of the rotating inertia of the SGs must be taken into account. To match the control of the SGs and the CIDG units, two approaches are possible. In the first approach, the control of the CIDG units is changed. For this, one possibility is to emulate inertia in P/f droop controlled CIDG units, which requires additional storage [127]. However, instead of altering the control of the CIDG units, here, the control strategy of the SGs is modified to comply with the VBD control. The reason to change the control strategy of the SGs instead of that of the CIDG units, is that the SGs generally form the minor part of the generators in the microgrid in which mostly a high share of (renewable-based, often) converter-interfaced units is present [131]. Converter behaviour is included in the SGs, which does not require additional storage in the DG units, is based on the P/V and Q/f droop control and takes into account the rotating inertia of the

SG.

5.2.2 Primary control: directly-coupled SGs: conventional method

The conventional active power control is largely based on the inertia of the SGs that are often large centralised units connected to the transmission network. The generators are equipped with a droop mechanism to change the mechanical power P_{m} dependent on the grid frequency f, which corresponds with their rotational speed:

$$P_m = P_{\mathrm{nom}} - K_{\mathrm{P,SG}}(f - f_{\mathrm{nom}}), \tag{5.1}$$

with $K_{\mathrm{P,SG}}$ the droop constant. For the reactive power sharing, the generators are equipped with a reactive power/voltage droop controller, with $K_{\mathrm{Q,SG}}$ the droop constant:

$$E = E_{\mathrm{nom}} - K_{\mathrm{Q,SG}}(Q - Q_{\mathrm{nom}}). \tag{5.2}$$

5.2.3 Synchronous generators in islanded microgrids

A. A change of control strategy of SGs

The major part of the generators in a microgrid are power-electronically interfaced [135]. However, a small share can be based on directly-coupled SGs with excitation winding. SGs include, for example, diesel generator sets that are used as backup or emergency power systems or to electrify remote places. In this PhD thesis, with SGs, directly-interfaced SGs are assumed. Converter-interfaced SGs can use the same control strategy as the CIDG units.

Despite the fact that the SGs form the minor part of the generators in the islanded microgrid, they can inject a significant amount of power during some periods (e.g., low sun and wind times). These different control strategies of SGs and CIDG units can pose problems in the microgrid.

In case the SGs use a grid-following control strategy, no conflict arises with the grid-forming CIDG units. However, then, the SGs are current-controlled and inject a pre-determined amount of power while following the grid voltage posed by the CIDG units. Hence, the SGs do not participate in the power sharing of the islanded microgrid. As these units are often dispatchable, opposed to a large share of the CIDG units that can be renewable-based, this is not an optimal situation and does not benefit the stability of the network.

Often, the SGs use a grid-forming strategy, namely the conventional P/f droop control. Hence, e.g., to change the output power, the controllers of the CIDG units ($P_{\mathrm{dc}}/V_{\mathrm{g}}$) and SGs ($P/f$) are triggered by different parameters. Consequently, ac-

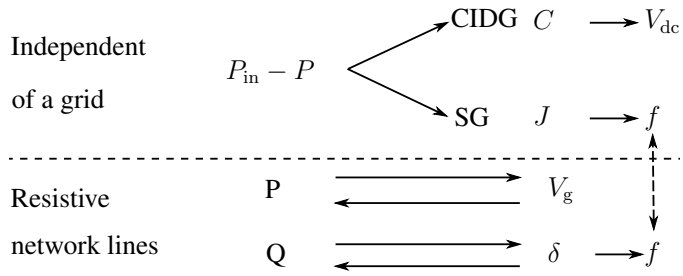

Figure 5.13: The energy balance and power flows in resistive networks

curate power sharing is not possible and the stability of the microgrid can be jeopardised. Next to different triggers to change the active power of the units, also active power changes in the network have a different effect on the units as clarified in Fig. 5.13. Firstly, for the CIDG units, in case of an unbalance between dc-power ($P_{\text{dc}} = P_{\text{in}}$) and delivered ac power P, the dc-bus capacitor C_{dc} absorbs the difference, which changes the dc-bus voltage. The $V_{\text{g}}/V_{\text{dc}}$ droop controller in turn changes V_{g}. For the SGs, a difference between P_{m} ($P_{\text{m}} = P_{\text{in}}$) and P is absorbed by the rotating inertia J of the generator, changing the terminal frequency. Therefore, active power changes in the network affect the frequency in case of SGs and voltage in case of CIDG units. Otherwise, in case of SGs, frequency changes are induced by active power changes, while in case of CIDG units, the frequency changes are induced by reactive power changes. This leads to an interference between the frequency changes of the units. The same is valid for grid voltage changes.
To avoid this interference, the control strategies of the SGs and CIDG units should be matched to each other for their integration in a resistive islanded microgrid. For this purpose, the control of the SGs is changed as they generally form the minor part of the units in the islanded microgrid [131].

B. SGs with converter behaviour

By changing the control strategy of the SGs to comply with the $P_{\text{dc}}/V_{\text{g}}$ droops of the CIDG units, SGs can take part in the active and reactive power sharing in the microgrid. For this purpose, P/V_{g} and Q/f droops are included in the SGs, and as such, converter behaviour is incorporated in the SGs.
A SG is, here, modelled by an inductance L in series with a back-emf E as depicted in Fig. 5.14. As depicted in this figure, two parameters of the SG can be controlled, namely the mechanical power P_m and the back-emf E. The frequency (or phase angle) of the terminal voltage V_{g} can only be controlled indirectly by changing the

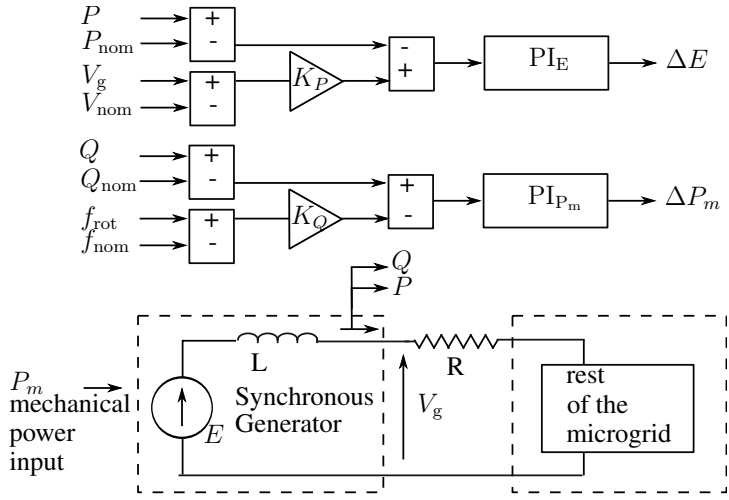

Figure 5.14: First order model of a SG in microgrid. PI controllers to control P_m and E. R represents the summation of the stator resistance of the SG and the line resistance of the line between the SG and the rest of the microgrid.

mechanical (input) power P_{m} of the SG. The amplitude of V_{g} can be controlled by changing E, which, in turn, is done indirectly by changing the excitation current. The automatic voltage regulator (AVR) of the SG can be used, but the set points are different compared to the conventional control of the AVRs.
Emulating converter behaviour, with P/V_{g} and Q/f droop controllers, in SGs is not evident. The main reasons are:

- the presence of rotational inertia. In a SG, when there is an unbalance between the ac-side power P and the input power P_{m}, the rotational speed of the SG will change. A changed rotational speed will affect the terminal frequency of the SGs. Because of the resistive microgrid lines, this will in turn influence the reactive power output of the generator. Hence, the active and reactive power changes of the SG are linked through the rotational inertia.

- the frequency and phase angle of the output voltage of a SG is more difficult to control compared to that of CIDG units, because the frequency is imposed by the rotational speed of the SG.

To solve this issue, the operating points of the SG are forced towards the P/V_{g} and Q/f droops by controlling E and P_{m} as depicted in Fig. 5.15. E is changed to include the P/V_{g} droop control for active power sharing as E and V_{g} only differ

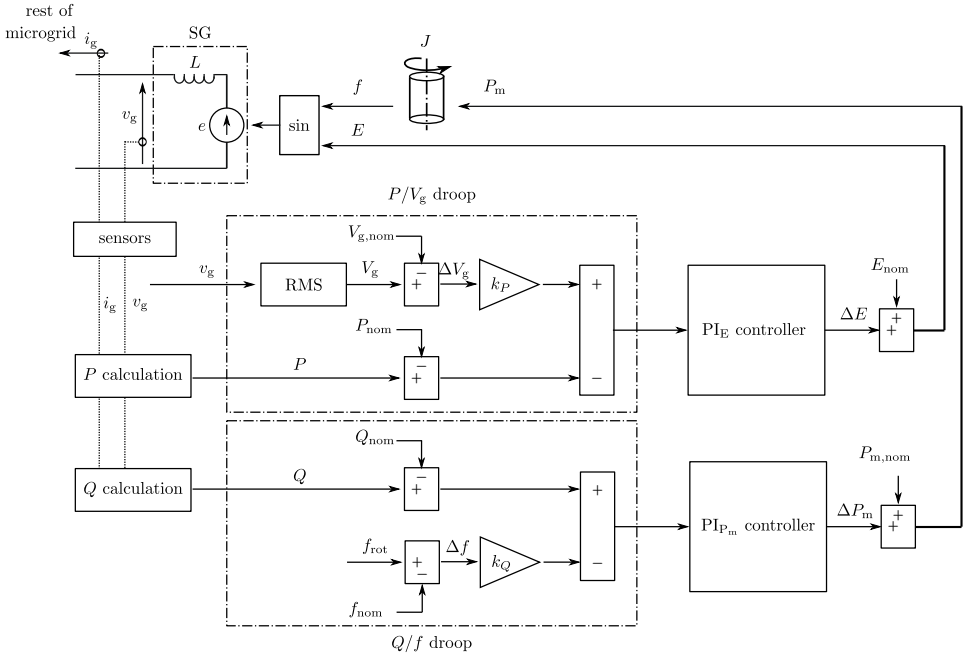

Figure 5.15: Overall SG control strategy and implementation of this strategy in SGs with VBD control

through the equivalent inductance of the SG. P_m is changed to use the Q/f droop control to achieve reactive power sharing between multiple SGs and CIDG units as P_m and frequency changes are interdependent through the rotational inertia. Because of the linkage between both, the controllers of E and P_m operate with a different bandwidth to avoid dynamical interactions between the controllers.

To shift the operation towards the P/V_g droop, a PI controller is included, operating on the back-emf E of the SG, with $E = E_\mathrm{nom} + \Delta E$. The input of this $\mathrm{PI_E}$ controller is:

$$-(P - P_\mathrm{nom}) + K_\mathrm{P}(V_\mathrm{g} - V_\mathrm{nom}) \tag{5.3}$$

with V_g the rms terminal voltage of the SG and P the ac-side active power, which are measured values. K_P represents the negative droop parameter. The back-emf E is, in turn, controlled by changing the excitation current of the SG. Because this is fast compared to changing P_m, the dynamics of this are neglected. Here, the SGs are not equipped with a constant-power band, they represent dispatchable units. Of course, if these SGs are not fully dispatchable, constant-power bands can be used

analogous as in the VBD control strategy for CIDG units.
The frequency f of the back-emf, referred to the stator, is determined by the inertia J of the SG according to:

$$P_m - P = \omega J \frac{d\omega}{dt}, \tag{5.4}$$

with P_{m} the input power and $\omega = 2\pi f_{\mathrm{rot}}$. In a SG, the mechanical speed is proportional with the electrical frequency f through the number of pole pairs. Here, the electrical speed is considered such that $f_{\mathrm{rot}} = f$. The grid frequency f can be forced towards the Q/f droop by changing the mechanical power P_{m} of the generator. Generally, P_{m} changes are relatively slow. Hence, a slower $\mathrm{PI}_{\mathrm{P_m}}$ controller with as output ΔP_{m} is implemented. The input of this PI controller is:

$$(Q - Q_{\mathrm{nom}}) - K_{\mathrm{Q}}(f_{\mathrm{rot}} - f_{\mathrm{nom}}), \tag{5.5}$$

with Q the ac-side power and K_{Q} the droop parameter. The mechanical power equals $P_m = P_{\mathrm{nom}} + \Delta P_{\mathrm{m}}$. If the mechanical power cannot be adjusted fast enough, some storage needs to be included. Except for the slow $\mathrm{PI}_{\mathrm{P_m}}$ controller and some small delay times, the dynamics of changing P_{m} are further neglected because of the small size of the SGs in low-voltage networks leading to relatively fast possible changes of P_{m} compared to the large central generators.

C. Discussion

Permanent-magnet synchronous machines (PMSMs) are not considered for two reasons. Firstly, PMSMs often use converter interfaces. Secondly, the reactive power of PMSMs cannot be controlled actively as the excitation field, that determines the back-emf E, can be assumed as largely constant. Therefore, they can not take part in the reactive power sharing in the microgrid, thus, the Q/f droop controller is not active. For the active power droop, an analogous PI controller as (5.3) can be included, but with output ΔP_{m} instead of ΔE. This is out of the scope of this PhD thesis.

5.2.4 Tuning of the controllers

In this paragraph, the model and PI controllers of the SG's VBD controller are discussed, taking into account the fast dynamics of the CIDG unit controllers and the slower response of the SGs. In the CIDG units, the $\mathrm{PI_I}$ of (3.44) and $\mathrm{PI_V}$ controllers of (3.46) are used.
An SG is, here, modelled by an inductance $L = 6$ mH in series with a back-emf E. A single-phase equivalent is considered for a three-phase SG. The $\mathrm{PI_E}$ controller

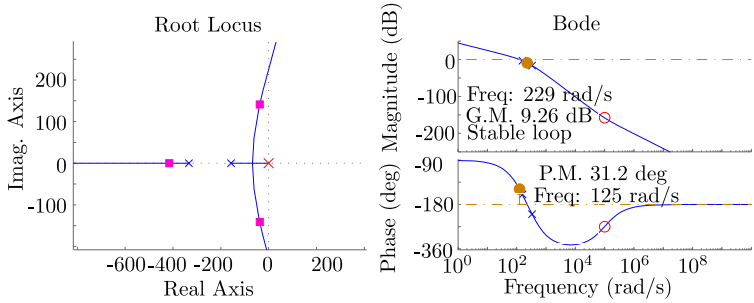

Figure 5.16: Root Locus of the $\mathrm{PI_E}$ *control loop*

is tuned by using the instantaneous power $p(\mathrm{t})$ equation:

$$p(\mathrm{t}) = e(\mathrm{t})i(\mathrm{t}), \tag{5.6}$$

with $e(\mathrm{t})$ the emf of the SG and $i(t)$ its output current. By using a low-pass filter, the active power can be derived:

$$p = E\frac{E-V}{R+sL}\frac{\omega_c}{s+\omega_c}, \tag{5.7}$$

with $\omega_c = 2\pi 25$ rad/s, V the load voltage and L and R the combined line and SG impedances. In small signal analysis:

$$P = \frac{2E_{\mathrm{nom}}\omega_c \Delta E}{(R+sL)(s+\omega_c)}, \tag{5.8}$$

with $E_{\mathrm{nom}} = 250$ V (calculated from $P_{\mathrm{nom}} = 1500$ W, $V_{\mathrm{g,nom}} = 230$ V, $R = 2\ \Omega$ and $L = 6$ mH) for the tuning of the controllers. The following $\mathrm{PI_E}$ controller is obtained:

$$\mathrm{PI_E} = 0.7\frac{1+10^{-5}s}{s}, \tag{5.9}$$

which has a bandwidth of 125 rad/s, a phase margin of 31.2 deg and a settling time of 0.098 s.

The $\mathrm{PI_{P_m}}$ controller is tuned according to the power balance equation through the rotating inertia J of the SG in (5.4). By assuming small derivations from ω compared to ω_{nom}:

$$P_m - P = \omega_{\mathrm{nom}} J\frac{\mathrm{d}\omega}{\mathrm{dt}} \tag{5.10}$$

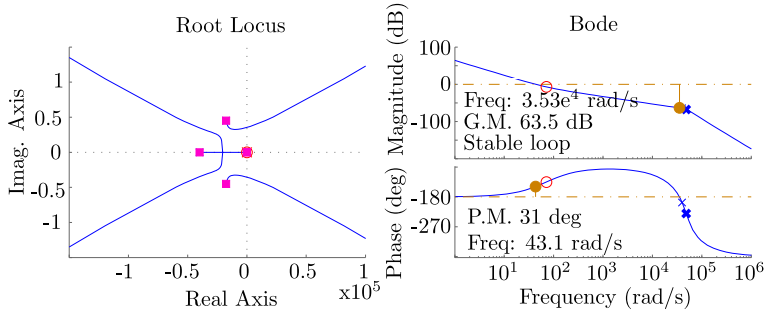

Figure 5.17: Root Locus of the $\mathrm{PI}_{\mathrm{P_m}}$ *control loop*

with $\omega_{\mathrm{nom}} = 2\pi 50$ rad/s and $J = 0.18\mathrm{kgm}^2$. By using the Padé approximation P, the following $\mathrm{PI}_{\mathrm{P_m}}$ controller is obtained:

$$\mathrm{PI}_{\mathrm{P_m}} = 9 \cdot 10^4 \frac{1 + 0.014s}{s}, \tag{5.11}$$

which has a bandwidth of 43.1 rad/s, a phase margin of 31 deg and a settling time of 0.377 s. A sufficiently different bandwidth between the PI_{E} and $\mathrm{PI}_{\mathrm{P_m}}$ control loops is obtained.

5.2.5 Concept

A simulation in a basic microgrid is discussed as a proof of concept. Two units of equal ratings are included, either both CIDG units or one CIDG unit and one SG in a microgrid with an RL load and a constant-power load. Further details are given in Fig. 5.18.

Two CIDG units In this first simulation, two CIDG units with nominal active and reactive power of 1500 W and 0 VAr respectively and with equal droops are considered. Also, both DG units represent dispatchable units without constant-power band ($b = 0$ %) and they use the VBD control strategy. The simulations start from an rms terminal voltage of 230 V and a frequency of 50 Hz. The droop coefficients are: $K_{\mathrm{V}} = -0.5$ V/V, $K_P = P_{\mathrm{nom}}/50$ W/V and $K_Q = 5 \cdot 10^{-5}$ Hz/VAr.
The simulation results depicted in Fig. 5.19 show that no difference in P, V_{g}, Q and f between the DG units is obtained, because of their equal ratings, equal droops and the symmetrical microgrid. After 0.6 s, when the constant-power load turns on, both units increase their power identically. This increase is slightly less than 250 W each, as also the grid voltage decreases, resulting in less consumption from

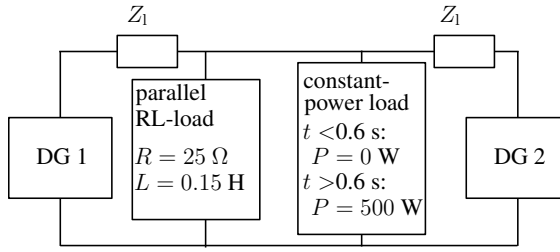

Figure 5.18: Symmetrical microgrid, equally rated CIDG units

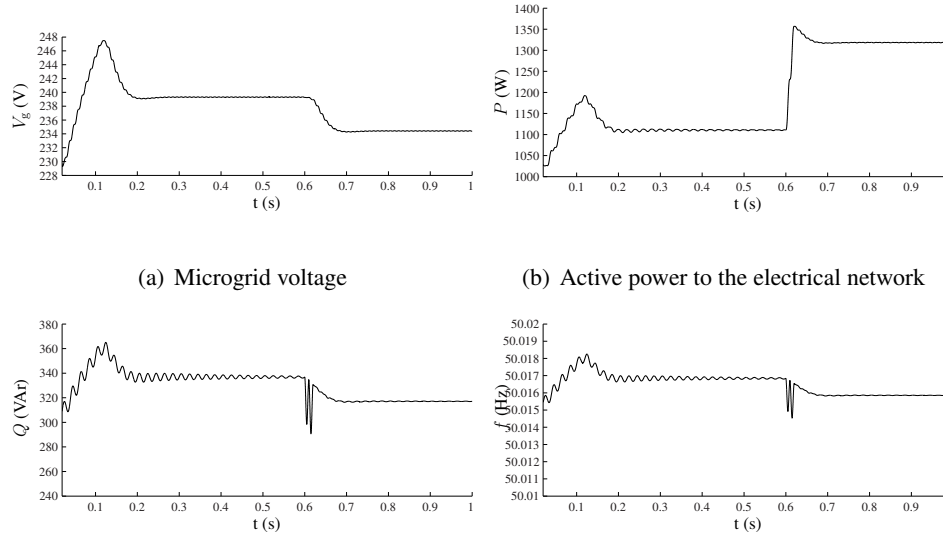

(a) Microgrid voltage

(b) Active power to the electrical network

(c) Reactive power to the electrical network

(d) Microgrid frequency

Figure 5.19: Proof of concept: Symmetrical microgrid, equally-rated CIDG units (— = CIDG 1; ---- = CIDG 2)

the RL load. The simulations show that in steady-state: $P_1 = P_2 = 1318$ W, $V_{g,1} = V_{g,2} = 234.5$ V, $f_1 = f_2 = 50.016$ Hz and $Q_1 = Q_2 = 317$ VAr.

One CIDG unit and a SG with control strategies not matched In this simulation, an SG is included instead of a CIDG unit. The SG is represented as an emf E in series with an inductance L of 6 mH. The SG uses conventional P/f and Q/V droop control and the CIDG unit uses the VBD control with $b = 0$ %.

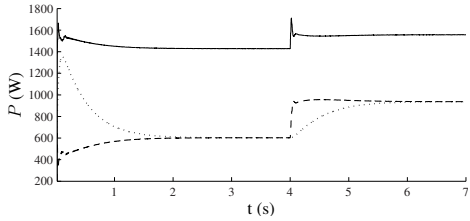

(a) Active power to the electrical network

Figure 5.20: Proof of concept: Symmetrical microgrid, CIDG unit and SG, control strategies not matched (— = CIDG; ---- = SG ac power, ... = SG mechanical power)

In case of a high rotating inertia of the SG, $J = 18$ kgm^2, which is a high value for a small low-voltage connected unit, a stable operation can be reached. However, steady-state is only reached slowly, as shown in Fig. 5.20. Mark the longer simulation time and the delayed load change in this figure. As in steady-state: $P_{\mathrm{CIDG}} = 1557.2$ W and $P_{\mathrm{SG}} = 937.1$ W, the power sharing is not according to the equal ratings of the units. In case the SG has a lower inertia J of 0.18 kgm^2, high power and voltage swings are obtained leading to an unstable operation because a low inertia does not provide sufficient damping in the system.

One CIDG unit and a SG with control strategies matched In this case, the control of the SG, with $J = 0.18$ kgm^2, uses converter behaviour with P/V_{g} and Q/f droop (thus VBD) control. Because the controllers are matched to each other, a stable operation is obtained, with equal ac-powers and terminal voltages, as depicted Fig. 5.21. In steady-state: $P_{\mathrm{CIDG}} = P_{\mathrm{SG}} = 1317$ W, $V_{\mathrm{g,CIDG}} = V_{\mathrm{g,SG}} = 234.4$ V, $Q_{\mathrm{CIDG}} = Q_{\mathrm{SG}} = 317$ VAr and $f_{\mathrm{CIDG}} = f_{\mathrm{SG}} = 50.016$ Hz. Still, higher P, V_{g}, Q and f swings are present in the transients compared to the case of only CIDG units.
These simulations show that implementing converter behaviour in SGs enables to incorporate the SGs in a converter-based microgrid and can lead to adequate power sharing between SGs and CIDG units.

5.2.6 Synchronous generator in the microgrid

In this simulation, the more extended microgrid of Fig. 5.22 is studied. One SG (with converter behaviour) and three CIDG units (with VBD controller) are included:

- G1 represents a fully dispatchable CIDG unit with $P_{\mathrm{dc,1,nom}} = 1500$ W and

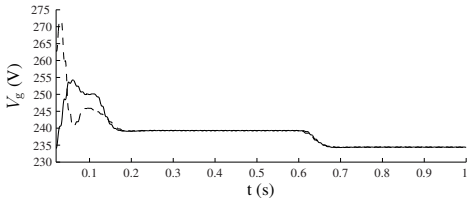

(a) Microgrid voltage

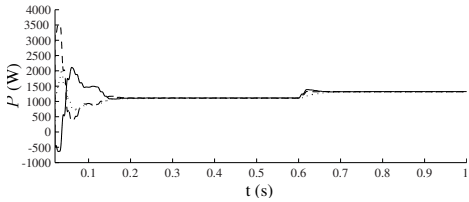

(b) Active power to the electrical network (— = CIDG 1; ---- = ac-power of SG, ... = mechanical power of SG)

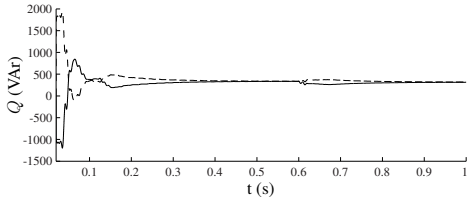

(c) Reactive power to the electrical network

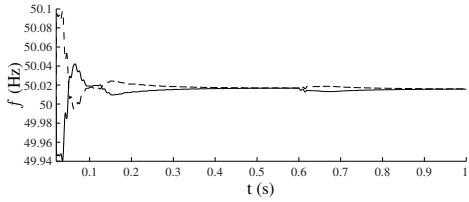

(d) Microgrid frequency

Figure 5.21: Proof of concept: CIDG unit and SG, control strategies matched (— = CIDG 1; ---- = SG)

$b = 0$ %.

- G2 represents an undispatchable CIDG unit (such as an intermittent renewable source) with $P_{\mathrm{dc,2,nom}} = 500$ W. Only the $V_{\mathrm{g}}/V_{\mathrm{dc}}$ droop control is used as a large constant-power band $b = 20$ %, which is larger than the absolute grid voltage limits, is included. After 0.6 s, the primary energy source changes the dc power to $P_{\mathrm{dc,2,nom}} = \frac{4}{3} \cdot 500$ W$= 667$ W.
- G3 represents a slightly dispatchable CIDG unit with $P_{\mathrm{dc,3,nom}} = 1000$ W and $b = 5$ %.
- The SG has nominal power 1500 W and is fully dispatchable.
- one of the loads turns on after 0.45 s.

The simulation results depicted in Fig. 5.23 show a stable operation. Also, the effect of the load change after 0.45 s and the generator change after 0.6 s are clearly visible. After the load change, the reaction of the SG (change of P_{m}) is slower than that of the CIDG units. This simulation shows that the mechanical power P_{m} of the SG lags compared to the ac power, the difference between both leads to a

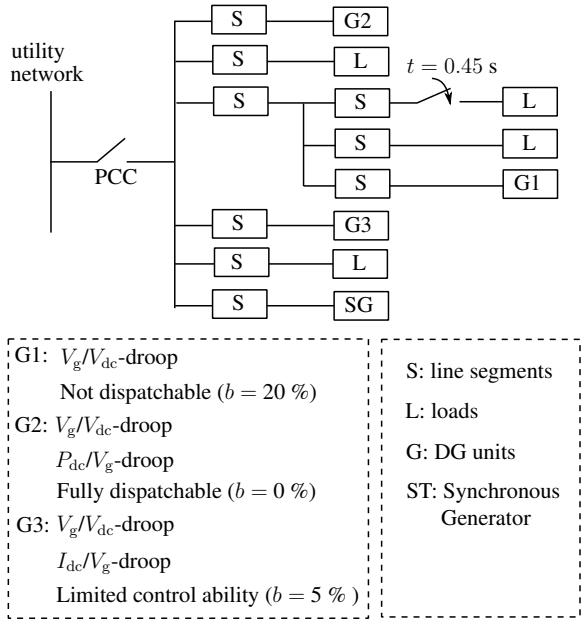

Figure 5.22: Islanded microgrid including synchronous generator

change of angular speed of the SG. The PI controllers of the SG enable to use this generator in a resistive microgrid with VBD controllers of the CIDG units. G1 has the largest output power, and its P_{dc}/V_g droop controller fully adjusts its output power according to the changes of the microgrid state. For example, at $t = 0.45$ s, when a load turns on, this generator significantly increases its output power. G2 on the other hand does not change its steady-state output power as it is not determined by the microgrid state but by its prime energy mover. For example, at $t = 0.45$ s, the ac-power P_2 increases, which is extracted from the dc-link capacitor because $P_{dc,2}$ remains constant. Hence, the dc-link voltage of G2 decreases such that the V_g/V_{dc} droop controller decreases V_g until a stable operation is obtained with $P_2 = P_{dc,2}$. The SG also adapts to the state of the microgrid and participates in the power sharing in the microgrid.

In steady-state, $P_1 = 2.18$ kW, $P_2 = 0.67$ kW, $P_3 = 1.20$ kW and $P_{SG} = 2.10$ kW. Therefore, good power sharing according to the ratings of the DG units (except for the undispatchable DG unit CIDG 2) is obtained, e.g., $P_1 \approx P_{SG}$, complying with their equal nominal power. Some inaccuracies in power sharing can exist because of the line impedances as, opposed to frequency, the grid voltage is not a global parameter. These are however small because of the small line impedances in small-scale networks and because the voltage is controlled between strict voltage limits.

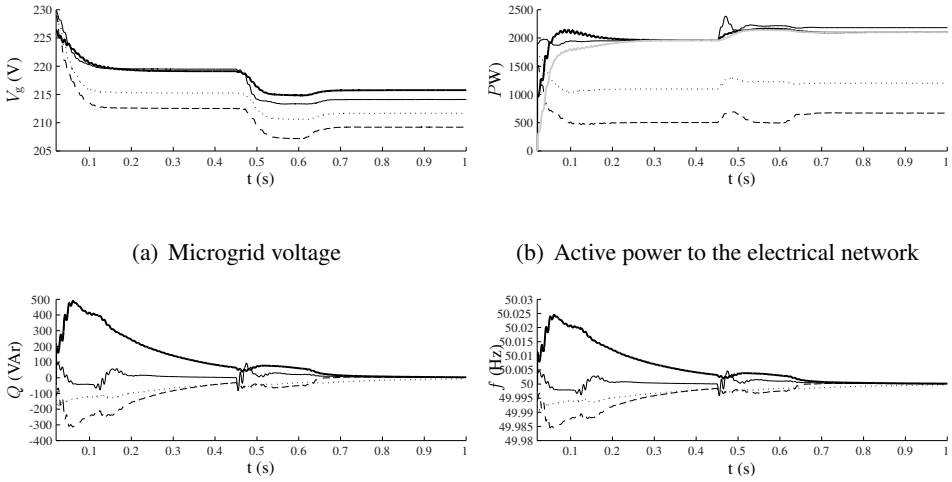

(a) Microgrid voltage

(b) Active power to the electrical network

(c) Reactive power to the electrical network

(d) Microgrid frequency

Figure 5.23: SG in the microgrid (— = CIDG 1; ---- = CIDG 2, $\cdots$ = CIDG 3, ▬ = SG. For the SG, in Fig. (b), the ac-side power P is given in black and the mechanical input power P_{m} in gray)

However, secondary control or the method of § 4.5 can be used to further optimise the power sharing and voltage control [109]. The units deliver equal reactive power because of their equal droops and nominal values of Q.

5.2.7 IEEE 13 Node Test Feeder

Also, a variant of the IEEE 13 Node Test Feeder is considered. The IEEE 13 Node Test Feeder is modified for application as a low-voltage network in islanded mode. This feeder is equal to the test feeder of Fig. 4.21, but now includes SGs. The simulation details of the nodes are summarised in Fig. 5.24, showing that a combination of various loads (resistive, inductive, constant-power and switching loads) is used. There are three CIDG units and two SGs connected to the feeder, with details summarised in Table 5.1 and with matched VBD controllers.
The current-controlled CIDG units use $I_{\mathrm{dc}}/V_{\mathrm{g}}$ droops with the resistive virtual output impedance $z_v = 3\ \Omega$ while the power-controlled CIDG unit has a $P_{\mathrm{dc}}/V_{\mathrm{g}}$ droop controller. The nominal dc-power of CIDG 1 and CIDG 3 can be calculated by taking into account z_v, and with $V_{\mathrm{dc,nom}} = 450$ V, $K_{\mathrm{V}} = 0.5$ V/V and $V_{\mathrm{g,nom}} = 230$ V. In nominal conditions: $P_{\mathrm{dc,1,nom}} = 2.1$ kW; $P_{\mathrm{dc,3,nom}} = 5.1$ kW in case $I_{\mathrm{dc,3,nom}} = 8$ A, and $P_{\mathrm{dc,3,nom}} = 3.0$ kW in case $I_{\mathrm{dc,3}} = 5.3$ A.

Table 5.1: CIDG units and SGs in test feeder: detail

CIDG	dc-side -controlled	value	constant-power band
CIDG1	current	$I_{\mathrm{dc},1,\mathrm{nom}} = 4$ A	$b = 0$ %
CIDG2	power	$P_{\mathrm{dc},2,\mathrm{nom}} = 3.5$ kW	$b = 0$ %
CIDG3	current	$I_{\mathrm{dc},3,\mathrm{nom}}$: t <0.4 s: 8 A t >0.4 s: 5.3 A	$b = 8$ %
SG1	power	$P_{\mathrm{m},1,\mathrm{nom}} = 5$ kW	
SG2	power	$P_{\mathrm{m},2,\mathrm{nom}} = 4$ kW	

In steady state, the simulation results give: $P_{\mathrm{CIDG1}} = 1.9$ kW, $P_{\mathrm{CIDG2}} = 3.5$ kW, $P_{\mathrm{CIDG3}} = 3.0$ kW, $P_{\mathrm{SG1}} = 4.3$ kW, $P_{\mathrm{SG2}} = 3.5$ kW; and $I_{\mathrm{dc,CIDG1}} = 3.6$ A, $I_{\mathrm{dc,CIDG2}} = 7.7$ A and $I_{\mathrm{dc,CIDG3}} = 5.3$ A. Hence, except for the undispatchable CIDG unit (voltage inside the constant-power band), a power sharing that is approximately according to the ratings of the units is obtained, for both CIDG units as well as the SGs. Analogously, in steady-state, all units deliver the same reactive power 757 VAr as the nominal Q and f, and thus, the droops are equal for all units. The figure also shows a clear delay in the changes of P_{m} compared to those of ac power P of the SGs. This delay is however restricted because of the small size of the SGs. At t =0.5 s, a resistive load turns off, which clearly results in a transient with decreasing power delivered by all DG units. At t =0.4 s, the generation decrease from CIDG 3 is met by an increase in P of the other generators, both CIDG units and SGs.

In Fig. 5.26, the same case is studied, but the SGs use the conventional P/f and Q/V droop control instead of VBD control. The steady-state results, e.g., of active power, show that the power sharing between the SGs and CIDG units is not according to the ratings: $P_{\mathrm{CIDG1}} = 2.4$ kW, $P_{\mathrm{CIDG2}} = 4.3$ kW, $P_{\mathrm{CIDG3}} = 3.0$ kW, $P_{\mathrm{SG1}} = 3.3$ kW, $P_{\mathrm{SG2}} = 2.3$ kW. From this, it is concluded that in order to provide accurate power sharing, a match between the control strategies of SGs and CIDG units is required. Also, the reactive power sharing between the SGs and CIDG units is not according to the ratings as the units have equal Q_{nom}, but the droops of the Q/f controllers of the CIDG units and the P/f controllers of the SGs are not equal. Also, Δf and ΔV_{g}, namely the triggers to change P for the SGs and CIDG units respectively can differ. Compared to the case with matched control strategies, larger transients are obtained in P with consequently, higher settling times.

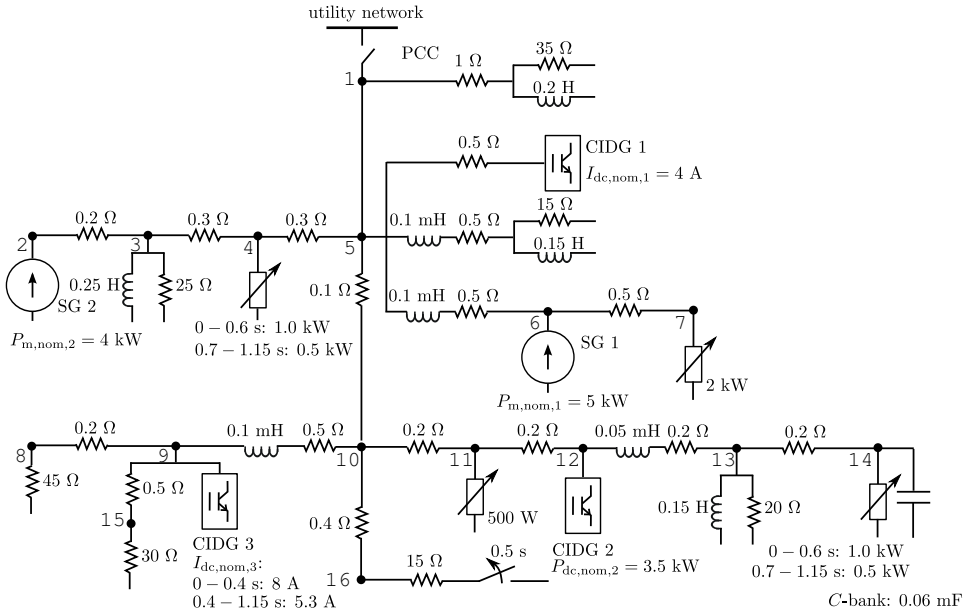

Figure 5.24: 13 Node Test Feeder

5.2.8 Conclusions

Because of an increasing share of DG units and the introduction of (islanded) microgrids, new control methods for the CIDG units in islanded microgrids are developed such as the VBD control strategy. However, still some SGs can be present in the microgrid, of which the P/f droop control does not comply with $P_{\mathrm{dc}}/V_{\mathrm{g}}$ droop control and the rotating inertia needs to be taken into account. Because SGs generally form the minor part of the generators in the microgrid, in this PhD thesis, the control strategy of the SGs is changed to comply with the CIDG unit control. This is implemented by including converter behaviour in the SGs. The results show a stable operation of islanded microgrids with a combination of SGs and CIDG units. The method also enables that both SGs and CIDG units can contribute to achieving an accurate power sharing.

5.3 Smart transformer

One of the main advantages of a microgrids is that they promise to become controllable entities within the electrical network [37,48,201]. This requires the ability of the utility grid to control or influence the power exchange with the microgrid by

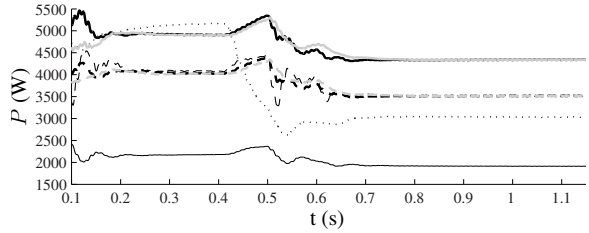

(a) Active power to the network

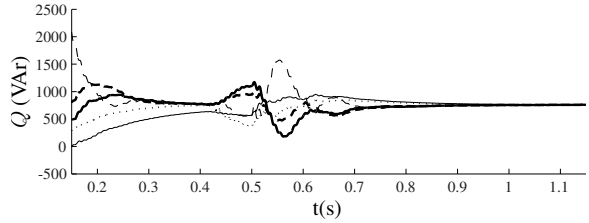

(b) Reactive power to the network

Figure 5.25: 13 node test feeder (— = CIDG 1; ---- = CIDG 2, ... = CIDG3, ▬ = SG1, ▬ ▬ = SG2) (Extra: ▬ = SG1, ▬ ▬ = SG2 with black = ac power and gray = mechanical power in Fig. (a))

communicating with only one unit. However, little research has been conducted on controlling the power transfer through the PCC, while more research concerning microgrids deals with either grid-connected or islanded operation or the transition between both [9, 45, 101, 121, 202]. One solution to control the PCC power is that the utility network communicates new set points to all (or specified) DG units and active loads, e.g., by using the multi-agent strategy of [203]. However, this does not comply with the concept of a microgrid as an entity from the grid's point of view. A possibility is, thus, that the utility network only needs to communicate to the PCC, and the microgrid controllers automatically respond, which significantly reduces the communication burden in the system.

This section addresses this possibility by introducing the concept of a smart transformer (ST), which is a tap-changing transformer located at the PCC. This unit controls the active power exchange between a microgrid and the utility grid dependent on the state of both networks and other information communicated to the ST. To control the active power, the ST uses its taps that change the microgrid-side voltage at the PCC. This voltage-based control of the ST is compatible with the VBD control of the generators, storage and controllable loads in the microgrid.

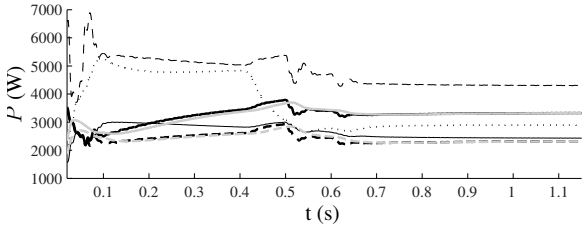

(a) Active power to the network

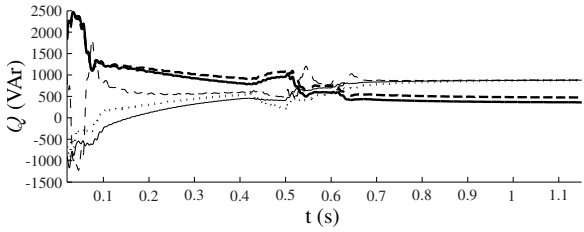

(b) Reactive power to the network

Figure 5.26: 13 node test feeder with SGs using P/f and Q/V droop control (— = CIDG 1; ---- = CIDG 2, ... = CIDG3, ▬ = SG1, ▬ ▬ = SG2) (Extra: ▬ = SG1, ▬ ▬ = SG2 with black = ac power and gray = mechanical power in Fig. (a))

In this way, firstly, the microgrid can automatically, without need for communication, adapt to changes of the ST set points, and vice versa. Secondly, the DG units and active loads can keep the same control method in the islanded mode and grid-connected mode. In this context, the usage of the ST can be implemented as a level between the primary control and the secondary control. For the actual secondary control, one possibility is to use a central controller with low-bandwidth communication with each DG unit to change their set points in order to minimise a cost function [201] or for economical reasons.

The main aspects of the ST are: 1) the ST controls the bidirectional power transfer between utility grid and microgrid, 2) the ST is able to aggregate information to determine its set point of power exchange, 3) the ST enables to exploit the microgrid as a controllable entity, because the utility network only needs to communicate to the ST instead of all microgrid elements.

5.3.1 Control principle: power transfer through smart transformer

Because of the high share of intermittent power sources and the small scale of the microgrid, inducing possibly high load peaks, new means of power flexibility are required. The droop control of the DG units, active loads and storage can provide this. In a grid-connected microgrid, another means to include flexibility is the usage of a ST.

1. Control strategy

To change the active power exchange ΔP_{PCC} between microgrid and utility grid, generally, a secondary central control approach is used that communicates changes of the set points to all the DG units $\Delta P_{\mathrm{set,i}}$, such that

$$\Delta P_{\mathrm{PCC}} = \sum_{i=1}^{N} \Delta P_{\mathrm{set,i}}. \tag{5.12}$$

Opposed to this general approach, here, the power transfer between a microgrid and the utility grid is actively controlled without the need for communication to all microgrid elements. Instead, only ΔP_{PCC} is communicated to the ST and the DG units automatically react. The ST is an on-load tap changer (OLTC) as depicted in Fig. 5.29, that can control its taps to alter the terminal voltage V_{PCC}. A comparison between the central control strategy and the ST strategy is shown in Fig. 5.27 and the ST is depicted in Fig. 5.28.

The control algorithm of the ST is based on the following discrete PI controller to force P_{PCC} to $P_{\mathrm{PCC,ref}}$, Fig. 5.30:

$$V_{\mathrm{PCC,k}} = V_{\mathrm{PCC,k-1}} + (e_k - e_{\mathrm{k-1}})K_1 + e_k K_2 \tag{5.13}$$

with $e_k = P_{\mathrm{PCC,ref,k}} - P_{\mathrm{PCC,k}}$, $V_{\mathrm{PCC,k}}$ the STs secondary voltage and k the discrete time step. The parameters K_1 and K_2 are derived from the proportional gain K_P and the integral gain K_i in a continuous PI controller by using:

$$V_{\mathrm{PCC}}(t) = K_p \left(e(t) + \frac{1}{T_i} \int_0^t e(\tau) d\tau \right) \tag{5.14}$$

which is transfered to discrete form by using backward finite difference:

$$\frac{dV_{\mathrm{PCC}}(t)}{dt} \approx \frac{V_{\mathrm{PCC,k}} - V_{\mathrm{PCC,k-1}}}{\Delta t}. \tag{5.15}$$

From this, it follows that $K_1 = K_p$ and $K_2 = K_P \Delta t / T_i$. Note that by using a tap-changing transformer, only discrete changes of V_{PCC} are possible. As here the compatibility of the presented control strategy in a microgrid is studied, the details of the ST are not considered. A higher power transfer from utility grid to microgrid,

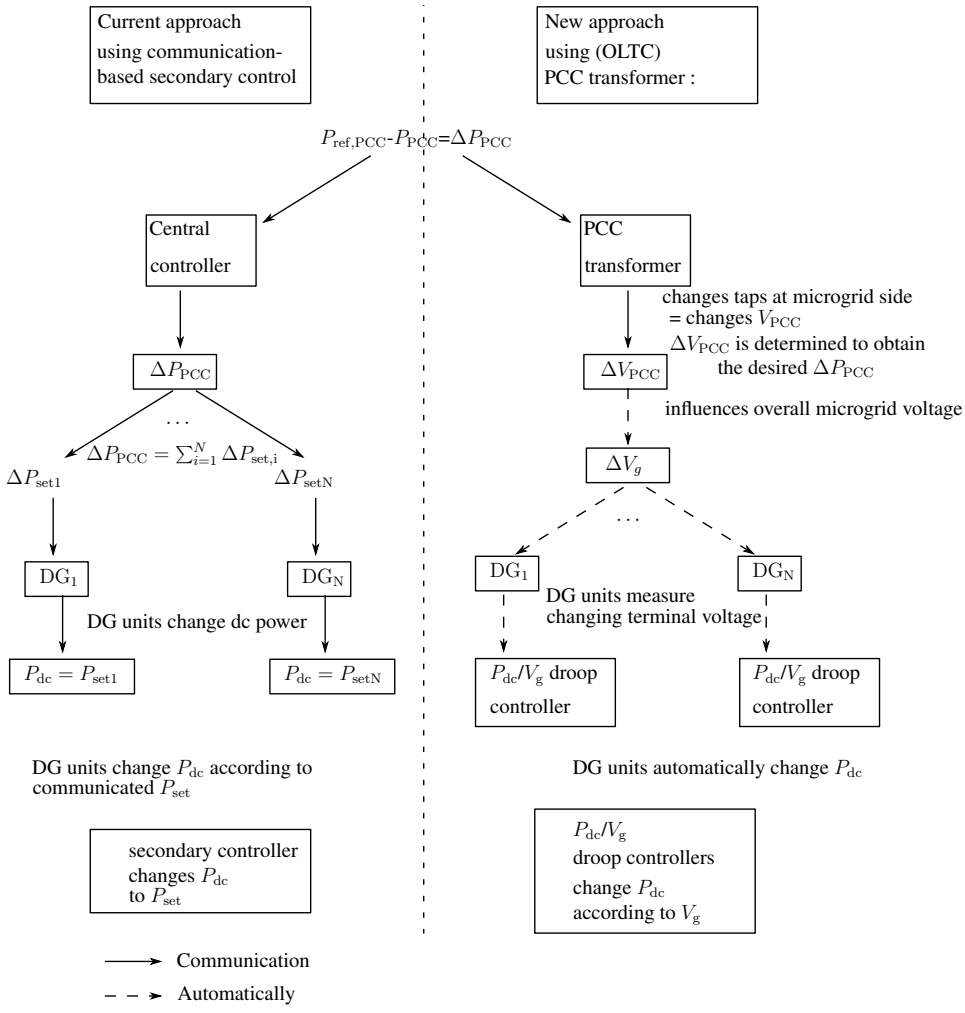

Figure 5.27: Smart transformer versus central control to change power export from microgrid to utility network

i.e., a higher P_{PCC}, can be achieved by increasing V_{PCC}, while of course, a lower V_{PCC} has the opposite effect. A consequence of a higher V_{PCC} is that the overall voltage in the microgrid increases. Therefore, the difference between the terminal voltages of the DG units and the overall microgrid voltage will decrease. The DG units will automatically deliver less ac power to the microgrid. Because initially, the dc-power remains the same, the dc-link voltage will increase. This increase will be sensed by the $V_{\mathrm{g}}/V_{\mathrm{dc}}$ droop controllers of the DG units, increasing their terminal

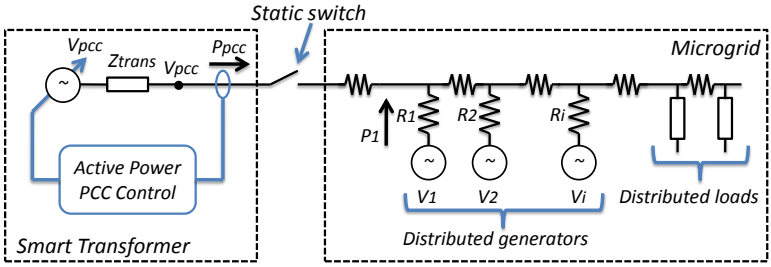

Figure 5.28: ST with the equivalent circuits of the resistive virtual lines and the generators

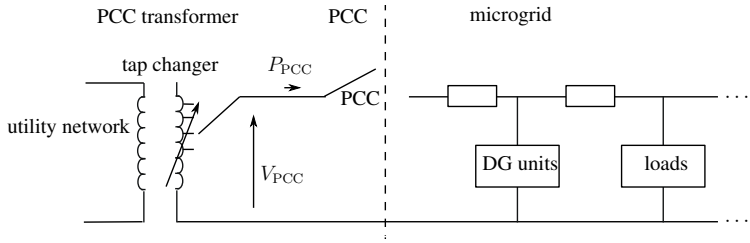

Figure 5.29: Smart transformer in microgrid

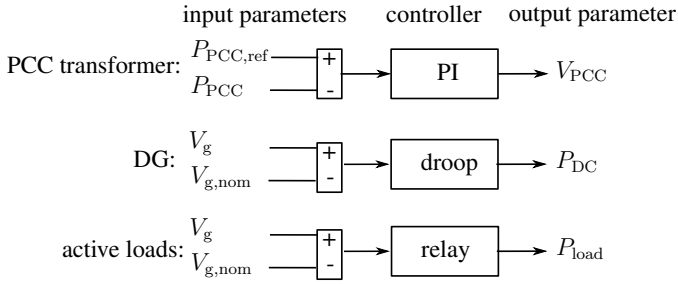

Figure 5.30: PI controller for smart transformer

voltage V_{g}. The $P_{\mathrm{dc}}/V_{\mathrm{g}}$ droop controllers in turn will decrease the dc-power in response to the increased V_{g}. In this way, the DG units automatically deliver less power when the power import into the microgrid is increased by increasing V_{PCC} with the ST.

Summarised, the power transfer P_{PCC} is altered by communicating $P_{\mathrm{PCC,ref}}$ to the ST. This ST uses a tap changer to influence its microgrid-side voltage V_{PCC}. This

directly influences the active power in the microgrid because 1) it is a low-voltage network with mainly resistive line parameters, leading to a linkage between P and V, 2) the active power control of both the generators and the active loads is voltage-triggered. Hence, these units automatically adapt to a change of V_{PCC}. Therefore, $P_{\mathrm{PCC,ref}}$ only needs to be communicated to a single unit and the rest of the microgrid elements adapt without communication. In this way, the microgrid can be exploited as a controllable entity within the electrical network for the primary control.

2. Reference power exchange between microgrid and utility network

The reference power exchange $P_{\mathrm{PCC,ref}}$ can be altered depending on 1) the status of the main grid, 2) the status of the microgrid (in case voltage-based control strategies are implemented, this state is visible in the microgrid voltage), 3) communication delivered by, e.g., a central controller (e.g., time-dependent price information, enabled by the smart grid concept). Overall, this information can be either communication-based or voltage-based. In case of voltage-based information, the microgrid-side voltage is used as the trigger to change $P_{\mathrm{PCC,ref}}$, e.g., in a droop-based control strategy analogous to the $P_{\mathrm{dc}}/V_{\mathrm{g}}$ droop control of the DG units. In this way, the utility can (help) balance the power in the microgrid by using the voltage-based method. In case of the communication-based information, in the literature, already some methods that determine OLTC set points are discussed, such as [204, 205]. These methods use an optimised power flow algorithm and an active management scheme. Also, in case of multiple microgrids, each microgrid can be seen as a single entity providing ancillary services, such as frequency regulation [206]. These services can be coordinated between the microgrids by means of communication resulting in new power set points for the ST. The ST aggregates all the available information, both voltage-based and communication-based, to determine $P_{\mathrm{PCC,ref}}$. The determination of $P_{\mathrm{PCC,ref}}$ is not the focus of this PhD thesis and the communication-based method is used for this.

3. Discussion

Using a ST than can change V_{PCC} according to $P_{\mathrm{PCC,ref}}$ has several advantages:

1. By using a controlled tap-changing ST located at the PCC in the grid-connected mode, the microgrid operates in a virtually islanded mode. The microgrid elements can use the same control strategy in grid-connected and islanded mode.

2. The control strategy of the smart transformer is compatible with the control of the loads and generators, because they are all voltage-based.

3. For P_{PCC} control, only communication between the utility grid and the smart transformer is required.

4. The microgrid adapts automatically to changes in the power transfer P_{PCC}. Therefore, the usage of a ST enables one of the main advantages of microgrids, namely that the microgrid can be seen as a controllable entity from the utility's point of view.

A disadvantage is that if the microgrid wants to deliver reactive power support to the grid, the reactive power control strategy in the microgrid must be changed when using the ST. In the islanded mode with Q/f droop control, the frequency is determined by the total reactive power. In the grid-connected mode with ST on the other hand, the microgrid frequency follows the grid frequency. As this can be assumed largely constant and nominal, all units operate at nominal reactive power. Generally, this involves unity power factor operation. This complies with the current operation of grid-connected units, but microgrid services regarding reactive power control are often required. Therefore, by using low-bandwidth communication, the reactive power of the DG units can be altered by changing the nominal Q or f set points, this can be included in a secondary control strategy, which is out of scope of this chapter.
Another option is the usage of a back-to-back (ac to ac) converter [207]. This configuration has an energy buffer in a dc-link capacitor, thus, gives more control flexibility. Opposed to a transformer, a back-to-back converter can control the frequency and phase angle of the microgrid voltage. Therefore, the converter can alter the reactive power exchange between the microgrid and the main grid. A back-to-back converter further renders dynamic decoupling to prevent voltage and frequency fluctuation in the utility side to impact the microgrid loads. The main disadvantage of a back-to-back converter is its high cost, because of the large rated power. This makes it impracticable for the power exchange control discussed in this chapter.

5.3.2 Proof of concept

For a proof of concept, a basic microgrid is considered. The simulation parameters are summarised in Table 5.2. The active power and voltage controllers start at $t = 0$ s with $V_{\mathrm{g}} = 230$ V rms. The microgrid consists of one ST located at the PCC, two DG units and two loads, as depicted in Fig. 5.31. Both DG units apply the $V_{\mathrm{g}}/V_{\mathrm{dc}}$ droop and $I_{\mathrm{dc}}/V_{\mathrm{g}}$ droop control strategies. The first DG unit, G1, has a wide constant-power band ($b = 8$ %), representing a slightly controllable DG unit, e.g., a renewable energy source with small storage capabilities. Here, the changes of, e.g., wind or sun, changing I_{dc} are not taken into account. The second one, G2, has a constant-power band b of 0 %, thus, represents a dispatchable unit. The dynamic effects of the changes of I_{dc} of this unit are not modelled in detail, the simplest way to do so is by including a low-pass filter that slows down the obtained

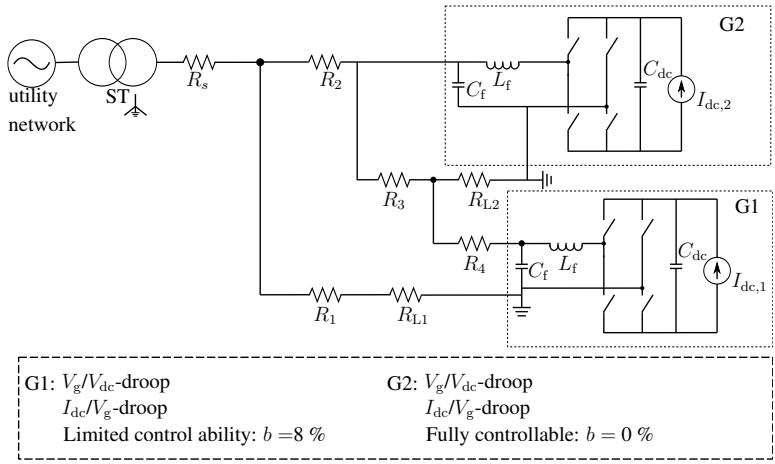

Figure 5.31: Microgrid configuration for proof of concept of smart transformer: single-line diagram

changes of I_{dc}. Here, the low-pass filter is omitted. The nominal input dc-currents are 1.5 A and 3 A for G1 and G2 respectively. Both loads are resistive loads. Furthermore, a resistive virtual output impedance is included in the DG units and the line impedances are purely resistive. The latter is a valid assumption as discussed above.
Three situations, depending on the reference active power through the ST, $P_{\mathrm{PCC,ref}}$, are investigated. Again, the method to determine $P_{\mathrm{PCC,ref}}$, e.g., based on an optimal power flow algorithm, is not considered.

- $P_{\mathrm{PCC,ref}} = 800$ W in Fig. 5.32. This simulation shows that the ST can track a reference active power by changing its microgrid-side voltage. Also, because of the voltage-based control of the DG units and the ST, the microgrid automatically responds to changes of the ST. The microgrid imports relatively much power from the main grid, for example, because of low energy prices in the main grid or off-times for the intermittent DG units in the microgrid. The obtained steady-state results are summarised in Table 5.3. The input dc-current of G1 remains 1.5 A as its terminal voltage, namely 226.8 V, remains in the constant-power band of $[(1-b)V_{\mathrm{g,nom}},(1+b)V_{\mathrm{g,nom}}]$ or [211.6, 248.4] V. The input dc-current of G2 has slightly increased to 3.26 A as this power source has a constant-power band of 0 % and its terminal voltage is slightly lower than the nominal voltage.

- $P_{\mathrm{PCC,ref}} = 0$ W in Fig. 5.33. The ST controls its secondary rms voltage such

Table 5.2: System parameters of basic case with ST. The line parameters are based on BAXB cables with phase resistance 0.41 Ω/km and neutral conductor with 0.71 Ω/km and $R_{\mathrm{phase}}/X \approx 5$.

parameter	value	parameter	value
$f_{\mathrm{s,VSI}}$	20 kHz	C_{f}	3 μF
$f_{\mathrm{s,ST}}$	1 kHz	L_{f}	2 mH
R_1	0.5 Ω	C_{dc}	1.5 mF
R_2	0.1 Ω	Droop K_{V}	0.5 V/V
R_3	0.3 Ω	Droop K_{Q}	$5\mathrm{e}^{-5}$ Hz/VAr
R_4	0.3 Ω	Droop K_{I}	$I_{\mathrm{dc,nom}}$/50
R_5	0.3 Ω	f_{nom}	50 Hz
R_{L1}	33 Ω	Q_{nom}	0 VAr
R_{L2}	33 Ω	$I_{\mathrm{dc,nom,1}}$	1.5 A
r_{v}	3 Ω	$I_{\mathrm{dc,nom,2}}$	3 A
$V_{\mathrm{dc,nom}}$	450 V	$V_{\mathrm{g,nom}}$	230 V rms

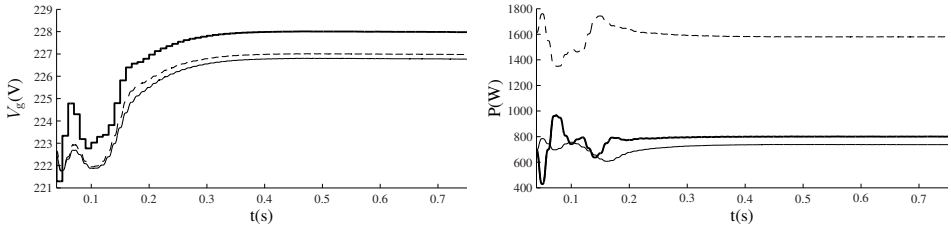

(a) Microgrid rms voltage

(b) Active power to the electrical network

Figure 5.32: Influence of smart transformer with $P_{\mathrm{PCC,ref}} = 800$ *W (— = G1; ---- = G2; ── = smart transformer)*

that there is no active power exchange between the main grid and the virtually islanded microgrid. Still, the PCC switch is closed, so reactive power exchange between both networks is possible.

As depicted in Table 5.3, the terminal voltage of the ST is lower to obtain a lower P_{PCC} compared to the case of Fig. 5.32. This low ST voltage influences the voltages of the rest of the microgrid. Hence, a lower terminal voltage $V_{\mathrm{g,2}}$ is obtained, and therefore, the flexible DG unit G2 increases the delivered dc-current. The inflexible unit G1 on the other hand, still delivers

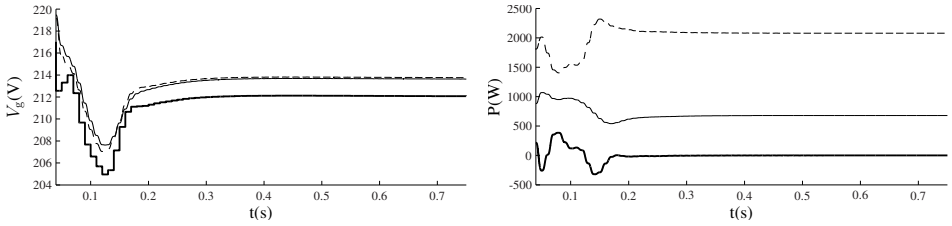

(a) Microgrid rms voltage

(b) Active power to the electrical network

Figure 5.33: Influence of smart transformer with $P_{\mathrm{PCC,ref}} = 0$ W (— = G1; ---- = G2; ▬ = smart transformer)

Table 5.3: Overview: influence of power exchange through smart transformer

	$P_{\mathrm{ref,PCC}}$		
	800 W	0 W	-800 W
P_1 (W)	737	678	789
P_2 (W)	1580	2078	2500
P_{PCC} (W)	800	0	-800
V_1 (V)	226.8	213.6	202.9
V_2 (V)	227.0	213.8	202.5
V_{PCC} (V)	228.8	212.1	197.6
$I_{\mathrm{dc},1}$ (A)	1.5	1.5	1.87
$I_{\mathrm{dc},2}$ (A)	3.26	4.38	5.34

nominal dc-current of 1.5 A because the grid voltage remains in the constant-power band. Furthermore, compared to the case with $P_{\mathrm{PCC,ref}} = 800$ W, the $I_{\mathrm{dc}}/V_{\mathrm{g}}$ droop controlled source G1 delivers slightly less power to the microgrid. This is due to the fact that the dc side of the DG unit is modelled as a constant current source and, hence, the lower microgrid voltage combined with the $V_{\mathrm{g}}/V_{\mathrm{dc}}$ droop control leads to lower dc-link voltages.
This simulation shows that the microgrid automatically adapts to the secondary voltage of the ST and that the ST can significantly influence the microgrid state.

- $P_{\mathrm{PCC,ref}} = -800$ W in Fig. 5.34. The islanded microgrid delivers active power to the main grid, hence, more power is generated in the microgrid. Op-

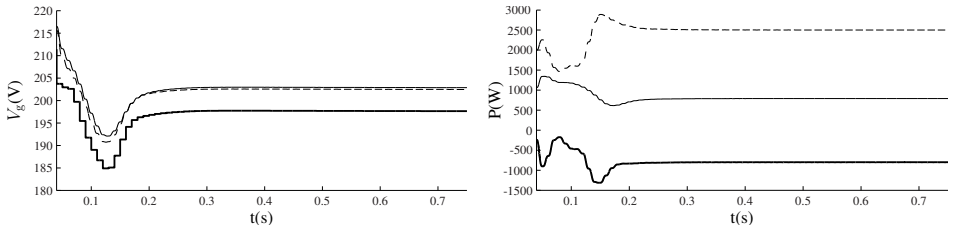

(a) Microgrid rms voltage

(b) Active power to the electrical network

Figure 5.34: Influence of smart transformer with $P_{\rm PCC,ref} = -800$ W (— = G1; ---- = G2; ▬ = smart transformer)

posed to the previous cases, the terminal grid voltages of both power sources are under the lower adjustment voltage, so both sources increase their dc-current. This shows the advantage of using the $I_{\rm dc}/V_{\rm dc}$ droop control with generator-dependent width of the constant-power band: the change of the dc-current of the less flexible DG unit G1 is delayed compared to that of the more flexible unit G2.

In the previous simulations, the voltage limits and usage of energy storage are not taken into account such that more extreme voltages compared to practical situations can be obtained, which is also due to the small scale of the considered microgrid. In this way, the effect of the ST and changes of the DG units can be studied. To take these voltage limits into account, the control signals of the ST can be influenced by the voltage state of the microgrid. Also, active load control and storage can be included, which is not the case in the previous simulation. Furthermore, a microgrid with only two DG units, one of them being inflexible was studied, so more flexibility in the DG units would lead to voltages closer to the nominal value.

In conclusion, by implementing the smart tap-changing transformer in the microgrid, the power exchange between a microgrid and the utility grid can be controlled by changing the microgrid-side voltage of the ST. It is also shown that the microgrid generators automatically (without need for communication) change their output power according to the microgrid-side voltage of the ST. In this way, the ST can significantly influence the microgrid state.

The usage of a ST is beneficial to enable operation in a virtually islanded microgrid. On the one hand, energy independence of for example a business area can be achieved without inter-unit communication, by only setting $P_{\rm PCC,ref} = 0$ W. On the other hand, the microgrid can participate in the markets and provide ancillary services by controlling its PCC power in a flexible manner.

5.3.3 Smart transformer delivers increased flexibility to the microgrid

In this example, a more realistic microgrid (four generators, different loads, smart transformer) is studied. The main purpose of this simulation is 1) to study the ST operation in the microgrid, 2) to compare the cases of a real islanded microgrid and a grid-connected microgrid. The microgrid configuration is depicted in Fig. 5.35 (i.e., slightly different from that in § 4.4 as here, it is a grid-connected microgrid). The microgrid sources have the following characteristics:

- G1: Constant-current source with a nominal dc-current $I_{\mathrm{dc,nom}}$ of 6 A. The active power control is performed by the $V_{\mathrm{g}}/V_{\mathrm{dc}}$ droop controller only, thus, a very large constant-power band is included.
- G2: G2 uses $V_{\mathrm{g}}/V_{\mathrm{dc}}$ and $P_{\mathrm{dc}}/V_{\mathrm{g}}$ droop control strategy and has limited control flexibility. Therefore, a constant-power band $b = 5$ % is included. The nominal power of this power-controlled source equals $P_{2,\mathrm{nom}} = 3000$ W.
- G3: Current-controlled source with $V_{\mathrm{g}}/V_{\mathrm{dc}}$ and $I_{\mathrm{dc}}/V_{\mathrm{g}}$ droop control, with $I_{3,\mathrm{nom}} = 5$ A and a constant-power band $b = 3$ %.
- G4: $V_{\mathrm{g}}/V_{\mathrm{dc}}$ and $I_{\mathrm{dc}}/V_{\mathrm{g}}$ droop control with $I_{3,\mathrm{nom}} = 3.5$ A, fully flexible current-controlled source as the constant-power band b equals 0 %.

Here, only linear loads are included as the focus is on the ST. The loads are 25 Ω loads. An analogous microgrid with nonlinear loads and inductive line elements has been considered in [184]. The other system parameters are equal as in the previous simulation, and are summarised in Table 5.2. The Q/f droop controller is only activated after 0.1 s, hence, before this instant, the DG units are not synchronised. This leads to large start-up transients. It is included to demonstrate the robustness of the controller.

A. Case without smart transformer

In this simulation case, the switch at the PCC is open, thus, an islanded microgrid is obtained. The simulation results in Fig. 5.36 show a stable microgrid operation. As G1 has no control flexibility, its dc-current remains the nominal value of 6 A. G2 on the other hand, which has some control flexibility, increases its output power from nominal 3000 W to 3122 W as its terminal voltage is lower than the lower adjustment voltage of $0.95V_{\mathrm{g,nom}} = 218.5$ V. The same is valid for G3 and G4.
Note that in this case, low nominal powers and a large load are chosen to obtain low output voltages. In this way, the impact of more control flexibility, namely provided by the ST, can be studied in detail in the next case. Still, a proper microgrid operation is obtained, despite the small scale of the microgrid, the low control flexibility in the generators and the ignored impact of energy storage and active load control.

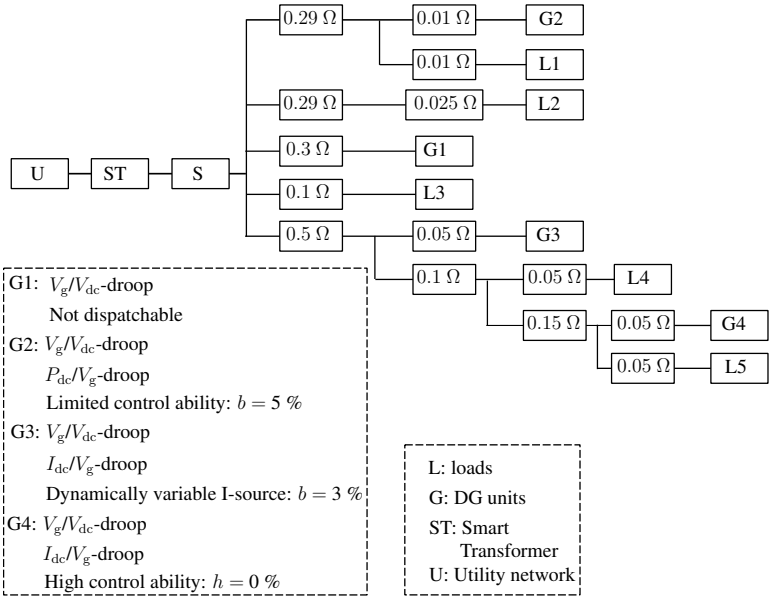

Figure 5.35: Microgrid configuration successive comparison by including a smart transformer and demand dispatch

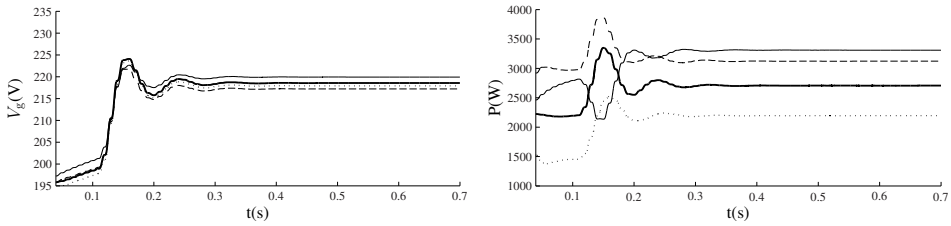

(a) Microgrid voltage (b) Active power to the electrical network

Figure 5.36: Smart transformer in microgrid: without smart transformer (— = G1; ---- = G2; ▬ = G3, . . . = G4)

B. Case with smart transformer

In this case, the PCC switch is closed to operate the microgrid in a grid-connected mode. Because of the low voltages obtained in the previous case, the reference power import in the microgrid, through the ST, equals 500 W (which is a chosen value dependent on the microgrid state only). The simulation results are shown in

Table 5.4: Overview: smart transformer in microgrid

	$P_{\mathrm{PCC,ref}}$	
	islanded	grid-connected with ST
P_1 (W)	3308	3407
P_2 (W)	3122	3040
P_3 (W)	2706	2560
P_4 (W)	2195	2121
P_{PCC} (W)	0	500
V_1 (V)	219.9	223.3
V_2 (V)	217.2	220.3
V_3 (V)	218.6	221.0
V_4 (V)	217.9	220.2
V_{PCC} (V)	-	219.9
$V_{\mathrm{L},1}$ (V)	213.3	216.6
$V_{\mathrm{L},2}$ (V)	217.0	220.1
$I_{\mathrm{dc},1}$ (A)	6	6
$I_{\mathrm{dc},2}$	6.3	6.1
$I_{\mathrm{dc},3}$ (A)	5.6	5.3
$I_{\mathrm{dc},4}$	4.7	4.5

Table 5.4 and Fig. 5.37.
Compared to the simulation case in islanded operating mode, the terminal voltages of all units are higher, thus closer to the nominal value, because of the power import through ST. For this reason, the dispatchable DG units also lower their I_{dc}. The simulations show that slightly more power is delivered by some (i.e., less dispatchable) DG units. The reason is that the ST increases the microgrid voltage and most generators here use current-controlled energy sources. For example, for the current-controlled source G1, because of the $V_{\mathrm{g}}/V_{\mathrm{dc}}$-droop control, an increase of V_{g} leads to higher V_{dc}. As the dc-link voltages increase, under constant I_{dc}, also the dc-power increases. In this way, the delivered ac active power is slightly increased as well. Because of the higher terminal voltages compared to the previous case, the dc-input currents are lower than in the previous case.
The simulations indicate that the ST can control the power exchange between the microgrid and the main grid. Also, the ST can effectively increase the power quality in the microgrid by forcing the voltage closer to its nominal value. Because of the ST, there is no need to change the power control method of the DG units between the islanded operating condition and the grid-connected operation with ST.

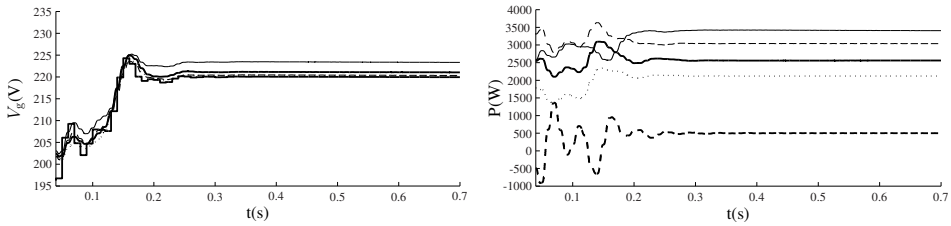

(a) Microgrid voltage

(b) Active power to the electrical network

Figure 5.37: Smart transformer in microgrid: with smart transformer (— = G1; ---- = G2; ▬ = G3, . . . = G4, ▬ ▬ = smart transformer)

5.3.4 Smart transformer in a microgrid with dynamical changes

In the following simulations, some dynamical events are included to study the effect of changing parameters in a microgrid that is connected to the utility network through a smart transformer. The microgrid configuration of Fig. 5.38 is studied, which is analogous as in § 5.1, but now in a virtually islanded operation. This microgrid consists of three power sources, the details of the sources are given in Fig. 5.38. The nominal generated dc currents are: $I_{\rm dc,1} = 7$ A, $I_{\rm dc,2} = 4.5$ A and $I_{\rm dc,3} = 3.5$ A. After 0.35 s, VSI 3 turns off and 0.35 s later it starts operating at 50 %. At $t = 1$ s, VSI falls down to 75 %. For the reactive power control, Q/f droop control is applied, with equal droops for the power sources. Again, this controller starts after 0.1 s to illustrate the robustness of the control strategy. The loads considered here are a combination of variable and non-variable loads. The simulations mimic a dynamic profile, with dynamic events such as losing a generator and changing the demand dispatch. The dynamic events included in the following simulation are described on page 184. For the loads, the demand dispatch starts at $t = 0.36$ s for both variable loads. Here basic demand dispatch is included: $R_{\rm var,1}$ can change from 25 Ω to 50 Ω with $V_{\rm g,o} = 0.91 V_{\rm g,nom}$ and $V_{\rm g,d} = 0.96 V_{\rm g,nom}$ in the relay function of Fig. 5.1. The second load with demand dispatch $R_{\rm var,2}$ can change from 25 Ω to 5000 Ω (i.e., turned off) with $V_{\rm g,o} = 0.93 V_{\rm g,nom}$ and $V_{\rm g,d} = 0.97 V_{\rm g,nom}$. The demand dispatch of $R_{\rm var,1}$ turns off at $t = 0.85$ s, such that then, $R_{\rm var,1} = 25$ Ω.

In the simulations presented below, firstly, the islanded microgrid without ST is studied. Secondly, this is compared with the case of a grid-connected microgrid with ST. The results are different from those in § 5.1.4D. as the DG units have other nominal powers.

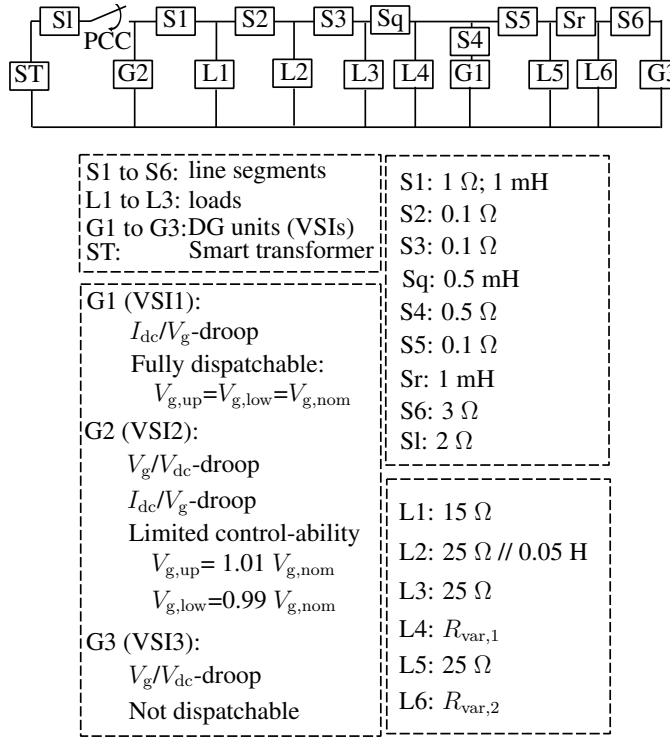

Figure 5.38: Microgrid configuration: extended example

A. Case without smart transformer

The simulation results for the case without smart transformer and with open PCC switch are depicted in Fig. 5.39.

- $0 < t < 0.35$ s: After a start-up transient, the terminal voltages reach $V_{g,1} = 218$ V, $V_{g,2} = 216$ V and $V_{g,3} = 236$ V.
- $0.35 < t < 0.7$ s: The demand signal for both variable loads turns on. Despite the loss of VSI 3, the contribution of the demand dispatch leads to a small voltage increase to $V_{g,1} = 218$ V and $V_{g,2} = 217$ V. For the same reason, the power sources deliver slightly less power to the microgrid. One remark according to the disconnection of G3 is that in the time span where G3 is turned off, the terminal voltage of this VSI slowly decreases. This has no practical value for the microgrid, as G3 is disconnected. The reason for this voltage decrease is that the disconnection of G3 is modelled with 1) $I_{dc,3} = 0$ A, 2) a switch located after the LC filter of G3 opens. Therefore,

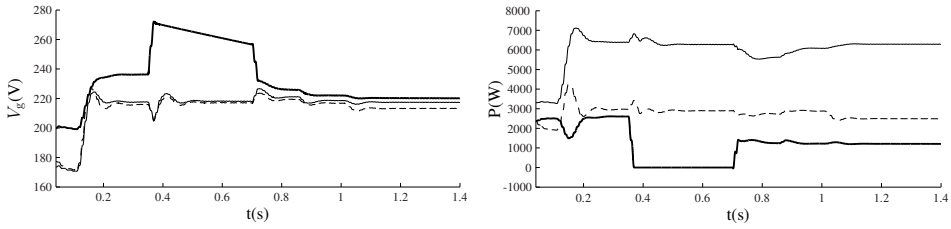

(a) Microgrid voltage

(b) Active power to the electrical network

Figure 5.39: Dynamic profile: without ST (— = G1; ---- = G2; ▬ = G3)

the LC-filter is not supplied and the filter capacitor voltage decreases across parasitic resistances, which are here simulated as a large resistance in parallel with this capacitor.

- $0.7 < t < 0.85$ s: Higher microgrid voltages are obtained because of the activation of VSI 3.
- $0.85 < t < 1$ s: At 0.85 s, the demand signal of $R_{\mathrm{var},1}$ is turned off, leading to a higher load burden. Therefore, the microgrid voltages are slightly decreased and G1 and G2 respond by increasing their output power.
- $t < 1$ s: Because less power is delivered by G2, the microgrid voltages are lower compared to the previous time span: with $V_{\mathrm{g},1} = 217$ V, $V_{\mathrm{g},2} = 213$ V and $V_{\mathrm{g},3} = 220$ V. Furthermore, because of the lower P_2, P_1 increases. In steady-state also, $I_{\mathrm{dc},1} = 9.5$ A, $I_{\mathrm{dc},2} = 5.2$ A and $I_{\mathrm{dc},3} = 1.8$ A.

B. Case with smart transformer

In this simulation, the feasibility of the ST concept in a microgrid with dynamic events is studied. The reference power of the ST starts at 800 W. At $t = 0.80$ s, P_{ref} decreases to -800 W. Generally, the state of the microgrid influences the determination of $P_{\mathrm{PCC,ref}}$, where the state of the microgrid is visible in the grid voltage. However, in order to study a more difficult case to control, here, $P_{\mathrm{PCC,ref}}$ is determined by external information only.
The simulation results for the case with ST are depicted in Fig. 5.40. From the simulations, it follows that in the first time span $0 < t < 0.35$ s, the terminal voltages are $V_{\mathrm{g},1} = 219$ V, $V_{\mathrm{g},2} = 221$ V, $V_{\mathrm{g},3} = 238$ V and $V_{\mathrm{g,ST}} = 228$ V. The obtained voltages are higher than in the previous case, because of the power input from the utility grid.

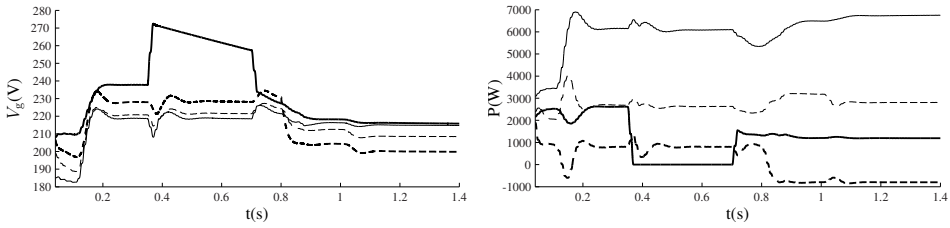

(a) Microgrid voltage

(b) Active power to the electrical network

Figure 5.40: Dynamic profile: with ST (— = G1; ---- = G2; ▬ = G3, ▬ ▬ = smart transformer)

At $t = 0.8$ s, the reference power of the ST decreases significantly, which can be triggered by the utility network because of, e.g., a sudden loss of a generator. From the simulations, it follows that the dispatchable DG units G‘and G2 increase their output power, without communication, to compensate for this change in the ST. The voltage in the microgrid decreases, such that normally, the microgrid voltage will trigger the ST to change $P_{\mathrm{PCC,ref}}$, in order to prevent under-voltage conditions. This is not included in this example in order to study the reaction of the DG units on the $P_{\mathrm{PCC,ref}}$ change rendered by the utility network.
In steady-state, $V_{\mathrm{g},1} = 215$ V, $V_{\mathrm{g},2} = 209$ V, $V_{\mathrm{g},3} = 216$ V and the delivered dc-currents are: $I_{\mathrm{dc},1} = 10.0$ A, $I_{\mathrm{dc},2} = 5.8$ A and $I_{\mathrm{dc},3} = 1.8$ A. $I_{\mathrm{dc},1}$ and $I_{\mathrm{dc},2}$ are higher than in the previous case to compensate for the power export to the main grid.
In conclusion, the examples indicate that the ST is able to operate in a microgrid with dynamic events. By adapting its $P_{\mathrm{PCC,ref}}$ to the microgrid state, a higher power quality (voltage quality) can be obtained. Furthermore, the microgrid generators and active loads automatically adjust to the state of the ST.

5.3.5 Conclusions

In conclusion, by implementing a smart transformer at the PCC, the power exchange between the microgrid and the utility grid can be controlled by altering the microgrid-side voltage of this transformer. It is also shown that the microgrid elements can use the same control algorithm in the grid-connected mode with smart transformer as in the islanded mode. The control strategies of the DG units, active loads and smart transformer are all voltage-based.
From the examples, it follows that the smart transformer gives more control flexibility to the microgrid. To control the power exchange between microgrid and utility

grid, the utility grid only needs to communicate to the smart transformer, instead of to all microgrid elements. The smart transformer aggregates this information with the voltage information of the microgrid to determine its power exchange. All microgrid elements automatically respond to changes of the ST. In this way, the smart transformer enables the microgrid to become a real controllable entity within the electrical network.

5.4 Conclusions

This chapter extends the VBD control that is developed for DG units to other microgrid elements. In § 5.1, the voltage is used as a trigger for active load changes. In this way, a primary demand dispatch strategy is developed that fully complies with the VBD control. The same control strategy is possible in the storage elements. It is concluded that the combination of the VBD strategy for the generators with the presented demand dispatch strategy allows reliable power supply without inter-unit communication for the primary control, leads to a more efficient usage of the renewable energy and can even lead to an increased share of renewables in islanded microgrids.
In § 5.2, the small share of SGs in the islanded microgrid is taken into account. In order to obtain an adequate power sharing between the CIDG units and SGs, the control strategy of the SGs is matched to the VBD control. Two PI controllers force the operation of the SG towards the $P_{\mathrm{dc}}/V_{\mathrm{g}}$ and Q/f droops.
In § 5.3, the microgrid is operated in a virtually islanded mode by using a smart transformer located at the PCC. The ST controls the PCC power and the microgrid elements automatically adapt. In this way, the microgrid can operate as a controllable entity in a virtually islanded mode, i.e., with predefined PCC power.
The content of this chapter has been published in the journal papers [208–210].

Chapter 6

Operating modes of a microgrid

The previous chapters focussed on the control of microgrids in a (virtually) islanded mode. Here, the grid-connected mode will be further analysed. This chapter does not study the grid-following converter control for units in grid-connected mode as this has already widely been studied in literature. It focusses on applying the VBD control in grid-connected mode in § 6.1. In § 6.2, the VBD controller is modified to enable a smooth transition between the grid-connected and the islanded operating conditions.

6.1 Grid-connected VBD control

Firstly, with respect to on-off oscillations, the power curtailment in renewables by using VBD control is compared with the state-of-the-art on-off control of these units. Secondly, the impact of VBD-controlled grid-connected DG units on the voltage level is studied. Thirdly, the beneficial impact of VBD control on the line losses in low-voltage networks is discussed.

6.1.1 Grid-connected VBD control to avoid on-off oscillations

A. Introduction

An increasing amount of renewable energy, often delivered by distributed generation (DG) units, is injected in the electrical power system. The traditional approach for integrating these DG units is by investing in more and stronger lines, which could lead to massive investments to cope with the huge rise of DG connection. Another common solution is to include hard curtailment, thus, on-off control of DG units in case the voltage limits are exceeded. However, hard curtailment potentially leads to on-off oscillations of DG and a significant loss of the available renewable energy as storage is often not economically viable. Except for this hard curtailment,

the grid-following DG units[1] generally do not contribute in the grid support, i.e., control of voltage amplitude and frequency, in contrast to the grid-forming units in islanded microgrids. Because of this passive operation of DG, local grid bottlenecks appear already today, e.g., for photovoltaic installations at the end of the lines or in areas with a high density of DG. Two central factors that restrict the available additional DG capacity in distribution networks are the voltage increase and voltage unbalance [27]. Therefore, the fit-and-forget strategy of installing DG is not a sustainable option and limits the further penetration of DG. In the future, DG will need to contribute in the grid support, e.g., to cooperate in the voltage control, power balancing and to provide other ancillary services like reserve. Because of the predominantly resistive lines, low-voltage networks mainly suffer from voltage problems in case of a large local penetration of DG units. Therefore, here, the voltage control by grid-connected DG units in low-voltage networks is discussed.

To provide voltage support, the conventional large power plants are equipped with reactive power/terminal voltage (Q/V_g) droop controllers. The grid-connected DG units can be equipped with analogous Q/V_g droop functions, e.g., the static voltage support of SMA inverters [211]. However, in low-voltage networks, voltage support through reactive power is generally inefficient as the grid voltage is linked with the active power, not the reactive power, because of the predominantly resistive lines. Hence, large amounts of Q are required to influence the voltage. This is further examined in § 6.1.2 and [212]. P/V_g droop controllers are more effective and straightforward to provide voltage support in a low-voltage network.

The conventional on-off control (hard curtailment) is compared with soft curtailment. In [213], hard curtailment is compared with communication-based soft curtailment, relying on a smart metering infrastructure. In this section, soft curtailment is analysed in a fast-acting primary control scheme, based on droops that do not depend on communication. On-off control can lead to power quality degradation (large voltage and current transients), loss of available renewable energy and problems with the inverters (damage or accelerated ageing). Therefore, soft curtailment is considered as well. An easy way to include soft curtailment in the DG units is by implementing a P/V_g droop controller. The current-controlled (grid-following) DG units can be equipped with P/V_g droops. An inherent disadvantage of grid-following units is that they need voltage tracking, generally by using a phase-locked loop (PLL), for the synchronisation of the unit to the grid. The P/V_g droop controller also depends on voltage tracking to extract the voltage amplitude. Grid-forming controllers in grid-connected DG units can be implemented as well. This is analogous to the transmission network in which the large central generators are grid-forming. In this paragraph, the VBD control, that is developed for grid-forming units in islanded microgrids [184], is used for voltage control by DG

[1] DG units in a grid-connected microgrid

units in grid-connected networks for two reasons. Firstly, the VBD control engages renewables in the voltage support while delaying the changes of the active power of the renewables to more extreme voltages compared to those of dispatchable DG units. Secondly, it presents a primary control operating without the need for inter-unit communication nor voltage tracking for synchronisation. It is shown that the VBD control is effective to avoid on-off oscillations (analogous to the P/V_{g} droops). With VBD control, the renewables also take part in the voltage control, but with a lower priority of power changes compared to that of the dispatchable DG units (in contrast to the P/V_{g} droops). In this way, the energy capturing of renewables is increased.
This section is structured as follows. In § B., an overview of the on-off and VBD control principles is given. In § C., these controllers are compared with respect to the renewable energy capturing, over-voltage occurrence and on-off oscillations. To further increase the renewable energy capturing, a Q/V droop is added to the VBD control strategy. In § D., some examples are studied to compare these methods with respect to the on-off oscillations, and voltage quality. The energy delivered by the different controllers is calculated, showing that on-off oscillations significantly reduce this energy. By using the VBD control and the VBD control with the extension of Q/V droops, the renewable energy capturing is significantly increased.

B. Voltage control by means of DG units

Currently, most DG units deliver an amount of power to the electrical network that is independent of the state of the network. This input power is determined solely by the energy source, e.g., maximum power point tracking in case of photovoltaic panels and wind turbines, or heat as primary driver in combined heat and power (CHP) units. Also, most units are current-controlled in a grid-following control strategy. In this paragraph, grid-forming and grid-following control strategies in grid-connected microgrids or utility feeders are considered.

Grid-following unit with on-off control Firstly, conventional grid-following controllers with on-off control as depicted in Fig. 6.1 are considered. The phase angle (θ in Fig. 6.1) of the reference current is obtained by tracking the terminal voltage by using a PLL. The current amplitude is obtained by a dc-link voltage controller keeping the dc-link voltage constant, while the input dc-power is independent of the state of the network. The on-off controller shuts down the DG unit in case the voltage exceeds a predefined value (e.g., 110% $V_{\mathrm{g,nom}}$), called the critical voltage.
Instead of implementing a 100 % change of active power (on-off) in case of over or under voltage, the delivered active power of the unit can be dependent on the local

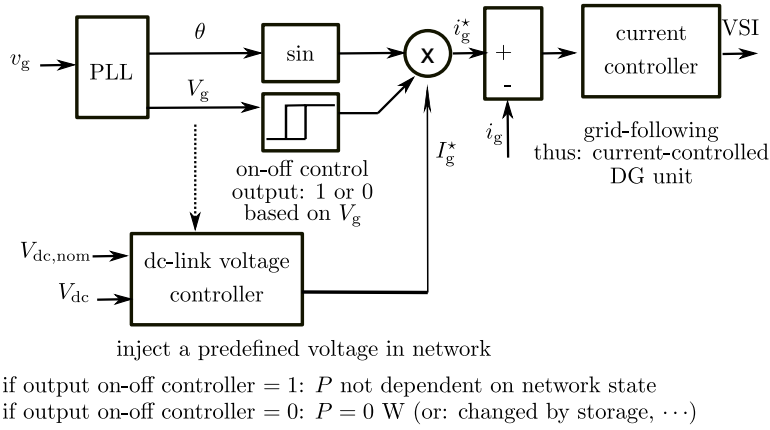

Figure 6.1: Grid-following unit with on-off control based on the terminal voltage

voltage ($P(V_g)$). For this, a grid-following P/V_g droop control strategy, that does not require a communication infrastructure, can be used.

Grid-forming unit with on-off control Next to the conventional grid-following controllers, it is shown that a grid-forming controller is possible in the grid-connected DG units as well. With grid-connected DG units, DG units that are connected to the utility network or a grid-connected microgrid are meant, not units connected to an islanded microgrid. In the control of the VSIs ac-side, always four parameters are present: the amplitude and phase angle of the terminal voltage and current. Two of these parameters can be controlled. Whereas the grid-following controllers are current-controlled (amplitude and phase of the current), the grid-forming controllers are voltage-controlled (amplitude and phase of the ac voltage), as is shown in Fig. 6.2. A PLL for voltage tracking is not required, which simplifies the control algorithm. The units are synchronised by the Q/f droop controllers, which measure the reactive power and change the frequency, thus phase angle, accordingly. This relies on the natural linkage between Q and phase angle differences in resistive networks.
Like in the grid-following units, these DG units can easily limit the injected current as their voltage control loop is often composed of an outer voltage and an inner current control loop. The grid-following DG units are mostly equipped with a power-factor-one controller. In the grid-forming controllers, this is inherently present as well. The reason is that the Q/f droop control operates at Q_{nom} in case $f = f_{\mathrm{nom}}$. The conventional generators force the grid frequency to its nominal value through secondary control. As Q_{nom} in most DG units equals zero, this means that these units operate at power-factor-one. This can be altered by changing Q_{nom}, for ex-

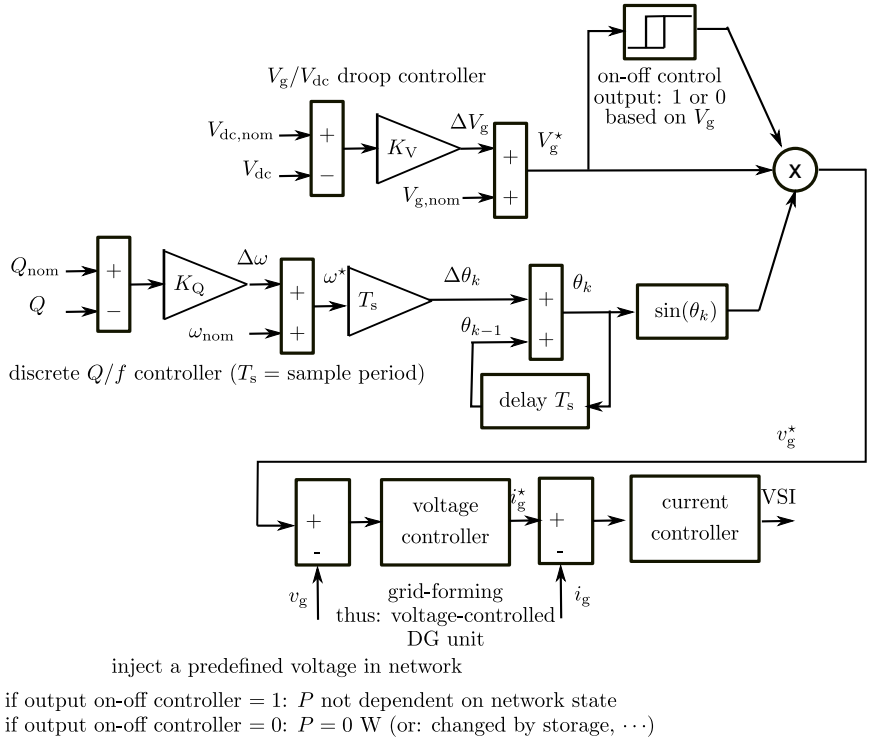

Figure 6.2: Grid-forming unit with on-off control based on the terminal voltage

ample in a secondary controller driven by smart grid communication and control. These grid-forming controllers also inject a predefined amount of active power in the network and operate with on-off control reacting on over-voltages. Like in the grid-following control, P/V_g droop control can be included in these units as well.

Grid-forming unit with VBD control The VBD control strategy, which has originally been developed for islanded microgrids, is applied in the grid-connected units to change their P based on the network state. The active power can be altered by changing the input from the energy source (biomass supply, changing the wind turbines pitch angle, or deviating from the maximum power point (MPP) in a photovoltaic system), by using energy storage or shifting the local load. The control principles of the VBD controller are summarised in Fig. 6.3.

C. Effect of the control algorithms on on-off oscillations

Grid-following controller

On-off control In the grid-following control, a PLL tracks the terminal

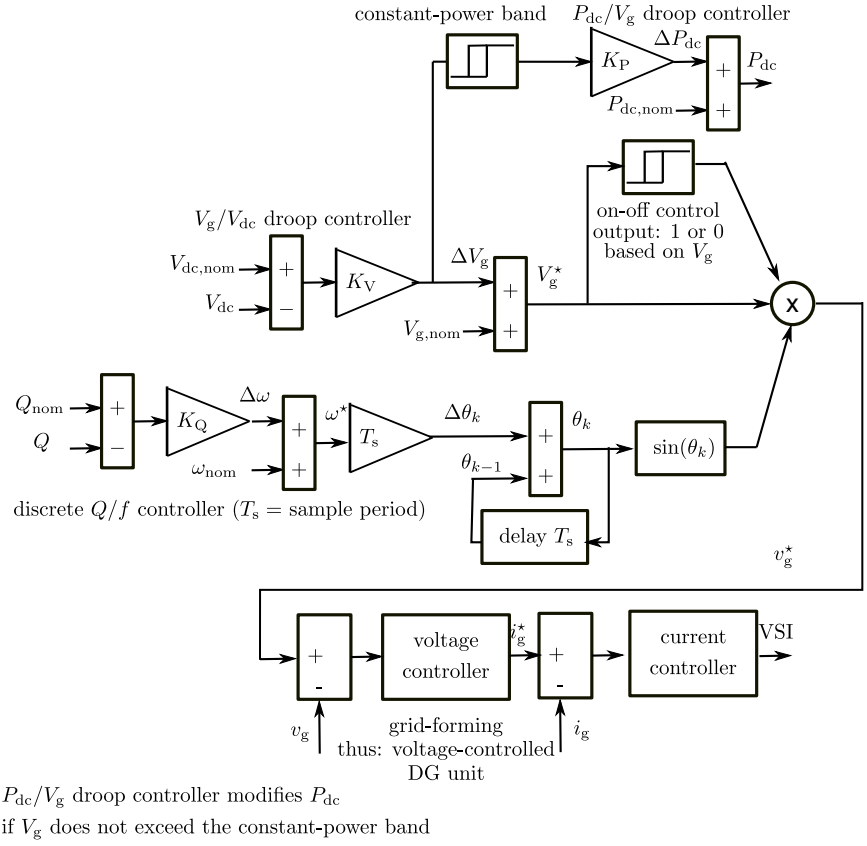

Figure 6.3: Grid-forming unit with VBD control

voltage of the DG units. The PLL calculates the phase angle θ of the voltage and the rms value (V_g). In order to inject a certain amount of power P (e.g., P determined by MPPT) into the microgrid, the reference current is calculated from:

$$i_{ref}(t) = \sqrt{2}\frac{P}{V_g}\sin(\theta). \tag{6.1}$$

Here, a power-factor-one control is used ($Q = 0$ VAr). The output power P equals $P_{dc,nom}$, except when the unit is turned off by its on-off controller, then, $P = 0$ W. The on-off control of the DG units is based on a hysteresis function. It turns the DG unit off when its terminal voltage exceeds a certain voltage and turns it back on when the voltage falls back to a lower voltage, and vice versa for under-voltage conditions. It is clear that when the DG unit turns off due to over-voltage, the voltage at the unit's terminals will drop. If the hysteresis function is not chosen

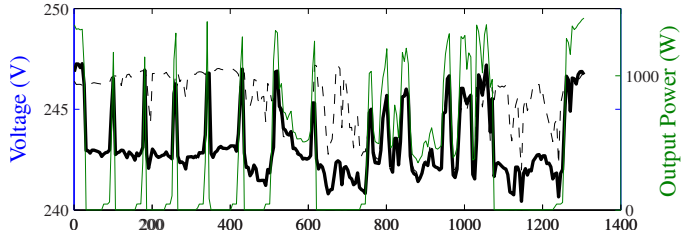

Figure 6.4: On/off control of DG leading to grid-oscillations: measurements of PV panels in Oostende, Belgium (— = DG unit 1, --- = DG unit 2, ━━ = V_{PCC})

properly, the voltage can drop below the turn-on voltage, turning the unit back on, which may lead to oscillations. An example of a measured voltage oscillation problem is depicted in Fig. 6.4. The first DG unit clearly shows an on-off oscillation. A proper choice of the parameters of the hysteresis function can solve the problem. However, as the network varies dynamically, this is difficult to achieve. Also, for all the DG units, the hysteresis function needs to be set according to the specific network characteristics of the network where the unit is connected to. This can be time consuming and not always fair (e.g., units at the end of the line are likely to turn off more frequently than other ones).

Trial strategy to limit power decrease In practice, the DG units turn off during a specified amount of time, e.g., 30 min, in case the number of on-off swings in a certain time period is higher than a threshold value. However, this may lead to even more renewable energy loss or over-sizing of the storage facilities. The reason is that, often, the DG unit should not have been turned off entirely in order to solve the voltage problem. A solution to avoid these oscillations is, hence, to change the hysteresis function's parameters online, for example, based on a trial and error strategy. Analogously, the percentage with which the DG units lower their output power, instead of turning off entirely, can be set based on a strategy that is here called the trial strategy. This strategy should determine the minimum amount of power reduction to avoid oscillations while still meeting the voltage limits. In [22], this optimal power change is determined by a smart grid algorithm. However, here, the controller should operate without communication as it involves a primary control such that optimal power cannot be determined in a straightforward manner. Therefore, the unit takes trial and error attempts by changing its power and, based on the according voltage change, searching for the minimum required power change.

In the trial strategy, when the voltage becomes too high, a drop of, for example 10 %, with a hysteresis function is implemented. If this is not sufficient to solve

the voltage problem, the drop is changed to 20 %, etc. This can avoid the on-off oscillations. For safety reasons, the controller can also start with a 100 % power drop and gradually lower this until no more oscillations occur while still avoiding voltage limit violation. As this method is not practical, it is merely included here to emphasise that fully turning off is not always required to avoid the voltage problem.

Soft curtailment Soft curtailment in all DG units can avoid the on-off oscillations, hence, achieves higher energy capturing of the renewable energy sources. Instead of turning off entirely when a voltage limit is exceeded, the output power can gradually be lowered when the terminal voltage rises, by using a P/V_{g} droop controller. However, this leads to renewable energy loss. The set-point of P automatically decreases with an increase of V_{g} even if other dispatchable DG units nearby have sufficient margin to solve the voltage problem. This is not compatible with the priority injection of renewables that should enable them to inject their generated power if the power quality can be maintained by other units.

Other methods to avoid oscillations The smart grid paradigm also covers mitigation of voltage problems. This is done by communicating new power set-points to the concerned DG units. However, this requires communication for the voltage control, which can reduce the reliability of the system. Hence, in this section, it is emphasised that with respect to the robustness of the system, communication should be avoided for primary control and protection issues. However, smart grid communication, management and control systems are very interesting for secondary issues and to support the automatic controllers for a more economical and optimal operation.

In the examples below, the on-off controller (hard curtailment) is compared with the VBD control. An optimal power change can be found by using communication and a smart metering infrastructure, implemented in a slow control scheme, overlaying the fast-acting primary control schemes that are analysed in this section.

VBD control to avoid oscillations As discussed above, the P/V_{g} droop controller, which can be implemented in both grid-following and grid-forming DG units, avoids the on-off oscillations. However, it does not distinct between the dispatchable and less dispatchable (e.g., renewable) DG units. Either no droops are implemented in the renewables, such that the oscillation problem is not solved in places with high renewable penetration. Or droops are implemented, solving the issue that on-off oscillations can occur when one unit has a large impact on the grid voltage, by changing the output of the unit depending on the voltage. However, this leads to a significantly lower renewable energy capturing as priority of power changes should be given to dispatchable DG units. Dispatchable units should act more and first to voltage rises, while the renewable energy sources should act only when absolutely necessary for the voltage control of the network. Therefore, the VBD

control sets an automatic priority based on the terminal voltage of the network. The output power changes of dispatchable DG units are prioritised over those of the less dispatchable ones. The automatic nature of the priority setting is crucial for the reliability of the system. Of course, smart grid features can change the settings of the VBD controller (e.g., the constant-power band width and the reference power) in an overlaying secondary control scheme.

VBD control with Q consumption In [22], the required amount of reactive power Q that a DG unit should consume to minimise its impact on the voltage variations is calculated. A minimal impact is achieved when the DG unit consumes (minus sign)

$$Q = -\frac{R}{X}P, \tag{6.2}$$

with R and X the line parameters and P the generated active power of the DG unit. Here, a uniform distribution of load along the feeder and a constant resistance and reactance per unit length are assumed. Still, a small impact remains due to the power losses associated with transport of power over the network, which are not included in (6.2). Here, low-voltage networks, which are mainly resistive, are considered, hence, with a high R/X, i.e., generally larger than three. Accordingly, such large amounts of reactive power can generally not be consumed by the generators without significant overrating. The reactive power consumed by the downstream load could be used to compensate part of the voltage rise, however, the load is generally unknown and variable in time. Therefore, a suboptimal amount of reactive power can be consumed by the generator, compromising between injecting more active power (which is analogous to limiting the impact of the unit's active power injection on the feeder voltage) and limiting the over-rating of the unit.

In order to improve the capturing of renewable energy, while still avoiding oscillations and over-voltages, in this section, a Q/V droop is included in the VBD control. In this way, the unit consumes reactive power when the voltage is out of the constant-power band. In Fig. 6.3, the value Q_{nom} (which is mostly 0 in the conventional VBD control) is dependent on ΔV_{g}. When the voltage is out of the constant power band Q_{nom} becomes $K_P \Delta V_{\mathrm{g}} \sin\theta$ ($\tan\theta = X/R$ and $K_P < 0$), otherwise Q_{nom} remains zero. By using θ, dependent on the line characteristics, Q_{nom} is not changed in purely resistive networks ($\theta = 0$) because Q consumption would have little effect on the voltage (hence, capturing of energy) as (6.2) reflects. Also, instead of using ΔV_{g} as input of the $P_{\mathrm{dc}}/V_{\mathrm{g}}$ droop controller, $\Delta V_{\mathrm{g}} \cos\theta$ is used.

Finding the absolute optimal value of Q to be consumed is not the focus of a primary control strategy. The VBD control succeeds in avoiding the on/off oscillations, while automatically giving priority to renewable injection. By changing

Q_{nom}, its impact on the voltage is decreased, which will increase the energy capturing (more power can be injected in the network). However, the optimal amount of reactive power is, in the considered resistive networks, often too high for the inverter. To optimise the network, secondary controllers, which can use communication (e.g., concerning the downstream load), can change the settings of the primary controllers.

D. Examples: on-off oscillations

The controllers discussed above, i.e., on-off control, VBD control and VBD control with Q/V droops, are compared with respect to the on-off oscillations and capturing of renewable energy. The grid-connected microgrid topology is depicted in Fig. 6.5. A typical EAXVB cable (150 mm^2) has a line resistance of 0.2-0.4 Ω/km. The higher the line resistance, the more significant the voltage problem in the network. Therefore, line resistance values (consisting of the resistance in the grid lines and the connection cables to the loads, which often have a smaller section, thus a higher resistance per km) on the upper margin are considered. The utility network is modelled as a 230 V rms and 50 Hz voltage source, i.e., a strong network. The DG units consist of a VSI with dc-bus ($V_{\mathrm{dc,nom}} = 700$ V, $C_{\mathrm{dc,nom}} = 1.5$ mF) and an LC filter ($L = 2$ mH, $C = 3$ μF). The microgrid consists of three DG units. The VSIs are modelled upto the level of the converter switches. The ac-side current and voltage controllers in Figs. 6.1, 6.2 and 6.3 consist of PI controllers. At the dc-side, the sources are modelled as constant-current sources, as the dc-side is not modelled in detail and relatively short time frames (transient changes) are studied. Hence, a $I_{\mathrm{dc}}/V_{\mathrm{g}}$ droop controller is used ($I_{\mathrm{dc}} = I_{\mathrm{dc,nom}} + K_P(V_{\mathrm{g}} - V_{\mathrm{g,nom}})$), which is completely analogous to the $P_{\mathrm{dc}}/V_{\mathrm{g}}$ droop controller for constant-power sources. DG 1 has a constant $I_{\mathrm{dc,nom}}$. DG 2 on the other hand has the initial $I_{\mathrm{dc,2,nom}}$ when $t < 1$ s and $0.5I_{\mathrm{dc,2,nom}}$ when $t > 1$ s. DG 3 has $I_{\mathrm{dc,3,nom}}$ when $t < 0.35$ s, $0.5I_{\mathrm{dc,3,nom}}$ when $0.35 < t < 0.70$ s and $1.25I_{\mathrm{dc,3,nom}}$ when $t > 0.70$ s, which is depicted in Fig. 6.6. Note that the actual dc current is equal to $I_{\mathrm{dc,nom}}$ in case the on-off controllers are used. In VBD control, this value is dependent on the terminal voltage according to the $I_{\mathrm{dc}}/V_{\mathrm{g}}$ droop controller.

Grid-following on-off control The on-off control of the three DG units is based on a hysteresis function that turns off the DG unit when its terminal voltage exceeds 109 % $V_{\mathrm{g,nom}}$ and turns it back on when the voltage again drops below 102 % $V_{\mathrm{g,nom}}$. An important remark concerning the following figures, is that the time scales are unrealistically short. The voltage measurements are assumed to be performed with the switching frequency of the units. Hence, the oscillations can also occur very fast. Of course, in practice, the oscillations follow up less quickly, firstly, because the voltage measurements can be slower, and secondly, because most units

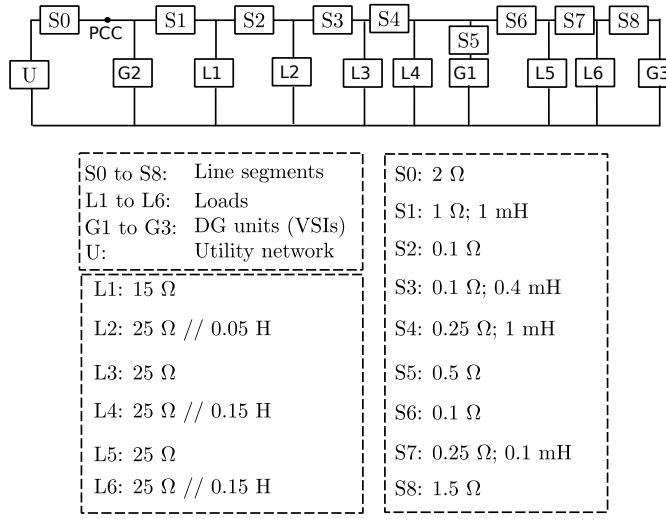

Figure 6.5: The considered microgrid topology, three DG units and six loads, grid-connected

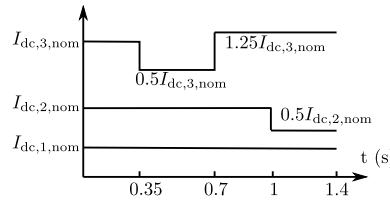

Figure 6.6: Changes of I_{dc} of the considered current sources, independent of state of network

turn off for a specified amount of time after over-voltage or under-voltage occurred. This is not included in the simulations to easily compare the controllers for equal boundary conditions in a limited simulation time. The fact that this is not included in the simulations, does not interfere with the general conclusions, focussing on comparing the different strategies. The time scale can be changed based on the real turn-off time of the DG units.

In the first case, the nominal dc currents equal 5 A, 7.5 A and 10 A for DG 1, DG 2 and DG 3 respectively. The simulation results are depicted in Fig. 6.7. A clear on-off oscillation of DG 3 is shown, except when $0.35 < t < 0.70$ s (low $I_{\mathrm{dc,nom,3}}$). When DG 3 disconnects, the grid voltage decreases significantly. The voltage falls below the 102 % $V_{\mathrm{g,nom}}$ voltage limit, such that the DG unit turns back on, etc. This is due to the high local penetration of DG units in a network with clearly resistive

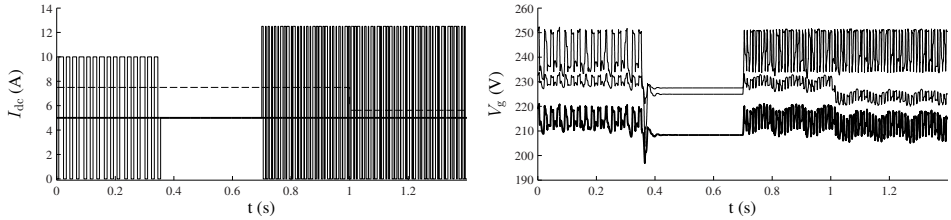

(a) Dc-input current of DG unit (b) Terminal voltage

Figure 6.7: Grid-following on-off control, first case $I_{\mathrm{dc,nom}}$: 5 A, 7.5 A and 10 A (— = DG 1; ---- = DG 2; — = DG 3, -.-.- = PCC in (b))

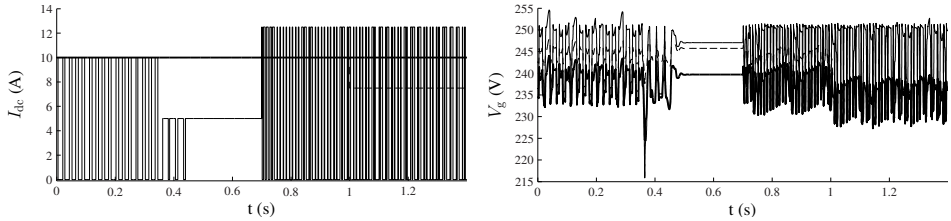

(a) Dc-input current of DG unit (b) Terminal voltage

Figure 6.8: Grid-following on-off control, second case $I_{\mathrm{dc,nom}}$: 10 A, 10 A and 10 A (— = DG 1; ---- = DG 2; — = DG 3, -.-.- = PCC in (b))

lines. On-off control is hence solely effective if the influence of one DG unit on the terminal voltage is not too large and the penetration of DG is sufficiently low. Therefore, this is not a sustainable situation in the context of achieving a higher penetration of renewable sources in the network, which are often small DG units.

In a second, more extreme case, the nominal dc-currents of the DG units equal 10 A for all three DG units. The results are shown in Fig. 6.8. Opposed to the previous case, the microgrid now delivers active power to the utility network. Although the voltage limits are not exceeded, this situation shows even larger voltage swings. Also, as will be discussed further, the delivered (renewable) energy of DG 3 has significantly been reduced due to a higher output power of the other DG units.

A solution to avoid the large renewable energy loss can be to replace the on-off controller with a strategy that decreases I_{dc} with, for example only 50 % instead of turning off entirely). Therefore, in the third case, the same hysteresis function to control the delivered power to the network is used, but instead of turning the

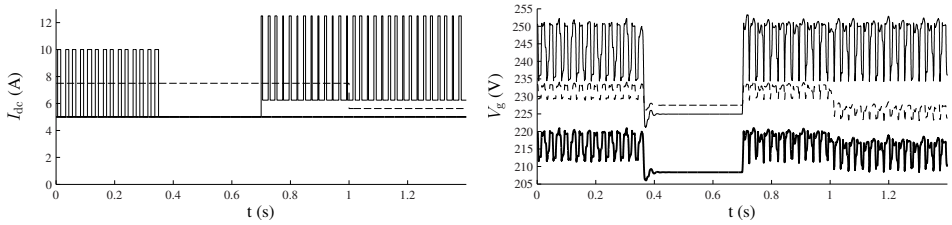

(a) Dc-input current of DG unit (b) Terminal voltage

Figure 6.9: Grid-following 50 % trial control, $I_{\mathrm{dc,nom}}$: 5 A, 7.5 A and 10 A (— = DG 1; ---- = DG 2; — = DG 3, -.-.- = PCC in (b))

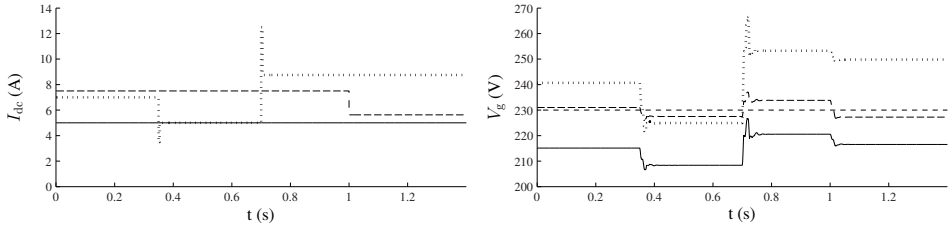

(a) Dc-input current of DG unit (b) Terminal voltage

Figure 6.10: Grid-following 70 % trial control, $I_{\mathrm{dc,nom}}$: 5 A, 7.5 A and 10 A (— = DG 1; ---- = DG 2; ··· = DG 3, -.-.- = PCC)

DG unit off in case of high voltages, a 50 % dc-current change is included (here called the 50 % trial control). Again, the nominal dc-currents of the DG units equal 5 A, 7.5 A and 10 A for DG 1, DG 2 and DG 3 respectively. The results are summarised in Fig. 6.9. The voltage profiles clearly still shows oscillations, but with a lower frequency. Therefore, it is expected that an optimal solution, with minimal power loss, can minimise the oscillations and hence, improve the renewable energy capture.

For a 70 % trial control, which decreases the I_{dc} with only 30 % by using an analogous hysteresis function, the simulation results are depicted in Fig. 6.10. With this 70 % control, the oscillations are no longer present. However, by using a primary control strategy, the percentage at which the power should decrease is hard to find in an elegant and all-around manner.

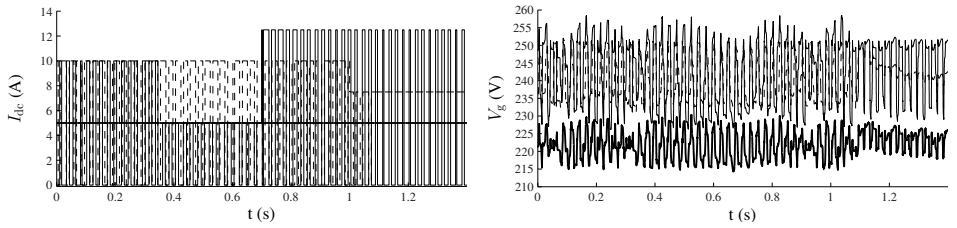

(a) Dc-input current of DG unit

(b) Terminal voltage

Figure 6.11: Grid-forming on-off control (— = DG 1; ---- = DG 2; — = DG 3, -.-.- = PCC in (b))

Grid-forming on-off control It is also possible to include grid-forming controllers with the on-off functionality. In this paragraph, the VBD control is included in the DG units with constant-power band $b = \infty$. This represents the control with delivered power independent on the state of the network, but implemented in a grid-forming controller. Again, on-off control is included for voltage limiting. This enables to prove that grid-forming control is possible in grid-connected units. As in grid-connected mode, $f \approx f_{\mathrm{nom}} = 50$ Hz, the DG units operate at power-factor-one, analogous to the grid-following controllers.
In the studied case, the nominal dc-currents of the DG units equal 5 A, 7.5 A and 10 A for DG 1, DG 2 and DG 3 respectively. Despite the on-off oscillations, the voltage limits are met, which is shown in Fig. 6.11. For other I_{dc}, analogous results are obtained as in the previous paragraph.
It is concluded that grid-forming control is possible in the grid-connected microgrids. The grid-forming and grid-following on-off controllers have analogous results concerning voltage swings.

VBD control In order to maintain the voltage limits and to provide a solution for the oscillation problem, VBD control where b is not infinite, thus, where I_{dc} depends on the state of the network, can be used. Opposed to the previous case, the $I_{\mathrm{dc}}/V_{\mathrm{g}}$ droop controller enables active power curtailment based on the terminal voltage without communication. Also, priority injection can be given to the renewables by setting a relatively large b in these units. Hence, the incentives for participating in voltage control should depend on the reaction time, power change and threshold voltage ($(1 \pm b)V_{\mathrm{g,nom}}$).
In Fig. 6.12, the nominal dc-currents of the DG units equal 5 A, 10 A and 10 A for DG 1, DG 2 and DG 3 respectively. Soft curtailment is included in these DG units by setting the constant-power band b equals 0, 4 and 7 %. The droops of the con-

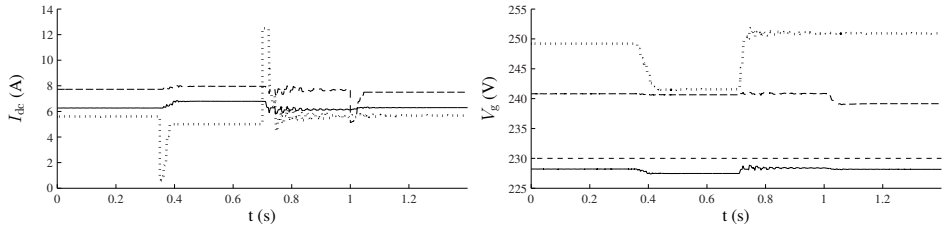

(a) Dc-input current of DG unit (b) Terminal voltage

Figure 6.12: VBD control, first case (— = DG 1; ---- = DG 2; ··· = DG 3, -.-.- = PCC)

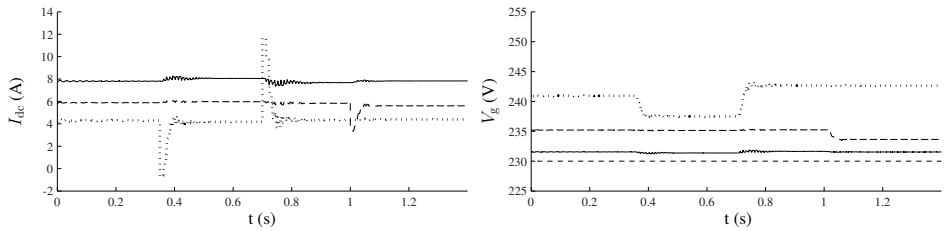

(a) Dc-input current of DG unit (b) Terminal voltage

Figure 6.13: VBD control, second case (— = DG 1; ---- = DG 2; ··· = DG 3, -.-.- = PCC)

trollers are set analogously as in [184], with $K_{\mathrm{P}} = -P_{\mathrm{dc,nom}}/10$, $K_V = -1$ V/V and $K_{\mathrm{Q}} = -25 \cdot 10^{-10}$ VAr·s. In the first 0.45 s, DG 2 and 3 deliver less than $I_{\mathrm{dc,nom}}$ to the network (by using fuel intake change, storage, deviation from MPPT, load shifting) as the local voltage exceeds the constant-power bands. Although the $I_{\mathrm{dc,nom}}$ values are higher than in the previous cases, making the voltage problem more stringent, the VBD controller avoids the voltage swings and the voltage limits are met. For the case with 5 A, 7.5 A and 10 A for DG 1, DG 2 and DG 3 respectively, analogous results are obtained except that DG 2 delivers $I_{\mathrm{dc,nom}}$ as the voltage does not exceed its constant-power band.

In Fig. 6.13, the nominal dc-currents of the DG units equal 10 A for all DG units. DG 2 and 3 deliver less power to the network compared to the previous case to cope with the increased delivery of DG 1.

In Fig. 6.14, the nominal dc-currents of the DG units equal 10 A for all DG units and all units are considered as renewable with a large constant-power band $b = 7\ \%$. As DG 1 and 2 react less on deviations of the voltage from the nominal value

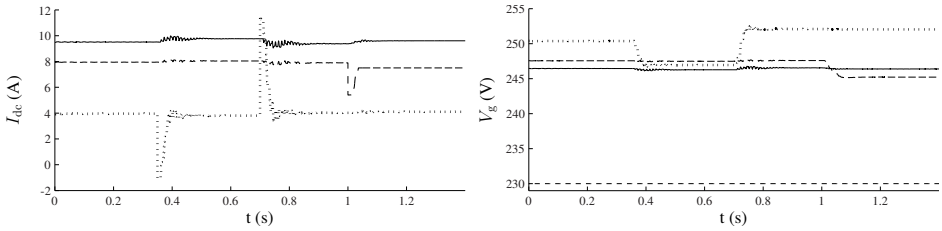

(a) Dc-input current of DG unit (b) Terminal voltage

Figure 6.14: VBD control, second case, but all units have constant-power band of 7 % (— = DG 1; ---- = DG 2; ··· = DG 3, -.-.- = PCC)

compared to the previous case, they deliver more power to the network. Hence, DG 3 contributes more to the voltage support compared to the previous case in Fig. 6.13. The simulations show that despite the higher nominal power of the DG units compared to the on-off control, the voltage remains in the 10 % limits and voltage oscillation is avoided.
VBD control with Q/V droops shows analogous results as the conventional VBD control with respect to the on-off oscillations. The main difference is in the renewable energy capturing, which is analysed in the next paragraph.

E. Examples: captured energy

Comparison between on-off and conventional VBD control Table 6.1 summarises the captured energy for all studied cases. DG 3 is highlighted as it is assumed as the renewable energy source most affected by voltage problems. In the grid-following control, when comparing the first three cases in the table, with the same $I_{\mathrm{dc,nom}}$ but with different power curtailment, the trial strategy with the 70 % controller captures significantly more of the available renewable energy of DG 3. Hence, on-off oscillations significantly lower the amount of captured renewable energy. However, as stated above, finding the optimal percentage of power decrease in this method is impractical. For the other DG units, there is no significant difference in the delivered energy in the three cases. In the fourth case, with higher $I_{\mathrm{dc,nom,1}}$ and $I_{\mathrm{dc,nom,2}}$, DG 2 delivers more energy to the network, while the captured energy of DG 3 is clearly diminished. This is especially disadvantageous if DG 3 is a renewable energy source.
For the grid-forming on-off controllers, analogous conclusions can be made. DG 3 is clearly negatively affected if the installed power of the other units increases.
In the VBD control, for the same $I_{\mathrm{dc,nom}}$, DG 3 delivers more power to the net-

Table 6.1: Captured energy (J)

Grid-foll. $I_{\mathrm{dc,nom}}$ (A)	on-off 5/7.5/10	50 % 5/7.5/10	70 % 5/7.5/10	on-off 10/10/10
DG 1 (E [J])	4896	4894	4893	9794
DG 2 (E [J])	6849	6848	6856	9122
DG 3 (E [J])	5775	6842	7991	4002

Grid-form. $I_{\mathrm{dc,nom}}$ (A)	on-off 5/7.5/10	on-off 5/10/10	on-off 10/10/10	
DG 1 (E [J])	5920	5963	8526	
DG 2 (E [J])	9661	10051	8081	
DG 3 (E [J])	5302	5208	4105	

Grid-form. $I_{\mathrm{dc,nom}}$ (A)	VBD 5/7.5/10	VBD 5/10/10	VBD 10/10/10	VBD-RE 10/10/10
DG 1 (E [J])	7087	6780	7942	11539
DG 2 (E [J])	7978	9166	8708	9402
DG 3 (E [J])	6691	6576	6279	4741

work than in the other two control strategies. Also, the renewable energy capturing of DG 3 is less affected if the other units are dispatchable, for which in the VBD only the value b needs to be altered. When all considered units are renewable energy-based, still DG 3 is affected most, because of the network configuration, but the renewable energy capturing is higher than in case of the other two controllers. Also, the total renewable energy capturing of the three units is higher such that less power needs to be imported from the utility network.

Comparison between VBD control without and with Q/V droops In order to compare the VBD control without and with Q/V droops, the network of Fig. 6.5 is used, but with a different line inductance. All DG units are renewable with $b = 7$ % and $I_{\mathrm{dc,nom}} = 10$ A. When compared in a purely resistive network, the impact of Q on the captured renewable energy is negligible. This is explained through (6.2) showing that a very large amount of reactive power is required to avoid the DG unit influencing the terminal voltage. In case the network has a realistic $R/X = 3$, the influence of the Q/V droops on the captured energy becomes larger as illustrated in Table 6.2. DG 1 and DG 2 consume no reactive power as their voltage is in the constant power bands. DG 3 consumes reactive power, hence, the increase in energy capturing is more significant for this unit.

Although VBD control is unconventional compared to the on-off controllers, as il-

Table 6.2: VBD without and with Q/V droops

	R-grid		$R/X = 3$	
	VBD	VBD+Q/V	VBD	VBD+Q/V
E_1 (J)	10760	11146	11813	11967
E_2 (J)	10303	10817	9233	9474
E_3 (J)	4486	4663	4920	5643
$V_{\mathrm{g},1}$ (V)	246.6	246.3	246.2	244.6
$V_{\mathrm{g},2}$ (V)	241.2	238.0	245.9	244.4
$V_{\mathrm{g},3}$ (V)	252.1	252.2	251.9	251.5
Q_1 (VAr)	0	-50	0	0
Q_2 (VAr)	0	0	0	0
Q_3 (VAr)	0	-1813	0	-1609
E_{trafo} (J)	-1775	-1121	-1922	-1290
Q_{trafo} (VAr)	5493	7279	6068	7905

lustrated above, a higher renewable energy capturing, less on/off oscillation and potentially a higher renewable energy source penetration (or equivalently, postponement/avoidance of investments in stronger lines for renewable energy connection) can be achieved. A drawback is that instead of a conventional on-off controller, the VBD control strategy needs to be implemented in the inverter, however, this is a one-time additional cost. By including Q/V droops as well, the energy capturing can further be increased.

The results above of adding Q consumption to increase the renewable energy capturing seem very promising. However, an important remark concerning the network losses should be made. In the VBD control without Q/V droops, 1922 J is injected into the utility network. With Q/V droops, this is only 1290 J, despite the higher renewable energy input and lower voltage level in the microgrid. Obviously, the consequence of this is a higher output current of the DG units, hence, more network losses. The profit gained in an increased renewable energy capturing is here completely absorbed in the network losses.

For a network with lower network resistances, the profit can be absolute. For the network of Fig. 6.5, where $S0 = 0.5\Omega$, $S1 = 0.25\Omega$, $S5 = 0.2\Omega$ and $S0 = 0.375\Omega$, with R/X again equal to 3, the results are given in Table 6.3. In this case, adding Q/V droops to the VBD controller is advantageous for the captured renewable energy, without losing the gained profit in increased network losses.

An important conclusion of this analysis is that reactive power consumption in resistive networks is generally not recommended. The effect on the network losses (and network overloading) can be significant.

Table 6.3: VBD without and with Q/V droops: low-resistance network

	VBD	VBD+Q/V
E_1 (J)	11801	11889
E_2 (J)	11111	11121
E_3 (J)	6982	7408
$V_{\mathrm{g},1}$ (V)	246.1	245.6
$V_{\mathrm{g},2}$ (V)	234.5	234.4
$V_{\mathrm{g},3}$ (V)	234.9	250.2
Q_1 (VAr)	0	0
Q_2 (VAr)	0	0
Q_3 (VAr)	0	-1230
E_{trafo} (J)	-6894	-7019
Q_{trafo} (VAr)	6982	7708

F. Conclusions

In this paragraph, the behaviour of grids with distributed energy sources is analysed. The on-off oscillations and diminished renewable energy capturing are studied in a low-voltage grid-connected microgrid with a high share of DG units. In case the units are grid-following and equipped with conventional on-off control, large voltage swings and renewable energy loss are observed. Hence, instead of completely shutting down the unit, the delivered power should be a function of the terminal voltage, while still communication should be avoided.
This section shows that using grid-forming units in the grid-connected system, with on-off controllers, is possible, but leads to analogous voltage problems. Therefore, the grid-forming VBD control, is used. This control strategy avoids voltage limit violation without the on-off swings that occurred in the other cases. It also retrieves a higher renewable energy capturing. Important is that VBD control does not require communication and automatically gives priority injection to the renewable energy sources.
Finally, the VBD control is extended with Q/V droops. By consuming reactive power, the impact of the DG unit on the terminal voltage is lowered. Relying on this, with Q/V droops, the renewable energy capturing is increased. However, because of the effect of reactive power consumption on the network losses, generally, it is better to use the VBD control without Q/V droops.

6.1.2 Grid-connected VBD control for voltage limiting by soft curtailment

The previous section studies on-off oscillations of renewables and compares the traditional on-off control with the VBD control. Here, voltage problems due to DG are analysed as they are becoming a major issue, especially in the low-voltage networks. Hence, to achieve voltage limiting, the DG units are sometimes equipped with Q/V droops, which is analogous as in the transmission network. However, it is shown in this section that the impact of reactive power on the voltage profile is limited in the considered low-voltage networks. The main reason is that in resistive networks, the voltage is mainly linked with active power, not reactive power. An indirect effect comes from the Q/V linkages in the overlaying networks, but the influence is difficult to predict in practice. Therefore, an effective way to avoid voltage limit violation in low-voltage networks is by implementing P/V droops and VBD control in the DG units.

A. Methods to avoid voltage-limit violation

Network investments Grid-upgrades are the historical approach to deal with the increasing demand. However, with the large increase of DG in the network, this demands for very large investments in the power system. Hence, the smart grid paradigm proposes to deal with the networks capacity in a smarter way to limit the required investments. Some solutions provided are demand response or curtailment of the output power of the DG units.

Hard curtailment For hard curtailment, the whole DG unit is disconnected in case the grid voltage exceeds a certain level, which is known as on-off control and analysed in § 6.1.1. This leads to a significant loss of the revenue, as generally, the units do not need to turn off entirely to solve the voltage problem. Also, a significant amount of the available renewable energy is lost, as the storage capacity is generally limited or absent. As discussed in the previous paragraph, it can lead to oscillation problems in the network.

Soft curtailment Another method is to use soft curtailment for voltage limiting in low-voltage networks.

1) Q/V droops

In the transmission network, the voltage is controlled through reactive power changes of the generators or of designated devices such as capacitor banks. Because of the experience in this strategy, analogous methods are pursued in the low-voltage networks. Therefore, new converters are sometimes equipped with Q/V curtailment strategies, e.g., the voltage support based on reactive power in [211] in a

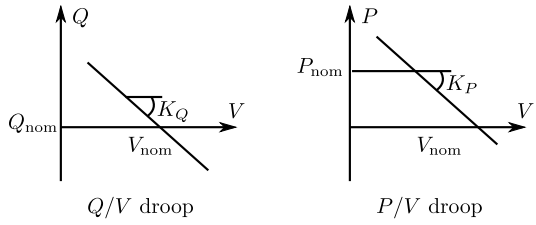

Figure 6.15: P/V or Q/V droops (without constant-power band)

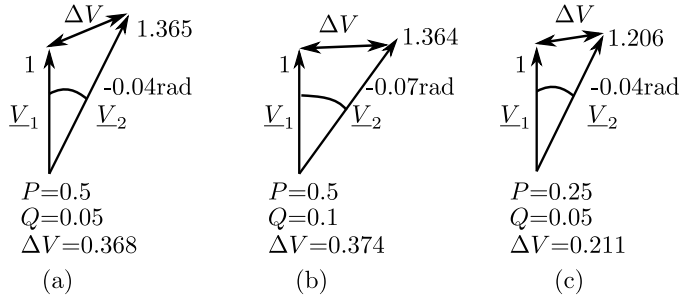

Figure 6.16: P/V linkage in resistive networks ($R = 1$ p.u.): p.u. values

droop as shown in Fig. 6.15. The effect of Q/V droops in a 10 kV network is also studied in [214].

However, from a theoretical point of view, there are limitations to this method. The considered low-voltage networks are predominantly resistive, such that the voltage magnitude mainly depends on the active power of the units, see (4.6a) and (4.6b). The P/V linkage is illustrated by Fig. 6.16 as well. In Fig. 6.16(b), compared to Fig. 6.16(a), the reactive power Q is doubled while the active power P remains the same. This clearly affects the phase difference δ while ΔV does not change significantly. In Fig. 6.16(c), P is halved compared to Fig. 6.16(a), which clearly affects ΔV, not δ. Eq. (6.2) also illustrates that in networks with a high R/X, a lot of reactive power is required to significantly influence the grid voltage.

Therefore, the impact of Q/V droops on the voltage profile is limited in low-voltage networks. Still, the reactive power can to some extent modify the terminal voltage, as:

- the lines are not perfectly resistive, always some inductance is present;
- Q can have an influence on the PCC voltage as the medium and low-voltage network lines are significantly more inductive than the microgrid itself.

Because of the latter reason, an indirect effect of Q on V is present. More de-

tails are given in [212]. Also, reactive power control does not involve active power changes, thus, the costs or revenue-losses are limited. One should however take into account that the current magnitude changes due to the reactive power control, which may restrict the delivered active power, again, indirectly. Also, often, there is an overrating of the VSI required to deliver the reactive power, and as discussed in the previous paragraph, the network losses may significantly increase due to the reactive power injection.

2) P/V droops

As discussed above, in predominantly resistive networks, the terminal voltage of the DG unit is directly affected by its active power. Therefore, the required active power change for a given voltage change is lower than the required reactive power change. To lower the voltage, the delivered active power of the DG units should decrease. For dispatchable DG units, this is easily done by decreasing the fuel intake. It often means less income from active power delivery and an operation that differs from the nominal operation, which is generally the most efficient. Lowering the generated power can also be implemented by deviating from the maximum power point operation, shifting the local load or by using storage equipment. There are several ways to encourage the voltage control by the DG units. Firstly, this ancillary service can be encouraged by the grid operator by means of incentives. Secondly, it may also become obliged for voltage limiting. Opposed to the central generators that have to participate in the primary control, presently, small DG units generally do not have this responsibility. However, with the increasing penetration of DG, this becomes an unsustainable situation. Thirdly, even without intervention of the operator, over-voltage conditions induce shut down of the units, which leads to a significantly higher loss of power generation compared to the soft curtailment. Hence, soft curtailment can lead to less revenue loss compared to full shut-down.

B. Case studies

Avoiding voltage-limit violation through reactive and active power changes is compared for the following control strategies: conventional grid-following (gr-foll) control, grid-following Q/V droop control, grid-following P/V droop control and grid-forming (gr-form) VBD control.

Strong network In this case, the microgrid is connected to a strong utility network $\underline{E_2}$ that is modelled as a 50 Hz voltage source of 230 V rms, which is not affected by the microgrid. The network is shown in Fig. 6.17.

Resistive microgrid lines

The microgrid lines are resistive, here 3 Ω. A large line resistance is chosen as it is a combination of the real line resistance and the resistive virtual output impedance

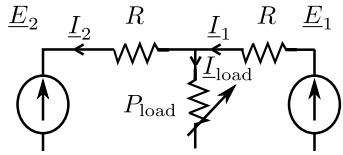

Figure 6.17: Microgrid topology, low-voltage microgrid

Table 6.4: Study of influence of control strategy: resistive lines

Case	P (kW)	Q (kVAr)	V_{DG} (V)
Gr-foll, undispatchable	3	0	271.0
Gr-foll, P/V	1.9	0	248.7
Gr-foll, Q/V	3	-2.2	266.1
Gr-form, VBD ($b = 0$ %)	1.7	0	245.2
Gr-form, VBD ($b = 5$ %)	2.1	0	252.6

of the DG unit. A load of 2 kW is connected to the network. The nominal power P_{nom} of the DG unit equals 3 kW. The rest is injected into the utility network.

First, an undispatchable grid-following controller is studied. The implementation of this controller is shown in Fig. 6.1 without the on-off functionality to illustrate the possible occurrence of overvoltages. The terminal voltage is tracked by using a Phase-Locked Loop (PLL). As power-factor-one control is generally implemented, the injected current is in phase with this voltage. The rms current is determined by a dc-link voltage controller keeping the dc-link voltage constant. The dc input power is determined externally, e.g., by using MPPT and as such, equals P_{nom}. Table. 6.4 shows that over-voltage ($V_{\text{g}} > 110\,\%V_{\text{g,nom}}$) occurs with the undispatchable units, such that this unit should shut down (e.g., on-off control).

Second, in the grid-following control algorithm, a P/V droop is included to restrict the delivered active power to the network based on the terminal voltage according to ((2.24), with $V_{\text{g,nom}} = 230$V rms and $K_P = -\frac{P_{\text{nom}}}{50\text{V}}$. Table 6.4 shows that the P/V droops avoid voltage limit violation.

In the third case, a Q/V droop is included in the grid-following control algorithm, according to (2.9) with $Q_{\text{nom}} = 0$ VAr and the same slope as in the previous case. Even without influence of the utility network, this control strategy slightly influences the terminal voltage. This is due to the changed rms current. Compared to the undispatchable DG unit, the reactive power of the unit has changed from zero to a negative value, i.e., consumption. Hence, for the same active power output, the

rms current increases. The voltage drop across the line (and virtual output resistance) increases. In this way, the terminal voltage of the unit lowers. However, the influence of Q on V is limited and here, still an over-voltage condition is present. The value of I_{rms} should be limited for protection of the converter and eventually, this can require a lower output active power.
Fourth, the VBD control can be implemented. An effective voltage-limiting is obtained. When comparing the dispatchable unit ($b = 0$ %) with the less dispatchable unit ($b = 5$ %), it is concluded that there is a trade-off between maximum injected power and voltage control. This trade-off can be set by adjusting b according to the characteristic of the unit.
The effectiveness of the Q/V droops in the case with inductive lines is further analysed in [212].
In conclusion, in the considered resistive networks, the VBD and P/V controllers are effective to avoid voltage limit violation. The Q/V droop controller has a limited effect on the terminal voltage of the DG units.

Utility network with Q/V dependence Practically, the utility network $\underline{E}_2$ in Fig. 6.17 is not a perfectly strong network. A Q/V linkage can be present, mainly through the Q/V droops in the central generators. In the previous case, it was shown that the Q/V droop-controlled grid-following units did not significantly affect the terminal voltage in the resistive microgrid. This does however not mean that Q/V droops are ineffective, as the Q dependence in the utility network should be considered as well. Here, the utility network is again represented as a voltage source, but now with a droop K_Q that is equal to that of the DG unit. Practically, the Q/V droop of the network is highly dependent on the local network state. It can be expected that it will be considerably lower because the voltage deviation of the PCC from its nominal value is further restricted by designated devices.
Table. 6.5 shows that Q/V droops become more effective because of the Q/V dependence in the network. The P/V droops and VBD controller are able to limit the voltage, analogously as in the previous case with resistive network lines. However, still, the effect of the DG units' reactive power on the local utility network is limited.

Constant-power bands In order to study the effect of the usage of constant-power bands, an analogous network as in the previous cases is considered. In Fig. 6.17, $\underline{E}_2$ remains the utility voltage and $\underline{E}_1$ represents DG 1. An additional DG unit (DG 2) is connected to DG 1 through a line resistance. Both units have a nominal power P_{nom} of 1500 W and $K_P = P_{\mathrm{nom}}/25\mathrm{V}$. Firstly, the grid-following P/V controller, here implemented as VBD control with $b = 0$ %, is studied. Secondly, the VBD controller is studied. In the VBD control, the first DG unit has a constant-

Table 6.5: Study of influence of control strategy: utility with Q-V dependence

Case	P (kW)	Q (kVAr)	V_{DG} (V)
Gr-foll, undispatchable	3	0	271.0
Gr-foll, P/V	1.9	0	248.7
Gr-foll, Q/V	3	-1.2	250.7
Gr-form, VBD	1.7	0	245.7

Table 6.6: Influence of constant-power bands (P in kW)

Case	P_1	P_2	$V_{\mathrm{DG},1}$ (V)	$V_{\mathrm{DG},2}$ (V)
Gr-foll, P/V	0.9	0.7	239.7	245.9
Gr-form, VBD	1.5	0.2	243.9	245.8

power band of 8 % while DG 2 operates without constant-power band. The results are summarised in Table 6.6. Both controllers lead to effective voltage limiting. Because of the usage of constant-power bands, the VBD controller clearly enables to capture the renewable energy potential, while the P/V controller lowers the output power of the renewable energy source.

C. Conclusions

In order to prevent voltage problems in low-voltage networks, the DG units should be equipped with an additional control strategy to change the injected power dependent on the local state of the network.
For this, analogous as in the high voltage networks, Q/V droops can be implemented. The lines in the considered networks are predominantly resistive. Hence, the impact of Q/V droops on the terminal voltage is limited. The effect is dependent on the Q/V linkage of the PCC voltage and the low, but non-zero value of X/R in the lines. This is often counteracted by (often expensive) designated devices such as tap changers that control V_{PCC}.
The P/V droops on the other hand affect the voltage in a direct manner and active power changes have a larger effect on the grid voltage compared to reactive power changes.
The VBD control also effectively affects the grid voltage amplitude through active power changes. This control strategy enables to delay changing the output power

of the renewables to more extreme voltages compared to those of the dispatchable DG units, thanks to the usage of constant-power bands.
Also, a combination of the three control strategies can be beneficial, as:

- Q/V droops: only reactive power changes are required. However, reactive power also changes the rms current of the DG unit, thus, when the DG units are not overrated, it also indirectly alters the maximum amount of active power that can be injected. Reactive power injection may also increase the line losses;
- P/V droops: are more effective for voltage control;
- VBD control: effective for voltage control and delayed response of renewables.

6.1.3 Grid-connected VBD control with beneficial power sharing modification

A problem often cited with droop controllers is that the grid voltage is not a global parameter. Therefore, there is an inherent trade-off between accuracy of active power sharing and output voltage control (deviation of voltage and frequency from the nominal values) [83, 108, 109, 215]. Accurate power sharing implies that the power changes of the loads are picked up by the units according to their droop, i.e., a combination of their power ratings and their ability to change their output power, analogous as the droop of the large central generators. Accurate power sharing implies that the line impedances do not influence the power sharing ratio. A solution to provide accurate power sharing by using inter-unit communication is given in § 4.5. Here, the VBD or P/V droop controllers without this functionality that requires communication, are further analysed.
The power sharing modification due to the line impedance effect is often mentioned as a disadvantage for P/V droops (and, thus, VBD control). Therefore, in this section, it is investigated whether this is actually a disadvantage of the control strategy. It is shown that with P/V droop control, the DG units that are located electrically far from the load centres automatically deliver a lower share of the power. This automatic power sharing modification can, thus, lead to decreased line losses, thus, an overall better efficiency compared to the methods that focus on perfect power sharing. In this section, the P/V and P/f droop control strategies are compared with respect to this power sharing modification and the line losses.

A. Power sharing in resistive networks

Fig. 6.18 is used to study the power sharing modification of P/V droop (and, thus, VBD) controllers in a low-voltage microgrid. A purely resistive microgrid is con-

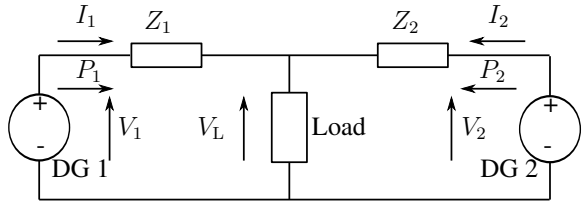

Figure 6.18: Two DG units in resistive network

sidered as P/V droops are based on the resistive character of the lines in low-voltage microgrids. For simplicity of the theoretical analysis and its conclusions, two equally-rated DG units (rated power P_{nom}) are connected to a load through line impedances Z_1 and Z_2. A discussion for different unit ratings is included on page 252. The power sharing in case of P/f and P/V droop control are considered. In this theoretical analysis, only the active power is taken into account, thus, only the working component of the current is calculated. The reactive power flow in the islanded microgrid should be limited. An abstraction of reactive power is made in the main part of the theoretical analysis, but the influence of reactive power is discussed briefly on page 252. Reactive power is also included in the extended simulation based on an 85-node microgrid.

A.1. Theoretical analysis

a) P/f droop control

For X-dominated lines, the $f(P)$ strategy of (2.7) can be used. The nominal power P_{nom} of a unit refers to the scheduled operating point (e.g., conventional generator) or MPP (e.g., renewable source). Subsequently, it does not directly reflect the rating or maximum output of the unit and its inverter. Therefore, like in conventional dispatchable generators, delivering more power than P_{nom} is possible. The droops are tuned such that $K_{\mathrm{f,i}} P_{\mathrm{nom,i}} = \Delta f_{\max}$, with $\Delta f_{\max}$ dependent on the network requirements: often a 1 % limit is postulated. As grid frequency is a global parameter: $f_1 = f_2$. Hence, equally-rated units deliver the same amount of active power to the network independent on the line impedance. For the reactive power sharing, the Q/V droop controller of (2.9) is used. With this controller, there is a line impedance effect producing reactive power sharing mismatches [110, 124].

b) P/V droop control

In resistive networks, there is a natural linkage between P and V, such that P/V droop controllers are effective. Accurate power sharing is obtained when after a load change, each DG unit changes its output power $\Delta P/P_{\mathrm{nom}}$ according to its ratings and specific characteristics, independent of the line impedance. In the conventional network, these ratings and characteristics are combined in the droop of

the generators. Small generators and less-dispatchable units (e.g., nuclear facilities) have a lower relative ΔP after a load change compared to other units. For droop controllers in DG units, the droops are equivalent to the droops of central generators. Here, only dispatchable DG units are considered. Renewable sources generally do not yet contribute to the power sharing according to the ratings and therefore, are not droop-controlled. The analysis where renewables are considered by setting proper constant-power bands in the VBD control leads to similar results. Generally, the P/V droop control strategy[2] of (2.24) ensures that the grid voltage is close to the nominal value throughout the power system. Hence, the active power sharing is good, but not perfect if the line resistances are considered. In Fig. 6.18 for example, the second DG unit is located at a distance that is electrically further from the load than DG 1, i.e., $R_1 < R_2$. Accurate power sharing would involve $P_1 = P_2$. This equal power would require $V_1 = V_2$ because of the P/V droop control with equal droops and equal nominal values for the two DG units. However, this leads to a contradiction with the different voltage drops over the line resistances, hence, $P_1 \neq P_2$. Therefore, in the P/V droop control, the DG units contribute to the load sharing dependent on both their ratings (droops) and the line impedances.
It is investigated whether this modification, namely $\frac{P_1}{P_2} \neq \frac{P_{\mathrm{nom},1}}{P_{\mathrm{nom},2}} = \frac{K_{P,2}}{K_{P,1}}$, is disadvantageous. If accurate power sharing is the primary goal, this inaccuracy can be solved by means of set point changes of the droop and nominal power/voltage settings. This can be done in a slower secondary control strategy that can be communication based or by the method provided in § 4.5.
Because the units have equal ratings ($K_{P,2} = K_{P,1} = K_P$):

$$V_1 - V_2 = -K_P P_1 + K_P P_2. \tag{6.3}$$

In the network:

$$V_i = V_{\mathrm{L}} + R_i I_i \tag{6.4}$$

Two distinct cases can be considered, with $R_1 < R_2$:

- $I_1 < I_2$. As R_1 is lower than R_2, according to (6.4), this implies that $V_2 > V_1$. For the active power, $P = VI$ is valid as the active component of the current is considered. Combined, this leads to $P_2 > P_1$. However, $V_2 > V_1$ combined with (6.3), involves $P_1 > P_2$. This is a contradiction, hence the case I_1 lower than I_2 is not possible.

- $I_1 > I_2$. Two subcases can be considered:

[2] VBD control is implicitly considered as well, it also uses P/V droops in the $P_{\mathrm{dc}}/V_{\mathrm{g}}$ droop controller.

- $R_2 I_2 > R_1 I_1$. Although $I_1 > I_2$, $R_2 I_2$ can be higher than $R_1 I_1$ because $R_2 > R_1$. According to (6.4), this leads to $V_2 > V_1$. Hence, because of the P/V droop control, $P_1 > P_2$.

- $R_2 I_2 < R_1 I_1$. For this, a proof by contradiction is given. If $R_2 I_2 < R_1 I_1$, from (6.4) it follows that $V_1 > V_2$. If also $I_1 > I_2$, then $P_1 > P_2$ using $P = VI$. However, $V_1 > V_2$ combined with (6.3) means that $P_2 > P_1$, which is in contradiction with the previous conclusion.

Hence:

$$\frac{R_2}{R_1} > 1 \Rightarrow \frac{P_2}{P_1} < \frac{P_{2,\text{nom}}}{P_{1,\text{nom}}}; I_1 > I_2. \tag{6.5}$$

From the previous equations, it follows that the unit that is located electrically furthest from the load centre takes a lower part in the power sharing. Although it seems obvious, no general conclusions about the line losses can be derived from this in the general case. However, as the electric power system is a voltage-controlled system, the voltage at each point is near its nominal value (or in strict limits), whereas the current variations can be significantly higher. Therefore, for constant power or current loads:

$$I_1 + I_2 \approx I_1' + I_2'. \tag{6.6}$$

The values with prime symbol (') refer to the case with P/f droop control, those without prime symbol refer to the P/V droop control. From the same assumption, voltage near its nominal value, it follows that $I_1' = I_2' = \frac{I_1 + I_2}{2}$ because of the equal power sharing with the P/f droops. In order to compare the losses in the network lines, the following comparison is made:

$$R_1 I_1^2 + R_2 I_2^2 \longleftrightarrow R_1 I_1'^2 + R_2 I_2'^2, \tag{6.7}$$

for the P/V and P/f controlled network respectively. This, combined with (6.6), gives:

$$\begin{aligned}\left[2R_1 I_1^2 + 2R_2 I_2^2 - 2R_1 I_1 I_2 - 2R_2 I_1 I_2\right] \\ + \left[R_1 I_1^2 + R_2 I_2^2 - R_1 I_2^2 - R_2 I_1^2\right] \longleftrightarrow 0.\end{aligned} \tag{6.8}$$

As discussed above, in the first term, $(2R_1 I_1 - 2R_2 I_2)(I_1 - I_2)$, the first factor is clearly negative and the second one positive. In the second term, $(R_1 - R_2)(I_1^2 - I_2^2)$, the first term is negative with a positive second term. Hence both terms are

negative, from which it can be concluded that the losses

$$R_1 I_1^2 + R_2 I_2^2 < R_1 I_1'^2 + R_2 I_2'^2. \tag{6.9}$$

Hence, the losses with P/V droops are lower than the case of P/f droops, under the aforementioned assumptions.
For units with different ratings, the droops P/V are tuned according to $K_{P,1} P_{\mathrm{nom},1} = K_{P,2} P_{\mathrm{nom},2}$. For the droop control,

$$V_1 - V_2 = -K_{P,1} P_1 + K_{P,2} P_2 \tag{6.10}$$

and in the network:

$$V_1 - V_2 = R_1 I_1 - R_2 I_2 \tag{6.11}$$

are valid. Again, two cases can be considered, with $R_2 > R_1$:

1. $V_1 < V_2$. Analogous to the previous case, this is advantageous for the power sharing as, then, $\frac{P_2}{P_1} < \frac{K_{P,1}}{K_{P,2}} = \frac{P_{\mathrm{nom},2}}{P_{\mathrm{nom},1}}$.

2. $V_1 > V_2$ is disadvantageous from the power sharing perspective: $\frac{P_2}{P_1} > \frac{K_{P,1}}{K_{P,2}} = \frac{P_{\mathrm{nom},2}}{P_{\mathrm{nom},1}}$ in (6.10) if no contradiction occurs. Together with $V_1 > V_2$, (6.11) implies that $I_1 > I_2$ and hence, $P_1 > P_2$.

   - $K_{P,1} > K_{P,2}$. In this case, the furthest unit is the largest one, $P_{\mathrm{nom},2} > P_{\mathrm{nom},1}$. From above, this leads to a contradiction. Hence, if the electrically furthest unit is the largest unit, the power sharing modification is advantageous.
   - $K_{P,1} < K_{P,2}$. This case does not lead to a contradiction and has a disadvantageous power sharing modification. As the furthest unit is the smallest one, the effect on the total line losses is however lower than in the previous case. The modification is advantageous to avoid voltage limit violation. Note also that the droop $K_{P,i}$ can be shifted by using a secondary controller that further optimises the system.

For the reactive power sharing, the Q/f droop controller of (2.25) is used. As the frequency f is a global parameter, the reactive power will be shared properly. In the previous paragraph, an abstraction was made of the reactive power. Still, Q has some influence on the power sharing. P and Q are not fully decoupled as there is always some inductance in the lines. However, in the considered low-voltage networks, the resistance of the lines is sufficiently high such that the decoupling of P and Q is a valid assumption. Q also affects the losses of the system, but the

Q flow is limited compared to P in islanded microgrids. For the P/V droops, it was shown that for equally-rated units with $R_2 > R_1$: $P_1 > P_2$. Because f is a global parameter in the related Q/f droop control: $Q_1 = Q_2$. For the P/f droops, with the same deduction: $P_1' = P_2'$ and $Q_1' > Q_2'$. From this, clearly, the reactive power has a tempering effect on the line losses of P/f droop controllers in the comparison of P/V - P/f droop control. As generally, the active power flow is significantly higher than the reactive power flow, the loss reduction because of the power sharing modification is still mostly more advantageous for P/V droops.

A.2. Analytical study

In this paragraph, the same network as in the previous case is analytically studied. The P/V and P/f droop controllers are compared with respect to the power sharing modification ($\alpha = \frac{P_1/P_2}{P_{1,\mathrm{nom}}/P_{2,\mathrm{nom}}}$) and the system efficiency ($\eta = 1 - \frac{R_1 I_1^2 + R_2 I_2^2}{P_1 + P_2}$) as a function of the dominant parameters R_1/R_2 and $P_{1,\mathrm{nom}}/P_{2,\mathrm{nom}}$. The values of R_1/R_2 change from 0.2 to 20 and $P_{1,\mathrm{nom}}/P_{2,\mathrm{nom}}$ varies from 0.5 to 20. The sum of those parameters, i.e., $R_1 + R_2$ and $P_{1,\mathrm{nom}} + P_{2,\mathrm{nom}}$ is kept constant.

The power sharing modification is analysed through the parameter α. A value α of one equals accurate power sharing according to the ratings, while for $\alpha > 1$, the first unit contributes more in the power sharing. Fig. 6.19 shows that for P/V droops, α increases when R_1/R_2 decreases. This implies that the power sharing is dependent on the line impedances, in a manner complying with the theoretical results above, i.e., the electrically closest unit will take a larger part in the power sharing. The figure shows that the power sharing modification α is dependent on R_1/R_2, as well as $P_{1,\mathrm{nom}}/P_{2,\mathrm{nom}}$. For $P_{1,\mathrm{nom}} < P_{2,\mathrm{nom}}$:

- if $R_1 \gg R_2$, i.e., the smallest unit is the furthest one, the power sharing becomes accurate with $\alpha \approx 1$ as shown in Fig. 6.19. Nevertheless, in this case, the power sharing modification would have a low effect on reducing the line losses as a highly efficient system is obtained in this case ($\eta \approx 1$) as shown in Fig. 6.20(a).

- if $R_2 > R_1$, i.e., the largest unit is the furthest one, the power sharing modification is beneficial with $\alpha > 1$ as shown in Fig. 6.19(b).

This also complies with the theoretical analysis. Fig. 6.19 shows that the power sharing modification has the largest influence when $P_{1,\mathrm{nom}} < P_{2,\mathrm{nom}}$ and $R_1 < R_2$ (and vice versa for $P_{1,\mathrm{nom}} > P_{2,\mathrm{nom}}$). There were precisely the cases with the lowest efficiency in Figs. 6.20(a) and (b). It are also the cases with the highest efficiency improvement as depicted in Figs. 6.20(c) and (d). The case with $P_{1,\mathrm{nom}} < P_{2,\mathrm{nom}}$ and $R_1 > R_2$ were already more efficient, and the power sharing modification is, thus, least effective in this case. For the P/f droop control, the results are

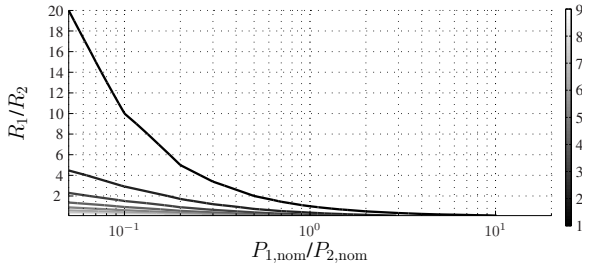

(a) Contour plot

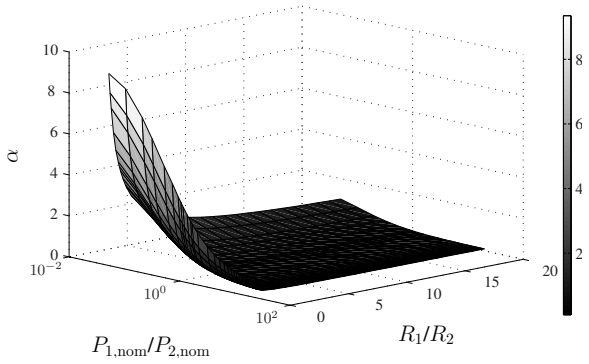

(b) 3D plot

Figure 6.19: Analytical results of the power sharing modification of P/V droops: $\alpha = \frac{P_1/P_2}{P_{1,\mathrm{nom}}/P_{2,\mathrm{nom}}}$ *as a function of* R_1/R_2 *and* $P_{1,\mathrm{nom}}/P_{2,\mathrm{nom}}$

not shown in Fig. 6.19 as a constant $\alpha = 1$ is obtained, thus, with power sharing according to the ratings and independent of the lines.
In Fig. 6.20, the line losses or equivalently, the system efficiency of both controllers are compared. From Fig. 6.20(c), it is concluded that the automatic power sharing modification leads to a higher efficiency of the P/V controllers compared to P/f control: $\eta_{\mathrm{PV}} - \eta_{\mathrm{PF}} > 0$.

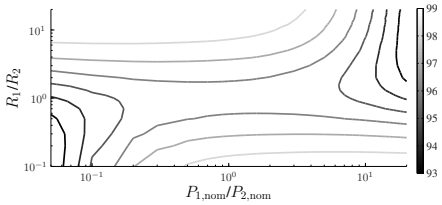

(a) η for P/V droops (η_{PV}) : contour plot

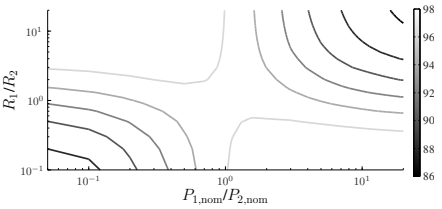

(b) η for P/f droops (η_{PF}) : contour plot

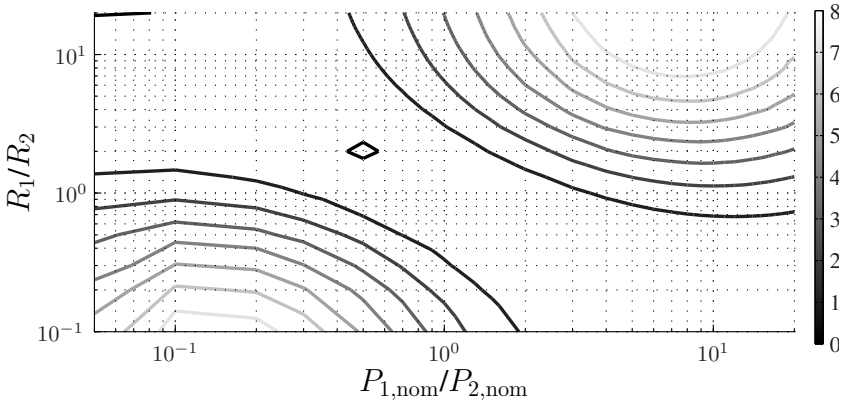

(c) $\eta_{\mathrm{PV}} - \eta_{\mathrm{PF}}$: contour plot

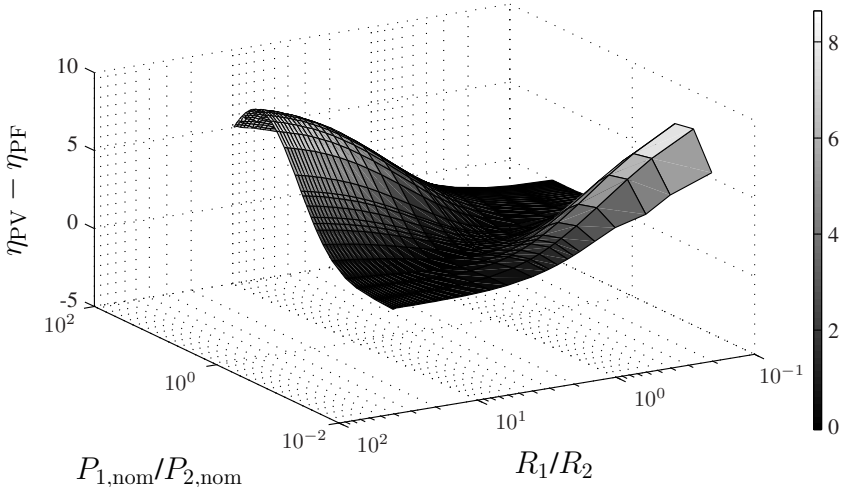

(d) $\eta_{\mathrm{PV}} - \eta_{\mathrm{PF}}$: contour plot

Figure 6.20: Analytical results of the system efficiency η

Table 6.7: Example P/V droop control versus P/f droop control ($R_2 > R_1$)

	P/V	P/f
V_1 (V)	229	222
V_2 (V)	233	238
I_1 (A)	14.16	11.08
I_2 (A)	3.55	10.35
P_1 (W)	3239	2119
P_2 (W)	827	2119
$P_{\text{line,loss}}$ (W)	65	239

B. Basic example

The theoretical results are verified on the basic microgrid example of Fig. 6.18 with $R_1 = 0.2\ \Omega$, $R_2 = 2\ \Omega$, $V_{\text{nom}} = 230$ V rms, $P_{\text{nom}} = 2.5$ kW and the load consumption $P_{\text{L}} = 4$ kW. Here, a purely resistive network is considered (low-voltage microgrid), but in the next paragraph (§ C), line inductance will be included as well.

In the P/V droop control, K_P equals $0.0025/\sqrt{2}$ V/W (i.e., $K_P = \frac{\Delta V_{\max}}{P_{\text{nom}}} = \frac{4.5V}{2500W}$) in (4.12) with $b = 0$ %, and a Q/f droop controller with droop 0.001 mrad/(s·VAr) is used. For the P/f - Q/V droop control (referred to as P/f), the droops are -$8 \cdot 10^{-6}$ Hz/W (i.e., $\frac{-0.125\text{rad/s}}{2500\text{W}}$) in the P/f droop control and -0.0035 V/VAr (i.e., $\frac{-8.8\text{Vrms}}{2500\text{VAr}}$) for the Q/V droop. Directly-coupled rotating inertia is lacking in the considered network, hence, the P/f controller is based on the inductive nature of the microgrid lines. As a resistive microgrid is studied in this example, a virtual inductive output impedance is included in the inverters, with 2 mH virtual inductance:

$$v_{\text{g,ref}} = v_{\text{g,droop}} - x_v i_g, \tag{6.12}$$

with x_v the virtual output impedance, $v_{\text{g,ref}}$ the reference voltage, $v_{\text{g,droop}}$ the voltage obtained by the P/f and Q/V droop controllers and i_g the output current.

The obtained results are summarised in Table 6.7 and comply with § A.

Both control strategies achieve $V \approx V_{\text{nom}}$, or at least, in the voltage limits of, e.g., 10 %. In the P/V droop control, the automatic modification in the power sharing, with higher output power of the DG unit that is electrically closest to the load, leads to lower line losses. According to the P/V droop, for example, $V_1 = 230\text{V} - 0.0025/\sqrt{2}(3239 - 2500)$, such that V_1 is indeed equal to 229 V

as shown in the table. Note that the droop of the P/V controller is determined according to a trade-off between the power control ($\frac{P_1}{P_2}$ close to $\frac{P_{\mathrm{nom},1}}{P_{\mathrm{nom},2}}$) and voltage control ($V$ close to V_{nom}). A higher absolute value of this droop leads to a higher difference of the voltage from its nominal value and a lower power difference. Then, a less accurate voltage control is obtained, e.g., with droop $0.005/\sqrt{2}$ instead of $0.0025/\sqrt{2}$ V/W: $V_1 = 228$ V, $V_2 = 235$ V, $P_1 = 2985$ W, $P_2 = 1093$ W and the line losses equal 77 W. In this case, the voltage of both units differ more from the nominal value of 230 V, but $\frac{P_1}{P_2} = 2.73$ is closer to $\frac{P_{\mathrm{nom},1}}{P_{\mathrm{nom},2}} = 1$ compared to the equivalent value of 3.9 in Table 6.7. Note that, here, the line resistances are chosen to be rather large to highlight the effect of power sharing modification. Practically, the line resistances will be lower leading to a lower modification of power sharing, but the same conclusions can be drawn.

As discussed above, the reactive power also has some effect on the line losses. Hence, a general comparison between P/f and P/V droops with respect to the line losses cannot be drawn, opposed to the effect on power sharing modification.

In this example, P/V-Q/f droops have no circulating current, opposed to the P/f-Q/V droops. In the Q/V droop, a lower absolute value of droop $K_{\mathrm{Q,v}}$ indicates a higher reactive power difference for the same voltage difference (compared to the nominal value), hence, an increased line loss. In the P/f droop control, circulating reactive power is obtained in the considered network (1249 VAr), which is avoided in the P/V controller. One remark concerning this circulating power, is that generally, it is practically not present. In this extreme theoretical case, pure active loads and a pure resistive network are considered, in which the P/f droop control is not the obvious approach because of the intrinsic linkage between P and V. The reason of this circulating reactive power in the theoretical case is the usage of the Q/V droop controller in the resistive network. This is clarified by the following example. In case I_1 would be lower than I_2, $V_1 < V_2$ as $R_1 < R_2$. This would lead to $P_1 < P_2$, which is contradictory with $P_1 = P_2$ because of the P/f droop control with equal droops and equal nominal values for the two DG units. Therefore, $I_1 > I_2$ and combined with $P_1 = P_2$, this leads to $V_1 < V_2$. Because of the negative Q/V slope, this leads to a difference in reactive power, namely $Q_1 > Q_2$. As the lines are purely resistive and a pure active power load is considered, this induces circulating power from one DG unit to the other.

C. 85-node distribution network

The previous basic example studied a simplified low-voltage network with purely resistive lines, pure active power loads and DG units of equal ratings. In order to verify the statement of automatic power sharing modification and reduced line losses in case of P/V droop control, in this section, a realistic distribution network is considered. In this network, inductive loads, consumption of reactive power,

Table 6.8: DG units placement and P_{nom}; and results obtained for the grid-connected system, where P_{nom} equals the delivered power

node	P_{nom} (kW)	node	P_{nom} (kW)
6	500	54	200
22	120	76	200
47	332	82	800

inductive-resistive lines and DG units of different ratings are considered.
The line losses are calculated in a 85-node distribution network, the data of the system are given in [216, 217]. This is summarised in Fig. 6.29 on page 273 and table 6.12 starting from page 274. The network has a nominal voltage of 11 kV and has 75 loads. The R/X value of the network lines equals 2.4. The loads are modelled as RL loads with

$$R = \frac{V_{\mathrm{nom}}^2}{P_{\mathrm{nom}}} \tag{6.13}$$

and $X/R = 1$. Analogous as in [216], the power factor of all loads is 0.7 lagging. The differences between the model of [216] and the model discussed below are limited:

- The distribution network in [216] is a balanced three-phase radial system. Here, it is seen in its single-phase equivalent.
- The network of [216] has no DG units, while here, six DG units are included. Their nominal power and node of location are shown in Table 6.8. The DG units are connected to the microgrid through a small line resistance of 0.1 Ω.

The following cases are compared:

- grid-connected system with six DG units modelled as PQ generators with power factor one
- islanded system with six DG units with P/V droop control
- islanded system with six DG units with P/f droop control

Grid-connected system with six DG units modelled as PQ generators with power factor one In this case, the DG units are grid-following PQ generators with a power factor of one. Grid-following units deliver their nominal power to the

network, i.e., P_{nom}, and do not change this value in case of load changes. Hence, these units are current-controlled. In steady-state, the grid delivers 870 kW and 2404 kVAr to the microgrid.

Islanded system with six DG units having P/V droop control In this case, the 85-node network is islanded. Since in the islanded mode, no main grid is available, at least one grid-forming unit is required. Here, all six DG units are considered as dispatchable DG units. Renewable sources can be included as well, but as they are generally not (yet) dispatched, they can be seen as negative loads, thus, do not influence the power sharing ratio of the dispatchable units. Droop control is used for the power sharing, thus, analogous as in the conventional network, the dispatchable units are voltage-controlled. Therefore, they are modelled as ac voltage sources. This is contrary to the grid-connected DG units in the previous case that had a grid-following control algorithm and, hence, where the DG units were modelled as ac current sources. The P/V of (4.12) with $b = 0$ % and Q/f of (4.14) droop controllers are used, with $K_P = \frac{700}{P_{\mathrm{nom}}}$ V/W, $K_Q = 1.5e^{-7}$ Hz/VAr for each DG unit, P_{nom} is given in table 6.8 and $Q_{\mathrm{nom}} = 0$ VAr. For the tuning, $\Delta V_{\max} = 700$ V has been used, reflecting a 6.5 % voltage limit. Also, a virtual resistive output impedance of $z_v = 3\Omega$ is included in the inverters, such that the output voltage v_{g} of the DG unit equals $v_{\mathrm{g}} = v_{\mathrm{g,droop}} - z_v i_{\mathrm{g}}$. All DG units deliver almost equal reactive power, namely 387 kVAr. The reason is the combination of equal droops, equal nominal reactive power and because f is a global parameter in the microgrid.
The simulation results for active power and terminal voltage are summarised in Table 6.9. In the grid-connected case, the utility network was delivering power to the microgrid. To cope with this loss of power input due to the islanding of the system, the DG units deliver more power compared to the grid-connected case, thus, P is higher than P_{nom}. From the line/load data and Fig. 6.29, clearly, DG 6 lies closer to the load centres compared to DG 82 which lies near the edges of the system. Hence, the equivalent line resistance $R_6 < R_{82}$. According to the power sharing modification studied here, it can be expected that $\Delta P_6 > \Delta P_{82}$. The value ΔP ($\Delta P = \frac{P - P_{\mathrm{nom}}}{P_{\mathrm{nom}}}$) of the DG units should be compared because of the different ratings of the DG units. This expected power sharing modification is indeed valid as P_6 has risen with 38 % while P_{82} has risen with only 17 %. Hence, $\frac{P_6}{P_{82}} = 0.74$ instead of the nominal value of 0.63. This is compatible with the electrical distance of the DG units from the load centres and hence, benefits the line losses in the system. The calculated line losses equal 35.9 kW.

Islanded system with six DG units having P/f droop control Analogous as in the previous case, the R/X value of the network lines in the considered 85-node system is approximately 2.4. Hence, in order to use P/f droop control, a virtual

Table 6.9: Islanded microgrid: DG with P/V droop control

node	P (kW)	node	P (kW)
6	690	54	290
22	180	76	319
47	427	82	933

Table 6.10: Islanded microgrid: DG with P/f droop control

node	P (kW)	node	P (kW)
6	663	54	265
22	159	76	265
47	441	82	1058

output inductance L_v of 50 mH needs to be included in the inverters. The DG units are equipped with the P/f droop control of (2.7) and Q/V droop control of (2.9), with $K_{\mathrm{f}} = \frac{-1}{2\pi P_{\mathrm{nom}}}$ Hz/W and $K_{\mathrm{Q,v}} = -6.5e^{-5}$ V/VAr for each DG.
The obtained results are summarised in Table 6.10. Perfect power sharing is obtained, e.g., $\frac{P_6}{P_{82}} = 0.63$, which equals the nominal value. Hence, P_i/P_j is equal to $P_{\mathrm{i,nom}}/P_{\mathrm{j,nom}}$ for all P/f droop controlled DG units. This is advantageous as the units always deliver power according to their ratings, but, opposed to the P/V controllers, no automatic power sharing modification is obtained. The overall line losses equal 47.04 kW, which is higher than in the case of the P/V droop control (31 %).
An important remark is that the line losses between the P/f and P/V droop control strategies are difficult to compare in general as these controllers normally operate in networks with different characteristics. P/f droops are generally used in inductive networks and/or networks with inertia. The P/V droops are fitted for inertialess resistive networks, which is often the case in the considered low-voltage microgrids.

D. Conclusions

In this section, the power sharing between multiple DG units is compared. Firstly, in P/V droop control, an inherent trade-off between accuracy of active power sharing and voltage regulation (voltage near the nominal value) is present. Hence, the ratio of delivered power of each two DG units can differ from the ratio of their

nominal active power because of the line parameters. This automatic power sharing modification is in the sense that the DG units that are near the load centres, when considering the electrical distance, automatically take a larger part in the power sharing than the ones further away. Hence, the power sharing modification of P/V controllers is beneficial with respect to the line losses.
Secondly, also P/f droop control is included in the DG units with a virtual inductive output impedance, to cope with the mainly resistive network lines in the considered low-voltage microgrids. The P/f droop controls strategy achieves accurate active power sharing. Hence, it does not have the automatic power sharing modification of the P/V droop control strategy.

6.2 Transition between grid-connected and islanded mode

This section focusses on modifying the VBD control strategy to enable a smooth transition between the islanded and the grid-connected mode of the microgrid. The VBD control can operate in both modes. Therefore, for islanding, no specific measures are required. To reconnect the microgrid to the utility network, the modified VBD control synchronises the voltage of a specified DG unit with the utility voltage. It is shown that this synchronisation procedure significantly limits the switching transient and enables a smooth mode transfer.
This section is structured as follows. In § 6.2.1, the VBD control principle is discussed for the different operating modes. First, the islanded mode, second the grid-connected mode and next, the transition from grid-connected to islanded mode and vice versa are analysed. The latter transition requires a synchronisation procedure. This paragraph also discusses the modifications in the VBD controller to enable the synchronisation. In § 6.2.2, some cases are studied to verify that, in a basic and an extended microgrid: (1) islanding does not require additional control modifications; (2) the synchronisation procedure leads to a smooth reconnection of the microgrid to the utility network.

6.2.1 Control strategies

A. VBD control in islanded microgrids

This is discussed in chapter 4.

B. VBD control in grid-connected microgrids

Although developed for islanded microgrids, the VBD controller can be used in grid-connected networks as well. The mains frequency, which is determined by

the droop controllers of the large conventional generators, will be little affected by the small grid-connected microgrid. Hence, the frequency of the microgrid units (f_{dg}) will converge to the mains frequency (f_{mains}). For example, if $f_{\mathrm{dg}} > f_{\mathrm{mains}}$, the phase angle of the microgrid units (δ for a specific unit) will keep increasing compared to that of the PCC ($\delta_{\mathrm{mains}} = 0$). From the power flow equations of a DG unit to the utility in a resistive network in (4.6b), it follows that the reactive power delivered by this unit to the utility will decrease. The DG unit measures its Q and droops it with a positive slope, which in turn leads to a lower set point of frequency f_{dg}. In this way, a steady-state is reached. Note that because of the small and temporarily differences between the frequencies, this problem should not be analysed in terms of frequency differences, but in terms of phase angle differences, as discussed above. In general, $f_{\mathrm{mains}} \approx f_{\mathrm{nom}}$, such that the reactive power of the unit will approximately equal its nominal value. If $Q_{\mathrm{nom}} = 0$ VAr in the VBD control, this is equal to the conventional control strategies of DG units with power-factor-one.
Like in the islanded microgrid, the $V_{\mathrm{g}}/V_{\mathrm{dc}}$ droop controller takes care of the balancing of the dc-bus. The $P_{\mathrm{dc}}/V_{\mathrm{g}}$ droop controller changes the active power of the unit to enable voltage limiting in the network.

C. Transition from grid-connected to islanded mode

When considering the transition from the grid-connected to islanded mode, two types of islanding are possible: planned and unplanned. Both types generally do not pose problems for the microgrid when using the VBD control. The control strategy can remain the same in both modes. In grid-connected mode, the terminal voltage and frequency of the units are generally near their nominal values. Hence, in this mode, the units deliver their nominal active and reactive power, analogous as in the grid-following strategies. If all the DG units would keep on delivering their nominal power to the network in islanded mode, this would lead to large variations of the voltage compared to its nominal value. Hence, the VBD controller acts on these deviations, limits them and takes care of the power sharing.
As the VBD control strategy can remain the same in the two modes, obviously, for islanding, no synchronisation is required. This is not valid when instead of VBD control, a grid-following control strategy is used. In this case, a change of control strategy is required as the islanded mode demands grid-forming control strategies for the voltage control and power sharing in the network.

D. Transition from islanded to grid-connected mode

Opposed to islanding, the transition from islanded to grid-connected mode is generally planned. Before the transition, the phase angle and rms value of the PCC

voltage at microgrid and utility side can differ. Moreover, the microgrid and utility network can operate at a different frequency, because the droop controllers in both networks do not force the frequency to its nominal value. Therefore, closure of the PCC switch without synchronisation would lead to large transients, i.e. sudden voltage and current changes. In order to realise a smooth mode transfer, a synchronisation procedure is required. Therefore, here, the VBD control strategy is changed to synchronise the utility and microgrid side rms voltage, phase angle and frequency before connecting the microgrid to the utility.

The synchronisation procedure can operate slower compared to the primary (VBD) control. Therefore, it is not necessary to avoid communication. The PCC voltage is measured and communicated to the synchronising DG unit that uses a PLL to obtain the rms voltage and its phase angle. One unit is selected for the synchronisation of the microgrid. To cope with this responsibility, this unit should be sufficiently large, dispatchable and close to the PCC.

The synchronisation strategy to synchronise the DG unit's voltage v_{g} to the PCC voltage at the utility side v_{util} is illustrated in Fig. 6.21. As the synchronising unit is electrically close to the PCC, it is assumed that $v_{\mathrm{g}} \approx v_{\mathrm{PCC}}$. The PCC switch closes at $t = t_{\mathrm{conn}}$ and the synchronisation procedure is active in $t_{\mathrm{conn}} - T_{\mathrm{sync}} < t < t_{\mathrm{conn}}$, with T_{sync} the duration of the synchronisation procedure. As discussed above, the VBD controller consists of a dc-power controller with the input coming from the $P_{\mathrm{dc}}/V_{\mathrm{g}}$ droop controller and a voltage controller with input from the $V_{\mathrm{g}}/V_{\mathrm{dc}}$ and Q/f droop controllers. Here, the VBD controller of the synchronising unit is modified by including an rms voltage synchronisation block, a droop limiting block and a phase synchronisation block, which are discussed further in this paragraph. The voltage, phase angle and frequency of the synchronising DG unit are controlled to their respective PCC values: $V_{\mathrm{g}} = V_{\mathrm{util}}$, $\theta_{\mathrm{g}} = \theta_{\mathrm{util}}$ and $f = f_{\mathrm{util}}$. These three synchronisation tasks are performed by the three different control blocks.
The rms voltage synchronisation block changes the output of the $P_{\mathrm{dc}}/V_{\mathrm{g}}$ droop controller gradually, thus, by using a ramp function, to force V_{g} to V_{util}.
Phase angle synchronisation is enabled by the phase synchronisation block that control θ_{g} towards θ_{util}. Again, a gradual synchronisation is obtained by using a ramp function. The output of this block is a frequency change, which according to (4.28) changes the phase angle of the voltage reference. The DG unit's frequency is controlled to the grid frequency by using the droop limiting block. This block turns off the Q/f droop ($f = f_{\mathrm{nom}}$) sufficiently before the synchronisation is performed. In Fig. 6.21, the gain of the droop is gradually lowered until it is off at $t = t_{\mathrm{conn}} - T_{\mathrm{sync}}/2$. Here, it is assumed that the grid frequency equals 50 Hz, the same strategy can be used for variable grid frequency, with the difference that during synchronisation, f_{nom} in Fig. 6.21 is changed to f_{util}, which can be obtained

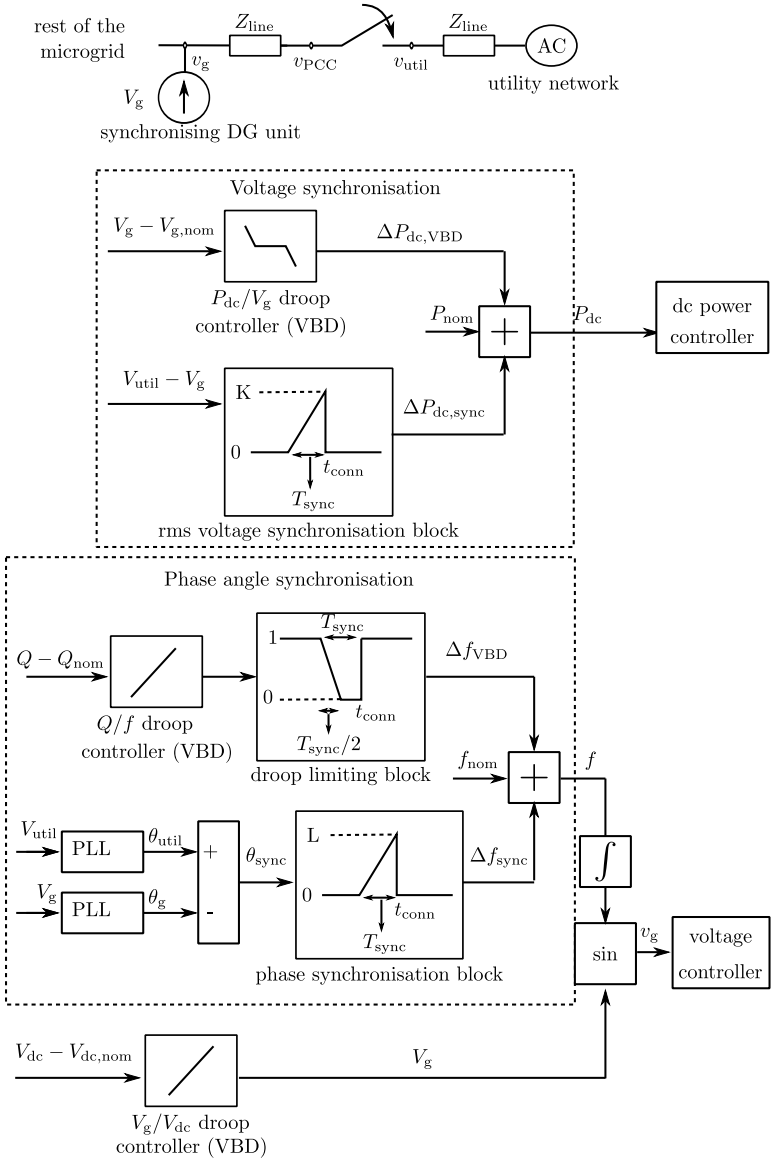

Figure 6.21: Synchronisation: control strategy in the VBD control, with V_{g} the rms value of the DG unit's terminal voltage $v_{\text{g}}(t)$

by using a frequency-locked loop (FLL).

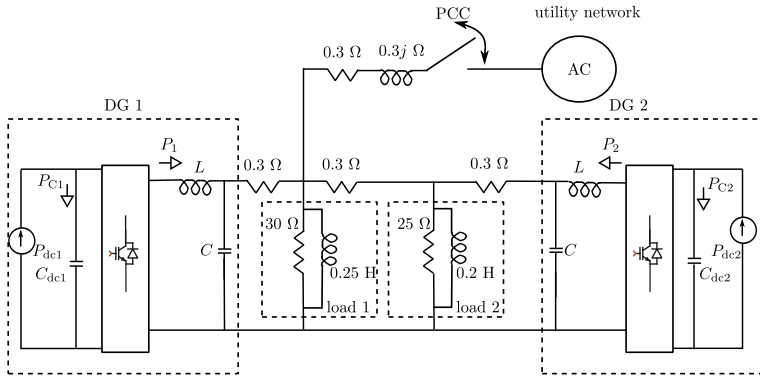

Figure 6.22: Basic microgrid configuration

6.2.2 Microgrid mode transfer with VBD control: results

A basic and an extended microgrid with mode transition are studied. First, the islanding procedure is discussed. Second, the transition from islanded to the grid-connected mode is discussed, and a comparison is made between the cases with and without synchronisation. It is shown that without synchronisation, large transients in voltage and current can occur and that the presented synchronisation procedure is effective to enable a smooth mode transition.

A. Basic microgrid

The considered microgrid, with two DG units and two RL loads, is depicted in Fig. 6.22. The utility network is modelled as a voltage source of 230 V rms and 50 Hz, i.e., a strong network connected to the microgrid through a line impedance (R/X = 1). A large parasitic resistance is present in parallel with the inductance of this line. The parameters of the DG units are: $L = 2$ mH, $C = 3$ μF and $C_{\mathrm{dc}} = 1.5$ mF. The nominal values are: $V_{\mathrm{dc,nom}} = 450$ V, $P_{\mathrm{dc,nom,1}} = 1.6$ kW, $P_{\mathrm{dc,nom,2}} = 800$ W, $Q_{\mathrm{dc,nom,1}} = Q_{\mathrm{dc,nom,2}} = 0$ VAr and the constant-power bands b equal 1 %. As a low-voltage microgrid is considered, the lines in the microgrid are resistive, here $0.3\ \Omega$ [104, 218].

VBD control with transition from grid-connected to islanded mode First, the transition from grid-connected to islanded mode, i.e., islanding, is considered. The transition takes place at $t = 0.505$ s.
The obtained results in Fig. 6.23 show an adequate transition, with limited switching transients. The DG units operate with VBD control in both modes. The voltage remains in the 10 % limits. The obtained voltage drop after switching is relat-

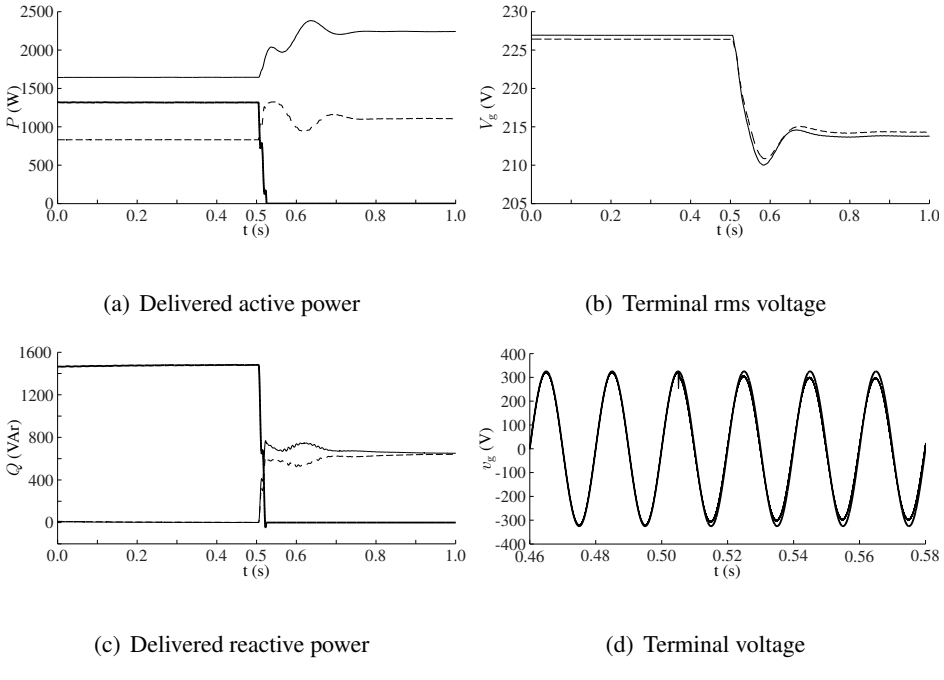

(a) Delivered active power

(b) Terminal rms voltage

(c) Delivered reactive power

(d) Terminal voltage

Figure 6.23: Basic microgrid: grid-connected to islanded (— = DG 1; ---- = DG 2; ▬ = utility network)

ively large due to the small scale of the microgrid studied here, the lack of storage equipment and the large load burden. Here, only primary control (stabilisation of the microgrid) is considered. If required, an overlaying secondary controller will change the set points of the primary controller to force the voltage closer to the nominal value, enabling voltage restoration on a longer term. This is out of the scope of this chapter.

The active power of both units is shared according to their ratings and droops. In steady state for the islanded operation, DG 1 delivers 2.2 kW, while DG 2 delivers 1.1 kW. In both modes, the DG units contribute in the voltage control because of their small constant-power band as they represent dispatchable units. Therefore, the active power differs from its nominal value. This enables soft curtailment by the VBD control in a primary controller. However, as in grid connected mode $V_\mathrm{g} \approx 230$ V, the DG units nearly deliver their rated power, $P_1 = 1.6$ kW and $P_2 = 830$ W. Note that less-dispatchable DG units, with a wider constant-power band, would exactly deliver their nominal power, i.e., MPP, in this case. In the grid-connected mode, the DG units operate with power-factor-one as $f = f_\mathrm{nom}$ because of the strong utility network. In islanded mode, the reactive power of the loads is

shared between the DG units. Here, the units deliver equal reactive power because of the equal droop and equal nominal values of f and Q chosen in this case.
Fig. 6.23(d) shows that in the grid-connected mode, the voltage of DG 1, which is electrically close to the PCC, differs little from the PCC voltage. After islanding, the difference becomes larger because of the droop controllers that enable power sharing.
The simulations show a small islanding transient and a proper operation of the VBD controller in both modes.

VBD control with transition from islanded to grid-connected mode The voltage v_{util}(t) is shifted with $\pi/3$ relative to v_{g}(t). In this way, synchronisation of v_{g} and v_{util} is required. The transition occurs at the zero-crossing of v_{util}, just before $t = 0.5$ s.

Without synchronisation procedure
In the first case, the DG units are not synchronised to the utility network, which is depicted in Fig. 6.24(d). Figs. 6.24(a-c) show extreme transients in P, Q and V_{g}. The over-current protection of the DG units or at the PCC may activate. Fig. 6.24(b) shows some variations in the terminal voltages of the units just after the switching. The reason is that in this case, there is no synchronisation and, thus, hard switching occurs.

With synchronisation procedure
In this case, the phase angle, frequency and rms voltage of $v_{\mathrm{g},1}$ and v_{util} are synchronised. The obtained results are depicted in Fig. 6.25. Fig. 6.25(d) shows synchronisation of the full waveform.
Note the different scale in the vertical axes of Figs. 6.25(a-c) compared to Figs. 6.24(a-c). The synchronisation transient is significantly lower than in the case without synchronisation. As the voltage in the islanded microgrid is lower than the nominal voltage, the power delivered by the dispatchable DG units is significantly larger than the nominal value, i.e., a large load burden. Therefore, in the grid-connected mode, the utility network injects power into the microgrid, forcing the voltage in the network and the active power of the DG units closer to the nominal values.
During synchronisation, the synchronising DG unit DG 1 delivers a significant amount of reactive power to synchronise its voltage phase angle with the PCC voltage. This is due to the large phase angle difference chosen in this case and the small T_{sync}. The other DG unit changes its reactive power to maintain a proper voltage quality and reactive power sharing. The active power of DG 1 increases during synchronisation to match its voltage with that of the PCC. In the basic microgrid, a large load, low P_{nom}, no secondary control to change the set points and a large initial phase angle difference are chosen such that before synchronisation

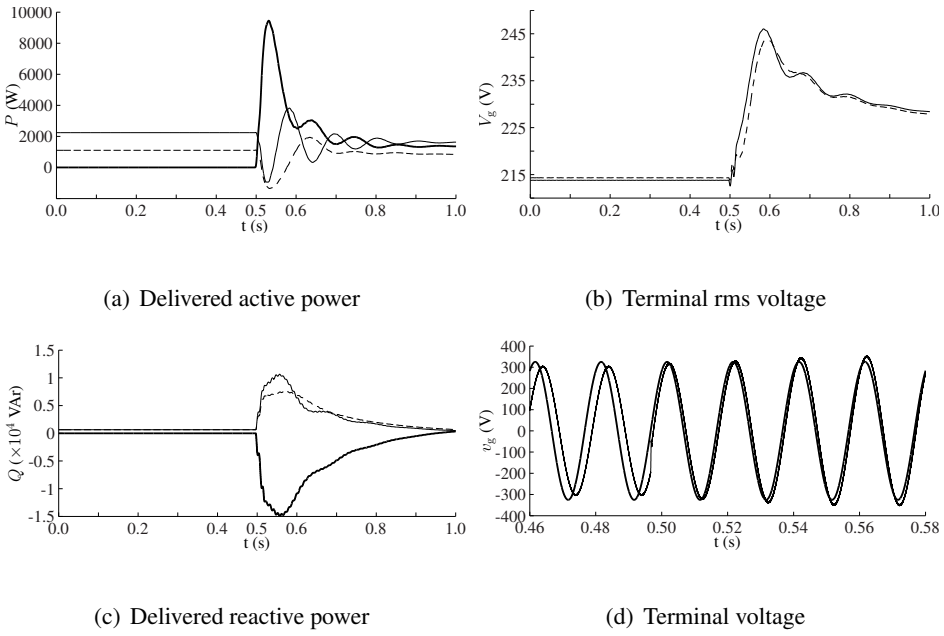

(a) Delivered active power

(b) Terminal rms voltage

(c) Delivered reactive power

(d) Terminal voltage

Figure 6.24: Basic microgrid: islanded to grid-connected, no synchronisation (— = DG 1; ---- = DG 2; ▬ = utility network)

the difference in $v_{\mathrm{dg},1}$ and v_{pcc} is large. In this way, the synchronisation procedure can be studied in an extreme case.

B. Extended microgrid

The microgrid configuration is depicted in Fig. 6.26 and the parameters are summarised in Table 6.11. The mode transition takes place at the zero crossing of the voltage just before 0.6 s. The microgrid consists of three constant-power loads with power factor 0.95. The first load $P_{\mathrm{load},1}$ equals 500 W, 150 VAr. The second load consumes 1 kW, 325 VAr and the third is a 2 kW, 650 VAr load. Also, two RL loads with the same power-factor are included. Further, the microgrid consists of three DG units. DG 1 and DG 2 are dispatchable, DG 3 is a unit with a wide constant-power band, representing a less dispatchable DG unit. The utility network is modelled as a strong network, with 230 V and 50 Hz and is connected to the microgrid through a line impedance. The transition from islanded to grid-connected mode is studied.

Without synchronisation

First, no synchronisation procedure is performed before connecting the microgrid

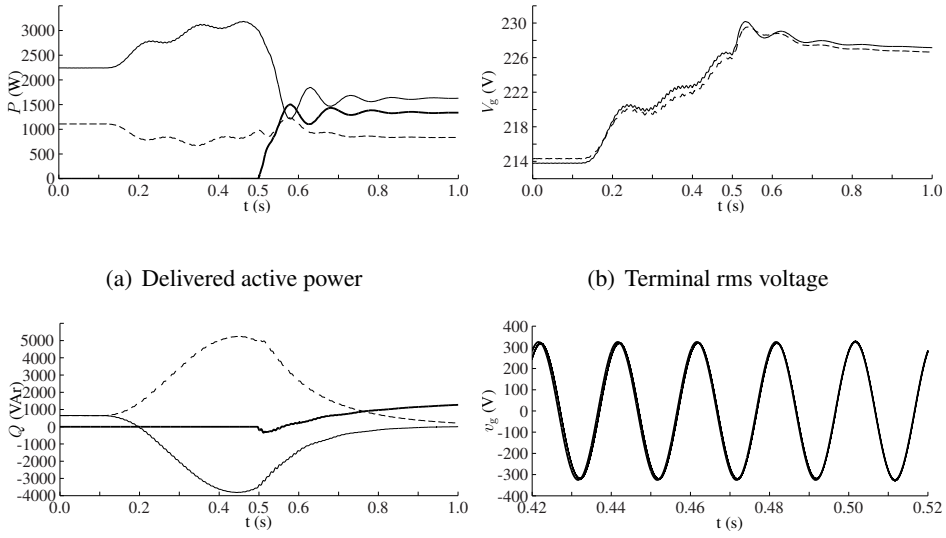

(a) Delivered active power

(b) Terminal rms voltage

(c) Delivered reactive power

(d) Terminal voltage

Figure 6.25: Basic microgrid: islanded to grid-connected, with synchronisation (— = DG 1; ---- = DG 2; ▬ = utility network)

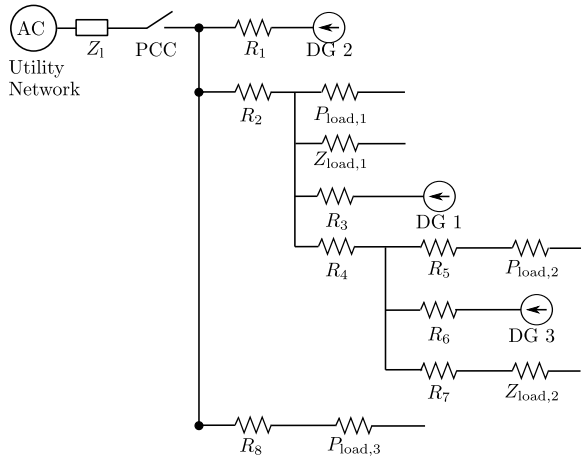

Figure 6.26: Extended microgrid configuration

to the utility network. The simulation results are depicted in Fig. 6.27. Clearly, the mode transfer transients are unacceptable and the protection devices may turn on.

Table 6.11: Microgrid case: parameters

Parameter	value	Parameter	value
C_{dc}	1.5 mF	$P_{\mathrm{nom},3}$	1.55 kW
$V_{\mathrm{dc,nom}}$	450 V	R_1, R_3, R_6	0.5 Ω
$V_{\mathrm{g,ref}}$	230 V	R_2, R_4, R_5, R_7, R_8	0.3 Ω
f_{nom}	50 Hz	$Z_{\mathrm{load},1}$	$50 + 16j$ Ω
$P_{\mathrm{nom},1}$	1.25 kW	$Z_{\mathrm{load},2}$	$75 + 25j$ Ω
$P_{\mathrm{nom},2}$	1.60 kW	Z_{l}	$0.5 + 0.5\mathrm{j}$ Ω

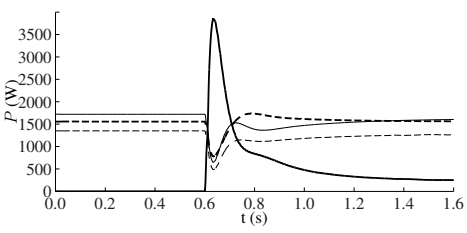

(a) Delivered active power

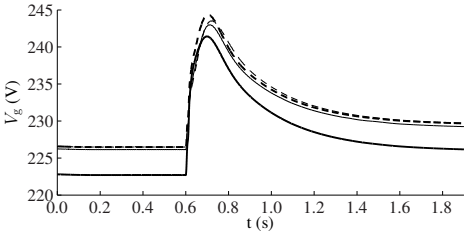

(b) Terminal rms voltage

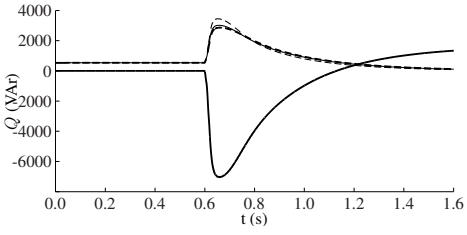

(c) Delivered reactive power

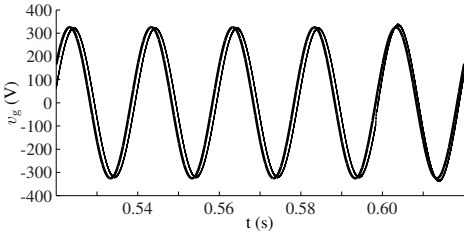

(d) Terminal voltage

*Figure 6.27: Extended microgrid: islanded to grid-connected, without synchronisation (— = DG 1; ---- = DG 2; **----** = DG 3; **—** = utility network)*

With synchronisation

Second, a synchronisation procedure in DG 1 is performed, with $T_{\mathrm{sync}} = 0.3\ s$. The simulation results are depicted in Fig. 6.28. The voltages remain in the 10 % limits in both modes. Fig. 6.28(d) shows that synchronisation of the PCC voltage and the voltage of DG 1 is achieved at the switching instant.

The synchronisation procedure leads to a significant reduction of transient voltages

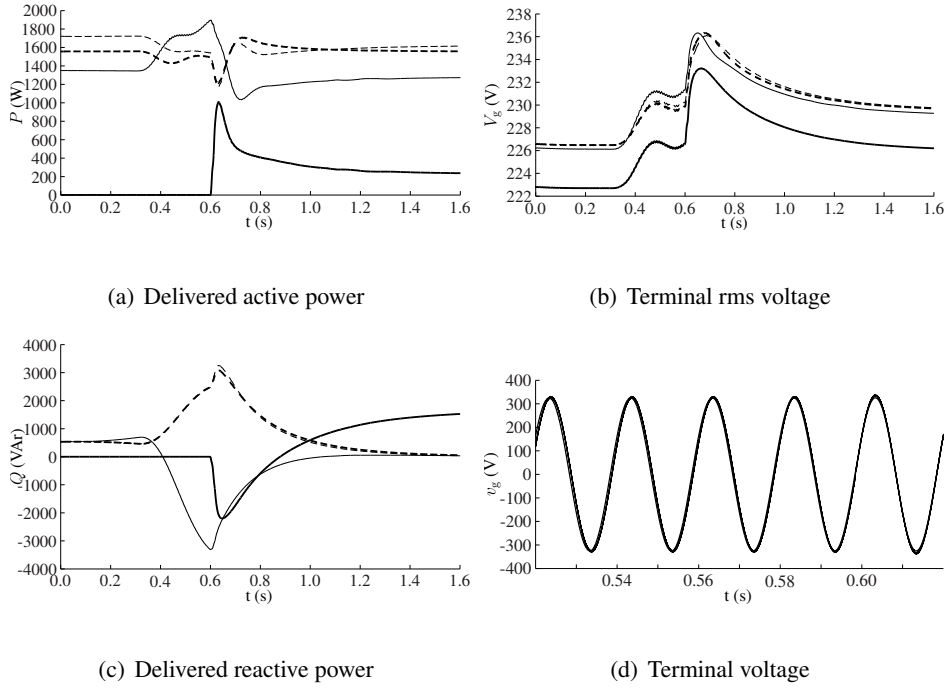

(a) Delivered active power

(b) Terminal rms voltage

(c) Delivered reactive power

(d) Terminal voltage

*Figure 6.28: Extended microgrid: islanded to grid-connected, with synchronisation (— = DG 1; ---- = DG 2; **----** = DG 3; **—** = utility network)*

and currents (Q, P and V_g) during the mode transfer. Note the different scales of the vertical axes of Figs. 6.27 and 6.28. In the islanded mode, the terminal voltages are significantly lower compared to in the grid-connected mode. The reason is that here, a large load burden is combined with a low total nominal power of the DG units. In this way, the operation in grid-connected and islanded mode differ significantly. The third DG unit, which is little dispatchable, clearly operates at nominal power, i.e., maximum power point, in both modes. The other units share the load in islanded mode and operate at rated power in the grid-connected mode as in this case, $V_\mathrm{g} \approx 230$ V.

6.2.3 Conclusions

It is shown that VBD control is possible in both modes. In the islanded microgrid, proper power sharing and voltage control are achieved. An optimised integration and capturing of the renewable energy is obtained because of the usage of constant-power bands. In the grid-connected mode, the control strategy does not need to be altered. Without need for communication, the renewables take part in the voltage

control by using soft curtailment in case of extreme voltages.
Islanding does not require additional measures as the control strategy does not need to be altered. For transition from islanded to grid-connected mode, which is a planned event, communication is used to announce the mode transition. The synchronising DG unit starts a procedure to synchronise its terminal voltage v_{g} with v_{util}. This synchronisation procedure is achieved by altering the VBD control with an additional term in the $P_{\mathrm{dc}}/V_{\mathrm{g}}$ and Q/f controllers. These controllers synchronise the rms voltage and the frequency/phase angle respectively. Hence, in this paragraph, a smooth mode-transfer is achieved by modifying the VBD control strategy with a synchronisation procedure to connect the islanded microgrid with the utility.

6.3 Conclusions

In this chapter, first, VBD control is used to avoid on-off oscillations of DG units. Avoiding on-off oscillations is a significant advantage of the controllers as it avoids a power quality degradation in the network, avoids life time reduction of the DG units and enables a larger capturing of the available renewable energy.
Second, VBD control achieves voltage limiting by including soft curtailment in the DG units. In resistive low-voltage networks, reactive power consumption has a limited effect on the voltage amplitude, opposed to soft curtailment.
Third, the power sharing modification with VBD and P/V droops is analysed, which is often mentioned as a disadvantage of P/V droop control. This section shows that this power sharing modification is often beneficial.
Finally, an additional module is added in the VBD algorithm to enable a smooth transition of a microgrid between the grid-connected and the islanded mode.
The content of this chapter has been published in [212, 219–221].

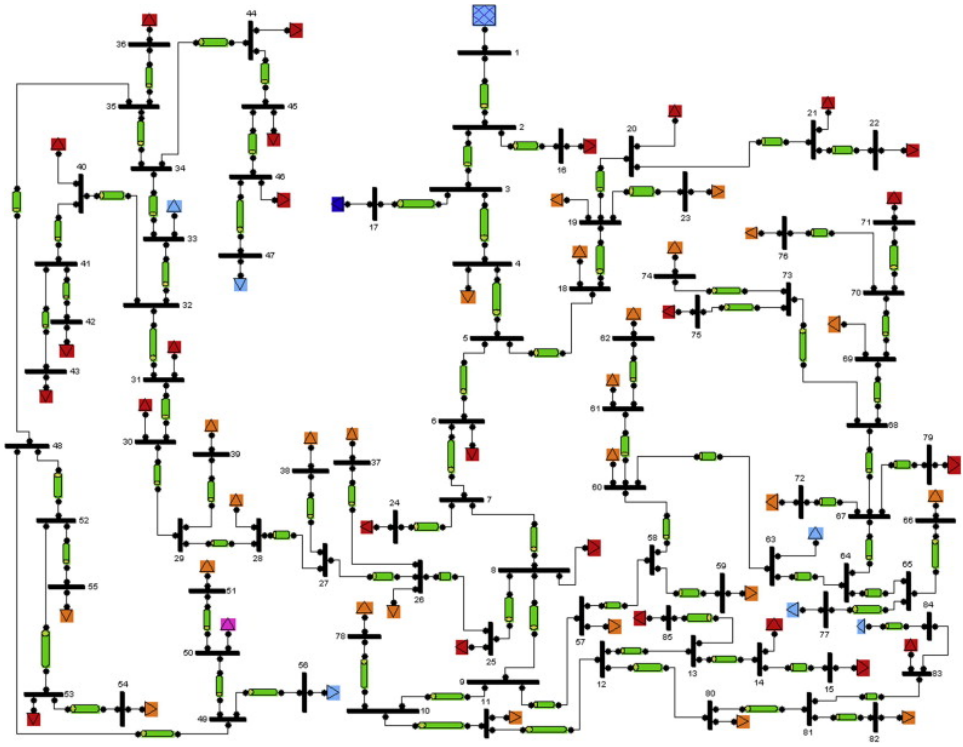

Figure 6.29: One line diagram of 85 node distribution network [216]

Table 6.12: Line and load data of 85 node distribution network [216, 217] (1)

	SN	RN	R_{l} (Ω)	X_{l} (Ω)	P_{RN} (kW)
1	1	2	0.108	0.075	0.00
2	2	3	0.163	0.112	0.00
3	3	4	0.217	0.149	56.00
4	4	5	0.108	0.074	0.00
5	5	6	0.435	0.298	35.28
6	6	7	0.272	0.186	0.00
7	7	8	1.197	0.820	35.28
8	8	9	0.108	0.074	0.00
9	9	10	0.598	0.410	0.00
10	10	11	0.544	0.373	56.00
11	11	12	0.544	0.373	0.00
12	12	13	0.598	0.410	0.00
13	13	14	0.272	0.186	35.28
14	14	15	0.326	0.223	35.28
15	2	16	0.728	0.302	35.28
16	3	17	0.455	0.189	112.00
17	5	8	0.820	0.340	56.00
18	18	19	0.637	0.264	56.00
19	19	20	0.455	0.189	35.28
20	20	21	0.819	0.340	35.28
21	21	22	1.548	0.642	35.28
22	19	23	0.182	0.075	56.00
23	7	24	0.910	0.378	35.28
24	8	25	0.455	0.189	35.28
25	25	26	0.364	0.151	56.00
26	26	27	0.546	0.226	0.00
27	27	28	0.273	0.113	56.00
28	28	29	0.546	0.226	0.00
29	29	30	0.546	0.226	35.28
30	30	31	0.273	0.113	35.28
31	31	32	0.182	0.075	0.00
32	32	33	0.182	0.075	14.00
33	33	34	0.819	0.340	0.00
34	34	35	0.637	0.264	0.00
35	35	36	0.182	0.075	35.28

Line and load data of 85 node distribution network [216, 217] (2)

	SN	RN	R_{l} (Ω)	X_{l} (Ω)	P_{load} (kW)
36	26	37	0.364	0.151	56.00
37	27	38	1.002	0.416	56.00
38	29	39	0.546	0.226	56.00
39	32	40	0.455	0.189	35.28
40	40	41	1.002	0.416	0.00
41	41	42	0.273	0.113	35.28
42	41	43	0.455	0.189	35.28
43	34	44	1.002	0.416	35.28
44	44	45	0.911	0.378	35.28
45	45	46	0.911	0.378	35.28
46	46	47	0.546	0.226	14.00
47	35	48	0.637	0.264	0.00
48	48	49	0.182	0.075	0.00
49	49	50	0.364	0.151	35.28
50	50	51	0.455	0.189	56.00
51	48	52	1.366	0.567	0.00
52	52	53	0.455	0.189	35.28
53	53	54	0.546	0.226	56.00
54	52	55	0.546	0.226	56.00
55	49	56	0.546	0.226	14.00
56	9	57	0.273	0.113	56.00
57	57	58	0.819	0.340	0.00
58	58	59	0.182	0.075	56.00
59	58	60	0.546	0.226	56.00
60	60	61	0.728	0.302	56.00
61	61	62	1.002	0.415	56.00
62	60	63	0.182	0.075	14.00
63	63	64	0.728	0.302	0.00
64	64	65	0.182	0.075	0.00
65	65	66	0.182	0.075	56.00
66	64	67	0.455	0.189	0.00
67	67	68	0.910	0.378	0.00
68	68	69	1.092	0.453	56.00
69	69	70	0.455	0.189	0.00
70	70	71	0.546	0.226	35.28

Line and load data of 85 node distribution network [216, 217] (3)

	SN	RN	R_{l} (Ω)	X_{l} (Ω)	P_{load} (kW)
71	67	72	0.182	0.075	56.00
72	68	73	1.184	0.491	0.00
73	73	74	0.273	0.113	56.00
74	73	75	1.002	0.416	35.28
75	70	76	0.546	0.226	56.00
76	65	77	0.091	0.037	14.00
77	10	78	0.637	0.264	56.00
78	67	79	0.546	0.226	35.28
79	12	80	0.728	0.302	56.00
80	80	81	0.364	0.151	0.00
81	81	82	0.091	0.037	56.00
82	81	83	1.092	0.453	35.28
83	83	84	1.002	0.340	14.00
84	13	85	0.819	0.340	35.28

Chapter 7

Integration of the proposed VBD control in a hierarchical control structure

The previous chapters focus on primary control in microgrids, e.g., in order to achieve a stable microgrid operation. Like in the conventional power system, the set points of the primary controllers should be altered based on non-local information, e.g., by means of a secondary controller. This controller can also modify the constant-power bands of the DG units, loads and storage elements in time, e.g., because of specific consumption constraints. This chapter does not discuss how to determine the secondary/tertiary controller's set points, how to implement these, nor the communication issues, etc. The chapter rather provides a general discussion about how to integrate the VBD controller in a hierarchical control structure. It also emphasizes and explains the need for a hierarchical control structure. For instance, the secondary/tertiary controller can address social issues of the producers if the physical position in the grid impacts the amount of power one can inject (and hence also impacts the financial remuneration for the energy delivered to the grid). Like the primary controller, the secondary controller can tackle technical issues, but extended with possible economical/societal/environmental objectives.

In § 7.1, the hierarchical control in the conventional electric power system is briefly revised and the objectives of hierarchical control in microgrids are summarised. In § 7.2, it is illustrated how the proposed primary VBD controller can be integrated in a hierarchical control in the DG units. Also, some examples of secondary control objectives in microgrids are given. In § 7.3, secondary control in active loads is discussed and § 7.4 reflects on the VPP concept and its positioning in the microgrid hierarchical control.

7.1 Introduction

The transmission network control is based on a hierarchical control scheme with primary, secondary and tertiary frequency controllers. In the European synchronous system, these three control strategies are characterised by their respective reserve [222]. The primary reserve, also called frequency containment reserve, comes available almost instantaneously (fully available in 30 s and stay available for at least 15 min) and keeps the system stable, e.g., when losing a generation unit or to cope with a wrong prediction. The primary control is based on the P/f droops of the large synchronous generators. The secondary reserve, also called frequency restoration reserve, comes available in 0.5-15 min (fully available in 15 min maximum) to compensate for frequency deviations from the nominal value. The secondary control is a centralised automatic control based on the area control error (ACE) signal to restore the operational balance in each control area and to compensate for prediction errors. It brings back the frequency and the interchange programs to their target values. The tertiary reserve, also called the replacement reserve, is reserve that requires more than 15 min to become available, and it replaces the primary and secondary reserves when they are depleted. Tertiary control is a manual change in the dispatching and unit commitment in order to restore the secondary control reserve, to manage congestions, and to bring back the frequency and the interchange programs to their target if the secondary control reserve is not sufficient. A long-term control is the time control. The Laufenburg control centre in Switzerland calculates the official Synchronous Time for the UCTE and issues the commands for its correction to bring it into line with UTC (Coordinated Universal Time) [222].
In microgrids, hierarchical control is analogous as in the conventional networks. Here, we only distinct between primary and secondary control, with the following aims:

- Primary control
  - Reliability
  - Fast, preferably without communication
- Secondary control
  - Can use communication
  - More global responsibilities: optimisation, emergencies, coordination of primary control actions, restoration of pre-agreed consumption patterns, restoration of nominal V and f, control of import/export of microgrid energy
  - Slower, smart grid

The microgrid hierarchical control is similar with the conventional hierarchical grid control. However, firstly, the microgrid primary controller should operate faster due to the lower system inertia, leading to a more dynamical system. Secondly, the control objectives of the secondary controllers are different: other than frequency restoration, the microgrid secondary controller can be addressed for economic optimisation and coordination of the control actions of the different units. In conventional grid control, economic issues are handled on beforehand, e.g., day-ahead, in the electricity markets. In islanded microgrids on the other hand, the same is valid, but the secondary controller can alter the scheduled power as well. The reason is the small scale of the microgrid, which makes the load and generation variations more distinct and less predictable. Also, the often high share of renewable power sources in microgrids compared to in conventional electric power systems increases the need for a secondary controller that may alter the power schedules. Another control objective of the secondary controller is to alter the rms grid voltage when it deviates too much from its nominal value, due to the primary control action. Thirdly, in the literature, there are generally three control levels defined, see table 7.1. Here, the second and third level are considered as one.

7.2 Secondary control of DG units

Secondary control in microgrids is analogous to the secondary control in the conventional network, as shown in Fig. 7.1. In the conventional network, frequency changes trigger the primary control. In a microgrid with VBD control, the voltage is the trigger. Secondary control takes over the primary control, when necessary (e.g., depletion of reserves) or when the control area is responsible for the unbalance, which is rarely an issue in microgrids as they mostly consist of a single area. In the microgrid, this control hierarchy is applicable for both the DG units and the active loads, with respectively, VBD control and voltage-based active load control for the primary control and with set point changes for the secondary control. In the conventional power system, active load control is not yet exploited profoundly and is mainly restricted to load shedding (as a last means to stabilise the system) and different day and night tariffs.

7.2.1 Examples of secondary control drivers

The secondary control changes the set points of the primary (VBD) controller, e.g., by shifting the droops. An example of droop shifts is shown in Fig. 7.2, where the secondary controller is implemented for fuel savings [223]. Fig. 7.2(a) shows the result of the primary controller, assuming $V_1 \approx V_2$. Accurate power sharing is obtained, but the two DG units operate at a low output power compared to the

Table 7.1: Control levels hierarhical microgrid control

level	operators	functions
grid	distribution network operator (DNO) and market operator (MO)	• manage operation with several microgrids • DNO communicates with MGCC • MO communicates with market
microgrid management	microgrid central controller (MGCC)	• restoration or improvement of voltage amplitude and frequency • synchronisation microgrid-utility • load shedding • optimum of production (market prices, grid security) • etc.
local management	local controllers (LC)	• inner control of DER to meet voltage and current references (chapter 3) • power generation control: power dispatch for a stable operation (chapters 2 and 4): to avoid circulating currents between the DG units and to establish the voltage and frequency of the grid.

ratings of the units. Hence, to operate more efficiently, one DG unit can be turned off. This is shown in Fig. 7.1(b), where the droop of DG 1 is shifted such that this unit turns off and DG 2 takes over the full load, and as such, operates closer to its nominal power. When the load increases again, the secondary controller shifts the droop of DG 1 again to the original position, such that this unit turns back on in Fig. 7.1(c). Shifting the droop can also be the responsibility of the primary control, i.e., in an automatic control for reliability reasons, triggered by a distinct change of the grid voltage.

A second example of secondary control is aiming at restoration of the nominal voltage amplitude and frequency in Fig. 7.3 [109]. In the market (day-ahead for example), the output power of the DG units is scheduled (P_{sched}). The droops are determined such that P_{sched} coheres with the desired (nominal) voltage V_{des}. However, when the load or a generator's output deviates from its scheduled value, the voltage (or frequency when using P/f droops) deviates from V_{des} in Fig. 7.3(a). To solve this issue, the droops of both DG units can be shifted as shown in Fig. 7.3(b).

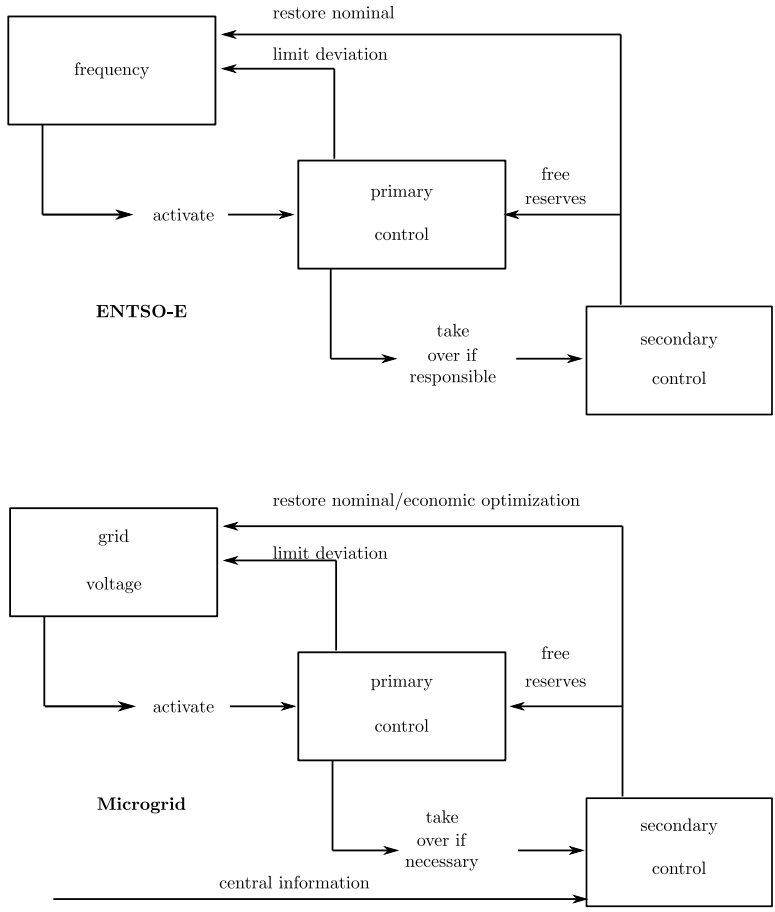

Figure 7.1: Secondary control takes over the primary control: hierarchical control analogous in the conventional grid and the microgrid

In this way, still perfect power sharing is obtained, i.e., $\frac{P_1}{P_2} = \frac{P_{\text{sched},1}}{P_{\text{sched},2}}$ while the voltage is restored to V_{des}. For this, an accurate coordination by means of secondary control is required as otherwise the situation of Fig. 7.4 can (temporarily) be obtained, leading to an inaccurate power sharing.

7.2.2 Secondary set point changes in VBD control

In this section, the usage of communication-based secondary control for DG units in a microgrid with primary VBD control is discussed. The secondary controller regulates the voltage or power at pilot points in the microgrid, the voltage at the

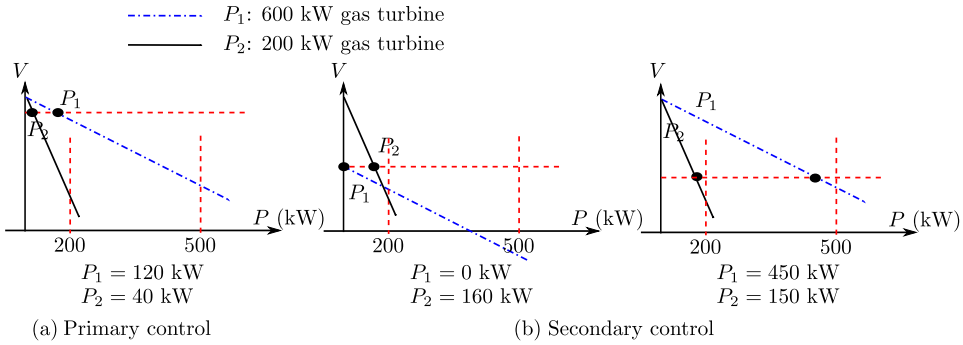

Figure 7.2: Droop shifting for economic optimisation: operation closer to the ratings

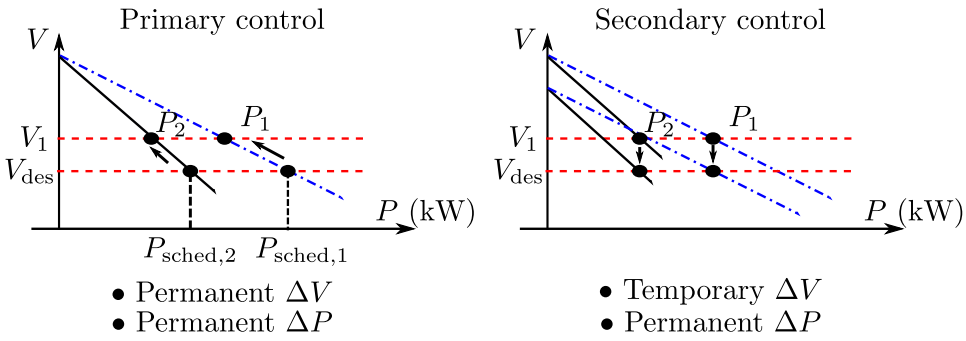

Figure 7.3: Coordinated droop shifting for nominal voltage restoration

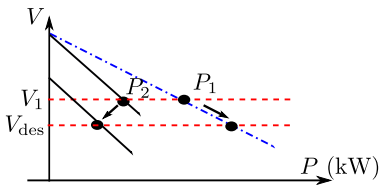

Figure 7.4: Uncoordinated droop shifting for nominal voltage restoration

PCC or the power exchange between microgrid and utility network. Note that the latter two objectives can also be achieved with the smart transformer of § 5.3, without communication inside the microgrid. The set points of the secondary controller are calculated based on an optimisation scheme (e.g., changing the desired power flow between the microgrid and the utility network, for loss reduction and to maximise economic revenue or for fuel optimisation) or based on power quality issues (e.g., changing voltages and frequencies in the microgrid). Secondary

control can help the DG units to provide ancillary services, which may become an important feature in the future power system.
Instead of focussing on determining the set points of secondary control, this section investigates the influence of the secondary control, its implementation in the DG units and its interactions with the primary VBD control. The cases of an islanded microgrid and (a cluster of) grid-connected microgrids are considered and the interaction between the primary control strategy and the secondary active power (voltage) control is studied. For the frequency control, linked with reactive power, an analogous approach can be followed, which is out of the scope of this section, but it is expected to be more straight-forward because frequency is a global parameter in the microgrid, opposed to voltage. Two options are considered:

1. The secondary voltage control:
    - determines a reference voltage for some pilot nodes in the microgrid. This reference voltage is obtained by modifying the droop or by shifting the $I_{\mathrm{dc}}/V_{\mathrm{g}}$ droop controller to change the nominal dc current of the VSI;
    - determines a reference voltage for the point of common coupling (PCC). As microgrids can be regarded as controllable entities from the grid operators point of view, the utility network only needs to communicate this reference to one point, the PCC. The secondary controller of the microgrid, in turn, determines new set points of the DG units in the microgrid and communicates those to the units.
2. The secondary power control determines a reference active power exchange between microgrid and utility network. Again, the grid operator only needs to communicate to the PCC, and the secondary control takes care of the control of the DG units in the microgrid.

The secondary control can be based on optimisation inside the microgrid or in the utility network consisting of multiple microgrids as clarified in Fig. 7.5. For optimisation in the microgrid, the reference voltages or the power references are determined for some pilot points. For multi-microgrid optimisation, a reference PCC voltage or power is determined.
As stated above, the output of the optimisation procedure can either be a reference voltage or a reference power, this is clarified by using Fig. 7.6. With the new set points, the secondary controller in the microgrid changes the active power of the DG units by using (low-bandwidth) communication. To change the active power, either the droop is changed or the droop function is shifted. As the latter approach is taken here, a controller with as output a modified $I_{\mathrm{dc,nom}}$ for the DG units is used.

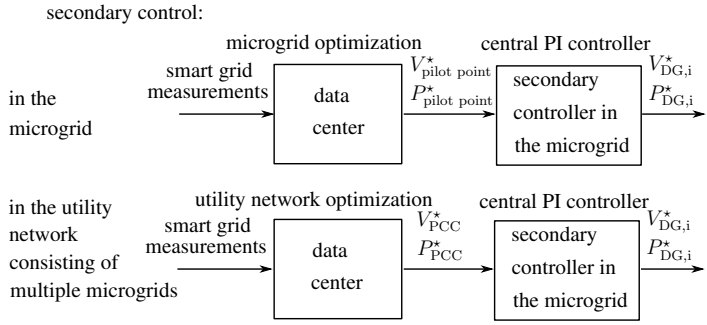

Figure 7.5: Secondary control for optimisation in the utility network or in the utility network

A. Secondary voltage control

According to the reference voltage, the secondary voltage control strategy calculates and communicates new set points of $I_{\text{dc,nom}}$ to the DG units. The secondary controller used in this paragraph consists of a centralised controller. This controller operates at a 100 Hz rate, with output u_{k}:

$$u_k = K_1 e_k + K_2 u_{\text{k}-1}, \tag{7.1}$$

with K_1 and K_2 the controller's parameters and $e_k = v_{\text{ref,k}} - v_{\text{meas,k}}$ in case of secondary voltage control. The value u_k is then distributed to the DG units, by taking into account their ratings (e.g., by sending $u_{\text{k,i}} = u_{\text{k}} \frac{P_{\text{dc,nom,i}}}{\sum_{i=1}^{N} P_{\text{dc,nom,i}}}$ to the respective DG units) as well as the width of their constant-power band. The dc current of the DG unit changes to:

$$I_{\text{dc}} = I_{\text{dc,nom}} + u_k + \Delta I_{\text{dc,droop}}, \tag{7.2}$$

with $\Delta I_{\text{dc,droop}}$ determined by the $I_{\text{dc}}/V_{\text{g}}$ droop control strategy.

Microgrid basic simulation $V^\star_{\text{PCC}}$
The microgrid configuration for this simulation is depicted in Fig. 7.7a with open PCC switch as a microgrid in islanded mode is studied. Both generators use an $I_{\text{dc}}/V_{\text{g}}$ and $V_{\text{g}}/V_{\text{dc}}$ droop control without constant-power band. Initially, they have nominal dc current 1.5 A. After 1.2 s, the dc current of DG 2 drops with 0.75 A, e.g., because of less solar input. Starting from 0.45 s, the secondary controller regulates the PCC voltage to 230 V rms. The output of this controller, a change of output power, is communicated to both DG units. Here, the case with $V^\star_{\text{PCC}}$ is studied, the case where $V^\star_{\text{g}}$ is set at a pilot node is analogous.

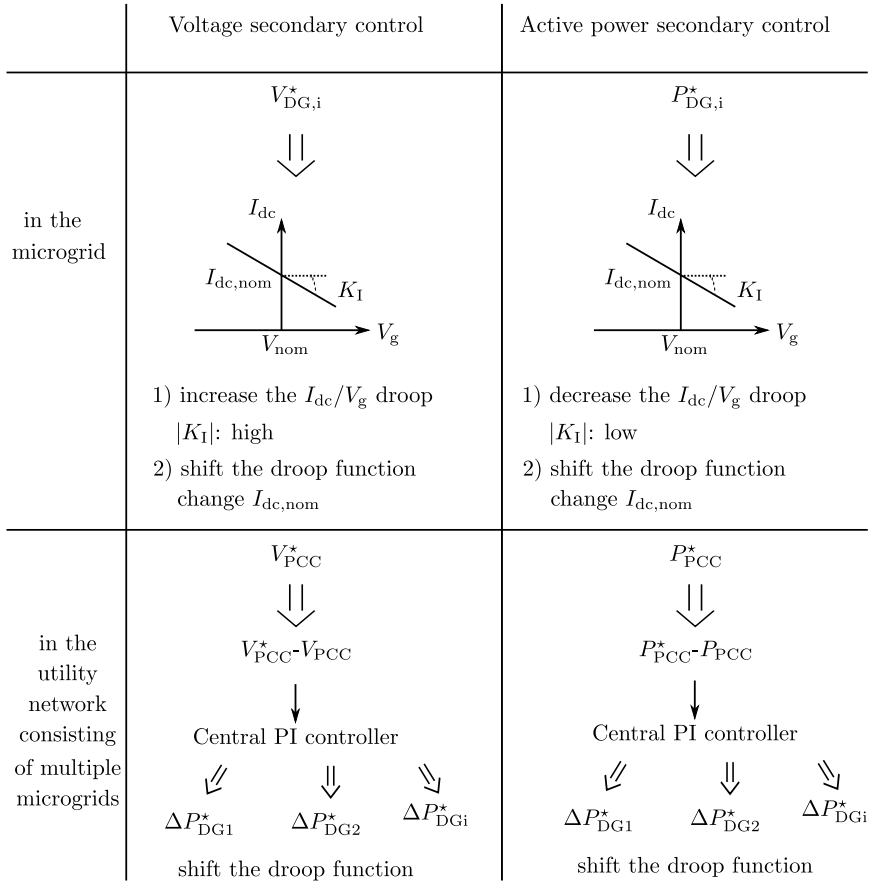

Figure 7.6: Secondary control overview: voltage secondary control versus power secondary control ("⇒" denotes communication)

The simulation results are depicted in Fig. 7.8. In the time span $0 < t < 0.45$ s, the DG units obtain a stable operation with $P_1 = P_2 = 1090$ W and $V_1 = V_2 = 234.6$ V, because of the symmetrical microgrid configuration and the equal generators. The initial transient is obtained because the DG units start from an equivalent grid-connected mode with 230 V rms. In the time span $0.45 < t < 1.2$ s, again the DG units have equal output, but the secondary controller sends negative set points of power change to these units in order to decrease the PCC voltage to 230 V rms. A stable operation is obtained and the simulation shows that the secondary controller reaches stable operation in 0.5 s. At $t = 1.2$ s, the output current of DG 2 decreases. Because of this decrease in output power, the dc-link voltage of DG 2 decreases and the $V_{\mathrm{g}}/V_{\mathrm{dc}}$ droop controller of this units lowers its terminal voltage.

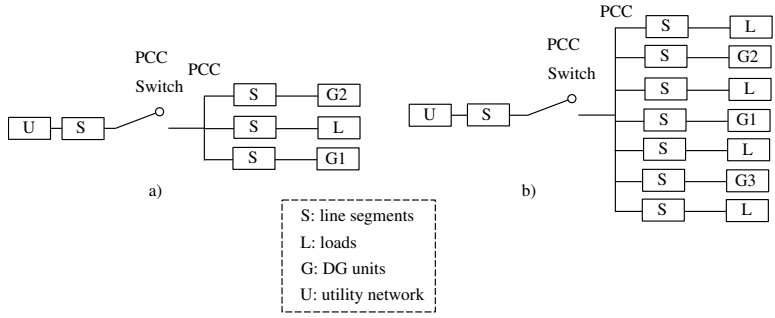

Figure 7.7: Microgrid configuration: a) basic and b) extended

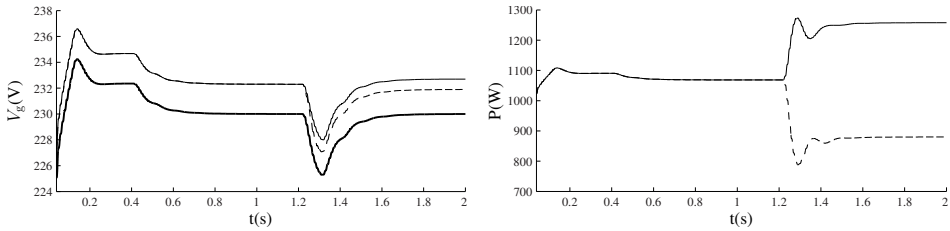

(a) Microgrid voltage (b) Active power to the electrical network

Figure 7.8: Microgrid basic simulation V_{PCC} (— = DG 1; ---- = DG 2; ▬ = PCC)

DG 1 also senses lower dc-link voltage and decreases the output voltage as well. Because of the lower V_{g}, the dc-current of DG 1 is increased by the primary $I_{\mathrm{dc}}/V_{\mathrm{g}}$ droop controller. The secondary controller operates at a lower rate to restore the PCC voltage. A stable operation is reached, again with $V_{\mathrm{PCC}} = 230$ V rms forced by the secondary controller, $V_{\mathrm{g1}} = 232.7$ V, $V_{\mathrm{g2}} = 231.9$ V, and $P_1 = 1257$ W, $P_2 = 880$ W.

Extended microgrid simulation with different kinds of DG units

This microgrid configuration is depicted in Fig. 7.7b. Three DG units are active, the first two DG units use an $I_{\mathrm{dc}}/V_{\mathrm{g}}$ and $V_{\mathrm{g}}/V_{\mathrm{dc}}$ droop control without constant-power band. Initially, they have nominal dc currents 5 A and 4 A respectively, but after 1.2 s the nominal dc current of DG 2 drops with 1 A. The third DG unit represents a non-dispatchable unit, e.g. driven by a renewable energy source, with dc current 3 A. Starting from 0.45 s, the secondary controller is used to control the PCC voltage to 230 Vrms.

From the simulations, it follows that the secondary control is able to control the

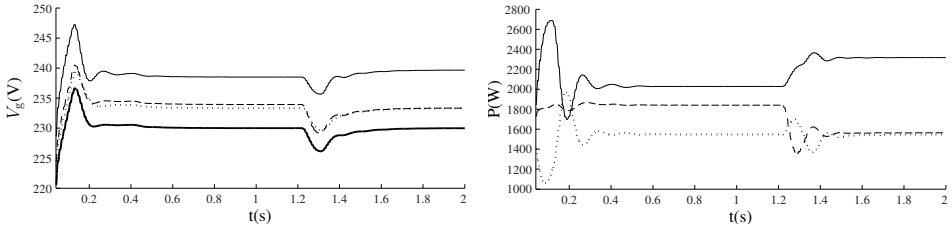

(a) Microgrid voltage (b) Active power to the electrical network

Figure 7.9: V_{PCC} control, extended microgrid (— = DG 1; ---- = DG 2; · · · =DG 3, ▬ = PCC)

voltage of a pilot point, here the PCC voltage, to a predefined value, even without the active participation of DG 3 in the power sharing and secondary control.

B. Secondary power control

Next to set points of voltage (in the microgrid or at the PCC), also a desired power exchange between a microgrid and the utility network can be determined. Again, dependent on this reference power, the secondary controller calculates new set points of power changes of the DG units and communicates these accordingly.
Another option, next to communication-based secondary control, can be the usage of a back-to-back converter [207] or a smart transformer.

Microgrid basic simulation $P^{\star}_{\mathrm{PCC}}$
The grid-connected microgrid configuration of Fig. 7.7a with closed PCC switch is considered. The same configuration parameters and transients are used as in the previous simulation.
The simulation results are depicted in Fig. 7.10. An initial transient is obtained because the DG units start operating at 230 V. In the time span $0 < t < 0.45$ s, a steady-state is reached, where $P_1 = P_2 = 1008$ W. The voltages of the generators are in the 10 % limits. In the time span $0.45 < t < 1.2$, the PCC power is controlled to a predefined value of 500 W. This forces the DG units to deliver less active power, namely 798 W each. From the simulation, it follows that the secondary control achieves steady-state after 0.5 s. The secondary control is, thus, sufficiently slower than the primary control to avoid interference between both. The settling time and overshoot of this P_{PCC} controller can easily be modified by changing the gain and integral term of the PI controller. Also, the change of output of DG 2 is accurately picked up by DG 1, while the reference PCC power exchange

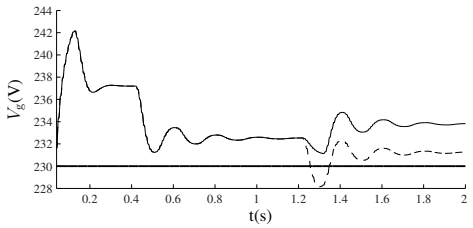

(a) Microgrid voltage

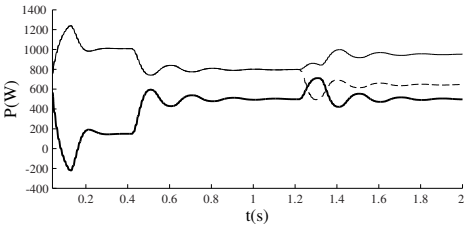

(b) Active power to the electrical network

Figure 7.10: P_{PCC} control, simple microgrid (— = DG 1; ---- = DG 2; ▬ = PCC)

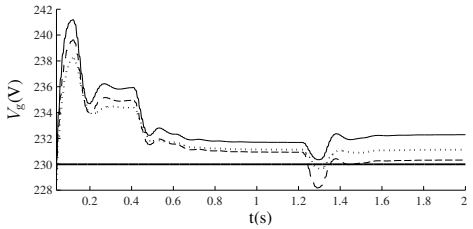

(a) Microgrid voltage

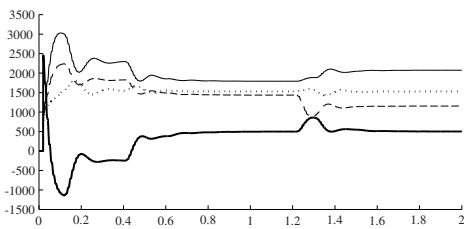

(b) Active power to the electrical network

Figure 7.11: P_{PCC} control, extended microgrid (— = DG 1; ---- = DG 2; · · · =DG 3, ▬ = PCC)

is maintained properly by the secondary controller.

Extended microgrid simulation with different kinds of DG units
The microgrid configuration is depicted in Fig. 7.7(b) with closed PCC switch. The same configuration parameters and transients as in the previous simulation are used.
From the simulations in Fig. 7.11, a stable operation is concluded. Also, the secondary controller is able to control the active power exchange between a microgrid and the utility network effectively.

7.3 Secondary control of active loads

The grid control is currently based on a “load following” strategy, where the generators follow the load changes without influencing the loads. In the load follow-

ing strategy, the loads are quasi blind to the state of the network. Interventions to change the demand are only used in emergency situations [224]. The advent of large amounts of DG units leads to a relative decrease of dispatchable generators compared to units with an intermittent variable character, which are often DG units (e.g., wind, solar). Therefore, the control flexibility of the generators to face the variability of the loads decreases. Both the production and demand become variable and to adjust them such that production exactly matches demand becomes more complex. This is especially an issue in small islanded microgrids, but becomes more important in the rest of the network as well. As the available storage capacity is mostly limited, a solution often presented is the usage of active load control to force the loads to react on the state of the electric power system. Some advantage of active load control are:

- it can reduce the need for future utility investments and generation assets;
- it can reduce/avoid congestion problems;
- it can reduce (individual) peak loads;
- it can reduce the stress on the network;
- it can avoid the high electricity prices on moments of high (average) load;
- it may increase the penetration limit for DG units while avoiding large system upgrades.

If load control is included in a high degree, the load following control strategy could reverse to a more "generation following" strategy in which the loads compensate the extra rigidity introduced at the supply side. Electrical vehicles (EVs) are expected to have a large impact on the electrical network, not only because they can become a large load but also as they can deliver ancillary services to the network. On one hand, EVs can contribute in the load control by operating as an energy buffer, thus, shifting the battery charging in time. On the other hand, EVs can add storage in the network by operating the batteries bidirectionally. An important aspect that needs to be dealt with is the impact on the life time of the batteries. The EV owners need to be refunded adequately.
The voltage-based demand dispatch strategy of § 5.1 and Fig. 7.12 operates without communication, is fast-acting, serves to increase the reliability of the microgrid and offers flexibility to deal with the increased penetration of renewables in microgrids. Therefore, it is called a primary load control analogous to the primary frequency control in the conventional electrical power system. Secondary active load control can be implemented on a longer time frame and can use communication by applying smart grid features, analogously as secondary DG control. In this way, the

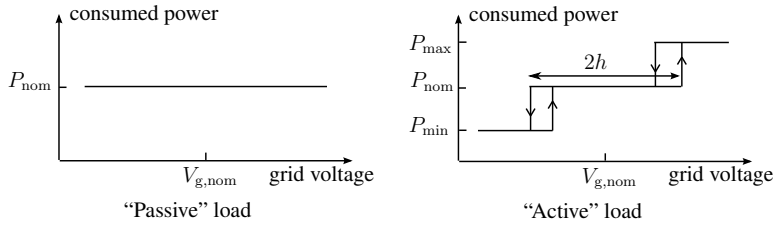

Figure 7.12: Active load control strategy based on the grid voltage

secondary controllers take over the primary controllers such that the impact of the latter on customers is restricted.

7.3.1 Drivers to enable secondary active load control

In order to encourage the loads to change their consumption based on external parameters, the drivers for the load participation should be considered. These drivers can be:

1. obligatory. This driver can achieve customer acceptance if it is absolutely necessary for the stability of the system (certainly in small scale systems). Therefore, in this case, an automatic load response should be obtained. It is analogous to the shedding of specific (rural) regions in order to avoid a total black out.

2. cost advantages: customers acquire financial benefits when participating in the active load control.

In general, there are two ways of electricity pricing to promote active load control: incentive-based and time-based pricing. In the incentive-based strategy, dedicated control systems are able to shed loads in response to a request from the utility. Incentive-based pricing generally deals with emergency/event-based active load control, avoiding outages. For time-based pricing, the best-known method is by using a two-tariff meter to have a lower price during the nights and weekends compared to the day times. In this case, still, the consumers are isolated from the real market-prices [224]. A newer concept is the smart meter with the ability for remote communication, which makes pricing based on near real-time prices possible. This may lead to a more market-based pricing strategy.
Several real-time tariff schemes already exist, such as

- Time-of-use (TOU) pricing with different prices defined over a day, with a fixed number of timeslots. TOU reflects the average cost of generating and

delivering power during those time periods. It encourages consumers to shift their consumption away from periods with high total load to periods with a lower demand. The prices are typically fixed on a monthly/seasonal basis. This is analogous to the two-tariff meter, but more differentiation is possible, e.g., to cope with seasonal effects.

- Real-time pricing (RTP) with typically hourly varying prices, related to the wholesale market price. Prices are typically fixed on a day-ahead or hour-ahead basis. RTP allows more gradation in the price compared to TOU pricing. Opposed to TOU pricing, next to seasonal effects, for example, also intra-day weather effects can play a major role.

- Critical peak pricing (CPP) uses trigger conditions that can change the price. CPP is often combined with TOU pricing.

For the primary load control, the real-time feature and a huge number of possible time slots is important, thus, the usage of communication should be kept minimal (or totally avoided). Primary active load control should, thus, involve an automatic load response. However, for time-based active load control, based on communication signals, there will always be a trade-off between communication burden and number of time slots/different prices/closeness of the information to the time of usage. Therefore, it is difficult to implement these kinds of communication-based active load control strategies if they are crucial for the stability of the system, e.g., in small scale systems. Consequently, they cannot be used as primary load control algorithms but merely contribute to the secondary load control.

7.3.2 Active load control in islanded microgrids

In islanded microgrids, the current two-tariff meter for electricity pricing could have adverse effects on the stability of the network. For example, in microgrids with a high penetration of photovoltaic panels, relatively much power is injected during the day-times. In such case, the consumption should be shifted to the sun-times instead of to the nights. As islanded microgrids are miniature, pilot versions of the future grids, we can expect the same issues in the conventional network with rising penetration of DG as well.
Therefore, in § 5.1, we have developed an active load control strategy especially for islanded microgrids to allow customer response that does not depend on communication. The active load control is included with a constant-power band $2h$, and generally the constant-power band width $2b$ of the renewable energy sources should be larger than that of the active loads. Again, the width of the constant power band is dependent on the nature of the load. Also, loads that allow a lower

smaller constant-power band should have more financial benefits than those with a wider band. The pricing for this load response should, thus, depend on:

- the width h of the constant-power band;
- the number and duration of the load shifts.

The primary active load control is effective in case of:

- islanded microgrids with VBD control such that high voltages are mainly due to generation from non-dispatchable DG units (renewable energy sources) and combined with a low load.
- grid-connected microgrids: non-dispatchable DG units (renewable energy sources) can cause over-voltage during periods of low load and high injection. Generally, this is mitigated by conservatively limiting the number of non-dispatchable DG units. The primary active load control can increase this maximum allowable number.

The smart grid features can deal with the pricing as the load response should be automatic and very fast, but the pricing involved may have some delay and can use bidirectional communication from the controllable load to an aggregation centre.
The secondary active load control can be included for optimisation reasons, and can operate on a larger time frame. The smart grid plays a major role in this secondary active load control as it offers bidirectional communication and smart sensors/devices. Some objectives of secondary active load control are discussed in [225]:

- communication about the availability of the load : bidirectional information between the smart appliances and the control centres;
- emergency actions (direct load control);
- coordination of primary active load control actions;
- restoration of pre-agreed consumption patterns after a change by the primary active load control.

7.4 Virtual power plants

7.4.1 VPP characteristics

Microgrids are an aggregation of DER that can operate both in grid-connected and islanded mode. An important benefit is that the microgrid presents itself to the

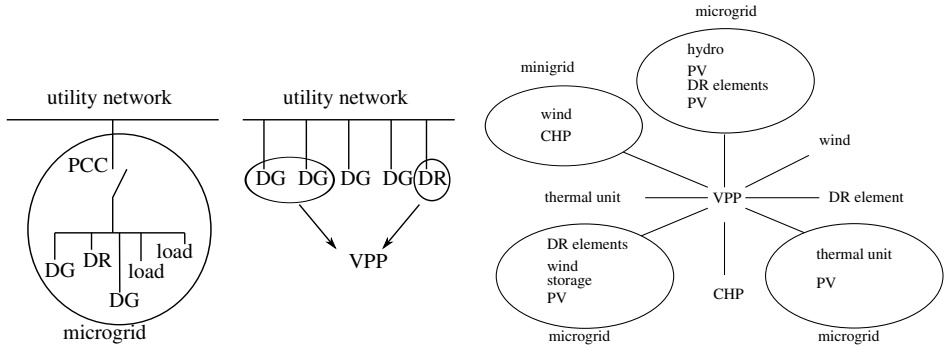

(a) Microgrids versus VPP: physical versus software-based aggregation of DER

(b) Microgrids and separate DER (DG units, demand response (DR) loads and storage elements) aggregated in a VPP

Figure 7.13: Virtual power plant characteristics

electrical network as a controllable entity. Virtual power plants (VPPs) form an aggregation of DER as well, but this aggregation can be virtual, thus, software-based as shown in Fig. 7.13. Hence, the geographical limits of microgrid systems are removed, but islanding of the whole VPP is often not possible as there is not a single PCC. VPPs can also consist of an aggregation of microgrids.
By aggregating DER, the VPP can participate in the electricity markets, deal with congestion problems and optimise voltage profiles in its feeders. As VPPs are software-based, they benefit from the communication functionalities delivered by the smart grid.

7.4.2 VPP classification

VPPs can be classified in technical and commercial VPPs (T-VPPs and C-VPPs). Of course, a VPP generally operates based on a combination of technical and commercial objectives. A C-VPP aggregates the DER in order to perform market-related activities, such as energy trading in different markets. The minimum trading volume in the Belpex day ahead market is 0.1 MWh/h, in the continuous intraday market segment, it is even 1 MWh/h. The minimum contract volumes are even larger. These capacity requirements are the biggest hurdles for the participation of DER in the markets. Therefore, aggregation of DER in a VPP can break the capacity threshold for electricity market entry [226]. A second hurdle is the importance of delivering a reliable service to the markets, for example, to avoid the unbalance penalties in case of wrong predictions of, e.g., intermittent energy sources. In this

context, mixed-asset VPPs are a main asset to reduce the risks of the individual DER technologies.

For T-VPPs, the aggregation is normally directed to provide specific power system support services, such as for the reliability and power quality of the grid.

Firstly, a T-VPP can contribute to the congestion management. Currently, the DER are installed in the electric power system without coordination and based on a fit-and-forget strategy. Because the network operators can often not change the output of the DER, they limit the installed DER capacity based on the worst-case scenario:

$$\sum P_{\mathrm{max,DER}} - \sum P_{\mathrm{min,load}} \leq \sum P_{\mathrm{max,grid}}. \tag{7.3}$$

Although this grid limit is only violated a few hours per year, the maximum installed capacity is limited permanently. By installing a VPP in a certain region, which requires a limited investment, the DNO and TNO can temporarily limit the DER capacity when necessary, while allowing for a higher installed energy capacity. As such, the real capacity factors and coincidence factors can be taken into account instead of using the conservative approach like in passively operated grids. This can prevent huge investments of both time and money in grid reinforcement and allows for a much larger share of renewable sources to be installed.

A T-VPP can also contribute to the voltage profile regulation. This can be done in a hierarchical control structure. In the primary control of the DG units, conventionally, over-voltage shut down is included. In the future, by means of a droop mechanism, which can be adopted analogous to the VBD control in islanded microgrids, voltage profile optimisation can be obtained by gradually changing the DG output power dependent on the terminal rms voltage, i.e., soft curtailment. In a secondary/tertiary control, the microgrid/VPP can coordinate the DG units in order to achieve an optimised voltage profile regulation (e.g., at a minimum cost).

Third, VPPs can play a major role in the oscillation clearance. The classical on-off control of DG can lead to oscillations in the network, which is demonstrated in Fig. 6.4. This primary safety function of the sources leads to unpredictable behavior. The first unit that reaches its voltage-limit will shut off. Due to tolerances in the components, it is hard to predict which unit this will be. This leads to low production rates on the days with the largest potential of renewable energy (e.g., wind or solar power). The VPP can solve this issue by providing coordination of the power changes. The DG output power does not change with 100 %, but with a value dependent on the terminal voltage of the units. Also, the power decreases due to over-voltages can be shared more evenly between the available resources, gaining more (predictable) production for the system as a whole.

Another aspect of VPPs is that aggregation of RES in VPPs makes it possible to engage the RES in reserve provision. This can be done by deviating from the MPP.

Solar panels, for example, can deliver a large contribution in the network stability because of their low inertia enabling a fast response time.

7.4.3 Hierarchical VPP/microgrid control

In this paragraph, a hierarchical control structure is presented in which, firstly, smart microgrids deal with local issues in a primary and secondary control (resource allocation, economic optimisation, control the power exchange between utility network and microgrid, frequency restoration and voltage profile improvements). Secondly, these microgrids are aggregated in a VPP that enables the tertiary control, forming the link with the electricity markets and dealing with issues on a larger scale. The VPP coordinator is responsible for supervision, balancing control, ancillary services and being the market interface.
For the VPP coordinator, microgrids offer the advantage of presenting themselves as entities, which reduces the communication and computational burden of the VPP coordinator. The VPP coordinator only adjusts the power through the PCC, while inside the microgrid, this power change can be dealt with taking into account all details of the microgrid in order to obtain an optimal operation.
The VPP coordinator calculates a total desired output power change of the VPP from information received from the DNO or from the VPP elements, e.g., for the balancing of the VPP. In order to realise this power change, two strategies are possible. In the direct control, the VPP coordinator determines a separate power change for each DER/microgrid and distributes this information to all the DER/microgrids in the system. The VPP coordinator has, thus, a direct control of its portfolio of DER and the performance of the system is highly linked with the intelligence of the VPP coordinator. It can however lead to problems of scalability, adaptability and computational burden. In case of a market-based control, the VPP coordinator uses a VPP market to send price signals to the DER or approves DER bids [227]. Opposed to the direct control strategy, the decisions for power changes are made by the DER units locally in order to maximise their profit. The VPP coordinator can not directly control the DER but has some controllability by changing the incentives. Both methods require two-way communication, intelligence and computational ability.
The hierarchical control approach is shown in Fig. 7.14. The primary control is not determined by the VPP coordinator, hence, analogous to primary control in microgrids, it is influenced by the DER locally. The output power of the DG units can be altered according to the state of the network by means of (modified) P/f, P/V and VBD controllers to enable the units to react on local voltage/frequency changes for local power quality improvements and a stable VPP operation. In primary control, only local measurements are used.
This primary control can be overlayed with a secondary control scheme. If applied

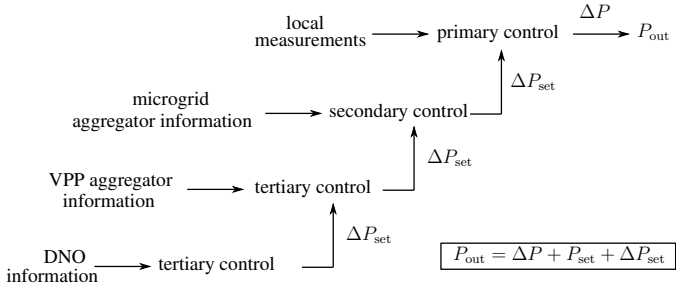

Figure 7.14: Hierarchical control in VPP with microgrids

to VPPs, the secondary control is a control for optimisation inside the microgrid (analogous to the microgrid secondary control). For example, the secondary controller can undo a primary P_{out} change of one unit by changing P_{out} of another unit, e.g., to reach an economic optimum.
The tertiary control deals with control signals from the DNO to the VPP coordinator or directly to the microgrids/DG units in case they are not part of a VPP. The tertiary control delivers new set points to the secondary control strategy, that in turn changes the nominal power in the primary control strategy.
By combining these different levels of controllers, a hierarchical control is formed where each control level delivers control signals to the lower levels. In case of a VPP with separate DER, the secondary VPP control can be omitted. In a microgrid without an overlaying VPP, the VPP tertiary control is omitted in Fig. 7.14. In an islanded microgrid, there is no tertiary control as defined in Fig. 7.14. In the state-of-the-art network, the renewable DG units have no secondary and tertiary control: $P_{\text{out}} = P_{\text{set}}$, with P_{set} merely determined by the DER, not by the state of the network.

7.5 Conclusions

In this chapter, the hierarchical control in a microgrid is considered. First, the secondary control of DG units is discussed. The influence of this secondary control, which changes the set values of the VBD controllers, on the system performance is considered. The secondary controller is able to obtain a reference power exchange between microgrid and utility (e.g., equal to the scheduled power in the markets) or a reference PCC voltage (e.g., voltage limiting). Next, the secondary control of active loads is discussed, which is analogous to secondary DG control. Finally, an overview of the VPP concept, focussing on hierarchical control, is briefly given.
The content of this chapter has been published in [228, 229].

Chapter 8

Concluding remarks and further research

In this chapter, the highlights of this work will be summarised, focussing on the innovative contributions of this PhD thesis. Further, some suggestions for further research subsequent to this work are given.

8.1 Concluding remarks

The increasing number and the increasing installed capacity of distributed generation (DG) units, poses a significant stress on the distribution networks and limits the further penetration of DG. Many of these problems arise because these DG units are not integrated in the networks in a coordinated manner and are not actively dispatched. Microgrids help to address these issues by aggregating generation, consumption and storage elements and controlling these assets as a single entity. A concurrent manner to tackle the actual problems in the electrical grids, is to make the electrical networks more intelligent, by including more monitoring, control and communication. It is expected that the grids will become smarter in an evolutionary manner, with smart microgrids as pioneers in a smarter grid.
An important aspect of microgrids is their ability to operate in islanded mode, which can increase the reliability of the local system or can enable electrification of remote regions in an economic manner. In this context, the main contribution of this PhD thesis is the development of the voltage-based droop (VBD) control for microgrids in islanded mode. This work focusses on small microgrids, hence, connected to the low-voltage networks. These networks have specific characteristics compared to the conventional networks, not only because of the low-voltage connection, but also because of their smaller scale and specific, mostly converter-interfaced, generators. Therefore, these networks need designated con-

trol strategies.

Some existing microgrid control strategies are discussed in chapter 2. The main contribution of this chapter is that the control strategies are explained by using coherent figures of the control strategies, making it easy to compare the strategies and point out the specific advantages and disadvantages. It is concluded that, except for very small microgrids, the research community is more and more converging to the control approach without inter-unit communication for the primary control, i.e., droop control.

The VBD control enables active and reactive power sharing in islanded microgrids, by determining a specific reference value of the terminal grid voltage. Hence, a voltage controller is required to control the grid voltage to this reference value. Chapter § 3 discusses the specific aspects of voltage control in islanded microgrids. PID-type control is considered and a comparison between direct PID control and cascaded PI control is made. Cascaded PI controllers are advantageous with respect to the robustness of the controller.

Chapter 4 presents the VBD control to enable active power sharing. This VBD controller uses the voltage as trigger for the active power changes of the DG units. The control strategy also includes constant-power bands to prioritise the power changes of the dispatchable DG units compared to the renewables. Hence, VBD control enables to dispatch the renewables, when necessary, in a primary control strategy to ensure a stable islanded microgrid operation. To also share the harmonic power, a harmonic power sharing strategy, based on the PR-SHI method developed in EELAB for grid-connected DG units is added to the VBD control.

In chapter 5, the other microgrid elements, such as loads/storage, synchronous generators and the transformer located at the point of common coupling of the microgrid and the utility grid are considered. Because of the small size of microgrids, sometimes, the DG units cannot ensure a stable microgrid operation. Therefore, a demand dispatch strategy, complying with the VBD control of the DG units, is presented. The primary control of the loads, generators and storage elements is triggered by the terminal voltage and based on constant-power bands, such that an automatic priority for power changes is implemented in all the grid elements.
In islanded networks, where the voltage is used to trigger active power changes, e.g., by using the VBD control, this control strategy can counteract with that of the directly-coupled synchronous generators. Therefore, a control strategy for synchronous generators in the context of VBD control is presented.
Next to the presentation of VBD control for DG units and extended to loads and storage equipment, another highlight in this PhD thesis is the development of the smart transformer concept. By using the smart transformer, it is now possible to live up to one of the most important advantages of microgrids, namely their operation as controllable entities. The smart transformer can control the power exchange

between a microgrid and the utility network without the need to change the control strategy in the microgrid, which can be operated as if it were in islanded mode.
In chapter 6, the grid-connected operating condition of a microgrid is considered. It is shown that the VBD control can operate in grid-connected mode as well, offering specific advantages in the voltage control of the distribution networks. When using VBD control, the renewables can actively participate in the voltage control, whereas now, they generally shut down entirely in response to overvoltages. Hence, the VBD control enables soft curtailment of renewables and avoids the on-off oscillations that can occur with the current on-off control of DG. This VBD control can also increase the capturing of the renewable energy potential compared to on-off control. It is also shown that VBD control leads to a beneficial power sharing compared to the conventional active power/frequency droop control, which can reduce the network losses. Finally, the transition between grid-connected and islanded mode is considered in this chapter. An additional control loop is added to the VBD control to enable a smooth mode transfer.
The former chapters focus on the primary control, hence, chapter 7 demonstrates how VBD control can be included in a secondary control concept by changing the primary VBD controller's set points. The microgrid's primary controller focusses on technical aspects in order to ensure a stable and reliable grid operation based on local information. Further technical, economical, societal and environmental objectives can be achieved by means of a secondary communication-based controller.
In this PhD thesis, the VBD control concept is presented in islanded microgrids, which was the main aim of this work. Additionally, the other aspects of microgrids were considered. First, the primary control of the other microgrid elements was discussed. Secondly, the operating modes other than the islanded mode were studied.

8.2 Further research

Microgrid research is relatively new and offers high potential to solve some issues the current electrical grid now faces, hence still, a lot of research in this field is required. Some suggestions for future research are given below.

- The VBD control is developed for single-phase microgrids. The extension to three-phase microgrids is an interesting research topic. In literature, often, the reference voltage (here, provided by the VBD control), is determined for one phase and then derived for the other phases by shifting this reference with 120°. However, when also taking unbalanced microgrids into account, some specific measures may be required. A possible action is to base the three-phase VBD control on the three-phase PR-SHI method in the PhD thesis of dr. ir. Bart Meersman.

- This PhD thesis discusses that a hierarchical control is absolutely necessary and showed that secondary/tertiary control can easily be fitted in with the developed VBD control concept by changing its set points. Future research is required to develop a strategy for determining these set points. A possibility is the usage of an optimisation procedure, e.g., optimising the economic income of the microgrid, taking into account the technical constraints, the specific wishes and needs of the grid elements (societal constraints) and the environmental objectives. In the context of grid-connected microgrids, the provision of ancillary services to the electric power system by means of microgrids is especially interesting. The ancillary services should be coordinated by the secondary/tertiary controllers.

- The main restriction to microgrids is the geographical one. Therefore, by aggregating microgrids into virtual power plants, further benefit can be taken from the microgrid concept, while still keeping advantage of the local nature and aggregation of a microgrid. Aggregated into a virtual power plant, microgrids can tackle grid issues that are not geographically confined by providing ancillary services to the grid operators. Analogous as the development of a management strategy for the hierarchical control in microgrids, VPP control can be studied. A central or agent-based controller can be envisioned. Some work concerning virtual power plants is being done by ing. Brecht Zwaenepoel.

- Finally, this PhD thesis is envisioned as a fundamental research project, based on an FWO grand. Together with Bart Meersman some experimental verification is made. Still, this laboratory set-up can be further extended in future research. Also, the step from a laboratory set-up to a demo-set up needs to be taken.

Appendix A

Voltage control in islanded microgrids: other control strategies

Next to the cascaded and direct PI(D) control, other, less conventional control strategies are possible as well. Some of these controllers, such as sliding-mode control and hysteresis control are discussed below.

A.1 Sliding-mode control

In the formulation of the voltage control problem, there is a discrepancy between the actual model and the mathematical model for controller design as the microgrid configuration is variable and not known in advance. Still, the required performance levels have to be met despite the existence of this system/model mismatch. This leads to the application of robust control strategies, such as the sliding-mode control technique, which is a nonlinear control. The purpose of the sliding-mode control law is to drive the system states $x(k)$ (or $x(t)$) onto a predefined surface s in the state space and to maintain those there for the subsequent time [230, 231]. Therefore, a control action is selected to ensure that

$$s(k) = Sx(k) = 0 \tag{A.1}$$

at a finite time $t_s = k_s T_s$, with T_s the sample period, and to maintain it there for $k > k_s$. For $k \leq k_s$, the system remains stable according to the Lyapunov method as will be shown further in this section. Also, initially or after a large disturbance, the bang-bang strategy is applied to drive the system states quickly to the switching surface with the maximum available control effort. Furthermore, the output of the

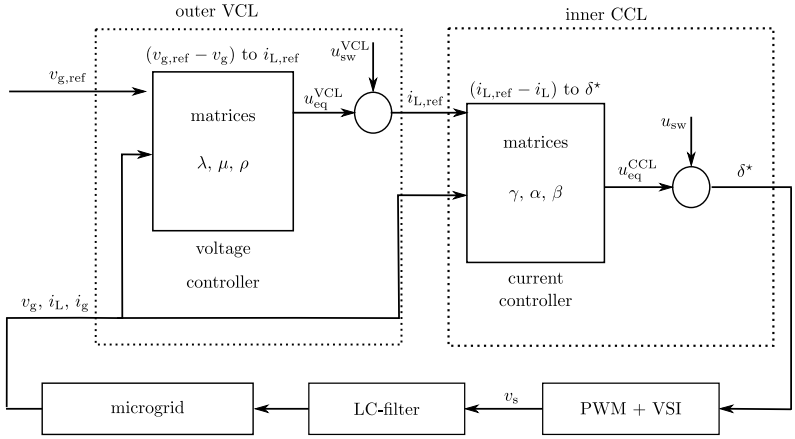

Figure A.1: Sliding-mode control using an inner current control loop and an outer voltage control loop, control scheme

sliding-mode controller, namely the duty ratio δ for the VSI, is limited to -1 and +1 by using a saturation function.

Sliding-mode control can be applied for the voltage control of an islanded microgrid as follows. The microgrid system has as controlled input the duty ratio $\delta^\star$ for the VSI with PWM as shown in Fig. A.1. The sliding-mode controller has as output this duty ratio and as input the difference between a reference grid voltage $v_g^\star$ and the obtained grid voltage v_g. The sliding-mode control is divided into two loops: an inner current-control loop (CCL) and an outer voltage-control loop (VCL). The outer VCL has as input the difference between $v_g^\star$ and v_g and its output $i_{L,ref}$ forms an input of the following inner CCL. The inner CCL controls i_L to $i_{L,ref}$ by changing the duty ratio $\delta^\star$ of the system. A state-space model of the system shown in Fig. 3.3 is derived from the basic equations (3.1), (3.2) and (3.3). The state-space representation of the system is

$$\dot{X}(t) = AX(t) + BU(t) + Ed(t) \tag{A.2}$$

with X the state vector, U the input vector of the microgrid system and d the state disturbances:

$$X = \begin{bmatrix} v_g \\ i_L \end{bmatrix} \qquad U = \begin{bmatrix} \delta^\star \end{bmatrix} \qquad d = \begin{bmatrix} i_g \end{bmatrix}. \tag{A.3}$$

The current i_g can be seen as a disturbance because the microgrid configuration is

not known. The state, input and disturbance matrices in (A.2) are given by:

$$A = \begin{bmatrix} 0 & \frac{1}{C} \\ -\frac{1}{L} & 0 \end{bmatrix} \qquad B = \begin{bmatrix} 0 \\ \frac{v_{\mathrm{dc}}}{L} \end{bmatrix} \qquad E = \begin{bmatrix} -\frac{1}{C} \\ 0 \end{bmatrix}. \tag{A.4}$$

In [232], discrete-time sliding-mode is proposed with an inner CCL and an outer VCL. Unlike in [232], the current i_{g} is measured in the approach presented in this section, for making a proper comparison between the different control methods and as it achieves a higher robustness. If this current is not measurable, estimators can be introduced in the control loop. The sliding-mode control strategy is derived from the discrete version of (A.2):

$$X(k+1) = A^* X(k) + B^* U(k) + E^* d(k) \tag{A.5}$$

where A^*, B^* and E^* are the discrete equivalents of the matrices A, B and E in (A.4), that are derived according to [233]:

$$A^* = e^{AT_s} \qquad B^* = \int_0^{T_s} e^{A(T_s-\tau)} B d\tau \qquad E^* = \int_0^{T_s} e^{A(T_s-\tau)} E d\tau. \tag{A.6}$$

Further,

$$y_1(k) = C_1 X(k) \qquad C_1 = \begin{bmatrix} 0 & 1 \end{bmatrix} \qquad y_1 = \begin{bmatrix} I_L \end{bmatrix} \tag{A.7}$$

$$e(k) = y_1(k) - y_{1,\mathrm{ref}}(k) \qquad y_{1,\mathrm{ref}} = \begin{bmatrix} I_{\mathrm{L,ref}} \end{bmatrix} \tag{A.8}$$

Discretisation of the continuous system gives:

$$A^* = \begin{bmatrix} \frac{1}{2} e^{\frac{T_s}{\sqrt{-CL}}} + \frac{1}{2} e^{\frac{-T_s}{\sqrt{-CL}}} & \frac{1}{2}\frac{\sqrt{-CL}}{C}\left(-e^{\frac{-T_s}{\sqrt{-CL}}} + e^{\frac{T_s}{\sqrt{-CL}}}\right) \\ -\frac{1}{2}\frac{\sqrt{-CL}}{L}\left(-e^{\frac{-T_s}{\sqrt{-CL}}} + e^{\frac{T_s}{\sqrt{-CL}}}\right) & \frac{1}{2} e^{\frac{T_s}{\sqrt{-CL}}} + \frac{1}{2} e^{\frac{-T_s}{\sqrt{-CL}}} \end{bmatrix} \tag{A.9}$$

$$B^* = \begin{bmatrix} -\frac{1}{2}\left\{1 + e^{\frac{2T_s}{\sqrt{-CL}}} - 2e^{\frac{T_s}{\sqrt{-CL}}}\right\} e^{\frac{-T_s}{\sqrt{-CL}}} \\ \frac{1}{2}\frac{\sqrt{-CL}}{L}\left\{e^{\frac{2T_s}{\sqrt{-CL}}} - 1\right\} e^{\frac{-T_s}{\sqrt{-CL}}}) \end{bmatrix} \tag{A.10}$$

$$E^* = \begin{bmatrix} -\frac{1}{2}\frac{\sqrt{-CL}}{C}\left\{e^{\frac{2T_s}{\sqrt{-CL}}} - 1\right\} e^{\frac{-T_s}{\sqrt{-CL}}}) \\ -\frac{1}{2}\left\{1 + e^{\frac{2T_s}{\sqrt{-CL}}} - 2e^{\frac{T_s}{\sqrt{-CL}}}\right\} e^{\frac{-T_s}{\sqrt{-CL}}} \end{bmatrix} \tag{A.11}$$

First, the inner CCL is derived and the switching surface s is given by

$$s(k) = y_1(k) - y_{1,\mathrm{ref}}(k) = i_{\mathrm{L}}(k) - i_{\mathrm{L,ref}}(k) = C_1 X(k) - i_{\mathrm{L,ref}}(k). \quad \text{(A.12)}$$

The control input should be designed so that the system can track the desired trajectory and consequently, i_{L} would track $i_{\mathrm{L,ref}}$. Ideal sliding-mode is achieved if the system input $U(k)$ is derived by setting $\dot{s}(t) = 0$ or in the discrete version: $s(k+1) - s(k) = 0$. Thus, with (A.1), $s(k+1) = 0$, with

$$s(k+1) = C_1 X(k+1) - i_{\mathrm{L,ref}}(k+1). \quad \text{(A.13)}$$

The state space equation (A.5) implies that

$$s(k+1) = C_1 \Big[A^* X(k) + B^* U(k) + E^* d(k) \Big] - i_{\mathrm{L,ref}}(k+1). \quad \text{(A.14)}$$

The input $u_{\mathrm{eq}}^{\mathrm{CCL}} = U = \delta^\star$ of the microgrid system, that is obtained from the output of the inner CCL, is the control input in order to achieve $s(k+1) = 0$, and therefore:

$$u_{\mathrm{eq}}^{\mathrm{CCL}}(k) = (C_1 B^*)^{-1} \Big[i_{\mathrm{L,ref}}(k+1) - S_1 A^* X(k) - S_1 E^* d(k) \Big], \quad \text{(A.15)}$$

or,

$$u_{\mathrm{eq}}^{\mathrm{CCL}}(k) = \gamma i_{\mathrm{L,ref}}(k+1) + \alpha X(k) + \beta d(k), \quad \text{(A.16)}$$

where $S_1 B^*$ is reversible since it is a non-zero scalar. Note that the matrices above are dependent on the filter parameters L and C, that can change due to component tolerances.

The Lyapunov method is commonly used to determine the stability properties of the sliding-mode controller. The Lyapunov function can be chosen as:

$$V(t) = 1/2 s^2(t). \quad \text{(A.17)}$$

For a stable sliding-mode, the Lyapunov function should satisfy the reaching law

$$\dot{V}(t) = s(t)\dot{s}(t) < -\eta \|s(t)\|, \quad \text{(A.18)}$$

as long as $s(\mathrm{t}) \neq 0$ and with η some strictly positive scalar. The discrete version of the reaching condition, with $s(\mathrm{k}) \neq 0$, can be evaluated from:

$$s(k)[s(k+1) - s(k)] < -\eta \|s(k)\|, \quad \text{(A.19)}$$

meaning that in case of a positive error s, this error will decrease, and vice versa

for a negative s, thus, the error decreases in absolute value. For this purpose, the equivalent control in (A.16) is augmented by a switching control term $u_{\mathrm{sw}}^{\mathrm{CCL}}(k)$ such that $U(k) = \delta^{\star}(k)$ becomes

$$U(k) = u_{\mathrm{eq}}^{\mathrm{CCL}}(k) + u_{\mathrm{sw}}(k) \tag{A.20}$$

With (A.14), (A.19) becomes

$$s(k)\Big[C_1\Big\{A^*X(k) + B^*\big[u_{\mathrm{eq}}^{\mathrm{CCL}}(k) + u_{\mathrm{sw}}^{\mathrm{CCL}}(k)\big] + E^*d(k)\Big\} - i_{L,ref}(k+1) - s(k)\Big] < -\eta\|s(k)\| \tag{A.21}$$

and by using (A.15):

$$s(k)\Big[C_1A^*X(k) + \big[i_{L,ref}(k+1) - C_1A^*X(k) - C_1E^*d(k) + C_1B^*u_{\mathrm{sw}}^{\mathrm{CCL}}(k)\big] + S_1E^*d(k) - i_{L,ref}(k+1) - s(k)\Big] < -\eta\|s(k)\| \tag{A.22}$$

or,

$$s(k)\Big[S_1B^*u_{\mathrm{sw}}^{\mathrm{CCL}}(k) - s(k)\Big] < -\eta\|s(k)\| \tag{A.23}$$

Therefore,

$$u_{\mathrm{sw}}^{\mathrm{CCL}}(k) = -K\mathrm{sign}(s(k)), \tag{A.24}$$

as C_1B^* is positive and reversible. The reaching condition becomes:

$$s(k)\Big[-(C_1B^*)K\mathrm{sign}(s(k)) - s(k)\Big] < -\eta\|s(k)\|, \tag{A.25}$$

which is valid for all possible C and L if $C_1B^*K > \eta$, defining K.
Also, other sliding surfaces can be introduced to achieve a satisfactory performance level [234]. Remaining on the switching surface may require infinitely fast switching. In practical microgrid applications however, the system has imperfections, such as parasitic dynamics and switching nonidealities. These can lead to chattering phenomena caused by the finite switching time in case of classical sliding-mode control. Chattering appears as a high frequency oscillation near the switching surface. It is undesirable, since it involves high control activity and may excite the neglected high-frequency dynamics of the microgrid system. Therefore, chattering must be reduced. Many approaches are proposed to counteract the effects of the chattering phenomenon, such as the continuous approximation to smoothen

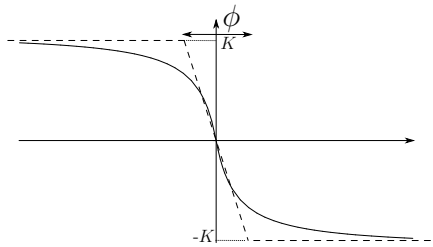

Figure A.2: Sliding-mode control: $u_{\rm sw}$ (—: continuous structure with (A.26), ----: boundary layer)

the discontinuity in (A.24) or the boundary layer method [235–239]. A boundary layer ϕ can be defined in which the discontinuous control input $u_{\rm sw}^{\rm CCL}$ is adapted, where if $|s|$ is small, the switching amplitude is lowered. The discontinuous $u_{\rm sw}^{\rm CCL}$ can be approximated by an appropriately chosen continuous structure for the sign-function [236, 237]:

$$u_{\rm sw}^{\rm CCL} = -\frac{Ks}{|s|+\delta}, \tag{A.26}$$

also shown in Fig. A.2 and with $\delta > 0$ and K a scalar.

For the outer voltage control loop, an analogous derivation is made. The value of U(k)= $u_{eq}^{\rm CCL}$(k) that is determined in the CCL, is included in the state equation (A.5) such that

$$X(k+1) = A^*X(k) + B^*\left[\gamma i^*_{\rm L,ref}(k) + \alpha X(k) + \beta d(k)\right] + E^*d(k). \tag{A.27}$$

The input of the outer VCL is the difference between $v_{\rm g}$ and $v_{\rm g,ref}$ and its output $u_{\rm eq}^{\rm VCL}$ is the reference current $i_{L,ref}$ that forms an input of the inner CCL. In the VCL, $u_{\rm eq}^{\rm VLC} = i_{\rm L,ref}$ and $y_2({\rm k}) = v_{\rm g}({\rm k}) = C_2X({\rm k})$. Hence,

$$X(k+1) = A_dX(k) + B_du_{\rm eq}^{\rm VLC}(k) + E_dd(k) \tag{A.28}$$

and

$$A_d = A^* - B^*(C_1B^*)^{-1}C_1A^* \qquad B_d = B^*(C_1B^*)^{-1} \tag{A.29}$$

$$E_d = E^* - B^*(C_1B^*)^{-1}C_1E^* \qquad C_2 = \begin{bmatrix}1 & 0\end{bmatrix} \tag{A.30}$$

The sliding-mode controller is determined according to

$$s(k+1) = 0 = y_2(k+1) - y_{2,ref}(k+1) \tag{A.31}$$

$$s(k+1) = 0 = C_2(A_d X(k) + B_d u_{\mathrm{eq}}^{\mathrm{VLC}}(k) + E_d d(k)) - v_{\mathrm{g,ref}}(k+1) \quad \text{(A.32)}$$

Such that:

$$u_{\mathrm{eq}}^{\mathrm{VLC}} = (C_2 B_d)^{-1} \left[v_{\mathrm{g,ref}}(k+1) - C_2 A_d X(k) - C_2 E_d d(k) \right] \quad \text{(A.33a)}$$

$$u_{\mathrm{eq}}^{\mathrm{VLC}} = \lambda v_{\mathrm{g,ref}}(k+1) + \mu X(k) + \rho d(k) \quad \text{(A.33b)}$$

The control strategy is summarised in Fig. A.1. Also in the VCL, $u_{\mathrm{sw}}^{\mathrm{VCL}}$ is determined according to the Lyapunov method. An advantage of sliding-mode over the direct and cascaded control strategies is that if changes in the filter parameters C and L occur, a simple change of the matrices in the previous equations can be made automatically. PID and PI regulators can also be tuned automatically by using heuristic rules such as the Ziegler and Nichols rules, but often, a better performance is obtained when manual tuning is applied. A disadvantage is that the sliding-mode control requires more computational burden as compared with the PID and PI regulators. However, all the matrices are calculated on beforehand, which limits the computational burden of the controllers.

A.2 Hysteresis Control

Second, the hysteresis control strategy can be applied for microgrid voltage control. In the basic implementation, a hysteresis controller changes its output states only when a given input leaves a given interval (hysteresis band). Therefore, if the microgrid voltage v_{g} exceeds the upper hysteresis limit $v_{\mathrm{g}}^{\star} + h$, the controller goes in the off-state, making v_{s} equal to -v_{dc}. In this case, the transistors T_1 and T_3 in Fig. 3.3 are blocked while T_4 and T_2 conduct, decreasing v_{g}. Then, if the lower voltage limit $v_{\mathrm{g}}^{\star} - h$ is reached, the controller goes in the on-state, making $v_{\mathrm{s}} = v_{\mathrm{dc}}$:

$$v_{\mathrm{s}} = \begin{cases} -v_{\mathrm{dc}} & \text{if} \quad \mathrm{v_g} \rightarrow > \mathrm{v_g^{\star}} + \mathrm{h} \\ v_{\mathrm{dc}} & \text{if} \quad \mathrm{v_g} \rightarrow < \mathrm{v_g^{\star}} - \mathrm{h} \end{cases} \quad \text{(A.34)}$$

The hysteresis control technique is easy to implement as it does not require any control system analysis, leading to an independence with respect to load parameters. This feature makes it interesting for microgrid applications, as the microgrid configuration is variable and unpredictable. Also, the simplicity of the controller is

an important factor as a large number of small DER are connected to the microgrid. Furthermore, a simple controller is often less expensive, making it interesting for small-scale, residential applications. The other main advantages of hysteresis control are good robustness, high control bandwidth, lack of tracking error, fast response and good accuracy [142,143,240]. Although simple and robust, this control technique is characterised by the disadvantage of producing a varying switching frequency. The actual switching frequency depends on the input filter of the VSI, the width $2h$ of the hysteresis band and the operating conditions [241]. An advantage of this control method is that the switching process is random by nature, avoiding switching peaks in the spectrum. However, the varying switching frequency is, in general, responsible for various problems, from the difficulty in designing the input filters to unwanted resonances in the microgrid [242]. A number of proposals are put forward to overcome this variable switching frequency [143,240,243,244], such as automatically adjusting the tolerance band. These however result in more complex control schemes. The other control strategies in this PhD thesis use a fixed switching frequency, but most require a control-oriented modelling of the system.
In the simulations of § A.5, the hysteresis controller is tuned with a hysteresis band of 0.2 V.

A.3 Linear Quadratic Regulator (LQR)

In the next control scheme, a linear-quadratic regulator (LQR) is used for the voltage control of an islanded microgrid. The state-space representation for tuning the LQR is derived by using (A.2):

$$\frac{\mathrm{d}}{\mathrm{dt}}\begin{bmatrix} i_{\mathrm{L}} \\ v_{\mathrm{g}} \end{bmatrix} = \begin{bmatrix} 0 & -\dfrac{1}{L} \\ \dfrac{1}{C} & 0 \end{bmatrix}\begin{bmatrix} i_{\mathrm{L}} \\ v_{\mathrm{g}} \end{bmatrix} + \begin{bmatrix} \dfrac{v_{\mathrm{dc}}}{L} \\ 0 \end{bmatrix}\begin{bmatrix} \delta^{\star} \end{bmatrix} + \begin{bmatrix} 0 \\ -\dfrac{1}{C} \end{bmatrix}\begin{bmatrix} i_{\mathrm{g}} \end{bmatrix}. \tag{A.35}$$

The matrices A, B and E in the state-space representation are transformed to their discrete equivalents $A^{\star}$, $B^{\star}$ and $E^{\star}$ by including the switching frequency of the VSI semiconductor switches, analogously as in § A.1.
The LQR method involves the determination of an input signal that takes a system from a given state to a final state while minimising a cost function J. This cost function is determined by:

$$J = \sum_{k=0}^{k=\infty} (X_k Q_k X_k + U_k R_k U_k + 2 X_k N U_k) \tag{A.36}$$

with $Q \geq 0$, $R > 0$ and here, $N = 0$. To minimise the cost function J, the

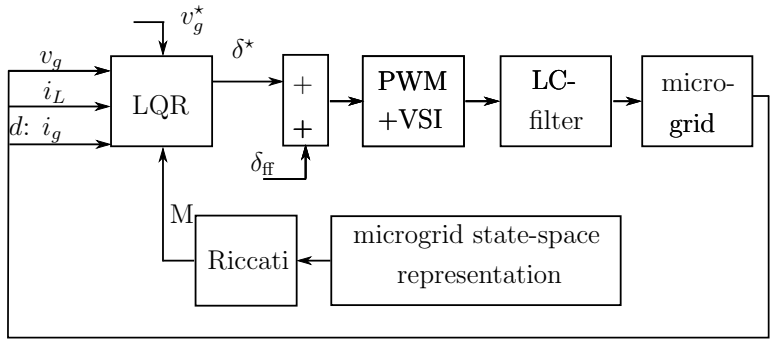

Figure A.3: LQR, control scheme

following state feedback law is presented:

$$U_k = -(R + B^{\star T} M B^{\star -1}) B^{\star T} (M A^\star X_k + M d + r) \\ = -K X_k - K'(M d + r), \quad \text{(A.37)}$$

with r an auxiliary variable depending on $A^\star$, $B^\star$, M, R, G and d; and M the solution of the algebraic Riccati-equation:

$$M = A^{\star T} M A^\star - A^{\star T} M B^\star (R + B^{\star T} M B^\star)^{-1} B^{\star T} M A^\star + Q. \quad \text{(A.38)}$$

As the system state is not controlled to zero, but v_{g} is controlled to $v_{\text{g}}^\star$, also this set value is included in the LQR controller as shown in Fig. A.3. Therefore, the state variable X_k in the cost function J of (A.36) is replaced by $X_k - X_{\text{k,ref}}$. The output U_{k} of the LQR in (A.37) now becomes $U_{\text{k,ref}} - K(X_k - X_{\text{k,ref}})$, with $U_{\text{k,ref}}$ derived from the feed-forward component δ_{ff}.

One of the disadvantages of LQR is the computational burden in finding an analytical solution of the Riccati equation, but this can be done off-line. An advantage of the LQR, is that the control is optimal with respect to the operating cost of the system. The standard LQR is inherently robust, which is derived from Nyquist as the phase margin is larger than $\pi/3$ and the gain margin is two. This is an important feature for the microgrid application. However, it should be noted that stability can only theoretically be guaranteed if the used model is in good agreement with the reality. The usage of observers or the occurrence of measurement error and the value of the maximal switching frequency of the VSI can affect this. Furthermore, this regulator requires a control-oriented modelling of the system. If a mismatch due to model inaccuracy, system changes or non-linearities occurs, the resulting controller can degrade. Therefore, also the robustness to parameter variations is

studied further in this paragraph. In this field, also adaptability can be studied, by adaptive LQ controllers. However, in this case, an on-line calculation concerning Riccati needs to be introduced, which is here avoided for the simplicity of the microgrid controllers.

A.4 Fuzzy Logic Controller

A disadvantage of PI and PID controllers is that they are fixed-gain feedback-controllers. Therefore, they cannot adapt to variations of the system parameters and also, the system modelling and the controller parameter tuning have to be done before implementing the controller. To have a controller that is well-tuned for a whole range of operating points without retuning the controller for different operating conditions, a fuzzy logic control system analogous to [245] is studied, which does not need a system model. In general, fuzzy logic does not require precise, noise-free inputs, is inherently robust and can control nonlinear systems that would be difficult to model.
A fuzzy control is a control based on rules rather than on mathematical equations and system models, which is advantageous for microgrid applications in limiting the computational burden and dependency on a system model. The controller is composed of three parts: fuzzification, calculation of the rule matrix membership degree and defuzzification. The error e and rate-of-change-of-error de are considered and divided into seven subsets: from negative big (nb) over zero (zr) to positive big (pb) as shown in Table A.1. During fuzzification, the measured values of e and de are associated with a weighting factor for each of the seven fuzzy subsets. Triangular membership functions as in Fig. A.4 are selected for these subsets. Here, the e-vector is derived by fuzzification of $er(k) = v_{\mathrm{g,ref}}(k) - v_{\mathrm{g}}(k)$. The nb value is chosen as -100, pb as +100, $zr = 0$, and analogous for the values inbetween. For example, if $er \leq$-100, $e = [1\ 0\ 0\ 0\ 0\ 0\ 0]$, if $er =$ -66: $e = [0\ 1\ 0\ 0\ 0\ 0\ 0]$ and if er is between -66 and -100: e becomes

$$[\frac{-er-66}{100-66}\ \frac{100+er}{100-66}\ 0\ 0\ 0\ 0\ 0]. \tag{A.39}$$

The de-vector is derived analogously, now with $er(k) = [v_{\mathrm{g,ref}}(k) - v_{\mathrm{g}}(k)] - [v_{\mathrm{g,ref}}(k-1) - v_{\mathrm{g}}(k-1)]$ and the pb value is here 10. After fuzzification, the rule matrix R of Table A.1 is formed, where the (i-j)-th element equals min(e_i,de_j). Further, the root-sum-square (RSS) method for defuzzification is applied to the rule matrix in order to determine the degree of membership for the output nb to pb, for example for the degree of membership of nm (D_{nm}):

$$D_{\mathrm{nm}} = \sqrt{R(1,5)^2 + R(2,4)^2 + R(3,3)^2 + R(4,2)^2 + R(5,1)^2} \tag{A.40}$$

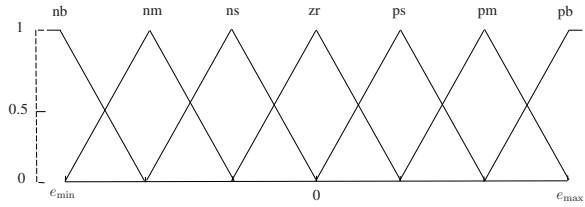

Figure A.4: Fuzzy Logic: membership functions e and de

Table A.1: Fuzzy Logic: Rule matrix with seven fuzzy subsets

e	de						
	nb	nm	ns	zr	ps	pm	pb
nb	nb	nb	nb	nb	nm	ns	zr
nm	nb	nb	nb	nm	ns	zr	ps
ns	nb	nb	nm	ns	zr	ps	pm
zr	nb	nm	ns	zr	ps	pm	pb
ps	nm	ns	zr	ps	pm	pb	pb
pm	ns	zr	ps	pm	pb	pb	pb
pb	zr	ps	pm	pb	pb	pb	pb

Finally, summation of these values with their respective degree of membership (given below) gives the input duty ratio $\delta^\star$ of the VSI with PWM:

$$\delta^\star = -1 \cdot D_{\mathrm{nb}} + \frac{-2}{3} \cdot D_{\mathrm{nm}} + \frac{-1}{3} \cdot D_{\mathrm{ns}} + 0 \cdot D_{\mathrm{zr}} + \frac{1}{3} \cdot D_{\mathrm{ps}} + \frac{2}{3} \cdot D_{\mathrm{pm}} + 1 \cdot D_{\mathrm{pb}} \quad \text{(A.41)}$$

An advantage of the fuzzy logic technique for microgrid voltage control is that it can easily be implemented as an offline pre-calculated lookup table. More computational burden is needed than for the hysteresis controller, but less compared to the other control strategies described in this chapter. Furthermore, no model is required for controller tuning, but the performance still depends on the knowledge and expertise of the designer in determining the fuzzy subsets nb to pb values of e, de and the membership degrees to calculate $\delta\star$.

A.5 Comparison of the regulators

In the following, the regulators are simulated and compared. According to the previous paragraphs, the controllers are tuned following current best-practice meth-

ods. From the previous paragraphs, it can be concluded that the controllers differ significantly in ease of implementation and computational burden. The hysteresis controller can easily be implemented and does not require complex computational effort or model knowledge. The fuzzy logic controller has also a reduced design complexity as no model is required, but here, some expertise is required to determine the fuzzy subsets. PI and PID controllers are rather easy to implement, but need parameter tuning and model knowledge. The computational burden of sliding-mode and LQR controllers is higher as more equations are to be solved. For the LQR, the nonlinear Riccati equation needs to be solved.
In [142], several current-control techniques for active power filters are compared. It is concluded that as the performances of all the studied controllers is rather similar, the best solution should strongly be influenced by the ease of implementation and the execution time. This further illustrates the advantages of the fuzzy logic, hysteresis and PI(D) controllers over the others. In [142], the steady-state and transient performance are considered, and here, this strategy will also be followed. Also, the robustness of the controllers, which is very important in microgrid applications, will be analysed.
The controllers are compared under different microgrid configurations, with the emphasis on the tracking performance and robustness. For these simulations, Matlab Simulink is used. First, the controllers step responses are studied, and next, the steady-state performance, transient performance and the noise sensitivity. Finally, a dynamic profile is given for checking the parameter sensitivity. As stated above, the power controller to determine the reference values of the grid voltage (frequency and amplitude) is not considered. As the focus is on the voltage control loop, the reference values are chosen in advance. The dc-bus voltage V_{dc} equals 400 V. In the simulations, the sampling frequency is 10 kHz. In general, increasing this sampling frequency can improve the controllers, but with higher VSI switching losses.

A.5.1 Step response

First, the voltage set value follows a step function that turns on from 0 to $230\sqrt{2} = 325$ V at a time $t = 20$ ms. The microgrid load consists of a resistive load R of 25 Ω in series with a line resistance R_l of 0.33 Ω, which is realistic in the low-voltage microgrid application.
In Fig. A.5, the step responses of the cascaded PI controllers, the direct PID controller and the hysteresis controller are compared. The cascaded controller shows a good tracking performance, but with some overshoot. The direct controller on the other hand has a slower response, also some overshoot and even a small tracking error, which is caused by the lack of system information. The direct controller controls the grid voltage under the assumption that the grid current i_{g} is zero. From

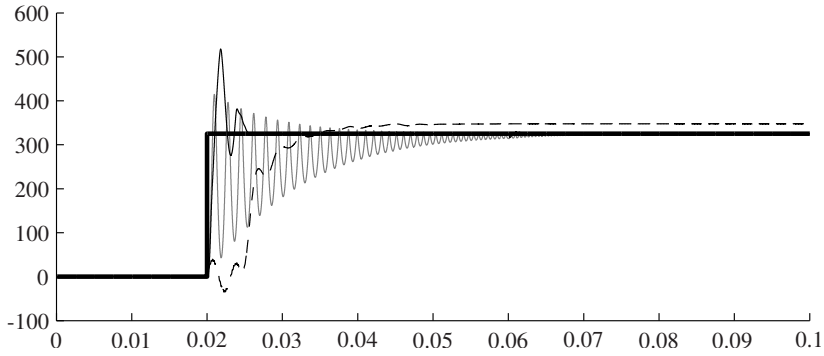

Figure A.5: Step response: grid voltage v_g with its reference value (━━ = desired, — = cascaded control strategy, ---- = direct control strategy, — = hysteresis control)

this, it can already be concluded that this lack of system information causes a deteriorated tracking performance. This illustrates the importance of the inner current control loop, where the cascaded control strategy is based upon. The hysteresis controller shows a good tracking performance but with oscillations and therefore, a larger settling-time. This was expected because of the simplicity of the controller that does not require a model. In general, these controllers show a promising performance as in the practical microgrid the voltage changes are much smaller.

In Fig. A.6, a comparison of the step responses of the cascaded, LQR, fuzzy logic and sliding-mode controllers is shown. Note the smaller simulation time in this figure as compared with Fig. A.5. These controllers show a better step response than the direct and hysteresis controllers. Especially, the LQR and sliding-mode control strategies obtain a smaller overshoot, rise time and settling time. The fuzzy logic controller also shows a good step response, even without the need for a system model.

As the microgrid does not operate in dc, comparison of the settling time, overshoot, rise time and tracking error is not sufficient for comparison and verification of the validity of the controllers. Furthermore, some controllers mentioned above are nonlinear controllers. For linear systems and linear controllers, standardised quality measures exist since the linearity makes it sufficient to check some cases and all possible behaviours of the regulated system are known as a linear combination of these basic cases. For nonlinear systems on the other hand, this is not possible.

Therefore, some possible worst-case options are studied. For example, as the controllers are applied for microgrid voltage control, it is not necessary to change the microgrid load with 100% as one single VSI is not burdened with the overall microgrid control. Also, the voltage and parameter changes can also be assumed to

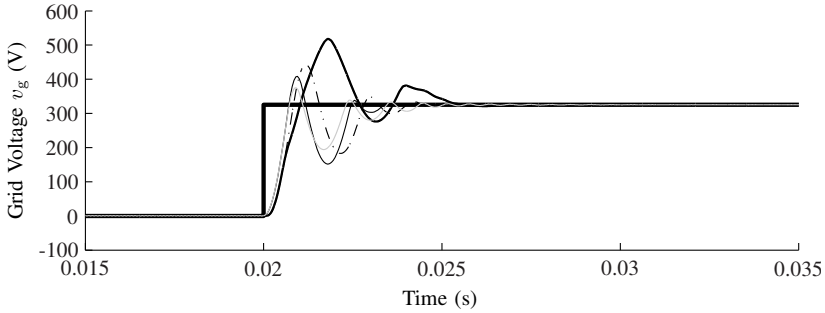

Figure A.6: Step response: grid voltage v_g with its reference value (━━ = desired, ── = cascaded control, -·-·-· = fuzzy logic control, ┄┄ = LQR, ── = sliding-mode control)

stay under the microgrid limits, e.g., the microgrid voltage should remain between -10% and +10% of the nominal voltage. The voltage limiting in microgrids is usually provided by power changes of the distributed generators, demand-side management, control of the storage elements and protective measures. Also, changes of the (filter) parameters can be assumed small, as good microgrid control assumes proper maintenance and parameter identification.

A.5.2 Sinusoidal response

In this simulation, the microgrid configuration is not changed, but the grid voltage set value is sinusoidal with 230 V rms value and 50 Hz frequency. The different $v_g(t)$ trajectories are compared in Fig. A.7.

In Fig. A.7(a), simulations are shown for the hysteresis control strategy. A zero phase error is obtained when considering a full period. The output voltage ripple is higher than the window of the hysteresis comparator, this is due to the discrete-time control, introducing delays [246]. The oscillations of the obtained voltage around the desired one were also shown in the step response and could be reduced by reducing the hysteresis band, but then, the switching losses would increase. The main disadvantage is the varying switching frequency and a somewhat rough operation. In [242], hysteresis and PI controllers are also compared in active filter applications, where, for this purpose, the hysteresis controller was superior. This was mainly due to the limitation of achievable regulator bandwidth for PI controllers.

The simulation results for the direct controller are depicted in Fig. A.7(b). A relatively good voltage tracking is obtained, but a small tracking error is shown. This amplitude error was also shown in the step response of this controller. As mentioned above, this is due to the lack of system information as compared with the

cascaded controllers.
From Fig. A.7(c), it follows that a good voltage tracking is obtained by using the cascaded controllers. The phase difference between the obtained and the desired grid voltage as well as the amplitude error are negligible. A small tracking error is inherent to the control of ac-values with PI controllers. Thanks to the feed-forward term included in the cascaded control algorithm, the cascaded control loops and the low frequency of the set value compared with the bandwidth of the controller, this error is however negligible in the application of microgrid voltage control. Also, resonant controllers[1] can be used and the results of Fig. A.7(c) are similar to this.
From the sliding-mode control depicted in Fig. A.7(d), a good voltage tracking with a phase error is concluded. This error is still very small, certainly if the choice of a very small scope in Fig. A.7(d) is taken into account.
The LQR control is depicted in Fig. A.7(e). In conclusion, in this control method, a higher amplitude error is obtained, but the voltage tracking performance and phase error are still good.
The voltage tracking with the fuzzy logic controller has a high quality as is depicted in Fig. A.7(f).
For comparison of the performances of the controllers, a performance indicator PerI, with

$$\mathrm{PerI} = \frac{1}{K} \frac{\sqrt{\sum_{k=k_0}^{k_0+K} (v_{\mathrm{g}}(k) - v_{\mathrm{g,ref}}(k))^2}}{230\sqrt{2}\mathrm{V}} \tag{A.42}$$

is proposed, determining the rms value of the error and here, k_0 denotes the time $t = t_0 = 0.045$ s and K corresponds with one fundamental period of 0.02 s. PerI is calculated for the different control strategies and this is summarised in Table A.2. All the control strategies have a PerI in the same order of magnitude, except the cascaded and the fuzzy logic controllers. Therefore, the performances of the controllers are similar, with a very low PerI, and thus a very good tracking performance for the cascaded control and the fuzzy logic control. The PerI of the sliding-mode control is higher due to the small phase lag. The PerI of the LQR is slightly lower as compared to the sliding-mode as the tracking error is mainly present in the peak values and not in the overall period.

A.5.3 Transient response: load change

While the steady-state performance of the studied controllers is similar, the transient performance can differ. Therefore, also the robustness to changing conditions of the studied grid is faced. A load change in the microgrid is studied. In the first

[1] Resonant controllers are equivalent to PI controllers, but achieve zero steady-state error at selected frequencies

Table A.2: Performance indicator (PerI) of the controllers: sinusoidal response

control strategy	PerI ($*10^{-4}$)
hysteresis control	2.3218
direct control	1.6716
cascaded control	0.0995
sliding-mode control	5.3120
LQR control	2.5343
fuzzy logic control	0.4863

0.06 s, the load equals the previous load of 25 Ω. After 0.06 s, a second resistance of 25 Ω switches on in parallel, meaning that the overall load resistance halves. The predefined grid voltage set-value remains unchanged.

The voltage transient with the hysteresis controller is negligible, and a good tracking performance is obtained under both conditions of load resistance. The transient is almost invisible in Fig. A.8(a). From this section and [143], it is concluded that the main advantages of the hysteresis controller compared to, e.g., the PI(D) controllers, are simplicity and independence of parameter changes.
The simulation results from the direct control are shown in Fig. A.8(b). A good voltage tracking with a small amplitude and phase difference between the reference and the obtained value of the grid voltage and a small transient are shown. Even here, with a 50% change of load, the transient does not induce stability problems as the voltage is quickly restored.
For the cascaded control, a good voltage tracking with a small transient is shown in Fig. A.8(c). A slightly better tracking performance than in the case of the direct controller is obtained, which is mainly achieved by the inner CCL.
The simulation results of the sliding-mode controller are depicted in Fig. A.8(d). The simulations show a good voltage tracking performance under variable load. The transient phenomenon shows some small, very quickly damped oscillations and the reaction quality to load change is comparable with the cascaded control strategy.
From the LQR control depicted in Fig. A.8(e), the transient behaviour is comparable with the cascaded control, but the error is larger, equivalently to Fig. A.7(e).
With the fuzzy logic control, a small transient is depicted in Fig. A.8(f). A good tracking performance is obtained without the necessity of a model of the system. The overall performance of the cascaded control is better, but a system model is crucial for tuning the PI controllers properly.
This chapter focusses on the most widely known control strategies, with the em-

phasis on simple and robust controllers that can be implemented in small distributed energy sources. Overall, for this changing microgrid configuration, possible further improvements could be made by including adaptive controllers. Adaptive control can be implemented to try to automate the whole tuning procedure of the controllers (self-tuning regulators) or to make it adaptive for time-varying system parameters. An adaptive regulator is inherently nonlinear and is more complicated than a fixed-gain regulator (requiring an on-line estimation of the time-varying parameters). In [233], it is stated that there are many cases in which a constant gain feedback can do as well as an adaptive regulator. In the microgrid, the cascaded control, for example, already provides good results, can cope well with the variation in system dynamics and can be implemented more easily. Therefore, here, adaptive controllers are not considered.

A.5.4 Noise sensitivity

The direct, hysteresis and fuzzy logic control strategies have the advantage that their robustness to measurement error or noise in the current i_{L} is infinite, because they do not depend on i_{L} as no measurements or estimations of this current are necessary. The cascaded, sliding-mode and LQR regulators on the other hand, depend on this measurement, but give sufficient robustness to i_{L}. In this paragraph, the noise sensitivity in v_{g} is studied by means of a white-noise error added to the measurement of v_{g}. This noise is a band-limited normally distributed noise with a maximum value of 15 V, which can be a very large measurement noise. In the next simulation, the load consists of the previous resistive load of 25 Ω.
The hysteresis control strategy of Fig. A.9(a) shows a low robustness to noise if compared with the other controllers. Large oscillations around the voltage set value are depicted.
The simulation results of the direct controller are shown in Fig. A.9(b). In this simulation, the voltage tracking performance is low. This is caused by the lack of the inner CCL loop, resulting in a controller that depends on the measurements of v_{g} only. Furthermore, the derivative term in the PID controller can give an amplification of the measurement noise. Therefore, the gain of the derivative can be limited according to [233].
The simulation results of the cascaded control are depicted in Fig. A.9(c). This control strategy shows a good tracking performance and low noise sensitivity as the difference between v_{g} and $v_{\mathrm{g}}^{\star}$ remains very small.
The simulation results of the sliding-mode controller in Fig. A.9(d) show that this controller is robust as the controller remains stable and the obtained oscillations are limited.
The LQR control depicted in Fig. A.9(e) shows low noise sensitivity as a small error between v_{g} and $v_{\mathrm{g,ref}}$ is obtained, but this error is larger compared with the

Table A.3: Performance indicator (PerI) of the controllers: noise sensitivity

control strategy	PerI ($*10^{-4}$)
hysteresis control	7.526
direct control	9.993
cascaded control	0.6697
sliding-mode control	10.69
LQR control	4.094
fuzzy logic control	1.859

cascaded controller.
From Fig. A.9(f), a good noise sensitivity of the fuzzy logic controller is concluded, even without the need for a model to tune this controller.
The fuzzy logic, LQR and cascaded controllers obtain the best voltage tracking performance under measurement inaccuracy. The noise sensitivity of all controllers can also be improved by using external measures, such as by including a well-tuned low-pass filter (LPF) before each measurement. This leads to the disadvantage of introducing a phase-lag, which should be compensated for. This LPF is omitted in the simulation of the noise sensitivity in order to make a good comparison between the controllers.
The PerI is also calculated in table A.3, the best PerIs are obtained by the cascaded control, LQR control and fuzzy logic control. Higher PerIs are calculated for the hysteresis control, direct control and sliding-mode control, the latter has a higher PerI as compared with the hysteresis controller due to the small phase lag occurring over the entire period.

A.5.5 Dynamic profile and parameter sensitivity

For the controllers with the best overall performance in this microgrid application, the cascaded, LQR and fuzzy logic controllers, a dynamic profile is implemented. It is interesting to study the robustness of the microgrid system to perturbations that may be introduced because of component tolerances.
Therefore, in the following simulations, the real filter capacitance is half the capacitance upon which the controllers are tuned. The implications are twofold. First, with this simulation, the robustness to parameter variation with a mistuned controller can be studied. Secondly, a lower filter capacitor indicates higher grid voltage changes, which is also disadvantageous for the voltage tracking and the overall grid stability.
Furthermore, at a time $t = 15$ ms, the microgrid load resistance halves analog-

ous as in § A.5.3 and at $t = 35$ ms, the grid voltage's set-value decreases with 100 V. The latter is a very high voltage change, which will not occur in realistic grid applications. In this way, a very high transient can be studied. Also, a longer simulation time is shown in Fig. A.10.
From Fig. A.10, it is concluded that these controllers show a good robustness to parameter variations as, despite the large parameter inaccuracy of 50%, still good tracking performance is obtained. Under the load change, the controllers show a very small, quickly-damped transient that is almost invisible in Fig. A.10. Also, after the 100 V change of set-value, the tracking is quickly restored. The LQR and fuzzy logic controllers show the smallest transient. In [143], fuzzy logic self-tuned PI controllers are compared with conventional PI controllers, where it is also shown that the transient overshoots can be reduced by implementing fuzzy logic. Note that also for the cascaded controllers, the tracking is sufficient as a 100 V change of set value is not tolerable in microgrids.

A.5.6 Summary and conclusions

In this paragraph, the grid voltage control is studied under different loads, transient effects, noise and other disturbances for six different control strategies. Furthermore, the principles, advantages and limitations of the controllers have been examined and a comparison of the design complexity has been made.
The implemented sliding-mode regulator has the advantage that an easy retuning is possible under changed filter parameters by adjusting the state matrices. A disadvantage of this controller is the presence of a small phase-lag between the desired and obtained grid voltage v_{g}.
The direct controller does not require an inner current control loop, hence does not depend on measurements or estimations of i_{g}. Some disadvantages of this regulator are the high noise sensitivity, the necessity of tuning a PID regulator and the lower system knowledge as i_g is unknown.
For more system knowledge, the cascaded control uses both an inner current and an outer voltage control loop. Therefore, a disadvantage is that two PI controllers (or at least a PI-P combination) need to be tuned, requiring a system model. An advantage is its good voltage tracking, overall good performance and also, usage of well-known PI controllers. However, the controllers are tuned under a particular operating condition and need to be designed to guarantee fast and stable voltage regulation under different microgrid configurations. It is shown that they show low noise and parameter sensitivity, if well-tuned.
The LQR configuration shows sufficiently good tracking performance and has the same advantages in retuning as the sliding-mode controller. Another advantage of LQR is that no inner current control loop needs to be implemented and still, a good performance is obtained. The noise and parameter sensitivity of LQR is better than

for the implemented hysteresis, direct and sliding-mode controllers, and comparable with the fuzzy logic and the cascaded control.
The hysteresis and fuzzy logic controllers show good tracking performance without the need for a model, hence the control is not distorted by model inaccuracy and parameter variations. This is an important advantage of these controllers. Furthermore, next to the good tracking performance of the fuzzy logic controller, its noise and parameter sensitivity is very good. However, it is noted that although no model is required, the fuzzy subsets have to be selected for the control. This requires some degree of system knowledge in advance and mostly needs an iterative process of retuning these values.

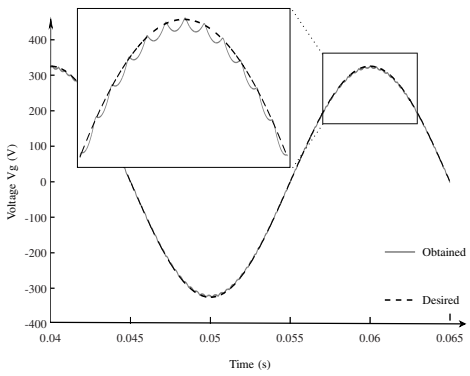

(a) Hysteresis control

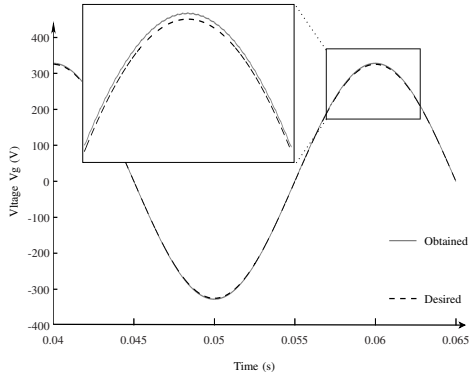

(b) Direct control

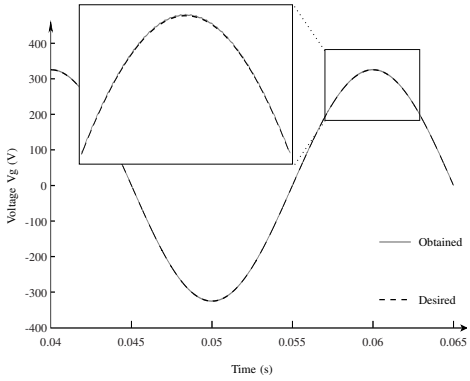

(c) Cascaded control

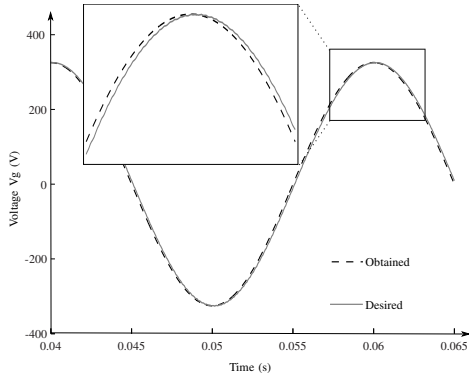

(d) Sliding-mode control

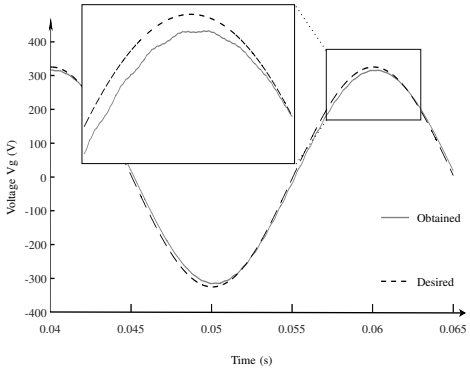

(e) LQR control

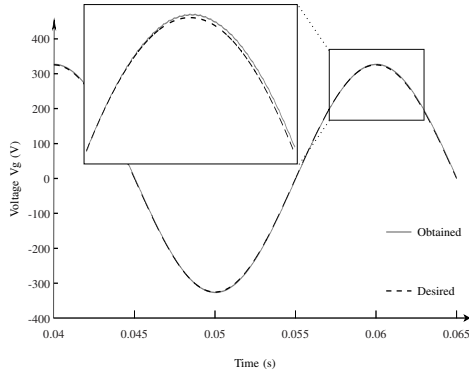

(f) Fuzzy logic control

Figure A.7: Resistive load: grid voltage v_g with its reference value

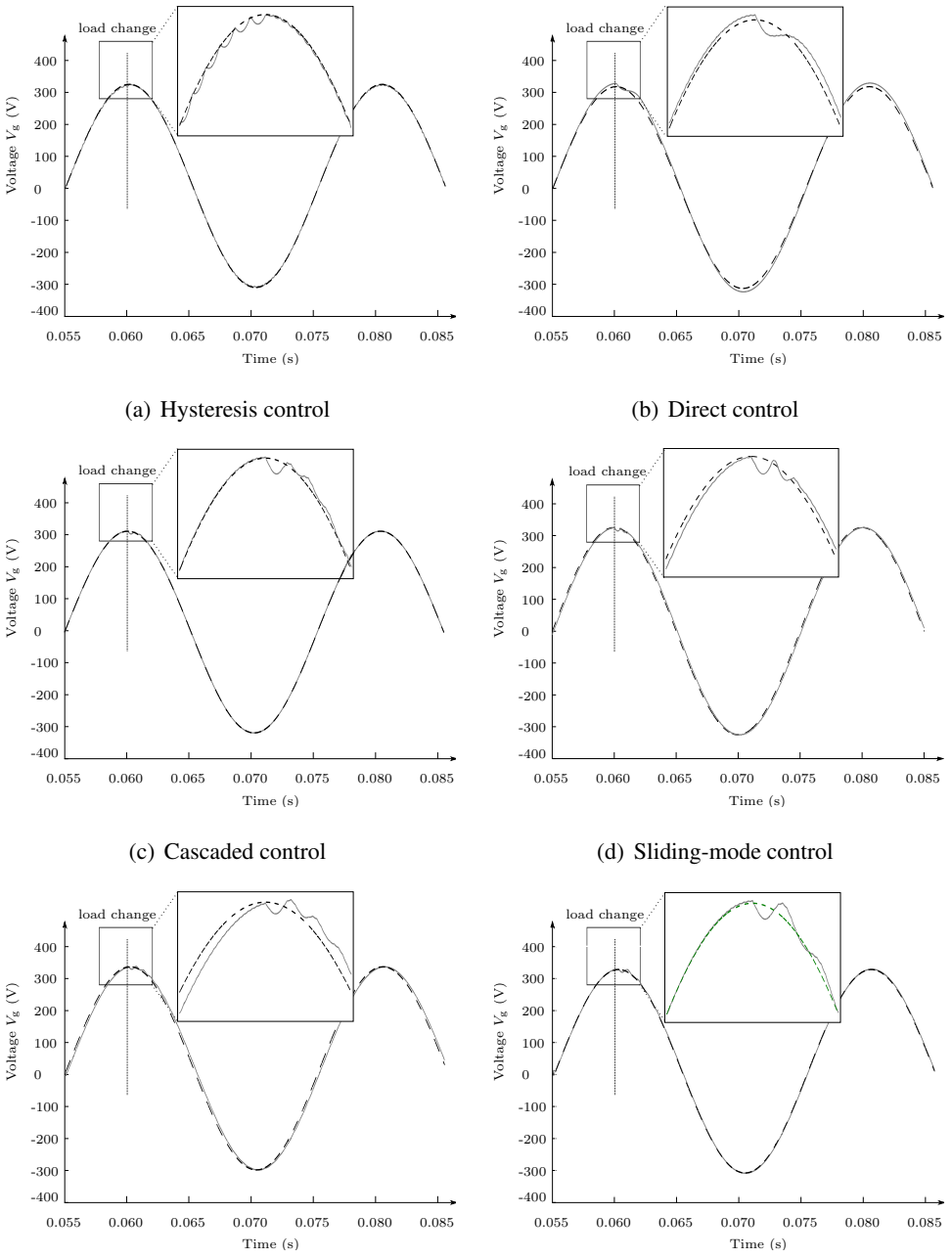

(a) Hysteresis control

(b) Direct control

(c) Cascaded control

(d) Sliding-mode control

(e) LQR control

(f) Fuzzy logic control

*Figure A.8: Load change: grid voltage v_g with its reference value (**----** = desired, — = obtained)*

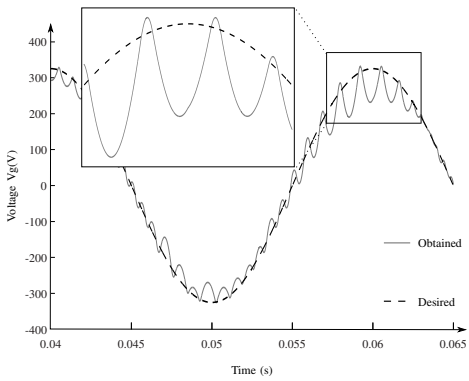

(a) Hysteresis control

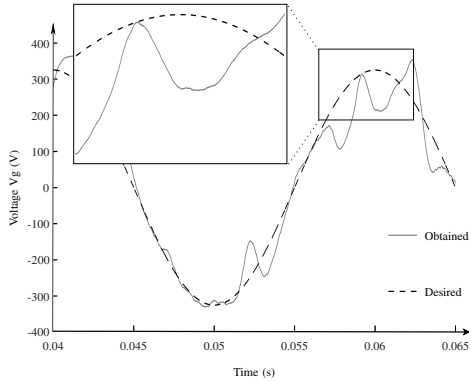

(b) Direct control

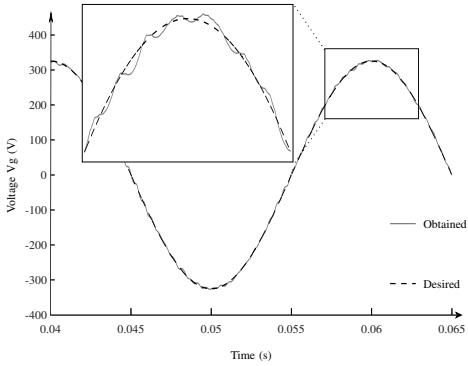

(c) Cascaded control

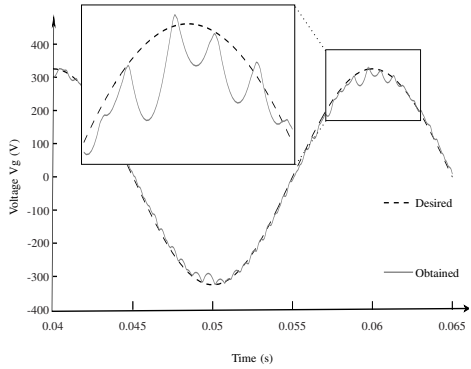

(d) Sliding-mode control

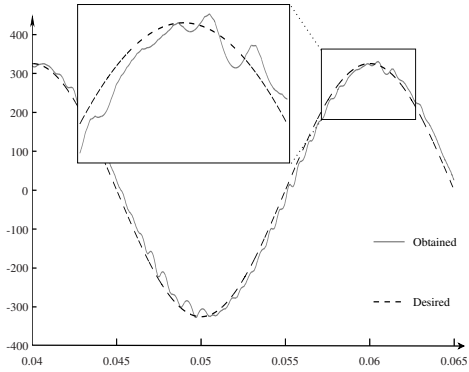

(e) LQR control

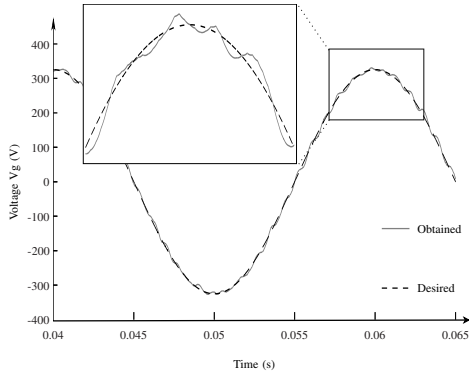

(f) Fuzzy logic control

Figure A.9: Measurement inaccuracy: grid voltage v_g with its reference value

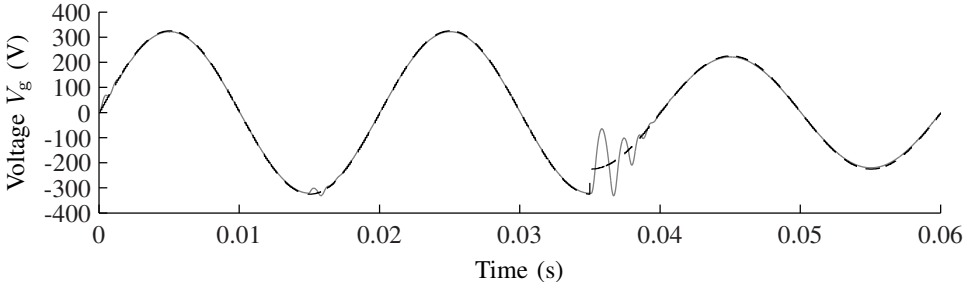

(a) Cascaded control

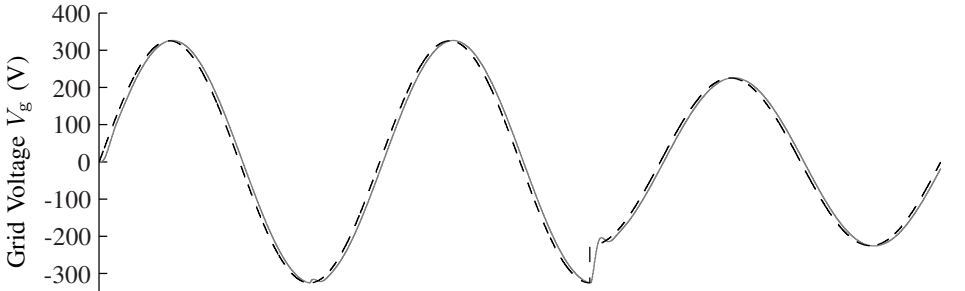

(b) LQR control

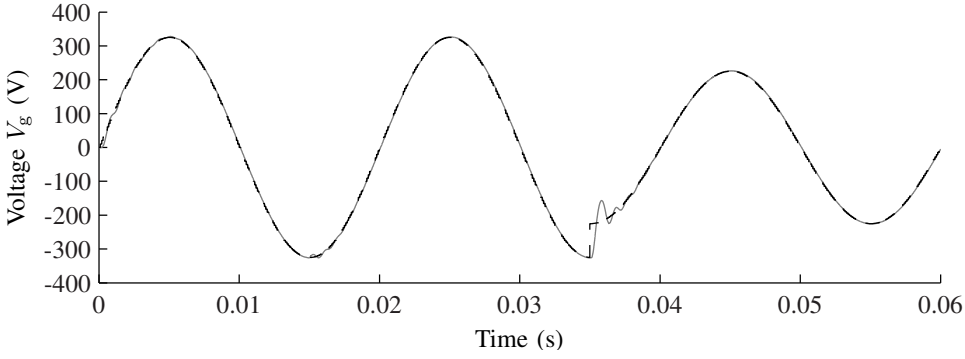

(c) Fuzzy Logic control

Figure A.10: Dynamic profile: grid voltage v_g with its reference value (---- = desired, — = obtained)

Bibliography

[1] N. Jenkins, R. Allan, P. Crossley, D. Kirschen, and G. Strbac, *Embedded Generation*, ser. IEE Power and Energy systems. The Institution of Electrical Engineers, Oct. 2000, vol. 31.

[2] A. F. Zobaa and C. Cecati, "A comprehensive review on distributed power generation," in *International Symposium on Power Electronics, Electrical Drives, automation and motion (SPEEDAM)*, Ischia, Italy, Jun. 11-13, 2008.

[3] W. Schellong, "Integrated energy management in distributed systems," in *International Symposium on Power Electronics, Electrical Drives, automation and motion (SPEEDAM)*, Ischia, Italy, Jun. 11-13, 2008.

[4] S. Barsali, M. Ceraolo, P. Pelacchi, and D. Poli, "Control techniques of dispersed generators to improve the continuity of electricity supply," in *Proc. IEEE PES Winter Meeting*, 2002, pp. 789–794.

[5] I. A. Hiskens and E. M. Fleming, "Control of inverter-connected sources in autonomous microgrids," in *American Control Conf.*, June 11-13, 2008, pp. 586–596.

[6] K. Iniewski, Ed., *Smart Grid Infrastructure & Networking*. McGraw-Hill Professional, 2012.

[7] European Commission. (2003) New ERA for electricity in Europe. Distributed generation: Key issues, challenges and proposed solutions.

[8] European Technology Platform Smart Grids. (2012, Mar.) Strategic research agenda: Smartgrids SRA 2035.

[9] P. Arboleya, D. Diaz., J. M. Guerrero, P. Garcia, F. Briz, C. Gonzalez-Moran, and J. G. Aleisxandre, "An improved control scheme based in droop characteristic for microgrid converters," *Electric Power Systems Research*, vol. 80, no. 10, pp. 1215 – 1221, Oct. 2010.

[10] Y. Mohamed and E. F. El-Saadany, "Adaptive decentralized droop controller to preserve power sharing stability for paralleled inverters in distributed generation microgrids," *IEEE Trans. Power Electron.*, vol. 23, no. 6, pp. 2806–2816, Nov. 2008.

[11] N. R. E. C. Association, "White paper on distributed generation," Aug. 2007.

[12] A. Piccolo and P. Siano, "Evaluating the impact of network investment deferral on distributed generation expansion," *IEEE Trans. Power Syst.*, vol. 24, no. 3, pp. 1559–1567, Aug. 2009.

[13] P. P. Barker and R. W. D. Mello, "Determining the impact of distributed generation on power systems. i. radial distribution systems," in *IEEE Power Engineering Society Summer Meeting*, vol. 3, Seattle, WA, 2000, pp. 1645 – 1656.

[14] T.-L. Lee and P.-T. Cheng, "Design of a new cooperative harmonic filtering strategy for distributed generation interface converters in an islanding network," *IEEE Trans. Power Electron.*, vol. 2, no. 5, pp. 1919–1927, Jul. 2007.

[15] M. Marwali, J.-W. Jung, and A. Keyhani, "Control of distributed generation systems – part II: Load sharing control," *IEEE Trans. Power Electron.*, vol. 19, no. 6, pp. 1551–1561, Nov. 2004.

[16] M. N. Marwali, J.-W. Jung, and A. Keyhani, "Stability analysis of load sharing control for distributed generation systems," *IEEE Trans. Energy Convers.*, vol. 22, no. 3, Sep. 2007.

[17] M. Prodanović, "Power quality and control aspects of parallel connected inverters in distributed generation," Ph.D. dissertation, University of London, Imperial College, 2004.

[18] R. H. Lasseter and P. Paigi, "Microgrid: A conceptual solution," in *Proc. IEEE Power Electron. Spec. Conf. (PESC 2004)*, Aachen, Germany, 2004.

[19] R. H. Lasseter and P. Piagi, "Control and design of microgrid components," Power Systems Engineering Research Center (PSERC), Tech. Rep., Jan. 2006.

[20] R. Lasseter, "Microgrids and distributed generation," *Journal of Energy Engineering*, vol. 133, no. 3, pp. 144–149, Sep. 2007.

[21] M. Ciobotaru, F. Iov, Y. Fan, S. Bifaretti, and P. Zanchetta, "Report on control strategies: advanced power converters for universal and flexible power

management in future electricity network (uniflex-pm)," Aalborg University and University of Nottingham, Tech. Rep., 2008.

[22] M. H. J. Bollen and F. Hassan, *Integration of Distributed Generation in the Power System*, ser. IEEE Press Series on Power Engineering. John Wiley & Sons, 2011.

[23] B. M. Weedy and B. J. Cory, *Electric Power Systems*. Wiley, 1998.

[24] M. Gauthier, C. Abbey, F. Katiraei, J.-L. Pepin, M. Plamondon, and G. Simard, "Planned islanding as a distribution system operator tool for reliability enhancement," in 19^{th} *International Conference on Electricity Distribution*, Vienna, May 21-24, 2007.

[25] S. M. Amin and B. F. Wollenberg, "Toward a smart grid," in *IEEE Power & Energy Magazine*, Sep./Oct. 2005, vol. 3, no. 5, pp. 34–41.

[26] R. Cossent, L. Olmos, T. Gómez, C. Mateo, F. Niewenhout, and O. Özdemir (IMPROGRES report). (2010, Mar.) The role of alternative network response options in minimising the costs of DG integration into power networks. [Online]. Available: www.improgres.org

[27] J. A. Peças Lopes, N. Hatziargyriou, J. Mutale, P. Djapic, and N. Jenkins, "Integrating distributed generation into electric power systems: A review of drivers, challenges and opportunities," *Electric Power Systems Research*, vol. 77, pp. 1189–1203, 2007.

[28] C. W. Gellings, *The Smart grid, enabling energy efficiency and demand response*. The Fairmont Press, 2009.

[29] M. K. an V. Vittal, S. Meliopoulos, and T. Mount, "The big picture," in *IEEE Power & Energy Magazine*, July/Aug. 2012, vol. 10, no. 4, pp. 22–34.

[30] G. Strbac, "Demand side management: Benefits and challenges," *Energy Policy*, vol. 36, pp. 4419–4426, 2008.

[31] R. N. Boisvert, P. A. Cappers, and B. Neenan, "The benefits of customer participation in wholesale electricity markets," *Electricity Journal*, vol. 15, no. 3, pp. 41–51, Apr. 2002.

[32] E-Energy. (2012) Smart energy made in germany - interim results of the E-Energy pilot projects towards the internet of energy. [Online]. Available: /www.e-energy.de

[33] H. Farhangi, "The path of the smart grid," in *IEEE Power & Energy Magazine*, Jan./Feb. 2010, vol. 8, no. 1, pp. 18–28.

[34] Siemens. (2011) Repair and retrofit - new life for aged transformers. [Online]. Available: www.siemens.com/energy

[35] A. Battaglini, J. Lilliestam, C. Bals, and A. Haas. (2008, June 18,) The SuperSmart Grid, European Climate Forum (ECF). [Online]. Available: www.supersmartgrid.net

[36] DNV KEMA, "Global ineventory and analysis of smart grid demonstration projects," Netbeheer Nederland, Tech. Rep., Oct. 22, 2012.

[37] R. H. Lasseter, A. Akhil, C. Marnay, J. Stephens, J. Dagle, R. Guttromson, A. Meliopoulous, R. Yinger, and J. Eto, "The CERTS microgrid concept, white paper on integration of distributed energy resources," in *California Energy Commission, Office of Power Technologies - U.S. Department of Energy, LBNL-50829, http://certs.lbl.gov*, Apr. 2002.

[38] R. H. Lasseter, J. H. Eto, B. Schenkman, J. Stevens, H. Vollkommer, D. Klapp, E. Linton, H. Hurtado, and J. Roy, "CERTS microgrid laboratory test bed," *IEEE Trans. Power Del.*, vol. 26, no. 1, pp. 325–332, Jan. 2011.

[39] M. Popov, H. Karimi, H. Nikkhajoei, and V. Terzija, "Modeling, control and islanding detection of microgrids with passive loads," in *14th Internat. Power Electronics and Motion Control Conf. (EPE/PEMC)*, Ohrid, Republic of Macedonia, Sept. 6-8, 2010.

[40] A. Engler, O. Osika, M. Barnes, N. Jenkins, and A. Arulampalam, *DB1 Local Micro Source controller strategies and algorithms*. www.microgrids.eu/micro2000, European Commission, Feb. 2004.

[41] J. Driesen and F. Katiraei, "Design for distributed energy resources: Microgrid planning and architectures for improved reliability and integration," *IEEE Power & Energy Magazine*, vol. 6, no. 3, pp. 30–40, May/June 2008.

[42] Y. W. Li and C. N. Kao, "An accurate power control strategy for power electronics interfaced distributed generation units operating in a low voltage multibus microgrid," *IEEE Trans. Power Electron.*, vol. 24, no. 12, pp. 2977–2988, Dec. 2009.

[43] M. Bollen, J. Zhong, O. Samuelsson, and J. Björnstedt, "Performance indicators for microgrids during grid-connected and island operation," in *Proc. IEEE Power Tech. Conf.*, Bucharest, Romania, June 28 - July 2, 2009.

[44] A. Vaccaro, M. Popov, D. Villacci, and V. Terzija, "An integrated framework for smart microgrids modeling, monitoring, control, communication, and verification," *Proc. IEEE*, vol. 99, no. 1, pp. 119 – 132, Jan. 2010.

[45] N. Pogaku, M. Prodanović, and T. C. Green, "Modeling, analysis and testing of autonomous operation of an inverter-based microgrid," *IEEE Trans. Power Electron.*, vol. 22, no. 2, pp. 613–625, Mar. 2007.

[46] M. A. Pedrasa and T. Spooner, "A survey of techniques used to control microgrid generation and storage during island operation," in *Australian Universities Power Engineering Conf. (AUPEC2006)*, Dec. 10-13, 2006.

[47] I.-K. Song, K.-D. Kim, J. Kelly, and C. Thomas, "Local green team - implementing smart communities in Illinois and Korea," in *IEEE Power & Energy Magazine*, jan./feb. 2011, vol. 9, no. 1, pp. 67–74.

[48] A. G. Tsikalakis and N. D. Hatziargyriou, "Centralized control for optimizing microgrids operation," *IEEE Trans. Energy Convers.*, vol. 23, no. 1, pp. 241–248, Mar. 2008.

[49] P. M. Costa and M. A. Matos, "Assessing the contribution of microgrids to the reliability of distribution networks," *El. Power Systems Research*, vol. 79, no. 2, pp. 382–389, Feb. 2009.

[50] K. De Brabandere, "Voltage and frequency droop control in low voltage grids by distributed generators with inverter front-end," Ph.D. dissertation, KU Leuven, Faculteit Ingenieurswetenschappen, Departement elektrotechniek, afdeling elektrische energie en computerarchitecturen, Kasteelpark Arenberg 10, B-3001 Leuven, België, Oct. 2006.

[51] X. Tan, Q. Li, and H. Wang, "Advances and trends of energy storage technology in microgrid," *Internat. Journal on Electrical Power and Energy Systems*, vol. 44, no. 1, pp. 179 – 191, 2013.

[52] K. H. LaCommare and J. H. Eto, "Understanding the cost of power interruptions to u.s. electricity consumers," Ernest Orlando Lawrence Berkely National Laboraty, Tech. Rep., 2004, http://eetd.lbl.gov/ea/EMP/EMP-pubs.html.

[53] C. Marnay and R. Firestone, "Microgrids: an emerging paradigm for meeting building electricity and heat requirements efficiently and with appropriate energy quality," Environmental Energy Technologies Division, U.S. Deparment of energy, presented at the European Council for an Energy Efficient Economy 2007 Summer Study, La Colle sur Loup, France, Tech. Rep., June 4-9, 2007.

[54] T. C. Green and M. Prodanovíc, "Control of inverter-based micro-grids," *Electric Power Systems Research*, vol. 77, no. 9, pp. 1204–1213, Jul. 2007.

[55] H. Jiayi, J. Chuanwen, and X. Rong, "A review on distributed energy resources and microgrid," *Renewable and Sustainable Energy Reviews*, vol. 12, no. 9, pp. 2472–2483, Dec. 2008.

[56] C. Marnay and G. Venkataramanan, "Microgrids in the evolving electricity generation and delivery infrastructure," in *Proc. IEEE PES General Meeting*, Montréal, Canada, June 18-22, 2006.

[57] P. Basak, A. K. Saha, S. Chowdhury, and S. P. Chowdhury, "Microgrid: control techniques and modelling," in *The 44th International Universities' Power Engineering Conference (UPEC 2009)*. Glasgow, Scotland, Sep. 1-4, 2009.

[58] H. Mohamad and P. Crossley, "Islanded operation of UK radial distribution earthing strategy," in *The 44th International Universities' Power Engineering Conference (UPEC 2009)*. Glasgow, Scotland, Sep. 1-4, 2009.

[59] F. Katiraei, M. R. Iravani, and P. W. Lehn, "Micro-grid autonomous operation during and subsequent to islanding process," *IEEE Trans. Power Del.*, vol. 20, no. 1, pp. 248–257, Jan. 2005.

[60] E. Planas, A. Gil-de-Muro, J. Andreu, I. Kortabarria, and I. Martínez de Alegría, "General aspects, hierarchical controls and droop methods in microgrids: a review," *Renewable and sustainable energy reviews*, vol. 17, no. 5, pp. 147–159, 2013.

[61] BC Hydro. Distribution power generator islanding guidelines. [Online]. Available: www.bchydro.com,Jun.2006

[62] F. Katiraei, C. Abbey, S. Tang, and M. Gauthier, "Planned islanding on rural feeders - utility perspective," in *IEEE PES 2008 General Meeting*, Pittsburgh, Pennsylvania, July 20-24, 2008.

[63] The World Bank, Washington DC. World development report 2010, development and climate change. [Online]. Available: go.worldbank.org/ZXULQ9SCC0,2010

[64] I. E. A. IEA. (2011) Access to electricity (weo-2011). [Online]. Available: www.worldenergyoutlook.org/

[65] I. Mitra, T. Degner, and M. Braun, "Distributed generation and microgrids for small island electrification in developing countries: a review," *SESI*

Journal, Journal of the Solar Energy Society of India, vol. 18, no. 1, pp. 6–20, Jan.-June 2008.

[66] N. Lidula and A. D. Rajapakse, "Microgrids research: A review of experimental microgrids and test systems," *Renewable and Sustainable Energy Reviews*, vol. 15, no. 1, pp. 186–202, 2011.

[67] M. Savaghebi, A. Jalilian, J. C. Vasquez, and J. M. Guerrero, "Secondary control scheme for voltage unbalance compensation in an islanded droop-controlled microgrid," *IEEE Trans. on Smart Grid*, vol. 3, no. 2, pp. 797–807, Jun. 2012.

[68] N. Hatziargyriou, H. Asano, R. Iravani, and C. Marnay, "Microgrids: an overview of ongoing research, development, and demonstration projects," in *IEEE Power & Energy Magazine*, Jul./Aug. 2007, vol. 5, no. 4, pp. 78–97.

[69] B. Kroposki, R. Lasseter, T. Ise, S. Morozumi, S. Papathanassiou, and N. Hatziargyriou, "A look at microgrid technologies and testing projects from around the world: making microgrids work," in *IEEE Power & Energy Magazine*, May/June 2008, vol. 6, no. 3, pp. 40–53.

[70] European Commission, "European smartgrids technology platform: vision and strategy for Europe's electricity networks in the future," Community Research, Tech. Rep., 2006.

[71] F. E. N. t. I. t. e. e. e. Fenix. (2005-2009) What is a virtual power plant. [Online]. Available: /www.fenix-project.org

[72] P. Asmus, "Microgrids, virtual power plants and our distributed energy future," *The Electricity Journal*, vol. 23, no. 10, pp. 72–82, Dec. 2010.

[73] F. Ueda, K. Matsui, M. Asao, and K. Tsuboi, "Parallel-connections of pulsewidth modulated inverters using current sharing reactors," *IEEE Trans. Power Electron.*, vol. 10, no. 6, pp. 673–679, Nov. 1995.

[74] B. T. Irving and M. J. Jovanovic, "Analysis, design, and performance evaluation of droop current-sharing method," in *IEEE Applied Power Electronics Conference and Exposition (APEC)*, vol. 1. New Orleans, USA, Feb. 6-10, 2000, pp. 235–241.

[75] A. Engler and N. Soultanis, "Droop control in LV-grids," in *Proc. Internat. Conf. On Future Power Systems*, The Netherlands, Nov. 16-18, 2005.

[76] A. Engler, "Control of parallel operating battery inverters," in *1st PV hybrid Power Systems Conference*, Aix-en-Provence, France, Sep. 2000.

[77] J.-F. Chen and C.-L. Chu, "Combination voltage-controlled and current-controlled PWM inverters for UPS parallel operation," *IEEE Trans. Ind. Electron.*, vol. 10, no. 5, pp. 547–558, Sep. 1995.

[78] K. Siri, C. Q. Lee, and T. F. Wu, "Current distribution control for parallel connected converters part ii," *IEEE Trans. Aerosp. Electron. Syst.*, vol. 28, no. 3, pp. 841–851, Jul. 1992.

[79] T. F. Wu, K. Siri, and J. Banda, "The central-limit control and impact of cable resistance in current distribution for parallel-connected DC-DC converters," in *25th Annual IEEE Power Electronics Specialists Conference (PESC '94)*, Taipei, Taiwan, Jun. 20-25 1994, pp. 694–702.

[80] J. Banda and K. Siri, "Improved central-limit control for parallel-operation of dc-dc power converters," in *IEEE Power Electronics Specialists Conference (PESC95)*, Atlanta, USA, Jun. 18-22, 1995, pp. 1104–1110.

[81] T. Kawabata and S. Higashino, "Parallel operation of voltage source inverters," *IEEE Ind. Appl. Mag.*, vol. 24, no. 2, pp. 281–287, Mar/Apr 1988.

[82] K. Siri, C. Q. Lee, and T. F. Wu, "Current distribution control for parallel connected converters part i," *IEEE Trans. Aerosp. Electron. Syst.*, vol. 28, no. 3, pp. 829–840, Jul. 1992.

[83] J. M. Guerrero, L. Hang, and J. Uceda, "Control of distributed uninterruptible power supply systems," *IEEE Trans. Ind. Electron.*, vol. 55, no. 8, pp. 2845–2859, Aug. 2008.

[84] R. Ramos, D. Biel, F. Guinjoan, and E. Fossas, "Master-slave sliding-mode control design in parallel-connected inverters," *Automatica*, vol. 42, no. 1-2, pp. 37–44, 2001.

[85] F. Petruzziello, P. D. Ziogas, and G. Joos, "A novel approach to paralleling of power converter units with true redundancy," in *The 21st Annual IEEE Power and Electron. Specialists Conf.* San Antonio, TX, USA, 1990.

[86] J. Holtz and K. Werner, "Multi-inverter UPS system with redundant load sharing control," *IEEE Trans. Ind. Electron.*, vol. 37, no. 6, pp. 506–513, Dec. 1990.

[87] W.-C. Lee, T.-K. Lee, S.-H. Lee, K.-H. Kim, D.-S. Hyun, and I.-Y. Suh, "A master and slave control strategy for parallel operation of three-phase UPS

systems with different ratings," in *Proc. IEEE The Applied Power Electronics Conference and Exposition (APEC'04)*, California, Feb. 22-26 2004, pp. 456–462.

[88] *Uninterruptible Power Supplies and Active Filters*. CRC Press, 2005.

[89] W. C. Lee, S. H. Lee, K. H. Kim, and D. S. Hyun, "Novel control strategy for parallel operation of UPS system," in *4th Internat. Power Electr. and motion control conf. (IPEMC'04)*, vol. 2, Xi'an, China, Aug. 14-16, 2004, pp. 983–988.

[90] Y. Pei, G. Jiang, X. Yang, and Z. Wang, "Auto-master-slave control technique of parallel inverters in distributed AC power systems and UPS," in *35th Annual IEEE Power Electronics Specialists Conference*, Aachen, Germany, 2004.

[91] X. Sun, Y.-S. Lee, and D. Xu, "Modeling, analysis, and implementation of parallel multi-inverter systems with instantaneous average-current-sharing scheme," *IEEE Trans. Power Electron.*, vol. 18, no. 3, pp. 844–856, May 2003.

[92] Y. Xing, L. Huang, and Y. Yan, "Redundant parallel control for current regulated inverters with instantaneous current sharing," in *IEEE 34th annual Power Electr. Specialist Conf (PESC'03)*, vol. 3, Acapulco, Mexico, Jun. 15-19, 2003, pp. 1438–1442.

[93] A. M. Roslan, K. H. Ahmed, S. J. Finney, and B. W. Williams, "Improved instantaneous average current-sharing control scheme for parallel-connected inverter considering line impedance impact in microgrid networks," *IEEE Trans. Power Electron.*, vol. 26, no. 3, pp. 702–716, Mar. 2011.

[94] Y.-K. Chen, Y.-E. Wu, T.-F. Wu, and C.-P. Ku, "ACSS for paralleled multi-inverter systems with DSP-based robust controls," *IEEE Trans. Aerosp. Electron. Syst.*, vol. 39, no. 3, pp. 1002–1015, Jul. 2003.

[95] H. Shan, Y. Kang, S. Duan, Y. Zhang, M. Yu, Y. Liu, G. Chen, and F. Luo, "Research on a novel digital parallel current sharing control technique of modularized ups," in *Internat. Conf. on Electrical Machines and Systems*, Seoul, Korea, Oct. 8-11, 2007, pp. 106–109.

[96] T. Fang, X. Ruan, L. Xiao, and A. Liu, "An improved distributed control strategy for parallel inverters," in *Power Electr. Specialist Conf. (PESC'08)*, Island of Rhodes, Greece, Jun. 15-19, 2008, pp. 3500–3505.

[97] Y.-K. Chen, Y.-E. Wu, T.-F. Wu, and C.-P. Ku, "CWDC strategy for paralleled multi-inverter systems achieving a weighted output current distribution," in *17th annual IEEE applied power el. conf. and exposition (APEC)*, Dellas, Texas, Mar. 10-14, 2002, pp. 1018–1023.

[98] Q. Chen, P. Ju, K. Q. Shi, Y. Tang, Z. Y. Shao, and W. Y. Yang, "Parameter estimation and comparison of the load models with considering distribution network directly or indirectly," *Electr. Power Syst. Res.*, vol. 32, 2010.

[99] C.-L. Chen, Y. Wang, J.-S. Lai, Y.-S. Lee, and D. Martin, "Design of parallel inverters for smooth mode transfer microgrid applications," *IEEE Trans. Power Electron.*, vol. 25, no. 1, pp. 6–15, Jan. 2010.

[100] T.-F. Wu, Y.-K. Chen, and Y.-H. Huang, "3C strategy for inverters in parallel operation achieving an equal current distribution," *IEEE Trans. Ind. Electron.*, vol. 47, no. 2, pp. 273–281, Apr. 2000.

[101] M. Prodanović and T. C. Green, "High-quality power generation through distributed control of a power park microgrid," *IEEE Trans. Ind. Electron.*, vol. 53, no. 5, pp. 1471–1482, Oct. 2006.

[102] R. Majumder, B. Chaudhuri, A. Ghosh, R. Majumder, G. Ledwich, and F. Zare, "Improvement of stability and load sharing in an autonomous microgrid using supplementary droop control loop," *IEEE Trans. Power Syst.*, vol. 25, no. 2, pp. 796–808, May 2010.

[103] E. Barklund, N. Pogaku, M. Prodanović, C. Hernandez-Aramburo, and T. C. Green, "Energy management in autonomous microgrid using stability-constrained droop control of inverters," *IEEE Trans. Power Electron.*, vol. 23, no. 5, pp. 2346–2352, Sep. 2008.

[104] A. Engler, O. Osika, M. Barnes, and N. Hatziargyriou, *DB2 Evaluation of the local controller strategies*. www.microgrids.eu/micro2000, Jan. 2005.

[105] F. Katiraei, R. Iravani, N. Hatziargyriou, and A. Dimeas, "Microgrids management: controls and operation aspects of microgrids," *Power and Energy Magazine*, vol. 6, no. 3, pp. 54–65, May/June 2008.

[106] M. C. Chandorkar, D. M. Divan, and R. Adapa, "Control of parallel connected inverters in standalone ac supply systems," *IEEE Trans. Ind. Appl.*, vol. 29, no. 1, pp. 136–143, Jan./Feb. 1993.

[107] F. A. Bhuiyan and A. Yazdani, "Multimode control of a DFIG-Based wind-power unit for remote applications," *IEEE Trans. Power Del.*, vol. 24, no. 4, pp. 2079–2089, Oct. 2009.

[108] J. M. Guerrero, J. Matas, L. García de Vicuña, M. Castilla, and J. Miret, "Wireless-control strategy for parallel operation of distributed-generation inverters," *IEEE Trans. Ind. Electron.*, vol. 53, no. 5, pp. 1461–1470, Oct. 2006.

[109] J. M. Guerrero, J. C. Vásquez, J. Matas, L. García de Vicuña, and M. Castilla, "Hierarchical control of droop-controlled AC and DC microgrids - A general approach towards standardization," *IEEE Trans. Ind. Electron.*, vol. 58, no. 1, pp. 158–172, Jan. 2011.

[110] A. Tuladhar, H. Jin, T. Unger, and K. Mauch, "Control of parallel inverters in distributed AC power systems with consideration of line impedance effect," *IEEE Trans. Ind. Appl.*, vol. 36, no. 1, pp. 131–138, Jan./Feb. 2000.

[111] J. M. Guerrero, L. García de Vicuña, J. Matas, M. Castilla, and J. Miret, "Output impedance design of parallel-connected UPS inverters with wireless load-sharing control," *IEEE Trans. Ind. Electron.*, vol. 52, no. 4, pp. 1126–1135, Aug. 2005.

[112] F. Katiraei and M. R. Iravani, "Power management strategies for a microgrid with multiple distributed generation units," *IEEE Trans. Power Syst.*, vol. 21, no. 4, pp. 1821–1831, Nov. 2006.

[113] J. M. Guerrero, J. Matas, L. García de Vicuña, M. Castilla, and J. Miret, "Decentralized control for parallel operation of distributed generation inverters using resistive output impedance," *IEEE Trans. Ind. Electron.*, vol. 54, no. 2, pp. 994–1004, Apr. 2007.

[114] J. M. Guerrero, J. C. Vásquez, J. Matas, M. Castilla, and L. García de Vicuña, "Control strategy for flexible microgrid based on parallel line-interactive UPS systems," *IEEE Trans. Ind. Electron.*, vol. 56, no. 3, pp. 726–736, Mar. 2009.

[115] J. C. Vasquez, R. A. Mastromauro, J. M. Guerrero, and M. Liserre, "Voltage-support provided by a droop-controlled multifunctional inverter," *IEEE Trans. Ind. Electron.*, vol. 56, no. 11, pp. 4510–4519, Nov. 2009.

[116] J. Matas, M. Castilla, L. G. de Vicuña, and J. C. Vasquez, "Virtual impedance loop for droop-controlled single-phase parallel inverters using a second order general integrator scheme," *IEEE Trans. Power Electron.*, vol. 25, no. 12, p. 2993, Dec. 2010.

[117] K. Debrabandere, B. Bolsens, J. Van den Keybus, A. Woyte, J. Driesen, and R. Belmans, "A voltage and frequency droop control method for parallel

inverters," *IEEE Trans. Power Electron.*, vol. 22, no. 4, pp. 1107–1115, July 2007.

[118] C.-T. Lee, C.-C. Chuang, C.-C. Chu, and P.-T. Chang, "Control strategies for distributed energy resources interface converters in the low voltage microgrid," in *IEEE Energy Conversion Congress and exposition (ECCE 2009)*, San Jose, CA, Sep. 20-24, 2009.

[119] X. Yu, H. H. Wang, A. M. Khambadkone, and S. T. Sing, "A hybrid control architecture for low voltage microgrid," in *IEEE Energy Conversion Congress and exposition (ECCE 2010)*, Atlanta, GA, Sep. 12-16, 2010, pp. 3161–3168.

[120] Y. Li and Y. W. Li, "Decoupled power control for an inverter based low voltage microgrid in autonomous operation," in *IEEE 6th Internat. Electron. and Motion Control Conf. (IPEMC'09)*. Wuhan, China, May 17-20, 2009, pp. 2490–2496.

[121] ——, "Power management of inverter interfaced autonomous microgrid based on virtual frequency-voltage frame," *IEEE Trans. on Smart Grid*, vol. 2, no. 1, pp. 30–40, Mar. 2011.

[122] J. C. Vasquez, J. M. Guerrero, A. Luna, P. Rodriguez, and R. Teodorescu, "Adaptive droop control applied to voltage-source inverters operating in grid-connected and islanded modes," *IEEE Trans. Ind. Electron.*, vol. 56, no. 10, pp. 4088–4096, Oct. 2009.

[123] H. Akagi, Y. Kanagawa, and A. Nabase, "Instantaneous reactive power compensator comprising switching devices without energy storage components," *IEEE Trans. Ind. Appl.*, vol. 20, no. 3, pp. 625–630, May/June 1984.

[124] A. Tuladhar, H. Jin, T. Unger, and K. Mauch, "Parallel operation of single phase inverter modules with no control interconnections," in *Applied power electronics Conference and Exposition 1997 (APEC'97)*. Atlanta, GA, USA, Feb. 23-27, 1997.

[125] T. K. Vrana and C. Hille, "A novel control method for dispersed converters providing dynamic frequency response," *Electrical Engineering Journal, Springer-Verlag*, vol. 93, pp. 217–226, May 2011.

[126] J. Driesen and K. Visscher, "Virtual synchronous generators," in *Proc. of the IEEE PES General Meeting*, Pittsburgh, PA, USA, July 20-24, 2008.

[127] K. Visscher. (2008, Jul.) Vsync - The virtual synchronous generator concept. [Online]. Available: www.vsycn.eu

[128] K. Sakimoto, Y. Miura, and T. Ise, "Stabilization of a power system with a distributed generation by a virtual synchronous generation function," in *8th Internat. Conf. on Power Electornics (ECCE)*, Korea, May 30- June 3, 2011.

[129] H.-P. Beck and R. Hesse, "Virtual synchronous machine," in *9th Internat. Conf. Electrical Power Quality and Utilisation (EPQU2007)*. Barcelona, Spain, Oct. 9-11, 2007.

[130] R. Hesse, D. Turschner, and H.-P. Beck, "Micro grid stabilisation using the Virtual Synchronous Machine (VISMA," in *Internat. Conf. on Ren. Energies and Power Quality (ICREPQ'09)*, Valencia, Spain, Apr. 15-17, 2009.

[131] Q.-C. Zhong and G. Weiss, "Synchronverters: inverters that mimic synchronous generators," *IEEE Trans. Ind. Electron.*, vol. 58, no. 4, pp. 1259–1267, Apr. 2011.

[132] D. Yan, S. Jianhui, and S. Yong, "A unified power controller for photovoltaic generators in microgrid," in *4th Internat. Conf. on Electric Utility Deregulation and Restructuring and Power Technologies (DRPT2011)*, Weihai, China, July 6-9, 2011, pp. 1121 – 1125.

[133] Y. Du, J. Su, M. Mao, and X. Yang, "autonomous controller based on synchronous generator dq0 model for micro grid inverters," in *8th Internat. Conf. on Power Electronics (ECCE Asia)*, The Shilla Jeju, Korea, May 30-June 3, 2011.

[134] C. Sao and P. Lehn, "Intentional islanded operation of converter fed microgrids," *Proc. IEEE Power Eng. Soc. General Meeting*, June 18-22, 2006.

[135] ——, "Control and power management of converter fed microgrids," *IEEE Trans. Power Syst.*, vol. 23, no. 3, Aug. 2008.

[136] J. Au-Yeung, G. M. A. Vanalme, J. M. A. Myrzik, P. Karaliolios, M. Bongaerts, J. Bozelie, and W. L. Kling, "Development of a voltage and frequency control strategy for an autonomous LV network with distributed generators," in *The 44th International Universities' Power Engineering Conference (UPEC 2009)*. Glasgow, Scotland, Sep. 1-4, 2009.

[137] M. Savaghebi and A. Jalilian, "A new control strategy for distributed generation interface converters to compensate for microgrid harmonics," in *Internat. Symp. on Power Electronics, Electr. Drives, Automation and motion (SPEEDAM2010)*, Pisa, Italy, Jun. 2010, pp. 908–913.

[138] T. L. Vandoorn, B. Meersman, J. D. M. D. Kooning, and L. Vandevelde, "Controllable harmonic current sharing in islanded microgrids: DG units with programmable resistive behavior towards harmonics," *IEEE Trans. Power Del.*, vol. 27, no. 2, pp. 831–841, Apr. 2012.

[139] D. J. Perreault, R. L. Selders, and J. G. Kassakian, "Frequency-based current-sharing techniques for paralleled power converters," *IEEE Trans. Power Electron.*, vol. 13, no. 4, pp. 626–634, Jul. 1998.

[140] D. J. Perreault, K. Sato, R. L. Selders, and J. G. Kassakian, "Switching-ripple-based current sharing for paralleled power converters," *IEEE Trans. Circuits Syst. I*, vol. 46, no. 10, pp. 1264–1274, Oct. 1999.

[141] T. L. Vandoorn, J. D. M. D. Kooning, B. Meersman, and L. Vandevelde, "Review of primary control strategies for islanded microgrids with power-electronic interfaces," *Ren. and Sust. Energy Reviews*, vol. 19, pp. 613–628, Mar. 2013.

[142] L. R. Limongi, R. Bojoi, G. Griva, and A. Tenconi, "Digital current-control schemes," *IEEE Ind. Electr. Magazine*, vol. 3, no. 1, pp. 20–31, Mar. 2009.

[143] M. P. Kazmierkowski and L. Malesani, "Current control techniques for three-phase voltage-source PWM converters: A survey," *IEEE Trans. Ind. Electron.*, vol. 45, no. 5, pp. 691–703, Oct. 1998.

[144] A. Y. Sendjaja and V. Kariwala, "Decentralized control of solid oxide fuel cells," *IEEE Trans. Ind. Informat.*, vol. 7, no. 2, pp. 163–170, May 2011.

[145] M. Ö. Efe, "Neural network assisted computationally simple $PI^{\lambda}DI^{\mu}$ control of a quadrotor UAV," *IEEE Trans. Ind. Informat.*, vol. 7, no. 2, pp. 354–361, May 2011.

[146] Á. Cuenca, J. Salt, A. Sala, and R. Pizá, "A delay-dependent dual-rate pid controller over an ethernet network," *IEEE Trans. Ind. Informat.*, vol. 7, no. 1, pp. 18–29, Feb. 2011.

[147] M. P. Kazmierkowski, M. Jasinski, and G. Wrona, "DSP-based control of grid-connected power converters operating under grid distortions," *IEEE Trans. Ind. Informat.*, vol. 7, no. 2, pp. 204–2011, May 2011.

[148] H. J. Avelar, W. A. Parreira, J. B. Vieira, L. C. Gomes de Freitas, and E. A. A. Coelho, "A state equation model of a single-phase grid-connected inverter using a droop control scheme with extra phase shift control action," *IEEE Trans. Ind. Electron.*, vol. 59, no. 3, pp. 1527–1537, Mar. 2012.

[149] N. Pogaku and T. Green, "Harmonic mitigation throughout a distribution system: a distributed-generator-based solution," *IEE Proc. Gener. Transm. Distrib.*, vol. 153, no. 3, pp. 350–358, May 2006.

[150] R. Teodorescu and F. Blaabjerg, "Flexible control of small wind turbines with grid failure detection operating stand-alone and grid-connected mode," *IEEE Trans. Power Electron.*, vol. 19, no. 5, pp. 1323–1332, Sep. 2004.

[151] R. D. Lorenz and D. B. Lawson, "Performance of feedforward current regulators for field-oriented induction machine controllers," *IEEE Trans. Ind. Appl.*, vol. 23, no. 4, pp. 597–602, July/Aug. 1987.

[152] J. D. M. De Kooning, *Balancering van het middelpunt van de busspanning bij driefasige netgekoppelde invertoren met neutrale geleider*, Universiteit Gent, 2010.

[153] David Van de Sype, "Kleinsignaalmodellering van digitaal gestuurde schakelende energie-omzetters," Ph.D. dissertation, Universiteit Gent, 2004.

[154] D. M. Van de Sype, K. De Gussemé, A. P. M. Van den Bossche, and J. A. Melkebeek, "Duty-ratio feed-forward for digitally controlled boost PFC converters," *IEEE Trans. Ind. Electron.*, vol. 52, no. 1, pp. 108–115, Feb. 2005.

[155] N. Nise, *Control System Engineering*. Wiley, 6th edition, 2010, isbn 978-0470547564.

[156] B. Renders, K. De Gussemé, W. R. Ryckaert, and L. Vandevelde, "Input impedance of grid-connected converters with programmable harmonic resistance," *IET Electr. Power Appl.*, vol. 1, no. 3, pp. 355–361, May 2007.

[157] Y. Li, D. M. Vilathgamuwa, and P. C. Loh, "Design, analysis, and real-time testing of a controller for multibus microgrid system," *IEEE Trans. Power Electron.*, vol. 19, no. 5, pp. 1195–1204, Sep. 2004.

[158] J. Schreel, "Spanningsregeling in een zelfstandig microgrid met convertor-gekoppelde productie-eenheden," Master's thesis, Universiteit Gent, 2011.

[159] T. L. Vandoorn, C. Ionescu, J. D. M. D. Kooning, R. D. Keyser, and L. Vandevelde, "Theoretical analysis and experimental validation of single-phase direct vs. cascade voltage control in islanded microgrids," *IEEE Trans. Ind. Electron.*, vol. 60, no. 2, pp. 789–798, feb 2013.

[160] B. Meersman, "Control of 3-phase inverter-connected distributed generators regarding the improvement of the power quality," Ph.D. dissertation, Ghent

University, Department of Electrical Energy, Systems and Automation, Sint-Pietersnieuwstraat 41, Ghent, Belgium, 2012.

[161] S. Conti, A. M. Greco, N. Messina, and U. Vagliasindi, "Generators control systems in intentionally islanded MV microgrids," in *International Symposium on Power Electronics, Electrical Drives, automation and motion (SPEEDAM)*, Ischia, Italy, Jun. 11-13, 2008.

[162] T. L. Vandoorn, B. Renders, B. Meersman, L. Degroote, and L. Vandevelde, "Power balancing in islanded microgrids by using a dc-bus voltage reference," in *20th Internat. Symp. on Power Electronics, Electrical Drives, Automation and Motion (SPEEDAM 2010)*, Pisa, Italy, June 14-16, 2010.

[163] F. M. L. L. De Belie, D. M. Van de Sype, K. De Gussemé, W. R. A. Ryckaert, and J. A. A. Melkebeek, "Digitally controlled boost PFC converter with improved output voltage controller," *Electr. Eng*, vol. 89, no. 5, pp. 363–370, May 2007.

[164] W. Yao, M. Chen, J. M. Guerrero, and Z.-M. Qian, "Design and analysis of the droop control method for parallel inverters considering the impact of the complex impedance on the power sharing," *IEEE Trans. Ind. Electron.*, vol. 58, no. 2, pp. 576–588, Feb. 2011.

[165] H. Akagi, H. Fujita, and k. Wada, "A shunt active filter based on voltage detection for harmonic termination of a radial power distribution line," *IEEE Trans. Ind. Appl.*, vol. 35, no. 3, pp. 638–645, May/June 1999.

[166] M. Cirrincione, M. Pucci, G. Vitale, and A. Miraoui, "Current harmonic compensation by a single-phase shunt active filter controlled by adaptive neural filtering," *IEEE Trans. Ind. Electron.*, vol. 56, no. 8, pp. 3128–3143, Aug. 2009.

[167] T. Green and N. Pogaku, "A model citizen approach to integrating inverter-based distributed generation," in *World Renewable Energy Congress (WREC)*, 2005, pp. 1101–1108.

[168] T. Takeshita and N. Matsui, "Current waveform control of PWM converter system for harmonic suppression on distribution system," *IEEE Trans. Ind. Electron.*, vol. 50, no. 6, pp. 1134–1139, Dec. 2003.

[169] P. N. Vovos, A. E. Kiprakis, A. R. Wallace, and G. P. Harrison, "Centralized and distributed voltage control: Impact on distributed generation penetration," *IEEE Trans. Power Syst.*, vol. 22, no. 1, pp. 476–483, Feb. 2007.

[170] B. Singh, K. A.-Haddad, and A. Chandra, "A review of active filters for power quality improvement," *IEEE Trans. Ind. Electron.*, vol. 46, no. 5, pp. 960–971, Oct. 1999.

[171] M. E.-Habrouk, M. K. Darwish, and P. Mehta, "Active power filters: A review," *IEE Proc. Electr. Power Appl.*, vol. 147, no. 5, pp. 403–413, Sep. 2000.

[172] H. Akagi, A. Nabae, and S. Atoh, "Control strategy of active power filters using multiple voltage-source PWM converters," *IEEE Trans. Ind. Appl.*, vol. IA-22, no. 3, May/June 1986.

[173] P. Jintakosonwit, H. Fujita, and H. Akagi, "Control and performance of a full-digital-controlled shunt active filter for installation on a power distribution system," *IEEE Trans. Power Electron.*, vol. 17, no. 1, pp. 132–140, Jan. 2002.

[174] Y. Li, D. M. Vilathgamuwa, and P. C. Loh, "Microgrid power quality enhancement using a three-phase four-wire grid-interfacing compensator," *IEEE Trans. Ind. Appl.*, vol. 41, no. 6, pp. 1707–1719, Nov./Dec 2005.

[175] N. Pogaku and T. Green, "Application of inverter-based distributed geneartors for harmonic damping throughout a distribution network," in *Proc. IEEE Power Electr. Spec. Conf. (PESC'05*.

[176] K. De Gussemé, W. R. Ryckaert, D. M. Van de Sype, J. A. Ghijselen, J. A. Melkebeek, and L. Vandevelde, "A boost PFC converter with programmable harmonic resistance," *IEEE Trans. Ind. Appl.*, vol. 43, no. 3, pp. 742–750, May/June 2007.

[177] B. Renders, W. R. Ryckaert, K. De Gussemé, K. Stockman, and L. Vandevelde, "Improving the voltage dip immunity of converter-connected distributed generation units," *Renew. Energy*, vol. 33, no. 5, pp. 1011–1018, May 2008.

[178] B. Meersman, B. Renders, L. Degroote, T. Vandoorn, and L. Vandevelde, "Three-phase inverter-connected dg-units and voltage unbalance," *Electric Power Systems Research*, vol. 81, no. 4, pp. 899–906, Apr. 2011.

[179] B. Renders, K. De Gussemé, W. R. Ryckaert, and L. Vandevelde, "Converter-connected distributed generation units with integrated harmonic voltage damping and harmonic current compensation function," *Electric Power Systems Research*, vol. 79, no. 1, pp. 65–70, Jan. 2009.

[180] ——, "Input impedance of grid-connected converters with programmable harmonic resistance," *IET Electr. Power Appl.*, vol. 1, no. 3, pp. 355–361, May 2007.

[181] B. Renders, "Convertor-gekoppelde decentrale generatoren en netkwaliteit in laagspanningsnetten," Ph.D. dissertation, Ghent University, Department of Electrical Energy, Systems and Automation, Sint-Pietersnieuwstraat 41, Ghent, Belgium, 2009.

[182] L. Degroote, B. Renders, B. Meersman, and L. Vandevelde, "Influence of converter-based distributed generators on the harmonic line losses," in *Internat. Conf. on Harmonics and Quality of Power (ICHQP 2008)*, Wollongong, NSW, Australia, Sept. 28 -Oct. 1, 2008.

[183] J. Desmet, "Study and analysis of losses in low voltage cables under harmonic loading," Ph.D. dissertation, KU Leuven, 2008.

[184] T. L. Vandoorn, B. Meersman, L. Degroote, B. Renders, and L. Vandevelde, "A control strategy for islanded microgrids with dc-link voltage control," *IEEE Trans. Power Del.*, vol. 26, no. 2, pp. 703–713, Apr. 2011.

[185] C. K. Sao and P. W. Lehn, "Autonomous load sharing of voltage source converters," *IEEE Trans. Power Del.*, vol. 20, no. 2, pp. 1009–1016, Apr. 2005.

[186] Q.-C. Zhong, "Robust droop controller for accurate proportional load sharing among inverters operated in parallel," *IEEE Trans. Ind. Electron.*, vol. 58, 2011, to appear.

[187] T. L. Vandoorn, B. Meersman, J. D. M. D. Kooning, and L. Vandevelde, "Analogy between conventional grid control and islanded microgrid control based on a global dc-link voltage droop," *IEEE Trans. Power Del.*, vol. 27, no. 3, pp. 1405–1415, Jul. 2012.

[188] T. L. Vandoorn, B. Renders, B. Meersman, L. Degroote, and L. Vandevelde, "Reactive power sharing in an islanded microgrid," in *45th International Universities Power Engineering Conference (UPEC 2010)*, Cardiff, Wales, Aug. 31 - Sep. 3, 2010.

[189] S. Abu-Skarkh, R. J. Arnold, J. Kohler, R. Li, T. Markvart, J. N. Ross, K. Steemers, P. Wilson, and R. Yao, "Can microgrids make a major contribuion to UK energy supply?" *Renewable and Sustainable Energy Reviews*, vol. 10, pp. 78–127, 2006.

[190] A. Brooks, E. Lu, D. Reicher, C. Spirakis, and B. Weihl, "Demand dispatch, using real-time control of demand to help balance generation and load," in *IEEE Power & Energy Magazine*, May/June 2010, vol. 8, no. 3, pp. 20–29.

[191] J. A. Peças Lopes, C. L. Moreira, and A. G. Madureira, "Defining control strategies for microgrids in islanded operation," *IEEE Trans. Power Syst.*, vol. 21, no. 2, pp. 916–924, 2006.

[192] J. Kirby, "Demand response for power system reliability: Faq," Oak Ridge National Laboratory, Tech. Rep., Dec. 2006.

[193] K. Hamilton and N. Gulhar, "Taking demand response to the next level," in *IEEE Power & Energy Magazine*, May/June 2010, vol. 8, no. 3, pp. 60–65.

[194] S. De Rijcke, K. De Vos, and J. Driesen, "Balancing wind power with demand-side response," in *5th IEEE Joint IAS,PELS & PES Benelux Chapter Young Researchers Symposium*, Leuven, Belgium, Mar 29-30, 2010.

[195] F. Rahimi and A. Ipakchi, "Demand response as a market resource under the smart grid paradigm," in *IEEE Trans. Smart Grid*, Jun. 2010, vol. 1, no. 1, pp. 82–88.

[196] I. J. Balaguer, Q. Lei, S. Yang, U. Supatti, and Z. Peng, "Control for grid-connected and intentional islanding operations of distributed power generation," *IEEE Trans. Ind. Electron.*, vol. to appear, 2010.

[197] May Mauseth Johnston, St. Vincent de Paul Society National Council. Direct load control and smart grid, customer issues for South Australia. [Online]. Available: www.vinnies.org.au,Jan.2010

[198] M. Parvania and M. Fotuhi-Firuzabad, "Demand response scheduling by stochastic SCUC," in *IEEE Trans. Smart Grid*, Jun. 2010, vol. 1, no. 1, pp. 89–98.

[199] T. Ericson, "Direct load control of residential water heaters," *Energy Policy*, vol. 37, pp. 3502–3512, 2009.

[200] L. Degroote, B. Renders, B. Meersman, and L. Vandevelde, "Neutral-point shifting and voltage unbalance due to single-phase DG units in low voltage distribution networks," in *2009 IEEE Bucharest PowerTech Conference*, Bucharest, Romania, June 28 - July 2, 2009.

[201] A. Mehrizi-Sani and R. Iravani, "Potential-function based control of a microgrid in islanded and grid-connected modes," *IEEE Trans. Power Syst.*, vol. 25, no. 4, pp. 1883–1891, Nov. 2010.

[202] F. Gao and M. R. Iravani, "A control strategy for a distributed generation unit in grid-connected and autonomous modes of operation," *IEEE Trans. Power Del.*, vol. 23, no. 2, pp. 850–859, Apr. 2008.

[203] M. Pipattanasomporn, H. Feroze, and S. Rahman, "Multi-agent systems in a distributed smart. grid: Design and implementation," in *Power systems conference and exposition (PSCE09)*. Seattle, Washington, Mar. 2009.

[204] P. Siano, P. Chen, Z. Chen, and A. Piccolo, "Evaluating maximum wind energy exploitation in active distribution networks," *IET Generation, Transmission & Distribution*, vol. 4, no. 5, pp. 598 – 608, May 2010.

[205] C. Cecati, C. Citro, A. Piccolo, and P. Siano, "Smart operation of wind turbines and diesel generators according to economic criteria," *IEEE Trans. Ind. Electron.*, vol. PP, no. 99 (forthcoming), pp. 1–1, 2011, digital Object Identifier: 10.1109/TIE.2011.2106100.

[206] C. Yuen, A. Oudalov, and A. Timbus, "The provision of frequency control reserves from multiple microgrids," *IEEE Trans. Ind. Electron.*, vol. 58, no. 1, pp. 173–183, Jan. 2011.

[207] R. Majumder, M. Dewadasa, A. Ghosh, G. Ledwich, and F. Zare, "Control and protection of a microgrid connected to utility through back-to-back converters," *Electr. Power Syst. Res.*, vol. 81, no. 7, pp. 1424 – 1435, 2011.

[208] T. L. Vandoorn, B. Renders, L. Degroote, B. Meersman, and L. Vandevelde, "Active load control in islanded microgrids based on the grid voltage," *IEEE Trans. on Smart Grid*, vol. 2, no. 1, pp. 139–151, Mar. 2011.

[209] T. L. Vandoorn, B. Meersman, J. D. M. D. Kooning, and L. Vandevelde, "Directly-coupled synchronous generators with converter behavior in islanded microgrids," *IEEE Trans. Power Syst.*, vol. 27, no. 3, pp. 1395 – 1406, aug 2012.

[210] T. L. Vandoorn, J. D. M. D. Kooning, B. Meersman, J. Guerrero, and L. Vandevelde, "Voltage-based control of a smart transformer in a microgrid," *IEEE Trans. Ind. Electron.*, vol. 60, no. 4, pp. 1291–1305, Apr. 2013.

[211] SMA Solar Technology. (2010, Jun.) SMA inverters as grid managers.

[212] T. L. Vandoorn, J. D. M. D. Kooning, B. Meersman, and L. Vandevelde, "Soft curtailment for voltage limiting in low-voltage networks through reactive or active power droops," in *IEEE Internat. Energy Conf. & Exhibition (Energycon 2012)*, Firenze Italy, Sep. 9-12, 2012.

[213] M. H. J. Bollen and N. Etherden, "Overload and overvoltage in low-voltage and medium-voltage networks due to renewable energy - some illustrative case studies," in *IEEE PES Innovative Smart Grid Technologies (ISGT 2011)*, Manchester, UK, Dec. 5-7, 2011.

[214] B. Bletterie, A. Goršek, T. Fawzy, D. Premm, W. Deprez, F. Truyens, A. Woyte, B. Blazič, and B. Uljanič, "Development of innovative voltage control for distribution networks with high photovoltaic penetration," *Progress in Photovoltaics: Research and Applications*, 2011.

[215] J. Kim, J. M. Guerrero, P. Rodriguez, R. Theodorescu, and K. Nam, "Mode adaptive droop control with virtual output impedances for inverter-based flexible AC microgrid," *IEEE Trans. Power Electron.*, vol. 26, no. 3, pp. 689–701, Mar. 2011.

[216] N. G. A. Hemdan and M. Kurrat, "Efficient integration of distributed generation for meeting the increased load demand," *Electrical Power and Energy systems*, vol. 33, pp. 1572–1583, 2011.

[217] D. Das, D. P. Kothari, and A. Kalam, "Simple and efficient method for load flow solution of radial distribution networks," *Int. J. Electr. Power Energy Syst.*, vol. 17, no. 335-346, pp. 717–731, Mar. 1995.

[218] A. Engler, "Applicability of droops in low voltage grids," *DER Journal*, no. 1, Jan. 2005.

[219] T. L. Vandoorn, J. D. M. D. Kooning, B. Meersman, J. M. Guerrero, and L. Vandevelde, "Automatic power sharing modification of p/v droop controllers in low-voltage resistive microgrids," *IEEE Trans. Power Del.*, vol. 27, no. 4, pp. 2317–2325, Oct. 2012.

[220] T. L. Vandoorn, B. Meersman, J. D. M. D. Kooning, and L. Vandevelde, "Transition from islanded to grid-connected mode of microgrids with voltage-based droop control," *IEEE Trans. Power Syst.*, 2012, accepted for publication.

[221] B. M. T. L. Vandoorn, J. D. M. De Kooning and L. Vandevelde, "Voltage-based droop control of renewables to avoid on-off oscillations caused by overvoltages," *IEEE Trans. Power Del.*, 2013, accepted for publication.

[222] UCTE. (2009, Mar. 19,) Operation handbook - policy 1: Load-frequency control and performance. [Online]. Available: http://www.entsoe.eu

[223] C. A. Hernandez-Aramburo, T. C. Green, and N. Mugniot, "Fuel consumption minimization of a microgrid," *IEEE Trans. Ind. Appl.*, vol. 41, no. 3, pp. 673–681, May/June 2005.

[224] M. Munson, G. Jaskulski, and C. Thomas, "If these walls could think - using smart buildings to unlock value in downtown Chicago," in *IEEE Power & Energy Magazine*, jan./feb. 2011, vol. 9, no. 1, pp. 50–55.

[225] K. Iniewski, Ed., *Smart Grid Infrastructure & Networking*. McGraw-Hill Professional, 2012, ch. 8. Voltage Based control of DG units and active loads in Smart Microgrids (by T. Vandoorn and L. Vandevelde), pp. 181–200.

[226] S. Ropenus and K. Skytte, "Regulatory review and barriers for the electricity supply system for distributed generation in eu-15," *Internat. Journal of distributed energy resources*, vol. 3, pp. 243–257, 2007.

[227] S. You, C. Træholt, and B. Poulsen, "Generic virtual power plant: management of distributed energy resources under liberalized electricity market," in *Internat. Conf. on Advances in Power System Control, Operation and Management (APSCOM 2009)*, Hong Kong, China, Nov. 8-11, 2009, pp. 1–6.

[228] T. L. Vandoorn, B. Zwaenepoel, J. D. M. D. Kooning, B. Meersman, and L. Vandevelde, "Smart microgrids and virtual power plants in a hierarchical control structure," in *IEEE PES Innovative Smart Grid Technologies (ISGT 2011)*, Manchester, UK, Dec. 5-7, 2011.

[229] T. Vandoorn, L. Vandevelde, G. Van Eetvelde, B. Meersman, and B. Zwaenepoel, "Slimme microgrids en virtual power plants, bouwstenen van het net van de toekomst," in *vakblad: elektrotechnisch ingenieur*, 2012, no. 140, pp. 18–22.

[230] L. Wu and H. Gao, "Sliding mode control of two-dimensional systems in roesser model," *IET Control Theory and Appl.*, vol. 2, no. 4, pp. 694–702, 2008.

[231] V. Utkin, J. Guldner, and J. Shi, *Sliding Mode Control in Electromechanical Systems*. Taylor & Francis Group, CRC Press, 1999.

[232] J.-W. Jung and A. Keyhani, "Control of a fuel cell based z-source converter," *IEEE Trans. Energy Convers.*, vol. 22, no. 2, pp. 467–476, Jun. 2007.

[233] K. J. Aström and B. Wittenmark, *Computer controlled systems : theory and design*. Englewood Cliffs (N.J.): Prentice-Hall, 1990.

[234] I. Eker and S. A. Akmal, "Sliding mode control with integral augmented sliding surface: design and experimental application to an electromechanical system," *Electr. Eng.*, vol. 90, no. 3, pp. 189–197, 2008.

[235] I. Boiko, L. Fridman, R. Iriarte, A. Pisano, and E. Usai, "Parameter tuning of second-order sliding mode controllers for linear plants with dynamic acturators," *Automatica*, vol. 42, no. 5, pp. 833–839, May 2006.

[236] R. Davies and S. K. Spurgeon, "Robust implementation of sliding mode control schemes," *Int. J. Sysems Sci.*, vol. 24, no. 4, pp. 733–743, 1993.

[237] G. Ambrosino, G. Celentano, and F. Garofalo, "Variable structure model reference adaptive control systems," *Int. J. Control*, vol. 39, no. 6, pp. 1339–1349, 1984.

[238] J. J. Slotine and S. S. Sastry, "Tracking control of non-linear systems using sliding surfaces, with application to robot manipulators," *Int. J. Control*, vol. 38, no. 2, pp. 465–492, 1983.

[239] K. D. Young, V. I. Utkin, and U. Özgüner, "A control engineer's guide to sliding mode control," *IEEE Trans. Control Syst. Technol.*, vol. 7, no. 3, pp. 328–342, May 1999.

[240] S. Buso, S. Faolo, and P. Mattavelli, "A dead-beat adaptive hysteresis current control," *IEEE Trans. Ind. Appl.*, vol. 36, no. 4, pp. 1174–1180, Jul./Aug. 2000.

[241] L. Dalessandro, U. Drofenik, S. D. Round, and J. W. Kolar, "A novel hysteresis current control for three-phase three-level PWM rectifiers," in *Applied Power Electronics Conference and Exposition, APEC 2005*, vol. 1, Austin Texas, Mar. 6-10, 2005, pp. 501– 507.

[242] S. Buso, L. Malesani, and P. Mattavelli, "Comparison of current control techniques for active filter applications," *IEEE Trans. Ind. Electron.*, vol. 45, no. 5, pp. 722–729, Oct. 1998.

[243] T. W. Chun and M. K. Choi, "Development of adaptive hysteresis band current control strategy of PWM inverter with constant switching frequency," in *Proc. IEEE APEC'96*, vol. 1, San Jose, CA, Mar. 3-7, 1996, pp. 194 – 199.

[244] L. Malesani, P. Mattavelli, and P. Tomasin, "Improved constant-frequency hysteresis current control of VSI inverters with simple feedforward bandwidth prediction," *IEEE Trans. Ind. Appl.*, vol. 33, no. 5, pp. 1194–1202, Sept./Oct. 1997.

[245] N. A. Gounden, S. A. Peter, H. Nallandula, and S. Krithiga, "Fuzzy logic controller with MPPT using line-commutated inverter for three-phase grid-connected photovoltaic systems," *Renewable Energy*, vol. 34, no. 3, pp. 909–915, Mar. 2009.

[246] M. Castilla, J. M. Guerrero, J. Matas, J. Miret, and J. Sosa, "Comparative study of hysteretic controllers for single-phase voltage regulators," *IET Power Electr.*, vol. 1, no. 1, pp. 132–143, 2008.

Publication list of T. L. Vandoorn

List of scientific publications

Journal papers

1. J. D. M. De Kooning, J. Van de Vyver, T. L. Vandoorn, B. Meersman and L. Vandevelde, "Impact of Speed Ripple on the Back-Emf Waveform of Permanent Magnet Synchronous Machines", in *IET Electric Power Applications*, 2013, accepted for publication

2. T. L. Vandoorn, J. D. M. De Kooning, B. Meersman and L. Vandevelde, "Voltage-Based Droop Control of Renewables to avoid On-Off Oscillations caused by Overvoltages", in *IEEE Trans. on Power Delivery*, 2013, accepted for publication

3. T. L. Vandoorn, J. D. M. De Kooning, B. Meersman, L. Vandevelde, "Review of Primary Control Strategies for Islanded Microgrids with Power-Electronic Interfaces", in *Renewable and Sustainable Energy Reviews*, Volume: 19, Pages: 613-628, Mar. 2013

4. T. L. Vandoorn, B. Meersman, J. D. M. De Kooning, L. Vandevelde, "Transition from Islanded to Grid-Connected Mode of Microgrids with Voltage-Based Droop Control", in *IEEE Trans. on Power Systems*, 2012, accepted for publication

5. T. L. Vandoorn, C. Ionescu, J. D. M. De Kooning, R. De Keyser and L. Vandevelde, "Theoretical Analysis and Experimental Validation of Single-Phase Direct vs. Cascade Voltage Control in Islanded Microgrids", in *IEEE Trans. on Industrial Electronics*, Volume: 60, Issue: 2, Pages: 789 - 798, Febr. 2013

6. T. L. Vandoorn, J. D. M. De Kooning, B. Meersman, J. M. Guerrero and L. Vandevelde, "Automatic Power Sharing Modification of P/V Droop Con-

trollers in Low-Voltage Resistive Microgrids", in *IEEE Trans. on Power Delivery*, Volume: 27 Issue: 4 Pages: 2318-2325, Oct. 2012

7. T. L. Vandoorn, B. Meersman, J. D. M. De Kooning, L. Vandevelde, "Analogy Between Conventional Grid Control and Islanded Microgrid Control Based on a Global DC-Link Voltage Droop", in *IEEE Trans. on Power Delivery*, Volume: 27 Issue: 3 Pages: 1405-1414, July 2012

8. T. L. Vandoorn, B. Meersman, J. D. M. De Kooning, L. Vandevelde, "Directly-Coupled Synchronous Generators With Converter Behavior in Islanded Microgrids", in *IEEE Trans. on Power Systems*, Volume: 27 Issue: 3 Pages: 1395-1406, Aug. 2012

9. T. L. Vandoorn, B. Meersman, J. D. M. De Kooning, L. Vandevelde, "Controllable Harmonic Current Sharing in Islanded Microgrids: DG Units with Programmable Resistive Behavior towards Harmonics", in *IEEE Trans. on Power Delivery*, Volume: 27 Issue: 2 Pages: 831-841, Apr. 2012

10. T. L. Vandoorn, J. D. M. De Kooning, B. Meersman, J. Guerrero and L. Vandevelde, "Voltage-Based Control of a Smart Transformer in a Microgrid", in *IEEE Trans. on Industrial Electronics*, Volume: 60 , Issue: 4, Pages: 1291 - 1305 , Apr. 2013

11. T.L. Vandoorn, B. Renders, L. Degroote, B. Meersman and L. Vandevelde, "Active Load Control in Islanded Microgrids based on the Grid Voltage", in *IEEE Trans. on Smart Grid*, Volume: 2 Issue: 1 Pages: 127-139, March 2011

12. T.L. Vandoorn, B. Meersman, L. Degroote, B. Renders and L. Vandevelde, "A Control Strategy for Islanded Microgrids with dc-link Voltage Control", in *IEEE Trans. Power Del.*, Volume: 26 Issue: 2 Pages: 703-713, Apr. 2011

13. B. Meersman, B. Renders, L. Degroote, T. Vandoorn, L. Vandevelde, "Three-phase inverter-connected DG-units and voltage unbalance", in *Electric Power Systems Research*, Volume: 81 Issue: 4 Pages: 899-906, Apr. 2011

14. T. L. Vandoorn, F. M. De Belie, T. J. Vyncke, J. A. Melkebeek and P. Lataire, "Generation of Multisinusoidal Test Signals for the Identification of Synchronous- Machine Parameters by Using a Voltage-Source Inverter", *IEEE Trans. Ind. Electron.*, vol. 57, no. 1, pp. 430 – 439, Jan. 2010

Book chapters

1. editor K. Iniewski, book: *Smart Grid Infrastructure & Networking*, chapter: 8. Voltage Based control of DG units and active loads in Smart Microgrids (by T. Vandoorn and L. Vandevelde), publisher McGraw-Hill Professional, pages = 181-200, 2012

Other publications

1. T. Vandoorn, L. Vandevelde, G. Van Eetvelde, B. Meersman and B. Zwaenepoel, "Slimme Microgrids en Virtual Power Plants, bouwstenen van het net van de toekomst", in *Vakblad Elektrotechnisch Ingenieur*, pages 18–22, number = 140, 2012

2. Tine Vandoorn, "Snelle en kostenbesparende identificatie van elektrische machines", in *Revue-E tijdschrift: Production décentralisée, decentrale productie*, vol. 126, no. 1, pp. 49 - 54, Feb. 2010

3. B. Zwaenepoel, T. L. Vandoorn, G. Van Eetvelde, J. I. Laveyne, B. Meersman and L. Vandevelde, "Solar Commercial Virtual Power Plant", in *2013 IEEE PES General Meeting (PESGM2013)*, Vancouver, Canada, Jul. 21-25, 2013

4. T. L. Vandoorn, J. D. M. De Kooning, B. Meersman and L. Vandevelde, "Improvement of active power sharing ratio of P/V droop controllers in low-voltage islanded microgrids", in *PES General Meeting (PES 2013)*, Vancouver, July 2013, under review

5. T. L. Vandoorn, J. D. M. De Kooning, B. Meersman and L. Vandevelde, "Soft curtailment for voltage limiting in low-voltage networks through reactive or active power droops", in *IEEE Internat. Energy Conf. & Exhibition (Energycon 2012)*, Firenze Italy, Sep. 9-12, 2012

6. T. L. Vandoorn, J. D. M. De Kooning, B. Meersman and L. Vandevelde, "Communication-Based Secondary Control in Microgrids with Voltage-Based Droop Control", in *2012 IEEE PES Transmission and Distribution Conference and Exposition (T &D 2012)*, Orlando, Florida, May. 7-10, 2012

7. T. L. Vandoorn, B. Zwaenepoel, J. D. M. De Kooning, B. Meersman and L. Vandevelde, "Smart Microgrids and Virtual Power Plants in a Hierarchical Control Structure", in *IEEE PES Innovative Smart Grid Technologies (ISGT 2011)*, Manchester, UK, Dec. 5-7, 2011

8. J. Agneessens, T. L. Vandoorn, B. Meersman, L. Vandevelde, "The use of Binary Particle Swarm Optimization to obtain a Demand Side Management

system", in *IET Renewable Power Generation Conference 2011 (RPG 2011)*, Edinburgh, UK, Sep. 5-8, 2011

9. M. Jacxens, B. Meersman, T. L. Vandoorn, J. D. M. De Kooning and L. Vandevelde, Overview of voltage control strategies in medium voltage networks with implementation of distributed generation, in *IET Renewable Power Generation Conference 2011 (RPG 2011)*, Edinburgh, UK, Sep. 5-8, 2011

10. K. Mets, T. Verschueren, C. Develder, T. L. Vandoorn and L. Vandevelde, "Integrated simulation of power and communication networks for smart grid applications", in *2011 IEEE 16th Internat. Workshop on Computer Aided Modeling and Design of Communication Links and Networks (CAMAD)*, Kyoto, Japan, pages 61-65, Jul. 10-11, 2011

11. T.L. Vandoorn, T. Loix, L. Vandevelde, B. Meersman and J. Driesen, "Influence of Power Control Strategies on the Voltage Profile in an Islanded Microgrid", in *14th IEEE International Conference on Harmonics and Quality of Power (ICHQP)*, Bergamo, Italy, Sep. 26-29, 2010

12. K. Martens, B. Meersman, J. De Kooning, B. Renders, T. Vandoorn and L. Vandevelde, "Influence of bus voltage variations on two Maximum Power Point control loops", in *14th IEEE International Conference on Harmonics and Quality of Power (ICHQP)*, Bergamo, Italy, Sep. 26-29, 2010

13. T. L. Vandoorn, B. Renders, B. Meersman, L. Degroote and L. Vandevelde, "Reactive Power Sharing in an Islanded Microgrid", in *45th International Universities Power Engineering Conference (UPEC 2010)*, Cardiff, Wales, Aug. 31 - Sep. 3, 2010

14. J. De Kooning, B. Meersman, T. L. Vandoorn, B. Renders and L. Vandevelde, "Comparison of Three-Phase Four-Wire Converters for Distributed Generation", in *45th International Universities Power Engineering Conference (UPEC 2010)*, Cardiff, Wales, Aug. 31 - Sep. 3, 2010

15. B. Meersman, J. De Kooning, T. L. Vandoorn, L. Degroote, B. Renders and L. Vandevelde, "Overview of PLL methods for Distributed Generation units", in *45th International Universities Power Engineering Conference (UPEC 2010)*, Cardiff, Wales, Aug. 31 - Sep. 3, 2010

16. T. L. Vandoorn, B. Renders, L. Degroote, B. Meersman and L. Vandevelde, "Grid voltage control in islanded microgrids with inverter-interfaced power sources", in *Second Innovation for Sustainable Production Conference (i-SUP 2010)*, Bruges, Belgium, Apr. 18-21, 2010

17. L. Degroote, B. Renders, K. Stockman, B. Meersman, T. L. Vandoorn and L. Vandevelde, “Impact of Distributed Generation on Three-Phase Voltage Dips”, in *Second Innovation for Sustainable Production Conference (i-SUP 2010)*, Bruges, Belgium, Apr. 18-21, 2010

18. B. Meersman, B. Renders, L. Degroote, T. L. Vandoorn, J. De Kooning and L. Vandevelde, “Overview of three-phase inverter topologies for distributed generation purposes”, in *Second Innovation for Sustainable Production Conference (i-SUP 2010)*, Bruges, Belgium, Apr. 18-21, 2010

19. B. Meersman, B. Renders, L. Degroote, T. Vandoorn and L. Vandevelde, “The influence of grid-connected three-phase inverters on voltage unbalance”, in *IEEE Power and Energy Society General Meeting*, Minneapolis, Minnesota USA, July 25-29, 2010

20. K. Vandemergel, F. De Belie, T. Vandoorn, T. Vyncke, P. Lataire and J. Melkebeek, “Improved Modelling of PMSMs Taking into Account Conductive Rotor Parts”, *Proceedings of the International Conference on Electrical Machines (ICEM)*, Rome, Italy, Sept. 6-8, 2010

21. T. L. Vandoorn, B. Renders, L. Degroote, B. Meersman and L. Vandevelde, “Voltage Control in Islanded Microgrids by means of a Linear-Quadratic Regulator”, in *5th IEEE Joint IAS,PELS & PES Benelux Chapter Young Researchers Symposium*, Leuven, Belgium, Mar 29-30, 2010

22. K. Vandemergel, F. De Belie, T. Vandoorn, T. Vyncke, P. Lataire and J. Melkebeek, “A General Test Platform to Identify the Parameters of a Wound-Rotor Synchronous Machine”, in *5th IEEE Joint IAS,PELS & PES Benelux Chapter Young Researchers Symposium*, Leuven, Belgium, Mar 29-30, 2010

23. T. L. Vandoorn, B. Renders, B. Meersman, L. Degroote and L. Vandevelde, “Power Balancing in Islanded Microgrids by using a dc-bus Voltage Reference”, in *20th Internat. Symp. on Power Electronics, Electrical Drives, Automation and Motion (SPEEDAM 2010)*, Pisa, Italy, June 14-16, 2010

24. L. Degroote, B. Renders, B. Meersman, T. L. Vandoorn and L. Vandevelde, “Power Quality Improvements through Power Electronic Interfaced Distributed Generation”, in *20th Internat. Symp. on Power Electronics, Electrical Drives, Automation and Motion (SPEEDAM 2010)*, Pisa, Italy, June 14-16, 2010

25. T. L. Vandoorn and L. Vandevelde, “Control of microgrids in island-mode with converter-interfaced generators”, in *PhD symposium, Ghent University*, Het Pand, Ghent, Belgium, Dec. 9, 2009

26. B. Meersman, B. Renders, L. Degroote, T. L. Vandoorn and L. Vandevelde, "Control design of grid-connected three-phase inverters for voltage unbalance correction", in *International Universities' Power Engineering Conference, 44th, Proceedings (UPEC 2009)*, Glasgow, Scotland, UK, Sept. 1-4, 2009

27. T. L. Vandoorn, B. Renders, F. M. L. L. De Belie, B. Meersman and L. Vandevelde, "A Voltage-source Inverter for Microgrid Applications with an Inner Current Control Loop and an Outer Voltage Control Loop", in *International Conference on Renewable Energies and Power Quality (ICREPQ'09)*, Valencia, Spain, Apr. 14-17, 2009

28. B. Meersman, B. Renders, L. Degroote, T. L. Vandoorn and L. Vandevelde, "DC-bus voltage controllers for a three-phase voltage-source inverter for distributed generation", in *International Conference on Renewable Energies and Power Quality (ICREPQ'09)*, Valencia, Spain, Apr. 14-17, 2009

29. F. M. De Belie, P. Sergeant, T. L. Vandoorn and J. A. Melkebeek, "Estimation errors in sensorless drives due to the magnetic interaction", in *Proceedings of the International Conference on Electrical Machines (ICEM)*, Vilamoura, Portugal, Sept. 6-9, 2008

30. T. L. Vandoorn, F. M. De Belie, T. J. Vyncke, J. A. Melkebeek and P. Lataire; "Generating Multisinusoidal Test Signals by using a VSI for the Identification of Synchronous Machines" in *Proceedings of the International Conference on Electrical Machines (ICEM)*, Vilamoura, Portugal, Sept. 6-9, pp. 495-500, 2008

From Oct. 2008 - Sept. 2009, this research has been funded by the Special Research Fund (BOF) of Ghent University. T. Vandoorn thanks Ghent University for the Fellowship received.

Since Oct. 2009, the research of Tine Vandoorn is financially supported by the FWO-Vlaanderen (Research Foundation - Flanders, Belgium). T. Vandoorn thanks the FWO for the Fellowship received.